Yuriy K. Sirenko
Staffan Ström
Editors

SPRINGER SERIES IN OPTICAL SCIENCES 153

Modern Theory of Gratings

Resonant Scattering: Analysis Techniques and Phenomena

Springer

Springer Series in
OPTICAL SCIENCES 153

founded by H.K.V. Lotsch

Springer Series in
OPTICAL SCIENCES

The Springer Series in Optical Sciences, under the leadership of Editor-in-Chief *William T. Rhodes*, Georgia Institute of Technology, USA, provides an expanding selection of research monographs in all major areas of optics: lasers and quantum optics, ultrafast phenomena, optical spectroscopy techniques, optoelectronics, quantum information, information optics, applied laser technology, industrial applications, and other topics of contemporary interest.
With this broad coverage of topics, the series is of use to all research scientists and engineers who need up-to-date reference books.

The editors encourage prospective authors to correspond with them in advance of submitting a manuscript. Submission of manuscripts should be made to the Editor-in-Chief or one of the Editors. See also www.springer.com/series/624

Yuriy K. Sirenko · Staffan Ström
Editors

Modern Theory of Gratings

Resonant Scattering: Analysis Techniques and Phenomena

With contributions of:
Jean Chandezon
Gerard Granet
Petr N. Melezhik
Anatoliy Ye. Poyedinchuk
Yuriy K. Sirenko
Daniel Sjöberg
Staffan Ström
Yury A. Tuchkin
Nataliya P. Yashina

With 120 Figures

Springer

Editors
Yuriy K. Sirenko
Ukrainian Academy of Sciences
Inst. Radiophysics and Electronics
Academician Proskura Street, 12
Kharkov 61085
Ukraine
yks@ire.kharkov.ua

Staffan Ström
Royal Institute of Technology
Alfven Laboratory
SE-100 44 Stockholm
Sweden
staffan.strom@alfvenlab.kth.se

ISSN 0342-4111 e-ISSN 1556-1534
ISBN 978-1-4419-1199-5 e-ISBN 978-1-4419-1200-8
DOI 10.1007/978-1-4419-1200-8
Springer New York Dordrecht Heidelberg London

Library of Congress Control Number: 2009938004

Preface

The first publication about the discovery of a diffraction grating by the American astronomer D. Rittenhouse dates back to 1786. It was not noticed by the scientific community of the day, and in the history of science the optician J. Fraunhofer was considered to be the creator of the diffraction grating (1821). Theoretical studies of this device, characterized by amazing dispersion properties were started by F.M. Schwerd in 1835. In those days, spectral analysis was coming into being. The needs from this new area stimulated making gratings with progressive enhancement of the resolution, and they encouraged relevant theoretical and experimental studies. The outstanding achievements of H.A. Rowland must be mentioned here. He developed a machine capable of making quite fine diffraction gratings (1882). Also, he suggested making ruling lines on a concave spherical surface and as a result spectrum dispersion and sharpness were elevated to a level that had not been seen before.

The progress in several scientific and technological fields is to a large extent guided by the performance of the presently available gratings which are so sophisticated that sometimes they seem to have little to do with their predecessors from the 19th century. Polarization converters and phase changers, filters and multiplexers, quantum and solid state oscillators, open quasi-optical dispersion resonators, and power compressors – these are only a few applications of periodic structures, which astonish us (up to now!) by their capabilities for controlled polarization, spatial and frequency selection of signals.

Different operating frequency ranges call for gratings differing in characteristic size (length of a period), and in their way of achieving the operating mode. The range is so wide that, say, if one end is a standard echelette optical reflection grating (3600 lines per millimeter on a 40 [cm] $\times$ 40 [cm] aluminium sheet) the other could be the antenna array of the unique decameter radio telescope UTR-2 developed and fabricated by the academician S.Ya. Braude's team at the Institute of Radio Physics and Electronics of the Ukrainian Academy of Sciences in 1966. This antenna field is developed by two multicomponent arrays. The first one, 1800 [m] long and 53 [m] wide, consists of 1440 wideband components making up 6 meridian aligned rows. The other, 900 [m] long and 40 [m] wide, is normal to the first one and carries 6 rows of 600 dipoles. All the dipoles (wire cylinders 8 [m] long and 1.8 [m] across) are horizontally arranged at a height of 3.5 [m] and east–west oriented.

Few countries could afford equipment for ruling optical gratings with thousand lines per millimeter. This process, expensive and time-consuming, failed to satisfy growing practical requirements. Rather good results have been achieved in making replicas of mechanically produced originals. An idea that diffraction gratings can be manufactured with the aid of holography was suggested by Yu.N. Denisyuk in 1962. The idea has been developed into holographic gratings intensively used in the making of spectral instruments. The advantages of holographic gratings consist in the fact that such gratings are free from grating ghosts (i.e., high orders caused by periodicity deviation), they are characterized by little occasional light diffusion and are easy to produce. Naturally, to get desired diffraction characteristics from holographic gratings is more difficult than, e.g., getting them from ruled echelette gratings whose geometry uniquely depends on the so-called blaze angle. Holographic gratings rank below ruled gratings in diffraction efficiency but, according to many authors, their wavefront quality in a working order (harmonic) is better. In addition, several observation were made in the 1980s that the employment of certain schemes of hologram recording and subsequent photoresist processing opened the way for design of blazed gratings, including echelettes.

Evidently effective employment of diffraction gratings cannot be achieved without thorough theoretical and experimental research into their diffraction properties. These investigations began early in the 20th century. R.W. Wood improved the diffraction grating by shaping the grooves to specific geometries. On this basis, he launched systematic studies of the energy distribution among different harmonics and experimentally found the property of anomalous scattering. Lord Rayleigh was the first to expand the field scattered from the grating into a series of plane waves. Studying the echelette wave diffraction in theoretical terms, he developed an approximate technique (known as the Rayleigh method) which has been one of the most widely used until rigorous techniques became available.

In the evolution of grating theory, one can identify several key periods. One falls within the last decades of the 20th century, characterized by the fact that relevant theoretical problems were approached using classical mathematical disciplines: mathematical physics, computational mathematics, theory of differential, and integral equations, etc. That the grating became a subject of adequate mathematical simulation has opened up new opportunities for reliable physical analysis and also new avenues of attack, on a rigorous theoretical base, on numerous applied problems. At this stage, the modern electromagnetic theory of gratings was greatly contributed by the scientific schools of Marseille, France (R. Petit, D. Maystre, M. Neviere, P. Vincent, A. Roger, J. Chandezon, et al.) and Kharkov, Ukraine (V.P. Shestopalov, L.N. Litvinenko, S.A. Masalov, V.G. Sologub, A.A. Kirilenko, et al.). The key chapters of the book largely proceed from their achievements from the early 1960s and onwards. Obviously, the growth of the research in the above-mentioned schools was heavily influenced by the results from other scientific centers the world over. We will address the most significant of them.

The methodology of modern radio physics is based on mathematical simulation and numerical experiment and it is realized by solving boundary value (frequency

domain) and initial boundary value (time domain) problems for Maxwell's equations. Time domain approaches (see, e.g., Chapter 4) offer more versatility and are more suited for the analysis of sophisticated electromagnetic structures of interest for applications. As a rule, the calculations here are reduced to implementation of explicit schemes (the schemes with the sequential passage of the time layers). There is a good agreement between the calculated results (results from analysis of electromagnetic field space–time transformations) and general human perception – the time domain is free of some idealizations, which are peculiar to the frequency domain. Moreover, time domain results are easy to change into the amplitude–frequency characteristics in the prescribed range of the frequency parameter $k = 2\pi/\lambda$, where λ is the free space wavelength. However, time domain methods are not used as extensively as one would expect for getting physical results proper. Thus, for example, all the power of the most popular at the moment FDTD-method is mainly applied to solution of particular engineering problems.

Far more examples of systematic and fruitful theoretical treatments can be met in time harmonic electromagnetics whose problems have been addressed much earlier in rigorous formulation. The last decades of the 20th century have brought some special powerful techniques for analysis and synthesis of various electromagnetic features. Numerous physical phenomena accompanying processes of monochromatic wave's radiation, propagation, and scattering have been identified, interpreted, and implemented into design of novel devices. Such advances have been assured by the fact that new theoretical methods have been developed being oriented to the solution to the specific applied problems. They have accounted the peculiarities of problems of interest and hence have provided with not only quantitative information, but they created also the base for qualitative analysis with further generalization. As an example, one may consider the authentic analytic regularization procedures (see Chapter 2) outperforming other frequency domain techniques in resonance situations. Actually, nearly all profound physical results gained from electromagnetic theory of gratings are due to use of analytic regularization procedures.

The long-wave specific case ($\kappa = l/\lambda \ll 1$, l is the grating period length), ending up with solutions of simple analytic representations and convenient approximations, has been understood most comprehensively by frequency domain methods. Here, the approach based on equivalent boundary conditions, possessing in the general case anisotropic properties, is widely applied (B.Ya. Moyzhes, L.A. Vainshtein, V.M. Astapenko and G.D. Malyuzhinetz; Ye.I. Nefedov, and A.N. Sivov, et al.). The theory of dense gratings based on this approach takes into account the influence of shape and relative size of the grating elements, the presence of sharp boundaries in the dielectric filling and allows one to make a correct limit transition as the conductors come infinitely close. A key point in the solution of the diffraction problem based on this theory is a search for the reflection and the propagation coefficients in terms of powers of a small parameter κ via considering a relevant static problem. The long-wavelength diffraction is implemented in many modern superhigh-frequency devices and units, thus the relevant theoretical studies are of current importance.

Simple and convenient analytic representations are very useful for the designers and, at the same time, they are an aid to general nature interpretations contributing to the electromagnetic theory of gratings. An example is the effect observed by G.D. Malyuzhinetz in the 1940s: given a certain angle of incidence on a dense grating arranged by metal bars of nonzero thickness, a plane H-polarized wave propagates through it with no reflection.

Of tremendous interest for physics and applications and a great problem for analysis is the resonance case $\kappa = O(1)$, i.e., the case when the wavelength is comparable with the grating period. When computer resources were limited, the research into the resonance domain had been restricted to some specific or limiting situations. They were studied by V.S. Ignatovskiy, E.A.N. Whitehead, F. Berz, J.F. Carlson, A.E. Heins, G.L. Baldwin, L.A. Vainshtein, V. Twersky, Yu.P. Lysanov, and others. These researchers laid a solid ground for the modern theory of resonant wave scattering by periodic structures. Indeed, the ideas and achievements gained in the 1940s–1960s are traced in almost every present-day method of mathematical modeling oriented to numerical experiments. First of all, it is the method of partial domains (or mode matching method) whose first fruitful implementation can be seen in L.N. Deryugin's works. Next are the potential-theory-based methods (integral equation techniques) whose present technique (N. Amitay, V. Galindo, and C.P. Wu; A.S. Il'inskiy and T.N. Galishnikova; A.I. Sukhov; Z.T. Nazarchuk, and others) is based on the quasi-periodic Green's function derived by V. Twersky. At a point of equivalent reformulation of the original boundary value problem, the authors of some analytic numerical methods (Ye.V. Avdeev and G.V. Voskresenskiy; R. Mittra and T. Itoh; S.M. Zhurav, and others) address, either implicitly or not, the technique and the results of the analytic solution to canonic diffraction problems similar to those considered by E.A.N. Whitehead, F. Berz, and others. Only few such problems have been solved rigorously. The most popular ones (see, e.g., works by E. Luneburg and K. Westpfahl; V.D. Luk'yanov; L.A. Vainshtein and V.I. Vol'man) have always been those about half-plane gratings and planar strip gratings. The enduring interest in elementary structures whose diffraction characteristics have long been thoroughly studied for arbitrary geometrical parameters and frequencies, from the long to the short wave regions, is indeed reasonable. The main significance of these considerations and the most valuable aspects of the outcomes consist in the search for new ideas and approaches and proving their potentials to be used in more sophisticated situations, which are far from standard.

In closing the issue of succession, it should be mentioned that the numerical solution of the problems concerning the plane wave diffraction by periodic corrugated surfaces has been the most frequently attempted by invoking the Rayleigh method (Rayleigh hypothesis). There are methods that take the Rayleigh representations for the scattered field and extend them in a straightforward manner from their region of validity directly to the grating surface. Furthermore, there are methods, prompted by the Rayleigh hypothesis, but resting on the fundamental results of I.N. Vekua about completeness of some systems of functions on curved contours. In the first case, difficulties in the proof of the principal step (it is necessary to

study singularities of the analytic continuation of the Rayleigh representation as a function of space coordinates) can be overcome only for shallow gratings, with the groove profile described by a sufficiently smooth one-valued function (see works of A.G. Kyurkchan). And even then a correct truncation of the resulting infinite system of algebraic equations for unknown amplitudes of the field space harmonics is not possible. In the other case, a principal feasibility exists to construct special linear combinations of functions that are asymptotically close to the solutions of the corresponding diffraction problems throughout the whole scattering domain. The central problem – development of stable computation schemes – is solved then with the adaptive (assignable by the groove shape and κ value) collocation technique.

In many works of electromagnetic theory of gratings the modern scientific methodology chain "object $\rightarrow$ mathematical model $\rightarrow$ algorithm $\rightarrow$ numerical experiment $\rightarrow$ physical interpretation of the results $\rightarrow$ formulation of general conclusions and recommendations" breaks down somewhere in the middle, at a level of standard illustrations of the efficiency of the algorithm. But nevertheless, after L.N. Deryugin's work who analyzed (in terms of some particular cases) the surface and double surface resonances on the comb gratings, issues do appear, which inform of experimental, analytic, and numerical results, concerning

- threshold phenomena (A. Hessel and A.A. Oliner; B.M. Bolotovskiy and A.N. Lebedev; E.A. Yakovlev and M.V. Robachevskiy);
- semitransparent grating effects of total resonant transition and reflection of plane waves (Ye.V. Avdeev and G.V. Voskresenskiy; A.F. Chaplin and A.D. Khzmalyan; R.S. Zaridze and G.M. Talakvadze; Yu.P. Vinichenko, A.A. Lemanskiy, and M.B. Mityashev);
- effects of total nonspecular wave reflection by reflective structures (E.V. Jull and G.R. Ebbeson; J.R. Andrewarsha, J.R. Fox, and I.J. Wilson; S.N. Vlasov and Ye.V. Koposova; and others).

Some authors (see, for example, works of E.V. Jull, D.C.W. Hi, N.C. Beaulieu, and P. Facq) have raised a very important question about the differences between the ideal (infinitely extending structure in the plane wave field) and actual (finite excitation field spot on the infinite periodic structure or finite structure in the plane wave field) operating modes of the grating.

Also nowadays the diffraction grating is still one of the central objects of electromagnetic analysis. Independent of how comprehensive the progress in our understanding of the grating is, continued research in this direction remains very important, indeed practical needs and the intrinsic logic of development of the modern grating theory present us with new problems, sending us to seek and hopefully find ways to their solution. Just so was formed during the recent years a new line of investigation, which is partially considered in this book (see Chapter 5) and associated with the analysis, synthesis, and determination of equivalent parameters of artificial materials – layers and coatings, which have a periodic structure and properties exhibited by natural materials in exceptional cases only.

Generally speaking, the book reflects those results which, in our opinion, are able to further pursue electromagnetic theory of gratings in pace with today's requirements of fundamental and applied science. The book gives the reader quite a comprehensive idea of:

- spectral theory of gratings (Chapter 1) giving reliable grounds for physical analysis of space–frequency and space–time transformations of the electromagnetic field in open periodic resonators and waveguides;
- authentic analytic regularization procedures (Chapter 2) that, in contradistinction to the traditional frequency domain approaches, fit perfectly for the analysis of resonant wave scattering processes;
- parametric Fourier method and C-method (Chapter 3) oriented on the effective numerical analysis of transformation properties of periodic interfaces and multilayer conformal arrays;
- new rigorous methods for analysis of spatial–temporal transformations of electromagnetic field that are grounded on the construction and incorporation into the standard finite-difference computational schemes, the so-called exact absorbing boundary conditions (Chapter 4);
- new solution variants to the homogenization problem (Chapter 5) – the central problem arising in the synthesis of metamaterials and metasurfaces;
- new physical and applied results (Chapters 2–5) about pulsed and monochromatic wave resonant scattering by periodic structures, including structures loaded on dielectric layers or chiral and left-hand medium layers, etc.

The authors hope that the reader will find that the discussed physical and applied results are presented in an illuminating way. Thus, for example, some figures in Chapter 4 are accompanied by **.exe** files which enable to watch in dynamics the space–time transformations of the electromagnetic field close to finite and infinite periodic structures. The archive with these files is open for downloading at http://www.ire.kharkov.ua/downloads/Figures_EXE_Files.zip.

The book is intended for researchers and graduate students in computational electrodynamics and optics, theoretical and applied radio physics. The material is also suitable for undergraduate courses in physics, computational physics, and applied mathematics.

The authors are representatives of a series of large European scientific and educational centers: Royal Institute of Technology, Stockholm, Sweden (Staffan Ström, the editor and the co-author of Chapter 4); *Blaise Pascal* University, Clermont-Ferrand, France (Jean Chandezon and Gerard Granet – Chapter 3); *Usikov* Institute of Radio Physics and Electronics of the National Academy of Sciences of Ukraine, Kharkov, Ukraine (Petr Melezhik – Sections 2.2, 2.4, 2.5; Anatoliy Poyedinchuk – Sections 2.1, 2.2, 2.4, 2.5, 3.6; Yuriy Sirenko – the editor, the author and co-author of Chapters 1, 4, and Section 2.3; Yury Tuchkin – Sections 2.1, 2.6; and Nataliya Yashina – Chapter 4 and Sections 2.4, 2.5, 3.6); Lund University, Lund, Sweden (Daniel Sjöberg – Chapter 5).

In this book, they are united by their profound interest in periodic structures, an area whose study has always been associated with burning scientific and engineering problems for the last one and a half hundred years.

Kharkov *Yuriy Sirenko*
Stockholm *Staffan Ström*

Contents

Chapter 1
Basic Statements

Abstract The principal results of modern electromagnetic theory of gratings are reviewed briefly in this chapter. The model initial boundary value problems and boundary value problems are formulated and supplied with basic equations, domains of analysis, boundary and initial conditions, and the condition providing their unambiguous resolution are determined. The analytic relations between problems in time and frequency domains are found out. The problems connected with the consideration of gratings as open periodic resonators and waveguides are formulated and analyzed. The actual essential results of spectral theory of gratings and resonant scattering theory by periodic structures are presented in concise form.

1.1 The Formulation of Boundary Value and Initial Boundary Value Problems in the Theory of Diffraction Gratings

1.1.1 Fundamental Equations

The initial boundary value problems and boundary value problems for the system of differential Maxwell equations form the corner stone of time domain and frequency domain electromagnetic theory. The solutions to these problems provide us with results, describing physical phenomena of spatio–temporal and spatial–frequency transformations of electromagnetic fields occurring in a large variety of structures: gratings, wave-guiding units, open resonators, radiating elements in antennas, etc. The adequacy and accuracy of the results depend in an essential way on the quality of the mathematical problems formulation and on the possibility of detailed analytic investigation of the solutions before the start of their numerical determination. In this chapter, we describe the problems of electromagnetic theory of gratings resulting from following system of equations:

$$\eta_0 \mathrm{rot}\vec{H} = \varepsilon\frac{\partial \vec{E}}{\partial t} + \sigma\vec{E} + \vec{J},\ \mathrm{rot}\vec{E} = -\eta_0\mu\frac{\partial \vec{H}}{\partial t}, \tag{1.1}$$

$$\mathrm{div}\left(\mu\vec{H}\right) = 0\,,\ \mathrm{div}\left(\varepsilon\vec{E}\right) = \rho, \tag{1.2}$$

Y.K. Sirenko, S. Ström (eds.), *Modern Theory of Gratings*, Springer Series in Optical Sciences 153, DOI 10.1007/978-1-4419-1200-8_1,

$$\mathrm{div}\vec{J} + \mathrm{div}\left(\sigma\vec{E}\right) + \frac{\partial \rho}{\partial t} = 0. \tag{1.3}$$

This is a complete system of Maxwell equations for electromagnetic waves propagating in stationary, locally inhomogeneous, isotropic, and nondispersive media. The system has to be supplemented with the equation of conservation of charge. Here, $\vec{E} \equiv \vec{E}(g,t) = \left\{E_x,E_y,E_z\right\}$ and $\vec{H} \equiv \vec{H}(g,t) = \left\{H_x,H_y,H_z\right\}$ are the vectors of the electrical and magnetic field strengths; $\eta_0 = (\mu_0/\varepsilon_0)^{1/2}$ is the free space impedance; ε_0 and μ_0 are the electric and magnetic vacuum constants; $\vec{J} = \eta_0\vec{j}$, $\vec{j} \equiv \vec{j}(g,t)$ is the extraneous current density; $\sigma = \eta_0\sigma_0$, $\sigma_0 \equiv \sigma_0(g) \geq 0$ is the specific conductivity of a locally inhomogeneous medium; $\varepsilon \equiv \varepsilon(g) \geq 1$ and $\mu \equiv \mu(g) \geq 1$ are its relative permittivity and magnetic permeability; $\rho = \rho_0/\varepsilon_0$, $\rho_0(g,t)$ is the volume density of the inducted and external electric charges; $g = \{x,y,z\}$ is a point in the space $\mathbf{R}^3$; x, y, and z are the Cartesian coordinates. We use SI for all physical parameters except t that is measured in meters ([m]) – it is the product of the natural time and the velocity of the propagation of light in vacuum.

If ρ in (1.2) and (1.3) is presented as the sum of two terms ρ_1 and ρ_2, denoting correspondingly the induced and external electric charge, then the continuity equation can be rewritten for each term separately: the induced charge ρ_1 corresponds to the conductivity current $\sigma\vec{E}$, external charge ρ_2 corresponds to external current $\vec{J}$. In the absence of external charges and currents, the induced electric charges and currents in homogeneous conducting media disappear rather quickly.

The first equation in (1.2) follows from the second one in (1.1), only if $\mathrm{div}\left(\mu\vec{H}\right) = 0\big|_{t=0}$. The second equation in (1.2) follows from the first equation in (1.1) and equation (1.3), only if $\mathrm{div}\left(\varepsilon\vec{E}\right) = \rho\big|_{t=0}$. Equation (1.3) follows from the first equation in (1.1) and the second one in (1.2). That means the divergence equations in (1.1), (1.2), and (1.3) are, in essence, conditions imposed on the initial data of the problem, but initial data for $\vec{E}$ and ρ have to be consistent [1]. Equation (1.3) makes the sources consistent (external electric charges and electric currents) for all observation times t. Generally, there are no formal reasons to assume that all the above-mentioned conditions are satisfied. That is why the system of equations describing electromagnetic processes is conventionally written in its complete form (1.1), (1.2), and (1.3).

If the problem is formulated correctly, all six components of the vectors $\vec{E}$ and $\vec{H}$ are defined by curl equations (1.1), which in Cartesian coordinates have the form

$$\begin{cases} \dfrac{\partial H_z}{\partial y} - \dfrac{\partial H_y}{\partial z} = \varepsilon\eta_0^{-1}\dfrac{\partial E_x}{\partial t} + \sigma_0 E_x + j_x \\ \dfrac{\partial H_x}{\partial z} - \dfrac{\partial H_z}{\partial x} = \varepsilon\eta_0^{-1}\dfrac{\partial E_y}{\partial t} + \sigma_0 E_y + j_y \\ \dfrac{\partial H_y}{\partial x} - \dfrac{\partial H_x}{\partial y} = \varepsilon\eta_0^{-1}\dfrac{\partial E_z}{\partial t} + \sigma_0 E_z + j_z \end{cases}, \quad \begin{cases} \dfrac{\partial E_z}{\partial y} - \dfrac{\partial E_y}{\partial z} = -\eta_0\mu\dfrac{\partial H_x}{\partial t} \\ \dfrac{\partial E_x}{\partial z} - \dfrac{\partial E_z}{\partial x} = -\eta_0\mu\dfrac{\partial H_y}{\partial t} \\ \dfrac{\partial E_y}{\partial x} - \dfrac{\partial E_x}{\partial y} = -\eta_0\mu\dfrac{\partial H_z}{\partial t} \end{cases}. \tag{1.4}$$

When the sources, that generate the field, and the structures, in which this field propagates, are homogeneous along the x-axis, we get $\partial/\partial x \equiv 0$, and the general problems for (1.1) splits into two mutually complementary problems: for E-polarized ($E_y = E_z = H_x = j_y = j_z \equiv 0$) and H-polarized ($H_y = H_z = E_x = j_x \equiv 0$) fields. In the case of E-polarization for $\mu\,(g) = \text{const}$ we get

$$\left[-\varepsilon\mu\frac{\partial^2}{\partial t^2} - \sigma\mu\frac{\partial}{\partial t} + \frac{\partial^2}{\partial y^2} + \frac{\partial^2}{\partial z^2}\right] E_x\,(g,t) = F\,(g,t) \equiv \mu\frac{\partial J_x}{\partial\, t}, \tag{1.5}$$

$$\frac{\partial H_y}{\partial t} = -\left(\eta_0\mu\right)^{-1}\frac{\partial E_x}{\partial z},\ \frac{\partial H_z}{\partial t} = \left(\eta_0\mu\right)^{-1}\frac{\partial E_x}{\partial y}. \tag{1.6}$$

When $\varepsilon\,(g) = \text{const}$ and $\sigma\,(g) = \text{const}$, equations of the same kind can be derived also for the components of the H-polarized field:

$$\left[-\varepsilon\mu\frac{\partial^2}{\partial t^2} - \sigma\mu\frac{\partial}{\partial t} + \frac{\partial^2}{\partial y^2} + \frac{\partial^2}{\partial z^2}\right] H_x\,(g,t) = F\,(g,t) \equiv \frac{\partial\, j_y}{\partial\, z} - \frac{\partial\, j_z}{\partial\, y}, \tag{1.7}$$

$$\varepsilon\frac{\partial E_y}{\partial t} + \sigma E_y + J_y = \eta_0\frac{\partial H_x}{\partial z},\ \varepsilon\frac{\partial E_z}{\partial t} + \sigma E_z + J_z = -\eta_0\frac{\partial H_x}{\partial y}. \tag{1.8}$$

In the general case, the vector functions $\vec{E}$ and $\vec{H}$ can be found either directly from (1.1) or from the equations, following from the system (1.1) after certain transformations (introducing various potentials, etc.). In this chapter, we consider the following vector problems that are equivalent (for $\mu\,(g) = \text{const}$) to (1.1):

$$\begin{cases} \left[\Delta - \operatorname{grad}\operatorname{div} - \varepsilon\,(g)\,\mu\dfrac{\partial^2}{\partial\, t^2} - \sigma\,(g)\,\mu\dfrac{\partial}{\partial\, t}\right]\vec{E}\,(g,t) = \\ \qquad = \mu\dfrac{\partial}{\partial\, t}\vec{J}\,(g,t) \equiv \vec{F}\,(g,t) \\ \dfrac{\partial}{\partial\, t}\vec{H}\,(g,t) = -\dfrac{1}{\eta_0\mu}\operatorname{rot}\vec{E}\,(g,t)\,; \qquad g \in \mathbf{R}^3 \end{cases}. \tag{1.9}$$

Here, Δ is the Laplace operator, which in Cartesian coordinates has the form

$$\Delta \equiv \frac{\partial^2}{\partial\, x^2} + \frac{\partial^2}{\partial\, y^2} + \frac{\partial^2}{\partial\, z^2}.$$

1.1.2 Domains of Analysis, Boundary and Initial Conditions

Equations (1.5), (1.7), and (1.9) are of hyperbolic type [2]. The initial boundary value problems for them have to include initial (at $t = 0$) and boundary (at all external and internal boundaries of the analysis domains $\mathbf{Q}$) conditions. In 3-D or 2-D (for case of $\partial/\partial x \equiv 0$) vector or scalar problems the domain of analysis $\mathbf{Q}$ is part

of the space $\mathbf{R}^3$ or the plane $\mathbf{R}^2$, bounded by surfaces $\mathbf{S}$ or by contours $\mathbf{S}_x$ that are the boundaries of the domains int $\mathbf{S}$ or int $\mathbf{S}_x$ ($\mathbf{S}_x$ is the trace of the surfaces $\mathbf{S}$ on the plane $x = \text{const}$), filled with a perfect conductor: $\mathbf{Q} = \mathbf{R}^3 \backslash \overline{\text{int}\,\mathbf{S}}$ or $\mathbf{Q} = \mathbf{R}^2 \backslash \overline{\text{int}\,\mathbf{S}_x}$. In so-called open problems, the analysis domains $\mathbf{Q}$ may extend to infinity along one or several space directions.

The system of boundary conditions for initial boundary value problems is formulated in the following way [3]:

- On a perfect conductor surface $\mathbf{S}$ the tangential component of the electric field density vector is equal to zero for all observation times t:

$$E_{tg}(g,t)\big|_{g\in\mathbf{S}} = 0,\ t \geq 0. \tag{1.10}$$

  From (1.10) and (1.1) follows:

$$H_{nr}(g,t)|_{g\in\mathbf{S}} = 0,\ \left.\frac{\partial H_{tg}(g,t)}{\partial \vec{n}}\right|_{g\in\mathbf{S}} = 0,\ t \geq 0;$$

  $\vec{n}$ is the outward normal with respect to the domain int$\mathbf{S}$. The function $H_{tg}(g,t)\big|_{g\in\mathbf{S}}$ defines so-called surface currents, generated on $\mathbf{S}$ by external electromagnetic field $\left\{\vec{E}(g,t), \vec{H}(g,t)\right\}$.
- On the surfaces $\mathbf{S}^{\varepsilon,\sigma}$ of discontinuities of the material properties of the medium, as well as all over the domain $\mathbf{Q}$, the tangential components $E_{tg}(g,t)$ and $H_{tg}(g,t)$ of the vectors of strength of the electrical ($\vec{E}$) and magnetic ($\vec{H}$) fields should be continuous. The normal components $\varepsilon\varepsilon_0 E_{nr}(g,t)$ and $\mu\mu_0 H_{nr}(g,t)$ of the vectors of electric and magnetic flux density are also continuous here.
- In the vicinity of singular points of the boundaries of the domain $\mathbf{Q}$ (points where the tangent and normal vectors are not defined) the density of the field energy has to be spatially integrable.
- If the domain $\mathbf{Q}$ is not bounded and the field $\left\{\vec{E}(g,t), \vec{H}(g,t)\right\}$ is generated by sources with supports that are bounded in $\mathbf{Q}$ then for any of finite time interval $(0;T)$ one can construct a virtual boundary $\mathbf{M} \subset \mathbf{Q}$ sufficiently remote from the sources, such that

$$\left\{\vec{E}(g,t), \vec{H}(g,t)\right\}\big|_{g\in\mathbf{M},\ t\in(0;T)} = 0. \tag{1.11}$$

Initial conditions (at the moment $t = 0$) give the starting state of the system, varying after (at times $t > 0$) according to the differential equations and the boundary conditions. The reference states $\vec{E}(g,0)$ and $\vec{H}(g,0)$ in the system (1.1) are the same as $\vec{E}(g,0)$ and $\left[\partial\vec{E}(g,t)/\partial t\right]\big|_{t=0}$ ($\vec{H}(g,0)$ and $\left[\partial\vec{H}(g,t)\big/\partial t\right]\big|_{t=0}$) in the differential forms of the second order (in the terms of t), to which (1.1) is transformed if the vector $\vec{H}$ (vector $\vec{E}$) is eliminated. Thus, (1.9) should be complemented with initial conditions of the kind

$$\vec{E}\,(g,0) = \vec{\varphi}\,(g)\,,\ \left.\frac{\partial}{\partial t}\vec{E}\,(g,t)\right|_{t=0} = \vec{\psi}(g),\ g \in \bar{\mathbf{Q}}. \tag{1.12}$$

The functions $\vec{\varphi}\,(g)$, $\vec{\psi}\,(g)$, and $\vec{F}\,(g,t)$, $t > 0$ (the instant and current source functions), usually have limited support in the closure of the domain $\mathbf{Q}$. Current sources can be divided into hard and soft [4]: soft sources do not have material supports and thus they are not able to scatter electromagnetic waves. Instant sources are used conventionally for pulsed excitation waves $\vec{U}^i\,(g,t)$ setting: $\vec{\varphi}\,(g) = \vec{U}^i\,(g,0)$ and $\vec{\psi}\,(g) = \left[\partial\ \vec{U}^i\,(g,t)\big/\partial t\right]\Big|_{t=0}$. The pulsed signal $\vec{U}^i\,(g,t)$ itself should satisfy the corresponding wave equation and the causality principle. One should also make sure that until the time $t = 0$ the pulsed signal does not make contact with the scattering object.

The latter is obviously impossible if infinite structures (gratings, for example) are excited by plane pulsed waves that propagate in a direction different from the normal to certain infinite boundary. Such waves are able to "sweep up" a part of the scatterer's surface by any moment of time. As a result, a mathematically correct modeling of the process becomes impossible: the input data required for the initial boundary value problem formulation are defined, as a matter of fact, by the solution of this problem.

1.1.3 Time Domain: Initial Boundary Value Problems

The vector problems describing the transient states of the field nearby the gratings with the geometry presented in Fig. 1.1a can be written in the form

$$\begin{cases} \left[\Delta - \operatorname{grad}\operatorname{div} - \varepsilon\,(g)\,\mu\,(g)\,\dfrac{\partial^2}{\partial\,t^2} - \sigma\,(g)\,\mu\,(g)\,\dfrac{\partial}{\partial\,t}\right]\vec{E}\,(g,t) = \vec{F}\,(g,t)\,; \\ \qquad g = \{x,y,z\} \in \mathbf{Q}, \quad t > 0 \\ \vec{E}\,(g,0) = \vec{\varphi}\,(g)\,, \qquad \left.\dfrac{\partial}{\partial t}\vec{E}\,(g,t)\right|_{t=0} = \vec{\psi}(g); \qquad g \in \bar{\mathbf{Q}} \\ E_{tg}\,(g,t)\big|_{g\in\mathbf{S}} = 0; \qquad t \geq 0 \end{cases} . \tag{1.13}$$

Here, $\mu\,(g)$ is a piecewise constant function and the surfaces $\mathbf{S}$ are assumed to be sufficiently smooth. It is also assumed (here and in consideration of other initial boundary value problems) that continuity conditions for tangential components of the vectors of electromagnetic fields density are satisfied, if required. The analysis domain $\mathbf{Q} = \mathbf{R}^3 \backslash \overline{\operatorname{int}\mathbf{S}}$ comprises essentially all of the space $\mathbf{R}^3$. For such domain the problems can be resolved efficiently only for two following cases:

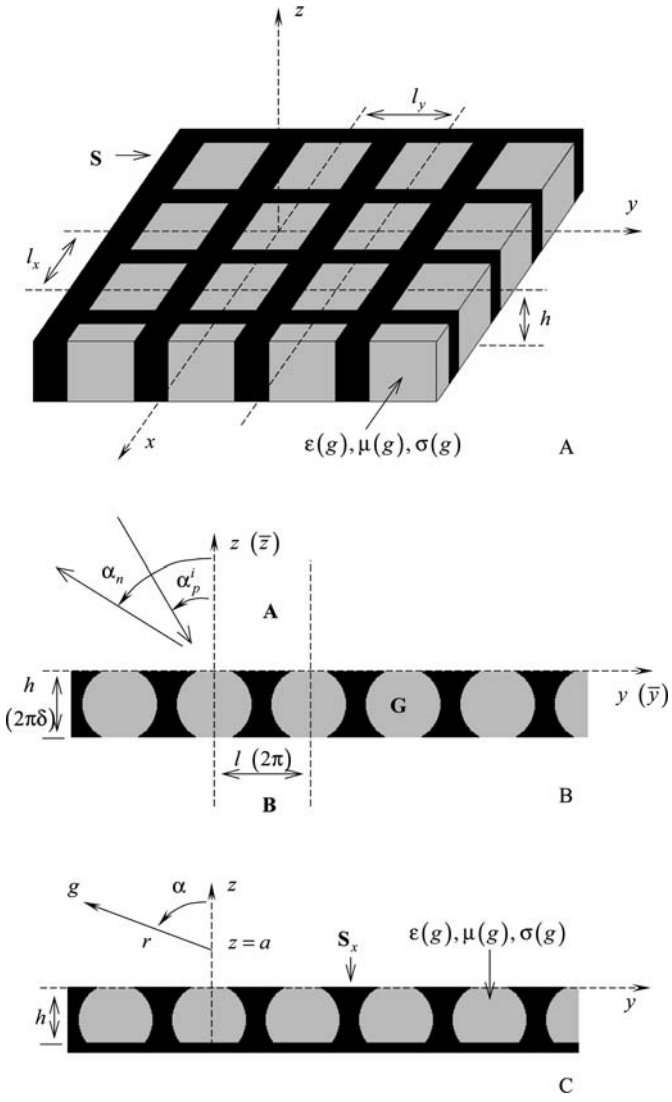

Fig. 1.1 The geometry of model problems in a right-handed coordinate system: (**a**) Three-dimensional grating; (**b**) semitransparent; and (**c**) reflecting plane gratings. Structures (**b**) and (**c**) are homogeneous along the *x*-axis

- The problem (1.13) degenerates into a conventional Cauchy problem ($\overline{\text{int}\,\mathbf{S}} = \emptyset$, medium is homogeneous, and the supports of the functions $\vec{F}\,(g,t)$, $\vec{\varphi}\,(g)$, and $\vec{\psi}(g)$ are bounded). With some inessential restriction for the source functions, the classical and generalized solution of the Cauchy problem does exist, is unique, and is described by the well-known Poisson formula [2].

- The functions $\vec{F}(g,t)$, $\vec{\varphi}(g)$, and $\vec{\psi}(g)$ have the same displacement symmetry as the periodic structure. In this case, the domain of analysis can be reduced to $\mathbf{Q}^{new} = \left\{g \in \mathbf{Q}: 0 < x < l_x; 0 < y < l_y\right\}$, completing problems (1.13) with periodicity conditions [1] on lateral surfaces of the rectangular Floquet channel $\mathbf{R} = \left\{g \in \mathbf{R}^3: 0 < x < l_x; 0 < y < l_y\right\}$.

The domain of analysis can be reduced to $\mathbf{Q}^{new}$ in more general case also. The objects of analysis are in this case not quite physical (complex sources, waves, and fields). However, by simple mathematical transformations, all the results can be presented in the customary, physically correct form. There are many reasons why the modeling of physically realizable situations in the electromagnetic theory of gratings should start with the analysis of initial boundary value problems for the images $f^{new}\left(g,t,\Phi_x,\Phi_y\right)$ of the functions $f(g,t)$ describing the true sources:

$$f(g,t) = \int_{-\infty}^{\infty}\int_{-\infty}^{\infty} \tilde{f}(z,t,\Phi_x,\Phi_x) \exp\left(2\pi i \Phi_x \frac{x}{l_x}\right) \exp\left(2\pi i \Phi_y \frac{y}{l_y}\right) d\Phi_x d\Phi_y$$

$$= \int_{-\infty}^{\infty}\int_{-\infty}^{\infty} f^{new}\left(g,t,\Phi_x,\Phi_y\right) d\Phi_x d\Phi_y. \tag{1.14}$$

From (1.14) it follows that

$$f^{new}\left\{\frac{\partial f^{new}}{\partial x}\right\}(x + l_x,y,z,t,\Phi_x,\Phi_x) = \mathrm{e}^{2\pi i \Phi_x} f^{new}\left\{\frac{\partial f^{new}}{\partial x}\right\}(x,y,z,t,\Phi_x,\Phi_x),$$

$$f^{new}\left\{\frac{\partial f^{new}}{\partial y}\right\}\left(x,y + l_y,z,t,\Phi_x,\Phi_x\right) = \mathrm{e}^{2\pi i \Phi_y} f^{new}\left\{\frac{\partial f^{new}}{\partial y}\right\}(x,y,z,t,\Phi_x,\Phi_x).$$

The use of the foregoing conditions restricts the analysis domain to the domain $\mathbf{Q}^{new}$, which is a part of the Floquet channel $\mathbf{R}$, and this allows us to rewrite the problems (1.13) in the following form:

$$\vec{E}(g,t) = \int_{-\infty}^{\infty}\int_{-\infty}^{\infty} \vec{E}^{new}(g,t)\left(g,t,\Phi_x,\Phi_y\right) d\Phi_x d\Phi_y,$$

$$\begin{cases} \left[\Delta - \operatorname{grad}\operatorname{div} - \varepsilon(g)\,\mu(g)\,\dfrac{\partial^2}{\partial t^2} - \sigma(g)\,\mu(g)\,\dfrac{\partial}{\partial t}\right]\vec{E}^{new}(g,t) = \vec{F}^{new}(g,t); \\ \qquad g \in \mathbf{Q}^{new}, \qquad t > 0 \\ \vec{E}^{new}(g,0) = \vec{\varphi}^{new}(g), \qquad \dfrac{\partial}{\partial t}\vec{E}^{new}(g,t)\Big|_{t=0} = \vec{\psi}^{new}(g); \qquad g \in \bar{\mathbf{Q}}^{new} \\ E_{tg}^{new}(g,t)\Big|_{g\in\mathbf{S}} = 0; \qquad t \geq 0 \\ \vec{E}^{new}\left\{\dfrac{\partial \vec{E}^{new}}{\partial x}\right\}(l_x,y,z,t) = \mathrm{e}^{2\pi i\Phi_x}\vec{E}^{new}\left\{\dfrac{\partial \vec{E}^{new}}{\partial x}\right\}(0,y,z,t); \qquad t \geq 0 \\ \vec{E}^{new}\left\{\dfrac{\partial \vec{E}^{new}}{\partial y}\right\}(x,l_y,z,t) = \mathrm{e}^{2\pi i\Phi_y}\vec{E}^{new}\left\{\dfrac{\partial \vec{E}^{new}}{\partial y}\right\}(x,0,z,t); \qquad t \geq 0 \end{cases} \tag{1.15}$$

Let us present the scalar problems for spatial–time transformations of E- and H-polarized field in near zone of a 1-D periodic grating (see Fig. 1.1b; $\partial/\partial x \equiv 0$) in the following form:

$$\begin{cases} P_{\varepsilon,\mu,\sigma}[U] \equiv \left[-\varepsilon\mu\dfrac{\partial^2}{\partial t^2} - \sigma\mu\dfrac{\partial}{\partial t} + \dfrac{\partial^2}{\partial y^2} + \dfrac{\partial^2}{\partial z^2}\right]U(g,t) = F(g,t); \\ \qquad g = \{y,z\} \in \mathbf{Q}, \qquad t > 0 \\ U(g,0) = \varphi(g), \qquad \dfrac{\partial}{\partial t}U(g,t)\Big|_{t=0} = \psi(g); \qquad g \in \bar{\mathbf{Q}} \\ E_{tg}(p,t)\big|_{p=\{x,y,z\}\in\mathbf{S}} = 0; \qquad t \geq 0 \end{cases} \tag{1.16}$$

Here, in the case of E-polarization – $U(g,t) = E_x(g,t)$ and $\mu(g)$ is a piecewise constant function. In the case of H-polarization – $U(g,t) = H_x(g,t)$ and now the functions $\varepsilon(g)$ and $\sigma(g)$ have to be piecewise constant. The surfaces $\mathbf{S} = \mathbf{S}_x \times [|x| \leq \infty]$ of the perfectly conducting elements in the geometry of the gratings are assumed to be sufficiently smooth. The domain of analysis in the problems (1.16) coincides with a part of the plane $\mathbf{R}^2$ limited by the contours $\mathbf{S}_x$: $\mathbf{Q} = \mathbf{R}^2 \backslash \overline{\operatorname{int}\mathbf{S}_x}$. We carry out its contraction to the domain $\mathbf{Q}^{new} = \{g \in \mathbf{Q} : 0 < y < l\}$, which is the part of the parallel-plane Floquet channel $\mathbf{R} = \{g \in \mathbf{R}^2 : 0 < y < l\}$, by going over in the analysis to the initial boundary value problems for the images $f^{new}(g,t,\Phi)$ of the functions $f(g,t)$ describing the true sources:

$$\begin{gathered} f(g,t) = \int_{-\infty}^{\infty} \tilde{f}(z,t,\Phi)\,\mathrm{e}^{2\pi i\Phi(y/l)}d\Phi = \int_{-\infty}^{\infty} f^{new}(g,t,\Phi)\,d\Phi \quad \leftrightarrow \\ \leftrightarrow \quad f^{new}(g,t,\Phi) = \frac{\exp\left(2\pi i\Phi y/l\right)}{l}\int_{-\infty}^{\infty} f(\bar{y},z,t)\,\mathrm{e}^{-2\pi i\Phi(\bar{y}/l)}d\bar{y}. \end{gathered} \tag{1.17}$$

In terms of the functions $f^{new}(g,t,\Phi)$, the problems (1.16) can be rewritten in the form:

$$U(g,t) = \int_{-\infty}^{\infty} U^{new}(g,t,\Phi)\, d\Phi,$$

$$\begin{cases} \left[-\varepsilon\mu\dfrac{\partial^2}{\partial t^2} - \sigma\mu\dfrac{\partial}{\partial t} + \dfrac{\partial^2}{\partial y^2} + \dfrac{\partial^2}{\partial z^2}\right] U^{new}(g,t) = F^{new}(g,t); \\ \qquad g = \{y,z\} \in \mathbf{Q}^{new}, \qquad t > 0 \\ U^{new}(g,0) = \varphi^{new}(g), \qquad \dfrac{\partial}{\partial t} U^{new}(g,t)\Big|_{t=0} = \psi^{new}(g); \qquad g \in \bar{\mathbf{Q}}^{new} \\ E_{tg}^{new}(p,t)\Big|_{p=\{x,y,z\}\in\mathbf{S}} = 0; \qquad t \geq 0 \\ U^{new}\left\{\dfrac{\partial U^{new}}{\partial y}\right\}(l,z,t) = \mathrm{e}^{2\pi i\Phi} U^{new}\left\{\dfrac{\partial U^{new}}{\partial y}\right\}(0,z,t); \qquad t \geq 0 \end{cases} . \quad (1.18)$$

In the case of the classical statement of the problems (1.13), (1.15), (1.16), and (1.18) (all the equations are satisfied in each point of the relevant domain), the solutions should have as many continuous derivatives as are present in the equations and that implies strict limitations on the smoothness for all the entries. The generalized solutions and statements are more suitable for a description of physical phenomena that are governed by differential equations and they make the analysis of the problem much simpler.

A generalized function is a generalization of the classical concept of a function. Roughly speaking, the generalized function is determined by its average values near each point, and this enables us to get a mathematically correct description of many idealized notions, e.g., intensity of a instant point source. A generalized function denotes any linear continuous functional (f,γ) on the space of functions $\mathbf{D} = \mathbf{D}(\mathbf{R}^n)$, i.e., on the space of all finite infinitely differentiable functions γ in $\mathbf{R}^n$. The linear set $\tilde{\mathbf{D}} = \tilde{\mathbf{D}}(\mathbf{R}^n)$ of all generalized functions, with weak convergence of sequences of functionals, becomes a complete space.

The generalized function f vanishes in the domain $\mathbf{G}\subset\mathbf{R}^n$ if $(f,\gamma)=0$ for all $\gamma\in\mathbf{D}(\mathbf{G})$. According to this definition, we introduce the definition of equal functions and generalized solutions to differential equations, boundary value, and initial boundary value problems. Thus, for instance, for the generalized solutions U of (1.16), the values of the functional $\left(P_{\varepsilon,\mu,\sigma}[U] - F,\gamma\right)$ should vanish for all $\gamma\in\mathbf{D}(\mathbf{Q}\times(0;\infty))$. A consistent, detailed, and comprehensive description of the properties of generalized functions and operations with them is given in [2]. Hereafter, we are going to refer frequently to this book.

Among all the generalized functions, our interest mostly concerns the simplest of them, i.e., the regular generalized functions. There is a one-to-one correspondence

between locally integrable functions and regular generalized functions. Therefore, the latter can be treated as conventional point functions, which is more suitable for the purposes of functional analysis and the theory of boundary value problems [5]. In the class $\tilde{\mathbf{D}}_r(\mathbf{G})$ of regular generalized functions, not all of the elements are infinitely differentiable. Due to their differential properties, they can be considered as elements of different functional spaces, in particular, the spaces $\mathbf{W}_m^l(\mathbf{G})$, consisting of functions $f(g) \in \mathbf{L}_m(\mathbf{G})$; $g \in \mathbf{G}$, that have generalized derivatives up to the order l from $\mathbf{L}_m(\mathbf{G})$, and others (see the Appendix for a list of the symbols and abbreviations).

Among all the singular generalized functions (viz., nonregular ones), we use only the Dirac δ-function ($\delta(g)$) and its generalized derivatives. However, we should make the following reservation. In cases when the standard mathematical operations (numerical implementation of computational schemes, finite-difference approximation of the initial boundary value problems, etc.) cannot be performed correctly because of the presence of such functions, then the regularization is achieved by substituting an appropriate locally integrable δ-approximating function for the δ-function (the "cap" function $\omega_\varepsilon(g)$, etc.; see [2]).

In some chapters of this book we often refer to the notion of a fundamental solution (principal function, Green's function) of the differentiation operator $B[U]$: the generalized function $G(g) \in \tilde{\mathbf{D}}(\mathbf{R}^n)$ is a fundamental solution of the operator $B[U]$, if $B[G] = \delta(g)$. Using the generalized function G, one can construct the solution of the equation $B[U] = f$ with an arbitrary right-hand part f: $U = (G * f)$. This scheme can also be applied to a partial inversion of the differentiation operator of a problem, followed by an equivalent presentation of the latter as an integro-differential equation. Fundamental solutions to classic differential operators, connected with the problems of electromagnetic theory are presented in the books [1, 2, 6, and 7] in a clear and useful way.

It is known [1, 2, 5] that initial boundary value problems for equations (1.5), (1.7), and (1.9) in the domain $\mathbf{Q}$ can be formulated in such way that they will be unambiguously resolved in Sobolev's space $\mathbf{W}_2^1(\mathbf{Q}^T)$, $\mathbf{Q}^T = \mathbf{Q} \times (0;T)$, $(0;T) = \{t\colon 0 < t < T < \infty\}$. Let us assume, for example, that the source functions $\varphi(g)$, $\psi(g)$, and $F(g,t)$ (for all $t > 0$) of the problem (1.16) are finite in $\bar{\mathbf{Q}}$ and that the functions $\partial\left[\varepsilon(g)\mu(g)\right]/\partial y$, $\partial\left[\varepsilon(g)\mu(g)\right]/\partial z$, and $\sigma(g)\mu(g)$, $g \in \mathbf{Q}$ are bounded. Then the following statement is true [5].

Statement 1.1 *Let* $F(g,t) \in \mathbf{L}_{2,1}(\mathbf{Q}^T)$, $\varphi(g) \in \overset{\circ}{\mathbf{W}}{}_2^1(\mathbf{Q})$, $\psi(g) \in \mathbf{L}_2(\mathbf{Q})$, $\mathbf{Q}^T = \mathbf{Q} \times (0;T)$. *Then problem (1.16) in the E-case for all* $t \in [0;T]$ *has a generalized solution from the energy class, and the uniqueness theorem is true in this class.*

By a generalized solution from the energy class we understand a function $U(g,t)$, belonging to $\overset{\circ}{\mathbf{W}}{}_2^1(\mathbf{Q})$ for any $t \in [0;T]$ and depending continuously on t in the norm of $\mathbf{W}_2^1(\mathbf{Q})$. Furthermore the derivative $\partial U/\partial t$ should exist as an element of the space $\mathbf{L}_2(\mathbf{Q})$ for any $t \in [0;T]$ and vary continuously with t in the norm of $\mathbf{L}_2(\mathbf{Q})$. The initial conditions should be continuous in the spaces $\overset{\circ}{\mathbf{W}}{}_2^1(\mathbf{Q})$ and

$\mathbf{L}_2(\mathbf{Q})$, respectively, and telegraph equation should be satisfied in terms of the identity

$$\int\limits_{\mathbf{Q}^T} \left\{ \varepsilon\mu \left(\frac{\partial}{\partial t}U\right) \left(\frac{\partial}{\partial t}\gamma\right) - \sigma\mu \left(\frac{\partial}{\partial t}U\right)\gamma - \left(\frac{\partial}{\partial y}U\right)\left(\frac{\partial}{\partial y}\gamma\right) - \left(\frac{\partial}{\partial z}U\right)\left(\frac{\partial}{\partial z}\gamma\right) \right\} dgdt +$$

$$+ \int\limits_{\mathbf{Q}} \varepsilon\,\mu\,\psi\,\gamma\,(g,0)\; dg \;=\; \int\limits_{\mathbf{Q}^T} F\,\gamma\, dgdt.$$

Here $\gamma = \gamma(g,t)$ is an arbitrary element from $\mathbf{W}^1_{2,0}\left(\mathbf{Q}^T\right)$ such that $\gamma(g,T) = 0$. This equality is derived in a formal way from the following identity

$$\left(P_{\varepsilon,\mu,\sigma}[U] - F, \gamma\right) = \int\limits_{\mathbf{Q}^T} \left(P_{\varepsilon,\mu,\sigma}[U] - F\right)\gamma\, dg\, dt = 0$$

by means of a single partial integration of the terms, containing second-order derivatives of the function $U(g,t)$. It has been proved in [5] that such a definition makes sense and is actually a generalized notion of the classic solution.

The class of generalized solutions, that has been called the energy class, is somewhat narrower than $\mathbf{W}^1_2\left(\mathbf{Q}^T\right)$. It is worth a more detailed study because this class is the only one where the following specific feature of hyperbolic equations can be determined: the solution $U(g,t)$ has the same differential features that are assumed to be satisfied at the initial moment of time (continuable initial conditions).

The initial boundary value problems for equations (1.5), (1.7), and (1.9) correctly formulated can be solved by the finite-difference method. The central difference approximation applied to these problems leads to explicit computational schemes without inversion of any matrix operators [5]. The correct choice of the steps of the grids over spatial and time variables guarantee the robustness of such schemes and the convergence of the sequences of solutions of grid problems to the solution of original problems. In corresponding criteria, the dimension of the problem and constants ξ and ζ, limiting the intervals of the variation of function $\left[\varepsilon(g)\,\mu(g)\right]^{-1}$ in the domain of computation $\mathbf{Q}$ or $\mathbf{Q}^{new}$ [1, 5], are the principal parameters.

1.1.4 Frequency Domain: Boundary Value Problems

The statements about the solutions of initial boundary value problems for equations (1.5), (1.7), and (1.9) (see, for example, Statement 1.1) can be formulated [5, 8] in terms of spaces of the type

$$\mathbf{W}^1_2\left(\mathbf{Q}^\infty,\beta\right) \equiv \left\{ \{U(g,t)\} :\; U(g,t)\exp(-\beta t) \in \mathbf{W}^1_2\left(\mathbf{Q}^\infty\right);\; \beta \geq 0 \right\}.$$

These results provide the background [2, 5, 8] for connection of the time domain and frequency domain solutions by means of the Laplace transform (image$\leftrightarrow$ original)

$$\tilde{f}(s) = L\left[f\right](s) \equiv \int\limits_0^\infty f(t)\mathrm{e}^{-st}dt \quad \leftrightarrow \quad f(t) = L^{-1}\left[\tilde{f}\right](t) \equiv \frac{1}{2\pi i}\int\limits_{\alpha-i\infty}^{\alpha+i\infty} \tilde{f}(s)\mathrm{e}^{st}ds. \tag{1.19}$$

Thus, the initial boundary value problems (1.18) can be juxtaposed with the boundary value problems

$$\begin{cases} \left[\dfrac{\partial^2}{\partial y^2} + \dfrac{\partial^2}{\partial z^2} + \tilde{\varepsilon}\mu k^2\right]\tilde{U}(g,k) = \tilde{f}(g,k); \qquad g = \{y,z\} \in \mathbf{Q}^{new} \\ \tilde{E}_{tg}(p,k)\big|_{p=\{x,y,z\}\in\mathbf{S}} = 0 \\ \tilde{U}\left\{\dfrac{\partial \tilde{U}}{\partial y}\right\}(l,z,k) = \mathrm{e}^{2\pi i\Phi}\tilde{U}\left\{\dfrac{\partial \tilde{U}}{\partial y}\right\}(0,z,k) \end{cases}. \tag{1.20}$$

Here $s = -ik$, k is a wave number (frequency parameter or just frequency); $\tilde{U}(g,k) \leftrightarrow U^{new}(g,t)$; $\tilde{E}_{tg}(g,k) \leftrightarrow E_{tg}^{new}(g,t)$; $\tilde{F}(g,k) \leftrightarrow F^{new}(g,t)$; $\tilde{\varepsilon}(g) = \varepsilon(g) + i\sigma(g)/k$; $\tilde{f}(g,k) = \tilde{F}(g,k) + ik\tilde{\varepsilon}(g)\mu(g)\varphi(g) - \varepsilon(g)\mu(g)\psi(g)$.

It is known [5, 8–11] that for values of k with positive imaginary part (k: $\mathrm{Im}k > 0$) and for any $\tilde{f}(g,k) \in \mathbf{L}_2(\mathbf{Q}^{new})$, the problems (1.20) are unambiguously solvable in $\mathbf{W}_2^1(\mathbf{Q}^{new})$; their resolvents in upper half-plane of the plane $\mathbf{C}$ of the complex variable k are analytic operator-functions. If $\mathrm{Im}k > \beta \geq 0$, and the function $\tilde{U}(g,k)$ is absolutely integrable over $\mathrm{Re}k$ along the axis $\mathrm{Im}k = \alpha > \beta$, then the solutions $U^{new}(g,t)$ to the problems (1.18) from the space $\mathbf{W}_2^1\left((\mathbf{Q}^{new})^\infty,\beta\right)$ and solutions $\tilde{U}(g,k)$ to the problems (1.20) from the space $\mathbf{W}_2^1(\mathbf{Q}^{new})$ are related according to

$$U^{new}(g,t) = \frac{1}{2\pi}\int\limits_{i\alpha-\infty}^{i\alpha+\infty} \tilde{U}(g,k)\mathrm{e}^{-ikt}dk, \; \tilde{U}(g,k) = \int\limits_0^\infty U^{new}(g,t)\mathrm{e}^{ikt}dt. \tag{1.21}$$

The answer to the question about the unambiguous solvability of the problem (1.20) for real values k (the domain of classic diffraction theory) may be found within the frame of one of three principles: radiation, limit absorption, or limit amplitude [1, 10, 12, 13]. Further, we shall consider only the radiation principle as it is more often used formally in papers devoted to the theory of diffraction gratings.

Let us divide the analysis domain $\mathbf{Q}^{new}$ of problems (1.20) into two parts: $\mathbf{Q}_a^{new} = \{g \in \mathbf{Q}^{new}: |z| < a\}$ – all scattering objects and sources are concentrated inside this domain – and ${}_a\mathbf{Q}^{new} = \{g \in \mathbf{Q}^{new}: |z| > a\}$. Obviously, the field $\tilde{U}(g,k)$ in the domain ${}_a\mathbf{Q}^{new}$ has to be free from waves coming from infinity $z = \pm\infty$. The representation [10]

$$\tilde{U}(g,k) = \sum_{n=-\infty}^{\infty} \left\{\begin{matrix} A_n(k) \\ B_n(k) \end{matrix}\right\}\mathrm{e}^{i[\Phi_n y \pm \Gamma_n(z\mp a)]}; \; \left\{\begin{matrix} z \geq a \\ z \leq -a \end{matrix}\right\}, \mathrm{Im}k \geq 0,$$

$$\Phi_n = \Phi_n(\Phi) = 2\pi(\Phi + n)/l,\ \Gamma_n = \Gamma_n(\Phi) = \sqrt{k^2 - \Phi_n^2},$$

$$\mathrm{Re}\Gamma_n \mathrm{Re}k \geq 0,\ \mathrm{Im}\Gamma_n \geq 0, \tag{1.22}$$

meets such requirements. It is sometimes called a partial radiation condition. Here, $A_n(k)$ and $B_n(k)$ are the complex-valued amplitudes of plane homogeneous and nonhomogeneous waves constituting the field $\tilde{U}(g,k)$.

Statement 1.2 (radiation principle) *Let* $\sigma(g) > 0$ *on an arbitrary set in* $\mathbf{Q}_a^{new} = \{g \in \mathbf{Q}^{new}: |z| < a\}$ *with nonzero measure. Then the radiation conditions (1.22) provide a unique solution to (1.20) for every* k: $\mathrm{Im}k \geq 0$. *If* $\sigma(g) \equiv 0$, *then the solution to (1.20) and (1.22) exists and is unique for every* k: $\mathrm{Im}k \geq 0$, *with the possible exception of not more than the countable set* $\left\{\bar{k}_n: \mathrm{Im}\bar{k}_n = 0\right\} \in \Omega_k$ *without finite accumulation points.*

The following statement [8, 11, 14, 15] allows us to examine in detail the question of solvability of the problems (1.20) and (1.22).

Statement 1.3 *The resolvent* $A^{-1}(k)$ *of the problem (1.20) and (1.22)* $A(k)\left[\tilde{U}\left(g,k,\tilde{f}\right)\right] = \tilde{f}(g,k)$, $g \in \bar{\mathbf{Q}}^{new}$ *is a meromorphic (in local variables on the surface* $\mathbf{K}$ *) operator-function of complex parameter* k . *For the resolvent's principal part* $\Xi\left[A^{-1}(k)\right]$ *in the vicinity of the pole* $k = \bar{k}$ *(in the vicinity of the characteristic number* $k = \bar{k}$ *of the operator-function* $A(k)$ *), that does not coincide with the branch point* $k_n^{\pm}$ *of the surface* $\mathbf{K}$ *, the following expansion*

$$\Xi\left[A^{-1}(k)\right] = \sum_{j=1}^{J}\sum_{m=1}^{M(j)}\left(k-\bar{k}\right)^{-m}\sum_{l=0}^{M(j)-m} w_l^{(j)}(\cdot)\, u_{M(j)-m-l}^{(j)} \tag{1.23}$$

is valid. Here,

$$u_0^{(j)}(g),\ u_1^{(j)}(g),\ \ldots,\ u_{M(j)-1}^{(j)}(g),\ j = 1,2,\ldots,J$$

is the canonical system of eigen and adjoint elements of the operator-function $A(k)$, *relevant to characteristic number* $\bar{k}$. *Its choice unambiguously defines the canonic system*

$$w_0^{(j)}(g),\ w_1^{(j)}(g),\ \ldots,\ w_{M(j)-1}^{(j)}(g),\ j = 1,2,\ldots,J$$

of eigen and adjoint elements of operator-function $\bar{A}(k) = \left[A(k^*)\right]^*$ *(* denotes complex conjugation), relevant to the characteristic number* $\bar{k}^*$.

The surface $\mathbf{K}$, mentioned in Statement 1.3, is a surface of analytic continuation of the canonical Green's function

$$\tilde{G}_0(g,g_0,k,\Phi) = -\frac{i}{2l}\sum_{n=-\infty}^{\infty} e^{i\left[\Phi_n(y-y_0)+\Gamma_n|z-z_0|\right]}\Gamma_n^{-1} \tag{1.24}$$

that is the fundamental solution to canonical problem (1.20) and (1.22), i.e., the problem, where $\overline{\text{int}\mathbf{S}} = \emptyset$, $\tilde{\varepsilon}(g)\,\mu(g) \equiv 1$, and $\text{Im}k = 0$. It is an infinite sheet Riemann surface consisting of the planes $k \in \mathbf{C}$ cut along the directions of $(\text{Re}k)^2 - (\text{Im}k)^2 - \Phi_n^2 = 0$, $n = 0, \pm 1, \pm 2,...$, $\text{Im}k \leq 0$ (see Fig. 1.2a). The first sheet of the surface $\mathbf{K}$ is unambiguously determined by the radiation conditions (1.22), i.e., by the choice of the values $\text{Re}\Gamma_n\text{Re}k \geq 0$ and $\text{Im}\Gamma_n \geq 0$, $n = 0, \pm 1, \pm 2,...$, at the axis $\text{Im}k = 0$. On this sheet, in the domain $0 < \arg k < \pi$, we have $\text{Im}\Gamma_n > 0$,

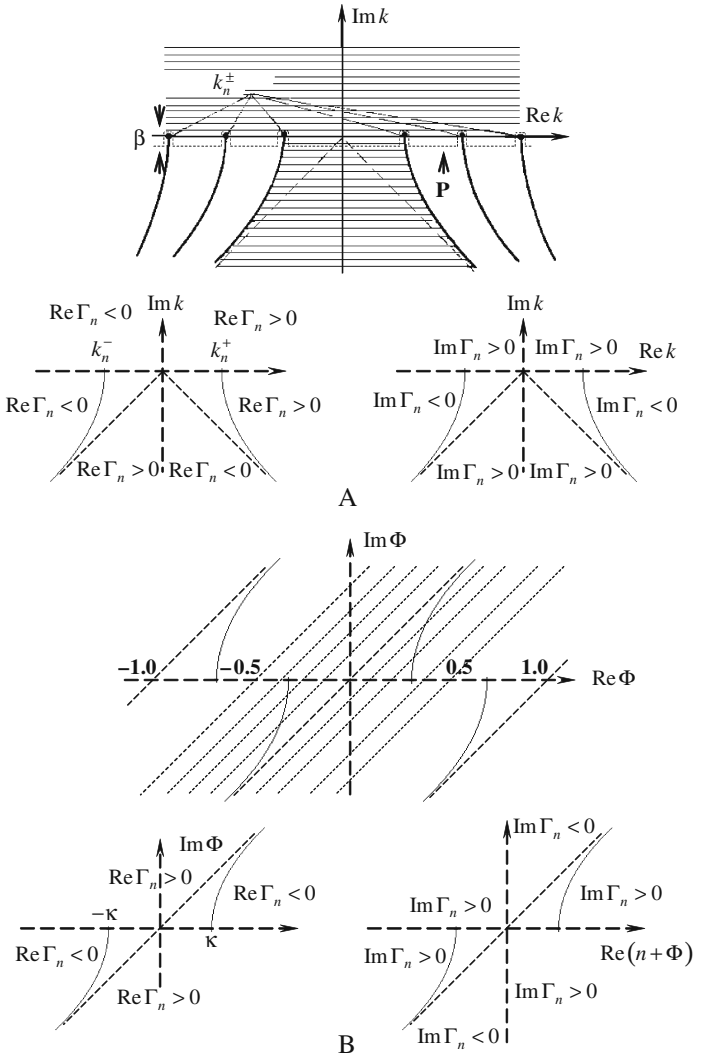

Fig. 1.2 The natural variation domains for the spectral parameters k, Φ and $\Gamma_n(k)$, $\Gamma_n(\Phi)$ values distribution: (**a**) First sheet of the **K** surface; (**b**) first sheet of the **F** surface

and $\mathrm{Re}\Gamma_n \geq 0$ for $0 < \arg k \leq \pi/2$ and $\mathrm{Re}\Gamma_n \leq 0$ for $\pi/2 \leq \arg k < \pi$. In the domain $3\pi/2 \leq \arg k < 2\pi$ for finite number of functions $\Gamma_n(k)$ (with relevant n such that $(\mathrm{Re}k)^2 - (\mathrm{Im}k)^2 - \Phi_n^2 > 0$) the relations $\mathrm{Im}\Gamma_n < 0$ and $\mathrm{Re}\Gamma_n > 0$ hold; for the rest of these functions we have $\mathrm{Im}\Gamma_n > 0$ and $\mathrm{Re}\Gamma_n \leq 0$. In the domain $\pi < \arg k \leq 3\pi/2$, the situation is similar only if the signs of $\mathrm{Re}\Gamma_n$ are opposite. The next sheets (each of them with its own set of relevant pairs $\{k \to \Gamma_n(k)\}$) have, unlike the first one, opposite signs (root branches) of $\Gamma_n(k)$ for a finite number of values of the index n. The cuts (solid lines in Fig. 1.2a) originate from the real algebraic branch points $k_n^{\pm}$: $\Gamma_n\left(k_n^{\pm}\right) = 0$ or $k_n^{\pm} = \pm|\Phi_n|$, $n = 0, \pm 1, \pm 2, \ldots$

Analytic continuation of the function $\tilde{G}_0(g,g_0,k,\Phi)$ preserves on the surface **K** all properties of the Green function for the canonical problem (1.20) and (1.22). It is easy to show also [10, 11] that on the first sheet of the surface **K**

$$\tilde{G}_0(g,g_0,k,\Phi) = \tilde{G}_0(g_0,g,k,-\Phi) = \tilde{G}_0^*\left(g,g_0,-k^*,-\Phi\right). \tag{1.25}$$

Let us come back now to the Fig. 1.1b and make one comment connected with formulation of 2-D initial boundary value problems for 1-D periodic structures. Sometimes these problems are considered (see, for example, Section 2.6) in the system of nondimensional time and spatial coordinates $\bar{y} = 2\pi y/l$, $\bar{z} = 2\pi z/l$, $\bar{t} = 2\pi t/l$, according to which the period of gratings is equal to 2π [1, 10, 16–18]. Such a trick simplifies certain mathematical expressions and allows us in the analysis to keep focus on the dimensionless parameter κ, characterizing the ratio between length of the period l and wavelength λ of the incident field. Many physical results of electromagnetic theory of gratings are formulated in terms of $\kappa = l/\lambda$, $\delta = h/l$, and other dimensionless parameters. Formally, the transition to the formulation corresponding to dimensionless parameters can be performed by means of the following substitutions in the conventional formulas: $y \to \bar{y}$, $z \to \bar{z}$, $t \to \bar{t}$, $l \to 2\pi$, $k \to \kappa$, and $h \to 2\pi\delta$.

1.2 The General Physical Picture: Principal Definitions and Consequences from Conservation Laws and Reciprocity Theorems

1.2.1 The Diffraction Problems for Plane Waves

Let us carry off the source $\tilde{f}(g,k)$ in problems (1.20) into infinity ($z = \infty$) and suppose that it generates in the reflection domain $z > 0$ (in the domain **A**) a plane homogeneous (p: $\mathrm{Im}\Gamma_p = 0$) or inhomogeneous (p: $\mathrm{Im}\Gamma_p > 0$) wave $\tilde{U}_p^i(g,k) = \exp\left[i\left(\Phi_p y - \Gamma_p z\right)\right]$ that excites a semitransparent, 1-D periodic structure (see Fig. 1.1b). If the source $\tilde{f}(g,k)$ is replaced by the incident plane wave $\tilde{U}_p^i(g,k)$, the problems (1.20) and (1.22) can be written as follows:

$$\begin{cases} \left[\dfrac{\partial^2}{\partial y^2}+\dfrac{\partial^2}{\partial z^2}+\tilde{\varepsilon}\mu k^2\right]\tilde{U}(g,k)=0; \qquad g=\{y,z\}\in\mathbf{Q}^{new} \\ \tilde{E}_{tg}(q,k)\big|_{q=\{x,y,z\}\in\mathbf{S}}=0 \\ \tilde{U}\left\{\dfrac{\partial\tilde{U}}{\partial y}\right\}(l,z,k)=\mathrm{e}^{2\pi i\Phi}\tilde{U}\left\{\dfrac{\partial\tilde{U}}{\partial y}\right\}(0,z,k) \\ \tilde{U}(g,k)=\begin{cases} \tilde{U}_p^i(g,k)+\displaystyle\sum_{n=-\infty}^{\infty}R_{np}^{\mathbf{AA}}\exp\left[i(\Phi_n y+\Gamma_n z)\right]; \qquad z\geq 0 \\ \displaystyle\sum_{n=-\infty}^{\infty}T_{np}^{\mathbf{BA}}\exp\left[i(\Phi_n y-\Gamma_n(z+h))\right]; \qquad z\leq -h \end{cases} \end{cases} . \tag{1.26}$$

Here, in the case of E-polarized field, $\mu(g)$ is a piecewise constant function, $\tilde{E}_y=\tilde{E}_z=\tilde{H}_x=0$, $\tilde{E}_x=\tilde{U}$, and

$$H_y=\frac{1}{ik\eta_0\mu}\frac{\partial\tilde{U}}{\partial z},\ H_z=-\frac{1}{ik\eta_0\mu}\frac{\partial\tilde{U}}{\partial y}. \tag{1.27}$$

For the H-case, $\tilde{\varepsilon}(g)$ is a piecewise constant function, $\tilde{H}_y=\tilde{H}_z=\tilde{E}_x=0$, $\tilde{H}_x=\tilde{U}$, and

$$E_y=-\frac{\eta_0}{ik\tilde{\varepsilon}}\frac{\partial\tilde{U}}{\partial z},\ \tilde{E}_z=\frac{\eta_0}{ik\tilde{\varepsilon}}\frac{\partial\tilde{U}}{\partial y}. \tag{1.28}$$

The surfaces $\mathbf{S}$ are assumed to be sufficiently smooth. The analysis domain $\mathbf{Q}^{new}$ coincides with the part of the parallel-plane Floquet channel $\mathbf{R}=\left\{g\in\mathbf{R}^2\colon 0<y<l\right\}$, limited with the contours $\mathbf{S}_x$: $\mathbf{Q}^{new}=\mathbf{R}\backslash\overline{\mathrm{int}\,\mathbf{S}_x}$.

The amplitudes $R_{np}^{\mathbf{AA}}=R_{np}^{\mathbf{AA}}(k,\Phi)$ and $T_{np}^{\mathbf{BA}}=T_{np}^{\mathbf{BA}}(k,\Phi)$ [see the last equation in (1.26)] form the so-called generalized scattering matrices of the grating: the reflection matrix $R^{\mathbf{AA}}=\left\{R_{np}^{\mathbf{AA}}\right\}_{n,p=-\infty}^{\infty}$ and the transmission matrix $T^{\mathbf{BA}}=\left\{T_{np}^{\mathbf{BA}}\right\}_{n,p=-\infty}^{\infty}$. The elements of these matrices specify the spatial–frequency distribution of the energy of the incident wave $\tilde{U}_p^i(g,k)$ in reflected and transferred via grating field. The rules for the upper indices are clear: from the domain whose identifier is on the right, into the domain with the identifier on the left. For the distribution over the modes (the lower indices) we have similarly: on the right there is the mode number of the incident wave, on the left there is the mode number of wave from the secondary field.

The elements of the generalized scattering matrices are connected by energy-balance relations

$$\sum_{n=-\infty}^{\infty}\left[\left|R_{np}^{\mathbf{AA}}\right|^2+\left|T_{np}^{\mathbf{BA}}\right|^2\right]\begin{Bmatrix}\mathrm{Re}\Gamma_n\\ \mathrm{Im}\Gamma_n\end{Bmatrix}=\begin{Bmatrix}\mathrm{Re}\Gamma_p+2\mathrm{Im}R_{pp}^{\mathbf{AA}}\mathrm{Im}\Gamma_p\\ \mathrm{Im}\Gamma_p-2\mathrm{Im}R_{pp}^{\mathbf{AA}}\mathrm{Re}\Gamma_p\end{Bmatrix}-\frac{k^2}{l\beta_0}\begin{Bmatrix}W_1\\ W_2\end{Bmatrix},\quad p=0,\pm1,\pm2,.... \tag{1.29}$$

and by reciprocity relations

$$\frac{R_{np}^{\mathbf{AA}}(\Phi)}{\Gamma_p(\Phi)}=\frac{R_{-p,-n}^{\mathbf{AA}}(-\Phi)}{\Gamma_{-n}(-\Phi)};\ \frac{T_{np}^{\mathbf{BA}}(\Phi)}{\Gamma_p(\Phi)}=\frac{T_{-p,-n}^{\mathbf{AB}}(-\Phi)}{\Gamma_{-n}(-\Phi)},\ n,p=0,\pm1,\pm2,..., \tag{1.30}$$

that are consequences from the complex power theorem (Poynting theorem) and the Lorentz lemma [10, 16, 18, 19].

Here,

$$W_1=\int\limits_{\mathbf{G}}\mathrm{Im}\tilde{\varepsilon}\varepsilon_0\left|\vec{E}\right|^2dg=\frac{1}{k}\int\limits_{\mathbf{G}}\sigma\varepsilon_0\left|\vec{E}\right|^2dg,$$

$$W_2=\begin{Bmatrix}+\\ -\end{Bmatrix}\int\limits_{\mathbf{G}}\left[\mu\mu_0\left|\vec{H}\right|^2-\mathrm{Re}\tilde{\varepsilon}\varepsilon_0\left|\vec{E}\right|^2\right]dg=\begin{Bmatrix}+\\ -\end{Bmatrix}\int\limits_{\mathbf{G}}\left[\mu\mu_0\left|\vec{H}\right|^2-\varepsilon\varepsilon_0\left|\vec{E}\right|^2\right]dg,$$

$$\beta_0=\begin{Bmatrix}\varepsilon_0\\ \mu_0\end{Bmatrix};\qquad\begin{Bmatrix}E-\text{case}\\ H-\text{case}\end{Bmatrix},$$

and $\vec{E}=\left\{\tilde{E}_x,\tilde{E}_y,\tilde{E}_z\right\}$, $\vec{H}=\left\{\tilde{H}_x,\tilde{H}_y,\tilde{H}_z\right\}$, $G=\{g\in\mathbf{Q}^{new}:\ -h\le z\le 0\}$.

Let now k be a real positive frequency parameter, and let an arbitrary semitransparent (Fig. 1.1b) or reflecting (Fig. 1.1c) grating be excited from the domain **A** by a homogeneous E- or H-polarized plane wave $\tilde{U}_p^i(g,k)$. The first term in the last equation in (1.26) for the reflection zone $z>0$ corresponds to a wave incident on the grating. The infinite series for the zones **A** and **B** determine the secondary (scattered) field. The terms of these series are usually referred to as partial components of the spatial spectrum of the structure or as spatial (diffraction) harmonics of a scattered field. The complex amplitudes $R_{np}^{\mathbf{AA}}$ and $T_{np}^{\mathbf{BA}}$ of the spatial harmonics composing the diffraction field in the reflection (**A**) and transmission (**B**) zones are complicated functions of k and Φ, as well as of the geometry and the material parameters of the grating. Every harmonic for which $\mathrm{Im}\Gamma_n=0$ and $\mathrm{Re}\Gamma_n>0$ is a homogeneous plane wave, propagating away from the grating at the angle $\alpha_n=-\arcsin\left(\Phi_n/k\right)$ in the reflection zone and at the angle $\alpha_n=\pi+\arcsin(\Phi_n/K)$ in the grating's transmission zone (all the angles are measured in the plane $y0z$, anticlockwise from the z-axis, see Fig. 1.1b). The angle $\alpha_p^i=\arcsin\left(\Phi_p/k\right)$ is an angle of incidence of the excitation wave $\tilde{U}_p^i(g,k)$ on the grating. It is obvious that the direction of propagation of the homogeneous harmonics of the secondary field depends on their number n and on the values of k and α_p^i. According to (1.29), the values $W_{np}^R=\left|R_{np}^{\mathbf{AA}}\right|^2\mathrm{Re}\Gamma_n/\Gamma_p$, $W_{np}^T=\left|T_{np}^{\mathbf{BA}}\right|^2\mathrm{Re}\Gamma_n/\Gamma_p$, and so on, determine energy content of the harmonics, that is, the relative part of the energy that is directed by

the structure into the relevant spatial radiation channel. The channel corresponding to the nth harmonic, we shall call "open" if $\mathrm{Im}\Gamma_n = 0$. The regime when only one channel for spatial harmonics is open ($n = p$) we shall call the single mode regime. For such a regime, the basic (or principal) spatial harmonic in the reflection zone is called the specular one, and its amplitude ($R_{pp}^{\mathbf{AA}}$) is called the reflection coefficient (clearly, $T_{pp}^{\mathbf{BA}}$ is called the transmission coefficient).

The angle between the directions of propagation of the primary and the minus mth reflected plane wave $\alpha_p^i - \alpha_{-m} = 2\alpha$ is determined from the equation $kl \sin\left(\alpha_p^i - \alpha\right) \cos\alpha = \pi\,(p + m)$. Particularly, at α=0 or at

$$kl \sin\left(\alpha_p^i\right) = \pi\,(p + m) \tag{1.31}$$

the corresponding harmonic propagates toward the incident wave. The creation of such a nonspecular reflecting mode is called autocollimation.

Not all the amplitudes $R_{np}^{\mathbf{AA}}$ and $T_{np}^{\mathbf{BA}}$ are equally useful for the physical analysis – in the far zone, the secondary field is formed only by the propagating harmonics with the numbers n such that $\mathrm{Re}\Gamma_n \geq 0$. But the radiation field in the immediate proximity of the grating requires taking into account the contribution of evanescent harmonics (n: $\mathrm{Im}\Gamma_n > 0$). Moreover, in some situations (resonance mode) this contribution is the dominating one.

The number of propagating harmonics $N = \sum_n \mathrm{Re}\Gamma_n \big/ |\Gamma_n|$ determines the number of channels that are open for radiation into free space and is the most general characteristic of the diffraction process. If the grating geometry is such that the channels in region **G** with the known wave propagation conditions can be chosen, then it is possible to introduce one more analogous identifier M which denotes the number of electromagnetically open channels at one period of the structure. These channels connect the domains of reflected and transferred via grating field. The joint qualitative characteristic $\{N, M\}$ taking into account the most common properties of gratings that are described by the consequences of the complex power theorem and the Lorentz lemma, enables us, in some cases, to predict, rather precisely, the feasibility of one or other scattering modes, whose specifics are determined by purely quantitative energy parameters. Thus, for example, it can easily be shown [18] that in the area of parameter values that corresponds to the vector $\{N, M\}$ with $N = M = 1$, a countable number of values $h \neq 0$ can always be found such that

$$\left|R_{00}^{\mathbf{AA}}\right| = 0, \qquad \left|T_{00}^{\mathbf{BA}}\right| = 1 \tag{1.32}$$

independent of the general configuration of the boundaries of a semitransparent structure. If (1.32) is fulfilled in some point in the region {1,1}, it means that the primary wave propagates entirely (without reflection) into the zone **B**. The value of $\arg T_{00}^{\mathbf{BA}}$ determines the equivalent phase incursion caused by the presence of the grating. The effect of complete transition is usually accompanied by an increased field strength in **G** and neighboring region, and the more pronounced it is, the

narrower the coupling channels and the higher the structure. Such observations suggested to many researchers the idea of a resonant nature of such fully transparent modes. However, this suggestion has been strictly proven only in [16]. This fact became the first in the chain of the results that afterward constituted the spectral theory of gratings (see Section 1.3).

1.2.2 The Simplest Physical Consequences from the Poynting Theorem and the Lorentz Lemma

From the relations (1.29) and (1.30), having rather general character, several simple and complex corollaries follow [18, 20]. Their usage allows controlling the results of numerical experiments and makes their physical interpretation easier. Sometimes these corollaries considerably reduce the volume of calculations or reduce the solution to one problem to the solution of another one that is mere simple or already resolved. Further, we shall list several of them relying for the most part on the results presented in [18]:

- The first line in (1.29) is the energy conservation law for propagating waves. In the case, when $\mathrm{Im}\Gamma_p = 0$, the energy of scattered field is connected in natural way with the energy of the incident wave. The energy of the wave $\tilde{U}_p^i(g,k)$ is partially absorbed by the grating (only if $W_1 \neq 0$), and the remaining part is distributed between spatial harmonics propagating in the domains **A** and **B** (it is reradiating into the directions $z = \pm\infty$). In the case of incidence by a plane inhomogeneous wave, the total (reradiated and absorbed) energy is defined by the imaginary part of reflection coefficient which in this case cannot be negative: $\mathrm{Im}R_{pp}^{\mathbf{AA}} \geq 0$.
- The relations in the second line in (1.29) restrict the value of density of near field of plane gratings ($h = 0$ and $W_2 = 0$); it cannot be big at frequencies remote from branch points of the surface **K** (far from grazing points $k_n^{\pm}$ or threshold points). In the case of incidence by a plane homogeneous wave, density of near field of plane gratings is defined by imaginary part of reflection coefficient which in this case cannot be positive: $\mathrm{Im}R_{pp}^{\mathbf{AA}} \leq 0$.
- For a perfect ($\sigma(g) \equiv 0$) semitransparent grating that is symmetric with respect to the plane $z = -h/2$, when $\mathrm{Re}\Gamma_0 > 0$ and $\mathrm{Im}\Gamma_n > 0$, $n \neq 0$, it follows from (1.29) that

$$\left|R_{00}^{\mathbf{AA}}\right|^2 + \left|T_{00}^{\mathbf{BA}}\right|^2 = 1, \quad \begin{cases} \left|R_{00}^{\mathbf{AA}} - T_{00}^{\mathbf{BA}}\right|^2 = 1; & E-\text{case} \\ \left|R_{00}^{\mathbf{AA}} + T_{00}^{\mathbf{BA}}\right|^2 = 1; & H-\text{case} \end{cases},$$

or

$$\mathrm{Re}\, R_{00}^{\mathbf{AA}} \mathrm{Re} T_{00}^{\mathbf{BA}} = -\mathrm{Im}\, R_{00}^{\mathbf{AA}} \mathrm{Im}\, T_{00}^{\mathbf{BA}}. \tag{1.33}$$

The equality (1.33) means that the difference between arguments of complex reflection and transmission coefficients can differ from the value $\pi/2$, only by a value that is multiple of π. We arrive at the same conclusion on estimating the values of $\arg R_{00}^{\mathbf{AA}} - \arg R_{-1,0}^{\mathbf{AA}}$ for perfectly reflecting gratings with planes of symmetry $y = \text{const} + nl$, $n = 0, \pm 1, \pm 2,...$, that is operating in regime of autocollimation reflection on minus first spatial harmonic ($\text{Im}\Gamma_n > 0, n \neq 0,-1$).

- Apparently, for periodic gratings with planes of symmetry $y = \text{const} + nl$, $n = 0, \pm 1, \pm 2,...$, $R_{np}^{\mathbf{AA}}(\Phi) = R_{-n,-p}^{\mathbf{AA}}(-\Phi)$ and $T_{np}^{\mathbf{BA}}(\Phi) = T_{-n,-p}^{\mathbf{BA}}(-\Phi)$. In this case, the following equalities hold together with (1.30):

$$R_{np}^{\mathbf{AA}}(\Phi)\,\Gamma_n(\Phi) = R_{pn}^{\mathbf{AA}}(\Phi)\,\Gamma_p(\Phi),\; T_{np}^{\mathbf{BA}}(\Phi)\,\Gamma_n(\Phi) = T_{pn}^{\mathbf{AB}}(\Phi)\,\Gamma_p(\Phi). \tag{1.34}$$

- The relation $W_{n0}^{R}(\Phi) = W_{0,-n}^{R}(-\Phi)$ is known in optics [19] as the reciprocity theorem for reflecting gratings. It follows from (1.30) that more general result takes place:

$$W_{np}^{R}(\Phi) = W_{-p,-n}^{R}(-\Phi), \tag{1.35}$$

which holds for all p and n, corresponding to propagating harmonics, and for all semitransparent and reflecting gratings.

- When $n = p = 0$ we derive from (1.30)

$$R_{00}^{\mathbf{AA}}\left(\alpha_0^i\right) = R_{00}^{\mathbf{AA}}\left(-\alpha_0^i\right). \tag{1.36}$$

That means that even in the case of an excitation of a semitransparent or reflecting grating that is nonsymmetric with respect to the planes $y = \text{const} + nl$, the reflection coefficient does not depend on the sign of the incidence angle. When $\text{Im}\Gamma_n > 0$, $n \neq 0$ and $\sigma(g) \equiv 0$, it follows from (1.29) that the value of $\left|T_{00}^{\mathbf{BA}}\right|$ is also independent of the sign of α_0^i.

- Consider the strip jalousie-type grating that is put in the field of H-polarized plane wave $\tilde{U}_0^i(g,k)$ incoming at an angle of $\alpha_0^i = -\vartheta$ (see Fig. 1.3a). This field is not disturbed by the grating, as the vector $\vec{E}(g,k)$ is perpendicular to infinitely thin, perfectly conducting strips. Hence for such a grating $R_{00}^{\mathbf{AA}}\left(\alpha_0^i\right) = 0$ and $\left|T_{00}^{\mathbf{BA}}\left(\alpha_0^i\right)\right| = 1$. It follows from (1.36) and (1.29) that in the case $\alpha_0^i = \vartheta$ there is no specularly reflected wave either, and in the frequency range where only principal harmonics are propagating ($\text{Im}\Gamma_n > 0$, $n \neq 0$) the total energy is still concentrated in the first transmitted spatial harmonic.
- An echelette grating with rectangular mounts has the ability to perform total reflection of H-polarized plane wave directly back in the case when incidence angle of the wave $\tilde{U}_0^i(g,k)$ is equal to the blaze angle (see Fig. 1.3b; $\alpha_0^i = 90^\circ - \vartheta$) and one higher-order harmonic (let it be $n = -m$) is in autocollimation mode ($kl\sin\left(\alpha_0^i\right) = \pi m$). This ability is widely exploited in numerous optical

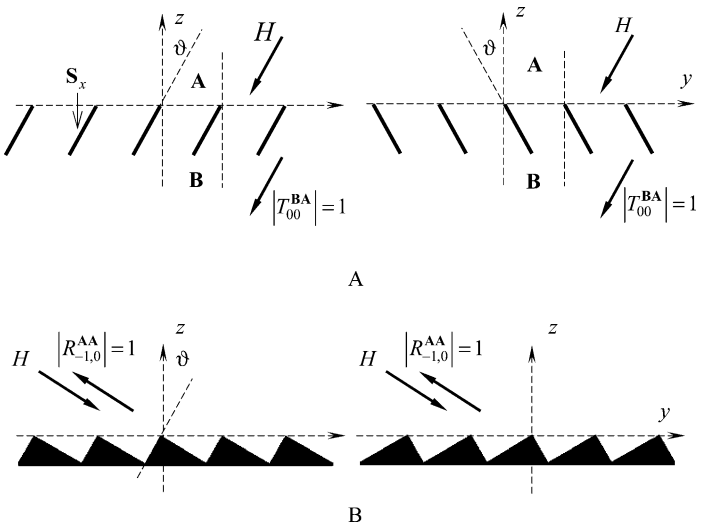

Fig. 1.3 Nontrivial consequences from reciprocity theorem: The effects of (**a**) total transmission and (**b**) total autocollimation reflection of the *H*-polarized plane wave

and microwave devices. The obvious geometrical resonance (the total field meeting all requirements of the problem (1.26) has the form of a sum of the fields for incident and reflected waves that are propagating in strictly opposite directions) allows one to write in this case: $\left|R^{\mathbf{AA}}_{-m,0}\left(\alpha^i_0\right)\right| = 1,\ R^{\mathbf{AA}}_{n0}\left(\alpha^i_0\right) = 0,\ n \neq -m$. Let $m = 1$ and the value of k is such that $\mathrm{Re}\Gamma_n\left(\alpha^i_0\right) = 0$ for all $n \neq 0, -1$. Then from (1.36) and (1.29), we obtain

$$R^{\mathbf{AA}}_{00}\left(\alpha^i_0\right) = R^{\mathbf{AA}}_{00}\left(-\alpha^i_0\right) = 0,\ \left|R^{\mathbf{AA}}_{+1,0}\left(-\alpha^i_0\right)\right| = 1. \tag{1.37}$$

The change of the angle α^i_0 to the angle $-\alpha^i_0$ is equivalent to turning the grating for 180° with respect to the z-axis (see Fig. 1.3b). It follows from (1.37) that as the case stands, echelette preserves the ability to reflect incident wave into back direction in spite of the distortion of the geometrical resonance relations.

- When $n = p = 0$, we derive from (1.30) the equality $T^{\mathbf{BA}}_{00}(\Phi) = T^{\mathbf{AB}}_{00}(-\Phi)$, that is, for any semitransparent grating the transmission coefficient stays the same when the direction of incident for wave $\tilde{U}^i_0(g,k)$ is changed to its opposite.
- The relations (1.29) and (1.30) give the possibility to formulate the following regularities for the theory of ideal asymmetrical reflecting gratings (see Fig. 1.1c). Let the parameters k and Φ be such that $\mathrm{Re}\Gamma_0(\Phi) > 0$ and $\mathrm{Re}\Gamma_n(\Phi) = 0$, $n \neq 0$. If the incident wave is an inhomogeneous plane wave $\tilde{U}^i_{\pm p}(g,k,\pm\Phi)$, then

$$\left|R^{\mathbf{AA}}_{0,\pm p}(\pm\Phi)\right|^2 \mathrm{Re}\Gamma_0(\pm\Phi) = 2\mathrm{Im}R^{\mathbf{AA}}_{\pm p,\pm p}(\pm\Phi)\,\mathrm{Im}\Gamma_{\pm p}(\pm\Phi). \tag{1.38}$$

In view of $R^{\mathbf{AA}}_{pp}(\Phi) = R^{\mathbf{AA}}_{-p,-p}(-\Phi)$, we derive from (1.38) $\left|R^{\mathbf{AA}}_{0p}(\Phi)\right| = \left|R^{\mathbf{AA}}_{0,-p}(-\Phi)\right|$ and

$$\left|R^{\mathbf{AA}}_{p0}(\Phi)\right| = \left|R^{\mathbf{AA}}_{-p,0}(-\Phi)\right|,\ \left|R^{\mathbf{AA}}_{p0}(0)\right| = \left|R^{\mathbf{AA}}_{-p,0}(0)\right|, p = \pm1, \pm2,.... \tag{1.39}$$

It is easy to get the physics that is described by equalities (1.39). The case of symmetrical incidence ($\Phi = 0$) is of specific interest: within the frequency range where only principal spatial harmonic can propagate, the absolute values of higher damped positive ($n = 1,2,...$) and negative ($n = -1, -2,...$) harmonics are equal to each other even for asymmetric gratings. Asymmetry only results in distortion of the phase symmetry of higher harmonic amplitudes. The symmetry of absolute values of amplitudes becomes invalid as k grows, just after the appearance of higher propagating modes.

1.3 The Spectral Theory of Gratings

1.3.1 Introduction

Every next book on the subject [16–19, 21] closed a certain further stage in the development of electromagnetic theory of gratings. The advancement has never been monotonous but it has provided results, which have spurred our interest, and it has furnished a basis for opening new scientific frontiers where we have managed to make progress and consolidate positions. The accomplishments have been accumulating, and so have certain inevitable problems whose thoughtful analysis has taken a long time. In our swift movement forward, we have always set them aside for the time being.

For the most part, the troubles we refer to have centered around the question of the uniqueness of the solution of the initial model boundary value problems, namely elliptic problems in nonclassical domains extended to infinity along one or more directions. To extract a unique physical solution, we must invoke some additional conditions. Their applicability (efficiency) is tested via one of the three classical principles – the radiation, limiting absorption, and limiting amplitude principles. For grating problems, it is common to take either partial radiation conditions or Rayleigh radiation conditions, suggesting a general analytic representation of the secondary field in terms of outgoing homogeneous and inhomogeneous plane waves in the reflection and transmission zones of the structure. The unique solvability of the boundary value problem completed with conditions of the above kind has been rigorously proved only in the absorbing medium case [16, 22]. In actuality, the model problems are formulated and solved in the limiting case of a lossless

medium. The existence and uniqueness of the solution is presumed (without hesitation), even if there are facts which speak against it [16]. These are weak spots in the theory of gratings, which reduce the sturdiness of the numerical algorithms for solving model boundary value problems and shake the reliability of the physical interpretation of the obtained numerical results. Owing to the so-called spectral theory of gratings [10] many questions have been cleared up. The topics of the spectral theory are

- research into characteristic features of the analytic continuation of the solutions to the elliptic boundary value problems to a complex (nonphysical) range of parameters;
- recognition of these peculiarities' role in the formation of a resonant response of a periodic structure to an external excitation by a monochromatic quasi-periodic or a compact source, or a wideband signal.

All mathematical models of resonant electromagnetic scattering are in conflict, bigger or smaller, with major physical principles. Abstract mathematical analysis concerned, for one, with the completion of the physical range of frequency, distance, energy, and other considered quantities offers expedients that can partly compensate for the conflict. The first trial of such an abstraction in classical electrodynamics – the transition to complex amplitudes, not existing in nature – was readily acknowledged, the benefits of dealing with these handy representations were promptly recognized. Complex functions (components of the field strength vectors) of real variables (frequency and spatial coordinates) have long been standard objects in the theory of stationary wave processes. Yet those who looked into the physics of resonant processes (spatial–frequency and spatial–temporal transformations of the field, with wave resonant scattering expected) were the first to feel uncomfortable in these frames. Also, problems were faced by those making efforts to justify the use of singular expansion technique or to get rid of idealizations like "a grating in the plane wave field or in the quasi-periodic source field" and to go over more practical situations, such as "a grating in the field of a plane waves beam or in the field of a finite duration signal." So, it was time to have the arguments (frequency and geometry parameters, the parameter Φ of the Floquet channel) complex-valued too, and to trace the features of the analytic continuation of the complex-valued solutions of the model boundary value problems. The motivation was quite clear – locally the behavior of a function of complex variable is completely determined by the character of singular points nearby. Yet it was not easy to realize. An obstacle arises when we try to come to nothing more than simple domains if we continue the classical boundary value problems in theory of gratings to the complex parameter range. As a result, the so-called continuous spectrum appears, an object unrelated to the physics of the processes analyzed. To avoid this difficulty, we have been seeking the analytic continuation within its natural boundaries, which gave rise to so exotic (at first glance) domains of complex frequency k and complex parameter Φ as infinite-sheeted Riemannian surfaces with algebraic branch points of the second order [10]. In these areas, the functions describing fields and complex amplitudes of

the fields are found to be usual meromorphic functions of the parameter k or Φ. The branch points only affect the appearance of the local (Riemannian surface-related) variable. This fact, that was shown by using the Fredholm theorem for compact finite-meromorphic operator-functions [15, 23, 24], opened for us a diversity of additional possibilities for the effective quantitative and qualitative examination of both steady-state and transient fields produced by gratings [1, 10].

1.3.2 The Grating as an Open Periodic Resonator

Let Φ have a fixed value. Then the following Statements 1.4–1.6 that qualitatively characterize the grating as an open periodic resonator are true [1, 10, 25–27].

Statement 1.4 (definition and qualitative characteristics of the frequency spectrum; see also Statement 1.3) *The analytic continuation of the solutions* $\tilde{U}(g,k)$ *of the problems (1.20), (1.22), and (1.26) into the domain of complex (nonphysical)* k *values produces the functions* $\tilde{U}(k)$ *with a natural domain of definition,* $\mathbf{K}$. *The sets of poles* $\left\{\bar{k}_n\right\} = \Omega_k$ *of the functions* $\tilde{U}(k)$, *which are meromorphic in the local variables on the surface* $\mathbf{K}$ *(just a countable sets without finite accumulation points) determine the complete frequency spectra of the gratings as the open periodic resonators: if* $k = \bar{k}_n$, *the homogeneous problems (1.20) and (1.22)* $(\tilde{f}(g,k) \equiv 0)$, *and (1.26)* $(\tilde{U}_p^i(g,k) \equiv 0)$ *are resolvable in a nontrivial way in* $\mathbf{K}$, *and the corresponding solutions* $u_0^{(j)}\left(g,\bar{k}_n\right), j = 1,2,...,J$ *have the meaning of free states (natural oscillations) of the structures field at the eigenfrequency* $\bar{k}_n$.

Reliable algorithms for the numerical solution of the spectral problems (the search of free oscillation eigenfrequencies and eigenfields) for open periodic resonators are conventionally [10, 28] based on the equivalent substitution of the homogeneous boundary value problems of (1.20) and (1.22) type by the homogeneous operator equations

$$B(k)\,b = 0;\ B(k) : l_2 \to l_2,\ b = \{b_n\} \in l_2,\ k \in \mathbf{K}, \tag{1.40}$$

l_2 is the space of the infinite sequences $a = \{a_n\} : \sum\limits_n |a_n|^2 < \infty$. It is important that the infinite matrix $B(k)$ should have the representation $B(k) = E + C(k)$, where E is the identity matrix and $C(k)$ is the finite-meromorphic matrix-valued function producing the kernel operator or the Koch matrix. Only in this case it is safe to believe that $\det[B(k)]$ [29] exists and an algorithm for finding the eigenfrequencies $\bar{k} \in \Omega_k$ can proceed from an approximate solution of the rigorous characteristic equation

$$d(k) = \det[B(k)] = 0,\ k \in \mathbf{K}. \tag{1.41}$$

Assume that a certain root $\bar{k}$ of the scalar equation (1.41) does not coincide with certain pole of the matrix-valued function $B(k)$. This root multiplicity determines

the multiplicity $M = M(1) + M(2) + ... + M(J)$ of the eigenvalue $\bar{k}$ of the operator equation (1.40), where (see also Statement 1.3) J is the number of linearly independent eigenfunctions $u_0^{(j)}(g,\bar{k})$ (the number of different free oscillations of the field) related to the eigenvalue (eigenfrequency) $\bar{k}$ and $M(j) - 1$ is the number of the associated functions $u_m^{(j)}(g,\bar{k})$, $m = 1,2,...,M(j) - 1$ for the eigenfunction $u_0^{(j)}(g,\bar{k})$. The pole order of the resolvent $A^{-1}(k)$ (the Green function $\tilde{G}(g,g_0,k,\Phi)$ or the fundamental solution of problems (1.20) and (1.22) at the point $k = \bar{k}$ is given by the maximum value $M(j)$.

In numerical experiments, problems (1.40) were separately solved for different symmetry classes of considered free oscillations, and no roots of above-unit multiplicity were found [10]. Under the assumption that the poles of the resolvent $A^{-1}(k)$ are simple (see, e.g., Statement 1.6), the multiplicity increase means the eigenfrequency $\bar{k}$ degeneration – one eigenfrequency corresponds to several linearly independent free oscillations of the open periodic resonator field. Normally there is little chance that changes of geometrical or constitutional parameters within their physical range will create a degeneration of this kind. Although a possibility exists for sufficiently close, in the metric of the corresponding complex space, relative position of two eigenfrequencies (for instance, $\bar{k}_1$ and $\bar{k}_2$) corresponding to free oscillations of different types but the same symmetry class. As some eigenfrequencies get close, the spectral characteristics of the "interacting" free oscillations experience local or global changes (see Section 1.3.4 and [1, 10, 30, 31]). A disturbance interferes in the regular run of the spectral curves $\bar{k}(\eta)$ realizing the zero lines of the function $d(k,\eta)$ as the mapping $d(k,\eta)\colon \mathbf{K} \times \mathbf{R}^1 \to \mathbf{C}$, where $\mathbf{C}$ is the complex plane and $\mathbf{R}^1$ is the real space of some varied parameter η of the problem. This means [32–34] that the trajectories $\bar{k}(\eta)$ pass near the isolated singular point $\{k_0,\eta_0\}$ of the mapping $d(k,\eta)\colon \mathbf{C} \times \mathbf{C} \to \mathbf{C}$ (here, as in the numerical experiment, the range of spectral parameter k is narrowed, while the physical range of the parameter η is expanded). The quantity $\gamma = d(k_0,\eta_0)$ evaluates the measure and the character of the mutual influence (coupling) of the oscillations as their eigenfrequencies come close. Also, it determines principal parameters of the anomalous and the resonant spatial–frequency transformations of the field $\tilde{U}(g,k,\eta)$ with real k and η values falling into the effective area of the critical point $\{k_0,\eta_0\}$ [31].

Statement 1.5 (rough localization of the spectrum Ω_k) *The spectrum* $\Omega_k(\eta)$ *of an open periodic resonator given by certain generalized parameter* η *is not empty in the bounded domain of the surface* $\mathbf{K}$. *The only exception may be the isolated points* η_m *from continuous range of parameter* η *at which all components of the spectrum* $\Omega_k(\eta_m)$ *tend to infinity.*

For volume gratings ($h \neq 0$) *with an ideal dielectric loading* ($\sigma(g) \equiv 0$), *the following statements are true.*

- *For* $\mathrm{Im}k \neq 0$, $\mathrm{Re}\,k \neq 0$, *the homogeneous problem (1.20) and (1.22) has no nontrivial solutions such that* $\mathrm{Im}k\mathrm{Re}\,k \sum_n \left(|A_n|^2 + |B_n|^2\right)\mathrm{Re}\Gamma_n > 0$. *In particular,*

there are neither outgoing ($\mathrm{Re}\Gamma_n \mathrm{Re}k > 0$ *for all n) solutions in the areas, where* $\mathrm{Im}k > 0$ *nor arriving (*$\mathrm{Re}\Gamma_n \mathrm{Re}k < 0$ *for all n) solutions, where* $\mathrm{Im}k < 0$.

- *For* $\mathrm{Im}k = 0$, $\mathrm{Re}\,k \neq 0$, *there are no nontrivial solutions such that* $\sum_n \left(|A_n|^2 + |B_n|^2\right)\mathrm{Re}\Gamma_n \neq 0$. *This specifically means that for both not arriving (*$\mathrm{Re}\Gamma_n \mathrm{Re}k \geq 0$ *for all n) and not outgoing (*$\mathrm{Re}\Gamma_n \mathrm{Re}k \leq 0$ *for all n) solutions, only those amplitudes* A_n *and* B_n *can be nonzero that are corresponding to* $\mathrm{Re}\Gamma_n = 0$.
- *For* $\mathrm{Im}k \neq 0$, $\mathrm{Re}\,k = 0$, *there are no nontrivial solutions such that* $\mathrm{Im}\Gamma_n > 0$ *for all* $n = 0, \pm 1, \pm 2, \ldots$
- *For* $|\mathrm{Im}k| \geq |\mathrm{Re}\,k|$, *there are no nontrivial solutions such that* $\sum_n \left(|A_n|^2 + |B_n|^2\right)\mathrm{Im}\Gamma_n \geq 0$. *In particular, there are no solutions with* $\mathrm{Im}\Gamma_n \geq 0$ *for all n.*

For plane gratings ($h = 0$), *the homogeneous problems (1.20) and (1.22) have no nontrivial solutions such that*

$$\sum_n \left(|A_n|^2 + |B_n|^2\right)\mathrm{Re}\Gamma_n \neq 0 \text{ and (or) } \sum_n \left(|A_n|^2 + |B_n|^2\right)\mathrm{Im}\Gamma_n \neq 0.$$

The spectrum of these gratings at the first sheet of the surface $\mathbf{K}$ *can include only the points* $\bar{k} = k_n^{\pm}$: $\Gamma_n\left(k_n^{\pm}\right) = 0$.

For any parameter values, the domains $0 < \arg k < \pi$ *and* $(5/4)\pi < \arg k < (7/4)\pi$ *on the first sheet of* $\mathbf{K}$ *(the cross-hatched area in Fig. 1.2a minus the segment* $|\mathrm{Re}k| \leq |\Phi_0|$*) do not contain points from the spectrum* Ω_k. *If* $\sigma(g) \equiv 0$ *and* $\bar{k} \in \Omega_k$, *the surface* $\mathbf{K}$ *has a sheet whose point* $-\bar{k}$ *will also belong to the set* Ω_k.

Statement 1.6 *Let* $\sigma(g) \equiv 0$ *and no real-valued eigenfrequency* $\bar{k}$ *on the first sheet of the surface* $\mathbf{K}$ *coincides with any branch point* $k_n^{\pm}$. *Then all poles of the Green function* $\tilde{G}(g,g_0,k)$, *that is the kernel of the resolvent* $A^{-1}(k)$, *or the fundamental solution to the problems (1.20) and (1.22) are simple at the points* $\bar{k}$.

Let us return to Statements 1.2–1.5. In general, the spectral theory results partly mentioned here make many previously obtained solutions ambiguous and enable us to study problems of the dynamic theory of open periodic resonators in terms of formally correct analytic and computational procedures, suggesting an optimal way to the goal. Thus, due to the fact that $\tilde{U}(g,k)$ (as well as $\tilde{G}(g,g_0,k)$; $A(k)$ and $B(k)$; $R_{np}^{\mathbf{AA}}(k)$ and $T_{np}^{\mathbf{BA}}(k)$) are meromorphic functions, one should inevitably, while studying any kind of singularity of the behavior of the relevant functions in the real frequency domain, pay attention first of all to singular points of the analytic continuation of the functions into the complex frequency domain. The analysis of local anomalous effects and phenomena is based on fundamental results of the theory of functions. In this way, it becomes possible to describe analytically the mechanisms of the resonant response of the structures in the form of local representations and expansion theorems. There are several simple examples [1, 10, 26, 35] confirming this statement.

The threshold effects in classical electromagnetics (first reported by R.W. Wood in 1902) have been studied intensively in numerous papers. However, it was the

analytic continuation of the solutions $\tilde{U}(g,k)$ of the elliptic boundary value problems (1.26) into the complex frequency domain that described in a most natural way the behavior of the complex amplitudes $R_{np}^{\mathbf{AA}}(k)$ and $T_{np}^{\mathbf{BA}}(k)$ of partial components of the diffraction field near the points $k_n^{\pm}$ where new homogeneous (propagating) waves emerge (see, for example, ref. [26]). This approach can lend itself well to the treatment of other local effects associated with electromagnetic radiation, propagation, and scattering. It is good enough to merit application to various methodological problems in theoretical radio physics. Take as an example problems related to the analysis of characteristic features of the field near singular points (edges) in the geometry of the structures or those concerned with the justification of the Rayleigh hypothesis. In the first case, the analytic continuation over the distance up to the edge will be natural. In the second, it is worth doing over spatial coordinates. So, different as they are, these problems share a common idea: in order to get rigorous results, one should abandon the framework of the conventional representations and set off for areas of physically unrealizable parameters in order to take advantage in full measure, of a mathematical apparatus adequate to the physics of the considered phenomena.

Let now a reflective grating (see Fig. 1.1c) be excited by an E- or H-polarized wave $\tilde{U}_0^i(g,k)$ in a regime with $|\Phi| \le 0.5$ (principal range of Φ). Assume that the scattered field possesses only one – principal – propagating harmonic ($\mathrm{Re}\Gamma_0 > 0$ and $\mathrm{Im}\Gamma_n > 0$ for $n = \pm 1, \pm 2, \ldots$ – it is the single-wave mode). For a reflective structure in such a regime $\left|R_{00}^{\mathbf{AA}}(k)\right| = 1$, i.e., $\left[R_{00}^{\mathbf{AA}}(k)\right]^* R_{00}^{\mathbf{AA}}(k) = 1$ (hereafter the asterisk $*$ indicates complex conjugation). We continue $R_{00}^{\mathbf{AA}}(k)$ into the domain of complex values of k on the first sheet of the surface $\mathbf{K}$. From $\ln\left[\left[R_{00}^{\mathbf{AA}}(k)\right]^* R_{00}^{\mathbf{AA}}(k)\right] = 0$ for $\mathrm{Im}k = 0$, using the symmetry principle [36], we obtain $\ln R_{00}^{\mathbf{AA}}(k^*) = -\ln\left[R_{00}^{\mathbf{AA}}(k)\right]^*$ or $R_{00}^{\mathbf{AA}}(k^*)\left[R_{00}^{\mathbf{AA}}(k)\right]^* = 1$. If the function $R_{00}^{\mathbf{AA}}(k)$ has a simple pole in the point $k = \bar{k}$, then $R_{00}^{\mathbf{AA}}\left(\bar{k}^*\right) = 0$. If only the first two terms in the expansion of $R_{00}^{\mathbf{AA}}(k)$ into the Laurent series are nonzero, we get, in view of the above, the following representation that is valid in a certain vicinity $\mathbf{D}$ of the point $\bar{k}$:

$$R_{00}^{\mathbf{AA}}(k) = \frac{r_{-1}}{k-\bar{k}} + r_0 = \mathrm{e}^{i\arg r_0}\frac{k-\bar{k}^*}{k-\bar{k}} = \mathrm{e}^{i\left(\arg r_0 - 2\arg\left(k-\bar{k}\right)\right)}; \quad \mathrm{Im}k = 0. \quad (1.42)$$

From (1.42) it follows that, if $\mathrm{Im}\bar{k} \ll 1$, by varying the real frequency parameter k in a small interval containing the point $k = \mathrm{Re}\bar{k}$, the phase of the reflection coefficient $R_{00}^{\mathbf{AA}}(k)$ changes approximately by 2π. This dynamic phase effect can be used in the design of tunable dispersive open resonators with selective grating mirrors and other radio-engineering devices in the millimeter and submillimeter wave range. From this effect one can also obtain reliable information about the eigenfrequency $\bar{k}$ of the structure.

Multipole representations like (1.42) are valid (see [1, 10, 35]) almost on the whole single-wave domain for both reflective and semitransparent structures symmetric about the $z{=}{-}h/2$ plane when the $R_{00}^{\mathbf{AA}}(k)$ (or $T_{00}^{\mathbf{BA}}(k)$) analytic continuation

from the corresponding real k interval into the **K** first sheet reveals a finite number of eigenfrequencies of free field oscillations. Any analytic error estimation is impossible for the solutions of the diffraction problems obtained by this method. But the error, according to computational experiments, is usually not over several percent throughout the whole single-wave domain. A most essential disagreement with rigorous results is far from the real parts of complex eigenfrequencies. The resonant behavior of the diffraction characteristics is described very accurately.

1.3.3 The Grating as an Open Periodic Waveguide

Change now the roles of the parameters k and Φ ($k > 0$ is fixed, Φ becomes a spectral parameter) and consider the grating as an open periodic waveguide. The following Statements 1.7–1.12 are true [10, 37, 38].

Statement 1.7 (definition and qualitative characteristics of eigenwaves) *The analytic continuation of the solutions* $\tilde{U}(g,k,\Phi)$ *of the problems (1.20), (1.22), and (1.26) into the complex domain of* Φ *yields the meromorphic functions* $\tilde{U}(\Phi)$ *whose natural domain of definition* **F** *is the infinite-sheeted Riemann surface consisting of planes* $\Phi \in \mathbf{C}$ *cut along the directions*

$$\begin{gathered}\kappa^2 - (n + \mathrm{Re}\Phi)^2 + (\mathrm{Im}\Phi)^2 = 0, \\ n = 0, \pm 1, \pm 2,..., \mathrm{Im}\Phi \mathrm{Re}(n + \Phi) \geq 0, \quad \kappa = kl/2\pi.\end{gathered} \tag{1.43}$$

The systems $\left\{\bar{\Phi}_n\right\} = \Omega_\Phi$ *of poles of the functions* $\tilde{U}(\Phi)$ *(no more than countable sets with no finite accumulation points) determine the complete spectra (eigenvalues) of the gratings as open periodic waveguides: if* $\Phi = \bar{\Phi}_n$ *, the homogeneous problems (1.20), (1.22), and (1.26) have nontrivial solutions in* **F***, and corresponding solutions* $u_0^{(j)}\left(g,\bar{\Phi}_n\right)$ *are eigenwaves of the periodic structures.*

The first sheet of the surface **F** (values of pairs $\{\Phi \to \Gamma_n(\Phi)\}$, $n = 0, \pm 1, \pm 2,...$) is determined by the radiation condition (1.22), which appears to be $\mathrm{Im}\Gamma_n(\Phi) \geq 0$, $\mathrm{Re}\Gamma_n(\Phi) \geq 0$, $n = 0, \pm 1, \pm 2,...$ on the axis $\mathrm{Im}\,\Phi = 0$ (see Fig. 1.2b). Here, $\Gamma_n(\Phi) = \Gamma_{-n}(-\Phi)$. The distinction of the next sheets is that for the finite number of values of the index n, the signs (root branches) of $\Gamma_n(\Phi)$ change to the opposite ones. The cuts (1.43) originate from the real algebraic branch points $\Phi_n^{\pm}$:$\Gamma_n\left(\Phi_n^{\pm}\right) = 0$ or $\Phi_n^{\pm} = \pm\kappa - n$. On these curves, $|\mathrm{Re}\Gamma_n(\Phi)| = |\mathrm{Im}\Gamma_n(\Phi)|$.

The properties of the eigenwaves of an open periodic waveguide are governed by the position on the surface **F** of the relevant propagation constants. Their fields in **A** and **B** domains can carry (in various combinations):

- harmonics not arriving onto the grating from $|z| = \infty$ ($\mathrm{Re}\Gamma_n \geq 0$) or not outgoing from it ($\mathrm{Re}\Gamma_n \leq 0$);
- harmonics not incrementing ($\mathrm{Re}\Gamma_n \mathrm{Im}\Gamma_n \geq 0$) or not decrementing ($\mathrm{Re}\Gamma_n \mathrm{Im}\Gamma_n \leq 0$) in the propagation direction z;

- harmonics that do not increment ($\mathrm{Re}\,(n+\Phi)\,\mathrm{Im}\Phi \geq 0$) and do not decrement ($\mathrm{Re}\,(n+\Phi)\,\mathrm{Im}\Phi \leq 0$) in the y-propagation direction.

Eigenwaves whose field decays exponentially away from the grating are known to be the surface waves. If not, the leaky waves take place. Eigenwaves whose field does not change in a direction perpendicular to the grating plane are piston waves. Waves whose eigenvalues $\bar{\Phi}$ are situated on the real axis of the first sheet of the surface $\mathbf{F}$ will be called real waves. Waves with complex eigenvalues $\bar{\Phi}$: $\mathrm{Im}\bar{\Phi} \neq 0$ will be called complex waves. Real waves fall into the slow ($\max\limits_n \left|k/\Phi_n\right| < 1$) and the fast ($\max\limits_n \left|k/\Phi_n\right| \geq 1$) waves. Here, of course, only those n are considered whose eigenwave field amplitudes A_n and B_n in the domains $\mathbf{A}$ and $\mathbf{B}$ are not zero.

Statement 1.8 *If there is an eigenwave* $u_0\left(g,\bar{\Phi}\right)$ *, there will also be an eigenwave* $u_0\left(g,\bar{\Phi}+p\right)$ *, with p being an arbitrary integer and* $u_0\left(g,\bar{\Phi}\right) = u_0\left(g,\bar{\Phi}+p\right)$ *. It means that all information about the eigenwaves associated with eigenvalues* $\overline{\Phi}$ *arbitrarily located on the surface* $\mathbf{F}$ *is available from the solution to the homogeneous problems (1.20), (1.22), or (1.26) in some spaces belonging to* $\mathbf{F}$ *sheets and separated by an arbitrary strip whose range of* $\mathrm{Re}\Phi$ *equals unity. One possible version of the selected strip is shown in Fig. 1.2b .*

Statement 1.9 *The spectrum* $\Omega_\Phi(\eta)$ *of an open periodic waveguide given by a generalized parameter* η *is not empty in a bounded part of the surface* $\mathbf{F}$ *. The only possible exception can be the isolated points* η_m *from the continuous range of the parameter* η*. At them, all components of the spectrum* $\Omega_\Phi(\eta_m)$ *tend to infinity.*

Statement 1.10 (rough localization of the spectrum Ω_Φ) *Let* $\mathrm{Im}\bar{\Phi} = 0$*. Then there exist no eigenwaves* $u_0\left(g,\bar{\Phi}\right)$ *such that*

$$\sum_{n=-\infty}^{\infty}\left[|A_n|^2+|B_n|^2\right]\left\{\begin{matrix}\mathrm{Re}\Gamma_n\left(\bar{\Phi}\right)\\ \mathrm{Im}\Gamma_n\left(\bar{\Phi}\right)\end{matrix}\right\} \neq -\frac{k^2}{l\beta_0}\left\{\begin{matrix}W_1\left(\bar{\Phi}\right)\\ W_2\left(\bar{\Phi}\right)\end{matrix}\right\};$$

$$W_1\left(\bar{\Phi}\right) = \frac{1}{k}\int\limits_{\mathbf{G}}\sigma\varepsilon_0\left|\vec{E}\right|^2 dg,$$

$$W_2\left(\bar{\Phi}\right) = \left\{\begin{matrix}+\\ -\end{matrix}\right\}\int\limits_{\mathbf{G}}\left[\mu\mu_0\left|\vec{H}\right|^2-\varepsilon\varepsilon_0\left|\vec{E}\right|^2\right]dg,\ \beta_0 = \left\{\begin{matrix}\varepsilon_0\\ \mu_0\end{matrix}\right\};\ \left\{\begin{matrix}E-\text{case}\\ H-\text{case}\end{matrix}\right\},$$

$$\mathbf{G} = \left\{g\in\mathbf{Q}^{new}:\ -h\leq z\leq 0\right\}.$$

This statement suggests the following conclusions.

- For $\sigma(g) \not\equiv 0$, the real axis of the first sheet of the surface $\mathbf{F}$ does not contain eigenvalues $\overline{\Phi}$. Eigenvalues $\overline{\Phi}$ of a plane grating ($h = 0$) can coincide here only with the branch points $\Phi_n^{\pm} = \pm\kappa - n$.
- If an ideal volume grating ($\sigma(g) \equiv 0$ and $h \neq 0$) supports a real eigenwave $u_0\left(g,\bar{\Phi}\right)$, then the amplitudes $A_n\left(\bar{\Phi}\right)$ and $B_n\left(\bar{\Phi}\right)$ of the partial components of

this wave field vanish for n such that $\mathrm{Re}\Gamma_n\left(\bar{\Phi}\right) > 0$. In the $E\,(H)$-polarization case, the electric field energy of this wave in the domain $\mathbf{G}$ is always greater (smaller) than the magnetic field energy.

- All eigenwaves whose eigenvalues belong to the real axis on the first sheet and do not coincide with branch points are the surface waves. Those propagating along the grating can only be the slow waves.
- For $\sigma\,(g) \not\equiv 0$, there are no surface waves $u_0\left(g,\bar{\Phi}\right)$ that transfer energy in the positive (for $\mathrm{Im}\bar{\Phi} < 0$) or negative (for $\mathrm{Im}\bar{\Phi} > 0$) directions of the y-axis.
- For $\sigma\,(g) \equiv 0$, there are no complex ($\mathrm{Im}\bar{\Phi} \neq 0$) surface waves $u_0\left(g,\bar{\Phi}\right)$ that transfer energy along the structure.
- If $u_0\,(g) = \sum\limits_m u_0\left(g,\bar{\Phi}_m\right)$, where $u_0\left(g,\bar{\Phi}_m\right)$ are different real surface waves, then $\mathrm{Re}P\left[u_0\,(g)\,,\vec{y},\tilde{y}\right] = \sum\limits_m \mathrm{Re}P\left[u_0\left(g,\bar{\Phi}_m\right),\vec{y},\tilde{y}\right]$. Here, $P\left[u_0\,(g)\,,\vec{y}\right]$ is the $\vec{y}$-directed flux of the Poynting vector of the wave field $u_0\,(g)$ crossing the complete $y = \tilde{y}$ section of the periodic structure.

Statement 1.11 *For perfect gratings ($\sigma\,(g) \equiv 0$) symmetric about the planes $y = \mathrm{const} + nl$, $n = 0, \pm 1, \pm 2,...$, points of the spectrum Ω_Φ are quadrupled, $\left\{\bar{\Phi}, -\bar{\Phi}, \bar{\Phi}^*, -\bar{\Phi}^*\right\}$, which is to say that if some point $\bar{\Phi}$ is located, for instance, on the first sheet of the surface $\mathbf{F}$, the points $-\bar{\Phi}$, $\bar{\Phi}^*$, $-\bar{\Phi}^*$ situated on a certain (the same or another) sheet of $\mathbf{F}$ also belong to the set Ω_Φ.*

A peculiar feature of the approach whose results have been partly formulated in Statements 1.7–1.11 distinguishes it from the previously used methods. Namely, the relevant boundary value problems are considered over the natural range of Φ. The complete Riemannian surface formulation of the spectral problems with a properly extended radiation conditions eliminates subjective elements inevitable in an effort to limit the Φ range to simple, physical regions. This approach is capable of dealing with any eigenwave type – surface, leaky, or piston. The classical method of formulating and solving self-adjoint problems ($\mathbf{L}_2$-theory) has similar possibilities. However, their realization imposes some additional difficulties, e.g., the continuation through continuous spectrum [39].

The results stated above qualitatively characterize the physical discrete spectrum Ω_Φ. Also, they substantially simplify the numerical analysis, reducing the search for eigenconstants and suggesting characteristic features of their dynamics under changes of parameters, providing thereby the necessary basis for constructing rigorous and efficient computational procedures [10]. Thus, e.g., from Statement 1.11 follows that the propagation constants $\bar{\Phi}$ of the eigenwaves move over the surface $\mathbf{F}$ in quadruples. If the imaginary part of $\bar{\Phi}$ is zero, then, in order for the respective eigenwave to be able to turn from a real into a complex one by variation of parameters, this wave should collide with another real eigenwave: only two waves from the point $\bar{\Phi} = \bar{\Phi}_1$, $\mathrm{Im}\bar{\Phi}_1 = 0$, where their propagation constants coincide, can simultaneously enter the domain of complex values of the spectral parameter $\bar{\Phi}$. Or, rather, only the projections of the propagation constants on the first sheet of the surface $\mathbf{F}$ coincide; the points $\bar{\Phi}_1$ themselves that are corresponding to both waves can in the general case belong to different sheets of $\mathbf{F}$. The collided real waves turn into

complex ones in different half-planes of the sheets of the surface **F**: the propagation constants have increments to the imaginary part that are equal in the absolute value, but with opposite signs.

We address some result from [1] (see Fig. 6.4 in [1]). In a rectangular metal grating, two real H_{013}-waves collide at the point $\bar{\Phi} = \bar{\Phi}_1 = 0.5$ as parameter k varies. Having collided, they turn into the complex waves, with the $\mathrm{Re}\bar{\Phi}$ values unchanged, both equal to 0.5, and the $\mathrm{Im}\bar{\Phi}$ values have opposite signs. The eigenwave field transformations also go in opposite directions until they take the H_{021}-wave typical appearance. Then, at a larger k, the waves collide again, the complex waves turn into the real ones classified as slow H_{021}-waves: on a short range of frequency parameter k, both waves change from H_{013} to H_{021}. All these behavioral features of grating spectrum Ω_Φ components reflect certain general regularities revealed by the qualitative analysis of spectral characteristics of open periodic waveguides [10, 37, 38]. However, the interaction of two eigenwaves whose eigenvalues come close in the complex space is of particular interest. The point is that usually the "interaction" either locally changes the wave modes (pure mode → hybrid mode → recovering of the preceding pure mode) or results in a wave mode exchange (two different pure modes → hybrid modes → exchange of the pure modes) [1, 10, 40]. The components of the spectrum Ω_Φ cannot vanish anywhere in the finite part of **F** under changes of the material and geometric parameters of the grating (see Statement 1.9 and [10, 11]). Hence, slow eigenwaves should, without exception, manage to pass the nontransmission zones of an open periodic waveguide. Turning for a while from real into the complex waves, they implement the only possible variant of a smooth transition into the domain of parameter values, where they can propagate again in their inherent mode.

Let now $\tilde{G}(g,g_0,\Phi)$ be the Green's function of a grating in the field of a quasi-periodic point source

$$\tilde{f}(g,\Phi) = \sum_{n=-\infty}^{\infty} \delta(y - y_0 - nl, z - z_0)\, \mathrm{e}^{i2\pi n\Phi};\ 0 < y_0 < l,\ g_0 = \{y_0,z_0\} \in \mathbf{Q}_a^{new}.$$

In other words, let $\tilde{G}(g,g_0,\Phi)$ be the fundamental solution of problems (1.20) and (1.22).

Using the superposition principle and taking into account the representation

$$\delta(y - y_0,\, z - z_0) = \int_{-0.5}^{0.5} \tilde{f}(g,\Phi) d\Phi, \tag{1.44}$$

we obtain

$$\underset{\circ}{\tilde{G}}(g,g_0) = \int_{-0.5}^{0.5} \tilde{G}(g,g_0,\Phi)\, d\Phi. \tag{1.45}$$

Here, $\tilde{\underset{\circ}{G}}(g,g_0)$ is the Green's function of the grating in the field of a point source (1.44), i.e., the fundamental solution of the operator of the problem of infinite periodic structure excitation by a compact source or a plane wave beam. These are the key problems in model synthesis of various quasi-optical devices (beam formers, absorbing and rescattering coatings, open dispersive resonators with substantially rarefied spectrum), where gratings act as resonant elements to efficiently select signals in frequency, polarization, and space [40, 41]. A correct analysis of these problems is only possible when the radiation condition has been taken into account, which provides, first, a physically valid solution and, second, admits the passage from differential to integral representations in standard methods of potential theory.

The formal approach to the problem using the transformation (1.45) does not yield quite accurate results [42, 43], as it is necessary to have some information on the singularities of the integrand (the function $\tilde{G}(g,g_0,\Phi)$) along the pass of integration, about acceptable ways of going around these singularities, etc. The information of the kind can be only obtained in terms of the spectral theory considering gratings as open periodic waveguides (see the previous results of the section and [10, 37, 38]). To simplify the case, the statement justified in [10] and based on results from [44] is presented below to fit the reflective grating geometry such as the one shown in Fig. 1.1c.

Statement 1.12 *Assume that the frequency $k > 0$ is not critical for a 1-D periodic waveguide, i.e., the section $|\Phi| \le 0.5$ does not contain any eigenvalues of $\bar{\Phi}$ corresponding to eigenwaves $u_0\left(g,\bar{\Phi}\right)$ that do not transfer energy along the structure. Assume also that among the elements of the set Ω_Φ there are no branch points of the surface* **F**. *Then, if $r \to \infty$ ($|\alpha| < \pi/2$) and $|y| \to \infty$ ($|\alpha| = \pi/2$),*

$$\tilde{\underset{\circ}{G}}(g,g_0) = \frac{l}{2\pi}\left(\frac{2\pi k}{r}\right)^{1/2} \mathrm{e}^{i(rk-\pi/4)} \left\{ \sum_{n:\ |\kappa \sin\alpha + n| \le 0.5} \eta_n A_n(g_0, -\kappa\sin\alpha - n) \right\} \cos\alpha +$$

$$+ \left\{ \begin{array}{ll} \pi i \sum\limits_{\overline{\Phi}_m \in M^+} \eta_m \mathrm{Res}\, \tilde{G}\left(g,g_0,\overline{\Phi}_m\right); & y > 0 \\ -\pi i \sum\limits_{\bar{\Phi}_m \in M^-} \eta_m \mathrm{Res}\, \tilde{G}\left(g,g_0,\overline{\Phi}_m\right); & y < 0 \end{array} \right. + O\left(r^{-1}\right). \qquad (1.46)$$

Here, $z - a = r\cos\alpha$ and $y = -r\sin\alpha$; η_m is a number (1 or 0.5) that is used for differentiating the contribution of poles and points of stationary phase depending on their location (inside or at the end of the integration interval); $A_n(g_0,\Phi)$ are the amplitudes of the Green's function $\tilde{G}(g,g_0,\Phi)$ harmonics in the expressions like (1.22); M^+ and M^- are the finite sets of the real eigennumbers $\left|\bar{\Phi}_m\right| \le 0.5$ corresponding to eigenwaves which transfer the energy along the grating in the positive and negative y directions, respectively.

By exciting the grating by a compact source (in the plane $\mathbf{R}^2$) and by scattering of plane waves, plane wave packets, and eigenwaves of a periodic open waveguide in

a system "grating – compact discontinuity," the radiation conditions following from relations like (1.46) single out the unique solution of the corresponding diffraction problems. This solution satisfies the physically valid requirement due to which the scattered field should be free from waves arriving from infinity into the zone where the sources and efficient scatterers are concentrated.

The first set of terms in the right-hand side of (1.46) represents a diverging cylindrical inhomogeneous wave with the amplitude (field pattern)

$$D(\alpha) = \cos\alpha \sum_{n:\ |\kappa \sin\alpha + n| \le 0.5} \eta_n A_n (g_0, -\kappa \sin\alpha - n). \tag{1.47}$$

Owing to (1.47), the field pattern in the far zone is completely determined by the amplitudes of the propagating harmonics of the quasi-periodic Green function $\tilde{G}(g,g_0,k,\Phi)$ for $\Phi = -\kappa \sin\alpha - n$, $|\Phi| \le 0.5$. In [43] a similar result was obtained. It is complemented here by the fields of real eigenwaves available from (1.46). They decrease exponentially for $z > a$ but have the order $O(1)$ for bounded z and $|y| \to \infty$.

1.3.4 Some Physical Results of Spectral Theory

In a number of cases, the spectral and scattering characteristics of different type gratings, thought of as open periodic resonators and waveguides, can be qualitatively analyzed by using results reported in Sections 1.3.2 and 1.3.3. However, the main tool for studying wave and oscillation processes in these structures, treated in terms of complex boundary value problems, is numerical experiment. The employed models enable us to obtain all necessary information quickly and with a desired accuracy. Physical results [1, 10, 40] based on the spectral theory have been obtained by numerical experiments on analytic regularization models (see [10, 11, 16, 17, 22, 45] and Chapter 2) for waveguide-type semitransparent and reflective gratings. Consideration was mostly given to free and forced oscillations for the case of E-polarization and for the structures with $\mu(g) \equiv 1$, $\sigma(g) \equiv 0$, and piecewise constant $\varepsilon(g)$. Often the joint qualitative characteristic $\{N,M\}$ (see Section 1.2.1) was invoked, which was readily calculated in those cases for any geometrical parameters and real-valued k and Φ. Thus, for the grating from Fig. 1.4, $N = \sum_n \mathrm{Re}\Gamma_n / |\Gamma_n|$ and $M = \sum_m \mathrm{Re}\gamma_m / |\gamma_m|$. Here, $\gamma_m = \sqrt{k^2\varepsilon - (m\pi/d)^2}$, $m = 1,2,...$, and $\mathrm{Re}\gamma_m \ge 0$, $\mathrm{Im}\gamma_m \ge 0$ are the propagation constants of the H_{0m}-waves within the $-h \le z \le 0$ section of a regular plane parallel waveguide (in channel **G**).

Let us briefly review the physical results from [1, 10, 40] for model structures like semitransparent rectangular metal gratings. The guiding channels **G** are filled with a homogeneous dielectric (see Fig. 1.4). Of concern will be free oscillations (E-polarization, $0 \le \Phi \le 0.5$) whose eigenfrequencies are situated on the first sheet of the surface **K**, more specifically, within $0 < k < k_0^+ = \Phi_0$, where all the radiation channels into the free space are closed ($N = 0$), and in the area $\mathrm{Im}k \le 0$ under segments of the real axis corresponding to the values $N = 1$

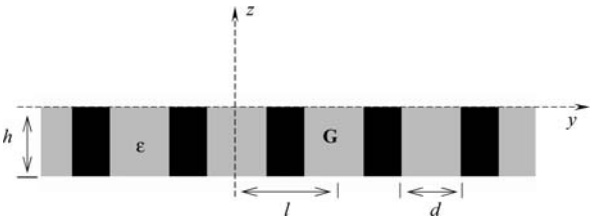

Fig. 1.4 A grating formed by *rectangular metal bars*

($k_0^+ < k < k_{-1}^- = -\Phi_{-1}$) and $N = 2$. These oscillations are identified as the H_{0mn}-oscillations, where $H_{0\,m}$ is the **G** channel wave dominating in the oscillation field, and n is the number of the field variations present along the structure height. The same-m oscillations belong to one and the same family, and n, the oscillation ordinal number in the family, determines its class of symmetry about the plane $z = -h/2$ (depending on whether the oscillation field configuration is symmetric or asymmetric with respect to this plane). For $\Phi = 0$ and $\Phi = 0.5$, the planes $y = pl$, $p = 0, \pm 1, \pm 2...$, also act as symmetry planes. The distribution of free oscillations between the two new symmetry classes is determined by the evenness of index m.

When solving spectral problems within $0 < k < \Phi_0$ ($N = 0$), where it can be that $M = 0$ ($0 < k < k_1$, k_m is the cutoff point of the H_{0m}-wave), $M = 1$ ($k_1 < k < k_2$), and $M = 2$ ($k_2 < k < \Phi_0 \le k_3$) and h values vary over a sufficiently wide range ($0 < h < H$), one finds that the number of free oscillation families is exactly equal to M, and each has its own bundle of the spectral curves $\bar{k}_{mn}(h)$, $m = 1,2$. So, the domain $(0;k_1) \times (0;H)$ carries no eigenfrequencies of an open periodic resonator. In the domain $(k_1;k_2) \times (0;H)$, we observe the bundle $\{\bar{k}_{1n}(h)\}$ (see Fig. 6.5 in [1]) all of whose components tend, as $h \to \infty$, to the cutoff point of the H_{01}-wave dominating in the field of the first-family free oscillations. The curves $\bar{k}_{1n}(h)$ run one above the other in order of increasing index n. For a given h, a larger n corresponds to a higher $\bar{k}_{1n}$ eigenfrequency. Quite rarefied when the grating height is small, the spectrum condenses as h increases.

When $\Phi = 0.5$, the bundle $\{\bar{k}_{2n}(h)\}$ of spectral curves for oscillations of the second family in the domain $(k_2;\Phi_0) \times (0;H)$ appears as the bundle $\{\bar{k}_{1n}(h)\}$ in the domain $(0;k_1) \times (0;H)$. As $h \to \infty$, all its components tend to the $H_{0\,2}$-wave cutoff point k_2, which is the boundary of the domain given by the vector $\{N,M\}$ with $N = 0$ and $M = 2$ (that is, plainly a $\{0,2\}$ vector). The spectral curves of the first- and the second-family oscillations meet. At their meeting points, one eigenfrequency corresponds to the two oscillations from two different symmetry classes (eigenfrequency degeneration): the field of one of them is symmetric about the plane $y = pl$ and the other oscillation field is asymmetric. When the symmetry provided by some special value of the parameter Φ disappears, the oscillations H_{01n} and H_{02n} of the same evenness of index n are found to share the same class of symmetry about the plane $z = -h/2$. Now their spectral curves go apart rather than meeting. In the space of

the expected meeting, they draw a Vienne-type chart (see, for example, Figs. 3.1 and 3.2 in [10]) that is characteristic of the "interacting" oscillations (responding to that their eigenfrequencies tend to come close). For small variations of h, the "interacting" oscillations exchange by their major spectral characteristics: by the dynamics of the eigenfrequency behavior and the mode type. Oscillations entering the interaction zone experience the following dynamic changes of their field structure: "two different pure modes → hybrid modes → exchange of the pure modes."

An approximate mathematical model of this phenomenon (the intermode coupling effect) for oscillations in closed resonators with excited boundaries was first given in [46]. There the results of classical excitation theory of self-adjoint operators are used. For gratings, the analysis of spectral characteristics is based on the solution of nonself-adjoint problems, i.e., eigenvalues in the general case are complex, and the eigenfunctions do not form a basis. Therefore, since the model from [46] cannot be applied, the main research tool here is the computational experiment. The results from [34, 47–52] prove the general character of the analyzed effect. Evidently, the conditions required for the existence of the effect can be created in almost any open resonator: waveguide, periodic, with compact or infinitely expanded boundaries. The effect of intermode coupling allows the spectral lines of the oscillations that are comparable regarding the diffraction Q-factor go apart in the complex space without intersecting, avoiding, in this way the degeneration, i.e., the possibility of existence of different oscillations from one symmetry class at one frequency $\bar{k}$. In [46], the deviation at the resonator boundaries and in its material parameters from ideal ones are considered to be necessary conditions for realization of this phenomenon. On the other hand, [53] proves the instability of degenerate states. The combination of these two results allow us to consider the intermode coupling effect as a reaction of an imperfect system (in our case – free field oscillations in an open periodic resonator) as it approaches an unstable state. The intermode coupling points out the possibility of degeneration of the oscillations in a certain ideal case that cannot be achieved by varying the values of parameters in the physical domain (real Φ, h, d, and so on). The search for degenerate states in open systems is normally associated with the requirement of analytic continuation of the solutions of the model spectral problems into the domain of complex (nonphysical) values of nonspectral parameters. In the simplest cases, the disappearance of degeneration and passage to the intermode coupling can be modeled in terms of parameters having conventional physical meaning, the same as discussed above in the case $\Phi = 0.5$ and real-valued eigenfrequencies $\bar{k} \in (0;\Phi_0)$.

Solving the spectral problems for $h \in (0;H)$ in the area $\mathrm{Im}k \leq 0$ under the real axis segment $\Phi_0 < k < -\Phi_{-1}$ corresponding to $N = 1$ and carrying one ($M = 1$), two ($M = 2$), or three ($M = 3$) cutoffs of the H_{0m}-waves, we obtain the spectral curves $\bar{k}_{mn}(h)$ for one ($m = 1$), two ($m = 1,2$), or three ($m = 1,2,3$) families of free field oscillations in the grating. As h increases indefinitely, all these curves tend to meet at the cutoff points k_m of the H_{0m}-waves. As generally $\mathrm{Im}\bar{k}_{mn}(h) \neq 0$ while $\mathrm{Im}k_n = 0$, we can state that the oscillation quality $Q_{mn} = \mathrm{Re}\bar{k}_{nm}/2\left|\mathrm{Im}\bar{k}_{nm}\right|$ infinitely increases as h does so. To simplify the situation, assume that $0 < \Phi < 0.5$,

i.e., all oscillations represent only two symmetry classes specified by the evenness of index n.

If $\Phi_0 < k_1 < k_2 < -\Phi_{-1}$ and $k_3 > -\Phi_{-1}$, the bundles $\left\{\mathrm{Re}\bar{k}_{1n}(h)\right\}$ and $\left\{\mathrm{Re}\bar{k}_{2n}(h)\right\}$ of spectral curves of the first and second families in the domain $(k_1; -\Phi_{-1}) \times (0;H)$ appear as the bundles $\left\{\bar{k}_{1n}(h)\right\}$ and $\left\{\bar{k}_{2n}(h)\right\}$ of real-valued eigenfrequencies in the domain $(0;\Phi_0) \times (0;H)$ when $\Phi = 0.5$ and $0 < k_1 < k_2 < \Phi_0 < k_3$ (see above). The Q-factor of the second-family oscillations is approximately two to three orders higher. That is why eigenfrequencies split up in the complex plane even where the curves $\mathrm{Re}\bar{k}(h)$ corresponding to oscillations from different families meet at certain h values. Before and after the intersection of $\mathrm{Re}\bar{k}(h)$ curves, all characteristic features of the related oscillations remain unchanged. However, near the coincidence of the real values of eigenfrequencies of the first- and second-family oscillations (and only for oscillations of similar symmetry classes), the field geometry of second-family oscillation gets essential distortions (hybrid mode), and its Q-factor increases rapidly and in some places seemingly toward infinity (see, for example, Fig. 6.6 in [1]). According to Statement 1.5 and a physically clear understanding of the case, at this moment, the amplitudes A_0 and B_0 of the partial components in the field of the corresponding H_{02n}-oscillation should become zero – the energy should not be radiated into the far zone. This fact has been verified numerically.

In the case considered, the Q-factors of the oscillations of the first and second families (let us denote the corresponding eigenfrequencies by $\bar{k}_1$ and $\bar{k}_2$, respectively) are determined by the radiation losses due to the radiation of both H_{01}- and H_{02}-waves. For distant $\bar{k}_1$ and $\bar{k}_2$, the radiation losses are dominating, which are integrally determined by the resonating waveguide wave (H_{01}-wave for the first family and H_{02}-wave for the second family). When $\mathrm{Re}\bar{k}_1$ and $\mathrm{Re}\bar{k}_2$ are close to each other, the H_{01}- and H_{02}-waves even up their related excitation levels in the oscillation fields, and so do their radiation loss contributions. This may reduce the resultant losses (and increase the Q-factor) when the phases of the contributors differ by π. Exactly such a mechanism, implying a compensation of contributions, results in an increased Q-factor of the oscillation of the second family under conditions that are close to those for existence of the oscillation of the first family. The fact that at this stage there are no significant changes in the oscillation of the first family is to be attributed to the incommensurability of the absolute values of its average radiation losses with the compensating contribution due to the intensified influence of H_{02}-waves. Note that super-high-Q oscillations occur in the region $k > \Phi_0$, where $N = 1$. Here the structure is generally open: harmonics propagating toward $|z| \to \infty$ can carry the field energy away without attenuation.

In regular situations, the oscillation mode described by the identifier H_{0mn} is a sufficiently stable characteristic provided that parameter variations are smooth. As mentioned above, the passage to the real axis of the eigenfrequency $\bar{k}_2(h)$ of the H_{02n}-oscillation when the spectral curves $\mathrm{Re}\bar{k}_1(h)$ and $\mathrm{Re}\bar{k}_2(h)$ meet ($\bar{k}_1(h)$ is the H_{01n}-oscillation eigenfrequency) causes the chain of the transformations “pure

modes → hybrid modes → recovery of the previous pure modes" that take place for the parameter h varying within small intervals. In anomalous situations occurring due to the eigenfrequency convergence of several free oscillations of one symmetry class in the corresponding complex space metric (clearly the Q-factors of these oscillations must be comparable), the "interacting" oscillation modes can be changed fundamentally. In the concerned situation, the realization of intermode coupling effect requires one more (the third) family of free oscillations with a bundle $\{\bar{k}_{3n}(h)\}$ of eigenfrequencies under the real axis segment $\Phi_0 < k < -\Phi_{-1}$ ($\Phi_0 < k_1 < k_2 < k_3 < -\Phi_{-1}$). The components of the bundles $\{\mathrm{Re}\bar{k}_{2n}(h)\}$and $\{\mathrm{Re}\bar{k}_{3n}(h)\}$ of different-evenness n indices will meet, and the corresponding oscillations having different classes of symmetry about the plane $-h/2$ will never respond to the convergence of their complex eigenfrequencies. The spectral curves $\mathrm{Re}\bar{k}_{2n}(h)$ and $\mathrm{Re}\bar{k}_{3n}(h)$ for equal-evenness n indices will go apart over the space $(k_3; -\Phi_{-1}) \times (0;H)$. Their divergence starts in a small vicinity of the point $\{\underline{k},\underline{h}\}$, which could have been a point of their meeting (see, for example, Figs. 2.12, 2.13, 2.14 in [10]). One of the curves $\mathrm{Im}\bar{k}_{2n}(h)$ or $\mathrm{Im}\bar{k}_{3n}(h)$ will go upward, coming to the real axis at the point $\underline{h}$ (super-high-Q oscillation in the region $k > \Phi_0$, where $N = 1$ and $M = 3$). The other will go down to the area $\mathrm{Im}k < 0$. The "interacting" oscillations exchange all their characteristics under changes of the parameters near the point $\{\underline{k},\underline{h}\}$. Having crossed the interaction zone, their field structure changes in the same way as in the real eigenfrequency case: "two different pure modes → hybrid modes → exchange of the pure modes."

Several general remarks on the super-high-Q oscillations in open resonators are in order. If we disregard the trivial case when the energy-radiating channels are electromagnetically closed (for gratings at $|\Phi| \leq 0.5$ it is the region $k < |\Phi_0|$), one can say that the super-high-Q oscillations are only possible in structures whose radiation field always contains only a finite number of "energy-consuming harmonics" (i.e., waves carrying energy to infinity). This illustrates the qualitative difference between the spectra of open periodic and waveguide resonators on the one hand and compact open resonators on the other. The latter can maintain on physical sheet of their own **K** surface the only attenuating ($\mathrm{Im}\bar{k} \neq 0$) oscillations of the field [8, 9, 11].

The super-high-Q oscillations ($\mathrm{Im}\bar{k} = 0$ on the first sheet of **K**) are, at the same time, the grating real (or slow) surface waves that propagate without attenuation toward the direction where the structure is periodical (see Statements 1.4 and 1.7). The area with one or several radiation channels open is given by the inequality $k > |\Phi_0|$ and classified in the literature as "forbidden" for these waves. If the channel is open only on principal harmonics ($\mathrm{Re}\Gamma_n > 0$ only for $n = 0$), then the amplitudes A_0 and B_0 of the plane waves – the partial field components of the real surface wave in the domains **A** and **B** (see (1.22)) – vanish (see Statements 1.5 and 1.10). In this case, the region $k > |\Phi_0|$ does not differ from the region $k < |\Phi_0|$ (the traditional region where real surface waves are present) as regards the energy exchange between the near grating zone and the free space, and here the existence of real waves is no more considered as an unusual effect. Thus, since super-high-Q oscillations have been revealed in a grating with open energy-radiating channels, the

traditional idea about the boundaries of the region of real surface wave existence for open periodic waveguides has been essentially extended. This result can be useful for solving many applied problems. It expands the area of applications of gratings as slowing and directing structures in various devices in microwave engineering, electronics, and optics.

The analytic continuation of the resolvents of diffraction problems (1.20), (1.22), and (1.26) into the domain of complex values of k reveals a certain set of singularities $\{\bar{k}_n\} = \Omega_k$, which according to Statement 1.4 may be qualified as isolated (for $|k| < \infty$) finite order poles of relevant operator-functions of local variables on the surface $\mathbf{K}$. This fundamental result of spectral theory allows us, in particular, to formulate a consistent and well-justified approach to the study of local anomalous changes of the diffraction grating electromagnetic field (see, for example, the dynamic phase effect described in Section 1.3.2). The changes of this type usually take place within extremely short intervals of variations of the free parameters and attended by sharp limiting (as much as possible) changes of the values of the principal diffraction characteristics. Below we will show several results of the spectral theory concerning analysis and treatment of most pronounced phenomena, including the total transition and the total reflection of electromagnetic waves (see

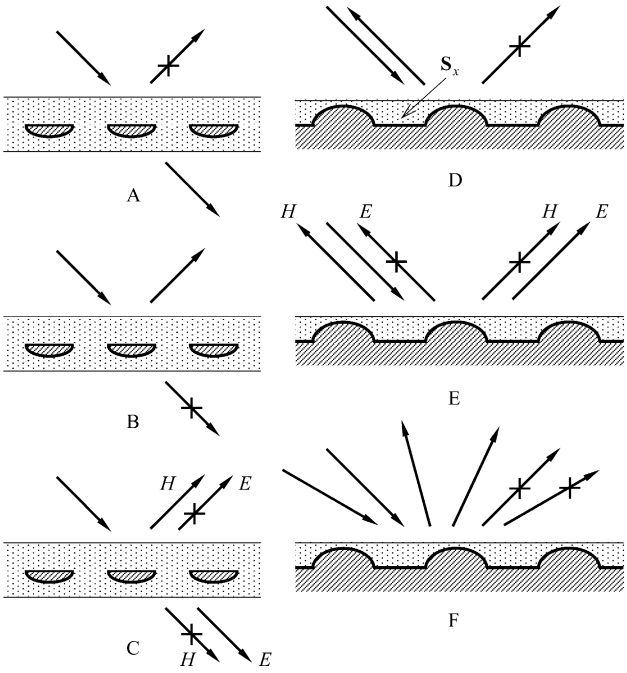

Fig. 1.5 The effects of (**a**) total transmission, (**b**) total reflection, and (**d**) total autocollimation reflection of an incident plane wave. The polarization selection of the signals by (**c**) semitransparent and (**e**) reflecting gratings. (**f**) The effect of total conversion of plane waves packets

Fig. 1.5) arising in the diffraction by semitransparent structures, the total conversion of wave packets by open periodic resonators and others [1, 10, 40, 54]. We do not dwell here on general (let us say regular) behavior of diffraction characteristics described rather explicitly in [16, 18, 19].

Let k be a real positive frequency parameter, and let an arbitrary semitransparent (Fig. 1.1b) or reflecting (Fig. 1.1c) structure be excited by E- or H-polarized plane wave $\tilde{U}_0^i(g,k)$, $2\pi\Phi/kl = \sin\alpha_0^i$, $|\alpha_0^i| < \pi/2$. The complex amplitudes $R_{n0}^{\mathbf{AA}}$, $T_{n0}^{\mathbf{BA}}$ of the spatial harmonics composing the diffraction field in zones **A** and **B** [see problems (1.26)] are complicated functions of k and α_0^i, geometrical and constitutive parameters of the grating. The methods aimed at the numerical solution of problems (1.26) [11, 16, 17, 19, 21, 43] suggest us regular patterns and characteristic features of these amplitudes as applied to a diversity of classical grating geometries. They have revealed and thoroughly analyzed a series of effects of both theoretical and practical importance [10, 16, 18, 19, 40]. Specifically there have been revealed:

- domains where grating ghosts exert anomalously large influence on the diffraction characteristics;
- conditions for periodic structures to act as a perfect selective system, with total transition or total reflection of the primary wave, total nonspecular reflection and total conversion of waves and wave packets, radical decomposition of cross-polarized fields to be separated into different spatial radiation channels;
- structures as candidates for diffraction electronics and antenna technique, solving the problems of effective surface to space wave conversion and so on.

These have inspired in large measure renewed interest in gratings as simple and versatile instruments for controllable frequency, and for spatial and polarization selection of signals. Abundant information is available now about what phenomena go on in the periodic structures. However the question "Why is it so?" has not been answered often enough. In this context, the spectral theory [1, 10, 40] serves the purpose of improving the situation. Thus, it has been able to uniquely associate some resonant wave-scattering regimes with a capability of periodic structures to maintain free oscillations of the field. In some simple cases, an analytic description could be obtained of mechanisms providing the grating resonant response to the external excitation by monochromatic or wideband signals.

By way of illustration, we return to the total transition effect briefly described in Section 1.2.1. The phenomenon is characteristic of any semitransparent structure in the area of parameter values that corresponds to the vector $\{N,M\}$ with $N = M = 1$. In the domain $(k_1; -\Phi_{-1}) \times (0;H)$ $(\Phi_0 < k_1 < -\Phi_{-1} < k_2; 0 \le \Phi \le 0.5)$, the curves $\left|T_{00}^{\mathbf{BA}}(k,h)\right| = 1$ define the locus $\{k,h\}$ where a rectangular metal grating (see Fig. 1.4) transmits the incident E-polarized plane wave into zone **B** without any reflection. Figure 6.9 in [1] plots these curves together with the spectral curves $\mathrm{Re}\bar{k}_{1n}(h)$ for the first-family free H_{01n}-oscillations of the field in the structure. The higher the Q-factor of free oscillations, the closer the spectral lines overlap with the curves $\left|T_{00}^{\mathbf{BA}}(k,h)\right| = 1$. The Q-factor of the $H_{0\,11}$-oscillation for a small h does not suffice to change the indicated at some $h = h_1$ behavioral trends of the

corresponding curve $\left|T_{00}^{\mathbf{BA}}(k,h)\right| = 1$. This curve at $h < h_1$ is almost parallel to the k-axis, thus indicating a minimum grating height that still allows the total transition, which here cannot be called resonant anymore. In any other case, the total transition effect in the region {1,1} is due to those oscillations that are close (by one's own structure) to the eigenoscillations.

The correspondence between spectral and anomalous diffraction characteristics has been established, but the mechanism which creates this correspondence has not yet been understood. The modeling of such a mechanism is in general quite intricate. However, in the case considered, it will not be so [10]. The application of a single pole representation of the type (1.42) to a structure symmetric about the plane $z = -h/2$ gives [10]

$$2R_{00}^{\mathbf{AA}}(k) = \exp\left(i\arg\left(r_0 \mp t_0\right)\right) + \exp\left(i\left[\arg\left(r_0 \pm t_0\right) - 2\arg\left(k - \bar{k}\right)\right]\right),\ \mathrm{Im}k = 0,$$
$$\left|k - \bar{k}\right| \ll 1. \tag{1.48}$$

Here, the upper sign is chosen if pole $\bar{k}$ stands for a symmetric free oscillation, and the lower sign is for an asymmetric one. The grating becomes completely transparent, when the contributions to the radiation field in the zone **A** (into only one propagating harmonic of the spatial spectrum of the structure), caused by the reflection of an incident wave from the grating aperture in plane $z = 0$ and the radiation of the propagating wave of the coupling channel **G**, are equal in magnitude but opposite in sign. As follows from (1.48), a full compensation is possible if the dynamic phase effect holds in the small neighborhood of the eigenfrequency $\bar{k}$.

A large number of practically interesting modes of the plane wave scattering by gratings are due to open-resonator complex eigenfrequencies situated on the first physical sheet of the surface **K**. In the case below, the scattered field from the grating is uniquely determined by the analytic continuation features of the resolvents of the diffraction problems (1.26), lying on upper, nonphysical sheets of the surface **K** [10, 54]. Since they usually have complex eigenfrequencies, open periodic and waveguide resonators have specific sets of real eigenfrequencies directly associated with the effects of total conversion of waves and wave packets.

Assume that at certain parameter values, one eigenfrequency $\bar{k}$ of a periodic open resonator comes to the real axis in the region $\mathrm{Re}k > 0$ of one of the higher-order sheets of the surface **K**. Consider the partial components of the free oscillation

$$u_0\left(g,\bar{k}\right) = \sum_{n=-\infty}^{\infty} \left\{ \begin{array}{l} R_n \exp\left[i\left(\Phi_n y + \Gamma_n z\right)\right] \\ T_n \exp\left[i\left(\Phi_n y - \Gamma_n\left(z + h\right)\right)\right] \end{array} \right\}; \qquad \left\{ \begin{array}{l} z \geq 0 \\ z \leq -h \end{array} \right\} \tag{1.49}$$

corresponding to the spectral point $\bar{k}$ (of the nontrivial solution of homogeneous problem (1.26) at $k = \bar{k}$). According to Statements 1.4 and 1.5, some of these

n- numbered partial components such that $\bar{k} < |\Phi_n|$ are inhomogeneous plane waves that either attenuate exponentially ($\mathrm{Im}\Gamma_n\left(\bar{k}\right) > 0$) or increase exponentially ($\mathrm{Im}\Gamma_n\left(\bar{k}\right) < 0$) with growth of $|z|$. A set of partial components (1.49) complementary to this set with n such that $\bar{k} > |\Phi_n|$ combines homogeneous plane waves arriving at the grating (if $\mathrm{Re}\Gamma_n\left(\bar{k}\right) < 0$) or propagating away from it into the free space (if $\mathrm{Re}\Gamma_n\left(\bar{k}\right) > 0$).

The expression (1.49) suggests the two wave packets $u_{01}\left(g,\bar{k}\right)$ and $u_{02}\left(g,\bar{k}\right)$ that never meet at the set n=0,±1,... Thus,

$$u_{0j}\left(g,\bar{k}\right) = \sum_{n\in N_j} \left\{ \begin{array}{l} R_n \exp\left[i\left(\Phi_n y + \Gamma_n z\right)\right] \\ T_n \exp\left[i\left(\Phi_n y - \Gamma_n\left(z+h\right)\right)\right] \end{array} \right\}; \qquad \left\{ \begin{array}{l} z \geq 0 \\ z \leq -h \end{array} \right\}, j = 1,2. \tag{1.50}$$

Here, $N_1 + N_2 = \{n\}_{-\infty}^{\infty}$, $N_1 = \left\{n{:}\mathrm{Im}\Gamma_n\left(\bar{k}\right) < 0 \quad \text{or} \quad \mathrm{Re}\Gamma_n\left(\bar{k}\right) < 0\right\}$, $N_2 = \left\{n{:}\mathrm{Im}\Gamma_n\left(\bar{k}\right) > 0 \quad \text{or} \quad \mathrm{Re}\Gamma_n\left(\bar{k}\right) > 0\right\}$, i.e., $u_{01}\left(g,\bar{k}\right) + u_{02}\left(g,\bar{k}\right) = u_0\left(g,\bar{k}\right)$.

Now consider the existence of the free field oscillation of the grating at the eigenfrequency $\bar{k}$ in terms of the problem of plane wave diffraction by a 1-D periodic structure [see problems (1.26)]. The grating is excited by a plane wave packet $u_{01}\left(g,k\right)$ at frequency $k = \bar{k}$ (here k is the projection of $\bar{k}$ onto the first sheet of the surface **K**). From (1.50) it follows that the secondary (scattered) field coincides with the plane wave packet $u_{02}\left(g,k\right)$. Thus, the point $\bar{k} \in \Omega_k$ determines the frequency at which the grating transforms one plane wave packet into the other. These packets are composed of different harmonics of the spatial spectrum of the structure.

Hence, the total conversion problem can be reduced to the search for the real eigenfrequency $\bar{k}$ on nonphysical sheets of the Riemann surface **K**. The characteristics of the packets $u_{01}\left(g,\bar{k}\right)$ and $u_{02}\left(g,\bar{k}\right)$ suggest the following search area: the surface sheet and the real axis segment (between two adjacent branch points). The efficiency of the spectral approach to the problem of synthesis of a structure, which is able to totally convert the wave packets of several harmonics propagating in different directions, is provided by its ability to obtain comprehensive data about the scattering process. These are the total diffraction field (free oscillation field), amplitudes of wave packets components (amplitudes of the partial field components in the radiation zones **A** and **B**), the working frequency (the projection of the real frequency $\bar{k}$ onto the first sheet of the surface **K**), and the structure parameters to realize the desired mode.

Chapter 2
Analytic Regularization Methods

Abstract The chapter is devoted to analytic regularization method, which main advantage is the ability to reduce equivalently in the mathematical sense the ill-conditioned problems to the well-conditioned ones.

In spite of its almost half a century history, the method seems to be not very well known in the West scientific community. It has been developed in Kharkov scientific school due to constant concern and inspiration of V.P. Shestopalov. Here we outline the key issues of the method and focus our attention at most recent results.

2.1 General Description and Classification of the Analytic Regularization Methods: History, Provenance, and Survey

The growth in qualitative analysis of boundary value problems in mathematical physics is among most pronounced trends in today's mathematics. Various practical needs have spurred the development of numerical techniques for solving problems of this kind. Yet a vast gap exists between the practical engineering and the experimental physics on one side and the capabilities of today's numerical techniques on the other. In radio physics, the same situation is found.

Among other factors, purely psychological reasons stand behind this gap. After the solvability of the boundary value problem has been proved and other qualitative characteristics of the problem operator have been revealed, mathematicians are often just bored with the further numerical solution of the problem. The background of engineers is, as a rule, not in mathematics. And if they make themselves employ numerical methods for solving boundary value mathematical physical problems and even take up the invention of new methods, they are simply not aware of the genuinely mathematical nature of the encountered numerical difficulties, even though the diffraction problem to solve is seemingly elementary, and therefore cannot cope with them.

For the past decades, the situation has been changing for the better due to a series of brilliant works [55, 56] (see also the references used there) spelling out why the

Y.K. Sirenko, S. Ström (eds.), *Modern Theory of Gratings*, Springer Series in Optical Sciences 153, DOI 10.1007/978-1-4419-1200-8_2,

innocent use of the method of moments or others fail to give a physically valid solutions.

In today's radio-physical community, a practice has spread that a numerical technique is not evaluated by criteria of its intrinsic features but via comparisons of the computation results with a full-scale experiment, as if geometrical theorems were proved by geodesic surveys. It is thought that the things should be quite the reverse. And if the physical adequacy of the employed mathematical model is certain, it is the numerical simulation results that must serve a standard for experiment accuracy estimations. In actual practice, however, one can see that the numerical solution techniques are so insecure that the authors and users of the methods prefer the measured results to the theoretical predictions and take the former as being accurate.

Another popular way of numerical method verification relies upon a comparison of computing results with analogous data owing to another author's technique. But if the techniques have the same-nature intrinsic instability, their numerical results, close or not, will be wrong. In particular, it is safe to say that every technique (the method of moments and others) based on the direct discretization of an integral equation of the first kind produces false solutions. Equations of this nature arising in some diffraction problems will be exemplified below.

A technique that works well for solving boundary value problems in diffraction theory and yet is little known in the West is the analytic regularization method [10, 11, 16, 17, 21, 22, 45, 48, 57–68] which, as we strongly believe, has capacity to bridge the above-mentioned gap between the qualitative and the quantitative means of boundary value problem analysis in radio physics. In cases, first of all for two-dimensional and axially symmetric problems, this method can satisfactorily solve by far the majority of engineering problems today. The conversion of the initial boundary value problem to the second-kind equation in the space l_2 is a characteristic feature of the method guaranteeing computational stability with any desired accuracy of the solution.

To be more specific, address the integral equation of the form

$$[D+S]\,z=f;z=z(\theta);f=f(\theta);\theta\in[-\pi;\pi],$$

where

$$[Dz]\ (\theta)=\frac{1}{2\pi}\int\limits_{-\pi}^{\pi}\left[1-2\ln\left|2\sin\frac{\theta-\tau}{2}\right|\right]z(\tau)\ d\tau;\theta\in[-\pi;\pi],$$

$$[Sz]\ (\theta)=\frac{1}{2\pi}\int\limits_{-\pi}^{\pi}K(\theta,\tau)\,z(\tau)\,d\tau;\theta\in[-\pi;\pi].$$

Here, $z=z(\theta),\theta\in[-\pi;\pi]$ is the unknown function, the right-hand side $f=f(\theta)$, $\theta\in[-\pi;\pi]$ is given, and the $K(\theta,\tau)$, $\theta,\ \tau\in[-\pi;\pi]$, is the kernel. The

kernel $K(\theta,\tau)$ is assumed to be smoother than the function $\ln\left|2\sin\left((\theta-\tau)/2\right)\right|$, say, suppose that it is continuously differentiable with respect to θ and τ.

This equation models essential features of the integral equations appearing in simplest two-dimensional diffraction problems.

We start with the problem formulation for this equation in the space $\mathbf{L}_2[-\pi,\pi]$, assuming that $z,\ f \in \mathbf{L}_2[-\pi;\pi]$. Let the solution $z_0 = z_0(\theta)$ to this equation exist for the right-hand side $f_0(\theta)$ given. Consider the family of functions $e_N(\tau) = N^{1/2}\exp(iN\tau)$, $N = 1,2,3$. Obviously the functions $z_N = z_0 + e_N$ will be solutions to the equations

$$[D+S]\,z_N = f_N; \quad f_N = f_0 + \tilde{e}_N + e_N^S, \quad \tilde{e}_N = De_N, \quad e_N^S = Se_N.$$

In the $\mathbf{L}_2([-\pi;\pi]\times[-\pi;\pi])$, the kernel of the operator D can be written in the form of its Fourier series

$$1-2\ln\left|2\sin\frac{\theta-\tau}{2}\right| = \sum_{n=-\infty}^{\infty}\frac{e^{in(\theta-\tau)}}{\tau_n^2}; \qquad \theta,\tau\in[-\pi;\pi], \quad \tau_n = \max\left(1,|n|^{1/2}\right).$$

Therefore $\tilde{e}_N(\theta) = N^{-1/2}\exp(iN\theta)$. The continuous differentiability of the kernel $K(\theta,\tau)$ lends $e_N^S = O\left(N^{-1}\right)$. Thus, $\|f_N - f_0\| \to 0, N\to\infty$ but $\|z_N - z_0\| \to \infty, N\to\infty$.

So, even if there is an infinitely small error in the right-hand side, the solution of the considered integral equation can be affected to an infinitely large extent. And, similarly, an infinitesimal in the $\mathbf{L}_2$ metric error in the $K(\theta,\tau)$ kernel calculation can infinitely affect the solution $z = z(\theta)$. Notice that the described instability of the solution toward $f(\theta)$ and $K(\theta,\tau)$ is not related to a particular solution technique but to the nature of the equation itself.

From a functional analysis standpoint, the discussed instability is easily explained. That the kernel of the integral operator $D + S$ is square integrable and entails the operator $D + S$ being compact in $\mathbf{L}_2[-\pi,\pi]$. Hence the equation $[D + S]s = f$ is ill conditioned (ill posed or incorrect, according to A.N. Tikhonov).

The problem with the numerical solution of the considered equation consists in the following. Whatever the algorithm, the numerical solution of this integral equation is subject to rounding-off errors caused by a finite-length mantissa of the arithmetic processor. These errors can be considered random, and the equivalent disturbances δf and δK belong to $\mathbf{L}_2$, but we cannot think of them as smooth anymore. Hence, beginning with a certain size of the system, the errors of this sort can fully destroy the solution (as it was already seen), and they really do it, which is confirmed by numerical experiment.

The solution practice of the considered integral equation consists in putting it through one or another discretization scheme and reducing it to the linear algebraic equation of a finite size. The condition number of the system tends to infinity as the system size grows, and so does a level of the solution error, which is proportional to the condition number. Thus, beginning with some critical size of the system, the numerical solution not only does not improve as a number of the equations

increases but, on the contrary, the error grows fast, ending up with a full collapse. This suggests that there exists an optimum size of the algebraic system with the solution accuracy at its best (actually not very good). Unfortunately this critical size is usually unknown.

In the theory of incorrect problems [69], the correctness set of the operator A:$\mathbf{H}\to\mathbf{H}$ is the pair $\mathbf{H}_1$ $\mathbf{H}_2$ of sets or spaces on which the operator A:$\mathbf{H}_1\to\mathbf{H}_2$ is bounded and has a bounded inverse operator. As a rule, $\mathbf{H}_1$ and $\mathbf{H}_2$ are built, respectively, as an extension and a contraction of $\mathbf{H}$, with $\mathbf{H}_2 \subseteq \mathbf{H} \subseteq \mathbf{H}_1$. At the same time, a choice of $\mathbf{H}$ and, consequently, $\mathbf{H}_1$ and $\mathbf{H}_2$ is not unique and dictated by the problem's physical sense.

Consider a Sobolev space $\mathbf{H}^s[-\pi;\pi]$ as a space of (generalized) functions $\varphi(\theta)$, $\theta\in[-\pi;\pi]$, with the norm $\|\varphi\|_{\mathbf{H}^s} = \left\{ \sum\limits_{n=-\infty}^{\infty} \tau^{4s} (\varphi_n)^2 \right\}^{1/2}$, where $\{\varphi_n\}_{n=-\infty}^{\infty}$ are the Fourier coefficients of the function $\varphi(\theta)$. One easily sees that the operator D realizes the isometric isomorphism of the spaces $\mathbf{H}^s$ and $\mathbf{H}^{s+1}$ for any real s according to the rule

$$\psi = D\varphi; \quad \varphi(\theta) = \sum_{n=-\infty}^{\infty} \varphi_n e^{in\theta}, \quad \psi(\theta) = \sum_{n=-\infty}^{\infty} \tau_n^{-2} \varphi_n e^{in\theta}, \quad \|\psi\|_{\mathbf{H}^{s+1}} = \|\varphi\|_{\mathbf{H}^s}.$$

Hence the operator D:$\mathbf{H}^s\to\mathbf{H}^{s+1}$ has its bounded inverse D^{-1}:$\mathbf{H}^{s+1}\to\mathbf{H}^s$ and

$$\varphi = D^{-1}\psi; \ \psi(\theta) = \sum_{n=-\infty}^{\infty} \psi_n e^{in\theta}, \ \varphi(\theta) = \sum_{n=-\infty}^{\infty} \tau_n^2 \psi_n e^{in\theta}, \ \|\psi\|_{\mathbf{H}^{s+1}} = \|\varphi\|_{\mathbf{H}^s}.$$

Correspondingly, the pair $\mathbf{H}^s$, $\mathbf{H}^{s+1}$ is the correctness set of the operator D.

For diffraction problems, picking $s = -1/2$ is most natural. Hence, the problem of solving the integral equation is formulated as

$$[D + S]z = f; \quad z \in \mathbf{H}^{-1/2}[-\pi;\pi], \quad f \in \mathbf{H}^{1/2}[-\pi;\pi].$$

It should be mentioned that Sobolev's spaces are very convenient for the theoretical analysis of the problem. However, for practical computational purposes, the sets $\mathbf{H}_1 = \mathbf{H}^{-1/2}[-\pi;\pi] \cap \mathbf{C}^{0,\alpha}[-\pi;\pi]$ and $\mathbf{H}_2 = \mathbf{H}^{1/2}[-\pi;\pi] \cap \mathbf{C}^{1,\alpha}[-\pi;\pi]$ are far more suitable. Moreover, taking $\mathbf{H}_2$ in the form $\mathbf{H}^{1/2} \cap \mathbf{C}^{m,\alpha}$ with an arbitrary m=2,3,... and even $\mathbf{H}_2 = \mathbf{H}^{1/2} \cap \mathbf{C}^{\infty}$ is still better (here the standard notation $\mathbf{C}^{m,\alpha}$ is used to indicate the class of m-times continuously differentiable functions whose mth derivative satisfies the Hölder condition with index α, see [9]). The designation $\mathbf{H}^{1/2} \cap \mathbf{C}^{m,\alpha}$ means that the space $\mathbf{C}^{m,\alpha}$ is considered with the metric of the space $\mathbf{H}^{1/2}$ ($\mathbf{C}^{m,\alpha}$ is not complete in this metric). Two factors stand behind the choice $\mathbf{H}_2 = \mathbf{H}^{1/2} \cap \mathbf{C}^{\infty}$. First, the more is m, the more effective can be the algorithm of the integral equation solution. Second, in all practical diffraction problems, the function f is governed by the incident field, which, being a solution of Helmholtz or Maxwell's equations, is infinitely differentiable (and even real analytic) in the spatial variables.

From the indicated structure of the operator D it follows that the numerical solution of the considered integral equation cannot in principle be stable on only one of the $\mathbf{H}$ spaces. The immunity of the solution to input data errors requires a pair of the spaces (or linear manifolds) $\mathbf{H}_1$ and $\mathbf{H}_2$ forming the correctness set of the considered equation operator. Broadly speaking, the latter means that the linear manifold $\mathbf{H}_2$ consists of all the derivatives of the functions from $\mathbf{H}_1$, and the norms of $\mathbf{H}_1$ and $\mathbf{H}_2$ are matching each other as shown above.

Returning to our instability example, it should be noticed that e_N does not increase in the $\mathbf{H}_1$ metric and $\tilde{e}_N$ does not decrease in the $\mathbf{H}_2$ metric. To be specific, $\|e_N\|_{\mathbf{H}^{-1/2}} = \|\tilde{e}_N\|_{\mathbf{H}^{1/2}} \equiv 1$. As a consequence, the described instability example collapsed in the new problem formulation.

It is needless to say that the discussed change in the problem formulation leaves the actual process of the computation of the solution unaffected. Therefore the next step, which is the analytic regularization, has to transform the considered integral equation in such a way that the input data inserted into the computer be a stable system of equations of the second kind in the space l_2 of square-summable sequences. It is in the space l_2 where the system stability is important. As it was already seen and it will be shown still further, the theoretical stability in any other space or a pair of spaces other than the l_2 inevitably leads to the numerical instability.

Having finished with the stability analysis of the previous simplest integral equation, consider the situation from a more general point of view.

Lots of publications are devoted to the numerical solution of boundary value problems in the stationary diffraction theory. In great many of them, the approximate solution depends on the reduction of the initial boundary value problem to the finite linear algebraic system of the kind

$$A_N x^N = b^N$$

with the matrix operator A_N of size N. This system, directly or indirectly, is the truncation result of the corresponding infinite system of the first kind in the form

$$Ax = b$$

or, which is the same, is the result of the algebraization of some functional (for one, integral) equation of the first kind. To decide whether this finite-dimensional system solution is worth solving at all, it is reasonable to answer the following two questions:

- Does the solution x^N of this system tend to the solution x^∞ of the initial infinite system?
- Will (or not) the "numerical catastrophe" $\left\|x^N - \bar{x}^N\right\| \Big/ \left\|x^N\right\| > 1$ come with N growing, where $\bar{x}^N$ is the approximate solution of the $A_N x = b^N$ system computed of necessity of a finite mantissa which carries only a finite m_c number of binary digit?

Clearly the second question is reasonable to consider only if the first question is answered positively, implying that $x^N \to x^\infty$ in a relevant metric coordinated with the metric of the functional space where the initial boundary value problem solution is sought. In its turn, in view of the applied aspect of the study, this metric has to be coordinated with the physical nature of the phenomenon modeled by the boundary value problem.

It is known [70] that in the general case, the first question is answered negatively. Broadly speaking, in any metric, a solution $\bar{x}^N$ of the system of the first kind does not tend to x^∞ as N grows. For boundary value diffraction problems, this situation is typical (see [56]).

Nevertheless let us assume that by virtue of some specific properties of the operator A this convergence somehow takes place, and, what is more, it does so in a desired metric. The standard definition (see [70, 71]) of condition number ν_N of the operator A_N is

$$\nu_N = \|A_N\|_2 \times \left\|A_N^{-1}\right\|_2,$$

where the operator norm $\|...\|_2$ is produced by the Euclidean metric of vectors of some N-dimensional space. Systems of the first kind are characterized by that $\|A_N\|_2 \to \infty$ or $\left\|A_N^{-1}\right\|_2 \to \infty$ as $N \to \infty$. That is, the operator A or A^{-1} is unbounded in the operator norm produced by the vector norm of the space l_2. Correspondingly $\nu_N \to \infty$ as $N \to \infty$.

It has been verified [71] that a number of right binary digits in components of the solution $\bar{x}^N$ does not exceed the value

$$m_r = m_c - \log_2 \nu_N,$$

where m_r is the number of right digits of the maximum-module component of the vector $\bar{x}^N$. Correspondingly, a relative error of components smaller in module is far larger. And if these components decrease fast, only a few of the first of them can carry right significant digits, the rest cannot be computed at all.

Thus, if $m_r \leq 0$, the solution $\bar{x}^N$ has none of significant digits right. In this case, the discrepancy $\delta^N \equiv A_N \bar{x}^N - b^N$ will be $\left\|\delta^N\right\|_2 \approx N 2^{-m_c} \left\|\bar{x}^N\right\|_2$ in the order of the value, which is evidently quite small. The accurate solution x^N rounded to m_c binary digits shows the same-order discrepancy.

It must be emphasized that a unique practical way to recognize that a "numerical catastrophe" is coming is through a straightforward ν_N and m_r calculation. Various indirect criteria such as energy balance (as δ^N is small, the energy conservation law can be satisfied with a very high accuracy even with $m_r < 0$ and $\bar{x}^N$ having no significant digits right) or stabilization of solution $\bar{x}^N$ with N (after $m_r < 0$ is reached, the $\bar{x}^N$ solutions can be either indifferent to N changes or varying very slowly, in compliance with the arithmetic processor rounding procedures) can, as a rule, only give an illusion of solution correctness of the initial boundary value problem.

Notice that the selection of the norm $\|...\|_2$ in the ν_N definition is not random, and there exist certain arguments behind the A or A^{-1} unboundedness in just the space l_2 operator norm. Though, as known [70], all finite-dimensional space norms are equivalent, their equivalence constants depend on N. And in some valuable sense the computer acts as if it modeled a metric close to the Euclidean metric [71]. That is, in the limit $N\to\infty$, it simulates the metric of the l_2. That is why the existence and the boundedness of the operators A and A^{-1} on the relevant pairs of spaces, mathematical justifications of the $\bar{x}^N$ convergence to $\bar{x}^\infty$ in the metrics of these spaces and such like are of no concern to the actual computation process: the computer interprets the algebraic system as if it were given on the l_2, demonstrating every delight of the "numerical catastrophe" as $\nu_N\to\infty$.

It is known that the "numerical catastrophe" can be delayed to large N by a proper choice of the basis in the method of moments, calling on special quadratic formulas, enhancing the arithmetic accuracy and such like. Yet these impediments cannot cancel characteristic features of equations of the first kind. Sooner or later the "numerical catastrophe" comes, excluding any possibility to solve the initial boundary value problem with an accuracy desired and cutting down possible intervals of variation of problem parameters.

It is a lack of understanding of the indicated difficulties and, first of all, the ignorance of the arithmetic routine of a particular machine (including such a bore as its specific rounding-off scheme), underestimating the difficulties preventing a stable numerical realization of many theoretically correct – in precision arithmetic – computational algorithms that seem to accompany a great body of publications inventing more and more methods intended for the numerical solution of boundary value problems in diffraction theory. And frequently the authors do not even mention the condition numbers of the algebraic schemes they use.

Let us turn to an alternative situation. Suppose that the original boundary value problem is equivalently reduced to the infinite system of algebraic equations of the form $Ax = b$; $x, b\in l_2$. The operator A takes the form $A=E + H$, where operator H is compact on the l_2 and E is the identity operator. A reasonably formulated boundary value problem has, as a rule, a unique solution, whence, by virtue of the indicated equivalence, it follows that the operator $A^{-1} = (E + H)^{-1}$ bounded on the l_2 space exists with a correct determination of the value

$$\nu_\infty = \|E + H\|_2 \times \left\|(E + H)^{-1}\right\|_2 < \infty.$$

As in the procedure above, consider the truncated systems

$$(E + H_N)\, x^N = b^N,$$

and in view of the compactness of H, the sequence of the finite-dimensional operators H_N can be chosen as

$$\|H - H_N\|_2 \to 0; \qquad N \to \infty.$$

It readily follows that the condition numbers ν_N tend to ν_∞: $\nu_N = \|E + H_N\|_2 \times \left\|(E + H_N)^{-1}\right\|_2 \to \nu_\infty$ as $N \to \infty$, and, hence, ν_N are uniformly bounded for any N large enough. In all practical situations of our knowledge that arise in the solution of a wide class of diffraction problems, the value ν_N varies within several tens or at most hundreds of units. Hence $\nu_N \ll 2^{m_c}$ for most modern computers.

So, compared to equations of the first kind, the second-kind equations have none of the indicated principal disadvantages preventing their effective solution. In particular, $x^N \to x^\infty$ and $\left\|\tilde{x}^N - x^N\right\| / \left\|x^N\right\| \to \nu_\infty 2^{-m_c+1}$ as $N \to \infty$ (see [70, 71]). The value $\nu_\infty 2^{-m_c+1}$ is so small that practically any accuracy can be achieved when N is large enough. The iterative refinement procedure [70] allows $\left\|\tilde{x}^N - x^N\right\|_2 / \left\|x^N\right\|_2 \approx 2^{-m_c}$ for any $\nu_\infty < 2^{m_c}$.

Thus, the equivalent conversion of the boundary value problem to an equation of the second kind in the l_2 can guarantee effective solution algorithms for this problem.

The techniques reducing the original boundary value problem to second-kind equations are built around the regularization of the problem operator. In functional analysis terms, this idea is well known and simple enough [72]. Let the linear operator $A:\mathbf{M}_1 \to \mathbf{M}_2$ be defined on a pair of functional (say, Banach) spaces $\mathbf{M}_1$ and $\mathbf{M}_2$. Additionally on some known space $\mathbf{M}$, the pair $L:\mathbf{M}_2 \to \mathbf{M}$ and $R:\mathbf{M} \to \mathbf{M}_1$ of bounded linear operators is given such that the inverse bounded operators L^{-1} and R^{-1} exist. It is evident that $LAR:\mathbf{M} \to \mathbf{M}$. If the relationship $LAR = E + H$ holds, with the operator H compact on $\mathbf{M}$, the pair L, R is referred to as a two-sided regularizer of the operator A.

This definition can be evidently extended to the case when the operators L, A, and R are only given on dense sets of the corresponding spaces. Then by $LAR = E + H$ is meant an operator obtained by the closure of the initial LAR.

When $\mathbf{M} = \mathbf{M}_1$ and $R = E$, the operator L is called a left-sided regularizer, and when $\mathbf{M} = \mathbf{M}_2$ and $L = E$, the operator R is a right-sided regularizer.

Take up the functional equation of the first kind $Ax = b$; $x \in \mathbf{M}_1$, $b \in \mathbf{M}_2$. Since the operator R^{-1} is bounded, any element $x \in \mathbf{M}_1$ is available in the form $x = Ry$ for some $y = R^{-1}x \in \mathbf{M}$. The usage of this representation yields $ARy = b$. Acting by the operator L on the left-hand side of this equation gives $LARy = Lb$. And in so far as the pair L, R is a two-sided regularizer of the operator A, we come up with the equation

$$(E + H)\, y = Lb; \qquad y, Lb \in \mathbf{M}$$

in the new unknown, y. With y constructed, the former unknown is expressed in the form $x = Ry$.

By the regularizer definition given right above, the equations $Ax = b$ and $(E + H)y = Lb$ are equivalent in the sense of the one-to-one correspondence existing between their solutions due to the operator R. At the same time, the second of these two is a second-kind equation.

Furthermore, let $\mathbf{M}$ be a Hilbert space. Having chosen a suitable basis there, we can match the Fourier coefficients in the left- and right-hand sides of the equation $(E + H)y = Lb$. By virtue of the well-known isomorphism of all Hilbert spaces, the

obtained equation is a second-kind equation belonging to the space l_2 and taking the form $\left(E+\tilde{H}\right)\tilde{y}=\tilde{b}$, where $\tilde{y},\ \tilde{b}\in l_2$ and $\tilde{H}\colon\ l_2\to l_2$ is a compact operator with necessity.

Thus, the analytic regularization method can be understood as a set of analytic transfoms coming up with a two-sided closed-form regularizer L, R in order for the first-kind equation $Ax=b$ to be analytically transformed to the equivalent second-kind equation $\left(E+\tilde{H}\right)\tilde{y}=\tilde{b};\tilde{y},\ \tilde{b}\in l_2$ with the operator $\tilde{H}$ compact in l_2. Of course, this is only an abstract sketch of the analytic regularization method. It does not answer the question how the procedure should be built for one or other boundary value diffraction problem, including specifications of functional spaces where the operator A should be defined (the boundary value problem formulation) in correspondence with a particular physical problem under modeling. The construction of the operators L and R in closed form is not in a priori evidence all the more. Therefore, any extension of the analytic regularization method to a further class of problems is an intellectual challenge.

Notwithstanding all gained experience, we cannot offer a readymade recipe but information about building blocks composing the analytic regularization method. They are:

- reduction of the initial boundary value problem to the integral or integral differential equation based on a more or less standard technology of Green's functions;
- singularity analysis of the obtained equation kernel, derivation of the so-called singular expansion as a finite sum of the leading singularities of the kernel;
- extraction of the leading singularities from the kernel until the rest becomes sufficiently smooth (the additive decomposition of the integral equation operator);
- conversion of the integral equation to the canonical form whose regularization algorithm is available or is known how to build;
- construction of a proper family of two-sided regularizers and selection of the best one out of them by criteria of computational efficiency.

In so far as the book is mainly concerned with the theory of periodic structures, we have little possibility to enlarge on these principal points of the method providing a successful solution of a great variety of problems. Yet in Section 2.6, we fill in many details about periodic structures. Now let us return to the elementary integral equation whose analysis has already been started.

So, we understand the analytic regularization method as a philosophy of numerical modeling as applied to sophisticated problems in diffraction theory rather than a set of theoretical formulas and technical expedients, even though we stock a whole arsenal of mathematical tools and computational algorithms. It is due to this philosophy that high-efficiency numerical models have been built, coming up with a wide diversity of diffraction problems solvable today. This philosophy directs our efforts to attack increasingly more difficult problems in diffraction theory.

For the reader's convenience, we will continue with the elementary equation taken up earlier, planning to construct one (simplest) of possible families of two-sided regularizers and discuss how the most suitable regularizer of this family should be chosen.

The Fourier series of the operator D kernel (the function $1-2\ln|2\sin(\theta-\tau)/2|$) was previously given. The Fourier series of the functions $K(\theta,\tau)$, $z(\tau)$, and $f(\theta)$ are

$$K(\theta,\tau)=\sum_{s=-\infty}^{\infty}\sum_{n=-\infty}^{\infty}K_{sn}e^{i(s\theta+n\tau)},\ z(\tau)=\sum_{n=-\infty}^{\infty}z_n e^{in\tau},$$

$$f(\theta)\quad=\sum_{n=-\infty}^{\infty}f_n e^{in\theta};\ \theta,\ \tau\in[-\pi;\pi].$$

Substitute the functions involved in the equation $[D+S]z=f$ by their Fourier series, interchange the orders of summation and integration and integrate them term by term on account of the orthogonality property of trigonometric functions (all the operations are legitimate for corresponding classes of functions). Matching the obtained coefficients in the left- and right-hand sides yields the algebraic system

$$\frac{z_s}{\tau_s^2}+\sum_{n=-\infty}^{\infty}K_{s,-n}z_n=f_s;\qquad s=0,\ \pm1,\ \pm2,\ ...$$

in the unknowns $\{z_n\}_{n=-\infty}^{\infty}$. The obtained infinite algebraic system is evidently a first-kind equation since the diagonal matrix $\left\{\delta_s^n\tau_s^{-2}\right\}_{s,n=-\infty}^{\infty}$ (δ_s^n being the Kronecker symbol) produces an operator compact in l_2. The same is clearly true for the matrix operator $\tilde{K}=\left\{K_{s,-n}\right\}_{s,n=-\infty}^{\infty}$.

For the considered equation, the following regularizer scheme seems evident. First, introduce the new unknowns $z_n^{\gamma}=\tau_n^{-\gamma}z_n$, where γ is some parameter to determine. Second, multiply each of the obtained equations of the number $s=0,\pm1,\pm2...$ by the factor $\tau_s^{2-\gamma}$. Finally,

$$z_s^{\gamma}+\sum_{n=-\infty}^{\infty}\left(\tau_s^{2-\gamma}\tau_n^{\gamma}K_{s,-n}\right)z_n=\tau_s^{2-\gamma}f_s;\qquad s=0,\ \pm1,\ \pm2,\ ...$$

The obtained system appears to be $(I+K_{\gamma})z^{\gamma}=f^{\gamma}$, where $z^{\gamma}=\left\{z_n^{\gamma}\right\}_{n=-\infty}^{\infty}$, $f^{\gamma}=\left\{\tau_n^{2-\gamma}f_n\right\}_{n=-\infty}^{\infty}$, and $K_{\gamma}=T^{2-\gamma}\tilde{K}T^{\gamma}$, with T being a diagonal matrix operator of the form $T=\left\{\tau_n\delta_s^n\right\}_{s,n=-\infty}^{\infty}$. Is this system a second-kind equation in l_2? Or, which is the same, is the operator K_{γ} compact in l_2? One easily verifies that the compactness of the operator K_{γ} depends, first, on how fast the coefficients $K_{s,n}$ decrease as $s,n\to\pm\infty$, which, in turn, depends on the smoothness of the kernel

$K(\theta,\tau)$ as a function that is 2π-periodic in both arguments. Second, one should properly choose a parameter γ according to the decrease character of the coefficients $K_{s,n}$ as $s,n\to\pm\infty$.

It is easy to see that the factor $\tau_s^{2-\gamma}\tau_n^{\gamma}$ degrades the decrease of the $K_{s,-n}$ coefficients for any γ. Therefore, it may happen that the operator K_γ is not compact whatever γ we use. This means that the logarithmic singularity removal from the kernel of the operator $D + S$ is inadequate to remedy this. And we have to derive such a leading singularity $K_0(\theta,\tau)$ from the function $K(\theta,\tau)$ that, first, the remainder $K(\theta,\tau)$–$K_0(\theta,\tau)$ will be sufficiently smooth and, second, the kernel $1 - 2\ln\left|2\sin\frac{\theta-\tau}{2}\right| + K_0(\theta,\tau)$ will have a sufficiently simple matrix (diagonal one is the best) of the Fourier coefficients. This expedient is employed for solving the diffraction problem of a corrugated surface in Section 2.6.

Now assume that the kernel $K(\theta,\tau)$ is so smooth as to have $\gamma = \gamma_0$ for which the operator K_γ is compact. Then it can be proved that there is a vicinity $(\gamma_1;\gamma_2)$ that contains γ_0 and provides compactness of the operator K_γ for any $\gamma\in(\gamma_1;\gamma_2)$. Thus, we get a family of regularizers rather than a single one and one of them is providing the fastest convergence of the reduction procedure for the relevant algebraic system.

Let us consider some examples. Let $K(\theta,\tau)$ be a continuous 2π-periodic function of its variables. If there is no more information about it, we cannot say that operator K_γ will be compact in l_2. Accept an extra assumption that the function $K(\theta,\tau)$ is continuously differentiable with respect to τ for any θ. Then the operator compactness will be provided by the choice $\gamma = 2$. In this case, $z_n^{\gamma} = \tau_n^{-2}z_n$. Analogously, if the function $K(\theta,\tau)$ is continuously differentiable with respect to θ (and is not differentiable with respect to τ), the operator K_γ is compact under the choice $\gamma = 0$, with $z_n^{\gamma} = z_n$. Finally, if $K(\theta,\tau)$ is continuously differentiable with respect to θ and τ, then any $\gamma\in[0;2]$ will be good enough to provide the operator K_γ compactness. To choose the best γ out of them, the differential properties of the $K(\theta,\tau)$ function should be studied in greater depth. For most (but not all) diffraction problems reduced to the equation of the concerned type, $\gamma = 1$ is an optimum choice.

At this stage of our explanation, the reader may feel disappointed about the simplicity of the analytic regularization scheme we have constructed (much ado about nothing). If so, we have to remind that, first, a most elementary integral equation was treated, coming up with a simplest-structure regularizer. Second, the disappointment, if any, should become amazement because we have so easily gained in such a vital characteristic as computational algorithm stability.

Concerning the evolution of the analytic regularization idea as applied to boundary value problems in diffraction theory (in particular, electrodynamical theory of gratings) and the relevant techniques for building regularizing operators, the following points are worth noting. The earliest boundary value problems solved substantially in terms of the above-described regularization idea were 2-D coordinate problems of wave diffraction by infinitely thin, perfectly conducting nonclosed screens (see [73–75] and the references used there), where the so-called semi-inversion method used to be employed. This method is a variant of the left-hand-sided regularization discussed here. Here, by coordinate problems we mean

boundary value problems proceeding from the Helmholtz equation and characterized by the fact that the boundary surface (or the contour), where the boundary conditions are applied, coincide with a part of the coordinate surface of one of the such special coordinate systems that the variables of the Helmholtz (or Maxwell's) equation can be separated.

By the partial domain (or sewing, or mode matching) method the coordinate problems are naturally reduced to the functional equations of the kind $Ax = b$, where the operator A depends on the excitation wave frequency and, of course, on other parameters, including the problem geometrical properties. The key point of the semi-inversion method is finding such an operator A_0 that, first, the bounded operator A_0^{-1} exists in a suitable functional space and, second, $A_0^{-1}A = E + H$, where H is a compact operator and E is the identity operator. For grating diffraction problems, one of the most common ways of building the operators A_0 and A_0^{-1} consists in the development of the operator part established by a single element of the grating to be extracted then from the operator A. When the considered diffraction problem for a single element can be solved in explicit form (for an arbitrary excitation field) or reduced to the equation of the second kind, one always arrives at the regularized equation $x + Hx = b$. It is easily understood that the resulting operator equation of the second kind is most suitable when periodic grating components are sufficiently spaced apart [16, 76–78].

One more variant of the semi-inversion method was originally suggested in [79] to solve diffraction problems of plane strip gratings. The key point is the development of the operator A_0 corresponding, conventionally speaking, to the electrostatic problem. In terms of the Riemann–Hilbert problem in theory of analytic functions [80] or using the integral transform method like the fractional integration (differentiation) technique [81], it was succeeded to explicitly construct the operator A_0^{-1} as a left-hand regularizer of the functional equations in the sewing method (some generalizations of this approach are discussed in Sections 2.2, 2.4, and 2.5). In this way, a wide class of diffraction problems for multielement and multilayer gratings, variously arrayed circular cylindrical screens, spherical segments, etc., has been examined (see [16, 18, 45, 74, 82] and references therein). In [22], the semi-inversion method was designed upon the development of the operator A_0 corresponding to the limiting value of one of the parameters of the initial diffraction problem. Thus, for instance, in the case of wave diffraction by jalousie-type gratings, the operator corresponding to the grating of semi-infinite planes was extracted from the sewing method operator. This operator inversion (A_0^{-1}) was due to the Wiener–Hopf method. In general, this variant of the semi-inversion method is based on the inversion of matrix convolution-type equations [17]. The employed mathematical technology is based on Mittag–Leffler's theorem about a meromorphic function representation (some aspects of the approach are given in Section 2.3). The results of this semi-inversion method variant are surveyed in [16–18].

An original variant of the semi-inversion method is suggested in references [83–85], where the wave diffraction is solved for a finite number of strip screens located in the same plane. The method develops from an explicit solution of the

Riemann–Hilbert problem for a finite number of real-axis segments [80], coming up with a single integral Fredholm equation of the second kind (for an arbitrary number of strip screens) with a smooth kernel of quite a simple appearance.

It seems that the most valuable methodological result concerning the semi-inversion method is that the so constructed regularization algorithms covering a wide diversity of model problems are unique in their speed, accuracy, efficiency, and reliability. With no additional expedients, these algorithms are capable of studying physical properties of different types of gratings from the long-wavelength and resonance regions to the really short-wave end of spectrum when the grating period measures several tens of the wavelengths.

It is these capabilities of the semi-inversion method that encouraged a lot of effort going into the further enhancement of the analytic regularization method. At the time when most algorithms for solving coordinate problems had been designed or so, the reasons providing their success were not clear enough. And soon it was discovered that the class of coordinate problems solved in this technology terms was coming to an end. In any event, the difficulties of further progress were enormous. It used to seem that a high computational efficiency of the developed algorithms had much to do with their specialization: each variant of the semi-inversion method used to be tailored for analyzing objects of essentially similar geometry. And, for instance, the solution of the electrostatic part $x_0 = A_0^{-1} b$ owing to the operator A_0^{-1} used to consider a specific character of a particular boundary value problem so comprehensively that the computation of the dynamical addition to the exact solution used to be a simple and effectively solved problem. Hence, the abandonment of narrow specialization had to lead to a severe decrease in efficiency.

With the things commonly adopted at that time, one could hardly expect a principal possibility for equally efficient and, at the same time, rather universal solution techniques for boundary value diffraction problems. Certain intellectual effort has been spared to overcoming this stereotype of thinking, recognition, and analysis of the key reasons providing a high quality of algorithms for coordinate diffraction problems, to elaboration of more general methods considering these reasons. Eventually far more general regularization procedures have come into being for quite an extensive class of boundary value diffraction problems. And the algorithms based on these principles are highly competitive in their computational efficiency with those commonly used for solving coordinate problems.

To this end, the regularization scenario suitable for coordinate problems had to be essentially modified [11]. First of all, it was no more possible to use the sewing (partial domain) method and enjoy the former simplicity of the algorithms as applied to arbitrarily shaped contours associated with the boundary conditions. It was found that the best alternative is the method of boundary integral equations based on familiar Green's functions (see, e.g., [86]). And in this case, both for closed and especially unclosed contours, the original boundary value problem should be reduced to integral equations of the first kind (see Section 2.6) rather than seemingly more convenient equations of the second kind. The next, and maybe the most important, is the idea of closing of the unclosed contour by imbedding it in some smooth closed configuration. This closure largely predetermines a principal

feasibility of a high computational efficiency of the developed algorithms (see [11]). The parametrization of the closed contour and analysis of the kernels of the constructed integral operators for the singular structure (differential properties) allow, via a relevant Fourier transform, reducing these integral equations to special-form dual series equations (some of them are examined in Section 2.2). The regularization of these dual series equations eventually gives the operator equations of the second kind.

A mention should be made that against the coordinate diffraction problems, we generally have to build the two-sided regularizer L and R whose analytic (closed form) derivation is closely related to the structure of kernel singularities of the above-mentioned integral operators and, also, to some properties of the closed contour parametrization. The computational efficiency of the outlined algorithmic scheme largely depends on the realization of the contour-closure procedure, choice of optimum (in a way) parametrization of the closed contour, method of computation of Fourier coefficients of integral operator kernels, summation procedures of slowly converging series for limiting values of the fields and their normal derivatives (i.e., for currents), etc. The mentioned range of ideas was originally applied in [63, 64] to the 2-D diffraction problem of infinitely thin perfectly conducting cylindrical screens. A detailed description of this approach to diffraction theory problems is the subject matter of book [11].

This brief schematic description of the analytic regularization method shows that the development of relevant computational algorithms and their computer realization are not a trivial activity. Therefore, the basic mathematical expedients and approaches will be considered in Sections 2.2, 2.3, 2.4, 2.5 and 2.6.

2.2 The Riemann–Hilbert Problem Method and Its Generalization

This subsection essentially portrays an approach (added on in subsequent sections) to solve boundary value problems of single-periodic gratings and different media interfaces (anisotropic dielectrics, chiral composites, metamaterials, etc.) in wave diffraction and propagation theory. In it, certain generalizations (modifications) are presented in regard to the classical variant of the Riemann–Hilbert problem method [45, 74] to deal with a wide class of dual series equations involving the functions $\exp(in\vartheta)$, $n = 0, \pm 1, \ldots$. It is these dual series equations that appear, e.g., in the electromagnetic wave diffraction by strip gratings located on an anisotropic dielectric interface (see Sections 2.4 and 2.5).

By means of regularization procedures specially designed for the case, all dual series equations considered in this section are equivalently reduced on a relevant l_2 space of quadratically summable sequences to the infinite system of linear algebraic equations of the form $x + Hx = b$, $x, b \in l_2$, with the operator H being compact on l_2. These systems are known to be effectively solved by various numerical methods.

Some of the results in this section (in a little different appearance), their modifications and relationships with corresponding boundary value problems in diffraction theory can be found in [75, 87–92].

2.2.1 Classical Dual Series Equations and the Riemann–Hilbert Problem

In this subsection, according to the major ideas of the references [45, 79], a study is conducted for one type of dual series equations, the simplest ones arising in modeling 2-D coordinate problems of the wave diffraction by systems of nonclosed infinitesimally thin screens, such as, in particular, single-periodic strip gratings [74]. From this point on, by a coordinate diffraction problem is meant a boundary value problem such that the structure interface coincides with a coordinate surface part referring to an orthogonal coordinate system enabling the separation of variables for the Helmholtz (Maxwell's) equation. The separation of variables (partial domain, or sewing method) reduces the coordinate problems to the dual series equations of the form

$$\sum_{n=-\infty}^{\infty} \gamma_n x_n \mathrm{e}^{in\vartheta} = F\left(\mathrm{e}^{i\vartheta}\right);\ |\vartheta| < \vartheta_0, \tag{2.1}$$

$$\sum_{n=-\infty}^{\infty} x_n \mathrm{e}^{in\vartheta} = G\left(\mathrm{e}^{i\vartheta}\right);\ |\vartheta| > \vartheta_0. \tag{2.2}$$

for the unknowns $x = \{x_n\}_{n=-\infty}^{\infty}$. Here, $F(\exp(i\vartheta))$ and $G(\exp(i\vartheta))$ are given functions, $\vartheta \in [-\pi;\pi]$, $\{\gamma_n\}_{n=-\infty}^{\infty}$ is a given sequence of complex numbers, and $\vartheta_0 \in [0;\pi]$ is a parameter.

Assume that the following conditions are satisfied:

- as $|n| \to \infty$, the values γ_n take on the form

$$\gamma_n = |n|\,(1 - \delta_n), \tag{2.3}$$

  where $\delta_n = O\left(n^{-2}\right)$;
- the given right-hand sides $F(\exp(i\vartheta))$ and $G(\exp(i\vartheta))$ are expanded into the Fourier series

$$F\left(\mathrm{e}^{i\vartheta}\right) = \sum_{n=-\infty}^{\infty} f_n \mathrm{e}^{in\vartheta}, \qquad G\left(\mathrm{e}^{i\vartheta}\right) = \sum_{n=-\infty}^{\infty} g_n \mathrm{e}^{in\vartheta}; \tag{2.4}$$

- all the series in (2.1) and (2.2) are the Fourier series of their sums: the series in (2.2) and (2.1) are Fourier series of the functions belonging, respectively, to the $\mathbf{L}_2[-\pi;\pi]$ and $\mathbf{L}_1[-\pi;\pi]$ spaces. The space $\mathbf{L}_p[-\pi;\pi]$, $p = 1,2$, is defined, e.g., in [70] (see also Appendix).

A solution of equations (2.1) and (2.2) will be sought in the infinite-sequence space $l_2(1)$, assuming that the Fourier coefficients of the functions $F(\exp(i\vartheta))$ and $G(\exp(i\vartheta))$ belong to the spaces $l_2(1)$ and $l_2(3)$, respectively. From here on, the infinite-sequence space $l_2(\eta)$ is defined as

$$l_2(\eta) = \left\{ \{x_n\}_{n=-\infty}^{\infty} : \sum_{n=-\infty}^{\infty} |x_n|^2 (1+|n|)^{\eta} < \infty \right\}. \tag{2.5}$$

The infinite series in the left-hand sides of (2.1) and (2.2) converge slowly (below one can see that $x_n = O\left(|n|^{-3/2}\right)$ as $|n| \to \infty$), making the dual series equations of little use for the direct analytic or numerical search of $x = \{x_n\}_{n=-\infty}^{\infty}$.

Let us show that the previous assumptions enable one to equivalently reduce these equations to an infinite system of linear algebraic equations of the second kind in the space $l_2 = l_2(0)$ (one easily finds that $l_2(1) \subset l_2$).

Introduce the new unknowns $y = \{y_n\}_{n=-\infty}^{\infty}$ by the formula

$$y_n = x_n - g_n;\ n = 0,\ \pm 1, \ldots. \tag{2.6}$$

Then equations (2.1) and (2.2) will take the appearance

$$\sum_{n=-\infty}^{\infty} |n|\, y_n e^{in\vartheta} = \sum_{n=-\infty}^{\infty} \psi_n e^{in\vartheta};\ |\vartheta| < \vartheta_0, \tag{2.7}$$

$$\sum_{n=-\infty}^{\infty} y_n e^{in\vartheta} = 0;\ |\vartheta| > \vartheta_0, \tag{2.8}$$

where

$$\psi_n = \begin{cases} f_0 - \gamma_0 (y_0 + g_0); & n = 0 \\ f_n + |n|\, \delta_n y_n + |n| (\delta_n - 1) g_n; & n \neq 0 \end{cases}. \tag{2.9}$$

Assume for a while that the function $\psi(\exp(i\vartheta)) = \sum_{n=-\infty}^{\infty} \psi_n \exp(in\vartheta)$ is available and construct a solution to equations (2.7) and (2.8) in explicit form (express y_n via ψ_n).

Differentiating equation (2.8) and taking $z_n = n y_n$ gives

$$\sum_{n \neq 0} z_n e^{in\vartheta} = 0;\ |\vartheta| > \vartheta_0, \tag{2.10}$$

$$\sum_{n \neq 0} z_n \frac{|n|}{n} e^{in\vartheta} = \psi\left(e^{i\vartheta}\right);\ |\vartheta| < \vartheta_0. \tag{2.11}$$

Equations (2.10) and (2.11) will be equivalent to equations (2.7) and (2.8) on the addition of the equality

$$\sum_{n\neq 0} \frac{(-1)^n z_n}{n} = -y_0, \tag{2.12}$$

coming from (2.8) at $\vartheta = \pi$.

Now let us show that the dual series equations (2.10) and (2.11) represent the well-known Riemann–Hilbert problem in the theory of analytic functions [79]. Indeed, according to [80], define the functions

$$X^+(z) = \sum_{n=1}^{\infty} z_n z^n, \quad X^-(z) = -\sum_{n=-\infty}^{-1} z_n z^n, \tag{2.13}$$

analytic, respectively, on inside and outside the circle $|z| \leq 1$.

From (2.10),

$$X^+\left(e^{i\vartheta}\right) - X^-\left(e^{i\vartheta}\right) = 0 \tag{2.14}$$

on the arc $\mathbf{P}_1$ of the unit circle connecting the points $\exp(-i\vartheta_0)$ and $\exp(i\vartheta_0)$ through the point $z = -1$. Hence, the function

$$X(z) = \begin{cases} X^+(z); & |z| < 1 \\ X^-(z); & |z| > 1 \end{cases} \tag{2.15}$$

is analytic in the complex plane with a cut along the arc $\mathbf{P}_2$ complementary to the arc $\mathbf{P}_1$. In view of (2.7), on the complementary arc $\mathbf{P}_2$,

$$X^+\left(e^{i\vartheta}\right) + X^-\left(e^{i\vartheta}\right) = \psi\left(e^{i\vartheta}\right); |\vartheta| < \vartheta_0, \tag{2.16}$$

where $X^+(\exp(i\vartheta))$ and $X^-(\exp(i\vartheta))$ are the function $X(z)$ limiting values, respectively, inside and outside the circle $|z| \leq 1$. Hence, equations (2.10) and (2.11) have been reduced to the problem of the function of the $X(z)$ determination by the sum of its limiting values on the arc $\mathbf{P}_2$. This is the Riemann–Hilbert problem whose simple solution was developed by T. Carleman [93].

The solution to this problem will be sought in the class of functions that have an integrable singularity at the points $z_0^{\pm} = \exp(\pm i\vartheta_0)$ and decrease as $|z| \to \infty$. The sought function $X(z)$ and the function $R(z) = \sqrt{\left(z - z_0^+\right)\left(z - z_0^-\right)}$ are analytic and unique in the complex plane cut along the arc $\mathbf{P}_2$. For $R(z)$, a root branch is chosen such that $R(0) = 1$. From (2.13), $X(z) = X^-(z) = z^{-1}(-z_{-1} + O(1))$ as $|z| \to \infty$. Therefore, the function $X(z)R(z)$ is bounded as $|z| \to \infty$, and upon the Cauchy theorem [94], we have

$$X(z)R(z) = \frac{1}{2\pi i} \oint_{\Gamma} \frac{X(\tau)R(\tau)}{\tau - z} d\tau + C. \tag{2.17}$$

Here, $\mathbf{\Gamma}$ is a sufficiently smooth closed contour to enclose the cut along the arc $\mathbf{P}_2$ and C is some constant proportional to the residue of the function $X(z)R(z)$ at an infinitely distant point $z = \infty$.

Refer to (2.17) and contract the contour $\mathbf{\Gamma}$ toward the arc $\mathbf{P}_2$. Considering (2.16), we obtain

$$X(z)R(z) = \frac{1}{2\pi i}\int\limits_{\mathbf{P}_2} \frac{\psi(\tau)R^+(\tau)}{\tau - z}d\tau + C, \tag{2.18}$$

where $R^+(\tau)$ is the $R(z)$ limiting value on the arc $\mathbf{P}_2$ as $z \to \tau$ from inside of the unit circle.

Formula (2.18) is a solution to the Riemann–Hilbert problem (2.16), and this formula is sufficient to solve equations (2.7) and (2.8). Applying the Sokhotskyi-Plemelj formulas [94] for limiting values of functions represented by the Cauchy-type integrals, from (2.18) it follows that

$$\sum_{n\neq 0} z_n e^{in\vartheta} = K\left(e^{i\vartheta}\right)\left[\frac{1}{\pi i}\int\limits_{\mathbf{P}_2}\frac{\psi(\tau)}{K(\tau)\left(\tau - e^{i\vartheta}\right)}d\tau + 2C\right]. \tag{2.19}$$

on the unit circle $|z| = 1$. Here the integral is understood as the Cauchy principal value, and

$$K\left(e^{i\vartheta}\right) = \begin{cases} \frac{1}{R^+\left(e^{i\vartheta}\right)}; & |\vartheta| < \vartheta_0 \\ 0; & |\vartheta| > \vartheta_0 \end{cases}. \tag{2.20}$$

Passing to the Fourier coefficients in (2.19) and removing the C constant in view of (2.12), one arrives at

$$y_0 = W_0\psi_0 + \sum_{n\neq 0}\psi_n\frac{V_{n-1}^{-1}}{n}, \tag{2.21}$$

$$y_m = \sum_{n=-\infty}^{+\infty}\psi_n\frac{V_{m-1}^{n-1}}{m} \tag{2.22}$$

with the notations [45, 74]

$$V_n(e^{i\vartheta}) = \frac{1}{\pi i}\int\limits_{\mathbf{P}_2}\frac{\tau^n d\tau}{K(\tau)\left(\tau - e^{i\vartheta}\right)},\ V_m^n = \frac{1}{2\pi}\int\limits_{-\pi}^{\pi} V_n\left(e^{i\vartheta}\right)K\left(e^{i\vartheta}\right)e^{-im\vartheta}d\vartheta \text{ and}$$

$$W_0 = \frac{1}{2\pi}\int\limits_{-\pi}^{\pi}\vartheta K\left(e^{i\vartheta}\right)d\vartheta.$$

The values W_0, V_m^n have been calculated in [45] by making use of the formulas

$$V_{m-1}^{n-1} = \frac{1}{2}\begin{cases} \frac{m}{m-n}\left[P_{m-1}(u)P_n(u) - P_m(u)P_{n-1}(u)\right]; & m \neq n \\ \sum_{s=0}^{n} \rho_{n-s}(u)P_{s-n}(u); & m = n \geq 0 \end{cases}, \qquad (2.23)$$
$$V_{-n-1}^{-n-1} = -V_{n-1}^{n-1}; \quad n \geq 1,\ W_0 = -\ln\frac{1+u}{2}.$$

Here $u = \cos\vartheta_0$ and $P_n(u)$ are the Legendre polynomials [95], which for negative n indices are defined by the formula

$$P_n(u) = P_{|n|-1}(u).$$

The functions $\rho_n(u)$, $n = 0,1,2,\ldots$, are expressed via the Legendre polynomials (see (2.66) below).

So, assuming that the Fourier coefficients $\{\psi_n\}_{n=-\infty}^{\infty}$ of the function $\psi(\exp(i\vartheta))$ [see (2.11)] are known, we have solved equations (2.10) and (2.11) in explicit form [see (2.21) and (2.22)]. Let us show how on the basis of this solution the infinite system of linear algebraic equations equivalent to equations (2.1) and (2.2.) should be derived. Evidently $\{y_n\}_{n=-\infty}^{\infty}$ and $\{\psi_n\}_{n=-\infty}^{\infty}$ in (2.21) and (2.22) should be substituted by their representations via $\{x_n\}_{n=-\infty}^{\infty}$ and $\{g_n\}_{n=-\infty}^{\infty}$, $\{f_n\}_{n=-\infty}^{\infty}$ [see (2.6) and (2.9)]. After some elementary manipulations,

$$x_m = \sum_{n=-\infty}^{\infty} a_{mn}x_n + b_m;\ m = 0,\ \pm 1,\ ..., \qquad (2.24)$$

with the matrix elements a_{mn} and the right-hand sides b_m being

$$a_{mn} = \begin{cases} -W_0\gamma_0; & m = n = 0 \\ \frac{|n|}{n}\delta_n V_{n-1}^{-1}; & m = 0, \quad n \neq 0 \\ -\gamma_0\frac{V_{m-1}^{-1}}{m}; & m \neq 0, \quad n = 0 \\ \frac{|n|}{m}\delta_n V_{m-1}^{n-1} & m \neq 0, \quad n \neq 0 \end{cases}, \qquad (2.25)$$

$$b_m = \begin{cases} g_0 + W_0 f_0 + \sum_{n\neq 0} \frac{V_{n-1}^{-1}}{n}\left(f_n - |n|\, g_n\right); m = 0 \\ g_m + \sum_{n=-\infty}^{+\infty} \frac{V_{m-1}^{n-1}}{m}\left(f_n - |n|\, g_n\right); m \neq 0 \end{cases}. \qquad (2.26)$$

Express the system of equations in vector form. For this, introduce the infinite-dimensional matrix $A = \{a_{mn}\}_{m,n=-\infty}^{\infty}$ and the column vectors $x = \{x_n\}_{n=-\infty}^{\infty}$, $b = \{b_m\}_{m=-\infty}^{\infty}$. In these denotations, (2.24) has the form

$$x = Ax + b. \qquad (2.27)$$

Equation (2.27) will be considered on the sequence space l_2. Let us show that the matrix A gives a compact operator on the space l_2, with the column vector $b \in l_2$. To this end, it is sufficient to ensure the convergence of the series $\sum_{m,n=-\infty}^{\infty} |a_{mn}|^2 < \infty$

and $\sum_{m=-\infty}^{\infty} |b_m|^2$. As it is known [95], Legendre polynomials obey the inequality

$$|P_n(u)| < \frac{2}{\sqrt{\pi |n| \left(1-u^2\right)}}; n = \pm 1, \pm 2, \ldots . \tag{2.28}$$

In view of (2.28), expression (2.23) readily gives as $|n|$, $|m| \to \infty$ the inequalities

$$\left|V_{m-1}^{n-1}\right| < \frac{C_1\sqrt{|m|}}{\sqrt{|n|}\,|m-n|}; m \neq n, \qquad \left|V_{m-1}^{m-1}\right| < C_2, \tag{2.29}$$

where C_1, C_2 are constants independent of m and n.

Now, considering (2.29) and upon the fact that $\delta_n = O(n^{-2})$ [see (2.3)], we obtain

$$|a_{mn}| < \frac{C_3}{\sqrt{|m|}\,|n|^{3/2}\,|m-n|}; \; m \neq n, \; |a_{mm}| < \frac{C_4}{m^2}. \tag{2.30}$$

Here C_3, C_4 are some constants. From (2.30) follows the convergence of the series $\sum_{m,n=-\infty}^{\infty} |a_{mn}|^2 < \infty$. Previously we assumed that the Fourier coefficients of the functions $F(\exp(i\vartheta))$ and $G(\exp(i\vartheta))$ satisfy the conditions $\{f_n\}_{n=-\infty}^{\infty} \in l_2$ (1) and $\{g_n\}_{n=-\infty}^{+\infty} \in l_2$ (3). On this account and in view of (2.23) and (2.29), we have from (2.26) that as $|m| \to \infty$

$$b_m = A_0 \frac{P_{m-1}(u)}{m} + A_1 \frac{P_m(u)}{m} + \frac{\widehat{b}_m}{|m|^{3/2}}, \tag{2.31}$$

where $A_s = \frac{(-1)^s}{2} \sum_{n=-\infty}^{\infty} (f_n - |n|\, g_n)\, P_{n-s}(u)$, $s = 0,1$, and $\widehat{b}_m$ are some values with $\sum_{m=-\infty}^{\infty} \left|\widehat{b}_m\right|^2 < \infty$. Hence the series $\sum_{m=-\infty}^{\infty} |b_m|^2 < \infty$ converges, which is the required result.

From the above discussion, it follows that equation (2.27) is a second-kind equation in the space l_2.

So, the initial dual series equations (2.1) and (2.2) have been reduced to the infinite system of linear algebraic equations of the second kind. These systems guarantee their numerical solution with any desired accuracy. Besides, the established properties of equation system (2.4) suggest the solvability and the uniqueness of the solution using, for instance, the corresponding Fredholm theory for operator equations of the second kind [70]. Furthermore, using (2.24), one arrives at an asymptotical estimation of the unknowns x_m as $|m| \to \infty$, which is identical to asymptotical estimation (2.31). Namely,

$$x_m = B_0 \frac{P_{m-1}(u)}{m} + B_1 \frac{P_m(u)}{m} + \frac{\widehat{x}_m}{|m|^{3/2}}, \tag{2.32}$$

where $B_s = A_s + C_s$, $C_s = 0.5(-1)^s \left[-\gamma_0 x_0 + \sum\limits_{n=-\infty}^{\infty} x_n \delta_n |n| P_{n-s}(u) \right]$, $s = 0,1$, and the values $\widehat{x}_m$ satisfy the condition $\sum\limits_{m=-\infty}^{\infty} \left| \widehat{x}_m \right|^2 < \infty$.

We will not go into details of the demonstration of (2.32) but only mention that the derivation of this asymptotic estimate rests on the explicit expression of V_{m-1}^{n-1} through the Legendre polynomials, inequality (2.28), and representation (2.3) for γ_n. Asymptotic estimates of this kind are found very useful in the summation of the x_m involving series, in particular, the series of the type (2.1) and (2.2). In diffraction theory (electrodynamics), they play the part of currents or charge densities, etc. These series, as seen from (2.1) and (2.2), have a slow rate of convergence so that their summation presents a problem. An evident means of the convergence improvement of these series is recognizing the x_m asymptotic behavior as $|m| \to \infty$ for the explicit summation of the asymptotic terms. The latter is possible in so far as in actual practice, the values γ_m, f_m, g_m usually satisfy stronger conditions than those above.

2.2.2 *Classical Dual Series Equations with "Matrix Perturbation"*

The elementary dual series equations discussed in the previous paragraph allow some generalizations. One such is the dual series equations

$$\sum_{n=-\infty}^{\infty} \left[\gamma_n x_n + (Vx)_n \right] e^{in\vartheta} = F(\vartheta);\ |\vartheta| < \vartheta_0, \tag{2.33}$$

$$\sum_{n=-\infty}^{\infty} \left[x_n + (Ux)_n \right] e^{in\vartheta} = G(\vartheta);\ \vartheta_0 < |\vartheta| \le \pi, \tag{2.34}$$

where $x = \{x_n\}_{n=-\infty}^{\infty}$ is the column vector of the unknowns, $U = \left\{U_{pq}\right\}_{p,q=-\infty}^{\infty}$ and $V = \left\{V_{pq}\right\}_{p,q=-\infty}^{\infty}$ are some given infinite-dimensional matrix operators with matrix elements U_{pq} and V_{pq} decreasing fast enough as $|p|,|q| \to \infty$. $(Ux)_n$ and $(Vx)_n$ are the nth components of the vector columns Ux and Vx, respectively, $F(\vartheta)$ and $G(\vartheta)$ are given functions, and $\vartheta_0 \in (0;\pi)$ is a fixed parameter. Concerning the given sequence γ_n, $n = 0,\pm1,\pm2\ldots$, it is assumed that

$$\gamma_n = |n| \begin{cases} C^+ \left[1 + O\left(n^{-2}\right) \right];\ n \to \infty \\ C^- \left[1 + O\left(n^{-2}\right) \right];\ n \to -\infty \end{cases} \tag{2.35}$$

with $C^{\pm}$ being some n-independent constants. In the general case, $C^+ \neq C^-$.

Below, the problem formulation for some classes of series equations is elaborated to recognize the spaces of the column vector x and the functions $F(\vartheta)$, $G(\vartheta)$, the sense of equations (2.33) and (2.34), and other specific points.

By the commonly accepted terminology, expressions (2.33) and (2.34) are dual series equations involving $\exp(in\vartheta)$ functions. We will call them standard equations when $U = V = 0$. If $U \neq 0$ and (or) $V \neq 0$, then (2.33) and (2.34) are matrix perturbation equations. And, finally, they are equations with diagonal matrix perturbation when U and V represent diagonal matrices.

It is not difficult to see that multiplying (2.33) and (2.34) by $\exp(im\vartheta)$, $m = 0,\pm1,\ldots$, and integrating between $(-\vartheta_0;\vartheta_0)$ and $(-\pi,\vartheta_0)$, $(\vartheta_0;\pi)$, respectively, yields the infinite system of linear algebraic equations, which is a functional equation of the first kind for x, with all notorious disadvantages of the equations of that kind.

Clearly any other straightforward algebraization of equations (2.33) and (2.34) will end up with a similar result, forcing us to invent a proper regularization procedure in an effort to solve equations (2.33) and (2.34). In this section, a regularization procedure of the kind will be developed for equations (2.33) and (2.34) in the case $C^+ = C^-$ [see (2.35)] [75, 92]. The regularization procedure described below is based on the development of a closed-form solution to the standard ($U = V = 0$) dual series equations by means of the Riemann–Hilbert boundary value problem theory [80]. With this knowledge, system (2.33) and (2.34) can be equivalently reduced to an infinite system of linear algebraic equations of the second kind to be effectively numerically solved by truncation.

If $C^+ = C^-$, dual series equations (2.33) and (2.34) appear to be

$$ax_0 + \sum_{n=-\infty}^{\infty} x_n |n| \, \mathrm{e}^{in\vartheta} + \sum_{n=-\infty}^{\infty} \left[\left(\bar{V}x \right)_n - f_n \right] \mathrm{e}^{in\vartheta} = 0; \ |\vartheta| < \vartheta_0, \tag{2.36}$$

$$\sum_{n=-\infty}^{\infty} x_n \mathrm{e}^{in\vartheta} + \sum_{n=-\infty}^{\infty} \left[(Ux)_n - g_n \right] \mathrm{e}^{in\vartheta} = 0; \ |\vartheta| > \vartheta_0, \tag{2.37}$$

where $a = \gamma_0/C^+, f = \{f_n\}_{n=-\infty}^{\infty}$ and $g = \{g_n\}_{n=-\infty}^{\infty}$ are the Fourier coefficients of the functions $(1/C^+)F(t)$ and $G(t)$, respectively. The matrix operator $\bar{V}$ is related to V as

$$\bar{V} = V + D, \tag{2.38}$$

where $D = \left\{ d_p \delta_p^q \right\}_{q,p=-\infty}^{\infty}$ is a diagonal matrix operator, $d_p = \gamma_p / C^+ - |p|$, $p = \pm1,\pm2,\ldots$, $d_0 = 0$ and δ_p^q is the Kronecker delta. From (2.35) it follows that $d_p = O\left(|p|^{-1}\right)$. As to the unknown column vectors x and the coefficients f and g, we assume that

$$x \in l_2(1); \tag{2.39}$$

$$g \in l_2(1), f \in l_2(-1). \tag{2.40}$$

In addition, all the series in (2.36) and (2.37) are assumed to be the Fourier series of their sums. That is, the series in (2.36) and (2.37) are [according to (2.39)] the Fourier series of the relevant functions belonging, respectively, to $\mathbf{L}_1[-\pi;\pi]$ and $\mathbf{L}_2[-\pi;\pi]$. Regarding the matrix operators $\bar{V}$, assume that the operators $T^{-1}\bar{V}T^{-1}$ and TUT^{-1} are compact as long as they act in the l_2 space, where the diagonal operator T is given by the matrix

$$T = \left\{\tau_n \delta_m^n\right\}_{m,n=-\infty}^{\infty};\ \tau_0 = 1, \tau_n = |n|^{1/2},\ n \neq 0. \tag{2.41}$$

Introduce the column vectors ψ,φ by the formulas

$$\varphi = \{\varphi_n\}_{n=-\infty}^{\infty}, \psi = \{\psi_n\}_{n=-\infty}^{\infty}, \tag{2.42}$$

$$\psi_n = (Ux)_n - g_n, \quad \varphi_n = ax_0\delta_0^n + \left(\bar{V}x\right)_n - f_n;\ n = 0, \pm 1, \pm 2,... \tag{2.43}$$

With this notation, equations (2.36) and (2.37) take the form

$$\sum_{n=-\infty}^{\infty} x_n \mathrm{e}^{in\vartheta} + \sum_{n=-\infty}^{\infty} \psi_n \mathrm{e}^{in\vartheta} = 0;\ |\vartheta| > \vartheta_0, \tag{2.44}$$

$$\sum_{n=-\infty}^{\infty} x_n |n| \mathrm{e}^{in\vartheta} + \sum_{n=-\infty}^{\infty} \varphi_n \mathrm{e}^{in\vartheta} = 0;\ |\vartheta| < \vartheta_0. \tag{2.45}$$

Now put aside formulas (2.42) and (2.43), assuming that the column vectors φ,ψ are known. Our immediate task is to construct for (2.44) and (2.45) a closed-form solution that satisfies condition (2.39). We will begin with a formal scheme for the derivation of the solution, ending with a brief mathematical justification (for details, see [11, 92]).

Introduce the new unknowns $y = \{y_n\}_{n=-\infty}^{\infty}$

$$y_0 = x_0 + \psi_0,\ y_n = n\left(x_n + \psi_n\right);\ n = \pm 1, \pm 2,... \tag{2.46}$$

Differentiate (2.44) with respect to ϑ term by term and, making use of (2.46), obtain from (2.44) and (2.45) the following system of equations:

$$\sum_{n\neq 0} y_n \mathrm{e}^{in\vartheta} = 0;\ |\vartheta| > \vartheta_0, \tag{2.47}$$

$$\sum_{n\neq 0} \frac{|n|}{n} y_n \mathrm{e}^{in\vartheta} = \sum_{n=-\infty}^{\infty} \left(|n|\,\psi_n - \varphi_n\right) \mathrm{e}^{in\vartheta};\ |\vartheta| < \vartheta_0, \tag{2.48}$$

$$\sum_{n\neq 0} (-1)^n n^{-1} y_n = -y_0. \tag{2.49}$$

Equation (2.49) comes directly from (2.44) at $\vartheta = \pi$ owing to (2.46). The fact is that the differentiation of (2.44) loses the zeroth Fourier coefficient information. To

avoid this error and guarantee an equivalent passage from (2.44), (2.45) to (2.47), (2.48), equation (2.44) is applied at some ϑ point, $|\vartheta| > \vartheta_0$, e.g., $\vartheta = \pi$. One easily checks that the solution of equations (2.44) and (2.45) does not depend on a particular choice of this point.

According to [92], the dual series equations (2.47), (2.48), and (2.49) can be converted to some Riemann–Hilbert boundary value problem. Indeed, define some two functions of the complex variable z as

$$X^+(z) = \sum_{n=1}^{\infty} y_n z^n, \quad X^-(z) = -\sum_{n=1}^{\infty} y_{-n} z^{-n}. \tag{2.50}$$

The functions $X^+(z)$ and $X^-(z)$ are analytic inside and outside, respectively, the circle $|z| = 1$. Let some arc $\mathbf{P}_2$ on the circle $|z| = 1$ connect the points $\exp(-i\vartheta_0)$ and $\exp(i\vartheta_0)$ through $z = -1$, with arc $\mathbf{P}_1$ complementing $|z| = 1$ to the full circle. With these functions, equations (2.47) and (2.48) take on the appearance ($z = \exp(i\vartheta_0)$)

$$X^+(z) - X^-(z) = 0; z \in \mathbf{P}_2, \tag{2.51}$$

$$X^+(z) + X^-(z) = \sum_{n=-\infty}^{\infty} (|n|\,\psi_n - \varphi_n)\, z^n; z \in \mathbf{P}_1. \tag{2.52}$$

From (2.51) it follows that the function

$$X(z) = \begin{cases} X^+(z); & |z| < 1 \\ X^-(z); & |z| > 1 \end{cases} \tag{2.53}$$

continues as a function analytic in the complex plane with a cut along $\mathbf{P}_1$ arc and decreases as $|z| \to \infty$ according to (2.50). Namely,

$$X(z) = -y_{-1} z^{-1} + O\left(z^{-2}\right). \tag{2.54}$$

As (2.36) and, consequently, (2.48) are assumed to be the series of their sums on $\mathbf{L}_1[-\pi;\pi]$, the limiting $X(z)$ values on the circle $|z| = 1$ belong to $\mathbf{L}_1[-\pi;\pi]$ as well. In this case, equations (2.47) and (2.48) are equivalent to the problem of the $X(z)$ reconstruction by the sum of its limiting values on arc $\mathbf{P}_1$, where the function $X(z)$ is not analytic. This problem represents an elementary variant of the Riemann–Hilbert boundary value problem (see [80]). Its solution is well known and available in the form (see [80])

$$X(z) = \frac{1}{2\pi i R(z)} \int_{\mathbf{P}_1} \frac{F(\tau) R(\tau)}{\tau - z} d\tau + \frac{y_{-1}}{R(z)}, \tag{2.55}$$

where

$$F(\tau) = \sum_{n=-\infty}^{\infty} (|n|\,\psi_n - \varphi_n)\ \tau^n, \tag{2.56}$$

$$R(z) = \left[\left(z - e^{i\vartheta_0}\right)\left(z - e^{-i\vartheta_0}\right)\right]^{1/2}. \tag{2.57}$$

The function $R(z)$ is analytic in the complex plane cut along arc $\mathbf{P}_1$, the root branch $R(0) = 1$ chosen.

Now let us show how dual series equations (2.47), (2.48), and (2.49) should be solved using (2.55). By virtue of the Sokhotskyi-Plemelj formulas (see [94]), from expression (2.55), it follows that for $|z| = 1$

$$X^+\left(e^{i\vartheta}\right) - X^-\left(e^{i\vartheta}\right) = \frac{K\left(e^{i\vartheta}\right)}{\pi i}\int\limits_{\mathbf{P}_1} \frac{F(\tau)\,R^+(\tau)}{\tau - e^{i\vartheta}}d\tau + 2y_{-1}K\left(e^{i\vartheta}\right), \tag{2.58}$$

where the integral is regarded as the Cauchy principal value, $R^+(\tau)$ denotes the limiting value of $R(z)$ on the inside of unit-circle arc $\mathbf{P}_1$: at $z = \tau(1–\varepsilon)$ and $\varepsilon \to +0$, and

$$K(\tau) = \begin{cases} \frac{1}{R^+(\tau)};\ \tau \in \mathbf{P}_1 \\ 0;\ \tau \in \mathbf{P}_2 \end{cases}. \tag{2.59}$$

Match the Fourier coefficients on both sides of equation (2.58) and on account of (2.56), get the relations

$$y_m = \sum_{n=-\infty}^{\infty} (|n|\,\psi_n - \varphi_n)\ V_m^n + 2y_{-1}R_m;\ m = \pm 1, \pm 2, \ldots, \tag{2.60}$$

$$0 = \sum_{n=-\infty}^{\infty} (|n|\,\psi_n - \varphi_n)\ V_0^n + 2y_{-1}R_0, \tag{2.61}$$

with V_m^n and R_m given below [see (2.63) and (2.64)]. Equations (2.60) and (2.61) should be completed with equation (2.49), which on the substitution of the right-hand side of equation (2.60) for y_m becomes

$$-y_0 = \sum_{n=-\infty}^{\infty} (|n|\,\psi_n - \varphi_n)\,V_\sigma^n + 2y_{-1}R_\sigma. \tag{2.62}$$

The coefficients V_m^n, R_m, V_σ^n, R_σ originally calculated in [45] are expressed via Legendre polynomials $P_n(u)$, (see [95] for their definition $P_0(u) = 1$, $P_1(u) = u, \ldots$)

$$V_m^n = \begin{cases} \frac{m+1}{2(m-n)}\left[P_m(u)P_{n+1}(u) - P_{m+1}(u)P_n(u)\right]; & m \neq n \\ \frac{1}{2}\sum\limits_{p=0}^{m+1} \rho_{m+1-p}(u); & n = m \geq 0 \\ -V_{|m|-2}^{|m|-2}(u); & n = m \leq -2 \\ 0; & n = m = -1 \end{cases}, \tag{2.63}$$

$$\begin{cases} R_m = \frac{1}{2}P_m(u); & m = 0, \pm 1, \pm 2, \ldots \\ P_{-n-1}(u) = P_n(u); & n = 0,1,2,\ldots \\ R_\sigma = -\frac{1}{2}\ln\frac{1+u}{2} \end{cases}, \tag{2.64}$$

$$V_\sigma^n = \begin{cases} \frac{1}{2}\rho_{\bar{n}}(u)\ln\frac{1+u}{2} + \frac{1}{2|n|}\left[P_{|n|}(u) - P_{|n|-1}(u)\right]; & n \neq 0, -1 \\ \frac{u-1}{2}\left(\ln\frac{1+u}{2} + 1\right); & n = -1 \\ \frac{1+u}{2}\ln\frac{1+u}{2}; & n = 0 \end{cases}, \tag{2.65}$$

where $u = \cos\vartheta_0$, $\bar{n} = \begin{cases} n+1; n > 0 \\ -n; \quad n < -1 \end{cases}$, $\rho_0(u) = 1$, $\rho_1(u) = -u$, and

$$\rho_n(u) = P_n(u) - 2uP_{n-2}(u) + P_{n-2}(u); \; n = 2,3,\ldots \tag{2.66}$$

In order to get y_m, $m = 0,\pm 1,\ldots$, in explicit form (recall that φ_n, ψ_n are assumed to be known), one only needs, on account of (2.61), to discard y_{-1} from (2.60) and (2.62). Indeed, substitute the expression

$$y_{-1} = 0.5R_0^{-1}\sum_{n=-\infty}^{\infty}(|n|\psi_n - \varphi_n)\; V_0^n \tag{2.67}$$

obtained from (2.61) into the right-hand sides of (2.60) and (2.62) to obtain

$$\begin{cases} y_m = \sum\limits_{n=-\infty}^{\infty}(|n|\psi_n - \varphi_n)\left(V_m^n - R_0^{-1}R_m V_0^n\right); & m = \pm 1, \pm 2, \ldots \\ y_0 = \sum\limits_{n=-\infty}^{\infty}(|n|\psi_n - \varphi_n)\left(R_0^{-1}R_\sigma V_0^n - V_\sigma^n\right) \end{cases}. \tag{2.68}$$

With formulas (2.63), (2.64), (2.65), and (2.66), it is not difficult to check the identities

$$V_{m-1}^{n-1} = V_m^n - R_0^{-1}R_m V_0^n,\; R_0^{-1}R_\sigma V_0^n - V_\sigma^n = \begin{cases} -\ln\frac{1+u}{2}; & n = 0 \\ n^{-1}V_{n-1}^{-1}; & n \neq 0 \end{cases}. \tag{2.69}$$

Substitute (2.69) into (2.68) and return to the unknowns $\{x_m\}_{m=-\infty}^{\infty}$. Then the solution to equations (2.44) and (2.45) with ψ_n, φ_n known is

$$x_0 = W_0\varphi_0 - \psi_0 + \sum_{n\neq 0}(|n|\psi_n - \varphi_n)\; n^{-1}V_{n-1}^{-1}, \tag{2.70}$$

$$x_m = -\psi_m + \sum_{n=-\infty}^{\infty} (|n|\,\psi_n - \varphi_n)\, m^{-1} V_{m-1}^{n-1}; \quad m = \pm 1, \pm 2, \ldots,$$
$$W_0 = \ln \frac{1+u}{2} \tag{2.71}$$

Thus, formulas (2.70) and (2.71) lend a closed-form solution to the standard dual series equations (2.44) and (2.45). On this basis, we will build an infinite system of linear algebraic equations of the second kind equivalent to the initial dual series equations (2.33) and (2.34) with matrix perturbation. For this, pass from the column vectors x, φ, ψ (see 2.43) assumed to satisfy the conditions [see (2.39) and (2.40)] $x \in l_2(1)$, $\psi \in l_2(1)$, and $\varphi \in l_2(-1)$, to the column vectors

$$\widehat{x} = \left\{\widehat{x}_n\right\}_{n=-\infty}^{\infty} = Tx \in l_2, \qquad \widehat{\psi} = \left\{\widehat{\psi}_n\right\}_{n=-\infty}^{+\infty} = T\psi \in l_2,$$
$$\widehat{\varphi} = \left\{\widehat{\varphi}_n\right\}_{n=-\infty}^{\infty} = T^{-1}\varphi \in l_2$$

lying on the l_2 space, the operator T is defined in (2.41).

Relations (2.70) and (2.71) are readily transformed to become

$$\widehat{x}_m = \sum_{n=-\infty}^{\infty} W_{mn}\left(\widehat{\psi}_n - \widehat{\varphi}_n\right) + \sum_{n=-\infty}^{\infty} P_{mn}\,\widehat{\psi}_n - \widehat{\psi}_m \qquad m = 0, \pm 1, \ldots \tag{2.72}$$

with

$$W_{mn} = \begin{cases} -W_0; \ m = n = 0 \\ \frac{\tau_n V_{n-1}^{-1}}{n}; \ n \neq 0, \quad m = 0 \\ \frac{\tau_n \tau_m V_{m-1}^{n-1}}{m}; \ m \neq 0 \end{cases}, P_{mn} = \begin{cases} W_0; \ m = n = 0 \\ -W_{m0}; \ m \neq 0, \quad n = 0 \\ 0; \ n \neq 0 \end{cases}. \tag{2.73}$$

Thus, by virtue of (2.73) with the matrix operators

$$W = \{W_{mn}\}_{m,n=-\infty}^{\infty}, \qquad P = \{P_{mn}\}_{m,n=-\infty}^{\infty}, \tag{2.74}$$

formulas (2.72) become

$$\widehat{x} = W\left(\widehat{\psi} - \widehat{\varphi}\right) + (P - E)\,\widehat{\psi}, \tag{2.75}$$

where E is the identity matrix operator.

Armed with formula (2.75) for solving equations (2.44) and (2.45) with φ, ψ known, proceed to the regularization of equations (2.73) and (2.37) on account of expressions (2.42) and (2.43) relating ψ_n, φ_n and f_n, g_n, x_n. To this end, define the column vectors

$$f = \{f_n\}_{n=-\infty}^{\infty}, \; g = \{g_n\}_{n=-\infty}^{\infty}, \tag{2.76}$$

$$\widehat{f} = \left\{\widehat{f}_n\right\}_{n=-\infty}^{\infty} = T^{-1}f, \quad \widehat{g} = \left\{\widehat{g}_n\right\}_{n=-\infty}^{\infty} = Tg. \tag{2.77}$$

Consequently, formulas (2.43) become

$$\widehat{\psi}_n = \left(\widehat{U}\,\widehat{x}\right)_n - \widehat{g}_n, \;\; \widehat{\varphi}_n = a\delta_0^n \widehat{x}_n + \left(\widehat{V}\,\widehat{x}\right)_n - \widehat{f}_n, \tag{2.78}$$

where $\widehat{U}$ and $\widehat{V}$ are the matrix operators

$$\widehat{U} = TUT^{-1}, \;\; \widehat{V} = T^{-1}\bar{V}T^{-1} \tag{2.79}$$

which are compact, by assumption, on the space l_2. Then relations (2.78) in the vector form are

$$\widehat{\psi} = \widehat{U}\,\widehat{x} - \widehat{g}\,, \;\widehat{\varphi} = a\,\widehat{E}\,\widehat{x} + \widehat{V}\,\widehat{x} - \widehat{f} \tag{2.80}$$

with the matrix operator $\widehat{E}$ defined as $\widehat{E} = \left\{\delta_m^0 \delta_n^0\right\}_{m,n=-\infty}^{\infty}$.

Considering (2.75) and (2.80) as a system of equations for the unknowns $\widehat{x}$, $\widehat{\varphi}$, $\widehat{\psi}$ and removing the unknowns $\widehat{\varphi}$, $\widehat{\psi}$ from (2.75) in view of (2.80), one arrives after some elementary transformations at the equation for $\widehat{x}$

$$(E + H)\,\widehat{x} = \widehat{b}\,, \tag{2.81}$$

with the matrix operator H and the column vector $\widehat{b}$ in the form

$$H = -aP + (E - P)\,\widehat{U} + W\left(\widehat{V} - \widehat{U}\right), \tag{2.82}$$

$$\widehat{b} = (E - P)\,\widehat{g} + W\left(\widehat{f} - \widehat{g}\right). \tag{2.83}$$

Now let us prove that the operator H available from (2.82) is compact on l_2 and, hence, equation (2.81) is a second-kind equation on l_2. In this case, we will assume that the matrix operators $\widehat{U}$, $\widehat{V}$ defined by formulas (2.79) are compact on l_2.

First of all we will show that the operator W is bounded on l_2. Put the column vector $x = \{x_n\}_{n=-\infty}^{\infty} \in l_2$ and prove that the column vector $y = \{y_m\}_{m=-\infty}^{\infty}$ such that $y{=}Wx$ belongs to l_2 for any $x{\in}l_2$. Indeed, in view of (2.73) and (2.63), we have

$$\begin{aligned} y_0 &= \sum_{n\neq 0} W_{0n}x_n = -W_0x_0 + \sum_{n\neq 0} \tau_n n^{-1} V_{n-1}^{-1} x_n = \\ &= -W_0x_0 + \tfrac{1}{2}\sum_{n\neq 0} \tau_n n^{-1}\left[P_{n-1}(u) - P_n(u)\right]x_n. \end{aligned}$$

On account of the inequality [see (2.60)]

$$|P_n(u)| < \frac{2}{\sqrt{\pi |n| \left(1-u^2\right)}}; \; n = \pm 1, \pm 2, \ldots \tag{2.85}$$

together with the Cauchy–Bunyakowsky inequality, the absolute convergence of the series (2.84) is ensured. Next let $m \neq 0$. Then

$$\begin{aligned} y_m = \sum_{n=-\infty}^{\infty} W_{mn} x_n = m^{-1} \tau_m^2 V_{m-1}^{m-1} x_m + \tfrac{P_{m-1}(u)}{2} \tau_m \sum_{m \neq n} \tfrac{\tau_n P_n(u)}{m-n} x_n - \\ - \tfrac{P_m(u)}{2} \tau_m \sum_{m \neq n} \tfrac{\tau_n P_{n-1}(u)}{m-n} x_n; \quad m = \pm 1, \pm 2, \ldots \end{aligned} \tag{2.86}$$

Make use of the fact that the matrix

$$\{\alpha_{mn}\}_{m,n=-\infty}^{\infty}: \; \alpha_{mn} = \begin{cases} 0; & m = n \\ \frac{1}{m-n}; & m \neq n \end{cases}$$

produces the bounded operator (see [70]) on l_2. Considering the estimate (2.85), we obtain from (2.86) that y_m can be written as

$$y_m = m^{-1} \tau_m^2 V_{m-1}^{m-1} x_m + \tau_m P_{m-1}(u) f_m^1 + \tau_m P_m(u) f_m^2, \tag{2.87}$$

where $\left\{f_m{}^j\right\}_{m=-\infty}^{\infty}, j = 1,2$, are some vector columns belonging to l_2. In view of the inequality

$$\left| V_{m-1}^{m-1} \right| < 2; \; m = \pm 1, \pm 2, \ldots$$

it immediately follows that the values y_m, $m = \pm 1, \pm 2, \ldots$, are quadratically summable.

The finite-valuedness of y_0 has been shown, proving, in turn, that the matrix W produces a linear operator defined everywhere on l_2. From the definition of W_{mn} [see (2.73)] it follows that the matrix W is self-adjoint. The previously established facts suggest, according to [70], that the operator W is bounded on l_2.

Now let us prove that the matrix $\{P_{mn}\}_{m,n=-\infty}^{\infty}$ produces a Hilbert–Schmidt operator on l_2. For this purpose, the convergence of $\sum\limits_{m,n} |P_{mn}|^2$ will suffice (see [70]). From (2.73),

$$\sum_{m,n} |P_{mn}|^2 = \sum_{m} \left|P_{m_0}\right|^2 = W_0^2 + \sum_{m \neq 0} m^{-2} \tau_m^2 \left(V_{m-1}^{-1}\right)^2 < W_0^2 + \text{const} \sum_{m \neq 0}^{\infty} m^{-3/2} < \infty.$$

Hence it immediately follows that the operator H defined by formula (2.82) is compact on l_2. Indeed, the operator P is compact as a Hilbert–Schmidt operator. Also, we have already shown that operator W is bounded, while the operators $\widehat{U}$

and $\widehat{V}$ are compact by assumption. Hence, the operator $W\left(\widehat{V}-\widehat{U}\right)$ is compact, too, which is what we set out to prove.

Based on the properties of operators P and W, one finds that, in view of (2.77) and (2.83), the column vectors $\widehat{b}$ and $\widehat{x}$ belong to l_2.

Thus, (2.81) represents an infinite system of linear algebraic equations of the second kind on l_2.

It is not difficult to extend the validity of the analytic regularization procedure designed for dual series equations (2.36) and (2.37) to the coupled system of a finite number of these equations below

$$\begin{cases} a_j x_0^j + \sum\limits_{n=-\infty}^{\infty} |n|\, x_n^j \mathrm{e}^{in\vartheta} + \sum\limits_{p=1}^{M} \sum\limits_{n=-\infty}^{\infty} \left[\left(V^{jp}x^p\right)_n - f_n^j\right] \mathrm{e}^{in\vartheta} = 0; \quad |\vartheta| < \vartheta_j \\ \sum\limits_{n=-\infty}^{\infty} x_n^j \mathrm{e}^{in\vartheta} + \sum\limits_{p=1}^{M} \sum\limits_{n=-\infty}^{\infty} \left[\left(U^{jp}x^p\right)_n - g_n^j\right] \mathrm{e}^{in\vartheta} = 0; \qquad |\vartheta| > \vartheta_j, j = 1,2,...,M \end{cases} \tag{2.88}$$

in the unknowns $x^j = \left\{x_n^j\right\}_{n=-\infty}^{\infty}, j = 1,2,\ldots, M$.

Both the values involved in (2.88) and the requirements imposed on them are the same as for equations (2.36) and (2.37), and therefore we avoid repetition of the details.

The regularization of equations (2.88), in other words, their reduction to an infinite system of linear algebraic equations of the second kind obeys the scheme developed for equations (2.36) and (2.37). First, the vectors

$$\psi^j = \sum_{p=1}^{M} U^{jp}x^p - g^j, \quad \varphi^j = a^j \widehat{E}\, x^j + \sum_{p=1}^{M} V^{jp}x^p - f^j \tag{2.89}$$

are assumed to be known and possessing the properties desired. By analogy with the previous case, equations of (2.44) and (2.45) type are obtained for every $j = 1,2,\ldots, M$. In view of (2.89), they are transformed to the analog of equation (2.81) in the form

$$\widehat{x}^j + \sum_{p=1}^{M} H^{jp}\, \widehat{x}^p = \widehat{b}^{\,j}; \; j = 1,2,...,M, \tag{2.90}$$

where

$$H^{jp} = -a^j P^j + \left(E - P^j\right) \widehat{U}^{jp} + W^j \left(\widehat{V}^{jp} - \widehat{U}^{jp}\right),$$
$$\widehat{b}^j = \left(E - P^j\right) \widehat{g}^j + W^j \left(\widehat{f}^j - \widehat{g}^j\right).$$

In equations (2.90), $\widehat{x}^j$, $\widehat{f}^j$, $\widehat{g}^j$ for all $j = 1,2,\ldots, M$ are expressed, respectively, through x^j, f^j, g^j via (2.76) and (2.77). The operators U^{jp} and V^{jp} are related to

U^{jp} and V^{jp} by formulas (2.79). Finally, the operators P^j, W^j for every $j = 1,2,\ldots,M$ come from formulas (2.63) to (2.66), (2.73), and (2.74), with ϑ_0 substituted by ϑ_j.

By construction, all the vectors in (2.90) belong to the l_2 space. It is easily proved that all the matrix operators involved in (2.90) and considered as operators acting on l_2 are compact. Hence, (2.90) is a system of equations of the second kind.

In closing mention should be made that the two-dimensional problem of electromagnetic (acoustic) wave diffraction by a grating consisting of finite-number elements like nonclosed arbitrarily shaped cylindrical screens is reduced to the systems of equations of (2.88) type [11].

2.2.3 Dual Series Equations with the Nonunit Coefficient of Conjugation

In this paragraph, the dual series equations (2.33) and (2.35) are examined in the case $C^{\pm} \neq C^{-}$ [see (2.35)]. Equations of this nature appear, to give one example, in problems of wave diffraction by a single-periodic perfectly conducting grating located on the interface of a gyrotropic medium (magnetoactive plasma, anisotropic dielectric, ferrite, etc.).

The regularization algorithm of these equations is designed to use the relevant standard equations solved in analytic (explicit) terms by considering the boundary value Riemann–Hilbert problem in theory of analytic functions. Suppose that we are given constants $C^{\pm}$ from (2.35) as complex numbers with the imaginary part other than zero (Im $C^{\pm} \neq 0$). The dual series equations (2.33) and (2.34) then take on the appearance

$$ax_0 + \sum_{n=1}^{\infty} nx_n e^{in\vartheta} - b \sum_{n=-\infty}^{-1} nx_n e^{in\vartheta} + \sum_{n=-\infty}^{\infty} \left[(\bar{V}x)_n - f_n\right] e^{in\vartheta} = 0;\ |\vartheta| < \vartheta_0, \tag{2.91}$$

$$\sum_{n=-\infty}^{\infty} x_n e^{in\vartheta} + \sum_{n=-\infty}^{\infty} \left[(Ux)_n - g_n\right] e^{in\vartheta} = 0;\ |\vartheta| > \vartheta_0, \tag{2.92}$$

where $a = \gamma_0/C_+$, $b = C_-/C_+$.

Evidently for b=1 ($C^+ = C^-$), these equations coincide with (2.36) and (2.37). Hereafter the parameter b will be called the conjugation coefficient of the dual series equations of the type (2.91) and (2.92). Assume that the imaginary part of the conjugation coefficient does not vanish (Im $b \neq 0$) and the column vectors $x = \{x_n\}_{n=-\infty}^{\infty}$, $f = \{f_n\}_{n=-\infty}^{\infty}$, and $g = \{g_n\}_{n=-\infty}^{\infty}$ are such that

$$x \in l_2(\eta), \tag{2.93}$$

$$g \in l_2(\eta), \quad f \in l_2(-\eta), \tag{2.94}$$

where $\eta = 1+(\arg b)\big/\pi, -\pi < \arg b < \pi$, and the space $l_2(\eta)$ is defined in (2.5). The matrix operators $\widehat{T}\,U\,\widehat{T}^{-1}$ and $\widehat{T}^{-1}\bar{V}\,\widehat{T}^{-1}$ are assumed to be compact in the space l_2, the matrix operator $\widehat{T}$ is given by the formula

$$\widehat{T} = \left\{\widehat{\tau}_n \delta_m^n\right\}_{m,\,n=-\infty}^{\infty}; \quad \widehat{\tau}_0 = 1, \quad \widehat{\tau}_n = |n|^{\eta/2}; \, n \neq 0. \tag{2.95}$$

Besides, the matrix operator $\bar{V}$, as opposed to (2.38), is

$$\bar{V} = V + D. \tag{2.96}$$

Here,

$$D = \left\{d_n \delta_m^n\right\}_{m,\,n=-\infty}^{\infty}; \quad d_0 = 0, \quad d_n = \begin{cases} \dfrac{\gamma_n}{C^+} - n; & n > 0 \\ \dfrac{\gamma_n}{C^+} + n\dfrac{C^-}{C^+}; & n < 0 \end{cases}.$$

The remaining requirements imposed on the values in (2.91) and (2.92) and, also, the Fourier series convergence are the same as for equations (2.31) and (2.37).

In view of (2.42) and (2.43), transform equations (2.91) and (2.92) to be similar to (2.47), (2.48), and (2.49) as follows:

$$\sum_{n\neq 0} y_n \mathrm{e}^{in\vartheta} = 0; \; |\vartheta| > \vartheta_0, \tag{2.97}$$

$$\sum_{n=1}^{\infty} y_n \mathrm{e}^{in\vartheta} - b \sum_{n=-\infty}^{-1} y_n \mathrm{e}^{in\vartheta} = \sum_{n=-\infty}^{\infty} \left(|n|\,\psi_n \delta_n - \varphi_n\right) \mathrm{e}^{in\vartheta}; \tag{2.98}$$

$$\sum_{n\neq 0} (-1)^n n^{-1} y_n = -y_0, \tag{2.99}$$

where

$$y_n = \delta_n^0 (x_0 + \psi_0) + n\,(x_n + \psi_n)\,, \; \delta_n = \begin{cases} 1; & n \geq 0 \\ b; & n < 0 \end{cases}.$$

Suppose that we are given the column vectors $\psi = \{\psi_n\}_{n=-\infty}^{\infty}$, $\varphi = \{\varphi_n\}_{n=-\infty}^{\infty}$ and check that equations (2.97), (2.98), and (2.99) are uniquely solvable for any value of the conjugation coefficient b, $\mathrm{Im}\, b \neq 0$. For this purpose, one only needs to know if the corresponding homogeneous equations ($\psi_n = \varphi_n = 0$; $n = 0, \pm 1, \ldots$) possess the trivial $y_n{=}0$, $n = 0, \pm 1, \ldots$, solution. Introduce the two functions

$$F_1(\vartheta) = \sum_{n\neq 0} y_n \mathrm{e}^{in\vartheta}, \qquad F_2(\vartheta) = \sum_{n=1}^{\infty} y_n \mathrm{e}^{in\vartheta} - b \sum_{n=-\infty}^{-1} y_n \mathrm{e}^{in\vartheta} \tag{2.100}$$

on the interval $[-\pi;\pi]$. Insofar as for $x = \{x_n\}_{n=-\infty}^{\infty}$, condition (2.93) must hold and the corresponding series in (2.91) and (2.92) are the Fourier series of their sums; functions (2.100) obey the Parseval equation

$$\int_{-\pi}^{\pi} F_1^* F_2 d\vartheta = 2\pi \sum_{n=-\infty}^{\infty} f_{1n}^* f_{2n}, \tag{2.101}$$

where $*$ indicates complex conjugation, f_{1n} and f_{2n} are the Fourier coefficients of the functions $F_1(\vartheta)$ and $F_2(\vartheta)$, respectively. From (2.97), (2.98), and (2.101), $\sum_{n=-\infty}^{\infty} f_{1n}^* f_{2n} = 0$. Therefore,

$$\sum_{n=1}^{\infty} |y_n|^2 - b \sum_{n=-\infty}^{-1} |y_n|^2 = 0. \tag{2.102}$$

After separation of the imaginary part

$$\sum_{n=-\infty}^{-1} |y_n|^2 \mathrm{Im} b = 0.$$

Hence $\sum_{n=-\infty}^{-1} |y_n|^2 = 0$ and $\sum_{n=1}^{\infty} |y_n|^2 = 0$. That is, $y_n = 0$, $n = 0,\pm1,\pm2\ldots$. From (2.99), $y_0 = 0$. And it has been shown that equations (2.97), (2.98), and (2.99) possess only a trivial solution for $\psi_n = \varphi_n = 0$, $n = 0,\pm1,\ldots$.

Now let us build a solution of these equations assuming that the column vectors $\varphi = \{\varphi_n\}_{n=-\infty}^{\infty}$ and $\psi = \{\psi_n\}_{n=-\infty}^{\infty}$ are known. To this end, reduce (2.97), (2.98), and (2.99) to the boundary value Riemann–Hilbert problem. Let $y = \{y_n\}_{n=-\infty}^{\infty}$ be the sought solution. Similar to (2.50) and (2.53), give the function $X(z)$ of a complex variable z by the formula

$$X(z) = \begin{cases} \sum_{n=-1}^{\infty} y_n z^n; |z| < 1 \\ -\sum_{n=-\infty}^{-1} y_n z^n; \quad |z| > 1 \end{cases}. \tag{2.103}$$

As follows from (2.97), this function is analytic on the complex plane with a cut along the unit-circle arc $\mathbf{P}$ connecting the points $\exp(-i\vartheta_0)$ and $\exp(i\vartheta_0)$ through the point $z = 1$. Denote by $X^+(z)$ and $X^-(z)$ the limiting values of $X(z)$ on the arc $\mathbf{P}$, correspondingly, inside and outside the unit circle $|z| \le 1$. Then from (2.98),

$$X^+(z) + bX^-(z) = \sum_{n=-\infty}^{\infty} (|n|\,\psi_n \delta_n - \varphi_n) z^n; z \in \mathbf{P}. \tag{2.104}$$

We have arrived at the boundary value Riemann–Hilbert problem: it is needed to construct the $X(z)$ function that is analytic everywhere but on the arc $\mathbf{P}$ and whose limiting values on this arc satisfy condition (2.72). The solution to this problem will be sought in the class of functions having an integrable singularity at the ends of the arc $\mathbf{P}$ and decreasing as $|z|\to\infty$. By the techniques suggested in [80], this problem solution is easily obtained in the form

$$X(z) = G(z)\left[\frac{1}{2\pi i}\int\limits_{\mathbf{P}} \frac{F(\tau)\,d\tau}{G^{+}(\tau)(\tau - z)} + C\right]; z \notin \mathbf{P}, \tag{2.105}$$

where $F(\tau) = \sum\limits_{n=-\infty}^{\infty} (|n|\,\psi_n\delta_n - \varphi_n)\,\tau^n$ and C is an arbitrary constant.

The function $G(z)$ from (2.105) is a solution of the homogeneous boundary value Riemann–Hilbert problem ($\psi_n = \varphi_n = 0$, $n = 0, \pm 1, \ldots$). It belongs to the above-mentioned class of functions and can be expressed in the form

$$G(z) = \left(z - e^{i\vartheta_0}\right)^{-1} \exp\left(\left(\frac{1}{2} - id\right)\int\limits_{\mathbf{P}} \frac{d\tau}{\tau - z}\right), \tag{2.106}$$

where $d = \ln b/2\pi$, $\ln b = \ln|b| + i\arg b$, $-\pi < \arg b < \pi$. The function $G^{+}(\tau)$ in (2.105) is the limiting value of the function $G(z)$ on the arc $\mathbf{P}$ inside the circle $|z| \le 1$.

Straightforward calculations show that the $G(z)$ function satisfies the following differential equation:

$$\frac{dG(z)}{dz} = \frac{2d\sin\vartheta_0 + \cos\vartheta_0 - z}{z^2 + 1 - 2z\cos\vartheta_0} G(z); \qquad z \neq e^{\pm i\vartheta_0}, G(0) = -e^{2\vartheta_0 d}. \tag{2.107}$$

On this basis, the $G(z)$ and $G^{-1}(z)$ functions can be expressed as the following series in terms of powers of the variable z:

$$G(z) = \begin{cases} -e^{2\vartheta_0 d}\sum\limits_{n=0}^{\infty} P_n(d,\vartheta_0)\,z^n; & |z| < 1 \\ \sum\limits_{n=0}^{\infty} P_n(d,-\vartheta_0)\,z^{-n-1}; & |z| > 1 \end{cases}, \tag{2.108}$$

$$G^{-1}(z) = \begin{cases} e^{-2\vartheta_0 d}\sum\limits_{n=0}^{\infty} Q_n(d,-\vartheta_0)\,z^n; & |z| < 1 \\ \sum\limits_{n=0}^{\infty} Q_n(d,\vartheta_0)\,z^{-n+1}; & |z| > 1 \end{cases}. \tag{2.109}$$

Here the function $P_n(d,\vartheta_0)$ satisfies the recurrence formulas

$$\begin{aligned} &P_0(d,\vartheta_0)=1, \quad P_1(d,\vartheta_0)=\cos\vartheta_0+2d\sin\vartheta_0,\\ &nP_n(d,\vartheta_0)=[(2n-1)\cos\vartheta_0+2d\sin\vartheta_0]P_{n-1}(d,\vartheta_0)-\\ &\quad-(n-1)P_{n-2}(d,\vartheta_0);\quad n=2,3,... \end{aligned} \tag{2.110}$$

and the functions $Q_n(d,\vartheta_0)$ are expressed via $P_n(d,\vartheta_0)$ as follows:

$$\begin{aligned} &Q_0(d,\vartheta_0)=1, Q_1(d,\vartheta_0)=-\cos\vartheta_0+2d\sin\vartheta_0,\\ &Q_n(d,\vartheta_0)=P_n(d,\vartheta_0)-2\cos\vartheta_0 P_{n-1}(d,\vartheta_0)+P_{n-2}(d,\vartheta_0);\\ &n=2,3,... \end{aligned} \tag{2.111}$$

Remark. For the conjugation coefficient $b=1$, it is easy to see that the functions $P_n(d,\vartheta_0)$ coincide with the Legendre polynomials and, furthermore, the function $G(z)$ is no different from the function $R^{-1}(z)$ [see (2.55), (2.56), and (2.57)].

For the next step toward the solution of equations (2.97), (2.98), and (2.99), take the Sokhotskyi-Plemelj formulas [94] for the Cauchy-type integral. The application of these formulas to (2.105) finally gives

$$\sum_{n\neq 0} y_n e^{in\vartheta}=\frac{b-1}{b}\widehat{F}\left(e^{i\vartheta}\right)+\widehat{G}\left(e^{i\vartheta}\right)\left[\frac{1}{2\pi i}\int\limits_{\mathbf{P}}\frac{F(\tau)\,d\tau}{G^{+}(\tau)\left(\tau-e^{i\vartheta}\right)}+C\right];-\pi\le t\le\pi, \tag{2.112}$$

where

$$\widehat{G}\left(e^{i\vartheta}\right)=G^{+}\left(e^{i\vartheta}\right)-G^{-}\left(e^{i\vartheta}\right);\ \widehat{F}\left(e^{i\vartheta}\right)=\begin{cases}0; & |\vartheta|>\vartheta_0\\ F\left(e^{i\vartheta}\right); & |\vartheta|<\vartheta_0\end{cases}\quad\text{and}$$
$$G^{-}\left(e^{i\vartheta}\right)=\lim_{\xi\to+0}G\left(e^{i\vartheta}(1+\xi)\right).$$

Calculate the singular integral in (2.112) (say, by using the Cauchy residue theorem [94] and expanding the functions $G(z)$ and $G^{-1}(z)$ from (2.108) and (2.109) into power series) and match the Fourier coefficients to have

$$y_0=\widehat{W}_0\varphi_0+\sum_{n\neq 0}n^{-1}\widehat{V}_{n-1}^{-1}(d,\vartheta_0)(|n|\psi_n\delta_n-\varphi_n), \tag{2.113}$$

$$y_m=\sum_{n=-\infty}^{\infty}\widehat{V}_{m-1}^{n-1}(d,\vartheta_0)(|n|\psi_n\delta_n-\varphi_n);m=\pm1,\pm2,... \tag{2.114}$$

The values $\widehat{W}_0$ and $\widehat{V}_{m-1}^{n-1}(d,\vartheta_0)$ are expressed via the functions $P_n(d,\vartheta_0)$ and $Q_n(d,\vartheta_0)$ by the formulas below. If $m=n$,

$$\widehat{V}_{m-1}^{m-1}(d,\vartheta_0)=\left(1+\mathrm{e}^{2\pi d}\right)^{-1}\begin{cases}0;m=0\\ \sum\limits_{n=0}^{m}Q_{m-n}(d,\vartheta_0)\,P_{n-m}(d,-\vartheta_0);m\geq 1\\ -\sum\limits_{n=0}^{|m|}Q_{|m|-n}(d,-\vartheta_0)\,P_{n+m}(d,\vartheta_0);\ m\leq -1\end{cases}. \tag{2.115}$$

If $m\neq n$,

$$\widehat{V}_{m-1}^{n-1}(d,\vartheta_0)=\left(1+\mathrm{e}^{2\pi d}\right)^{-1}\times \\ \times\begin{cases}\dfrac{\mathrm{e}^{2d\vartheta_0}m}{m-n}[P_{m-1}(d,\vartheta_0)\,P_n(d,\vartheta_0)-P_m(d,\vartheta_0)\,P_{n-1}(d,\vartheta_0)];n\neq 0\\ \mathrm{e}^{2d\vartheta_0}P_{m-1}(d,\vartheta_0)-P_m(d,\vartheta_0);n=0\end{cases}, \tag{2.116}$$

$$\widehat{W}_0=\left(1+\mathrm{e}^{2\pi d}\right)^{-1}\sum_{n=1}^{\infty}\frac{(-1)^n}{n}[\mathrm{e}^{2d\vartheta_0}P_{n-1}(d,\vartheta_0)+\mathrm{e}^{-2d\vartheta_0}P_{n-1}(d,-\vartheta_0)+ \\ +P_n(d,-\vartheta_0)+P_n(d,\vartheta_0)]. \tag{2.117}$$

By definition, for the $P_n(d,\vartheta_0)$ functions with negative n indices, we have

$$P_n(d,\vartheta_0)=\mathrm{e}^{-2d\vartheta_0}P_{|n|-1}(d,-\vartheta_0);n=-1,-2,... \tag{2.118}$$

So, formulas (2.113), (2.114), and (2.115), (2.116), (2.117), and (2.118) give a closed-form solution to equations (2.97), (2.98), and (2.99). This solution makes it possible to reduce the initial equations (2.91) and (2.98) to an infinite system of linear algebraic equations of the second kind.

Indeed, pass to the unknowns $x=\{x_n\}_{n=-\infty}^{\infty}$ in (2.113) and (2.114) and introduce the new column vectors $\widehat{x}=\left\{\widehat{x}_n\right\}_{n=-\infty}^{\infty}$, $\widehat{\psi}=\left\{\widehat{\psi}_n\right\}_{n=-\infty}^{\infty}$, $\widehat{\varphi}=\left\{\widehat{\varphi}_n\right\}_{n=-\infty}^{\infty}$ according to the formulas

$$\widehat{x}=\widehat{T}x,\quad \widehat{\psi}=\widehat{T}\psi,\quad \widehat{\varphi}=\widehat{T}^{-1}\varphi. \tag{2.119}$$

Let us remind that the operator $\widehat{T}$ is defined in (2.95). Then (2.113) and (2.114) can be expressed in the vector form

$$\widehat{x}=\widehat{W}\left(\widehat{D}\,\widehat{\psi}-\widehat{\varphi}\right)+\left(\widehat{P}-E\right)\widehat{\psi}. \tag{2.120}$$

The matrix operators $\widehat{W},\widehat{D},\widehat{P}$ are defined as $\widehat{W} = \left\{\widehat{W}_{mn}\right\}_{m,n=-\infty}^{\infty}$, $\widehat{P} = \left\{\widehat{P}_{mn}\right\}_{m,n=-\infty}^{\infty}$, $\widehat{D} = \left\{\delta_n\delta_n^m\right\}_{m,n=-\infty}^{\infty}$, with

$$\widehat{W}_{mn} = \begin{cases} -\widehat{W}_0; & m=n=0 \\ \dfrac{\widehat{\tau}_n\,\widehat{V}_{n-1}^{-1}(d,\vartheta_0)}{n}; & n\neq 0, \quad m=0 \\ \dfrac{\widehat{\tau}_n\,\widehat{\tau}_m\,\widehat{V}_{m-1}^{n-1}(d,\vartheta_0)}{m}; & m\neq 0 \end{cases}, \quad \widehat{P}_{mn} = \begin{cases} \widehat{W}_0; & m=n=0 \\ -\widehat{W}_{m0}; & m\neq 0, \quad n=0 \\ 0; & n\neq 0 \end{cases},$$

and

$$\delta_n = \begin{cases} 1; & n\geq 0 \\ b; & n<0 \end{cases}, \quad \widehat{\tau}_n = \begin{cases} 1; & n=0 \\ |n|^{\eta/2}; & n>0 \end{cases}, \quad \eta = 1+\frac{\arg b}{\pi}.$$

In view of (2.80), exclude $\widehat{\varphi}$ and $\widehat{\psi}$ from (2.120) to obtain the following equation for the unknown column vectors $\widehat{x}$:

$$\left(E+\widehat{H}\right)\widehat{x} = \widehat{b}\,, \tag{2.121}$$

where

$$\widehat{H} = -a\,\widehat{P} + \left(E-\widehat{P}\right)\widehat{U} + \widehat{W}\left(\widehat{V}-\widehat{D}\,\widehat{U}\right), \quad \widehat{b} = \left(E-\widehat{P}\right)\widehat{g} + \widehat{W}\left(\widehat{f}-\widehat{D}\,\widehat{g}\right).$$

The compactness of the matrix operator $\widehat{H}$ in the space l_2 is shown using the asymptotic estimates of the functions $P_n(d,\vartheta_0)$ at a large index $|n|\to\infty$, the same as it was done in the case when the conjugation coefficient is $b=1$, saving us from having to go into the details. A mention should be only made that the asymptotic estimates of the $P_n(d,\vartheta_0)$ function can be obtained by the method of generating functions [94]. For $n\to+\infty$,

$$P_n(d,\vartheta_0) = \left[\Gamma\left(\frac{1}{2}+id\right)\right]^{-1}\left(1-\mathrm{e}^{i2\vartheta_0}\right)^{-1/2+id}\mathrm{e}^{-in\vartheta_0}n^{-1/2+id}\left(1+O\left(\frac{1}{n}\right)\right), \tag{2.122}$$

where $d=(\ln b)/2\pi$ and $\Gamma(\ldots)$ is the gamma function. The asymptotical estimation for $n\to-\infty$ comes directly from (2.118). It is easily checked that for $b=1$, formula (2.122) agrees with the Legendre polynomial asymptotical estimation $P_n(\cos\vartheta_0)$.

Thus, it has been demonstrated that the dual series equations (2.91) and (2.92) are reduced to an infinite system of linear algebraic equations of the second kind of the type (2.121). In the subsequent sections, this fact will be used for designing numerical algorithms to solve the problem of plane electromagnetic wave diffraction by perfectly conducting strip gratings located on the interface of a magnetoactive plasma-type medium.

2.2.4 The System of Dual Series Equations and Riemann–Hilbert Vector Problem

So far, we have dealt with such dual series equations whose regularization algorithm is effectively constructed using the explicit solution of the conjugation (Riemann–Hilbert) problem in theory of analytic functions. However, in diffraction problems of single-periodic gratings one often faces systems of dual equations whose nature differs from what was discussed in Sections 2.2.1, 2.2.2, and 2.2.3. Generally, they can be written in the form

$$\sum_{n=-\infty}^{\infty} x_n \mathrm{e}^{in\vartheta} = 0;\ |\vartheta| < \vartheta_0, \tag{2.123}$$

$$\sum_{n=-\infty}^{\infty} |n|\,(bx_n + y_n)\,\mathrm{e}^{in\vartheta} + \sum_{n=-\infty}^{\infty} \left[\left(V^{11}x\right)_n + \left(V^{12}y\right)_n - f_{1n}\right]\mathrm{e}^{in\vartheta} = 0;\ |\vartheta| < \vartheta_0, \tag{2.124}$$

$$\sum_{n=-\infty}^{\infty} y_n \mathrm{e}^{in\vartheta} = 0;\ |\vartheta| > \vartheta_0, \tag{2.125}$$

$$\sum_{n=-\infty}^{\infty} |n|\,(ay_n + x_n)\,\mathrm{e}^{in\vartheta} + \sum_{n=-\infty}^{\infty} \left[\left(V^{21}x\right)_n + \left(V^{22}y\right)_n - f_{2n}\right]\mathrm{e}^{in\vartheta} = 0;\ |\vartheta| > \vartheta_0. \tag{2.126}$$

Here, $x = \{x_n\}_{n=-\infty}^{\infty}$, $y = \{y_n\}_{n=-\infty}^{\infty}$ are the unknown column vectors, $V^{pq} = \left\{V_{mn}^{pq}\right\}_{m,n=-\infty}^{\infty}$, $p,q = 1,2$, are the given infinite-dimensional matrix operators, $(V^{pq}x)$ $(V^{pq}y)$ are the nth components of the column vectors $(V^{pq}x)_n$ and $(V^{pq}y)_n$, respectively, $f_1 = \{f_{1n}\}_{n=-\infty}^{\infty}$ and $f_2 = \{f_{2n}\}_{n=-\infty}^{\infty}$ are some given column vectors, $\vartheta_0 \in (0;\pi)$, and a and b are, in general, some complex numbers.

The assumptions about the Fourier series convergence in (2.123), (2.124), (2.125), and (2.126) are identical to those in Section 2.2.2. The matrix operators V^{pq}, $p,q = 1,2$, meet the condition that the operators $T^{-1}V^{pq}T^{-1}$ are compact in the space l_2, with operator T defined by formula (2.41). A solution of system (2.123)–(2.126) will be sought in the space $l_2(1)$ [see (2.37)], the known column vectors are assumed to be $f_1, f_2 \in l_2(-1)$. The standard equation system corresponding to (2.123), (2.124), (2.125), and (2.126) is provided by putting $V^{pq} = 0$, $p,q = 1,2$. The nearest task is to derive an analytic solution to the standard equations, the column vectors x and y expressed explicitly via the column vectors f_1 and f_2. After that it will be shown how the infinite system of linear algebraic equations of the second kind, equivalent to system (2.123), (2.124), (2.125), and (2.126), should be constructed.

The basic idea of the explicit solution of the system of standard dual series equations is the conversion to some Riemann–Hilbert vector problem (the conjugation problem in theory of vector analytic functions). Generally speaking, this problem cannot be explicitly solved for arbitrary values of the parameters a and b, which

forces us to restrict the consideration to the case $0 \le ab < 1$ [see (2.124) and (2.126)]. Later on, we will see that this condition is actually satisfied for problems of wave diffraction by a single-periodic grating located on the chiral plane layer interface (Section 2.6).

The interested reader can easily check that system (2.124), (2.125), and (2.126) with $a = b = 0$ is identical to equations (2.33) and (2.34), which makes it possible to use the results from Section 2.2.2 as such.

Proceed to the case $a \neq 0$ and $b \neq 0$. The first thing to do is to verify the unique solvability of the system of standard equations in the space $l_2(1)$ [see (2.124), (2.125), and (2.126) with $V^{pq} = 0$].

Let $f_1 = f_2 = 0$. To prove the unique solvability of the system of standard equations, the existence of the trivial solution $x = 0$ and $y = 0$ will suffice. Assume the contrary, implying that a solution of the standard equations is $x \neq 0$, $y \neq 0$ rather than x, $y = 0$. Introduce the functions

$$F_1(\vartheta) = \sum_{n=-\infty}^{\infty} |n| (ay_n + x_n) \mathrm{e}^{in\vartheta}, \quad F_2(\vartheta) = \sum_{n=-\infty}^{\infty} |n| (bx_n + y_n) \mathrm{e}^{in\vartheta}, \tag{2.127}$$

$$F_3(\vartheta) = \sum_{n=-\infty}^{\infty} x_n \mathrm{e}^{in\vartheta}, \quad F_4(\vartheta) = \sum_{n=-\infty}^{\infty} y_n \mathrm{e}^{in\vartheta}. \tag{2.128}$$

Complying with the previous assumptions about the Fourier series appearing in (2.124), (2.125), and (2.126), these functions obey the equality

$$\int_{-\pi}^{\pi} F_1(\vartheta) F_4^*(\vartheta) \, d\vartheta = 0, \quad \int_{-\pi}^{\pi} F_2(\vartheta) F_3^*(\vartheta) \, d\vartheta = 0. \tag{2.129}$$

As before, the asterisk $*$ indicates complex conjugation. Substituting (2.127) and (2.128) into (2.129) yields

$$\sum_{n=-\infty}^{\infty} |n| \left(ay_n x_n^* + |x_n|^2 \right) = 0, \quad \sum_{n=-\infty}^{\infty} |n| \left(bx_n y_n^* + |y_n|^2 \right) = 0 \tag{2.130}$$

whence

$$b \sum_{n=-\infty}^{\infty} |n| \, |x_n|^2 = a \sum_{n=-\infty}^{\infty} |n| \, |y_n|^2. \tag{2.131}$$

Now it will suffice to address the Cauchy–Bunyakowsky inequality

$$\left| \sum_{n=-\infty}^{\infty} |n| \, x_n y_n \right|^2 \le \sum_{n=-\infty}^{\infty} |n| \, |x_n|^2 \sum_{n=-\infty}^{\infty} |n| \, |y_n|^2,$$

which, in view of (2.131), leads to the inequality $ab \ge 1$ for a and b values.

Thus, the assumption $x \neq 0$ and $y \neq 0$ results in a contradiction, which affirms that the system of standard equations is uniquely solved for $0 \leq ab < 1$.

To construct an analytic solution to these equations, write the standard equations as

$$\sum_{n=-\infty}^{\infty} nx_n \mathrm{e}^{in\vartheta} = 0;\ |\vartheta| < \vartheta_0, \tag{2.132}$$

$$\sum_{n=-\infty}^{\infty} |n|\,(bx_n + y_n)\,\mathrm{e}^{in\vartheta} = \sum_{n=-\infty}^{\infty} f_{1n}\mathrm{e}^{in\vartheta};\ |\vartheta| < \vartheta_0, \tag{2.133}$$

$$\sum_{n=-\infty}^{\infty} ny_n \mathrm{e}^{in\vartheta} = 0;\ |\vartheta| > \vartheta_0, \tag{2.134}$$

$$\sum_{n=-\infty}^{\infty} |n|\,(ay_n + x_n)\,\mathrm{e}^{in\vartheta} = \sum_{n=-\infty}^{\infty} f_{2n}\mathrm{e}^{in\vartheta};\ |\vartheta| > \vartheta_0, \tag{2.135}$$

$$\sum_{n\neq 0} x_n = -x_0,\ \ \sum_{n\neq 0} (-1)^n y_n = -y_0. \tag{2.136}$$

They are evidently equivalent to (2.123), (2.124), (2.125), and (2.126) for $V^{pq} = 0$, $p,q = 1,2$.

Let us show that (2.132), (2.133), (2.134), and (2.135) can be reduced to the Riemann–Hilbert vector problem in the theory of analytic functions [80]. Introduce some piecewise analytic vector functions $\Phi^{\pm}(z)$ as follows:

$$\Phi^{\pm}(z) = \left\{ \begin{matrix} X^{\pm}(z) \\ Y^{\pm}(z) \end{matrix} \right\}, \tag{2.137}$$

with

$$X^{+}(z) = \sum_{n=1}^{\infty} nx_n z^n,\ \ Y^{+}(z) = \sum_{n=1}^{\infty} ny_n z^n, \qquad X^{-}(z) = -\sum_{n=-\infty}^{-1} nx_n z^n.$$
$$Y^{-}(z) = -\sum_{n=-\infty}^{-1} ny_n z^n.$$

The functions $\Phi^{+}(z)$ and $\Phi^{-}(z)$ are clearly analytic, respectively, inside and outside the unit circle. From (2.132), (2.133), (2.134), and (2.135), it follows that the limiting values of these functions on the circle $|z| = 1$ satisfy the conditions

$$\Phi^{+}\left(\mathrm{e}^{i\vartheta}\right) = G_1 \Phi^{-}\left(\mathrm{e}^{i\vartheta}\right) + F_1\left(\mathrm{e}^{i\vartheta}\right);\ |\vartheta| < \vartheta_0, \tag{2.138}$$

$$\Phi^{+}\left(\mathrm{e}^{i\vartheta}\right) = G_2 \Phi^{-}\left(\mathrm{e}^{i\vartheta}\right) + F_2\left(\mathrm{e}^{i\vartheta}\right);\ |\vartheta| > \vartheta_0 \tag{2.139}$$

with G_1, G_2 being quadratic matrices of the appearance

$$G_1 = \begin{Bmatrix} 1 & 0 \\ -2b & -1 \end{Bmatrix}, G_2 = \begin{Bmatrix} -1 & -2a \\ 0 & 1 \end{Bmatrix} \tag{2.140}$$

and with the vector functions

$$F_1\left(\mathrm{e}^{i\vartheta}\right) = \begin{Bmatrix} 0 \\ f_1\left(\mathrm{e}^{i\vartheta}\right) \end{Bmatrix}, F_2\left(\mathrm{e}^{i\vartheta}\right) = \begin{Bmatrix} f_2\left(\mathrm{e}^{i\vartheta}\right) \\ 0 \end{Bmatrix},$$

where

$$f_1\left(\mathrm{e}^{i\vartheta}\right) = \sum_{n=-\infty}^{\infty} f_{1n}\mathrm{e}^{in\vartheta} \text{ and } f_2\left(\mathrm{e}^{i\vartheta}\right) = \sum_{n=-\infty}^{\infty} f_{2n}\mathrm{e}^{in\vartheta}.$$

So, we have arrived at the Riemann–Hilbert vector problem to determine the two vector functions $\Phi^+(z)$ and $\Phi^-(z)$ that are analytic, respectively, inside and outside the circle $|z| < 1$. On the circle, the limiting values of these functions satisfy conditions (2.138) and (2.139). With the restriction $0 < ab < 1$ imposed on the a and b values, the solution to this problem is available in explicit form. Let us derive it on the assumption that the sought vector functions $\Phi^{\pm}(z)$ have an integrable singularity at the discontinuity points of the matrix coefficients G_1 and G_2, that is, at $z = \exp(\pm i\vartheta_0)$.

Introduce the new vector functions

$$\begin{gathered} \widehat{\Phi}^+(z) = \Phi^+(z) - F_2^+(z), \quad \widehat{\Phi}^-(z) = G_2\Phi^-(z) + F_2^-(z); \\ F_2^{\pm}(z) = \begin{Bmatrix} f_2^{\pm}(z) \\ 0 \end{Bmatrix}, \end{gathered} \tag{2.141}$$

where $f_2^+(z) = \sum_{n=0}^{\infty} f_{2n}z^n$ for $|z| \le 1$ and $f_2^-(z) = \sum_{n=-\infty}^{-1} f_{2n}z^n$ for $|z| \ge 1$. With these $\widehat{\Phi}^{\pm}(z)$ functions, relations (2.106) and (2.107) become

$$\widehat{\Phi}^+\left(e^{i\vartheta}\right) = G_1G_2\,\widehat{\Phi}^-\left(\mathrm{e}^{i\vartheta}\right) + \widehat{F}\left(\mathrm{e}^{i\vartheta}\right); \ |\vartheta| < \vartheta_0, \tag{2.142}$$

$$\widehat{\Phi}^+\left(\mathrm{e}^{i\vartheta}\right) = \widehat{\Phi}^-\left(\mathrm{e}^{i\vartheta}\right); \ |\vartheta| > \vartheta_0, \tag{2.143}$$

where

$$\widehat{F}\left(\mathrm{e}^{i\vartheta}\right) = F_1\left(\mathrm{e}^{i\vartheta}\right) - F_2^+\left(\mathrm{e}^{i\vartheta}\right) - G_1G_2F_2^-\left(\mathrm{e}^{i\vartheta}\right).$$

Direct calculations suggest that the square matrix G_1G_2 can be written

$$G_1G_2 = PDP^{-1}, \tag{2.144}$$

with

$$D = \left\{ \begin{matrix} \lambda_+ & 0 \\ 0 & \lambda_- \end{matrix} \right\}; \lambda_\pm = 2ab - 1 \pm i2\sqrt{ab - a^2b^2}$$

and the matrices

$$P = \left\{ \begin{matrix} 1 & -\frac{2a}{1+\lambda_-} \\ -\frac{2b}{1+\lambda_-} & 1 \end{matrix} \right\}, P^{-1} = (1-\lambda_+)^{-1} \left\{ \begin{matrix} 1 & \frac{2a}{1+\lambda_-} \\ \frac{2b}{1+\lambda_-} & 1 \end{matrix} \right\}.$$

In view of representation (2.144), introduce the vector functions $\tilde{\Phi}^{\pm}(z) = P^{-1}\,\widehat{\Phi}^{\pm}(z)$. Then (2.142) and (2.143) take on the appearance

$$\tilde{\Phi}^{+}\left(e^{i\vartheta}\right) = D\tilde{\Phi}^{-}\left(e^{i\vartheta}\right) + \tilde{F}\left(e^{i\vartheta}\right);\ |\vartheta| < \vartheta_0, \tag{2.145}$$

$$\tilde{\Phi}^{+}\left(e^{i\vartheta}\right) = \tilde{\Phi}^{-}\left(e^{i\vartheta}\right);\ |\vartheta| > \vartheta_0, \tag{2.146}$$

where

$$\tilde{F}\left(e^{i\vartheta}\right) = P^{-1}\,\widehat{F}\left(e^{i\vartheta}\right) = P^{-1}F_1\left(e^{i\vartheta}\right) - P^{-1}F_2^{+}\left(e^{i\vartheta}\right) - DP^{-1}F_2^{-}\left(e^{i\vartheta}\right).$$

Thus, by equivalent transformations, we arrived at the Riemann–Hilbert vector problem (2.145) and (2.146), with the conjugation coefficient being the diagonal matrix D. Clearly this problem falls into the two Riemann–Hilbert scalar problems similar to those considered in Section 2.2.3. Namely,

$$\tilde{X}^{+}\left(e^{i\vartheta}\right) = \lambda_+\tilde{X}^{-}\left(e^{i\vartheta}\right) + \tilde{f}_1\left(e^{i\vartheta}\right);\ |\vartheta| < \vartheta_0, \tag{2.147}$$

$$\tilde{X}^{+}\left(e^{i\vartheta}\right) = \tilde{X}^{-}\left(e^{i\vartheta}\right);\ |\vartheta| > \vartheta_0, \tag{2.148}$$

$$\tilde{Y}^{+}\left(e^{i\vartheta}\right) = \lambda_-\tilde{Y}^{-}\left(e^{i\vartheta}\right) + \tilde{f}_2\left(e^{i\vartheta}\right);\ |\vartheta| < \vartheta_0, \tag{2.149}$$

$$\tilde{Y}^{+}\left(e^{i\vartheta}\right) = \tilde{Y}^{-}\left(e^{i\vartheta}\right);\ |\vartheta| > \vartheta_0. \tag{2.150}$$

Here, $\tilde{X}^{\pm}(\exp(i\vartheta))$, $\tilde{Y}^{\pm}(\exp(i\vartheta))$ and $\tilde{f}_1(\exp(i\vartheta)), \tilde{f}_2(\exp(i\vartheta))$ are components of the vector functions $\tilde{\Phi}^{\pm}(\exp(i\vartheta))$ and $\tilde{F}(\exp(i\vartheta))$, respectively.

The solution to problems (2.147), (2.148), (2.149), and (2.150) is [80]

$$\tilde{X}(z) = G_x(z)\left[\frac{1}{2\pi i}\int\limits_{\mathbf{P}} \frac{\tilde{f}_1(\vartheta)\,d\vartheta}{G_x^{+}(\vartheta)(\vartheta - z)} + C_x\right], \tag{2.151}$$

$$\tilde{Y}(z) = G_y(z)\left[\frac{1}{2\pi i}\int\limits_{\mathbf{P}} \frac{\tilde{f}_2(\vartheta)\,d\vartheta}{G_y^{+}(\vartheta)(\vartheta - z)} + C_y\right], \tag{2.152}$$

where $\mathbf{P}$ is the arc connecting $z = \exp(-i\vartheta_0)$ and $z = \exp(i\vartheta_0)$ points through the point $z = 1$ on the circle $|z\hat{o} = 1$, C_x and C_y are arbitrary constants. The functions

$G_{x,y}(z)$ are solutions of the homogeneous Riemann–Hilbert problems ($\tilde{f}_1 = \tilde{f}_2 = 0$) coming from (2.106) upon the substitution $d = d_{\pm} = \ln(-\lambda_{\pm})/2\pi$. The functions $G^{+}{}_{x,y}(\vartheta)$ give the limiting values of $G_{x,y}(z)$ on the arc **P** inside the circle, $|z| < 1$. Now let us show how a solution of standard equations (2.132), (2.133), (2.134), (2.135), and (2.136) should be constructed using (2.151) and (2.152).

First of all, take advantage of the relationship between the vector functions $\Phi^{+}(z)$ and $\tilde{\Phi}^{\pm}(z)$

$$\Phi^{+}(z) = P\tilde{\Phi}^{+}(z) + F_2^{+}(z);\ |z| \le 1, \tag{2.153}$$

$$\Phi^{-}(z) = G_2 P\tilde{\Phi}^{-}(z) + G_2 F_2^{-}(z);\ |z| \ge 1. \tag{2.154}$$

Substituting the expressions of quadratic P and G_2 matrices into (2.153) and (2.154) and making some equivalent transformations, one gets the difference $\Phi^{+}(\exp(i\vartheta))$–$\Phi^{-}(\exp(i\vartheta))$ of the vector function limiting values on the unit circle as follows:

$$\begin{cases} X^{+}\left(e^{i\vartheta}\right) - X^{-}\left(e^{i\vartheta}\right) = \tilde{X}^{+}\left(e^{i\vartheta}\right) - \lambda_{+}\tilde{X}^{-}\left(e^{i\vartheta}\right) - \frac{2a}{1+\lambda_{-}}\left(\tilde{Y}^{+}\left(e^{i\vartheta}\right) - \lambda_{-}\tilde{Y}^{-}\left(e^{i\vartheta}\right)\right) \\ \qquad\qquad + f_2^{+}\left(e^{i\vartheta}\right) - f_2^{-}\left(e^{i\vartheta}\right) \\ Y^{+}\left(e^{i\vartheta}\right) - Y^{-}\left(e^{i\vartheta}\right) = \tilde{Y}^{+}\left(e^{i\vartheta}\right) - \tilde{Y}^{-}\left(e^{i\vartheta}\right) - \frac{2b}{1+\lambda_{-}}\left(\tilde{X}^{+}\left(e^{i\vartheta}\right) - \tilde{X}^{-}\left(e^{i\vartheta}\right)\right) \end{cases}. \tag{2.155}$$

Matching the Fourier coefficients in (2.155) yields

$$\begin{cases} x_m = \frac{\delta_m^{+}}{m}\tilde{x}_m - \frac{2a\delta_m^{-}}{(1+\lambda_{-})m}\tilde{y}_m + \frac{f_{2m}}{|m|} \\ y_m = \frac{\tilde{y}_m}{m} - \frac{2b\tilde{x}_m}{(1+\lambda_{-})m} \end{cases};\ m \ne 0, \tag{2.156}$$

$$\tilde{x}_0 = -\frac{f_{20}}{1-\lambda_{+}},\quad \tilde{y}_0 = -\frac{2bf_{20}}{\lambda_{-}-\lambda_{+}}. \tag{2.157}$$

Here $\{\tilde{x}_m\}_{m=-\infty}^{\infty}$ and $\{\tilde{y}_m\}_{m=-\infty}^{\infty}$ are the Fourier coefficients of the functions $\tilde{X}^{+}(\exp(i\vartheta)) - \tilde{X}^{-}(\exp(i\vartheta))$ and $\tilde{Y}^{+}(\exp(i\vartheta)) - \tilde{Y}^{-}(\exp(i\vartheta))$, respectively, and

$$\delta_m^{\pm} = \begin{cases} 1; & m \ge 0 \\ \lambda_{\pm}; & m < 0 \end{cases}.$$

Now, determine the Fourier coefficients $\{\tilde{x}_m\}_{m=-\infty}^{\infty}$ and $\{\tilde{y}_m\}_{m=-\infty}^{\infty}$ from (2.151) and (2.152). For this, it is sufficient to implement the results from Section 2.2.3 [see (2.113), (2.114), (2.115), (2.116), and (2.117)]. Finally,

$$\tilde{x}_m = \sum_{n=-\infty}^{\infty} \tilde{f}_{1n}\,\hat{V}_{m-1}^{n-1}(d_{+},\vartheta_0) + \tilde{x}_0 P_m(d_{+},\vartheta_0), \tag{2.158}$$

$$\tilde{y}_m = \sum_{n=-\infty}^{\infty} \tilde{f}_{2n}\,\hat{V}_{m-1}^{n-1}(d_{-},\vartheta_0) + \tilde{y}_0 P_m(d_{-},\vartheta_0);\ m = \pm 1, \pm 2, \ldots, \tag{2.159}$$

where the values $\widehat{V}_{m-1}^{n-1}(d_-,\vartheta_0)$ come from (2.115) and (2.116), and the functions $P_m(\mathrm{d}_\pm,\vartheta_0)$ are found by formula (2.78) upon the substitution $d = d\pm = \ln(-\lambda_\pm)/2\pi$. The sequences $\left\{\tilde{f}_{1n}\right\}_{n=-\infty}^{\infty}$ and $\left\{\tilde{f}_{2n}\right\}_{n=-\infty}^{\infty}$ in $\{f_{1n}\}_{n=-\infty}^{\infty}$ and $\{f_{2n}\}_{n=-\infty}^{\infty}$ terms are

$$\tilde{f}_{1n} = -\frac{\delta_n^+ f_{2n}}{1-\lambda_+} + \frac{2af_{1n}}{\lambda_- - \lambda_+}, \quad \tilde{f}_{2n} = -\frac{2b\delta_n^- f_{2n}}{\lambda_- - \lambda_+} + \frac{f_{1n}}{1-\lambda_+}. \tag{2.160}$$

Substitute (2.160) and (2.158), (2.149) into (2.156), (2.155) in view of (2.136). Then

$$x_m = \sum_{n=-\infty}^{\infty} W_{mn}^{11} f_{1n} + \sum_{n=-\infty}^{\infty} W_{mn}^{12} f_{2n}, \tag{2.161}$$

$$y_m = \sum_{n=-\infty}^{\infty} W_{mn}^{21} f_{1n} + \sum_{n=-\infty}^{\infty} W_{mn}^{22} f_{2n};\ m = 0, \pm 1, \pm 2,..., \tag{2.162}$$

the coefficients W_{mn}^{pq}, $p,q = 1,2$ are available from the formulas

$$W_{mn}^{11} = \frac{2a}{\lambda_- - \lambda_+} \begin{cases} \frac{1}{m}\left[\delta_m^+ \widehat{V}_{m-1}^{n-1}(d_+,\vartheta_0) - \delta_m^- \widehat{V}_{m-1}^{n-1}(d_-,\vartheta_0)\right]; & m \neq 0 \\ W_{n1}(d_-,\vartheta_0) - W_{n1}(d_+,\vartheta_0); & m = 0 \end{cases},$$

$$W_{mn}^{12} = \begin{cases} \frac{\delta_{mn}}{|m|} - \frac{1}{m}\left[\frac{\delta_m^+\delta_n^+ \widehat{V}_{m-1}^{n-1}(d_+,\vartheta_0)}{1-\lambda_+} + \frac{\delta_m^-\delta_n^- \widehat{V}_{m-1}^{n-1}(d_-,\vartheta_0)}{1-\lambda_-}\right] - \\ \quad -\frac{\delta_{0n}}{m}\left[\frac{\delta_m^+ P_m(d_+,\vartheta_0)}{1-\lambda_+} + \frac{\delta_m^- P_m(d_-,\vartheta_0)}{1-\lambda_-}\right]; \quad m \neq 0 \\ \frac{\delta_n^+ W_{n1}(d_+,\vartheta_0)}{1-\lambda_+} + \frac{\delta_n^- W_{n1}(d_-,\vartheta_0)}{1-\lambda_-} - \frac{1}{|n|}; \ m = 0, \quad n \neq 0 \\ \frac{W_{01}(d_+,\vartheta_0)+R_1(d_+,\vartheta_0)}{1-\lambda_+} + \frac{W_{01}(d_-,\vartheta_0)+R_1(d_-,\vartheta_0)}{1-\lambda_-}; \quad m = 0, \quad n = 0 \end{cases}$$

$$W_{mn}^{21} = \begin{cases} \frac{1}{m}\left[\frac{\widehat{V}_{m-1}^{n-1}(d_+,\vartheta_0)\lambda_+}{\lambda_+ - 1} + \frac{\widehat{V}_{m-1}^{n-1}(d_-,\vartheta_0)\lambda_-}{\lambda_- - 1}\right]; & m \neq 0 \\ \frac{W_{n2}(d_+,\vartheta_0)}{\lambda_+ - 1} + \frac{W_{n2}(d_-,\vartheta_0)}{\lambda_- - 1}; & m = 0 \end{cases},$$

$$W_{mn}^{22} = \frac{2b}{\lambda_- \lambda_+}, \begin{cases} \frac{1}{m}\left[\delta_n^+ \widehat{V}_{m-1}^{n-1}(d_+,\vartheta_0) - \delta_n^- \widehat{V}_{m-1}^{n-1}(d_-,\vartheta_0)\right] + \\ \quad + \frac{\delta_0^n}{m}\left[P_m(d_+,\vartheta_0) - P_m(d_-,\vartheta_0)\right]; m \neq 0 \\ \delta_n^- W_{n2}(d_-,\vartheta_0) - \delta_n^+ W_{n2}(d_+,\vartheta_0); \quad m = 0, \quad n \neq 0 \\ W_{02}(d_-,\vartheta_0) - W_{02}(d_+,\vartheta_0) + R_2(d_-,\vartheta_0) - R_2(d_+,\vartheta_0); \\ \quad m = 0, \quad n = 0 \end{cases}.$$

Here $W_{np}(d_\pm,\vartheta_0)$, $R_p(d_\pm,\vartheta_0)$, $p = 1, 2$, represent the series

$$W_{n1}(d_{\pm},\vartheta_0)=\sum_{m\neq 0}\frac{\delta_m^{\pm}\widehat{V}_{m-1}^{n-1}(d_{\pm},\vartheta_0)}{m},\quad W_{n2}(d_{\pm},\vartheta_0)=\sum_{m\neq 0}\frac{(-1)^m V_{m-1}^{n-1}(d_{\pm},\vartheta_0)}{m},$$
$$R_1(d_{\pm},\vartheta_0)=\sum_{m\neq 0}\frac{\delta_m^{\pm}P_m(d_{\pm},\vartheta_0)}{m},\quad R_2(d_{\pm},\vartheta_0)=\sum_{m\neq 0}\frac{(-1)^m P_m(d_{\pm},\vartheta_0)}{m}.$$

Formulas (2.161) and (2.162) provide an explicit solution of the system (2.132), (2.133), (2.134), (2.135), and (2.136) of standard dual series equations. Now this solution will be used to derive the infinite system of linear algebraic equations of the second kind for the unknown column vectors $x=\{x_n\}_{n=-\infty}^{\infty}$, $y=\{y_n\}_{n=-\infty}^{\infty}$, which is equivalent to system (2.91), (2.92), (2.93), and (2.94).

The algebraic scheme of this derivation is as follows. In the first place, we intend to express (2.161) and (2.162) in vector form. Introduce the infinite-dimensional matrices $W^{pq}=\left\{W_{mn}^{pq}\right\}_{m,n=-\infty}^{\infty}$, $p,q=1,2$, and the column vectors $f_p=\left\{f_{pn}\right\}_{n=-\infty}^{\infty}$, $p=1,2$. Then, taking care of the multiplication of a matrix by a column vector, we have expressions (2.161) and (2.162) in the form

$$x=W^{11}f_1+W^{12}f_2, \tag{2.163}$$

$$y=W^{21}f_1+W^{22}f_2. \tag{2.164}$$

Rewrite (2.123), (2.124), (2.125), and (2.126) to get

$$\begin{cases}\sum\limits_{n=-\infty}^{\infty}x_n\mathrm{e}^{in\vartheta}=0; & |\vartheta|<\vartheta_0\\ \sum\limits_{n=-\infty}^{\infty}|n|\,(bx_n+y_n)\,\mathrm{e}^{in\vartheta}=\sum\limits_{n=-\infty}^{+\infty}g_{1n}\mathrm{e}^{in\vartheta}; & |\vartheta|<\vartheta_0\\ \sum\limits_{n=-\infty}^{\infty}y_n\mathrm{e}^{in\vartheta}=0; & |\vartheta|>\vartheta_0\\ \sum\limits_{n=-\infty}^{\infty}|n|\,(ax_n+x_n)\,\mathrm{e}^{in\vartheta}=\sum\limits_{n=-\infty}^{\infty}g_{2n}\mathrm{e}^{in\vartheta}; & |\vartheta|>\vartheta_0\end{cases},$$

where $g_{1n}=f_{1n}-\left(V^{11}x\right)_n-\left(V^{12}y\right)_n$, $g_{2n}=f_{2n}-\left(V^{21}x\right)_n-\left(V^{22}y\right)_n$.

Let us solve these equations as if the column vectors $g_1=\{g_{1n}\}_{n=-\infty}^{\infty}$, $g_2=\{g_{2n}\}_{n=-\infty}^{\infty}$ were known. In view of (2.163) and (2.164),

$$x=W^{11}g_1+W^{12}g_2, \tag{2.165}$$

$$y=W^{21}g_1+W^{22}g_2. \tag{2.166}$$

Now one only needs to replace g_1, g_2 in (2.165) and (2.166) by their expressions in f_1, f_2 and x, y terms. The result is

$$x=-\left(W^{11}V^{11}+W^{12}V^{21}\right)x-\left[\left(W^{11}V^{12}+W^{12}V^{22}\right)y+W^{11}f_1+W^{12}f_2\right], \tag{2.167}$$

$$y = -\left(W^{21}V^{11} + W^{22}V^{21}\right)x - \left[\left(W^{21}V^{12} + W^{22}V^{22}\right)y + W^{21}f_1 + W^{22}f_2\right]. \tag{2.168}$$

Let us show how equation system (2.167) and (2.168) should be transformed to the system of equations of the second kind in the space l_2. Seeking a solution to system (2.123), (2.124), (2.125), and (2.126) in the $l_2(1)$ space makes us use the column vectors

$$\widehat{x} = Tx, \quad \widetilde{y} = Ty, \tag{2.169}$$

with the matrix operator T given by (2.41). One easily finds that $\widehat{x}\,, \widehat{y} \in l_2$.

Introduce the new matrices $\widehat{W}^{pq}$ and the column vectors $\widehat{b}_1$, $\widehat{b}_2$

$$\widehat{W}^{pq} = TW^{pq}T, \quad \widehat{V}^{pq} = -T^{-1}V^{pq}T^{-1}; \quad p,q = 1,2, \tag{2.170}$$

$$\widehat{b}_1 = \widehat{W}^{11}T^{-1}f_1 + \widehat{W}^{12}T^{-1}f_2, \quad \widehat{b}_2 = \widehat{W}^{21}T^{-1}f_1 + \widehat{W}^{22}T^{-1}f_2 \tag{2.171}$$

and substitute (2.169) into (2.167) and (2.168) in view of (2.170) and (2.171). Then

$$\widehat{x} = \left(\widehat{W}^{11}\,\widehat{V}^{11} + \widehat{W}^{12}\,\widehat{V}^{21}\right)\widehat{x} + \left(\widehat{W}^{11}\,\widehat{V}^{12} + \widehat{W}^{12}\,\widehat{V}^{22}\right)\widehat{y} + \widehat{b}_1, \tag{2.172}$$

$$\widehat{y} = \left(\widehat{W}^{21}\,\widehat{V}^{11} + \widehat{W}^{22}\,\widehat{V}^{21}\right)\widehat{x} + \left(\widehat{W}^{21}\,\widehat{V}^{12} + \widehat{W}^{22}\,\widehat{V}^{22}\right)\widehat{y} + \widehat{b}_2. \tag{2.173}$$

Make sure that the matrix operators in (2.172) and (2.173) are compact in l_2. Indeed, the operator $\widehat{V}^{pq}$, $p, q = 1, 2$, is compact by assumption, and the matrix $\widehat{W}^{pq}$ produces the bounded operator in l_2. The latter follows from the analytic estimates of the function $P_n(d_\pm,\vartheta_0)$ as $|n|\to\infty$ [see (2.122)] and formulas (2.116) and (2.117) for $\widehat{V}^{n-1}_{m-1}(d_\pm,\vartheta_0)$. Hence, the matrix operator $\widehat{W}^{\bar{p}\bar{q}}\,\widehat{V}^{pq}$, $p, \bar{p}, q, \bar{q} = 1,2$ is compact as a product of bounded and compact operators [70].

Thus, system (2.172) and (2.173) is an operator equation of the second kind in the space l_2, which guarantees that the solution of this equation can be obtained with any preassigned accuracy by truncation [70]. It means that infinite system (2.172) and (2.173) can be replaced by the finite system for the N unknowns. This method is used in working relevant diffraction problems of single-periodic gratings and yields solid numerical results.

2.3 Inversion of Convolution-Type Matrix Operators in System of Equations in the Mode Matching Technique

The analytic regularization procedure for the inversion of convolution-type matrix operators of infinite system of equations obtained by the mode matching (partial

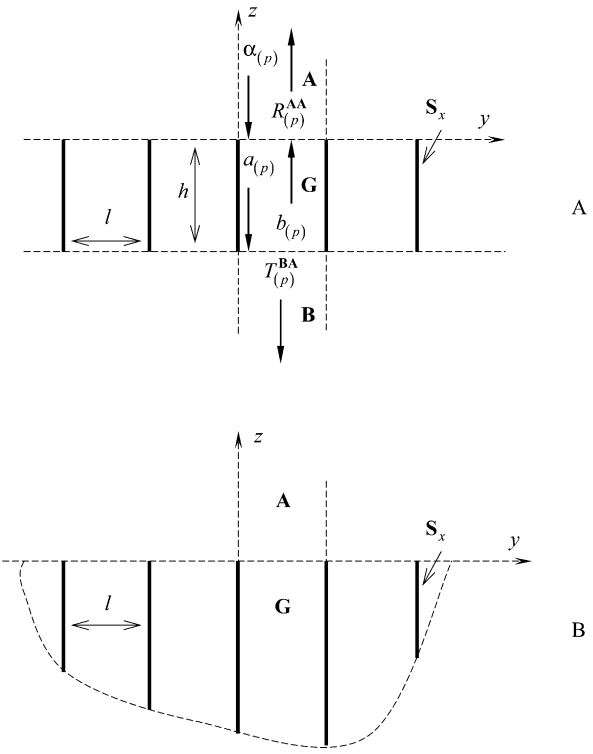

Fig. 2.1 The geometry of gratings: (**a**) Lamellar (or knife) grating and (**b**) grating of perfectly conducting half-planes

domain) method was originally suggested in [22]. Thus, the problem of plane-wave diffraction by a grating made up of vertical metal strips (see Fig. 2.1a) has been solved, and any improvement of that solution does not seem possible. The solution obtained in this way (see Section 2.3.1) is easy to transform to closed-form analytic expressions [16, 18], whether k be small or large or related to the long-wave piece of the resonant range. It can be numerically obtained by the truncation method, with the error decreasing exponentially whatever values the dimensionless parameter kl takes.

The method has been intensively promoted in electrodynamical theory of gratings. Thus, effective solutions to diffraction problems have been built for jalousie-type gratings [16, 17, 97, 98] and echelette gratings [16, 17, 99], lamellar gratings with a sophisticated periodic pattern [17, 100] and echelette gratings with obtuse and acute teeth [17, 101, 102], for dielectric echelettes with one interface metallized [17, 103] and echelettes with two absorbing interfaces [104]. The studies of these structures mainly kept in focus the resonant frequencies and had to rely on computers with limited resources. That is why every algorithmic and computational detail was elaborated very carefully. Such operating characteristics of the method as its actual convergence rate, compliance with the problem conditions,

etc., which were less open to analytic inspection, were examined by means of specially invented procedures during numerical experiments. Great efforts went into the computational realization of the algorithms. In parallel, intensive studies were conducted for their comprehensive mathematical justification [17, 105], including development of a qualitative theory of ill-posed infinite systems of linear algebraic equations resulted from the mode matching method [17, 106–108] and extension of the scope of canonical structures for which the diffraction problem solution is available in explicit analytic form [109]. The new analytic solutions essentially add to the capability of the considered method and extend its possible area of application (see Section 2.3.2).

All these results have been summarized in the books [17, 18]. The first one fully concentrates on approaches, algorithms, and relevant computational schemes. The other one presents the physical results of the theory of wave scattering by diffraction gratings achieved within 1972–1985. The present book is focused on a thorough analysis of various diffraction phenomena. It traces general, common nature scenarios of resonant and nonresonant wave scattering processes and, also, carefully studies some specific situations of both fundamental and applied significance. The main body of the book is composed of authors' original works performed in cooperation with their fellow contributors. It includes analysis of the plane-wave total transition through semitransparent structures and the total reflection from them, threshold effects (Wood's anomalies), "ghosts of grating" phenomena, regimes of the total nonspecular (autocollimation, in particular) wave reflection from nontransparent structures, analysis and synthesis of grating polarization converters for half-plane and semi-sphere scanning, etc.

2.3.1 *Lamellar Gratings: Systems of First-Kind Equations and Analytic Regularization of the Problem*

Let a lamellar grating (see Fig. 2.1a) be illuminated by a plane E-polarized wave $\tilde{U}_p^i(g,k) = \exp\left[i\left(\Phi_p y - \Gamma_p z\right)\right]$, $k > 0$ and let p be an integer. The general solution of boundary value problem (1.26) in domains **A**, **B**, and **G** is

$$\tilde{U}(g,k) = \begin{cases} \tilde{U}_p^i(g,k) + \sum\limits_{n=-\infty}^{\infty} R_{np}^{\mathbf{AA}} \exp\left[i\left(\Phi_n y + \Gamma_n z\right)\right]; & g = \{y,z\} \in \mathbf{A} \\ \sum\limits_{m=1}^{\infty} \left[a_{mp}\exp\left[-i\gamma_m z\right] + b_{mp}\exp\left[i\gamma_m (z+h)\right]\right] \sin\left(\frac{m\pi y}{l}\right); & g \in \mathbf{G} \\ \sum\limits_{n=-\infty}^{\infty} T_{np}^{\mathbf{BA}} \exp\left[i\left(\Phi_n y - \Gamma_n (z+h)\right)\right]; & g \in \mathbf{B} \end{cases} . \tag{2.174}$$

Here, $\tilde{U}(g,k) = \tilde{E}_x(g,k)$, $\gamma_m = \sqrt{k^2 - \left(m\pi/l\right)^2}$, $m = 1,2,\ldots$, are the propagation constants of the H_{0m}-waves in the regular parallel-plate waveguide segment $-h \le z \le 0$ (channel **G**) connecting the reflection and transition zones of the periodic structure, and $\mathrm{Re}\gamma_m \ge 0$, $\mathrm{Im}\gamma_m \ge 0$.

Matching the tangential components $\tilde{E}_x(g,k)$ and $\tilde{H}_y(g,k)$ of the field strength vectors on the partial domain boundaries $z=0$ and $z=-h$ yields the infinite system of linear algebraic equations of the first kind

$$\sum_{n=-\infty}^{\infty}\frac{S_{np}^{\pm}}{\Gamma_n-\gamma_m}=\frac{1}{\Gamma_p+\gamma_m}\mp e^{i\gamma_m h}\left[\sum_{n=-\infty}^{\infty}\frac{S_{np}^{\pm}}{\Gamma_n+\gamma_m}-\frac{1}{\Gamma_p-\gamma_m}\right];\ m=1,2,... \tag{2.175}$$

with the recalculation formula

$$\left(a_{mp}\pm b_{mp}\right)\frac{\gamma_m l^2}{m\pi\left[1-(-1)^m\exp\left(i2\pi\Phi\right)\right]}=\frac{1}{\Gamma_p-\gamma_m}-\sum_{n=-\infty}^{\infty}\frac{S_{np}^{\pm}}{\Gamma_n+\gamma_m};\ m=1,2,... \tag{2.176}$$

Here, $S_{np}^{\pm}=R_{np}^{\mathbf{AA}}\pm T_{np}^{\mathbf{BA}}$.

A part of the solution $\left\{S_{np}^{\pm}\right\}_n$ of problem (2.175) will be extracted that satisfies the system of equations

$$\sum_{n=-\infty}^{\infty}\frac{S_{np}}{\Gamma_n-\gamma_m}=\frac{1}{\Gamma_p+\gamma_m};\ m=1,2,... \tag{2.177}$$

and determines the generalized reflection matrix $R^{\mathbf{AA}}(\infty)=\left\{S_{np}\right\}_{n,p=-\infty}^{\infty}$ of the knife grating for $h\to\infty$. Let the amplitudes S_{np} be determined by the residual calculation technique [42] based on the Mittag-Leffler theorem about the expansion of a meromorphic function into a series of principal parts [36]. Assume that in the plane $\mathbf{C}$ of a complex variable w, there exist functions $f_p(w)$ such that:

- $f_p(w)$ have simple poles at the points $w=\Gamma_n$, $n=0,\pm1,\pm2,\ldots$, and $w=-\Gamma_p$;
- $f_p(\gamma_m)=0$, $m=1,2,\ldots$;
- $\operatorname{Res} f_p(-\Gamma_p)=1$;
- $f_p(w)\to0$ on a regular system of closed contours $\mathbf{C}_{|w|}$ in the plane $\mathbf{C}$ if $|w|\to\infty$.

Under these assumptions,

$$S_{np}=\operatorname{Res} f_p(\Gamma_n);\ n=0,\pm1,\pm2,... \tag{2.178}$$

Indeed, as for all $m=1,2,\ldots$ [36],

$$\lim_{|w|\to\infty}\frac{1}{2\pi i}\oint_{\mathbf{C}_{|w|}}\left[\frac{f_p(w)}{w-\gamma_m}\right]dw=\sum_{n=-\infty}^{\infty}\frac{\operatorname{Res} f_p(\Gamma_n)}{\Gamma_n-\gamma_m}+\frac{\operatorname{Res} f_p\left(-\Gamma_p\right)}{-\Gamma_p-\gamma_m}+f_p(\gamma_m)=0, \tag{2.179}$$

the set $\{S_{np}\}_n$ from (2.178) lends a solution to problem (2.177). The functions $f_p(w)$ possessing all the above-mentioned properties will be expressed as [16, 17]

$$f_p(w) = e^{i\ln 2(w+\Gamma_p)l/\pi} \frac{(\Gamma_0+\Gamma_p)}{(w+\Gamma_p)(\Gamma_0-w)} \prod_{s=1}^{\infty} \frac{(\gamma_s-w)(\Gamma_s+\Gamma_p)(\Gamma_{-s}+\Gamma_p)}{(\gamma_s+\Gamma_p)(\Gamma_s-w)(\Gamma_{-s}-w)}.$$

For large $|w|$ and $|n|$, one arrives at the following estimations:

$$f_p(w) = O\left[(w+\Gamma_p)^{-1} w^{-1/2}\right] \text{ and } S_{np} = \operatorname{Res} f_p(\Gamma_n) = O\left(n^{-3/2}\right).$$

An examination of the integral

$$\lim_{|w|\to\infty} \frac{1}{2\pi i} \oint_{C_{|w|}} \left[\frac{f_p(w)}{w+\gamma_m}\right] dw = \sum_{n=-\infty}^{\infty} \frac{\operatorname{Res} f_p(\Gamma_n)}{\Gamma_n+\gamma_m} + \frac{\operatorname{Res} f_p(-\Gamma_p)}{-\Gamma_p+\gamma_m} + f_p(-\gamma_m) = 0,$$

yields

$$\sum_{n=-\infty}^{\infty} \frac{S_{np}}{\Gamma_n+\gamma_m} - \frac{1}{\Gamma_p-\gamma_m} = -f_p(-\gamma_m);\ m = 1,2,... \tag{2.180}$$

Introduce the new unknowns $\bar{S}^{\pm}_{np} = S^{\pm}_{np} - S_{np}$, $n = 0, \pm 1, \pm 2, \ldots$, and change via (2.177) and (2.180) from problems (2.175) and (2.176) to the problem

$$\sum_{n=-\infty}^{\infty} \frac{\bar{S}^{\pm}_{np}}{\Gamma_n-\gamma_m} = \mp e^{i\gamma_m h}\left[\sum_{n=-\infty}^{\infty} \frac{\bar{S}^{\pm}_{np}}{\Gamma_n+\gamma_m} - f_p(-\gamma_m)\right] = e^{i\gamma_m h/2}\beta^{\pm}_{mp};\ m = 1,2,..., \tag{2.181}$$

$$(a_{mp} \pm b_{mp}) \frac{\gamma_m l^2}{m\pi\left[1-(-1)^m \exp(i2\pi\Phi)\right]} = f_p(-\gamma_m) - \sum_{n=-\infty}^{\infty} \frac{\bar{S}^{\pm}_{np}}{\Gamma_n+\gamma_m} = \pm\beta^{\pm}_m e^{-i\gamma_m h/2};$$
$$m = 1,2,... \tag{2.182}$$

It has not been possible to identify a pair of infinite-sequence spaces on which the operators of problems (2.175), (2.177), and (2.181) are bounded and have bounded inverses [17, 105, 108]. That is, algorithms for an approximate solution of these infinite systems of linear algebraic equations of the first kind (truncation solution algorithms, for one) withstand justifications [110]. Yet there have been obtained results [17, 42, 106, 107] sufficiently interesting to expect that in some cases an approximate solution of the operator equation of the nature can converge weakly (in coordinate-wise fashion) to the exact solution. Thus, for instance, the values $\bar{S}^{\pm}_{np}(N)$ found from system (2.181) truncated to the order N ($m = 1,2,\ldots,N$) converge to the

exact $\bar{S}_{np}^{\pm}$ values for each $n = -M, -M+1,...,N-M-1$ with increasing N. Yet the convergence rate essentially depends on:

- the n value;
- whether a module or a phase of the complex amplitude $\bar{S}_{np}^{\pm}(N)$ is calculated;
- a choice of the main diagonal of the system constituted by a finite number of equations (a choice of M).

When passing from lamellar gratings to jalousie gratings (see, for example, Fig. 1.3a; $\vartheta \neq 0$), the information provided by the truncated first-kind equation systems corresponding to these asymmetrical structures will be, at best, relatively true only for amplitude modules of several fundamental spatial harmonics.

A rigorous solution of boundary value problems (and, specifically, problems in electromagnetic theory of gratings) proposes algorithms where an approximate problem solution converges to the exact solution in the metric of an appropriate Hilbert space. Thus, for instance, if the solution represented by the amplitude sets $\left\{R_{np}^{\mathbf{AA}}\right\}_n$ and $\left\{T_{np}^{\mathbf{BA}}\right\}_n$, the analysis is most conveniently carried out in the infinite-sequence space $\tilde{l}_2 = \left\{a = \{a_n\}: \ \|a\|_{\tilde{l}_2}^2 = \sum_n |a_n|^2 (1+|n|) < \infty\right\}$. It acts as an energy space in processes relative to the plane-wave scattering by periodic structures [see, for example, relations (1.29)]. And the fulfillment of the conditions $\left\{R_{np}^{\mathbf{AA}}\right\}_n \in \tilde{l}_2$, $\left\{T_{np}^{\mathbf{BA}}\right\}_n \in \tilde{l}_2$ provides the uniqueness of the solution to the (1.26) type of problems for gratings with edges like interface segments where both tangents and normals are undetermined [16, 17, 42].

Return to problem (2.181) to seek its rigorous solution via the analytic inversion of the operator part given by the matrix $A = \left\{(\Gamma_n - \gamma_m)^{-1}\right\}_{m=1,\, n=-\infty}^{\infty}$. Assume the existence of meromorphic functions $\varphi_r(w)$ such that:

- $\varphi_r(w)$ have simple poles at points $w = \Gamma_n$, $n = 0,\pm1,\pm2,...$;
- $\varphi_r(\gamma_m) = -\delta_m^r$, $m,r = 1,2,...,$ δ_m^r is the Kronecker delta;
- $\varphi_r(w) \to 0$ on some regular system of closed contours $\mathbf{C}_{|w|}$ in the plane $\mathbf{C}$ if $|w| \to \infty$;
- the series $\sum_r \varphi_r(w)\, e^{i\gamma_r h/2} \beta_{rp}^{\pm}$ converges uniformly within the analyticity domain of the functions $\varphi_r(w)$.

Let us show that by these assumptions, the operator equation (2.181) is equivalent to the following operator equation of the second kind:

$$\bar{S}_{np}^{\pm} = \sum_{r=1}^{\infty} \operatorname{Res} \varphi_r(\Gamma_n)\, e^{i\gamma_r h/2} \beta_{rp}^{\pm};\ n = 0, \pm 1, \pm 2,... \tag{2.183}$$

Indeed, since

$$\lim_{|w|\to\infty}\frac{1}{2\pi i}\oint\limits_{\mathbf{C}_{|w|}}\left[(w-\gamma_m)^{-1}\sum_{r=1}^{\infty}\varphi_r(w)\,\mathrm{e}^{i\gamma_r h/2}\beta_{rp}^{\pm}\right]dw=$$
$$=\sum_{n=-\infty}^{\infty}\left(\sum_{r=1}^{\infty}\operatorname{Res}\varphi_r(\Gamma_n)\,\mathrm{e}^{i\gamma_r h/2}\beta_{rp}^{\pm}\right)\frac{1}{(\Gamma_n-\gamma_m)^{-1}}+$$
$$+\sum_{r=1}^{\infty}\varphi_r(\gamma_m)\,\mathrm{e}^{i\gamma_r h/2}\beta_{rp}^{\pm}=0;\ m=1,2,...,$$

each solution of the operator equation (2.183) will be a solution of equation (2.181). Additionally, the regularization on the left (as the previous operation is called) does not lose any solution from the solution set [111]. That is, each solution of equation (2.181) will also simultaneously be a solution of equation (2.183).

The functions $\varphi_r(w)$ that possess all the mentioned properties take the appearance [16, 17]

$$\varphi_r(w)=-\mathrm{e}^{i\ln 2(w-\gamma_r)l/\pi}\frac{(\Gamma_0-\gamma_r)}{(\Gamma_0-w)}\prod_{s=1}^{\infty(r)}\frac{(\gamma_s-w)(\Gamma_s-\gamma_r)(\Gamma_{-s}-\gamma_r)}{(\gamma_s-\gamma_r)(\Gamma_s-w)(\Gamma_{-s}-w)}.$$

Here, the index (r) over the sign of the infinite product indicates that the term $(\gamma_s-w)(\gamma_s-\gamma_r)^{-1}$ corresponding to $s=r$ is discarded. Large $|w|$ and r values satisfy the estimate [17]

$$\varphi_r(w)=O\left[\frac{\gamma_r^{1/2}}{(w-\gamma_r)\,w^{1/2}}\right]. \tag{2.184}$$

From (2.181) and (2.183), in view of the equality

$$\lim_{|w|\to\infty}\frac{1}{2\pi i}\oint\limits_{\mathbf{C}_{|w|}}\left[\frac{\varphi_r(w)}{w+\gamma_m}\right]dw=\sum_{n=-\infty}^{\infty}\frac{\operatorname{Res}\varphi_r(\Gamma_n)}{\Gamma_n+\gamma_m}+\varphi_r(-\gamma_m)=0;\ m=1,2,...,$$

one obtains

$$\begin{aligned}\beta_{mp}^{\pm}&=\mp\mathrm{e}^{i\gamma_m h/2}\left[\sum_{n=-\infty}^{\infty}\frac{\bar{S}_{np}^{\pm}}{\Gamma_n+\gamma_m}-f_p(-\gamma_m)\right]=\\&=\mp\mathrm{e}^{i\gamma_m h/2}\left[\sum_{n=-\infty}^{\infty}\left[\frac{1}{\Gamma_n+\gamma_m}\sum_{r=1}^{\infty}\mathrm{e}^{i\gamma_r h/2}\operatorname{Res}\varphi_r(\Gamma_n)\,\beta_r^{\pm}\right]-f_p(-\gamma_m)\right]=\\&=\mp\mathrm{e}^{i\gamma_m h/2}\left[\sum_{r=1}^{\infty}\mathrm{e}^{i\gamma_r h/2}\beta_r^{\pm}\sum_{n=-\infty}^{\infty}\frac{\operatorname{Res}\varphi_r(\Gamma_n)}{\Gamma_n+\gamma_m}-f_p(-\gamma_m)\right]=\\&=\pm\mathrm{e}^{i\gamma_m h/2}\left[\sum_{r=1}^{\infty}\mathrm{e}^{i\gamma_r h/2}\beta_r^{\pm}\varphi_r(-\gamma_m)+f_p(-\gamma_m)\right];\ m=1,2,...\end{aligned} \tag{2.185}$$

So, the initial problem has been reduced [see (2.181), (2.182), and (2.185)] to the infinite systems of linear algebraic equations of the second kind

$$\beta_{mp}^{\pm} = \pm e^{i\gamma_m h/2}\left[\sum_{r=1}^{\infty} e^{i\gamma_r h/2}\beta_{rp}^{\pm}\varphi_r(-\gamma_m) + f_p(-\gamma_m)\right]; m = 1,2,... \quad (2.186)$$

(to the operator equations $\left[E + B^{\pm}(k)\right]\beta_{(p)}^{\pm} = b_{(p)}^{\pm}$, where E is the identity matrix, $B^{\pm}(k) = \left\{B_{mr}^{\pm} = \mp e^{i(\gamma_m+\gamma_r)h/2}\varphi_r(-\gamma_m)\right\}_{m,r=1}^{\infty}$, $b_{(p)}^{\pm} = \left\{b_{mp}^{\pm} = \pm f_p(-\gamma_m)e^{i\gamma_m h/2}\right\}_m$, and $\beta_{(p)}^{\pm} = \left\{\beta_{mp}^{\pm}\right\}_m$ are the unknown vectors) with the recalculation formulas

$$R_{np}^{\mathbf{AA}} \pm T_{np}^{\mathbf{BA}} = \sum_{r=1}^{\infty} \operatorname{Res}\varphi_r(\Gamma_n)e^{i\gamma_r h/2}\beta_{rp}^{\pm} + \operatorname{Res} f_p(\Gamma_n); n = 0, \pm 1, \pm 2,..., \quad (2.187)$$

$$\left(a_{mp} \pm b_{mp}\right) = \pm\beta_{mp}^{\pm}\frac{e^{-i\gamma_m h/2}m\pi\left[1 - (-1)^m \exp(i2\pi\Phi)\right]}{\gamma_m l^2}; m = 1,2,... \quad (2.188)$$

The estimates

$$B_{mr}^{\pm} = O\left[e^{-\pi(m+r)h/2l}\frac{r^{1/2}}{(m+r)m^{1/2}}\right], b_{mp}^{\pm} = O\left[e^{-\pi mh/2l}m^{-3/2}\right]; m,r \to \infty \quad (2.189)$$

suggest [70] that the operator equation (2.186) is a Fredholm equation in the sequence space $\tilde{l}_2$. This means that for all $k \notin \Omega_k$ (see Section 1.3.2), bounded inverse operators $\left[E + B^{\pm}(k)\right]^{-1}$ do exist, the unknown vectors $\beta_{(p)}^{\pm} \in \tilde{l}_2$, and infinite systems (2.186) can be solved by the truncation method converging in $\tilde{l}_2$ space norm. The evident equality

$$\beta_{(p)}^{\pm} - \beta_{(p)}^{\pm}(N) = \left(E + B^{\pm}(k)\right)^{-1}\left[\left(B^{\pm}(k) - B^{\pm}(k,N)\right)\beta_{(p)}^{\pm}(N) + \left(b_{(p)}^{\pm} - b_{(p)}^{\pm}(N)\right)\right]$$

and estimates (2.189) suggest that

$$\left\|\beta_{(p)}^{\pm} - \beta_{(p)}^{\pm}(N)\right\|_{\tilde{l}_2} = O\left[e^{-\pi(N+1)h/2l}\right]; N \to \infty,$$

$$R_{np}^{\mathbf{AA}}, T_{np}^{\mathbf{BA}} = O\left(|n|^{-3/2}\right); |n| \to \infty,$$

$$a_{mp}, b_{mp} = O\left(m^{-3/2}\right); m \to \infty.$$

Here, $\beta_{(p)}^{\pm}(N) = \left\{\beta_{mp}^{\pm}(N)\right\}_{m=1}^{N}$ is the solution of the system of equations (2.186) truncated to order N ($\left[E + B^{\pm}(k,N)\right]\beta_{(p)}^{\pm}(N) = b_{(p)}^{\pm}(N)$), $B^{\pm}(k,N) = \left\{B_{mr}^{\pm}\right\}_{m,r=1}^{N}$, and $b_{(p)}^{\pm}(N) = \left\{b_{mp}^{\pm}\right\}_{m=1}^{N}$.

2.3.2 Matrix Scheme of Analytic Regularization Procedure

The algorithmization of the problems in terms of the discussed analytic regularization procedure can be fairly simplified by the application of generalized scattering matrix technique [16, 17, 42, 112]. Let us confirm this statement by two simple examples.

First, assume the availability of the scattering matrices (see Section 1.2.1) $R^{\mathbf{AA}}(\infty) = \left\{R^{\mathbf{AA}}_{np}(\infty)\right\}^{\infty}_{n,p=-\infty}$, $T^{\mathbf{GA}}(\infty) = \left\{T^{\mathbf{GA}}_{mp}(\infty)\right\}^{\infty}_{m=1,p=-\infty}$, $R^{\mathbf{GG}}(\infty) = \left\{R^{\mathbf{GG}}_{ms}(\infty)\right\}^{\infty}_{m,s=1}$, and $T^{\mathbf{AG}}(\infty) = \left\{T^{\mathbf{AG}}_{ns}(\infty)\right\}^{\infty}_{n=-\infty,s=1}$ that provide through the relationships

$$A = R^{\mathbf{AA}}(\infty)\,\alpha + T^{\mathbf{AG}}(\infty)\,\beta,\ B = T^{\mathbf{GA}}(\infty)\,\alpha + R^{\mathbf{GG}}(\infty)\,\beta;$$
$$A = \{A_n\},\ B = \{B_m\},\ \alpha = \left\{\alpha_p\right\},\ \beta = \{\beta_s\}$$

all the amplitude–frequency characteristics of a grating made up of thin metal half-planes (see Fig. 2.1b) in the field of the E-polarized waves

$$\tilde{U}^i(g,k) = \begin{cases} \sum\limits_{p=-\infty}^{\infty} \alpha_p \exp\left[i\left(\Phi_p y - \Gamma_p z\right)\right]; & g = \{y,z\} \in \mathbf{A}, \quad k > 0 \\ \sum\limits_{s=1}^{\infty} \beta_s \exp\left(i\gamma_s z\right) \sin\left(\frac{s\pi y}{l}\right); & g \in \mathbf{G} \end{cases}. \tag{2.190}$$

Here, $A = \{A_n\}$ and $B = \{B_m\}$ are the amplitudes of the secondary field

$$\tilde{U}^s(g,k) = \begin{cases} \sum\limits_{n=-\infty}^{\infty} A_n \exp\left[i\left(\Phi_n y + \Gamma_n z\right)\right]; & g \in \mathbf{A} \\ \sum\limits_{m=1}^{\infty} B_m \exp\left(-i\gamma_m z\right) \sin\left(\frac{m\pi y}{l}\right); & g \in \mathbf{G} \end{cases}$$

($\tilde{U}(g,k) = \tilde{U}^i(g,k) + \tilde{U}^s(g,k)$) in the grating reflection zone ($\mathbf{A}$) and in the regular parallel-plate waveguide ($\mathbf{G}$).

Now, return to the lamellar grating problem (see Fig. 2.1a) considered in Section 2.3.1. Evidently (see [42, 112]) all amplitudes of waves composing the field (2.174) are related as

$$\begin{cases} R^{\mathbf{AA}}_{(p)} = R^{\mathbf{AA}}(\infty)\left[\alpha_{(p)}\right] + T^{\mathbf{AG}}(\infty)\,E(h)\left[b_{(p)}\right] \\ a_{(p)} = T^{\mathbf{GA}}(\infty)\left[\alpha_{(p)}\right] + R^{\mathbf{GG}}(\infty)\,E(h)\left[b_{(p)}\right] \\ b_{(p)} = R^{\mathbf{GG}}(\infty)\,E(h)\left[a_{(p)}\right] \\ T^{\mathbf{BA}}_{(p)} = T^{\mathbf{AG}}(\infty)\,E(h)\left[a_{(p)}\right] \end{cases}. \tag{2.191}$$

Here, $R^{\mathbf{AA}}_{(p)} = \left\{R^{\mathbf{AA}}_{np}\right\}_n$, $T^{\mathbf{BA}}_{(p)} = \left\{T^{\mathbf{BA}}_{np}\right\}_n$, $a_{(p)} = \left\{a_{mp}\right\}_m$, $b_{(p)} = \left\{b_{mp}\right\}_m$, $\alpha_{(p)} = \left\{\delta^p_n\right\}_n$, and $E(h) = \left\{\delta^s_m e^{i\gamma_m h}\right\}^{\infty}_{m,s=1}$. Formula (2.191) describes all the stages

of the formation of the response of the periodic structure to the excitation by the plane E-polarized wave $\tilde{U}_p^i(g,k) = \exp\left[i\left(\Phi_p y - \Gamma_p z\right)\right]$ (by signal $\alpha_{(p)}$). Thus, for instance, the first equation of system (2.191) can be interpreted in the following way. The signal $R_{(p)}^{\mathbf{AA}}$ (the waves $\left\{R_{np}^{\mathbf{AA}} \exp\left[i\left(\Phi_n y + \Gamma_n z\right)\right]\right\}_n$) is a sum of two signals. One of them is caused by the reflection of the primary signal $\alpha_{(p)}$ from the aperture $z = 0$ of the half-plane grating. The other is defined by the signal $b_{(p)}$ (by the waves $\left\{b_{mp}\exp\left[i\gamma_m(z+h)\right]\sin\left(m\pi y/l\right)\right\}_m$) that have arisen in the plane $z = -h$, experienced (during the propagation from the plane $z = -h$ to the plane $z = 0$) the action of the regular domain $\mathbf{G}$ (operator $E(h)$), and after that partly penetrated through the aperture $z = 0$ into domain $\mathbf{A}$. From (2.191),

$$R_{(p)}^{\mathbf{AA}} \pm T_{(p)}^{\mathbf{BA}} = R^{\mathbf{AA}}(\infty)\left[\alpha_{(p)}\right] \pm T^{\mathbf{AG}}(\infty)\,E(h)\left[a_{(p)} \pm b_{(p)}\right], \tag{2.192}$$

$$a_{(p)} \pm b_{(p)} = T^{\mathbf{GA}}(\infty)\left[\alpha_{(p)}\right] \pm R^{\mathbf{GG}}(\infty)\,E(h)\left[a_{(p)} \pm b_{(p)}\right]. \tag{2.193}$$

Let us introduce by the relations

$$a_{(p)} \pm b_{(p)} = \pm E\left(-h/2\right)E(\Phi)\left[\beta_{(p)}^{\pm}\right];\; E(\Phi) = \left\{\delta_m^s \frac{m\pi\left[1-(-1)^m\,\mathrm{e}^{i2\pi\Phi}\right]}{\gamma_m l^2}\right\}_{m,s=1}^{\infty} \tag{2.194}$$

[(2.194) is a matrix form of expressions (2.188)] the new unknowns $\beta_{(p)}^{\pm} = \left\{\beta_{mp}^{\pm}\right\}_m$ and pass from (2.192) and (2.193) to the equations

$$R_{(p)}^{\mathbf{AA}} \pm T_{(p)}^{\mathbf{BA}} = R^{\mathbf{AA}}(\infty)\left[\alpha_{(p)}\right] + T^{\mathbf{AG}}(\infty)\,E\left(h/2\right)E(\Phi)\left[\beta_{(p)}^{\pm}\right], \tag{2.195}$$

$$\beta_{(p)}^{\pm} = \pm E\left(h/2\right)E^{-1}(\Phi)\left\{T^{\mathbf{GA}}(\infty)\left[\alpha_{(p)}\right] + R^{\mathbf{GG}}(\infty)\,E\left(h/2\right)E(\Phi)\left[\beta_{(p)}^{\pm}\right]\right\}. \tag{2.196}$$

Invoking familiar representations [17] of the operators $R^{\mathbf{AA}}(\infty)$, $T^{\mathbf{GA}}(\infty)$, etc., one finds that equations (2.195) and (2.196) coincide with (2.187) and (2.186). The final result obtained in the matrix scheme formalism becomes the same but takes, at the same time, less analytic efforts.

Such a good rate of convergence as in the previous example is not always the case when the final operator equations obtained via the analytic regularization procedure are solved by the truncation method. The errors in the determination of the field amplitudes are exponentially small only when elementary scatterers in the structure geometry are separated by regular wave propagation regions, such as Floquet channel segments or segments of parallel-plate waveguides. Here those scatterers are called elementary whose diffraction problem solution is available in closed (explicit) form (see, for example [17, 104, 109, 113]). These are:

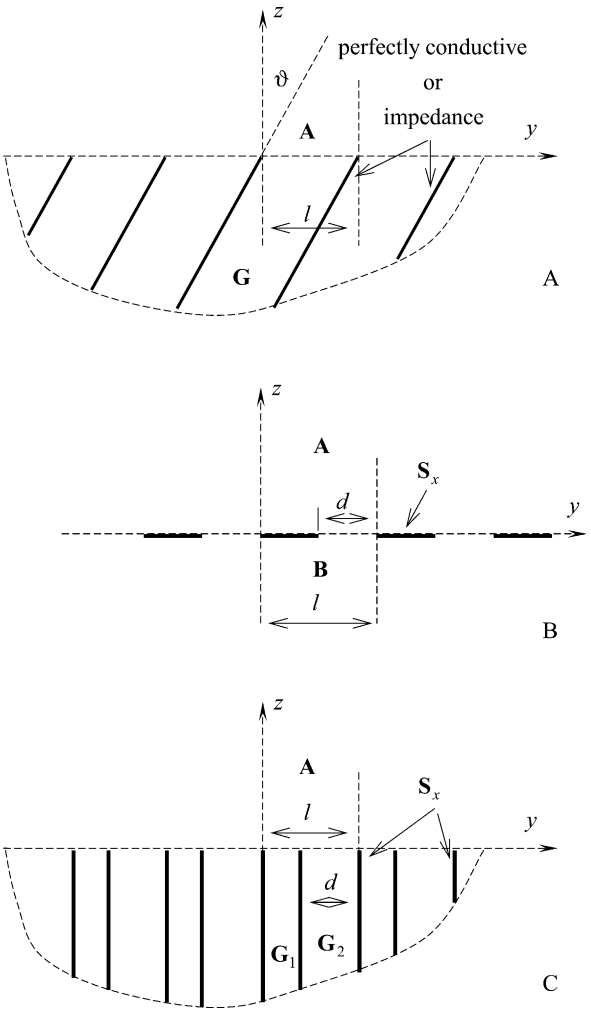

Fig. 2.2 (**a**) Gratings made of vertical and inclined half-planes, (**b**) plane strip gratings, and (**c**) grating with two half-planes in the period

- gratings of vertical or oblique half-planes, both perfectly conducting and absorbing (see Figs. 2.1b and 2.2a);
- planar half-filling strip gratings ($l = 2d$) and gratings with two half-planes per period (see Fig. 2.2b and c) – the half-integer Φ case;
- bifurcation of a parallel-plate waveguide;
- lateral (across Floquet channel or parallel-plate waveguide) interfaces, etc.

The analysis of the final operator equations of the type $[E + B(k)]\beta = b$ in the method gets much more complicated when the elementary inhomogeneities carried by the considered periodic structure cannot be spaced out with a regular wave propagation domain between them. In this case, a simpler, matrix-formalism scheme

of the analytic regularization procedure is more efficient for the following facts. The spectrum and the norm of the operators produced by the generalized scattering matrices of elementary inhomogeneities and defining [by relations like (2.192), (2.193), (2.194), (2.195), and (2.196)] all the qualitative characteristics of the problem $[E + B(k)]\beta = b$ can be evaluated in terms of the energy balance and the reciprocity relations (see Section 1.2.1 and works [17, 42, 105, 108, 114]). By functional analysis techniques [70, 110, 115], this information can be translated into the knowledge needed to prove that the operator equations $[E + B(k)]\beta = b$ are correct and solvable by truncation. It is the route that will be taken to solve the next problem.

Let an echelette grating with perfectly conducting interfaces and a 90° tooth angle (see Fig. 2.3a) be excited by a plane E-polarized wave $\tilde{U}_p^i(g,k) = \exp\left[i\left(\Phi_p y - \Gamma_p z\right)\right]$, with $k > 0$, and p an integer. Imagine the echelette wider wall shifted down along the perfectly conducting half-planes $\{g = \{y,z\}:\ y = z\mathrm{tg}\vartheta + nl;\ n = 0, \pm 1, \pm 2, ...,\ z \le 0\}$. The regular domain obtained in this way is denoted as **G** (see Fig. 2.3b). The general solution of boundary value problem (1.26) for this new structure is

$$\tilde{U}(g,k) = \begin{cases} \tilde{U}_p^i(g,k) + \sum\limits_{n=-\infty}^{\infty} R_{np}^{\mathbf{AA}} \exp\left[i\left(\Phi_n y + \Gamma_n z\right)\right]; & g = \{y,z\} \in \mathbf{A} \\ \sum\limits_{m=1}^{\infty} \left[a_{mp}\exp\left[-i\bar{\gamma}_m \bar{z}\right] + b_{mp}\exp\left[i\bar{\gamma}_m\left(\bar{z} + \bar{h}\right)\right]\right] \sin\left(\frac{m\pi\bar{y}}{l\cos\vartheta}\right); & g \in \mathbf{G} \end{cases} . \tag{2.197}$$

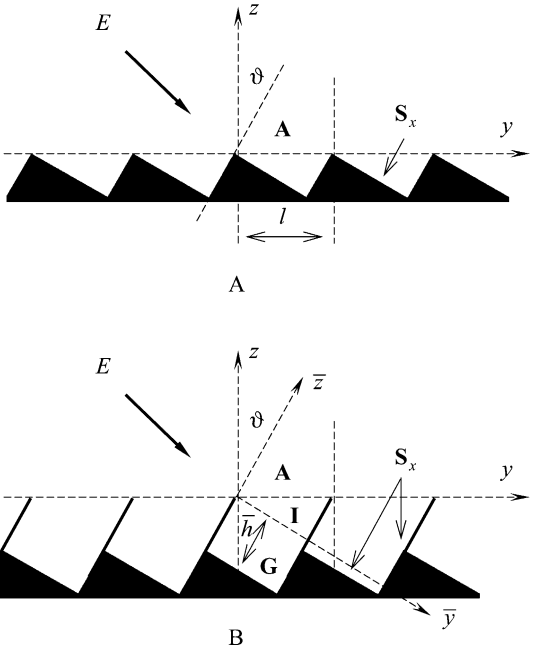

Fig. 2.3 Echelette with *rectangular tooth*: (**a**) original geometry and (**b**) modified geometry

Here, $\bar{\gamma}_m = \sqrt{k^2 - \left(m\pi/l\cos\vartheta\right)^2}$, $m = 1,2,\ldots$, $\mathrm{Re}\bar{\gamma}_m \geq 0$, $\mathrm{Im}\bar{\gamma}_m \geq 0$ are the propagation constants of the H_{0m}-waves in the segment $-\bar{h} \leq \bar{z} \leq 0$ of the regular parallel-plate waveguide (domain $\mathbf{G}$). The generalized scattering matrix method relates the amplitudes of the field (2.197) as follows:

$$\begin{cases} R^{\mathbf{AA}}_{(p)} = R^{\mathbf{AA}}(\mathrm{I})\left[\alpha_{(p)}\right] + T^{\mathbf{AG}}(\mathrm{I})\,E\left(\bar{h}\right)\left[b_{(p)}\right] \\ a_{(p)} = T^{\mathbf{GA}}(\mathrm{I})\left[\alpha_{(p)}\right] + R^{\mathbf{GG}}(\mathrm{I})\,E\left(\bar{h}\right)\left[b_{(p)}\right] \\ b_{(p)} = -E\left(\bar{h}\right)\left[a_{(p)}\right] \end{cases}. \tag{2.198}$$

Here, $E\left(\bar{h}\right) = \left\{\delta^s_m \mathrm{e}^{i\bar{\gamma}_m\bar{h}}\right\}^{\infty}_{m,s=1}$, $R^{\mathbf{AA}}_{(p)} = \left\{R^{\mathbf{AA}}_{np}\right\}_n$, $a_{(p)} = \left\{a_{mp}\right\}_m$, $b_{(p)} = \left\{b_{mp}\right\}_m$, and $\alpha_{(p)} = \left\{\delta^p_n\right\}_n$, $T^{\mathbf{GA}}(\mathrm{I}) = \left\{T^{\mathbf{GA}}_{mp}(\mathrm{I})\right\}^{\infty}_{m=1,p=-\infty}$, $R^{\mathbf{GG}}(\mathrm{I}) = \left\{R^{\mathbf{GG}}_{ms}(\mathrm{I})\right\}^{\infty}_{m,s=1}$, etc., are the scattering matrices defining all amplitude–frequency characteristics of elementary inhomogeneity $\mathbf{I}$ (grating of oblique perfectly conducting half-planes). The explicit form of these matrix operators examined by the methods of the complex variable function theory can be found in the books [16, 17] including also the estimations

$$\begin{gathered} R^{\mathbf{AA}}_{np}(\mathrm{I}) = O\left[\frac{p^{1/2}}{(|n|+|p|)n^{1/2}}\right],\ T^{\mathbf{GA}}_{mp}(\mathrm{I}) = O\left[\frac{p^{1/2}}{(m/2\cos\vartheta - |p|)m^{1/2}}\right], \\ R^{\mathbf{GG}}_{ms}(\mathrm{I}) = O\left[\frac{s^{1/2}}{(m+s)m^{1/2}}\right],\ T^{\mathbf{AG}}_{ns}(\mathrm{I}) = O\left[\frac{s^{1/2}}{(s/2\cos\vartheta - |n|)|n|^{1/2}}\right]; \\ |n|,\ |p|,\ m,\ s \to \infty. \end{gathered} \tag{2.199}$$

They suggest that for $\bar{h} > 0$ and $k \notin \Omega_k$, the system of equations (2.198) is uniquely solvable in the space $\tilde{l}_2$ and numerically solvable by the truncation method converging in $\tilde{l}_2$ space norm [70, 110]. The error in the determination of the amplitude set $R^{\mathbf{AA}}_{(p)}$ in the metric of this space is equal to $O\left[\mathrm{e}^{-\pi(N+1)h/l\cos\vartheta}\right]$.

Letting $\bar{h} \to 0$ in (2.198) (returning to the initial structure geometry) yields the second-kind operator equation

$$a_{(p)} + R^{\mathbf{GG}}(\mathrm{I})\left[a_{(p)}\right] = T^{\mathbf{GA}}(\mathrm{I})\left[\alpha_{(p)}\right] \tag{2.200}$$

and the recalculation formula

$$R^{\mathbf{AA}}_{(p)} = R^{\mathbf{AA}}(\mathrm{I})\left[\alpha_{(p)}\right] - T^{\mathbf{AG}}(\mathrm{I})\left[a_{(p)}\right]. \tag{2.201}$$

It is essential to show the invertibility of the operator $\left[E + R^{\mathbf{GG}}(\mathrm{I})\right] : \tilde{l}_2 \to \tilde{l}_2$, or the existence and boundedness of the operator $[E + R^{\mathbf{GG}}(\mathbf{I})]^{-1}$. There are no other ways to guarantee an orthonormalized basis of the $\tilde{l}_2$ space in which the infinite equation system (2.200) can be solved by truncation [110]. However, the operator $R^{\mathbf{GG}}(\mathbf{I})$ is not totally continuous, being a Hilbert-type operator in the $\tilde{l}_2$ space [see [116] and estimations (2.199)], it is only bounded in this space. Also, there

hardly exists a direct way to get the estimate $\left\|R^{\mathbf{GG}}(\mathrm{I})\right\| < 1$ justifying (the same as the total continuity of the operator $R^{\mathbf{GG}}(\mathbf{I})$) the unique solvability of problem (2.200). The last possibility is to prove that the full spectrum of the operator $R^{\mathbf{GG}}(\mathbf{I})$ is enclosed by the circle $|w|=1$ in the plane $\mathbf{C}$ of complex variable w. This possibility is realized via the energy relationships that are obtained as a result of the complex power theorem applied to the volume of elementary inhomogeneity $\mathbf{I}$ [17, 42, 114].

Thus, it has been shown that for $k\notin\Omega_k$, the spectrum of the operator $R^{\mathbf{GG}}(\mathbf{I})$ is enclosed by the circle $|w|=1$, $w\in\mathbf{C}$. Hence [70, 115], the operator $[E + R^{\mathbf{GG}}(\mathbf{I})]$ is invertible, the sets $a_{(p)}$ and $R^{\mathbf{AA}}_{(p)}$ belong to the space $\tilde{l}_2$ (all scattering operators of the inhomogeneity $\mathbf{I}$ are bounded on the pair of spaces $\tilde{l}_2 \to \tilde{l}_2$ [116]), and a solution of the operator equation (2.200) can be obtained for any parameters l and ϑ by the successive approximation approach:

$$a_{(p)}(M) = \sum_{m=0}^{M} \left(-R^{\mathbf{GG}}(\mathrm{I})\right)^m T^{\mathbf{GA}}(\mathrm{I})\left[\alpha_{(p)}\right]; M \to \infty.$$

One more consequence of the invertibility of the operator $[E + R^{\mathbf{GG}}(\mathbf{I})]$ refers to the possibility to solve equation (2.200) by the truncation method converging in $\tilde{l}_2$ space norm. Indeed, the use of the evident equality

$$a_{(p)} - a_{(p)}(N) = -\left[E(N) + E(N) R^{\mathbf{GG}} E(N)\right]^{-1} E(N) R^{\mathbf{GG}} [E - E(N)]\left[a_{(p)}\right],$$

yields

$$\left\|a_{(p)} - a_{(p)}(N)\right\| \le \text{const}\left\|[E - E(N)]\left[a_{(p)}\right]\right\|. \tag{2.202}$$

Here, $E(N) = \left\{\delta^s_m\right\}^N_{m,s=1}$ and $a_{(p)}(N)$ is the solution of the truncated system

$$a_{(p)}(N) + E(N) R^{\mathbf{GG}}(\mathrm{I}) E(N)\left[a_{(p)}(N)\right] = E(N) T^{\mathbf{GA}}(\mathrm{I})\left[\alpha_{(p)}\right].$$

Since for any $a_{(p)} \in \tilde{l}_2$, $\left\|[E - E(N)]\left[a_{(p)}\right]\right\| \to 0$ as $N\to 0$, then

$$\left\|a_{(p)} - a_{(p)}(N)\right\| \to 0; N \to 0.$$

The scattered field of the grating meets the Meixner condition near the singular points in the structure geometry (near the points where the tangents and the normals to the contour $\mathbf{S}_x$ are not defined). In the considered case of an echelette grating with a 90° tooth angle, this means that $a_{mp} = O\left(m^{-5/3}\right)$, $R^{\mathbf{AA}}_{np} = O\left(|n|^{-5/3}\right)$ for m and $|n|$ large enough [42]. Knowing the rate of decrease of the secondary field amplitude and addressing (2.202), one can estimate the rate of convergence of the truncation method as follows:

$$\left\|a_{(p)} - a_{(p)}(N)\right\| = O\left[(N+1)^{-2/3}\right]; N \to 0.$$

2.4 Electromagnetic Wave Diffraction by Gratings in Presence of a Chiral Isotropic Medium

Chiral composites possessing spatial dispersion have unusual electromagnetic characteristics, such as optical activity and circular dichroism [117, 118]. Certain advances in the technologies used to manufacture chiral materials open up new fields for their application, including effective microwave absorbers, microstrip antenna substrates, chirally filled waveguides, switches, and modulators. In these applications, it is the presence of chiral materials that allow us to vary, and in some cases essentially improve, the characteristics of electrodynamical systems beyond those based on more conventional materials.

Thus, for example, a chiral substrate in place of a dielectric one in a microstrip antenna suppresses the surface wave power [119], and so enhances radiation efficiency, widens the transmission band, and reduces mutual coupling between the antenna elements. Results demonstrating the behavior of chiral materials as substrates and covers for antenna applications are found in [120, 121]. In [120], a chiral substrate is reported to be reducing the pattern size of the patch antenna for a given frequency. The chirality of a microstrip antenna cover makes the antenna more compact, increases gain performances, magnifies the radiation resistance and the antenna efficiency, and also reduces the radar cross-section around the resonance [121]. The analysis carried out in [122] of the scattering by a chiral periodic structure showed that the structure can be used as both a frequency-selective device and a mode-conversion device. Using their polarization properties, chiral materials can be used for filters, polarization converters, and lenses. In view of the circular polarization of chiral medium eigenwaves, a chiral medium couples both linear polarizations of the field, and so gives rise to new and interesting polarization effects.

A chiral inclusion may impart novel properties also in well-known structures. For example, when a linearly polarized wave is normally incident on a perfectly conducting strip grating attached to an isotropic chiral half-space, it is shown in this chapter (see also [123]) that the reflected field contains cross-polarized harmonics; the diffracted field character depends on the direction of the elliptic polarization of the incident wave, and the nature of chiral media losses is responsible for specific features of the diffracted field, which correspond to dichroism.

The phenomenon of nearly total transformation of an elliptically polarized wave into a linearly polarized wave is described herein (also see [124]). It is achieved by reflection from a structure comprising a perfectly conducting ground plate overlaid with a chiral layer and a magnetodielectric layer, and topped off with a perfectly conducting strip grating. This reflecting structure has potential application in various microwave devices. The complete transformation of an obliquely incident linearly polarized wave to a specularly reflected cross-polarized wave may be achieved with this structure [125]; also regimes of essential autocollimation reflection and nearly total nonspecular reflection, with a high-telescopicity factor, have been found [126, 127].

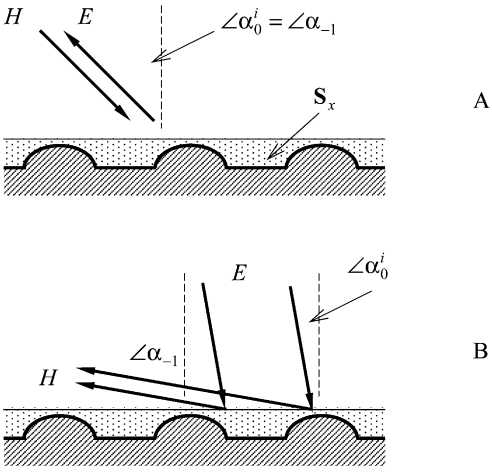

Fig. 2.4 The nonspecular reflection with polarization conversion: (**a**) autocollimation reflection and (**b**) high-telescopicity reflection (telescopicity factor is $r_t = \cos\alpha_0^i / \cos\alpha_{-1}$)

In the autocollimation regime (see Fig. 2.4a), the minus first harmonic of cross-polarization propagates in a direction opposite to the primary incident wave of linear polarization. Thus, in this regime, the structure acts as a frequency-selecting mirror with polarization conversion. The nonspecular reflection regime with a high telescopicity factor (see Fig. 2.4b) is characterized by a quasi-complete conversion of the nearly normally incident wave into the minus first cross-polarized harmonic, which almost skims above the grating surface. In this regime, the energy flux density of the wave is greatly increased and a high-purity polarization transformation is obtained. Thus, the structure can be used as an antenna component.

The determination of those structure parameters, which give the desired reflection regime, faces serious computational difficulties, even ignoring the polarization conversion. While an optimization may be carried out by examining the controlling parameters in a wide band of variation, it must be recognized that the phenomena occurs within narrow limits and often has a resonance nature. The phenomena associated with the polarization transformation are even more narrowly limited and have a striking resonance nature. Therefore an effective and reliable numerical procedure is required.

The presence of a chiral medium complicates the problem mathematically, making it a fully vectorial problem. The analysis of the diffraction in presence of chiral materials has been recently carried out using a variety of numerical methods, such as the finite difference frequency domain formulation [128] used for scattering from arbitrarily shaped chiral objects; the hybrid finite element-boundary integral method [129] applied to scattering of three-dimensional chiral objects above a perfect conducting plane; the T-matrix analysis [130] used to model semicircular channels filled with chiral materials in a conducting plate; etc. Approaches based on these methods are widely used because of their high flexibility when applied to scatterers of different, rather complicated shapes. Although, as a rule, they require high memory and computer resources (in other words, they are computationally expensive), recent developments in computer systems have made the use of such methods

efficient. Actually only one problem, but an essential one, remains. These conventional approaches are based on the numerical solution of a first-kind Fredholm equation which is ill posed, and often displays unpredictable accuracy and possible instability with an increase in the number of iterations. That is why, for example, the authors of [130] stress how carefully their empirical choice of proper truncation number must be followed to get acceptable accuracy in their T-matrix method. The primary concern with these disadvantages is that they most strongly feature in the areas of greatest interest in technical applications, namely, the resonant domain characterized by energetically pronounced effects.

Thus, it is highly desirable to transform this equation into a second-kind Fredholm equation, which provides a stable and fast-converging computational algorithm with the required accuracy of computation. For a certain class of scatterers this transformation can be implemented by the idea of analytic regularization described above (see Section 2.2, and [57]). The use of an analytic regularization [57, 61] allows us to obtain an effective and reliable calculation procedure that overcomes the difficulties mentioned; this procedure solves the optimization problems for obtaining desired characteristics of diffracted field in the resonance regimes.

2.4.1 Field Presentation in Chiral Medium

The unusual electromagnetic characteristics of chiral medium are caused by the essential spatial dispersion which cannot be neglected as in conventional media. The spatial dispersion leads to the results that the field in the chiral medium, i.e., the vectors of electromagnetic induction ($\vec{D}$ and $\vec{B}$), is defined not only by the correspondent strength vectors ($\vec{E}$ and $\vec{H}$), but as well by the rotors of these vectors. The constitutive relations, determining the electromagnetic induction in a homogeneous reciprocal chiral medium for harmonic temporal dependence exp(–*ikt*), are presented in the following form [117]:

$$\vec{D} = \varepsilon_0\, \tilde{\varepsilon}\, \vec{E} + i\gamma\sqrt{\varepsilon_0 \mu_0}\vec{H},\ \vec{B} = \mu_0 \tilde{\mu}\, \vec{H} - i\gamma\sqrt{\varepsilon_0 \mu_0}\vec{E}. \tag{2.203}$$

Here, ε_0 and μ_0 are the electric and magnetic constants, respectively; $\tilde{\varepsilon} = \tilde{\varepsilon}' + i\tilde{\varepsilon}''$ and $\tilde{\mu} = \tilde{\mu}' + i\tilde{\mu}''$ are the relative permittivity and permeability of the chiral medium; and $\gamma = \gamma' + i\gamma''$ is the chirality parameter responsible for the magnetic–electric interaction. We consider an isotropic medium, i.e., $\tilde{\varepsilon}$, $\tilde{\mu}$, and γ are scalars. Due to the composite nature of the artificial chiral medium all its constitutive parameters exhibit frequency dispersion.

In view of the constitutive relations (2.203), we rewrite the system of Maxwell's equations for time-harmonic fields $\vec{E} \equiv \vec{E}\,(g,k) = \left\{\tilde{E}_x, \tilde{E}_y, \tilde{E}_z\right\}$ and $\vec{H} \equiv \vec{H}\,(g,k) = \left\{\tilde{H}_x, \tilde{H}_y, \tilde{H}_z\right\}$, $p = \{x,y,z\}$ in the form

$$\begin{cases} \operatorname{rot}\vec{H} = a_{11}\,\vec{E} + a_{12}\,\vec{H} \\ \operatorname{rot}\vec{E} = a_{21}\,\vec{H} + a_{22}\,\vec{E} \end{cases}, \tag{2.204}$$

where $a_{11} = -ik\eta_0^{-1}\,\tilde{\varepsilon}$, $a_{12} = k\gamma$, $a_{21} = ik\eta_0\,\tilde{\mu}$, $a_{22} = k\gamma$.

The field analysis in an unbounded homogeneous chiral medium is usually based on the introduction of new vectors [131] that allow decoupling of the Maxwell's equations into two independent systems of differential equations of the first order.

Separate the vector of magnetic field strength in (2.204):

$$\begin{cases} \vec{H} = \frac{1}{a_{21}} \left(\mathrm{rot}\vec{E} - a_{22}\vec{E} \right) \\ \mathrm{rotrot}\vec{E} = a_{11}a_{21}\vec{E} - a_{12}a_{22}\vec{E} + a_{12}\,\mathrm{rot}\vec{E} + a_{22}\,\mathrm{rot}\vec{E} \end{cases}.$$

Introducing the operator $M = \mathrm{rotrot} - a_{12}\mathrm{rot} - a_{22}\mathrm{rot} - a_{11}a_{21} + a_{12}a_{22}$, we arrive at the vector Helmholtz's equation

$$M\vec{E} = 0. \tag{2.205}$$

Taking into account $a_{12} = a_{22}$, the operator of the second-order M can be rewritten as

$$M = [\mathrm{rot} - a_{12}]^{\,2} - a_{11}a_{21} = \left[\mathrm{rot} - \left(\sqrt{a_{11}a_{21}} + a_{12}\right)\right]\left[\mathrm{rot} + \left(\sqrt{a_{11}a_{21}} - a_{12}\right)\right]$$

$$= M^{+}M^{-}.$$

Thus, the operator M can be represented as a product of two operators of the first order M^{+} and M^{-}, which commute. Seeking for solution of equation (2.205) in the form of sum $\vec{E} = \vec{E}^{+} + \vec{E}^{-}$, we have

$$M^{+}M^{-}\left(\vec{E}^{+} + \vec{E}^{-}\right) = 0.$$

Since the operators M^{+} and M^{-} commute, this equation is split into the equations $M^{+}\vec{E}^{+} = 0$, $M^{-}\vec{E}^{-} = 0$ or

$$\mathrm{rot}\vec{E}^{+} = -k^{+}\vec{E}^{+}, \qquad \mathrm{rot}\vec{E}^{-} = k^{-}\vec{E}^{-}. \tag{2.206}$$

Here, $k^{\pm} = -\left(\sqrt{a_{11}a_{21}} \pm a_{12}\right) = -k\sqrt{\tilde{\varepsilon}\,\tilde{\mu}}\,(1 \pm \eta)$ and $\eta = \gamma \Big/ \sqrt{\tilde{\varepsilon}\,\tilde{\mu}}$ is the relative chirality parameter.

Thus, the factorization of the vector wave equation (2.205) allowed reducing the problem to the two equations of the first order (2.206). Express the vector of magnetic strength $\vec{H}$ in terms of the vectors $\vec{E}^{\pm}$:

$$\vec{H} = \frac{1}{a_{21}}\left(-\left(k^{+} + a_{22}\right)\vec{E}^{+} + \left(k^{-} - a_{22}\right)\vec{E}^{-}\right) = -\frac{i}{\rho}\left(\vec{E}^{+} - \vec{E}^{-}\right) = \vec{H}^{+} + \vec{H}^{-},$$

where $\rho = \sqrt{\mu_0\,\tilde{\mu}\,\big/\varepsilon_0\,\tilde{\varepsilon}}$.

Therefore, the electromagnetic field in the chiral medium is defined by the linear combinations of the so-called wave fields $\vec{E}^{\pm}$. Uncoupled plane waves $\vec{E}^{+}$, $\vec{H}^{+}$ and $\vec{E}^{-}$, $\vec{H}^{-}$ of left- and right-hand circular polarizations with propagation constants k^{+} and k^{-} are shown to be eigenwaves of the unbounded homogeneous chiral medium.

In the case of two-dimensional problems (when, for example, $\partial/\partial x \equiv 0$), we obtain the following field representation in the chiral medium:

$$\begin{aligned} &\vec{E} = \vec{E}^{+} + \vec{E}^{-}, \vec{H} = \vec{H}^{+} + \vec{H}^{-} = -\tfrac{i}{\rho}\left(\vec{E}^{+} - \vec{E}^{-}\right), \\ &\tilde{E}_x^{\pm} = \tilde{U}^{\pm}, \quad \tilde{E}_y^{\pm} = \mp\tfrac{1}{k^{\pm}}\tfrac{\partial \tilde{U}^{\pm}}{\partial z}, \quad \tilde{E}_z^{\pm} = \pm\tfrac{1}{k^{\pm}}\tfrac{\partial \tilde{U}^{\pm}}{\partial y} \end{aligned} \tag{2.207}$$

and

$$\left[\frac{\partial^2}{\partial y^2} + \frac{\partial^2}{\partial z^2}\right]\tilde{U}^{\pm}\left(g, k^{\pm}\right) + \left(k^{\pm}\right)^2 \tilde{U}^{\pm}\left(g, k^{\pm}\right) \equiv \Delta_{y,z}\tilde{U}^{\pm} + \left(k^{\pm}\right)^2 \tilde{U}^{\pm} = 0;\ g = \{y,z\}.$$

Thus, the components $\tilde{E}_x^{\pm}$ are those through which all the other field components can be represented. In the case of a bounded chiral medium, the wave fields $\vec{E}^{\pm}$ are connected to meet the corresponding boundary conditions for total fields $\vec{E}$ and $\vec{H}$. Even for the two-dimensional case, the equations for the sought field show that all the components are coupled, so the problem is a vectorial one.

2.4.2 Formulation of the Problem

At first, let us consider the model problem of electromagnetic wave diffraction from a strip grating placed above (or on) a chiral half-space. The problem geometry is shown in Fig. 2.5a. A periodic grating of infinitely thin and perfectly conducting strips parallel to the x-axis lies in the plane $z = h_1$. The grating period is l, the slot width is d. The interface between the chiral $z < 0$ and nonchiral $z > 0$ media is

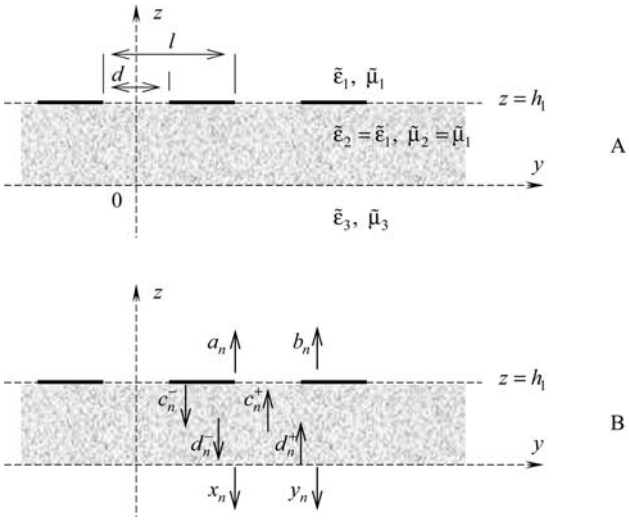

Fig. 2.5 (**a**) The structure profile and (**b**) the secondary field harmonics

given by the plane $z = 0$; $\tilde{\varepsilon}_1$ and $\tilde{\mu}_1$ are the relative permittivity and permeability of the magnetodielectric filling the upper half-space ($z > 0$), and $\tilde{\varepsilon}_3$, $\tilde{\mu}_3$, and $\eta = \gamma \Big/ \sqrt{\tilde{\varepsilon}_3\, \tilde{\mu}_3}$ are the constitutive parameters of the chiral half-space.

A plane electromagnetic wave normally incident on the grating from above is characterized by $\vec{E}^i = \vec{E}_0 \exp(-i(k_1 z + kt))$ and $\vec{H}^i = \vec{H}_0 \exp(-i(k_1 z + kt))$, where $k_1 = k\sqrt{\tilde{\varepsilon}_1\, \tilde{\mu}_1}$ is the wave number of the upper half-space. The diffracted field is to be found.

We will seek the solution in the form of a total field equal to the sum of the incident and secondary fields. Since the incident field is independent of the x-coordinate and the grating is uniform with respect to the x-axis, the desired field is independent of this coordinate. Thus, the problem is the two-dimensional ($\partial/\partial x \equiv 0$) one. Concerning the orientation of the incident wave, the original problem can be reduced to special cases of an E-polarized field where $\vec{E}_0 = \{\tilde{e},0,0\}$ or a H-polarized field where $\vec{H}_0 = \left\{\tilde{h},0,0\right\}$.

For the existence and uniqueness of the solution, it is necessary [45] that the solution obeys the Maxwell equations, the boundary conditions, the radiation condition at infinity, the quasi-periodicity condition, and the condition that the field energy is finite within any bounded volume of space.

2.4.3 The Systems of Dual Series Equations

The geometry of the structure allows us to solve the considered boundary value problem by the method of separation of variables. Assuming that the solution exists, we will seek it in the form of a Fourier series expansion for domains D_j ($j = 1,2,3$), where $D_1{:}h_1 < z$, $D_2{:}0 < z < h_1$, and $D_3{:}z < 0$. Substituting the series into Helmholtz's equation ($\Delta_{yz}\tilde{U}(g) + k_1^2\tilde{U}(g) = 0$ for $z > 0$ and $\Delta_{y,z}\tilde{U}^{\pm}(g) + \left(k^{\pm}\right)^2\tilde{U}^{\pm}(g) = 0$ for $z < 0$), we can represent the field components as follows (see Fig. 2.5b):

$$
\begin{cases}
\tilde{E}_x^1 = \tilde{e}\exp(-ik_1 z) + \sum\limits_{n=-\infty}^{\infty} a_n \exp\left(i\Gamma_n^1 (z - h_1)\right)\, \exp\left(i\,\Phi_n y\right) \\
\tilde{H}_x^1 = \tilde{h}\exp(-ik_1 z) + \sum\limits_{n=-\infty}^{\infty} b_n \exp\left(i\Gamma_n^1 (z - h_1)\right)\, \exp\left(i\,\Phi_n y\right)
\end{cases} ; z > h_1,
$$

$$
\begin{cases}
\tilde{E}_x^2 = \sum\limits_{n=-\infty}^{\infty} \left[c_n^+ \exp\left(i\Gamma_n^2 z\right) + c_n^- \exp\left(-i\Gamma_n^2 (z - h_1)\right)\right] \exp\left(i\,\Phi_n y\right) \\
\tilde{H}_x^2 = \sum\limits_{n=-\infty}^{\infty} \left[d_n^+ \exp\left(i\Gamma_n^2 z\right) + d_n^- \exp\left(-i\Gamma_n^2 (z - h_1)\right)\right] \exp\left(i\,\Phi_n y\right)
\end{cases} ; \quad 0 < z < h_1,
$$

$$
\begin{cases}
\tilde{E}_x^3 = \sum\limits_{n=-\infty}^{\infty} \left[x_n \exp\left(-i\Gamma_n^+ z\right) + y_n \exp\left(-i\Gamma_n^- z\right)\right] \exp\left(i\Gamma_n^1 h_1\right) \exp\left(i\Phi_n y\right) \\
\tilde{H}_x^3 = \frac{-i}{\rho_3} \sum\limits_{n=-\infty}^{\infty} \left[x_n \exp\left(-i\Gamma_n^+ z\right) - y_n \exp\left(-i\Gamma_n^- z\right)\right] \exp\left(i\Gamma_n^1 h_1\right) \exp\left(i\Phi_n y\right)
\end{cases} ; \quad z < 0.
\tag{2.208}
$$

Here, we have denoted the propagation constant of the nth field harmonic by Φ_n in the y-direction and by $\Gamma_n^j; j \neq 3$, $\Gamma_n^{\pm}; j = 3$ in the z-direction for the domain D_j:

$$\Phi_n = \frac{2\pi}{l} n\,, \qquad \Gamma_n^j = \sqrt{k_j^2 - (\Phi_n)^2}, \qquad \Gamma_n^{\pm} = \sqrt{\left(k^{\pm}\right)^2 - (\Phi_n)^2}. \tag{2.209}$$

The root branches with $\mathrm{Im}\left(\Gamma_n^{j,\pm}\right) \geq 0$ are chosen to fit the radiation condition at infinity, $k_j = k\sqrt{\tilde{\varepsilon}_j \tilde{\mu}_j}$, and $\rho_j = \sqrt{\mu_0\,\tilde{\mu}_j / \varepsilon_0\,\tilde{\varepsilon}_j}$, $j = 1,2,3$.

The obtained field representation (2.208) satisfies the quasi-periodicity condition and corresponds to the Rayleigh expansion of the diffracted field in a superposition of partial harmonics of spatial spectrum. This superposition, which consists of a finite number of plane uniformly propagating waves (for which Γ_n^j, $\Gamma_n^{\pm}$ are real) and an infinite number of slow nonuniform surface waves (with Γ_n^j, $\Gamma_n^{\pm}$ complex), is localized near the inhomogeneity planes $z = h_1$, $z = 0$. The propagation direction and decay character of these waves are given by (2.209), while the wave amplitudes and phases are determined by the unknown Fourier coefficients: a_n, b_n, $c_n^{\pm}$, $d_n^{\pm}$, and x_n, y_n. It is possible to show that each number n in the series describing the chiral medium field is assigned to a couple of circularly polarized waves with amplitudes x_n, y_n and wave vectors $\vec{k}_n^{\pm} = \left\{0, \Phi_n, -\Gamma_n^{\pm}\right\}$. Note that, complex coefficients a_n, $c_n^{\pm}$ correspond to E-polarization and b_n, $d_n^{\pm}$ to H-polarization. Thus, the problem is to find these coefficients.

Satisfying the boundary condition, that the tangential components of the electric field are equal over the grating period gives

$$\begin{aligned} a_n &= c_n^{+} \exp\left(i\Gamma_n^1 h_1\right) + c_n^{-} - \delta_0^n\,\tilde{e}\,\exp\left(-ik_1 h_1\right) \text{ and} \\ b_n &= d_n^{+} \exp\left(i\Gamma_n^1 h_1\right) - d_n^{-} + \delta_0^n\,\tilde{h}\,\exp\left(-ik_1 h_1\right). \end{aligned} \tag{2.210}$$

Using the obtained relations (2.210) and applying the boundary condition that the magnetic field components are continuous over the grating slot yields the series equation valid on the interval $|y| < d/2$

$$\begin{cases} \sum\limits_{n=-\infty}^{\infty} \Gamma_n^1 c_n^{-} \exp\left(i\Phi_n y\right) = \tilde{e} k_1 \exp\left(-ik_1 h_1\right) \\ \sum\limits_{n=-\infty}^{\infty} d_n^{-} \exp\left(i\Phi_n y\right) = \tilde{h} \exp\left(-ik_1 h_1\right) \end{cases}; \; |y| < d/2.$$

Imposing the boundary condition that the electric field tangential components vanish on the metal strips results in another couple of the series equation valid on the interval $d/2 < |y| < l/2$. Thus, the boundary conditions corresponding to the strip grating at $z = h_1$ allows us to obtain two systems of functional equations

$$\begin{cases} \sum\limits_{n=-\infty}^{\infty} \Gamma_n^1 \, c_n^- \exp\left(i\Phi_n y\right) = \tilde{e} k_1 \exp\left(-ik_1 h_1\right); & |y| < d/2 \\ \sum\limits_{n=-\infty}^{\infty} \left\{c_n^+ \exp\left(i\Gamma_n^1 \, h_1\right) + c_n^-\right\} \exp\left(i\Phi_n y\right) = 0; & d/2 < |y| \le l/2 \end{cases}, \quad (2.211)$$

$$\begin{cases} \sum\limits_{n=-\infty}^{\infty} d_n^- \exp\left(i\Phi_n y\right) = \tilde{h} \exp\left(-ik_1 h_1\right); & |y| < d/2 \\ \sum\limits_{n=-\infty}^{\infty} \Gamma_n^1 \left\{ d_n^+ \exp\left(i\Gamma_n^1 \, h_1\right) - d_n^- \right\} \exp\left(i\Phi_n y\right) = 0; & d/2 < |y| \le l/2 \end{cases}. \quad (2.212)$$

System (2.211) of dual series equations is for E-polarization, and system (2.212) for H-polarization. The continuity of the tangential components of the field at $z = 0$ enables us to determine $c_n^{\pm}$, $d_n^{\pm}$ via the complex amplitudes x_n, y_n of the field in the chiral medium:

$$c_n^+ = \frac{1}{2} \exp\left(i\Gamma_n^1 h_1\right) \left[\left(A_n^{11} - A_n^{12}\right) x_n + \left(A_n^{21} - A_n^{22}\right) y_n\right],$$

$$c_n^- = \frac{1}{2} \left[\left(A_n^{11} + A_n^{12}\right) x_n + \left(A_n^{21} + A_n^{22}\right) y_n\right],$$

$$d_n^+ = -\frac{i}{2\rho_3} \exp\left(i\Gamma_n^1 h_1\right) \left[\left(B_n^{11} - B_n^{12}\right) x_n + \left(B_n^{21} - B_n^{22}\right) y_n\right],$$

$$d_n^- = \frac{i}{2\rho_3} \left[\left(B_n^{11} + B_n^{12}\right) x_n + \left(B_n^{21} + B_n^{22}\right) y_n\right].$$

Here, we have introduced the coefficients

$$A_n^{11} = 1, \quad A_n^{12} = \frac{\tilde{\mu}_1}{\tilde{\mu}_3 \, (1+\eta)} \, \frac{\Gamma_n^+}{\Gamma_n^1}, \quad A_n^{21} = 1, \quad A_n^{22} = \frac{\tilde{\mu}_1}{\tilde{\mu}_3 \, (1-\eta)} \, \frac{\Gamma_n^-}{\Gamma_n^1},$$

$$B_n^{11} = -\frac{\tilde{\varepsilon}_1}{\tilde{\varepsilon}_3 \, (1+\eta)} \, \frac{\Gamma_n^+}{\Gamma_n^1}, \quad B_n^{12} = -1, \quad B_n^{21} = \frac{\tilde{\varepsilon}_1}{\tilde{\varepsilon}_3 \, (1-\eta)} \, \frac{\Gamma_n^-}{\Gamma_n^1}, \quad B_n^{22} = 1.$$

Systems (2.211) and (2.212) for the coefficients x_n, y_n take the form

$$\begin{cases} \sum\limits_{n=-\infty}^{\infty} \Gamma_n^1 \left\{x_n \left[A_n^{11} + A_n^{12}\right] + y_n \left[A_n^{21} + A_n^{22}\right]\right\} \exp\left(i\Phi_n y\right) = \\ = 2k_1 \tilde{e} \exp\left(-ik_1 h_1\right); & |y| < d/2 \\ \sum\limits_{n=-\infty}^{\infty} \left\{x_n \left[\Omega_n^+ A_n^{11} + \Omega_n^- A_n^{12}\right] + y_n \left[\Omega_n^+ A_n^{21} + \Omega_n^- A_n^{22}\right]\right\} \exp\left(i\Phi_n y\right) = \\ = 0; & d/2 < |y| \le l/2 \end{cases}, \quad (2.213)$$

$$\begin{cases} \sum\limits_{n=-\infty}^{\infty} \left\{ x_n \left[B_n^{11} + B_n^{12} \right] + y_n \left[B_n^{21} + B_n^{22} \right] \right\} \exp\left(i\Phi_n y \right) = \\ = -2i\rho_3 \tilde{h} \exp\left(-ik_1 h_1 \right); \qquad |y| < d/2 \\ \sum\limits_{n=-\infty}^{\infty} \Gamma_n^1 \left\{ x_n \left[\Omega_n^+ B_n^{11} + \Omega_n^- B_n^{12} \right] + y_n \left[\Omega_n^+ B_n^{21} + \Omega_n^- B_n^{22} \right] \right\} \exp\left(i\Phi_n y \right) = \\ = 0; \qquad d/2 < |y| \le l/2 \end{cases}, \tag{2.214}$$

where $\Omega_n^{\pm} = 1 \pm \exp\left(i2\Gamma_n^1 h_1 \right)$. Systems (2.213) and (2.214) of dual series equations involving exponential functions are equivalent to an operator equation of the first kind in the Hilbert space given by the Meixner condition [132].

The obtained systems are coupled, and describe fields of both linear polarizations. Let, for example, the grating be excited by an E-polarized wave ($\tilde{h} = 0$), then without chirality ($\gamma = 0$), i.e., when lower half-space ($z < 0$) is magnetodielectric, we have $k^+ = k^-$ and $A_n^{11} = A_n^{21}$, $A_n^{12} = A_n^{22}$ and also $B_n^{11} = -B_n^{21}$, $B_n^{12} = -B_n^{22}$. Then systems (2.213) and (2.214) become decoupled, and the homogeneous equations of system (2.214) imply $x_n = y_n$. If so, the H-polarized field disappears, and system (2.213) gives the solution to the scalar diffraction problem in the E-polarization case. The presence of chirality ($\gamma \neq 0$) will give rise to additional field polarization. The appearance of additional polarization is attributed to the fact that the chiral medium eigenwaves represent circularly polarized waves produced by the superposition of E- and H-polarized fields. So despite the two-dimensional problem formulation, the sought field contains components of both polarizations, which are coupled in this problem. Therefore, the vector problem is considered.

2.4.4 An Algebraic System of the Second Kind

In order to separate a series with slow convergence rate, we introduce the new unknown coefficients

$$X_n = x_n \left[B_n^{11} + B_n^{12} \right] + y_n \left[B_n^{21} + B_n^{22} \right] + \delta_0^n 2i\rho_3 \tilde{h} \exp\left(-ik_1 h_1 \right) \text{ and}$$

$$Y_n = x_n \left[\Omega_n^+ A_n^{11} + \Omega_n^- A_n^{12} \right] + y_n \left[\Omega_n^+ A_n^{21} + \Omega_n^- A_n^{22} \right].$$

Now, in the case of $h_1 \neq 0$, i.e., for the grating placed above the chiral half-space, systems (2.213) and (2.214) can be represented in the following form:

$$\begin{cases} \sum\limits_{n=-\infty(n\neq 0)}^{\infty} |n| X_n \exp\left(in\vartheta \right) = F^1\left(\vartheta; X_n, Y_n \right); \qquad |\vartheta| > \vartheta_0 \\ \sum\limits_{n=-\infty}^{\infty} X_n \exp\left(in\vartheta \right) = 0; \qquad |\vartheta| < \vartheta_0 \end{cases}, \tag{2.215}$$

$$\begin{cases} \sum\limits_{n=-\infty}^{\infty} Y_n \exp\left(in\vartheta \right) = 0; \qquad |\vartheta| > \vartheta_0 \\ \sum\limits_{n=-\infty(n\neq 0)}^{\infty} |n| Y_n \exp\left(in\vartheta \right) = F^2\left(\vartheta; X_n, Y_n \right); \qquad |\vartheta| < \vartheta_0 \end{cases}, \tag{2.216}$$

where $\vartheta = 2\pi y/l$ and $\vartheta_0 = \pi d/l$. Then the inequality $|\vartheta| < \vartheta_0$ indicates the grating slot and $\vartheta_0 < |\vartheta|$ refers to the strip. The right-hand sides of the systems $F^{1,2}(\vartheta; X_n, Y_n) = \sum_{n=-\infty}^{\infty} f_n^{1,2}(X_n, Y_n) \exp(in\vartheta)$ are sufficiently smooth functions of ϑ, belonging to the $\mathbf{L}_2[-\pi;\pi]$ space. Their Fourier coefficients are:

$$f_0^1 = i\kappa_1 \left\{ X_0 + \left(x_0 \left[B_0^{11} - B_0^{12} \right] + y_0 \left[B_0^{21} - B_0^{22} \right] \right) \exp(i2k_1 h_1) \right\}$$

$$+2\chi_1 \rho_3 \tilde{h} \exp(-ik_1 h_1),$$

$$f_n^1 = |n| \left\{ \xi_n X_n - (1-\xi_n) \left(x_n \left[B_n^{11} - B_n^{12} \right] + y_n \left[B_n^{21} - B_n^{22} \right] \right) \exp\left(i2\Gamma_n^1 h_1 \right) \right\},$$

$$f_0^2 = i\kappa_1 \left\{ Y_0 - \left(x_0 \left[A_0^{11} - A_0^{12} \right] + y_0 \left[A_0^{21} - A_0^{22} \right] \right) \exp(i2k_1 h_1) \right\}$$

$$-2i\kappa_1 \tilde{e} \exp(-ik_1 h_1),$$

$$f_n^2 = |n| \left\{ \xi_n Y_n + (1-\xi_n) \left(x_n \left[A_n^{11} - A_n^{12} \right] + y_n \left[A_n^{21} - A_n^{22} \right] \right) \exp\left(i2\Gamma_n^1 h_1 \right) \right\}.$$

Here, $\xi_n = 1 + i\sqrt{\left(\kappa_1/n\right)^2 - 1}$ is the smallness parameter, $\kappa_1 = l\lambda^{-1}\sqrt{\tilde{\varepsilon}_1 \tilde{\mu}_1}$, and λ is the wavelength in vacuum.

The asymptotic estimates of the coefficients $A_n^{rs} = O(1)$, $B_n^{rs} = O(1)$, $r, s = 1,2$, and the smallness parameter $\xi_n = O(n^{-2})$ show that as $|n| \to \infty$

$$f_n^{1,2} \underset{|n|\to\infty}{=} \frac{\sigma_n^{1,2}}{|n|} + O(|n| \exp(-\sigma\ |n|)),$$

where $\sigma = 4\pi h_1 l^{-1} \left[1 - 0.5 \left(\kappa_1 n^{-1} \right)^2 \right] > 0$, and the sequences $\left\{ \sigma_n^{1,2} \right\}_{n=-\infty}^{\infty}$ belong to l_2 space with weight $(|n| + 1)$. Therefore, the systems' right-hand sides, containing the Fourier expansions of the functions $F^{1,2}$, converge well. The left-hand sides of the systems are the series with slow convergence rate; they correspond to the principal part of the problem operator possessing the singularity. Taking the right-hand sides of (2.215) and (2.216) as known allows us to assume that the obtained functional systems are decoupled. Thus, we have not only extracted the singularity in the left-hand sides of the equations but also managed to decouple the systems in terms of the principal part of the operator.

It should be stressed that such decoupling is possible only for $h_1 \neq 0$, i.e., in the case of the grating placed above the chiral half-space. For $h_1 = 0$, the decoupling of the systems is impossible, and we have to solve the systems jointly. This required the development of an essentially new mathematical approach described above in Section 2.2.4.

For the case $h_1 \neq 0$, systems (2.215) and (2.216) are equivalent to a scalar Riemann–Hilbert boundary value problem (see [45] and Section 2.2.1). Applying this well-known method to the solution of this problem for each system individually yields the following infinite system of linear algebraic equations [133]:

$$\begin{cases} Y_m = \sum\limits_{n=-\infty}^{\infty} V_{mn}(u)\left\{\alpha_n Y_n + \beta_n X_n\right\} + b_m \\ X_m = \sum\limits_{n=-\infty}^{\infty} \tilde{V}_{mn}(\tilde{u})\left\{\tilde{\alpha}_n Y_n + \tilde{\beta}_n X_n\right\} + \tilde{b}_m \end{cases}; \quad m = 0, \pm 1, ... \tag{2.217}$$

The values $V_{mn}(u)$, $\tilde{V}_{mn}(\tilde{u})$, and α_n, β_n, b_m; $\tilde{\alpha}_n$, $\tilde{\beta}_n, \tilde{b}_m$ that appears in system (2.217) have the form

$$u = \cos\delta,\ V_{00} = -\ln\frac{1+u}{2},\ V_{0n} = \frac{1}{n}V_{n-1}^{-1}(u),\ V_{mn} = -\ V_{m-1}^{n-1}(u),$$

$$\tilde{u} = \cos\tilde{\delta},\ \tilde{V}_{00} = -\ln\frac{1+\tilde{u}}{2},\ \tilde{V}_{0n} = \frac{(-1)^n}{n}V_{n-1}^{-1}(\tilde{u}),$$

$$\tilde{V}_{mn} = \frac{(-1)^{m+n}}{m}V_{m-1}^{n-1}(\tilde{u}),\ \alpha_0 = i\kappa_1\frac{R_0^+}{T_0^+},$$

$$\alpha_n = |n|\left\{\xi_n\frac{R_n^+}{T_n^+} + \frac{R_n^-}{T_n^+}\exp\left(i2\Gamma_n^1 h_1\right)\right\},\ \beta_0 = 2i\kappa_1\frac{A_0}{T_0^+}\exp(i2k_1h_1),$$

$$\beta_n = -2|n|(1-\xi_n)\frac{A_n}{T_n^+}\exp\left(i2\Gamma_n^1 h_1\right),\ \tilde{\alpha}_0 = 2i\kappa_1\frac{B_0}{T_0^+}\exp(i2k_1h_1),$$

$$\tilde{\alpha}_n = -2|n|(1-\xi_n)\frac{B_n}{T_n^+}\exp\left(i2\Gamma_n^1 h_1\right),\ \tilde{\beta}_0 = i\kappa_1\frac{C_0}{T_0^+},$$

$$\tilde{\beta}_n = |n|\left\{\xi_n\frac{C_n}{T_n^+} - \frac{T_n^-}{T_n^+}\exp\left(i2\Gamma_n^1 h_1\right)\right\},$$

$$b_m = -2i\kappa_1 V_{m0}(u)\left[\tilde{e}\exp(-ik_1h_1) + 2i\rho_3\tilde{h}\frac{A_0}{T_0^+}\exp(ik_1h_1)\right],$$

$$\tilde{b}_m = 2\rho_3\tilde{h}\kappa_1\tilde{V}_{m0}(\tilde{u})\left[\exp(-ik_1h_1) + \frac{T_0^-}{T_0^+}\exp(ik_1h_1)\right],$$

where the matrix $V_m^n(u)$ is defined in Section 2.2.1, and

$$A_n = A_n^{11}A_n^{22} - A_n^{12}A_n^{21}, \qquad B_n = B_n^{11}B_n^{22} - B_n^{12}B_n^{21},$$

$$C_n = \left[\Omega_n^+A_n^{11} + \Omega_n^-A_n^{12}\right]\left[\Omega_n^+B_n^{21} + \Omega_n^-B_n^{22}\right] - \left[\Omega_n^+A_n^{21} + \Omega_n^-A_n^{22}\right]$$
$$\left[\Omega_n^+B_n^{11} + \Omega_n^-B_n^{12}\right],$$

$$R_n^{\pm} = \left[A_n^{11} \pm A_n^{12}\right]\left[B_n^{21} + B_n^{22}\right] - \left[A_n^{21} \pm A_n^{22}\right]\left[B_n^{11} + B_n^{12}\right],$$

$$T_n^{\pm} = \left[\Omega_n^{+} A_n^{11} + \Omega_n^{-} A_n^{12}\right]\left[B_n^{21} \pm B_n^{22}\right] - \left[\Omega_n^{+} A_n^{21} + \Omega_n^{-} A_n^{22}\right]\left[B_n^{11} \pm B_n^{12}\right].$$

The asymptotic estimates of the coefficients $\alpha_n, \tilde{\beta}_n = 1/|n|$; $\tilde{\alpha}_n, \beta_n = |n| \exp(-\sigma|n|)$ as $|n| \to \infty$, and the behavior of V_m^n for $|m|, |n| \to \infty$, allow us to conclude that (2.217) is a Fredholm-type system of the second kind. This system is the rigorous solution to the formulated vector problem, it finds X_n and Y_n and consequently all the unknowns.

Now we turn to the case when the grating is placed on the chiral half-space, i.e., $h_1 = 0$. We will show herein that the system of equations (2.213) and (2.214) is reducible to the form of the system of equations (2.123), (2.124), (2.125), and (2.126) described in Section 2.2.4. Really, after elementary transformations, equations (2.213) and (2.214) can be represented as

$$\begin{cases} \sum\limits_{n=-\infty}^{\infty} X_n \exp(in\vartheta) = 0; \qquad |\vartheta| < \vartheta_0 \\ \sum\limits_{n=-\infty(n\neq 0)}^{\infty} \Gamma_n^1 \bar{c}_n \left(\bar{b}_n X_n + Y_n\right) \exp(in\vartheta) + k_1 \left(\frac{\rho_1+\rho_3}{\rho_3} Y_0 + 2\tilde{e}\right) = 0; \quad |\vartheta| < \vartheta_0 \end{cases}, \tag{2.218}$$

$$\begin{cases} \sum\limits_{n=-\infty}^{\infty} Y_n \exp(in\vartheta) = 0; \qquad |\vartheta| > \vartheta_0 \\ \sum\limits_{n=-\infty(n\neq 0)}^{\infty} \Gamma_n^1 \bar{d}_n \left(X_n + \bar{a}_n Y_n\right) \exp(in\vartheta) + \frac{k_1\rho_3}{\rho_1+\rho_3}\left(X_0 - i2\rho_1\tilde{h}\right) = 0; \quad |\vartheta| > \vartheta_0 \end{cases}. \tag{2.219}$$

Here, we introduced the coefficients

$$\bar{a}_n = \frac{B_n^{11} + B_n^{21}}{B_n^{21} - B_n^{11}}, \qquad \bar{b}_n = \frac{A_n^{22} - A_n^{12}}{\left(1 + A_n^{12}\right)\left(1 + B_n^{21}\right) + \left(1 + A_n^{22}\right)\left(1 - B_n^{11}\right)},$$

$$\bar{c}_n = \frac{\left(1 + A_n^{12}\right)\left(1 + B_n^{21}\right) + \left(1 + A_n^{22}\right)\left(1 - B_n^{11}\right)}{2 + B_n^{21} - B_n^{11}}, \qquad \bar{d}_n = \frac{B_n^{21} - B_n^{11}}{2 + B_n^{21} - B_n^{11}}. \tag{2.220}$$

Using the explicit expressions for A_n^{pq} and B_n^{pq}, it is possible to obtain the following asymptotic estimates for (2.220) as $|n| \to \infty$:

$$\bar{a}_n = \eta + O\left(n^{-2}\right), \qquad \bar{b}_n = \frac{\tilde{\varepsilon}_3\tilde{\mu}_1\eta}{(\tilde{\varepsilon}_1+\tilde{\varepsilon}_3)(\tilde{\mu}_1+\tilde{\mu}_3)-\tilde{\varepsilon}_3\tilde{\mu}_3\eta^2} + O\left(n^{-2}\right),$$

$$\bar{c}_n = \frac{(\tilde{\varepsilon}_1+\tilde{\varepsilon}_3)(\tilde{\mu}_1+\tilde{\mu}_3)-\tilde{\varepsilon}_3\tilde{\mu}_3\eta^2}{\tilde{\mu}_3\left(\tilde{\varepsilon}_1+\tilde{\varepsilon}_3\left(1-\eta^2\right)\right)} + O\left(n^{-2}\right),$$

$$\bar{d}_n = \frac{\tilde{\varepsilon}_1}{\tilde{\varepsilon}_1+\tilde{\varepsilon}_3\left(1-\eta^2\right)} + O\left(n^{-2}\right). \tag{2.221}$$

Now, taking into account the estimates (2.221) and that $\Gamma_n^1 = |n|\frac{2\pi i}{l}\left[1+O\left(n^{-2}\right)\right]$ as $|n|\to\infty$, we write the system of equations (2.218) and (2.219) in the following form:

$$\begin{cases} \sum\limits_{n=-\infty}^{\infty} X_n \exp(in\vartheta) = 0; \qquad |\vartheta| < \vartheta_0 \\ \sum\limits_{n=-\infty}^{\infty} |n|(bX_n + Y_n)\exp(in\vartheta) + \\ \qquad + \sum\limits_{n=-\infty}^{\infty}\left(V_n^{11}X_n + V_n^{12}Y_n - f_{1n}\right)\exp(in\vartheta); \qquad |\vartheta| < \vartheta_0 \end{cases}, \tag{2.222}$$

$$\begin{cases} \sum\limits_{n=-\infty}^{\infty} Y_n \exp(in\vartheta) = 0; \qquad |\vartheta| > \vartheta_0 \\ \sum\limits_{n=-\infty}^{\infty} |n|(X_n + aY_n)\exp(in\vartheta) + \\ \qquad + \sum\limits_{n=-\infty}^{\infty}\left(V_n^{21}X_n + V_n^{22}Y_n - f_{2n}\right)\exp(in\vartheta); \qquad |\vartheta| > \vartheta_0 \end{cases}. \tag{2.223}$$

Here,

$$a = \eta,\ b = \frac{\tilde{\varepsilon}_3\tilde{\mu}_1\eta}{(\tilde{\varepsilon}_1+\tilde{\varepsilon}_3)(\tilde{\mu}_1+\tilde{\mu}_3)-\tilde{\varepsilon}_3\tilde{\mu}_3\eta^2}. \tag{2.224}$$

The coefficients V_n^{pq} (p,q = 1,2) can be expressed in terms of A_n^{pq}, B_n^{pq}, and Γ_n^1. As $|n|\to\infty$ they satisfy the conditions

$$V_n^{pq} = O\left(|n|^{-1}\right), p,q = 1,2. \tag{2.225}$$

Coefficients f_{1n} and f_{2n} are of the form

$$f_{1n} = -\frac{i\kappa_1\tilde{\mu}_3\left(\tilde{\varepsilon}_1+\tilde{\varepsilon}_3\left(1-\eta^2\right)\right)}{(\tilde{\varepsilon}_1+\tilde{\varepsilon}_3)(\tilde{\mu}_1+\tilde{\mu}_3)-\tilde{\varepsilon}_3\tilde{\mu}_3\eta^2}\tilde{e}\delta_0^n, \tag{2.226}$$

$$f_{2n} = -\frac{2\kappa_1\rho_1\rho_3\left(\tilde{\varepsilon}_1+\tilde{\varepsilon}_3\left(1-\eta^2\right)\right)}{\tilde{\varepsilon}_1(\rho_1+\rho_3)}\tilde{h}\delta_0^n. \tag{2.227}$$

It follows from expressions (2.225), (2.226), and (2.227) that the coefficients of dual series equations (2.222) and (2.223) meet the conditions for applying the analytic regularization method which uses the explicit solution of the vectorial Riemann–Hilbert boundary value problem, described in detail in Section 2.2.4. Namely, the asymptotic estimates (2.225) for the elements V_n^{pq} show that the matrix operators $V^{pq} = \left\{V_n^{pq}\delta_m^n\right\}_{m,\,n=-\infty}^{\infty}$ specify compact operators in l_2 space. From formulas (2.226) and (2.227), it follows that vector columns $f_1 = \{f_{1n}\}_{n=-\infty}^{\infty}$ and $f_2 = \{f_{2n}\}_{n=-\infty}^{\infty}$ belong to the space $l_2(-1)$ (see Section 2.2).

In addition, in the case of real-valued constitutive parameters $\tilde{\varepsilon}_j$, $\tilde{\mu}_j$, and $\eta = \gamma\Big/\sqrt{\tilde{\varepsilon}_3\,\tilde{\mu}_3}$, the coefficients a and b satisfy the inequality $0 \le ab < 1$. Let us prove it. From (2.224) we have

$$ab = \frac{\tilde{\varepsilon}_3\tilde{\mu}_1\eta^2}{(\tilde{\varepsilon}_1+\tilde{\varepsilon}_3)\;(\tilde{\mu}_1+\tilde{\mu}_3)-\tilde{\varepsilon}_3\tilde{\mu}_3\eta^2}. \tag{2.228}$$

It is known [117], that $\eta < 1$, therefore $(\tilde{\varepsilon}_1+\tilde{\varepsilon}_3)\,(\tilde{\mu}_1+\tilde{\mu}_3) - \tilde{\varepsilon}_3\tilde{\mu}_3\eta^2 > 0$. Suppose, that $ab \ge 1$, then from (2.228) we have $\tilde{\varepsilon}_3\,(\tilde{\mu}_1+\tilde{\mu}_3)\,\eta^2 \ge (\tilde{\varepsilon}_1+\tilde{\varepsilon}_3)\,(\tilde{\mu}_1+\tilde{\mu}_3)$ and consequently $\eta \ge \sqrt{1+\left(\tilde{\varepsilon}_1\big/\tilde{\varepsilon}_3\right)}$. Thus, the inequality $0 \le ab < 1$ holds.

Thus, on the basis of the results described in Section (2.2.4.), the system of dual series equations (2.222) and (2.223) is equivalent to the system of linear algebraic equations of the second kind, which has the form as that of (2.172) and (2.173).

2.4.5 Numerical Analysis for Grating and Chiral Half-Space

Introduce the reflection coefficients (a_0^x, a_0^y) and the transmission coefficients (b_0^x, b_0^y) for the x- and y-components of the electric field as follows: $a_0^x = a_0$ and $a_0^y = -\rho_1 b_0$ for $z > h_1$; $b_0^x = \left(x_0 + y_0\right)\exp\left(ik_1h_1\right)$ and $\quad b_0^y = -i\left(x_0 - y_0\right)\exp\left(ik_1h_1\right)$ for $z < 0$. These coefficients determine the field averaged over the grating period. The upper indices x and y relate, respectively, to the field of E-polarization and H-polarization. The incident field polarization is called the principal polarization, and the polarization perpendicular to the principal is called the cross-polarization. Using the boundary conditions, one obtains the following relations:

$$a_0^x + \tilde{e}\exp\left(-ik_1h_1\right) = \Omega b_0^x, \quad a_0^y + \rho_1\tilde{h}\exp\left(-ik_1h_1\right) = \Omega b_0^y,$$

where

$$\Omega = \frac{1}{2}\left[\left(1-\frac{\rho_1}{\rho_3}\right)\exp\left(ik_1h_1\right) + \left(1+\frac{\rho_1}{\rho_3}\right)\exp\left(-ik_1h_1\right)\right].$$

Note that the coefficients introduced are related by the functional dependence imposed by the boundary conditions.

The distinctive feature of the behavior of reflection coefficients as functions of the frequency parameter $\kappa = l/\lambda$ is the presence of peculiarities analogous to the classical Wood anomalies [45] at the so-called grazing points $\kappa_{1n} = n\Big/\sqrt{\tilde{\varepsilon}_1\tilde{\mu}_1}$ and peculiarities in the vicinity of the points $\kappa_{3n}^{\pm} = n\mathrm{Re}\left(1\Big/\left(\sqrt{\tilde{\varepsilon}_3\tilde{\mu}_3}\pm\gamma\right)\right)$ where $n = 0,\pm1,\ldots$. It is seen from the field representation that the quantities κ_{1n} and $\kappa_{3n}^{\pm}$ determine the frequency parameter values for which the nth harmonic of the nonchiral and chiral half-spaces, respectively, becomes propagating. Figure 2.6a shows the reflection coefficients of the principal-polarized field as a functions of κ. If $\kappa_{31}^{\pm} < \kappa < \kappa_{11}$, then the number of waves propagating in the chiral medium, which is assumed to be optically denser, is greater than that in the nonchiral medium. For small h_1, the surface harmonics decaying with distance from the grating become propagating upon entering the chiral medium and carry away a fraction of the energy. Such an energy redistribution explains the distinctive features of the reflection coefficients of the principal-polarized field in the vicinity of the points $\kappa_{3n}^{\pm}$.

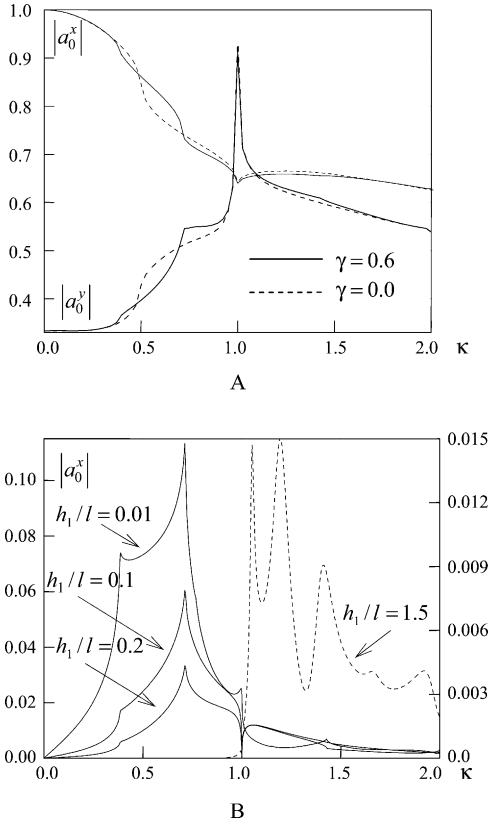

Fig. 2.6 The reflection coefficients versus frequency $\kappa = l/\lambda$ for (**a**) principal polarization field ($h_1/l = 0.05$) and (**b**) cross-polarized field (the *solid* and the *dashed curves* refer to the *left* and *right* vertical axes, respectively; $\gamma = 0.6$): $\tilde{\varepsilon}_1 = 1$, $\tilde{\mu}_1 = 1$, $\tilde{\varepsilon}_3 = 4$, $\tilde{\mu}_3 = 1$, $d/l = 0.5$

The frequency dependences of the reflection coefficients of cross-polarized waves are shown in Fig. 2.6b. The appearance of new propagating circularly polarized waves in the chiral medium at $\kappa_{3n}^{\pm}$ explains the increase in the reflection coefficients of the cross-polarized field at these points. The magnitudes of these coefficients depend on the amount of energy transferred by decaying surface waves to the chiral medium. For small distances, these coefficients decrease with increasing h_1. For $\left|\Gamma_1^1\right| h_1 \gg 1$, the surface field of the grating does not enter the second medium and the zero-order principal-polarized wave propagating normally does not produce the reflection of the cross-polarized field. Hence, the cross-polarized field is absent until the harmonic of the order $n = 1$, propagating at an angle to the z-axis, appears in the upper half-space for $\kappa > \kappa_{11}$.

Now we analyze the frequency dependences of the reflection coefficients in the case where the E- and H-polarized waves are incident simultaneously (see Fig. 2.7). The difference of the phases of the E- and H-polarized waves is $\delta\phi = \arg\left(\rho_1 \tilde{h} \Big/ \tilde{e}\right)$. The superposition of the incident waves will have different polarizations for different values of $\delta\phi$. Let $|\tilde{e}| = 1$ and $\left|\rho_1 \tilde{h}\right| = 1$. In-phase waves yield a linearly polarized wave, whereas for $\delta\phi = \pm\pi/2$, we have waves with right- and left-hand circular polarizations, respectively.

If a wave with right-hand circular polarization is incident, then the peculiarity in the vicinity of κ_{31}^{-} is more pronounced than the one in the vicinity of κ_{31}^{+}. This is explained by the efficient energy transfer in the case when the frequencies and polarizations of the incident wave and the propagating harmonic appearing in the chiral medium in the vicinity of κ_{31}^{-}, having also a right-hand circular polarization, are identical. In the vicinity of κ_{31}^{+}, the incident wave and the corresponding harmonic of the chiral medium interact weakly due to the fact that their field vectors rotate in opposite directions, although they both have circular polarization. For an incident linearly polarized wave, the above-mentioned features in the vicinity of κ_{31}^{+} are equally pronounced.

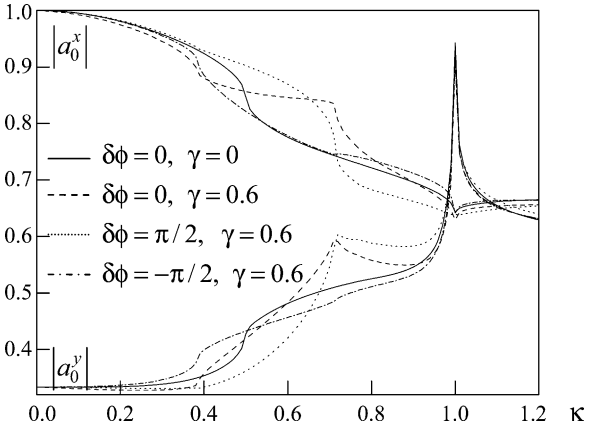

Fig. 2.7 The reflection coefficients versus frequency $\kappa = l/\lambda$ at the simultaneous incidence of E- and H-polarized waves: $\tilde{\varepsilon}_1 = 1$, $\tilde{\mu}_1 = 1$, $\tilde{\varepsilon}_3 = 4$, $\tilde{\mu}_3 = 1$, $d/l = 0.5$, $h_1/l = 0.05$

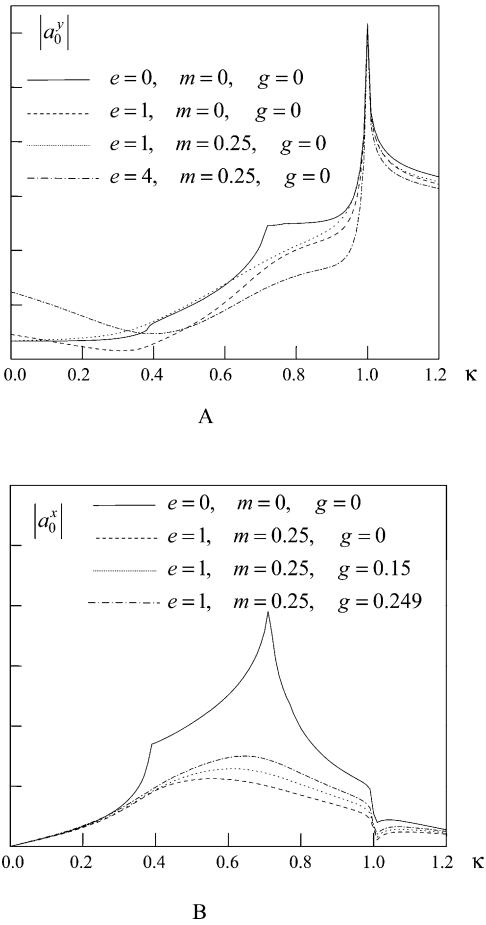

Fig. 2.8 The reflection coefficients versus frequency in the case of (**a**) principal and (**b**) cross-polarizations with damping presence: $\tilde{\varepsilon}_1 = 1$, $\tilde{\mu}_1 = 1$, $\tilde{\varepsilon}_3 = 4 + ie$, $\tilde{\mu}_3 = 1 + im$, $\gamma = 0.6 + ig$, $d/l = 0.5$, $h_1/l = 0.05$

Figure 2.8 shows the frequency dependences of the reflection coefficients in the presence of damping. Presence of losses results in decreasing and smoothing the absolute values of the reflection coefficients. In this case, the effect of losses on the principal-polarized field (Fig. 2.8a) is weaker than that on the cross-polarized field (Fig. 2.8b). The complex-valued chirality parameter stipulates that waves with right- and left-hand circular polarizations propagate with different attenuations since the waves with right- and left-hand circular polarizations have a greater attenuation for $\gamma'' > 0$ and $\gamma'' < 0$, respectively. Therefore, the wave diffraction at the parameter values for which the propagating harmonics are less attenuated is affected by losses to a smaller degree.

Figure 2.9 shows the reflection coefficients as functions of the relative chirality parameter $\eta = \gamma \Big/ \sqrt{\tilde{\varepsilon}_3 \tilde{\mu}_3}$ for $\kappa = \kappa_{31}^{-}(\eta)$ in the case when H-polarized wave is incident. An increase in η leads to an increase in $\kappa_{31}^{-}(\eta)$, and results in the

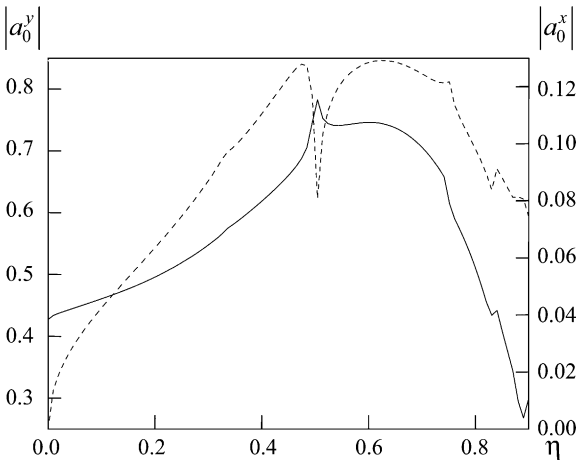

Fig. 2.9 The reflection coefficients as the functions of relative chirality parameter $\eta = \gamma/\sqrt{\tilde{\varepsilon}_3\tilde{\mu}_3}$ for $\kappa = \kappa_{31}^-$: the *solid* and the *dashed curves* refer to the *left* and *right* vertical axes, respectively; $\tilde{\varepsilon}_1 = 1$, $\tilde{\mu}_1 = 1$, $\tilde{\varepsilon}_3 = 4$, $\tilde{\mu}_3 = 1$, $d/l = 0.5$, $h_1/l = 0.05$

transition to the short-wavelength range where the considered reflection coefficient of principal polarization $|a_0^y|$ is generally increasing. The amplitude $|a_0^x|$ of the cross-polarized field caused by the chiral medium is increasing monotonically with increasing η in the single-wave region of the nonchiral half-space ($\kappa < \kappa_{11}$). The reflection coefficients $|a_0^{x,y}|$ exhibit distinctive features at the points of appearance of new propagating harmonics, i.e., under the condition $\kappa_{31}^-(\eta) = \kappa_{1n}$ (see Fig. 2.9).

Figure 2.10 shows the reflection coefficient of the cross-polarized field as function of the grating transparency $\Theta = d/l$ for the case when an *H*-polarized wave is incident. If $\kappa < \kappa_{11}$ and $|\Gamma_1^1| h_1 < 1$, then the excitation of the cross-polarized field is related to the existence of the higher-order spatial harmonics of the grating. In

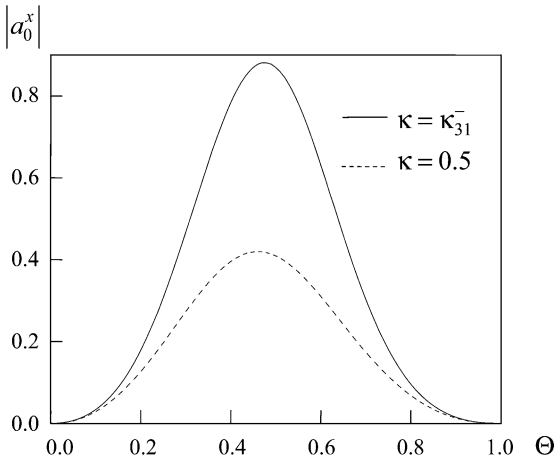

Fig. 2.10 The reflection coefficients versus the grating transparency $\Theta = d/l$ in the cross-polarization case: $\tilde{\varepsilon}_1 = 1$, $\tilde{\mu}_1 = 1$, $\tilde{\varepsilon}_3 = 4$, $\tilde{\mu}_3 = 1$, $\gamma = 0.6$, $h_1/l = 0.05$

this situation, the value of $|a_0^x|$ has a maximum if $\Theta = 0.5$ since this coefficient is mainly determined by the spatial harmonic of order $n = 1$, whose amplitude has a maximum if $\Theta = 0.5$ [45].

2.4.6 Strip Grating with Layered Medium

Consider the diffraction problem for the layered structure composed of a strip grating, a magnetodielectric layer, a chiral layer, and a screen (see Fig. 2.11). Let the grating lie in the plane $z = h_1$, and a perfectly conducting screen is placed in the plane $z = -h_2$. The domains D_1: $h_1 < z$ and D_2: $0 < z < h_1$ are magnetodielectric with relative permittivities $\tilde{\varepsilon}_1$, $\tilde{\varepsilon}_2$ and permeabilities $\tilde{\mu}_1$, $\tilde{\mu}_2$; the domain D_3: $-h_2 < z < 0$ is a chiral layer with the chirality parameter γ and relative permittivity and permeability $\tilde{\varepsilon}_3$, $\tilde{\mu}_3$.

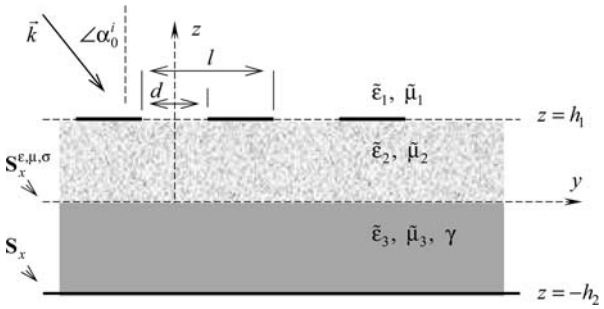

Fig. 2.11 The structure profile and the wave incidence

Suppose, that the monochromatic elliptically polarized plane wave $\vec{E}^i = \vec{E}_0 \exp\left(i\left[\left(\vec{k}\cdot\vec{r}\right) - kt\right]\right)$, $\vec{H}^i = \vec{H}_0 \exp\left(i\left[\left(\vec{k}\cdot\vec{r}\right) - kt\right]\right)$ is obliquely incident on the grating such that

$$\vec{E}_0 = \left\{\tilde{e},\ \rho_1\,\tilde{h}\cos\alpha_0^i\,,\ \rho_1\,\tilde{h}\sin\alpha_0^i\right\} \text{ and } \vec{H}_0 = \left\{\tilde{h},\ -\frac{\tilde{e}}{\rho_1}\ \cos\alpha_0^i,\ -\frac{\tilde{e}}{\rho_1}\ \sin\alpha_0^i\right\}.$$

Here, $\vec{k} = k\sqrt{\tilde{\varepsilon}_1\tilde{\mu}_1}\left\{0, \sin\alpha_0^i, -\cos\alpha_0^i\right\}$, α_0^i is the angle between the incident wave vector $\vec{k}$ and the z-axis (see Fig. 2.11); the values $\tilde{e}$, $\tilde{h}$, and ρ_1 have the same meaning as defined above.

As before, we present the diffracted field in the form of a Rayleigh expansion, i.e., an infinite series of the spatial harmonics. In the case of an oblique wave incidence that is under consideration, the propagation constant of the nth harmonic in the y-direction is $\Phi_n = 2\pi l^{-1}\left(n - \kappa\sqrt{\tilde{\varepsilon}_1\tilde{\mu}_1}\sin\alpha_0^i\right)$, and the field components have a form similar to the representation (2.208). For example, in the chiral layer (D_3) the x-components of the field may be represented as:

$$\left\{\begin{matrix}\tilde{E}_x^3\\ \tilde{H}_x^3\, i\rho_3\end{matrix}\right\} = \sum_{n=-\infty}^{\infty}\left[\left(x_n^+\exp\left(i\Gamma_n^+ z\right)+x_n^-\exp\left(-i\Gamma_n^+ z\right)\right)\pm\right. \quad ; \qquad -h_2 < z < 0\,.$$
$$\left.\pm\left(y_n^+\exp\left(i\Gamma_n^- z\right)+y_n^-\exp\left(-i\Gamma_n^- z\right)\right)\right]\exp\left(i\,\Phi_n y\right) \tag{2.229}$$

The boundary conditions at each inhomogeneity planes relates the sought complex amplitudes of the Rayleigh harmonics in all domains of the structure. Also the boundary conditions allow us to obtain two coupled systems of dual series equations to determine the unknown coefficients. The obtained systems being some generalization of systems (2.213) and (2.214) are equivalent to an operator equation of the first kind. It was shown in [123] that these systems can be reduced to

$$\begin{cases}\sum\limits_{n=-\infty\, n\neq 0}^{\infty} X_n\exp\left(in\vartheta\right)+\theta\, X_0=0; & \vartheta_0<|\vartheta|<\pi\\ \sum\limits_{n=-\infty\, n\neq 0}^{\infty}\frac{|n|}{n}X_n\exp\left(in\vartheta\right)+\theta\, X_0=\sum\limits_{n=-\infty}^{\infty} f_n^1\exp\left(in\vartheta\right); & |\vartheta|<\vartheta_0\ ,\\ \sum\limits_{n=-\infty\, n\neq 0}^{\infty}\frac{(-1)^n}{n+\theta}X_n+X_0=0; & \vartheta=\pi\end{cases} \tag{2.230}$$

$$\begin{cases}\sum\limits_{n=-\infty\, n\neq 0}^{\infty} Y_n\exp\left(in\vartheta\right)+\theta\, Y_0=0; & \tilde{\vartheta}_0<|\vartheta|<\pi\\ \sum\limits_{n=-\infty\, n\neq 0}^{\infty}\frac{|n|}{n}Y_n\exp\left(in\vartheta\right)+\theta\, Y_0=\sum\limits_{n=-\infty}^{\infty} f_n^2\exp\left(in\vartheta\right); & |\vartheta|<\tilde{\vartheta}_{00}\ .\\ \sum\limits_{n=-\infty\, n\neq 0}^{\infty}\frac{(-1)^n}{n+\theta}Y_n+Y_0=0; & \vartheta=\pi\end{cases} \tag{2.231}$$

Here, $\tilde{\vartheta}_0=\pi-\vartheta_0$; the value $\theta\in[-0.5;\,0.5)$ is chosen so that $\theta=-m_0+\kappa\,\sin\alpha_0^i$, where m_0 is the nearest integer to $\kappa\,\sin\alpha_0^i$; X_n and Y_n are certain linear combinations of the unknowns x_n^-, y_n^- which are the Fourier coefficients describing the complex amplitudes of the nth order spatial spectrum harmonics in the chiral medium (see (2.229)). The rest of the Fourier coefficients can be expressed in terms of x_n^-, y_n^-; the coefficients $f_n^{1,2}$ are linear combinations of X_n and Y_n.

Using the asymptotic estimates, it is possible to show that

$$f_n^{1,2}\underset{|n|\to\infty}{=}\sigma_n^{1,2}n^{-2}+O\left(\exp\left(-\sigma\,|n|\right)\right),$$

where $\sigma\approx 4\pi\left(h_1/l\right)>0$, and the values $\sigma_n^{1,2}$ satisfy the conditions $\sum\limits_{n=-\infty}^{\infty}\left|\sigma_n^{1,2}\right|^2<\infty$. These representations show that the series in the right-hand sides of (2.230) and (2.231) are uniformly and rapidly convergent series. So for the given problem the singularities, which correspond to the principal part of the operator of

the problem, have been isolated on the left-hand sides of the equations. The obtained functional systems are coupled only through the right-hand sides.

In the form (2.230) and (2.231), the systems are equivalent to the well-known scalar Riemann–Hilbert problem [45]. The method for its solution allows us to obtain the system of linear algebraic equations

$$\begin{cases} \theta X_0 = \sum\limits_{p=-\infty}^{\infty} V_{0p} \left\{ \alpha_p^0 X_p + \beta_p Y_p \right\} + b_0 \\ X_n = \sum\limits_{p=-\infty}^{\infty} V_{np} \left\{ \alpha_p^n X_p + \beta_p Y_p \right\} + b_n \\ \theta Y_0 = \sum\limits_{p=-\infty}^{\infty} \tilde{V}_{0p} \left\{ \tilde{\alpha}_p X_p + \tilde{\beta}_p^0 Y_p \right\} + \tilde{b}_0 \\ Y_n = \sum\limits_{p=-\infty}^{\infty} \tilde{V}_{np} \left\{ \tilde{\alpha}_p X_p + \tilde{\beta}_p^n Y_p \right\} + \tilde{b}_n \end{cases}, \tag{2.232}$$

where the values V_{np}, $\tilde{V}_{np}$; α_p^n, β_p; and $\tilde{\alpha}_p$, $\tilde{\beta}_p^n$ are given in [123]. From the asymptotic estimates of the coefficients α_p^n, $\tilde{\beta}_p^n = O\left(p^{-2}\right)$ and $\tilde{\alpha}_p$, $\beta_p = O\left(\exp\ (-\sigma\,|\mathrm{p}|)\right)$, and from the behavior of V_{np}, $\tilde{V}_{np}$ as $|n|, |p| \to \infty$ it follows that (2.232) is equivalent to a Fredholm system of the second kind. Such a system can be effectively solved by appropriate truncation to meet any preassigned accuracy.

2.4.7 *Electromagnetic Properties of a Strip Grating with Layered Medium in the Resonant Frequency Range*

The diffraction grating changes the incident field into a superposition of spatial spectrum waves. This superposition consists of a finite number of propagating harmonics and an infinite number of surface harmonics decaying in the z-direction. The mth surface harmonic of the jth domain becomes a propagating wave once the frequency parameter κ is such that $\Gamma_m^j(\kappa) = 0$, $j = 1,2$, and $\Gamma_m^{\pm}(\kappa) = 0$ $(j = 3)$. We denote such value of parameter κ by κ_{jm} for $j = 1,2$, and $\kappa_{3m}^{\pm}$ for the chiral domain $(j = 3)$.

Due to the presence of the grating, different harmonics from all domains can interact with each other, and an energy redistribution between harmonics takes place. For certain values of the structure parameters, significant energy redistribution may be achieved, in which the field of one polarization dominates over the field of other polarizations. Such essential energy redistribution is caused by the resonant interaction of harmonics in all domains of the structure.

The far field of the structure is represented as a sum of a finite number of propagating harmonics. Let us introduce the efficiencies in the n-order of the spectrum R_n^x, R_n^y, determining the relative fraction of scattered energy density that is spread from the structure to the upper half-space by propagating harmonics of nth order that has the wave vector $\vec{k}_n^1 = \left\{0, \Phi_n, \Gamma_n^1\right\}$. The superscript x corresponds to the E-polarized field and the superscript y to the H-polarized field.

Our interest is focused on the diffraction properties associated with the conversion of the incident field of principal polarization into the cross-polarized reflected field. Also the phenomenon of nearly total transformation of an elliptically polarized incident wave into a linearly polarized reflected wave is investigated. The efficiency $R_n^{x,y}$ as a function of the frequency parameter κ and the relative thickness of the chiral layer $H_2 = h_2/l$ will be studied numerically in the cases of specular and nonspecular reflections.

2.4.7.1 Specular Reflection

Figure 2.12 presents efficiency $R_0^{x,y}$ in the case of normal incidence of the *E*-polarized wave. For the upper half-space $h_1 < z$, the single-mode region (when

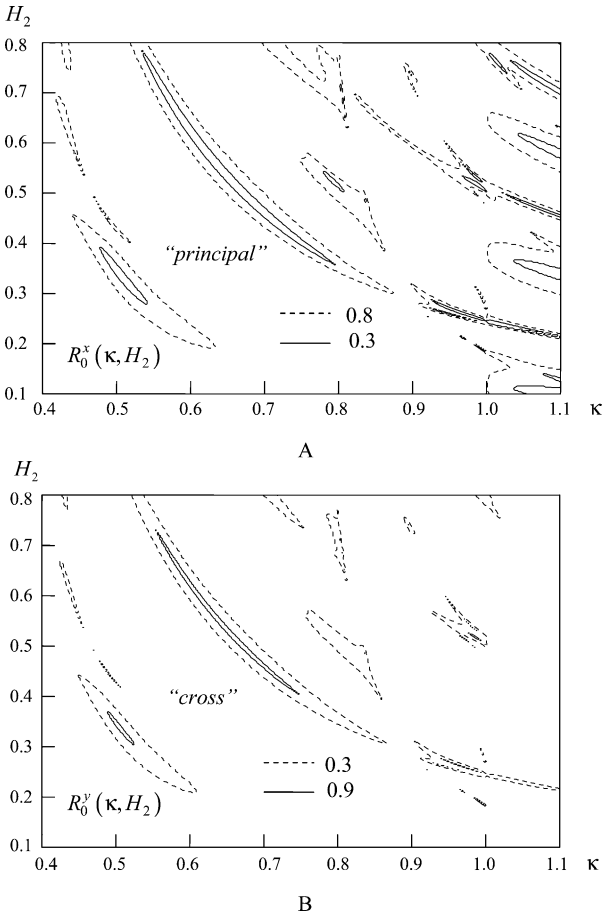

Fig. 2.12 (**a**) The principal and (**b**) cross-polarization efficiency in the normal incidence case: $\tilde{e} = 1.0$, $\tilde{h} = 0$, $\alpha_0^i = 0$, $\tilde{\varepsilon}_1 = 1.0$, $\tilde{\mu}_j = 1.0$, $\tilde{\varepsilon}_2 = \tilde{\varepsilon}_3 = 4.0$, $\eta = 0.3$, $d/l = 0.5$, $h_1/l = 0.03$

$N_1 = 1$) is determined by the condition $-\kappa < \kappa_{11}$, $\kappa_{11}=1$, when $\alpha_0^i = 0$ and $\tilde{\varepsilon}_1 = \tilde{\mu}_1 = 1$. In this region, the minima of efficiency R_0^x of the principal polarization correspond to the maxima of the efficiency R_0^y of the cross-polarization, and the equality $R_0^x + R_0^y = \tilde{e}^2 + \left(\rho_1 \tilde{h}\right)^2$ holds. In the parameter region of existence of the higher propagating harmonics of the first medium, i.e., when $\kappa \geq \kappa_{11}$, this picture is changed because of the energy redistribution between the higher harmonics. The vicinities of frequencies $\kappa_{3n}^{\pm}$ are characterized by effective polarization conversion, which is most pronounced in the interval $\kappa \in [0; \kappa_{11}]$.

In the case of the oblique incidence ($\alpha_0^i \neq 0$) of the *E*-polarized wave, the cross-polarization efficiency R_0^y is presented in Fig. 2.13. A linearly polarized wave normally incident on a chiral medium produces the left- and right-hand circularly

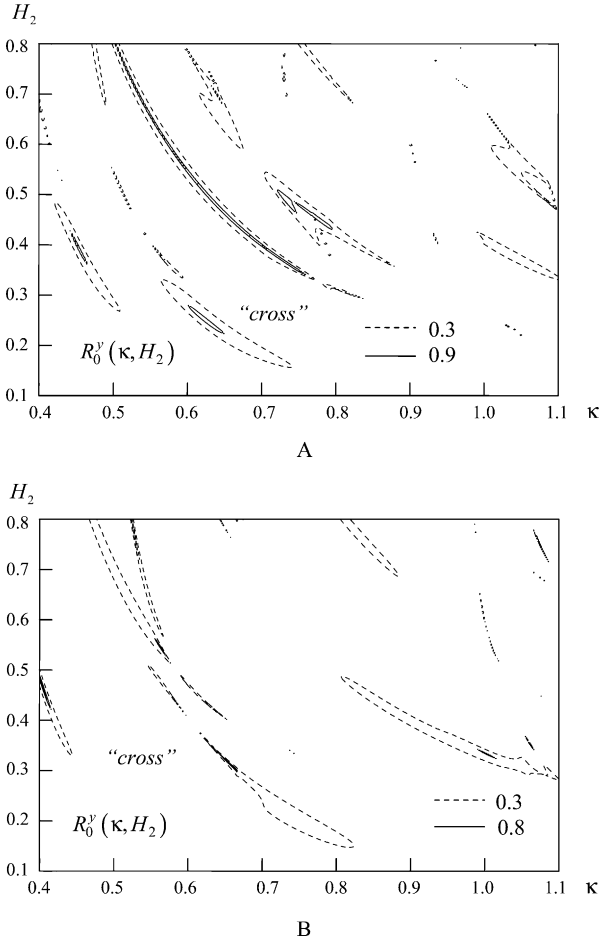

Fig. 2.13 The cross-polarization efficiency in the oblique incidence case: $\tilde{e} = 1.0$, $\tilde{h} = 0$, $\tilde{\varepsilon}_1 = 1.0$, $\tilde{\mu}_j = 1.0$, $\tilde{\varepsilon}_2 = \tilde{\varepsilon}_3 = 4.0$, $\eta = 0.3$, $d/l = 0.5$, $h_1/l = 0.03$, (**a**) $\alpha_0^i = 15°$ and (**b**) $\alpha_0^i = 30°$

polarized waves in it. For normal incidence, they propagate in the same direction as the incident wave, and their superposition would be a linear-polarized wave, with the rotation of polarization plane as the propagation proceeds inside the chiral medium. In the case of oblique incidence, the circularly polarized waves propagate in the different directions, and their superposition is not a linearly polarized wave. In the case of normal incidence, the nth and $(-n)$th harmonics appear at the same frequency. But they do not behave like that in the case of the oblique incidence. As α_0^i increases, the points of appearance of the higher harmonics move away from $\kappa_{jn} = \kappa_{j(-n)}$, $j = 1,2$, and $\kappa_{3n}^{\pm} = \kappa_{3(-n)}^{\pm}$: to the left for the positive harmonics and to the right for the negative. The phase velocities of the plus and minus nth harmonics are different when $\alpha_0^i \neq 0$. Hence the resonances split, and their number is doubled. The splitting is most evident at small angles. Since at the oblique incidence, the higher harmonics of the chiral medium appear before those at $\alpha_0^i = 0$; the polarization conversion region extends along κ to the left (to the low frequency region) as α_0^i grows. The most broadband conversion is observed at $\alpha_0^i = 0$. The efficiency in the zeroth order of spectrum for the cross-polarization is the same, whether an E- or H-polarized wave is incident.

The performed numerical analysis [125] shows that the incident linearly polarized wave can be nearly completely converted into the specularly reflected wave of cross-polarization almost at any incident angle α_0^i.

The combination of the nth propagating harmonics of E- and H-polarization generally gives an elliptically polarized wave. Now our concern will be with the diffraction features associated with the change of the incident elliptically polarized wave into a specularly reflected zero-order harmonic of linear (E- or H-) polarization. The value $\Delta R_0 = R_0^x - R_0^y$ as a function of the structure parameters will be considered. Let the energy density of the incident elliptically polarized wave, which is proportional to $\tilde{e}^2 + \left(\rho_1 \tilde{h}\right)^2$, equal 100%. Thus, when $\Delta R_0 = 100\%$, the total transformation from an incident elliptically polarized wave into a specularly reflected zero-order harmonic of linear E-polarization with the energy density 100% occurs. Similarly, $\Delta R_0 = -100\%$ means a total transformation into an H-polarized wave with the density 100%. Thus, the value ΔR_0 measures the efficiency of elliptical to linear polarization transformation.

The complex amplitudes $\tilde{e}$, $\tilde{h}$ define a character of elliptical polarization of incident wave. For example, if $|\tilde{e}| = \left|\rho_1 \tilde{h}\right|$ and $\delta\phi = \arg\left(\rho_1 \tilde{h} \Big/ \tilde{e}\right) = \pm\pi/2$, the resultant is a right-handed or left-handed circularly polarized incident wave; when $\tilde{e} = 0$ or $\tilde{h} = 0$, then the incident wave, respectively, has linear H- or E-polarization.

The value ΔR_0 as a function of κ and $H_2 = h_2/l$ for the different relations of the E- and H-polarized field components in three incident wave of elliptical polarization is presented in Fig. 2.14. The domains of high-purity polarization transformation, in which $|\Delta R_0| > 90\%$, may be identified for different polarizations in the incident wave [124]. The domains of transformation into E- and H-polarized specularly reflected waves are situated close to each other, and their extent depends on the content of E- and H-polarized field components in the incident wave. These domains

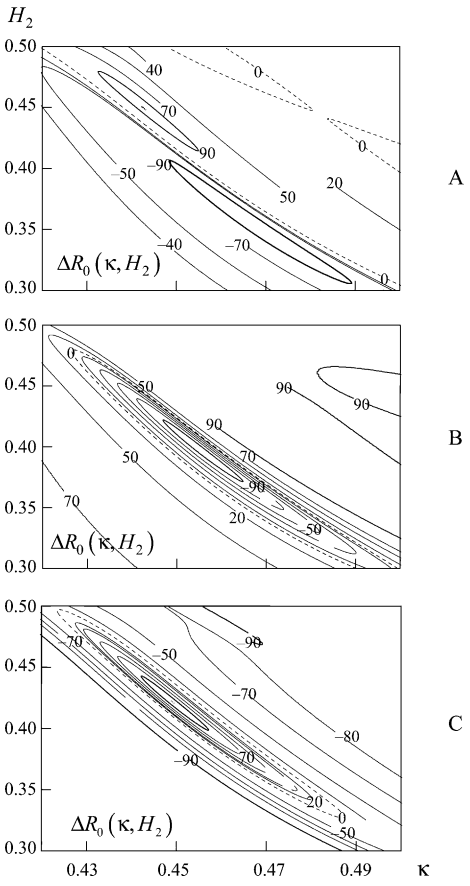

Fig. 2.14 The polarization transformation efficiency ΔR_0 versus κ and H_2 for different polarizations of the incident wave: $\tilde{\varepsilon}_1 = 1.0$, $\tilde{\mu}_j = 1.0$, $\tilde{\varepsilon}_2 = \tilde{\varepsilon}_3 = 4.0$, $\eta = 0.3$, $d/l = 0.5$, $h_1/l = 0.015$, $\alpha_0^i = 15°$, $\delta\phi = -\pi/2$; (**a**) $|\tilde{e}| = \left|\rho_1 \tilde{h}\right|$; (**b**) $|\tilde{e}| = 4\left|\rho_1 \tilde{h}\right|$; and (**c**) $4|\tilde{e}| = \left|\rho_1 \tilde{h}\right|$

as a whole are rather wide and their location depends on the elliptical polarization parameters of the incident wave.

When the efficiency of elliptical to linear polarization transformation does not take extreme values ($\Delta R_0 \neq \pm 100\%$, i.e., the scattered field has both *E*- and *H*-polarized components), a wave of some elliptical polarization is specularly reflected from the structure. Its elliptical polarization may be described by the Stokes parameters [134]. These parameters for the reflected elliptically polarized wave of zero order may be expressed in terms of ΔR_0 and the phase difference ΔF_0 between the zero-order harmonics of *E*- and *H*-polarizations.

The efficiency of the polarization transformation for different incident wave angles is illustrated in Fig. 2.15. Nearly total polarization transformation ($|\Delta R_0| > 97\%$) is seen to take place in a wide range $\left(\Delta\alpha_0^i \approx 20°\right)$ of incident wave angles. Considering the values of ΔR_0 and ΔF_0, one can analyze how the reflected field polarization depends on frequency.

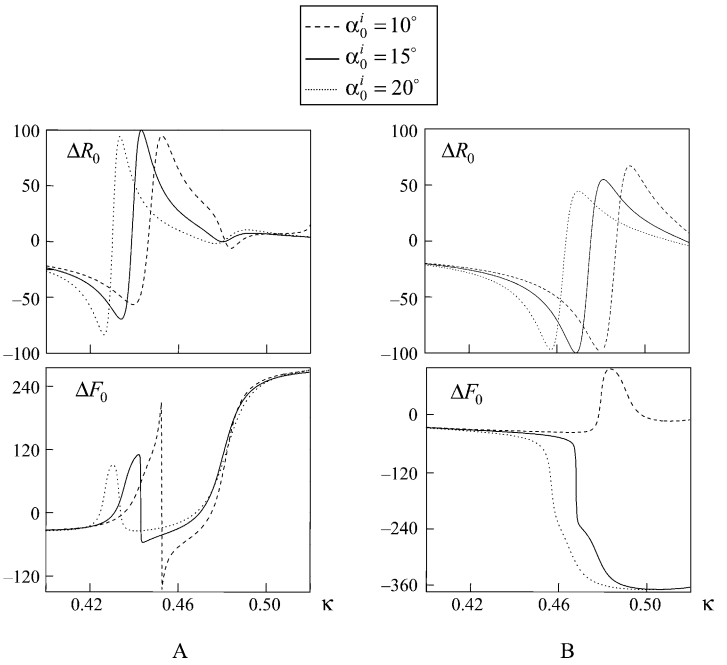

Fig. 2.15 The polarization transformation efficiency ΔR_0 and the phase difference ΔF_0 versus κ for different incident angles: $\tilde{\varepsilon}_1 = 1.0$, $\tilde{\mu}_j = 1.0$, $\tilde{\varepsilon}_2 = \tilde{\varepsilon}_3 = 4.0$, $\eta = 0.3$, $d/l = 0.5$, $h_1/l = 0.015$, $|\tilde{e}| = \left|\rho_1 \tilde{h}\right|$, $\delta\phi = -\pi/2$; (**a**) $H_2 = 0.448$; and (**b**) $H_2 = 0.354$

The dependence of the transformation of the elliptical to linear polarization on geometrical and constitutive parameters of the considered structure was studied. It was found that the polarization transformation might be effectively controlled by an appropriate choice of the structure parameters. For instance, a small decrease of the magnetodielectric layer thickness increases the polarization transformation bandwidth, and a change of the grating slot width allows frequency tuning.

2.4.7.2 Nonspecular Reflection

The information about the direction of the wave vector $\vec{k}_n^1$ allows us to define a difference between the angles of the primary wave arrival and the secondary nth harmonic departure. Given the angle difference, we can specify the κ to α_0^i relationship. In particular, from the condition $\vec{k}_n^1 = -\vec{k}$, we derive the relation

$$\alpha_0^i = -\arcsin\left(n/2\kappa_1\right),$$

which defines the autocollimation reflection regime of the nth spatial harmonic. In the regime, the nth wave of the upper half-space propagates in the direction opposite

to the primary wave, that is, $\alpha_0^i = \alpha_n$, where α_n is the nth harmonic angle of propagation. An energy concentration in this nth wave may be achieved by optimizing the structure parameters.

Denote by N_j the number of the propagating waves in jth domain harmonics with different propagation constants. The scattering regime can be characterized by the vector $N(\kappa) = \{N_1, N_2, N_3\}$.

Further on, nonspecular reflection accompanied by polarization conversion will be traced [127] as applied to the minus fist propagating harmonic with the wave vector $\vec{k}_{-1}^{1} = \left\{0, \Phi_{-1}, \Gamma_{-1}^{1}\right\}$.

For an incident H-polarized wave, the cross-polarization efficiency R_{-1}^{x} in the autocollimation regime is illustrated in Figs. 2.4a and 2.16. As seen, within $1.283 < \kappa < 1.289$ (which matches $22°56' > \alpha_{-1} > 22°50'$) and $0.760 < H_2 < 0.767$, there exists a zone where the efficiency for cross-polarization exceeds 0.9. The R_{-1}^{x} maximum reaches 0.933, it is found to be at $\kappa = 1.285$ ($\alpha_{-1} = 22°54'$) and $H_2 = 0.765$. This effect takes place in the frequency zone specified by $N(\kappa) = \{2,6,9\}$. A similar regime can be also observed for the E-polarized wave incidence. The autocollimation regime with no polarization conversion may have both explicit and implicit resonance character. But the autocollimation regime with the polarization conversion has sharp resonances.

The excitation of the structure at $\alpha_0^i = 87°$ when the incident H-polarized wave nearly skims the structure is illustrated in Figs. 2.4b and 2.17a. In this regime, one observes a quasi-complete conversion of the incident, nearly surface-parallel wave into the $n = -1$ cross-polarized harmonic propagating at $\alpha_{-1} = 8°12'$. The telescopicity coefficient ($r_t = \cos\alpha_{-1} / \cos\alpha_0^i$) amounts to 18.925. The maxima of R_{-1}^{x} is 0.99 at $\kappa = 0.876$ and $H_2 = 0.313$. The zone of this effect at a level of $R_{-1}^{x} > 0.9$

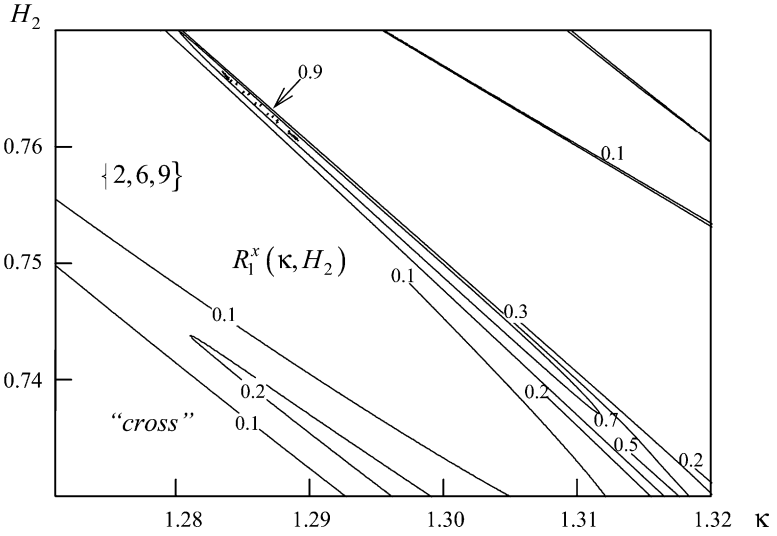

Fig. 2.16 The cross-polarization efficiency in the autocollimation regime: $\tilde{e} = 0$, $\rho_1 \tilde{h} = 1.0$, $\alpha_0^i = -\arcsin(1\ 2\kappa)$, $\tilde{\varepsilon}_1 = 1.0$, $\tilde{\mu}_j = 1.0$, $\tilde{\varepsilon}_2 = \tilde{\varepsilon}_3 = 4.0$, $\eta = 0.3$, $d/l = 0.448$, $h_1/l = 0.015$

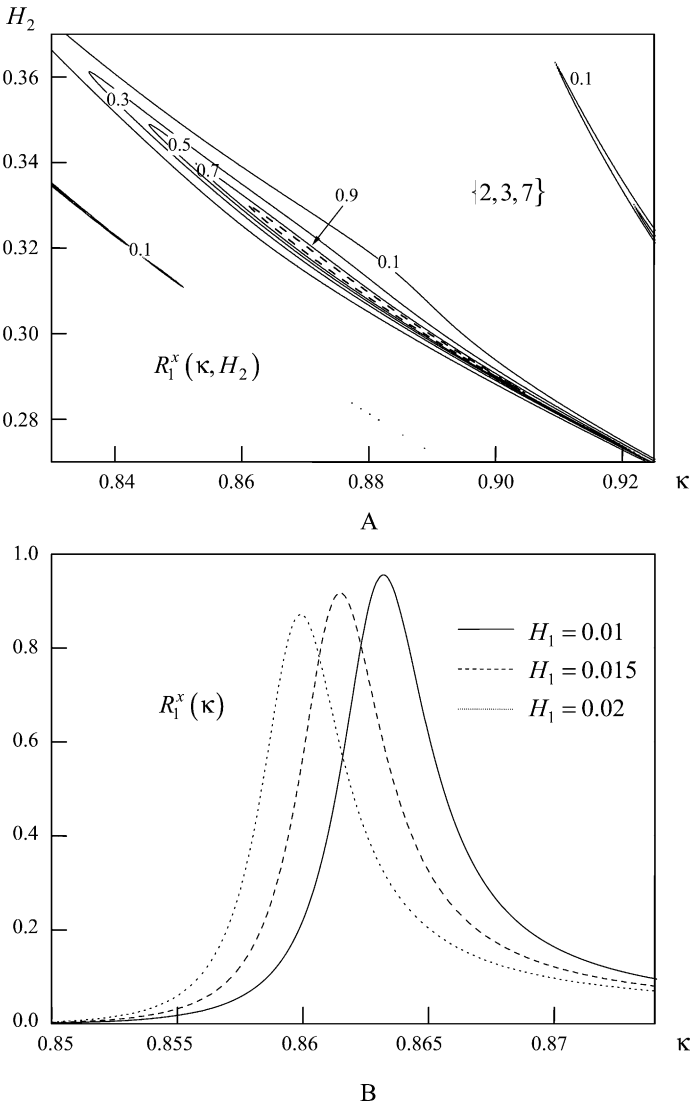

Fig. 2.17 The cross-polarization efficiency in enhanced-telescopicity regime: $\tilde{e} = 0$, $\rho_1 \tilde{h} = 1.0$, $\alpha_0^i = 87°$, $\tilde{\varepsilon}_1 = 1.0$, $\tilde{\mu}_j = 1.0$, $\tilde{\varepsilon}_2 = \tilde{\varepsilon}_3 = 4.0$, $\eta = 0.3$, $d/l = 0.9$, (**a**) $H_1 = h_1/l = 0.015$, and (**b**) $H_2 = 0.313$

with the telescopicity coefficient r_t from 18.827 to 19.009 lies within $0.853 < \kappa < 0.904$ and $0.287 < H_2 < 0.340$. In this case, the number of the harmonics propagating in the media is {2,3,7}. For the *E*-polarized wave incidence, the telescopicity regime has not been found.

The broadband property of the regimes of polarization transformation is effectively controlled by the distance h_1 ($H_1 = h_1/l$) between the grating and the chiral layer (see, for example, Fig. 2.17b). The value of this distance defines the electromagnetic coupling between the grating and the chiral layer via the higher harmonics. As h_1 increases, the higher surface harmonics of the grating cannot reach the chiral layer. Only when h_1 is small, such that $\left|\Gamma_1^2 h_1\right| \ll 1$, the higher harmonics localized near the grating are able to participate in the energy transport and redistribution actions essential for the discussed processes. In this case, the magnetodielectric layer thickness is too small ($h_1 \ll \lambda$) to have any valuable effect on the location of the considered regimes in the plane κ, H_2. As h_1 increases, the grating to chiral layer coupling weakens, the quality of the resonance effects goes up, and the zones of existence of the effects shrink. Thus, the broadband property of the regime can be effectively controlled by small h_1 variations.

The phenomenon of polarization transformation is caused by the presence of the chiral medium. The discussed structure can be considered as an open resonator where the grating and the screen act as the mirrors and the chiral and dielectric layers are the resonator fillings. On the one hand, being a periodical inhomogeneity, the grating converts the incident wave into a superposition of an infinite number of spatial harmonics and thus excites higher order oscillations in the resonator layers. On the other hand, the grating makes different oscillations interact with each other and so establishes electromagnetic coupling between different Floquet harmonics both inside and outside the resonator.

Due to the circular polarization of a chiral medium eigenwaves, the *E*- and *H*-polarized waves are coupled in the chiral layer, and that makes possible the polarization transformation. At a given frequency and with a suitable choice of the structure parameters, the wave interference redistributes the energy between the propagating harmonics so that the discussed regimes of polarization transformation occur. Effective polarization transformation occurs when the number of the harmonics propagating in the "resonator layers" is more than in free space. This phenomenon is of resonance character, and it is a response to the oscillatory excitations which are close to the structure eigenmodes that are described in [135].

2.5 Resonant Scattering of Electromagnetic Waves by Gratings and Interfaces Between Anisotropic Media and Metamaterials

This section is concerned with the boundary value diffraction problem of a strip grating located on different media interfaces: anisotropic dielectric, ferrite, metamaterial, etc. The solution strategy begins with the partial domain (sewing) method to reduce the initial boundary value problem in terms of Helmholtz (Maxwell's) equations to dual series equations. Owing to the regularization theory of dual series equations outlined in Section 2.2, we arrive at an infinite system of linear algebraic equations of the second kind solvable by truncation to any accuracy desired.

Examples illustrating the computation of various physical characteristics (transition and reflection coefficients, eigenfrequencies, diffraction fields, etc.) are given. For more details about the processes of the electromagnetic wave interaction with a strip grating located on a medium interface, we refer to the original papers [18, 136–148].

2.5.1 Resonant Wave Scattering by a Strip Grating Loaded with a Metamaterial Layer

The knowledge of characteristic features of wave processes in metamaterial-loaded open structures (open resonators and waveguides, diffraction gratings, etc.) will lend us fresh opportunities in forming new physical principles of electromagnetic wave generation, amplification, and channeling. A very important stage is explorations into resonance phenomena occurring when monochromatic electromagnetic waves interact with single-periodic metamaterial-loaded structures. The present section is concerned with resonant effects arising during the electromagnetic wave scattering by a strip grating backed by a metamaterial layer such that its effective permittivity depends on the excitation wave frequency. It is shown that in the frequency region where the real part of the metamaterial effective permittivity takes on negative values, the open structure of this kind has an infinite number of complex eigenfrequencies with a finite accumulation point. These frequencies match eigenoscillations whose amplitudes decay exponentially with time. When the frequency of the monochromatic linearly polarized incident wave coincides with the real part of one of the eigenfrequencies of the structure, effects of nearly total reflection and transition of the wave energy arise.

The process of monochromatic plane-wave interaction with a strip grating located on a metamaterial surface will be modeled in terms of the following boundary value problem:

Let the layer $-h < z < 0$ (Fig. 2.18) be filled with some isotropic metamaterial whose effective permittivity depends on frequency as follows

$$\tilde{\varepsilon}(\omega) = 1 - \frac{\omega_p^2}{\omega(\omega + i\nu)}, \tag{2.233}$$

where $\omega = kc$ is the circular frequency, $k = 2\pi/\lambda$, c and λ are the velocity of light and wavelength in a vacuum, ω_p is the characteristic frequency established by the parameters of the metamaterial constituents, and $\nu \geq 0$ is the frequency responsible for the losses. The permeability is $\mu = 1$. The metamaterial boundary ($z = 0$) supports an x-infinite and x-homogeneous perfectly conducting strip grating with d-wide grooves and a period l (see Fig. 2.18). We assume that the excitation wave and the diffraction field are also x-independent. The time dependence is $\exp(-ikt)$. From the half-space $z > 0$ and along the z-axis, an H-polarized unit-amplitude plane electromagnetic wave

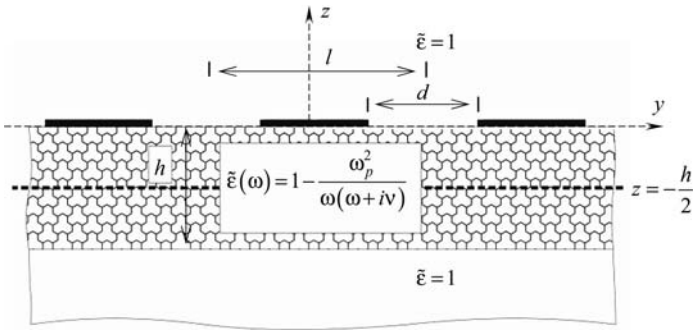

Fig. 2.18 The problem geometry

$$\tilde{H}_x^i = \mathrm{e}^{-ikz}, \qquad \tilde{E}_y^i = \mathrm{e}^{-ikz}, \qquad \tilde{E}_x^i = \tilde{E}_z^i = \tilde{H}_y^i = \tilde{H}_z^i = 0$$

is incident.

The diffraction field $\left\{\vec{E}^s, \vec{H}^s\right\}$ satisfies the homogeneous system of Maxwell's equations and satisfies the Meixner condition, radiation condition at infinity ($z \to \pm\infty$), periodicity condition, boundary condition on perfectly conducting grating strips, and the conjugation condition on the metamaterial surface. Under these assumptions, the diffraction field $\left\{\vec{E}^s, \vec{H}^s\right\}$ is governed by the unique nonzero component $\tilde{H}_x^s$ of the magnetic field as follows:

$$\tilde{E}_y^s = -\frac{1}{ik\tilde{\varepsilon}} \frac{\partial \tilde{H}_x^s}{\partial z}, \qquad \tilde{E}_z^s = \frac{1}{ik\tilde{\varepsilon}} \frac{\partial \tilde{H}_x^s}{\partial y}.$$

The other components of the field $\left\{\vec{E}^s, \vec{H}^s\right\}$ vanish, suggesting that the diffraction field is H-polarized.

Introduce the function $\tilde{U}(g,k)$, $g = \{y, z\}$, coinciding with the magnetic component of the total field $\tilde{H}_x^i + \tilde{H}_x^s$. As follows from Maxwell's equations, everywhere but on the grating strips and the metamaterial surface this function satisfies the Helmholtz equation

$$\Delta_{y,z} \tilde{U}(g,k) + k^2(z)\, \tilde{U}(g,k) = 0; \qquad k^2(z) = \begin{cases} k^2; & z > 0 \quad \text{and} \quad z < -h \\ k^2\tilde{\varepsilon}; & -h < z < 0 \end{cases}. \tag{2.234}$$

In addition, the $\tilde{U}(g,k)$ function is periodic with period l along the y-axis and meets the radiation condition in the half-spaces $z > 0$ and $z < -h$. The functions $\tilde{U}(g,k)$ and $(k(z))^{-2}\, \partial \tilde{U}(g,k) \big/ \partial z$ are required to be continuous across the grating slots $\left\{g:\ z = 0,\ \left|2\pi y l^{-1} + n\right| > \pi\left(1 - dl^{-1}\right);\ n = 0, \pm 1, \pm 2, \ldots.\right\}$ and across the interface between the metamaterial and the free space at $z = -h$. On the grating strips $\left\{g:\ z = 0,\ \left|2\pi y l^{-1} + n\right| < \pi\left(1 - dl^{-1}\right);\ n = 0, \pm 1, \pm 2, \ldots.\right\}$, they satisfy the boundary conditions

$$\left.\frac{\partial \tilde{U}(g,k)}{\partial z}\right|_{z=0+0}=0, \qquad \left.\frac{\partial \tilde{U}(g,k)}{\partial z}\right|_{z=0-0}=0. \tag{2.235}$$

On this basis, the sought function $\tilde{U}(g,k)$ can be expressed via its Fourier series in the Y-variable in the three domains: the half-spaces $\mathbf{A}$ ($z>0$) and $\mathbf{B}$ ($z<-h$) and the layer $-h<z<0$, taking the appearance

$$\tilde{U}(g,k)=\begin{cases} \mathrm{e}^{-ikz}+\sum\limits_{n=-\infty}^{\infty} R_{n0}^{\mathbf{AA}}\mathrm{e}^{i(\Phi_n y+\Gamma_{1n}z)}; & z>0 \\ \sum\limits_{n=-\infty}^{\infty} \mathrm{e}^{i\Phi_n y}\left(C_{1n}\mathrm{e}^{i\Gamma_{2n}(z+h)}+C_{2n}\mathrm{e}^{-i\Gamma_{2n}z}\right); & -h<z<0 \\ \sum\limits_{n=-\infty}^{\infty} T_{n0}^{\mathbf{BA}}\mathrm{e}^{i(\Phi_n y-\Gamma_{1n}(z+h))}; & z<-h \end{cases}. \tag{2.236}$$

Here $\Gamma_{1n}=\sqrt{k^2-\Phi_n^2}$, $\Gamma_{2n}=\sqrt{k^2\tilde{\varepsilon}-\Phi_n^2}$, $\Phi_n=2\pi n/l$. The root branches are chosen via the radiation condition (cf. Section 1.1.4) to have $k\mathrm{Re}\Gamma_{1n}\geq 0$, $\mathrm{Im}\Gamma_{1n}\geq 0$. Notice that any branch of the root Γ_{2n} can be adopted. For definiteness sake, let $k\mathrm{Re}\Gamma_{2n}\geq 0$, $\mathrm{Im}\Gamma_{2n}\geq 0$.

Now we will reduce the boundary value diffraction problem to dual series equations for the unknown coefficients $\left\{R_{n0}^{\mathbf{AA}}\right\}_{n=-\infty}^{\infty}$ of the $\tilde{U}(g,k)$ expansion into the Fourier series in the half-space $z>0$ [see (2.236)]. Indeed, using (2.236) and applying the conjugation conditions on the metamaterial boundaries yields the relationships between the coefficients $\left\{C_{pn}\right\}_{n=-\infty}^{\infty}$, $p=1,2$, $\left\{T_{n0}^{\mathbf{BA}}\right\}_{n=-\infty}^{\infty}$, and $\left\{R_{n0}^{\mathbf{AA}}\right\}_{n=-\infty}^{\infty}$ in the form

$$T_{n0}^{\mathbf{BA}}=\frac{2\tilde{\varepsilon}\Gamma_{1n}\exp(i\Gamma_{2n}h)}{\Gamma_n}\left(R_{n0}^{\mathbf{AA}}-\delta_0^n\right). \tag{2.237}$$

$$C_{1n}=\frac{\tilde{\varepsilon}\Gamma_{1n}(\Gamma_{2n}-\tilde{\varepsilon}\Gamma_{1n})}{\Gamma_{2n}\Gamma_n}\left(R_{n0}^{\mathbf{AA}}-\delta_0^n\right) \tag{2.238}$$

$$C_{2n}=\frac{\tilde{\varepsilon}\Gamma_{1n}(\Gamma_{2n}+\tilde{\varepsilon}\Gamma_{1n})}{\Gamma_{2n}\Gamma_n}\left(R_{n0}^{\mathbf{AA}}-\delta_0^n\right) \tag{2.239}$$

Here, $\Gamma_n=\exp(i2\Gamma_{2n}h)(\Gamma_{2n}-\tilde{\varepsilon}\Gamma_{1n})-\Gamma_{2n}-\tilde{\varepsilon}\Gamma_{1n}$ and δ_m^n is the Kronecker delta.

Satisfying the strip and slot boundary conditions yields

$$1+\sum_{n=-\infty}^{\infty} R_{n0}^{\mathbf{AA}}\mathrm{e}^{i\Phi_n y}=\sum_{n=-\infty}^{+\infty}\left(C_{1n}\mathrm{e}^{i2\Gamma_{2n}h}+C_{2n}\right)\mathrm{e}^{i\Phi_n y}; \qquad |y|>\frac{l-d}{2}, \tag{2.240}$$

$$k-\sum_{n=-\infty}^{\infty} R_{n0}^{\mathbf{AA}}\Gamma_{1n}\mathrm{e}^{i\Phi_n y}=0; \qquad |y|<\frac{l-d}{2}. \tag{2.241}$$

Having denoted $\vartheta = 2\pi y/l$ and $\vartheta_0 = \pi(1–d/l)$ and substituting (2.238) and (2.239) into (2.240), we finally obtain

$$1 + d_0 + \sum_{n=-\infty}^{\infty} R_{n0}^{\mathbf{AA}} (1 - d_n) \, \mathrm{e}^{in\vartheta} = 0; \qquad |\vartheta| > \vartheta_0, \tag{2.242}$$

$$k - \sum_{n=-\infty}^{\infty} R_{n0}^{\mathbf{AA}} \Gamma_{1n} \mathrm{e}^{in\vartheta} = 0; \qquad |\vartheta| < \vartheta_0, \tag{2.243}$$

where

$$d_n = \frac{\tilde{\varepsilon}\Gamma_{1n}\left[\exp\left(i2\Gamma_{2n}h\right)\left(\Gamma_{2n} - \tilde{\varepsilon}\Gamma_{1n}\right) + \Gamma_{2n} + \tilde{\varepsilon}\Gamma_{1n}\right]}{\Gamma_{2n}\left[\exp\left(i2\Gamma_{2n}h\right)\left(\Gamma_{2n} - \tilde{\varepsilon}\Gamma_{1n}\right) - \Gamma_{2n} - \tilde{\varepsilon}\Gamma_{1n}\right]}. \tag{2.244}$$

Let us demonstrate that equations (2.242) and (2.243) are dual series equations of the same type as equations (2.36) and (2.37) in Section 2.2.2. Represent the coefficients Γ_{1n} and d_n from (2.242) and (2.243) in the form

$$\Gamma_{1n} = i\frac{2\pi}{l} |n| \left(1 + \delta_{1n}\right); \qquad n \neq 0, \tag{2.245}$$

$$d_n = -\tilde{\varepsilon} + \delta_{2n}. \tag{2.246}$$

It is easily seen that as $n \to \pm\infty$, the coefficients δ_{1n} and δ_{2n} are

$$\delta_{1n} = O\left(n^{-2}\right), \qquad \delta_{2n} = O\left(n^{-2}\right). \tag{2.247}$$

Indeed, from (2.245),

$$\delta_{1n} = \frac{l\Gamma_{1n}}{i2\pi\,|n|} - 1 = \sqrt{1 - \frac{\kappa^2}{n^2}} - 1 = -\frac{\kappa^2}{n^2\left(\sqrt{1 - \frac{\kappa^2}{n^2}} + 1\right)} = O\left(n^{-2}\right).$$

Here, $\kappa = lk/2\pi = l/\lambda$. Substitute (2.245) and (2.246) into (2.242) and (2.243). Finally,

$$\sum_{n=-\infty}^{\infty} R_{n0}^{\mathbf{AA}} \mathrm{e}^{in\vartheta} - \sum_{n=-\infty}^{\infty} R_{n0}^{\mathbf{AA}} \frac{\delta_{2n}}{1 + \tilde{\varepsilon}} \mathrm{e}^{in\vartheta} + \frac{1 + d_0}{1 + \tilde{\varepsilon}} = 0; \qquad |\vartheta| > \vartheta_0, \tag{2.248}$$

$$\sum_{n=-\infty}^{\infty} |n| \, R_{n0}^{\mathbf{AA}} \mathrm{e}^{in\vartheta} + \sum_{n=-\infty}^{\infty} R_{n0}^{\mathbf{AA}} \, |n| \, \delta_{1n} \mathrm{e}^{in\vartheta} + i\kappa\left(1 - R_{00}^{\mathbf{AA}}\right) = 0; \qquad |\vartheta| < \vartheta_0. \tag{2.249}$$

To make it clear that equations (2.247) and (2.248) are similar to equations (2.36) and (2.37) in Section 2.2.2, introduce the matrix operators $V = \{V_{mn}\}_{m,n=-\infty}^{\infty}$ and $U = \{U_{mn}\}_{m,n=-\infty}^{\infty}$ by the formulas

$$V_{mn} = |n|\,\delta_{1n}\delta_m^n, \qquad U_{mn} = -\frac{\delta_{2n}}{1+\varepsilon}\delta_m^n, \tag{2.250}$$

and the column vectors $f = \{f_n\}_{n=-\infty}^{\infty}$ and $g = \{g_n\}_{n=-\infty}^{\infty}$; $f_n = -i\kappa\delta_0^n$, $g_n = -\frac{1+d_0}{1+\tilde{\varepsilon}}\delta_0^n$. With these notations, equations (2.248) and (2.249) are written as

$$aR_{00}^{\mathbf{AA}} + \sum_{n=-\infty}^{\infty} R_{n0}^{\mathbf{AA}}\,|n|\,e^{in\vartheta} + \sum_{n=-\infty}^{\infty}\left[(VR)_n - f_n\right]e^{in\vartheta} = 0; \qquad |\vartheta| < \vartheta_0, \tag{2.251}$$

$$\sum_{n=-\infty}^{\infty} R_{n0}^{\mathbf{AA}} e^{in\vartheta} + \sum_{n=-\infty}^{\infty}\left[(UR)_n - g_n\right]e^{in\vartheta} = 0; \qquad |\vartheta| > \vartheta_0, \tag{2.252}$$

where $a = -i\kappa$ and $R = \left\{R_{n0}^{\mathbf{AA}}\right\}_{n=-\infty}^{\infty}$.

Asymptotical formulas (2.247) suggest that the matrix operators $T^{-1}VT^{-1}$ and TUT^{-1} are compact in the space l_2, and the column vectors f and g are such that $g \in l_2(1), f \in l_2(-1)$ (see definitions for matrix T and space $l_2(\eta)$ in Section 2.2).

Hence the dual series equations (2.251) and (2.252) allow the analytic regularization procedure outlined in Section 2.2.2. The application of this procedure provides the infinite system of linear algebraic equations

$$(1+\tilde{\varepsilon})\,R_{m0}^{\mathbf{AA}} + \sum_{n=-\infty}^{\infty} H_{mn}R_{n0}^{\mathbf{AA}} = b_m; \qquad m = 0, \pm 1, ... \tag{2.253}$$

The matrix $H = \{H_{mn}\}_{m,n=-\infty}^{\infty}$ of this system and its right-hand side $b = \{b_m\}_{m=-\infty}^{\infty}$ are given by the expressions

$$b_m = (1+\tilde{\varepsilon})\begin{cases} \dfrac{1+d_0}{d_0-1} + \dfrac{i\kappa W_0\,(1+\tilde{\varepsilon})}{1-d_0}; & m = 0 \\ -\dfrac{i\kappa V_{m-1}^{-1}}{m}; & m \neq 0 \end{cases}, \tag{2.254}$$

$$H_{mn} = \begin{cases} \dfrac{i\kappa W_0\,(1+\tilde{\varepsilon})^2}{1-d_0}; & m = n = 0 \\ \dfrac{\delta_n\,|n|\,(1+\tilde{\varepsilon})}{(d_0-1)\,n}V_{n-1}^{-1}; & m = 0, \quad n \neq 0 \\ -\dfrac{i\kappa}{m}V_{m-1}^{-1}; & m \neq 0, \quad n = 0 \\ \dfrac{|n|\,\delta_n}{m}V_{m-1}^{n-1}; & m, n \neq 0, \quad m \neq n \\ d_m + \tilde{\varepsilon} + \dfrac{|m|\,\delta_m}{m}V_{m-1}^{m-1}; & m = n, \quad m \neq 0 \end{cases}, \tag{2.255}$$

where $\delta_n = -\delta_{2n} - \delta_{1n}(1+\tilde{\varepsilon})$, and the coefficients W_0, V_{m-1}^{n-1} are calculated in Section 2.2. From the asymptotic formula (2.247), $\delta_n = O(n^{-2})$ as $n \to \pm\infty$. Hence,

based on the results from Section 2.2.2, one finds that the matrix operator H of system (2.253) is compact in the l_2 space.

Thus, with $R = \left\{R_{n0}^{\mathbf{AA}}\right\}_{n=-\infty}^{\infty}$ coming from system (2.253) and using formulas (2.236), (2.237), (2.238), and (2.239), the initial diffraction problem has been solved. Here an important point should be mentioned. For a lossless metamaterial layer ($\nu = 0$), the solution of the initial diffraction problem readily comes from (2.253) for all excitation wave frequencies but $\omega = \omega_p/\sqrt{2}$, which is equivalent to $\tilde{\varepsilon} = -1$. In some sense, this frequency is especial. As $\omega \to \omega_p/\sqrt{2}$, the matrix operator $\left[(\tilde{\varepsilon}+1)E + H\right]$ of system (2.253) becomes compact, having, consequently, no bounded inverse and thus forbidding a direct application of the truncation method to system (2.253). By a solution is meant the limit to which the solution $\left\{R_{n0}^{\mathbf{AA}}\right\}_{n=-\infty}^{\infty}$ of system (2.253) proceeds as the metamaterial becomes lossless, $\nu \to 0$.

Now turn to the spectral problem describing peculiar features of the analytic continuation of the diffraction field to the complex frequency domain. The mathematical formulation of the spectral problem differs from the statement of the diffraction problem. In the first place, the former is independent of the excitation wave. Second, the function $\tilde{U}(g,k)$ in (2.236) forms accounting for the radiation condition is analytically continued from the real-valued frequency domain to the corresponding infinite-sheeted Riemannian surface (see, for instance, Section 1.3). So, the spectral problem of the grating backed by the metamaterial layer with the effective permittivity in (2.233) form is a problem about eigenfrequencies and eigenoscillations bearing an l-periodic dependence on the grating spatial coordinate y. The sought spectral parameter is the wave number k (or normalized frequency $\varkappa = l/\lambda = kl/2\pi$) belonging to the Riemannian surface $\mathbf{K}$ (or $\mathbf{K}_\varkappa$). From this point on, the metamaterial is assumed lossless ($\nu = 0$), its effective permittivity is

$$\varepsilon(\omega) = 1 - \frac{\omega_p^2}{\omega^2},$$

and the spectral parameter $\varkappa$ belongs to the first – physical – sheet of the Riemannian surface $\mathbf{K}_\varkappa$ (see Section 1.3).

The discussed spectral problem is equivalent to equation (2.253) with $b = 0$ (the excitation wave is absent), the matrix elements in the (2.254) form are considered as a function of the spectral parameter $\varkappa$ varying on the physical sheet of the surface $\mathbf{K}_\varkappa$. The problem of the kind means finding the characteristic numbers and the eigenvectors of the operator-function $E + B(\varkappa)$, where $B(\varkappa) = (1+\tilde{\varepsilon})^{-1}H(\varkappa)$. The results from Section 1.3 let us establish that the matrix operator $B(\varkappa)$ is a finite-meromorphic kernel operator-function of the complex variable $\varkappa$ on the physical sheet of the Riemannian surface excepting the points $\varkappa = 0$ and $\varkappa = \pm\varkappa_p/\sqrt{2}$ ($\varkappa_p = \omega_p l/2\pi c$) and, also, the branch points $\varkappa_n^{\pm}$:$\Gamma_{1n}(\varkappa_n^{\pm}) = 0$; $n = \pm 1, \pm 2, \ldots$. The poles of the operator-function $E + B(\varkappa)$ coincide with the point $\varkappa = 0$ and the roots of the equations

$$\exp(i2\Gamma_{2n}h)(\Gamma_{2n} - \varepsilon\Gamma_{1n}) - \Gamma_{2n} - \tilde{\varepsilon}\Gamma_{1n} = 0; \qquad n = 1,2,\ldots. \tag{2.256}$$

Then the characteristic numbers and, hence, the eigenfrequencies are roots of the equation

$$\det\left[E + B\left(\kappa\right)\right] = 0, \tag{2.257}$$

where det[...] is the infinite determinant of the operator $E + B(\kappa)$. Evidently the function det[E+$B(\kappa)$] is meromorphic in any bounded domain not carrying the points $\kappa = 0$, $\kappa = \pm\kappa_p/\sqrt{2}$ and the branch points $\kappa = \kappa_n^{\pm}$. Hence the set of the roots of equation (2.257) is nothing more than a denumerable set on the physical sheet of the surface $\mathbf{K}_\kappa$ with probable accumulation points coinciding with either $\kappa = 0$, $\kappa = \pm\kappa_p/\sqrt{2}$, or the poles coming from (2.256).

Consider some qualitative properties of the root set of equation (2.257). Suppose that the grating strips are sufficiently small, $1 - d/l \ll 1$ (at $d/l = 1$ the grating disappears). Represent the operator-function $B(\kappa)$ as a sum of two operator-functions so that $B(\kappa) = B_1(\kappa)$+$B_2(\kappa)$, where $B_1(\kappa) = \left\{\delta_m^n \gamma_m\right\}_{m,n=-\infty}^{\infty}$, $\gamma_0 = 0$, $\gamma_m = \frac{d_m + \tilde{\varepsilon}}{1+\tilde{\varepsilon}}$ for $m \neq 0$. Estimating the values of W_0, V_{m-1}^{n-1} when $d/l \to 1$ (see, e.g., [45]) one finds that the operator-function $B_2(\kappa)$ obeys the condition

$$\|B_2(\kappa)\| < \text{const}\ \sin\left[\pi\left(1 - \frac{d}{l}\right)\right], \tag{2.258}$$

where $\|...\|$ is the norm of the operator-function $B_2(\kappa)$ in l_2. Hence as $d/l \to 1$, the norm of $B_2(\kappa)$ tends to zero in any bounded domain of κ values except for $\kappa = 0$, $\kappa = \pm\kappa_p/\sqrt{2}$ the branch points, and the poles. It is easy to check that the characteristic numbers of the operator-function $E + B_1(\kappa)$ match the roots of the equations

$$\exp\left(i\Gamma_{2n}h\right)\left(\Gamma_{2n} - \tilde{\varepsilon}\Gamma_{1n}\right) \pm \left(\Gamma_{2n} + \tilde{\varepsilon}\Gamma_{1n}\right) = 0; \qquad n = 1,2,... \tag{2.259}$$

Next it can be shown that the κ domain where $\mathrm{Re}(\tilde{\varepsilon}) < 0$ allows real-valued roots of equation (2.259). Figure 2.19 plots results from (2.259) computed for different $n = 1,2,....$ (squares for the plus and circles for the minus). As $n \to \infty$, these roots asymptotically tend to $\kappa = \kappa_p/\sqrt{2}$ (Fig. 2.19, dotted line), indicating that $\kappa = \kappa_p/\sqrt{2}$ is the accumulation point. It is notable that equation (2.259) suggests some metamaterial characteristic frequency $\tilde{\kappa}_p = x_0 l/2\pi h$, where $x_0 \approx 1.325$ satisfies the equation

$$x\mathrm{e}^{-0.5\sqrt{x^2+4}} + 2 - \sqrt{x^2+4} = 0.$$

For $\kappa_p \leq \tilde{\kappa}_p$, some finite number of the roots of equation (2.259) exceed $\kappa_p/\sqrt{2}$ (Fig. 2.19) and for $\kappa_p > \tilde{\kappa}_p$, no one is over $\kappa_p/\sqrt{2}$ (Fig. 2.19b).

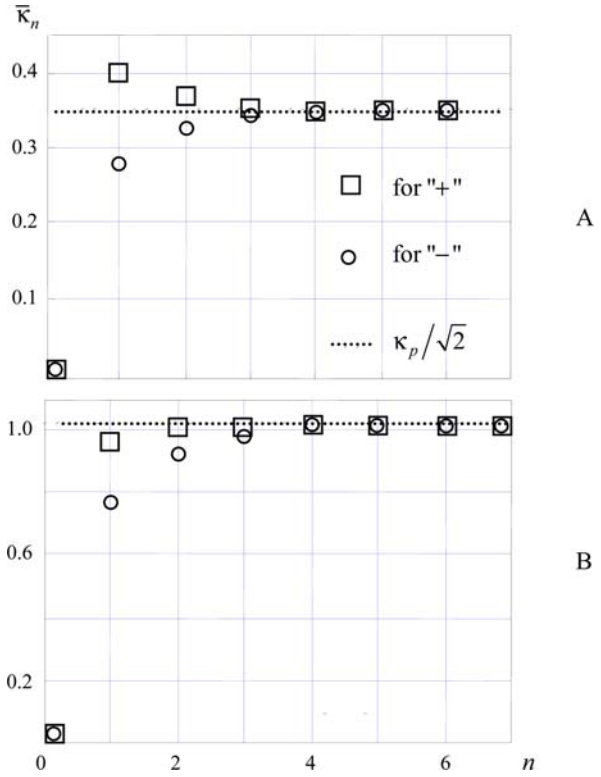

Fig. 2.19 The roots $\bar{\kappa}_n$ of equation (2.259) for different n values: $h/l = (2\pi)^{-1}$, (**a**) $\kappa_p = 0.5$, and (**b**) $\kappa_p = 1.45$

Now let $1–d/l$ be a small number and $\bar{\kappa}_0$ be a characteristic number of the operator-function $E + B_1(\kappa)$, i.e., $\det[E + B_1(\bar{\kappa}_0)] = 0$. Evidently there is a circle with the point $\bar{\kappa}_0$ as center and a radius so small that the operator-function $[E + B_1(\kappa)]^{-1}$ is bounded on the circumference line. Then from (2.257) it follows that if $1–d/l$ is small enough, the inequality

$$\left\| [E + B_1(\kappa)]^{-1} B_2(\kappa) \right\| < 1$$

is true on the circumference line. Through the operator generalization provided by the Rouche theorem [15], one finds that the mentioned circle carries a characteristic number of the operator-function $E + B_1(\kappa) + B_2(\kappa)$, suggesting, at least phenomenologically, that the characteristic numbers of the operator-function $E + B(\kappa)$ and, hence, the characteristic numbers of the examined electrodynamical structure (a grating loaded with a metamaterial layer) have the accumulation point $\kappa = \kappa_p/\sqrt{2}$.

The eigenfrequency computation for $0 < d/l \leq 1$ follows the algebraic scheme outlined below. Let a finite-dimensional matrix operator-function $B_N(\kappa)$ represent

the $N \times N$ truncation of the matrix $B(\kappa)$. In view of the compactness of $B(\kappa)$ for any $\delta > 0$ as small as desired and in any bounded domain of κ (excluding $\kappa = 0, \pm\kappa_p/\sqrt{2}$ and the branch points $\kappa = \kappa_n^{\pm}$), a natural number N exists such that

$$\|B(\kappa) - B_N(\kappa)\| < \delta. \tag{2.260}$$

The eigenfrequencies of the finite-dimensional operator-function $E + B_N(\kappa)$ can be sought as roots of the determinant-function $\det[E + B_N(\kappa)]$. By virtue of (2.260), each solution $\bar{\kappa}_m$ of spectral problem (2.257) is approximated to any desired accuracy by the solution $\bar{\kappa}_m^N$ of the equation $\det[E + B_N(\kappa)] = 0$ provided that N is large enough. Using the compactness property of the operator-function $B(\kappa)$, one easily verifies [11] that the procedure described right above is computationally stable as N rises.

To analyze the solution of the spectral problem (2.257), the domain $\mathrm{Re}(\kappa) > 0$ of the spectral parameter will suffice. From formulas (2.238), we have

$$\det[E + B(\kappa)] = \left(\det\left[E + B(-\kappa^*)\right]\right)^*,$$

where the $*$ indicates complex conjugation. Therefore, if $\bar{\kappa}$ is an eigenfrequency with $\mathrm{Re}(\kappa) > 0$, then $-\bar{\kappa}^*$ is an eigenfrequency with $\mathrm{Re}(\kappa) < 0$ (for details, refer to Section 1.3). From the considered structure symmetry with respect to the plane $y = 0$ (see Fig. 2.18) it follows that there are two classes of eigenoscillations: even and odd with respect to y variable. Besides, when the metal strips of the grating disappear, leaving the metamaterial layer alone, the structure acquires an additional symmetry about the plane $z = -h/2$, thus giving rise to two more solution types: even and odd in the coordinate z about the plane $z = -h/2$. They correspond to the characteristic equations (2.259) with the minus and the plus signs, respectively.

Figures 2.20 and 2.21 illustrate the dependence of the real and imaginary parts of the first three eigenfrequencies $\bar{\kappa}$ on the geometrical parameter d/l (grating slot normalized width). These were obtained by the numerical solution of equation (2.257), with specially designed algorithms and programs. The eigenfrequencies of the oscillations which in the limiting case $d/l = 1$ are symmetric about the plane $z = -h/2$ [minus in equation (2.259)] are shown in Fig. 2.20. The eigenfrequencies of the oscillations asymmetric about the plane $z = -h/2$ [plus in (2.259)] are shown in Fig. 2.21. The solid line plots the eigenfrequencies of oscillations symmetric with respect to the plane $y = 0$, the dashed line is for asymmetric oscillations. Notice that the imaginary parts of the eigenfrequencies of oscillations asymmetric about the plane $y = 0$ practically vanish and are not visible in Figs. 2.20b and 2.21b. The dotted curves in Figs. 2.20a and 2.21a correspond to $\kappa_p/\sqrt{2}$. As seen from Figs. 2.20 and 2.21, for $d/l = 1$ (i.e., the grating is absent), the imaginary parts of eigenfrequencies vanish (the metamaterial layer is lossless, $\nu = 0$).

The real parts of the eigenfrequency oscillations symmetric and asymmetric with respect to the plane $z = -h/2$ for prescribed $\kappa_p = 0.5 < \tilde{\kappa}_p$ are, as shown above, located on different sides of the point $\kappa = \kappa_p/\sqrt{2}$ and match at $d/l = 1$, the corresponding $\bar{\kappa}_n$ values presented in Fig. 2.19a. In Fig. 2.22, one observes the equal

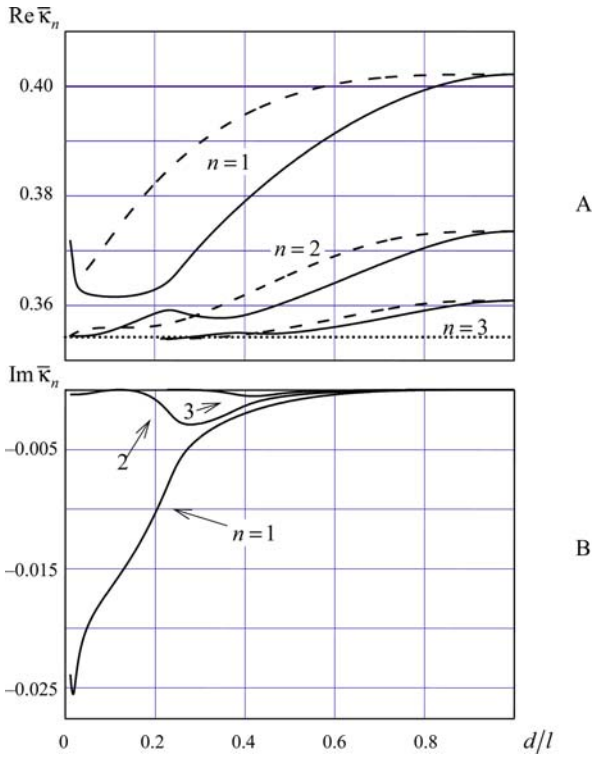

Fig. 2.20 The eigenfrequencies $\bar{\kappa}_n$ versus d/l for oscillations cophasal about $z = -h/2$: (**a**) Real and (**b**) imaginary parts; $\kappa_p = 0.5$, $h/l = (2\pi)^{-1}$

module $\left|\tilde{H}_x\right| = \text{const}$ and the equal phase $\arg\left(\tilde{H}_x\right) = \text{const}$ lines of the unique nonzero component $\tilde{H}_x(y,z)$ of the magnetic field for some eigenoscillations of the grating backed by the metamaterial layer. The oscillation with the eigenfrequency $\bar{\kappa} = 0.36565 - i10^{-12}$ in Fig. 2.22a is asymmetric about the plane $y = 0$ and in phase at $d/l = 1$ with respect to the plane $z = -h/2$ (the same oscillation phase on both interfacial sides of the metamaterial). The oscillation with the eigenfrequency $\bar{\kappa} = 0.35173 - i7.079 \cdot 10^{-5}$ in Fig. 2.22b is symmetric about the plane $y = 0$ and opposite in phase with respect to the plane $z = -h/2$ at $d/l = 1$ validating the above-made division of the examined structure eigenoscillations into classes of symmetry.

Interestingly also that as $d/l \to 1$ (the grating changes into a perfectly conducting plane), the real parts of some eigenfrequencies tend to the poles of the operator-function $E+B(\kappa)$, which are the roots of equation (2.256), the imaginary parts vanishing. This numerical result resists analytic justification because the d/l dependence of the matrix elements [see (2.255)] of the operator-function $H(\kappa)$ and, hence, of $B(\kappa) = (1 + \tilde{\varepsilon})^{-1}H(\kappa)$ is singular at $d/l = 0$.

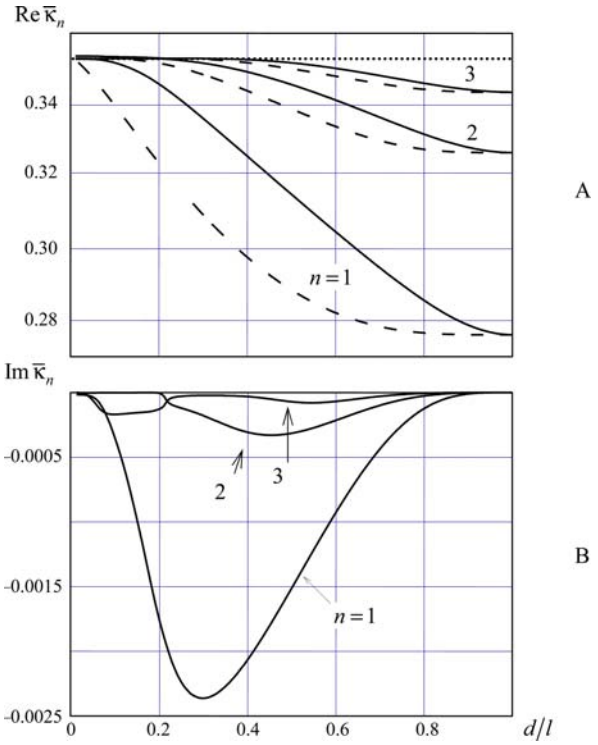

Fig. 2.21 The eigenfrequencies $\bar{\kappa}_n$ versus d/l for oscillations antiphasal about $z = -h/2$: (**a**) Real and (**b**) imaginary parts; $\kappa_p = 0.5$, $h/l = (2\pi)^{-1}$

Next we consider the eigenfrequency behavior as the metamaterial characteristic frequency varies. As the characteristic frequency $\kappa_p \to 0$, the eigenfrequencies of all oscillation types tend to zero (see Fig. 2.23). This is attributed to the fact that the grating has no eigenfrequencies in free space (at $\kappa_p = 0$, the effective permittivity of our metamaterial is $\tilde{\varepsilon} = 1$) [10]. The increase $\kappa_p \to \infty$ leads to different results for eigenfrequencies of different oscillation types. Thus, the real parts of eigenfrequencies corresponding to oscillations opposite in phase with respect to the plane $z = -h/2$ asymptotically tend to the branch point $\kappa_{\pm 1}^{+} = 1$ (see Fig. 2.23a). They asymptotically tend to the line $\mathrm{Re}\bar{\kappa} = \kappa_p/\sqrt{2}$ for oscillations in phase with respect to the plane $z = -h/2$. In this case, for both oscillation types, the imaginary parts of the eigenfrequency tend to zero as $\kappa_p \to \infty$ (see Fig. 2.23b). For other values of the metamaterial layer normalized thickness and the grating slot width, the indicated eigenfrequency behavior persists.

Examine the eigenfrequency behavior as the normalized thickness h/l of the metamaterial layer changes, whereas the grating slot width $d/l = 0.5$ and the characteristic frequency κ_p=0.5 are fixed. Begin with the case $d/l \approx 1$, where the roots of equations (2.259) approximate the real parts of the eigenfrequency rather well.

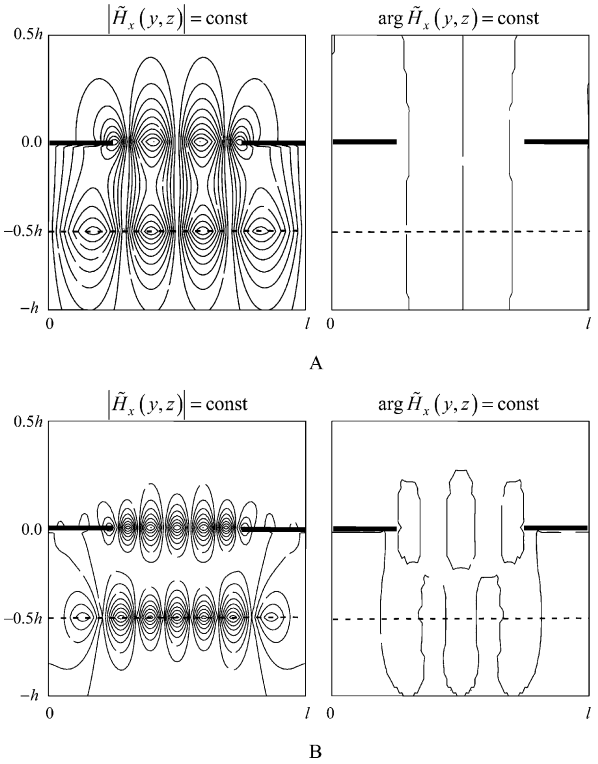

Fig. 2.22 The structure of some eigenoscillation types for (**a**) $\bar{\kappa} = 0.36565 - i10^{-12}$; and (**b**) $\bar{\kappa} = 0.35173 - i7.079 \cdot 10^{-5}$: $\kappa_p = 0.5$, $h/l = (2\pi)^{-1}$, $d/l = 0.5$

At a sufficiently small layer thickness $\bar{h} = 2\pi h/l \ll 1$ and for $\kappa_p < 1$, we arrive at the following eigenfrequency approximations:

$$\bar{\kappa}_{n+} \approx \kappa_p \sqrt{\frac{n\bar{h}}{2}}, \qquad \bar{\kappa}_{n-} \approx \kappa_p \left(1 - \frac{n^2 \bar{h}}{2\sqrt{n^2 - \kappa_p^2}}\right). \tag{2.261}$$

Here, κ_n^+ and κ_n^- are the roots of equations (2.259) for the minus and plus signs, respectively. As seen, $\bar{\kappa}_{n+} \to 0$ and $\bar{\kappa}_{n-} \to \kappa_p$ as $\bar{h} \to 0$. It has been shown numerically that this eigenfrequency behavior is also typical for $d/l \neq 1$ (see Fig. 2.24a). When the real parts of eigenfrequencies $\bar{\kappa}$ satisfy $\mathrm{Re}\bar{\kappa} > \kappa_p/\sqrt{2}$, they asymptotically tend to κ_p as the layer becomes thin and to $\bar{\kappa} = \kappa_p/\sqrt{2}$ as it becomes thick. It was already mentioned that the eigenfrequency accumulation point is $\kappa = \kappa_p/\sqrt{2}$. If for the indicated κ_p and d/l values, the eigenfrequencies are such that $\mathrm{Re}\bar{\kappa} < \kappa_p/\sqrt{2}$, they tend to zero as $h/l \to 0$ and approach the relevant eigenfrequencies of the grating

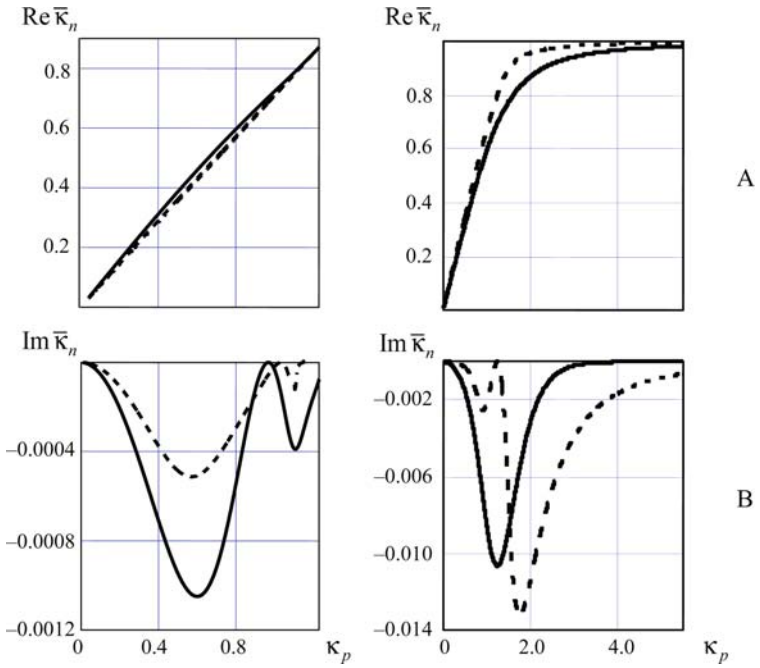

Fig. 2.23 The eigenfrequencies $\bar{\kappa}_n$ versus κ_p: (**a**) Real and (**b**) imaginary parts; $h/l = (2\pi)^{-1}$, $d/l = 0.5$

backed by a metamaterial half-space as $h/l \to \infty$ [145]. When $h/l \to 0$, the imaginary parts typically tend to zero for both oscillation types $\mathrm{Re}\bar{\kappa} > \kappa_p/\sqrt{2}$ and $\mathrm{Re}\bar{\kappa} < \kappa_p/\sqrt{2}$ (Fig. 2.24b). As the layer thickness grows, the imaginary parts of eigenfrequencies such that $\mathrm{Re}\bar{\kappa} < \kappa_p/\sqrt{2}$ approach those of the grating backed by a metamaterial half-space [145]. For other values of the characteristic frequency κ_p and the grating slot width, this dependence of the structure eigenfrequency on the metamaterial layer thickness still remains.

We proceed to a description of the solution of the diffraction of a plane H-polarized wave by a strip grating placed on a metamaterial layer surface. We consider the case that the normalized frequency κ of the excitation wave is less than κ_p. First of all, we mention again that the real part of the metamaterial permittivity in this frequency region is negative, $\mathrm{Re}\tilde{\varepsilon} < 0$. Second, it is a region that contains real parts of the eigenfrequencies of the spectral problem. Assume that $\kappa_p/\sqrt{2} \leq 1$, which is actually realized by a proper choice of the grating period. Then from (2.236) it follows that the diffraction field in the reflection (**A**) and the transition (**B**) zones is a superposition of the traveling zeroth harmonic and an infinitely large number of surface harmonics exponentially decaying away from the grating along the z-axis ($z \to \pm\infty$). Hence the diffraction field away from the grating is solely governed by the zeroth traveling harmonic characterized by the amplitude $R_{00}^{\mathbf{AA}}$ (reflection coefficient) in the reflection zone ($z > 0$) and the amplitude $T_{00}^{\mathbf{BA}}$

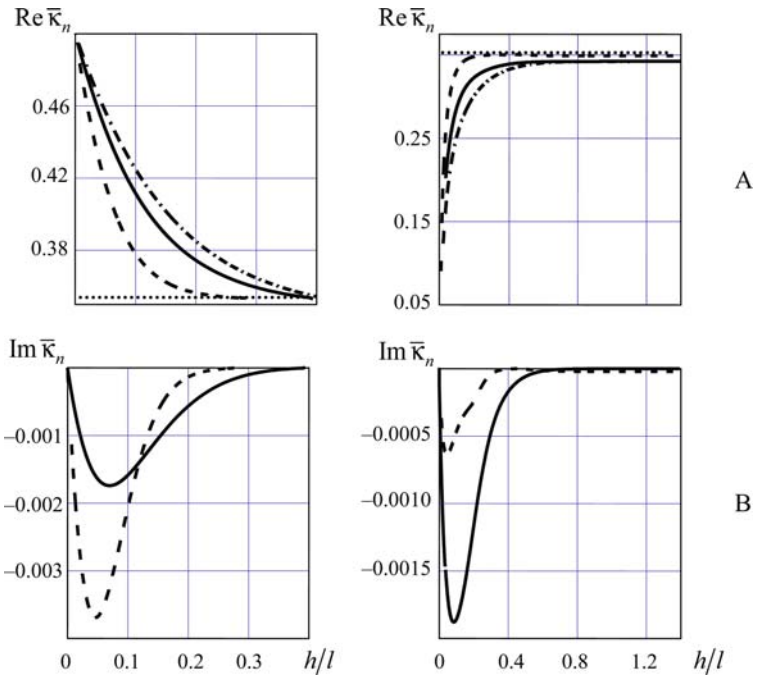

Fig. 2.24 The eigenfrequencies $\bar{\kappa}_n$ versus h/l: (**a**) Real and (**b**) imaginary parts; $d/l = 0.5$, $\kappa_p = 0.5$. The *dotted curves* in (**a**) correspond to $\kappa_p/\sqrt{2}$

(transition coefficient) in the transition zone ($z < -h$). In the case of plane electromagnetic wave incidence, Fig.2.25a plots the transition coefficient module versus frequency for: a metamaterial layer and a grating with $\kappa_p = 0.5$, $v = 10^{-5}$, $d/l = 0.5$, $h/l = 1/(2\pi)$ (solid line), a metamaterial layer single with $\kappa_p = 0.5$, $v = 10^{-5}$, $d/l = 0.5$, $h/l = 1/(2\pi)$ (dashed line), and a grating in a vacuum with $\kappa_p = 0$, $d/l = 0.5$ (dotted line).

It is seen that neither the grating nor the metamaterial layer exhibits resonance properties in the indicated domain $0.3 \le \kappa \le 0.41$ of the normalized frequency parameter. The incident plane-wave energy is practically completely transmitted with $\left|T_{00}^{\mathbf{BA}}\right| > 0.9$. But the incorporation of the grating with the metamaterial layer makes a clearly resonant structure in the indicated κ region, and a discrete set of κ values exists when this construction either almost completely reflects the excitation field energy, $\left|T_{00}^{\mathbf{BA}}\right| \approx 0$ or practically completely transmits it, $\left|T_{00}^{\mathbf{BA}}\right| \approx 1$. A comparison of these κ values with the real parts of the eigenfrequencies at corresponding problem parameters (Figs. 2.20a and 2.21a) indicates that the resonances of the transmission coefficient module keep pace with the excitation of structure eigenoscillations. The excitation fields at some resonance κ values are illustrated in Fig. 2.25b and c. Figure 2.22 demonstrates that the oscillation structure at the resonances of the transmission coefficient $\left|T_{00}^{\mathbf{BA}}\right|$ resembles the eigenoscillation field of

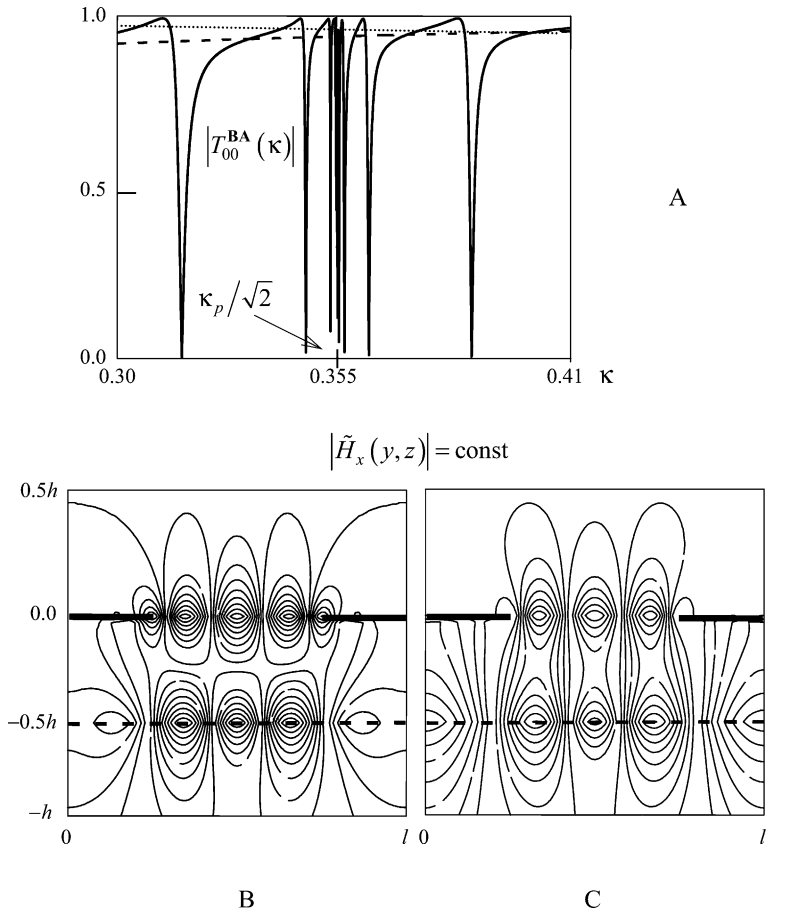

Fig. 2.25 (**a**) The transition coefficient module $\left|T_{00}^{\mathbf{BA}}\right|$ versus normalized frequency $\kappa = l/\lambda$. (**b** and **c**) The excitation field structure at resonance frequencies: $\kappa_p = 0.5$, $v = 10^{-5}$, $d/l = 0.5$, $h/l = (2\pi)^{-1}$, (**b**) $\kappa = 0.34576$; and (**c**) $\kappa = 0.36106$

an open electrodynamical structure – a strip grating backed by a metamaterial layer. Owing to the fact that the excitation field is symmetric about the $y = 0$ plane, only eigenoscillations symmetric about the plane $y = 0$ are excited.

2.5.2 The Plane-Wave Diffraction from a Strip Grating with Anisotropic Medium

In this section, the analytic regularization method (see Section 2.2.3) will be discussed as applied to the monochromatic plane-wave diffraction from a perfectly

conducting strip grating located on the boundary of an anisotropic dielectric half-space. The sewing (partial domain) method is adopted to reduce this problem to the dual series equations of (2.91) and (2.92) type (see Section 2.2.3). The regularization procedure turns them into an infinite system of linear algebraic equations of the second kind in the space l_2, which can be solved effectively.

Let us formulate the diffraction problem. A plane wave is incident along the z-axis on an infinite grating composed of infinitely thin perfectly conducting strips as that in Fig. 2.26. The incident field is assumed to be H-polarized in the x-direction. If so, the magnetic field of the incident wave has only the $\tilde{H}_x^i = \exp(-ikz)$ component. The electric field components lie in the plane x=const. The time dependence is $\exp(-ikt)$. Also, it is assumed that the grating is located in the plane $z = 0$ and extends infinitely along the x-axis. The half-space $z < 0$ is filled with a homogeneous anisotropic medium whose permeability is $\mu = 1$ and whose permittivity is given by the second-rank tensor

$$\tilde{\varepsilon} = \begin{pmatrix} \varepsilon_3 & 0 & 0 \\ 0 & \varepsilon_1 & -i\varepsilon_2 \\ 0 & i\varepsilon_2 & \varepsilon_1 \end{pmatrix}. \tag{2.262}$$

It is required to find the diffraction field $\{\vec{E}^s, \vec{H}^s\}$ governed by a homogeneous system of Maxwell's equations and meeting the radiation condition at infinity $z \to \pm\infty$, the Meixner condition, the periodicity condition, the boundary conditions on the grating perfectly conducting strips, and the field conjugation condition on the anisotropic half-space boundary. The incident wave is x-independent. So, in view of the uniqueness theorem for the solution and the infinity and the homogeneity of the grating in the x-direction, the diffraction field is also x-independent, suggesting us a two-dimensional problem, $\partial/\partial x \equiv 0$.

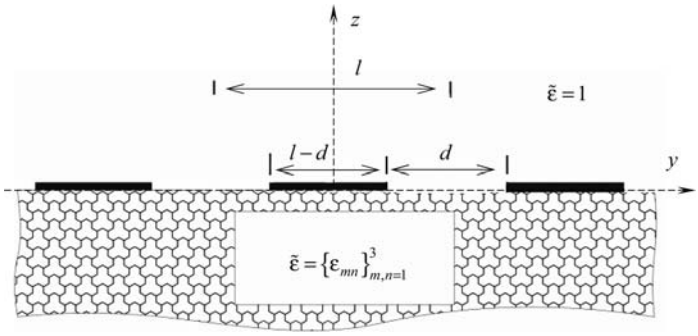

Fig. 2.26 The problem geometry

Using (2.262) and considering the listed assumptions, one easily verifies that the diffraction field components $\{\vec{E}^s, \vec{H}^s\}$ are expressed via the unique nonzero component $\tilde{H}_x^s$ of the magnetic field as follows:

$$\tilde{E}_y^s = \frac{1}{ik\varepsilon_\perp}\left(i\frac{\varepsilon_2}{\varepsilon_1}\frac{\partial \tilde{H}_x^s}{\partial y} - \frac{\partial \tilde{H}_x^s}{\partial z}\right), \qquad \tilde{E}_z^s = \frac{1}{ik\varepsilon_\perp}\left(\frac{\partial \tilde{H}_x^s}{\partial y} + i\frac{\varepsilon_2}{\varepsilon_1}\frac{\partial \tilde{H}_x^s}{\partial z}\right), \qquad (2.263)$$

where $\varepsilon_\perp = \left(\varepsilon_1^2 - \varepsilon_2^2\right)\varepsilon_1^{-1}$ is the effective permittivity of the anisotropic half-space. For the half-space $z > 0$, put $\varepsilon_1 = 1$, $\varepsilon_2 = 0$. From (2.263) it follows that the diffraction field is H-polarized.

For the sake of convenience, introduce the function $\tilde{U}(g,k)$

$$\tilde{U}(g,k) = \begin{cases} \tilde{H}_x^i + \tilde{H}_x^s; & z > 0 \\ \tilde{H}_x^s; & z < 0 \end{cases}. \qquad (2.264)$$

By the Maxwell's equations, everywhere but at the anisotropic half-space boundary this function satisfies the Helmholtz equation

$$\Delta_{y,z}\tilde{U}(g,k) + k^2(z)\,\tilde{U}(g,k) = 0;\ g = \{y,z\},\ k^2(z) = k^2\begin{cases} 1; & z > 0 \\ \varepsilon_\perp; & z < 0 \end{cases}. \qquad (2.265)$$

Rewrite the boundary condition on the grating strips and the conjugation condition on the anisotropic half-space boundary in terms of the function $\tilde{U}(g,k)$. On the perfectly conducting grating strips the tangential electric field component $\tilde{E}_y$ has to vanish, giving

$$\left.\frac{\partial \tilde{U}(g,k)}{\partial z}\right|_{z=0+0} = 0, \qquad \left.\left(\frac{\partial \tilde{U}(g,k)}{\partial y} + i\frac{\varepsilon_2}{\varepsilon_1}\frac{\partial \tilde{U}(g,k)}{\partial z}\right)\right|_{z=0-0} = 0 \qquad (2.266)$$

for $|2\pi y/l + n| < \pi(1 - d/l);\ n = 0, \pm 1, \pm 2, ...$

As the tangential components $\tilde{H}_x$ and $\tilde{E}_y$ are continuous across the grating slots, the relationships (2.263) yield

$$\begin{array}{c} \left.\frac{\tilde{U}(g,k)}{\partial z}\right|_{z=0+0} = \frac{1}{\varepsilon_\perp}\left.\left(\frac{\partial \tilde{U}(g,k)}{\partial z} - i\frac{\varepsilon_2}{\varepsilon_1}\frac{\partial \tilde{U}(g,k)}{\partial y}\right)\right|_{z=0-0}, \\ \left.\tilde{U}(g,k)\right|_{z=0+0} = \left.\tilde{U}(g,k)\right|_{z=0-0} \end{array} \qquad (2.267)$$

for $|2\pi y/l + n| > \pi(1 - d/l);\quad n = 0, \pm 1, \pm 2, ...$ Here, l and d are, respectively, the period and the width of the grating slots (see Fig. 2.2b).

Take the Fourier series expansion of the function $\tilde{U}(g,k)$ in the variable y for the half-spaces $z > 0$ (domain **A**) and $z < 0$ (domain **B**). Considering that $\tilde{U}(g,k)$ must satisfy equation (2.265) and implying the radiation condition, we have

$$\tilde{U}(g,k) = \begin{cases} e^{-ikz} + \sum\limits_{n=-\infty}^{\infty} R_{n0}^{\mathbf{AA}} e^{i(\Phi_n y + \Gamma_{1n} z)}; & z > 0 \\ \sum\limits_{n=-\infty}^{\infty} T_{n0}^{\mathbf{BA}} e^{i(\Phi_n y - \Gamma_{2n} z)}; & z < 0 \end{cases}. \qquad (2.268)$$

Here, $\left\{R_{n0}^{\mathbf{AA}}\right\}_{n=-\infty}^{\infty}$ and $\left\{T_{n0}^{\mathbf{BA}}\right\}_{n=-\infty}^{\infty}$ are the sought unknown coefficients and $\Gamma_{1n} = \sqrt{k^2 - \Phi_n^2}$, $\Gamma_{2n} = \sqrt{k^2\varepsilon_\perp - \Phi_n^2}$. The choice of the root branches Γ_{1n} and Γ_{2n} is governed by the radiation condition (see Section 2.5.1): $k\mathrm{Re}\Gamma_{pn} \geq 0$, $\mathrm{Im}\Gamma_{pn} \geq 0$, $p = 1,2$, $n = 0,\pm1,\pm2,\ldots$

So, we have arrived at the problem of finding the coefficients $\left\{R_{n0}^{\mathbf{AA}}\right\}_{n=-\infty}^{\infty}$ and $\left\{T_{n0}^{\mathbf{BA}}\right\}_{n=-\infty}^{\infty}$ in the Fourier series expansion of the function $\tilde{U}(g,k)$. Use boundary conditions (2.266) and (2.267) and derive the equations these coefficients satisfy.

Substitute (2.268) into (2.266) and (2.267) to arrive at the dual series equations

$$\sum_{n=-\infty}^{\infty} T_{n0}^{\mathbf{BA}} \left(in\frac{2\pi\varepsilon_2}{l\varepsilon_1} + \Gamma_{2n} \right) \mathrm{e}^{in\vartheta} = 0; \qquad |\vartheta| < \vartheta_0, \tag{2.269}$$

$$\sum_{n=-\infty}^{\infty} \left(R_{n0}^{\mathbf{AA}} - T_{n0}^{\mathbf{BA}} + \delta_0^n \right) \mathrm{e}^{in\vartheta} = 0; \qquad |\vartheta| > \vartheta_0, \tag{2.270}$$

where $\vartheta = (2\pi y)/l$, $\vartheta_0 = \pi(1 - d/l)$.

From (2.266) and (2.267), one easily finds that the coefficients $\left\{R_{n0}^{\mathbf{AA}}\right\}_{n=-\infty}^{\infty}$ and $\left\{T_{n0}^{\mathbf{BA}}\right\}_{n=-\infty}^{\infty}$ are related as

$$R_{n0}^{\mathbf{AA}} = \delta_0^n - \frac{in\frac{2\pi\varepsilon_2}{l\varepsilon_1} + \Gamma_{2n}}{\varepsilon_\perp \Gamma_{1n}} T_{n0}^{\mathbf{BA}}; \qquad n = 0, \pm 1, \pm 2, \ldots \tag{2.271}$$

Introduce the new unknowns $x = \{x_n\}_{n=-\infty}^{\infty}$ by the formula

$$x_n = R_{n0}^{\mathbf{AA}} - T_{n0}^{\mathbf{BA}} + \delta_0^n; \qquad n = 0, \pm 1, \pm 2, \ldots \tag{2.272}$$

Use (2.271) and bring equations (2.269) and (2.270) to the form

$$\sum_{n=-\infty}^{\infty} x_n \gamma_n \mathrm{e}^{in\vartheta} - \frac{2\kappa}{1 + \sqrt{\varepsilon_\perp}} = 0; \qquad |\vartheta| < \vartheta_0, \tag{2.273}$$

$$\sum_{n=-\infty}^{\infty} x_n \mathrm{e}^{in\vartheta} = 0; \qquad |\vartheta| > \vartheta_0. \tag{2.274}$$

Here, as before, $\kappa = kl/2\pi = l/\lambda$ and

$$\gamma_n = \frac{\Gamma_{1n}\left(in\frac{\varepsilon_2}{\varepsilon_1} + \frac{l}{2\pi}\Gamma_{2n} \right)}{\varepsilon_\perp \Gamma_{1n} + \Gamma_{2n} + in\frac{2\pi\varepsilon_2}{l\varepsilon_1}}. \tag{2.275}$$

Let us show that equations (2.273) and (2.274) can be expressed in the form of equations (2.91) and (2.92) (see Section 2.2.3). First of all, notice that Γ_{1n} and Γ_{2n} obey the following asymptotical formulas as $n \to \pm\infty$ [see (2.245) and (2.247)]:

$$\Gamma_{1n} = i\frac{2\pi}{l}\,|n|\,(1+\delta_{1n})\,, \tag{2.276}$$

$$\Gamma_{2n} = i\frac{2\pi}{l}\,|n|\,(1+\delta_{2n})\,, \tag{2.277}$$

where $\delta_{pn} = O\left(n^{-2}\right)$; $p = 1, 2$. Using (2.276) and (2.277) one finds that the coefficient γ_n from (2.275) can be written as

$$\gamma_n = i\,|n| \begin{cases} C^+\left[1+O\left(n^{-2}\right)\right]; & n\to+\infty \\ C^-\left[1+O\left(n^{-2}\right)\right]; & n\to-\infty \end{cases}, \tag{2.278}$$

where $C^+ = (1+\varepsilon_1-\varepsilon_2)^{-1}$, $C^- = (1+\varepsilon_1-\varepsilon_2)^{-1}$. Now substitute (2.278) into (2.273). After some elementary manipulations, one obtains

$$ax_0 + \sum_{\substack{n=1 \\ |\vartheta|<\vartheta_0}}^{\infty} nx_n e^{in\vartheta} - b\sum_{n=-\infty}^{-1} nx_n e^{in\vartheta} + \sum_{n=-\infty}^{\infty} |n|\,\delta_n x_n e^{in\vartheta} + \frac{i2\kappa(1+\varepsilon_1-\varepsilon_2)}{1+\sqrt{\varepsilon_\perp}} = 0; \tag{2.279}$$

$$\sum_{n=-\infty}^{\infty} x_n e^{in\vartheta} = 0; \qquad |\vartheta| > \vartheta_0. \tag{2.280}$$

Here,

$$a = -\frac{i\kappa\,(1+\varepsilon_1-\varepsilon_2)}{1+\sqrt{\varepsilon_\perp}}; \tag{2.281}$$

$$b = \frac{1+\varepsilon_1-\varepsilon_2}{1+\varepsilon_1+\varepsilon_2}, \tag{2.282}$$

$$\delta_n = \begin{cases} \dfrac{\gamma_n}{i\,|n|\,C^+} - 1; & n>0 \\ \dfrac{\gamma_n}{i\,|n|\,C^+} - \dfrac{C^-}{C^+}; & n<0 \end{cases}. \tag{2.283}$$

From (2.278) it follows that $\delta_n = O(n^{-2})$ as $n\to\pm\infty$. Introduce the matrix operator $V = \{V_{mn}\}_{m,n=-\infty}^{\infty}$ and the column vector $f = \{f_n\}_{n=-\infty}^{\infty}$ by the formulas

$$V_{mn} = |n|\,\delta_n\delta_m^n, \qquad f_n = -\frac{i2\kappa\,(1+\varepsilon_1-\varepsilon_2)}{1+\sqrt{\varepsilon_\perp}}\delta_0^n. \tag{2.284}$$

Substituting (2.284) into (2.279) yields

$$ax_0 + \sum_{n=1}^{\infty} nx_n e^{in\vartheta} - b\sum_{n=-\infty}^{-1} nx_n e^{in\vartheta} + \sum_{n=-\infty}^{\infty}\left[(Vx)_n - f_n\right]e^{in\vartheta} = 0; \qquad |\vartheta|<\vartheta_0, \tag{2.285}$$

$$\sum_{n=-\infty}^{\infty} x_n e^{in\vartheta} = 0; \qquad |\vartheta| > \vartheta_0. \tag{2.286}$$

One easily checks that equations (2.284) and (2.285) match (2.91) and (2.92) with $U = 0$ and $g = 0$. Now it will suffice to verify that the matrix operator $\widehat{V} = \widehat{T}^{-1} V \widehat{T}^{-1} = \left\{\widehat{V}_{mn}\right\}_{m,n=-\infty}^{\infty}$ is compact on the space l_2, where the operator $\widehat{T}$ is given by (2.95). From (2.284) and (2.91), it follows that the matrix elements of the operator $\widehat{V}$ have the appearance

$$\widehat{V}_{mn} = |n|^{1-\eta}\, \delta_n \delta_m^n; \quad n \neq 0 \qquad \text{and} \qquad \widehat{V}_{00} = 0, \tag{2.287}$$

where $\eta = 1 + \arg b/\pi$, $-\pi \leq \arg b < \pi$.

As soon as $\delta_n = O(n^{-2})$, then $\widehat{V}_{nn} \to 0$ for $n \to \pm\infty$, suggesting that the operator $\widehat{V}$ is compact on the l_2 [70].

So, the analytic regularization method outlined in Section 2.2.3 is acceptable for the dual series equations (2.285) and (2.286). As a result, they are equivalent to the infinite system of linear algebraic equations of the second kind on the space l_2 and can be written in the form

$$\left(E + \widehat{H}\right) \widehat{x} = \widehat{b}\,, \tag{2.288}$$

where the operator $\widehat{H} = -a\,\widehat{P} + \widehat{W}\,\widehat{V}$ is compact on the l_2, $\widehat{b} = \widehat{W}\,\widehat{f}$, $\widehat{x} = \widehat{T}\,x$, $\widehat{f} = \widehat{T}^{-1} f$, and the matrix elements of the operators $\widehat{P}$ and $\widehat{W}$ are available from (2.115), (2.117), and (2.121). System (2.288) can be solved with any preassigned accuracy by truncation [144].

Owing to the discussed technique, we have obtained a vast collection of numerical results. Some of them are published in references [144, 145].

Let us analyze some results coming from the numerical solution of equation (2.282). For an anisotropic dielectric medium, we will take a cold electron plasma confined in a constant magnetic field $\vec{H}_0 = \{H_0,0,0\}$ aligned with the x-axis ($\vec{H}_0$ is parallel to the grating edges). Then the components of the permittivity tensor are

$$\varepsilon_1 = 1 - \frac{\omega_p^2\,(\omega + i\nu)}{\omega\left[(\omega + i\nu)^2 - \omega_c^2\right]}, \qquad \varepsilon_2 = -\frac{\omega_p^2 \omega_c}{\omega\left[(\omega + i\nu)^2 - \omega_c^2\right]}, \; \varepsilon_3 = 1 - \frac{\omega_p^2}{\omega\,(\omega + i\nu)}. \tag{2.289}$$

Here ω_p is the plasma frequency, $\omega_c = eH_0/mc$ is the electron cyclotron frequency, ν is the effective collision frequency of electrons, with e and m being, respectively, the electron charge and mass, and c is the speed of light in vacuum.

In the subsequent discussion it will be convenient to use the dimensionless parameters $\kappa = l\omega/2\pi c = l/\lambda$, $\kappa_p = \omega_p l/2\pi c$, $\kappa_c = \omega_p l/2\pi c$ (we recall that l is the grating period).

The computations mainly refer to the excitation frequency band $0 < \kappa < 3$. In this case, as follows from (2.268), the field in the half-space $z > 0$ is a superposition of the incident field and the diffraction field consisting of an infinite series of spatial harmonics of the form $\tilde{U}_n^s(g,k) = R_{n0}^{\mathbf{AA}} \exp\left[i(\Phi_n y + \Gamma_{1n} z)\right]$, $n = 0,\pm1,\pm2,\ldots$. A finite number of harmonics whose numbers satisfy the condition $|n| < \kappa$ are plane H-polarized waves outgoing away from the grating. When $\kappa < 1$, only one wave $\tilde{U}_0^s(g,k) = R_{00}^{\mathbf{AA}} \exp(ikz)$ goes out from the grating. An infinite number of harmonics with numbers $|n| \geq 1$ are surface waves decaying exponentially as $z \to \pm\infty$ and traveling along the grating with phase velocities whose absolute values are less than the speed of light. Hence far away from the grating (the half-space $z > 0$), the diffraction field is governed only by the principal spatial harmonic $\tilde{U}_0^s(g,k)$. The principal harmonic amplitude $R_{00}^{\mathbf{AA}}$ normalized to the incident wave amplitude is a complex coefficient representing the reflection of the field from the grating lying on the boundary of the anisotropic half-space ($z > 0$).

Consider the behavior of the reflection coefficient depending on the excitation wave frequency, grating parameters, and the characteristic frequencies κ_p, κ_c of the anisotropic half-space. For definiteness sake, suppose that $\kappa_p < 1$ and $\kappa_c < 1$ (this is always possible via a reasonable choice of the grating period). The calculations from the numerical solution of (2.288) reveal the frequency range $\alpha_- < \kappa < \kappa_c$; $\alpha_\pm = 0.5\left(\sqrt{\kappa_c^2 + 2\kappa_p^2} \pm \kappa_c\right)$ where even if grating slots are very narrow, the electromagnetic field almost completely transmitted to the anisotropic medium (the reflection coefficient module is $\left|R_{00}^{\mathbf{AA}}\right| \leq 0.3$). Typical dependences of the reflection coefficient module are given in Fig. 2.27a and b, showing a pronounced negative peak of the reflection coefficient amplitude. Thus, at the excitation wavelength more than 10^3 times as large as the grating slot width, the reflection coefficient module is $\left|R_{00}^{\mathbf{AA}}\right| \approx 0.3$. Compare it with the module of the reflection coefficient of a grating free from the anisotropic medium ($\kappa_p = \kappa_c = 0$; dashed line).

As is known [45], a metal strip grating is practically transparent to plane H-polarized waves in the long-wavelength part ($\kappa \ll 1$) of spectrum. The reflection coefficient grows fast as κ increases ($\kappa \to 1$) (see Fig. 2.27a). With the anisotropic half-space present, there is a range of variation of κ ($\kappa < 1$) when even for very narrow slots ($\lambda/d \sim 10^3$), the reflection coefficient module can be substantially less than that of a grating in free space. Also, it is interesting that the characteristic frequency κ_c can effectively control the reflection coefficient (see Fig. 2.27b).

Consider now the behavior of the reflection coefficient in the resonance range $\kappa \approx 1$ (the excitation field wavelength is comparable with the grating period). In this case the well-known resonances (Wood's anomalies) [45] coexist with the resonances caused by the anisotropic medium. In support of this, see Fig. 2.27c for $\left|R_{00}^{\mathbf{AA}}\right|$ curves corresponding to various characteristic frequencies κ_p of the anisotropic medium. The first resonance, $\kappa \approx 1$ (the excitation field wavelength equals the grating period) does not depend on κ_p (Wood's anomaly). The second occurs at

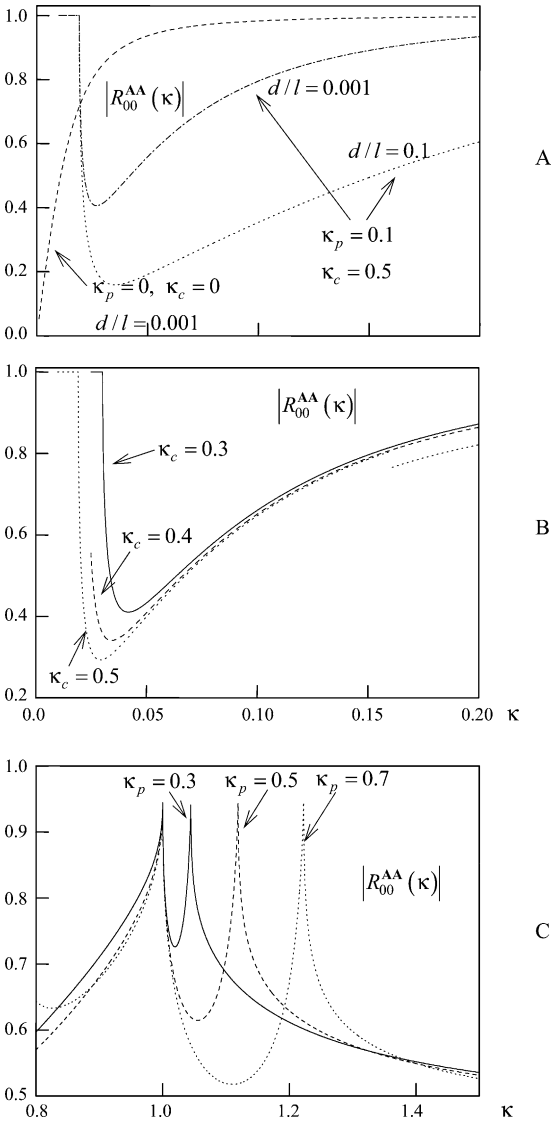

Fig. 2.27 (**a**) The reflection coefficients $\left|R_{00}^{AA}\right|$ versus frequency $\kappa = l/\lambda$ for different structure parameters: (**b**) $\kappa_p = 0.1$, $d/l = 0.01$; (**c**) $\kappa_c = 0.1$, $d/l = 0.5$

$\kappa \approx 1/\sqrt{\varepsilon_\perp}$, where $\varepsilon_\perp = \left(\varepsilon_1^2 - \varepsilon_2^2\right)/\varepsilon_1$ is the effective permittivity of the anisotropic half-space. And it disappears when $\kappa_p \to 0$ and $\kappa_c \to 0$. Attention is drawn to the fact that as κ_p (the plasma frequency) increases, the frequency at which this resonance is possible moves toward the short-wavelength end. This behavior of the reflection coefficient can be used for the determination of the physical characteristics (such as κ_p) of an anisotropic medium. Indeed, knowing the grating geometrical parameters (d and l), the cyclotron frequency κ_c and the frequency κ_{res} at which the reflection

coefficient module is at a maximum, one finds the plasma frequency

$$\omega_p = \frac{2\pi c}{l}\sqrt{\frac{2\kappa_{res}^2 - 1 + \sqrt{1 + 4\kappa_c^2\left(\kappa_{res}^2 - 1\right)}}{2}},$$

and, consequently, the cold electron plasma density from $\kappa_{res}\sqrt{\varepsilon_\perp} \approx 1$.

Now, examine the features of the reflection coefficient behavior with the anisotropic lossy medium [see (2.289), $\nu \neq 0$]. Figure 2.28 shows characteristic dependences of the module of the reflection coefficient in frequency bands where the real part of the effective permittivity takes on positive values. By numerical calculations it was found that these frequency bands carry particular frequencies $\kappa = \alpha_\pm$ in whose vicinities the reflection coefficient can exhibit resonances, and these are due to the surface waves existing on the anisotropic half-space boundary (with the grating absent). At the frequency $\kappa = \alpha_\pm$, the phase velocities of these surface waves become zero. The resonances are most pronounced when the grating slots are

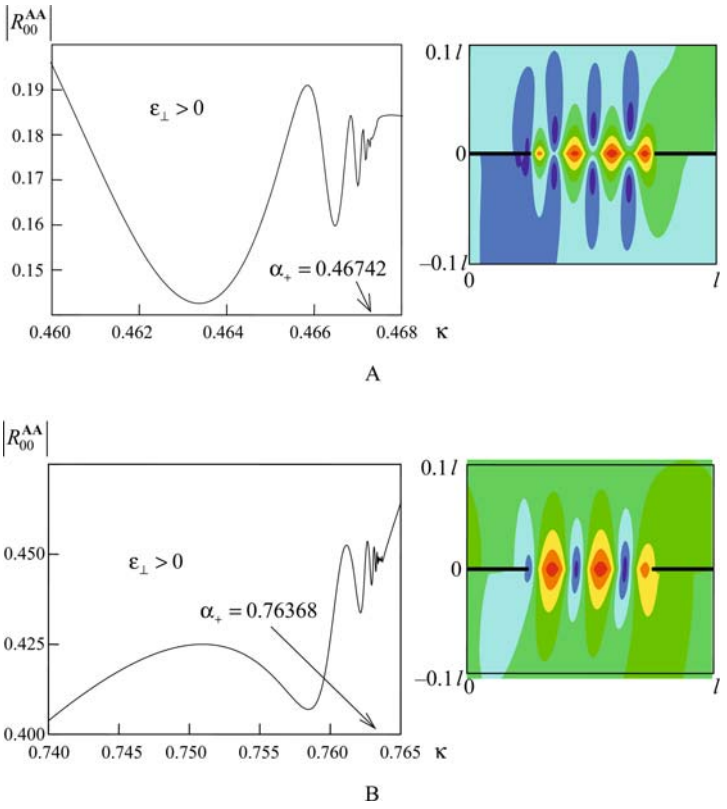

Fig. 2.28 The reflection coefficient module versus frequency and the field structure at resonance frequencies: (**a**) $\kappa_p = 0.5$, $\kappa_c = 0.2$; and (**b**) $\kappa_p = 0.5$, $\kappa_c = 0.6$

sufficiently wide ($d/l \geq 0.5$). Figure 2.28 shows the $\tilde{H}_x$ component distribution at some resonance frequencies, $d/l = 0.5$. As seen, the field is concentrated near the grating slots.

Another resonance type is due to the surface wave supported by the interface between the perfectly conducting metal and an anisotropic half-space. The frequency at which the phase velocity of this wave vanishes matches the cyclotron frequency κ_c. In its vicinity, the reflection coefficient can be resonant (Fig. 2.29). In this frequency region, the real part of the effective permittivity takes on negative values. Therefore with losses absent ($\nu = 0$), the reflection coefficient module equals unity ($\left|R_{00}^{\mathbf{AA}}\right| = 1$). The situation changes completely when the anisotropic half-space is lossy. Namely, the reflection coefficient module as a function of frequency demonstrates clear negative peaks (see Fig. 2.29a) which are most pronounced when the grating slots are sufficiently narrow ($d/l \leq 0.1$). For the field structure at some

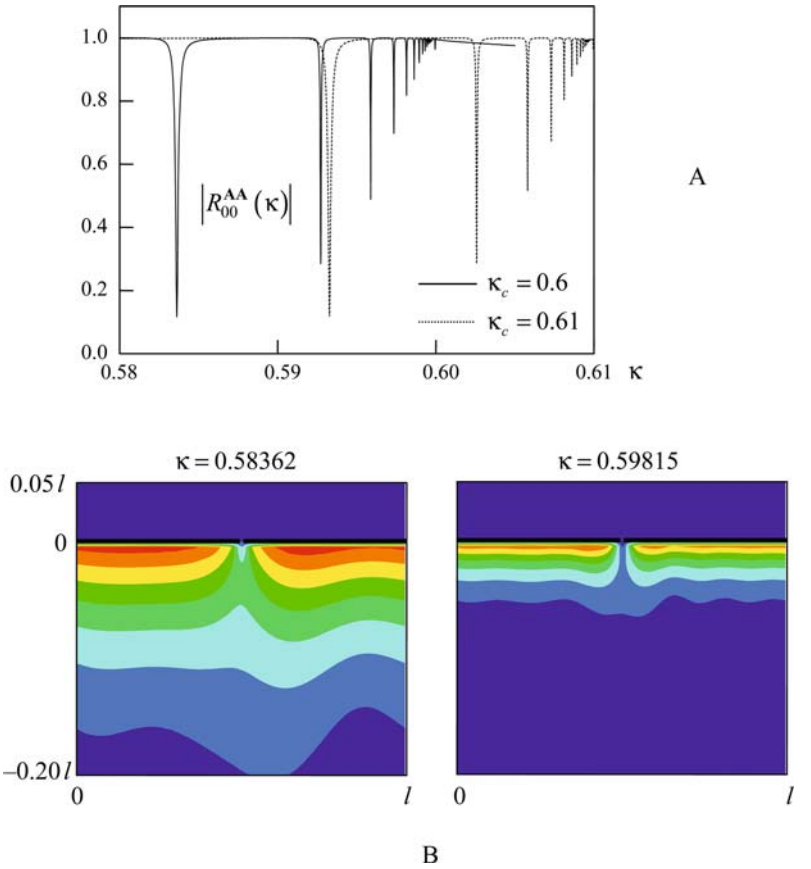

Fig. 2.29 (**a**) The reflection coefficient module versus frequency for $d/l = 0.01$, $\kappa_p = 0.5$, $\kappa_c = 0.6$, and $\kappa_c = 0.61$; and (**b**) the field structure at some resonance frequencies

frequencies corresponding to minima of the amplitude of the reflection coefficient, see Fig. 2.29b. The resonance field is concentrated in the anisotropic medium near the grating metal strips.

At this point, our presentation of numerical results obtained with the aid of the analytic regularization method has come to an end, in the present context. We hopefully appreciate that the cited results provide at least a partial answer to the long-standing question of what is the practical use of all these analytic regularization procedures with their sometimes complicated transformations and bulky constructions.

2.6 Diffraction of Quasi-Periodic Waves by Obstacles with Cylindrical Periodical Wavy Surfaces

The purpose of this section is the demonstration of the simplest initial technique of the analytic regularization method. That is why the subject of our consideration herein is mathematical modeling of simple, but key problems of electromagnetic wave diffraction by obstacles with infinite and smooth one-dimensional periodical wavy surfaces (see Fig. 2.30). We study these problems in the system of nondimensional time and spatial coordinates $\bar{y} = 2\pi y/l$, $\bar{z} = 2\pi z/l$, $\bar{t} = 2\pi t/l$, according to which the period of gratings is equal to 2π.

Such a cylindrical surface $\bar{\mathbf{S}}$ is supposed to be 2π-periodical with respect to the space variable $\bar{y}$ and homogeneous in the longitudinal $\bar{x}$-direction. The cross-section $\bar{\mathbf{S}}_x$ of $\bar{\mathbf{S}}$ by the plane $\bar{x} = \text{const}$ can be described as the set of contours:

$$\bar{\mathbf{S}}_x = \bigcup_{j=-\infty}^{\infty} \bar{\mathbf{S}}_{x,j} \in \mathbf{C}^{\infty};\ \bar{\mathbf{S}}_{x,j} = \left\{\bar{g}_j = \{\bar{y} + 2\pi j, \bar{z}\} :\ \bar{g} = \{\bar{y}, \bar{z}\} \in \bar{\mathbf{S}}_{x,0};\ 0 \le \bar{y} \le 2\pi\right\}. \tag{2.290}$$

We assume that contour $\bar{\mathbf{S}}_x$ is nonself-crossing and (just for simplicity) infinitely smooth. Contour $\bar{\mathbf{S}}_{x,0}$ is supposed to be of finite length.

Corresponding parameterizations of contours $\bar{\mathbf{S}}_x$ and $\bar{\mathbf{S}}_{x,0}$ play an essential role in our future explanation. Necessary constructions and assumptions can be summarized as follows.

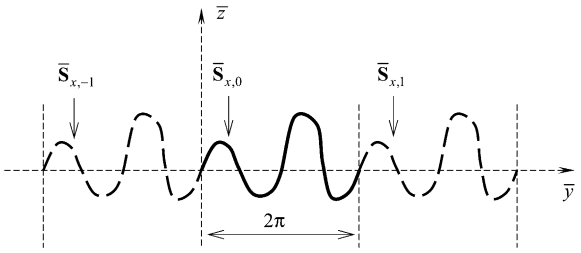

Fig. 2.30 Perfectly conducting metallic 2π-periodic grating of arbitrary profile

- The vector function

$$\eta^0(\vartheta) \equiv \{\bar{y}(\vartheta), \bar{z}(\vartheta)\}; \vartheta \in [-\pi;\pi] \tag{2.291}$$

is assumed to be given as a smooth parameterization of the contour $\bar{\mathbf{S}}_{x,0}$. It means that $\bar{y}(\vartheta)$ and $\bar{z}(\vartheta)$ are such functions that for every $\vartheta \in [-\pi;\pi]$ they give corresponding to this ϑ point $\bar{g} = \{\bar{y}, \bar{z}\} = \{\bar{y}(\vartheta), \bar{z}(\vartheta)\} \in \bar{\mathbf{S}}_{x,0}$ with the property that function $l(\vartheta) \equiv \left\{\left[d\bar{z}(\vartheta)/d\vartheta\right]^2 + \left[d\bar{y}(\vartheta)/d\vartheta\right]^2\right\}^{1/2}$ is finite and strongly positive (one-to-one mapping condition):

$$0 < l(\vartheta) < \infty. \tag{2.292}$$

- The parameterization $\eta^j(\vartheta) \equiv \left\{\bar{y}_j(\vartheta), \bar{z}_j(\vartheta)\right\}$, $j = 0, \pm 1, \pm 2, \ldots$, for every contour $\bar{\mathbf{S}}_{x,j}$ is constructed according to (2.290) and (2.291):

$$\bar{y}_j(\vartheta) = \bar{y}(\vartheta - 2\pi j), \bar{z}_j(\vartheta) = \bar{z}(\vartheta - 2\pi j); \vartheta \in \left[-\pi + 2\pi j; \pi + 2\pi j\right]. \tag{2.293}$$

- The parameterization $\eta(\vartheta)$ of the contour $\bar{\mathbf{S}}_x$ is

$$\eta(\vartheta) \equiv \eta^j(\vartheta); \vartheta \in \left[-\pi + 2\pi j; \pi + 2\pi j\right], \bar{y}(\vartheta + 2\pi) = \bar{y}(\vartheta) + 2\pi, \quad \bar{z}(\vartheta + 2\pi) = \bar{z}(\vartheta), \tag{2.294}$$

and, due to the construction,

$$\eta: (-\infty;\infty) \leftrightarrow \bar{\mathbf{S}}_x \tag{2.295}$$

is a one-to-one mapping of $(-\infty;\infty)$ to $\bar{\mathbf{S}}_x$.

- The parameterization $\eta(\vartheta)$ thus obtained is infinitely smooth:

$$\eta(\vartheta) \in \mathbf{C}^\infty(-\infty;\infty). \tag{2.296}$$

We will say that the function $f(\vartheta)$ is a 2π-quasi-periodical one (with respect to variable ϑ) if the function satisfies the condition

$$f(\vartheta + 2\pi) = e^{i2\pi\Phi} f(\vartheta) \tag{2.297}$$

for each ϑ in the domain of the function definition. Parameter Φ is introduced in Section 1.1.3 and it is known as the parameter of quasi-periodicity. According to (2.291), Φ in (2.297) can be always chosen (by means of adding or extraction of an integer number) satisfying the inequalities that we assume to be valid below:

$$-1/2 < \Phi \leq 1/2. \tag{2.298}$$

For concreteness, we assume also that the surface $\bar{\mathbf{S}} = \bar{\mathbf{S}}_x \times [-\infty < x < \infty]$ is excited by an electromagnetic plane wave

$$\tilde{U}_p^i(\bar{g},\kappa)=\exp\left[i\left(\bar{\Phi}_p\bar{y}-\bar{\Gamma}_p\bar{z}\right)\right];\ \bar{g}\in\mathbf{R}^2 \tag{2.299}$$

(p is integer), which is 2π-quasi-periodical with respect to $\bar{y}$, does not depend on $\bar{x}$, and comes from the upper half-space. Here [see also (1.22)], $\bar{\Phi}_n=\Phi+n$, $\bar{\Gamma}_n=\sqrt{\kappa^2-\bar{\Phi}_n^2}$, $\mathrm{Re}\bar{\Gamma}_n\mathrm{Re}\kappa\geq 0$, and $\mathrm{Im}\bar{\Gamma}_n\geq 0$. As well, $\tilde{U}_p^i(\bar{g},\kappa)$ can be, in principal, any 2π-quasi-periodical in respect to $\bar{y}$, not depending on $\bar{x}$, and smooth in some vicinity $\mathbf{V}$ of $\bar{\mathbf{S}}$ function.

The incident field, the obstacle's material parameters, and the geometrical structure do not depend on the space variable $\bar{x}$, then, evidently, the scattered field $\tilde{U}^s(\bar{g},\kappa)$ does not depend on $\bar{x}$ either. Consequently, the electromagnetic fields can be expressed by means of two scalar functions $\tilde{E}_x$ (E-polarization) and $\tilde{H}_x$ (H-polarization) satisfying homogeneous Helmholtz equations. Thus, the problems under consideration are scalar and two-dimensional ones.

There are three typical kinds of boundary conditions on the surface $\bar{\mathbf{S}}$, namely, Dirichlet, Neumann, and transmission ones. When $\bar{\mathbf{S}}$ is the surface of a perfectly conducting screen, we have Dirichlet or Neumann boundary value problems (BVPs) for E- or H-polarization, respectively. For the case when the surface separates two media with different material parameters (it will be the surface $\bar{\mathbf{S}}^{\varepsilon,\mu,\sigma}$), we arrive at transmission problems (for both polarizations).

In this section, we restrict ourselves at rather brief consideration of the Dirichlet and Neumann problems only. There is a big similarity in construction of analytic regularization method for the other BVPs mentioned above. Also, it is necessary to have much more room for going into all details even for a Dirichlet BVP only. That is why we recommend our reader to look at the publications [10, 11, 57, 58, 63, 64, 149, 150], where similar and more complicated problems are investigated.

In Section 2.6.1, we consider a Dirichlet BVP. Section 2.6.2 is devoted to reducing the BVP to a standard integral equation of the first kind. Differential and singular properties of the transformed integral equation kernel are the subject of the analysis in Section 2.6.3. In Section 2.6.4, we discuss the splitting of the integral equation kernel and the requirements for the result of the splitting. In Section 2.6.5, we reduce the integral equation to an infinite system of the first kind. In Section 2.6.6, we use the splitting constructed for obtaining the algebraic system of the second kind, which forms functional equations of the type $(E+H)\,x=b$, x, $b\in l_2$ with identity operator E and compact operator H in the space l_2 of square-summable sequences. Section 2.6.7 outlines the difference in application of the analytic regularization method for the Neumann BVP in comparison with the Dirichlet one. Here we obtain similar result: the Neumann BVP is reduced to the algebraic system of the second kind, which is qualitatively the same as one mentioned above for the Dirichlet BVP.

As it is well known, solving such an algebraic system of the second kind by means of the reduction method is numerically stable process that gives principal possibility to obtain the solution with any predetermined accuracy (in contrast to many popular, but unstable methods like the family of Galerkin and the other direct methods).

2.6.1 The Dirichlet Diffraction Problem

The initial version of the algorithm explained herein can be found in publication [149]. Similar problem, but for semitransparent grating, is the subject of publication [150].

Let the above-mentioned $\bar{\mathbf{S}}$ be a surface of a perfectly conducting screen, which is illuminated by an E-polarized wave with given 2π-quasi-periodical component $\tilde{E}_x^i(\bar{g},\kappa) = \tilde{U}_p^i(\bar{g},\kappa)$ [see formula (2.299) and the next paragraph].

We pose the Dirichlet BVP in the same way as it is explained in Chapter 1 – see (1.20) and (1.22). Nevertheless, some details of the boundary conditions and their exact mathematical sense must be added. We use the problem posing in the classical sense similar to [9]. That is why we assume that unknown and seeking for 2π-quasi-periodical function $\tilde{U}^s(\bar{g},\kappa)$, $\bar{g} \in \mathbf{R}^2$, i.e., scattering field, belongs to the following functional class:

$$\tilde{U}^s(\bar{g},\kappa) \in \mathbf{C}^2\left(\mathbf{R}^2 \backslash \bar{\mathbf{S}}_x\right) \cap \mathbf{C}^{1,\alpha}\left(\overline{\mathbf{R}^{2(+)}}\right) \cap \mathbf{C}^{1,\alpha}\left(\overline{\mathbf{R}^{2(-)}}\right). \tag{2.300}$$

Here, $\mathbf{R}^{2(\pm)}$ are open parts of $\mathbf{R}^2$ placed over and under the contour $\bar{\mathbf{S}}_x$ correspondingly, and $\overline{\mathbf{R}^{2(\pm)}}$ are their closures. This description (2.300) of the class of functions means, in particular, the existence of the following limits, uniform on $\mathbf{S}$:

$$\tilde{U}^{s(\pm)}(\bar{g},\kappa) = \lim_{h\to+0} \tilde{U}^s\left(\bar{g} \pm h\vec{n}_{\bar{g}},\kappa\right);\ \bar{g} \in \bar{\mathbf{S}}_x, \tag{2.301}$$

$$\frac{\partial \tilde{U}^{s(\pm)}(\bar{g},\kappa)}{\partial \vec{n}_{\bar{g}}} = \lim_{h\to+0} \frac{\partial \tilde{U}^{s(\pm)}\left(\bar{g} \pm h\vec{n}_{\bar{g}},\kappa\right)}{\partial \vec{n}_{\bar{g}}};\ \bar{g} \in \bar{\mathbf{S}}_x, \tag{2.302}$$

where $\vec{n}_{\bar{g}}$ is unit outward (directed from $\mathbf{R}^{2(+)}$ to $\mathbf{R}^{2(-)}$) normal to $\bar{\mathbf{S}}_x$ in point $\bar{g} \in \bar{\mathbf{S}}_x$, and, in general, the $(\pm)$ limits are not equal, but can be equal, of course [as this takes place, for example, in condition (2.303)].

We assume also that Dirichlet boundary condition is satisfied, which corresponds to E-polarized wave diffraction by a perfectly conductive cylindrical wavy surface $\bar{\mathbf{S}}_x$:

$$\tilde{U}^{s(\pm)}(\bar{g},\kappa) + \tilde{U}_p^i(\bar{g},\kappa) = 0;\ \bar{g} \in \bar{\mathbf{S}}_x. \tag{2.303}$$

As follows from (1.24), the canonic Green function $\tilde{G}_0(\bar{g},\bar{g}_0,\kappa,\Phi)$ becomes infinite for $\bar{\Gamma}_n = 0$ (that corresponds to branch points of the BVP operator). That is why we will assume below that κ and Φ are chosen in such a way that $\bar{\Gamma}_n \neq 0$.

2.6.2 Reduction of the Dirichlet BVP to the Integral Equations

It can be proved by standard technique of Green's formulas that the scattered field $\tilde{U}^s(\bar{g},\kappa)$ has the following representation:

$$\tilde{U}^s(\bar{g}_1,\kappa) = \int\limits_{\bar{\mathbf{S}}_{x,0}} \tilde{G}_0(\bar{g}_1,\bar{g}_2,\kappa,\Phi)\, M_D(\bar{g}_2)\, dl_{\bar{g}_2};\ \bar{g}_1 \in \mathbf{R}^2 \backslash \bar{\mathbf{S}}_x. \tag{2.304}$$

Here,

$$M_D(\bar{g}) = \frac{\partial \tilde{U}^{s(+)}(\bar{g},\kappa)}{\partial \vec{n}_{\bar{g}}} - \frac{\partial \tilde{U}^{s(-)}(\bar{g},\kappa)}{\partial \vec{n}_{\bar{g}}};\ \bar{g} \in \bar{\mathbf{S}}_x, \tag{2.305}$$

and $M_D(\bar{g})$ is quasi-periodic function satisfying the integral identity

$$\int\limits_{\bar{\mathbf{S}}_{x,0}} \tilde{G}_0(\bar{g}_1,\bar{g}_2,\kappa,\Phi)\, M_D(\bar{g}_2)\, dl_{\bar{g}_2} = -\tilde{U}^i_p(\bar{g}_1,\kappa);\ \bar{g}_1 \in \bar{\mathbf{S}}_{x,0}. \tag{2.306}$$

$\tilde{G}_0(\bar{g}_1,\bar{g}_2,\kappa,\Phi)$ is the canonic Green's function (1.24) of free space for Helmholtz equation and for 1-D periodical structures, but written with respect to nondimensional normalized spatial coordinates $\bar{g} = \{\bar{y},\bar{z}\}$ and points $\bar{g}_j$, $j = 1, 2$. Here, $\kappa = l/\lambda$, where l is the realistic grating period and λ is the wavelength of the incident wave. This function has view (1.24), but value l in factor $-i/2l$ before the symbol of the sum must be changed by $-i/4\pi$, because the grating period in respect to normalized value $\bar{y}$ is equal to 2π (value l in (1.24) has nothing common with function $l(\vartheta)$ in (2.292) that should not be a cause of any confusion, because nowhere below in this section notation l is used as the grating period, but only function $l = l(\vartheta)$ may appear in formulas).

It is noteworthy that series (1.24) is absolutely useless for numerical calculation of $\tilde{G}_0(\bar{g}_1,\bar{g}_2,\kappa,\Phi)$ in domain $|\bar{z}_1 - \bar{z}_2| \ll 1$, because of the series' slow convergence. In a number of papers their authors used extraction of the main asymptotic part of the common term of the series in the form ρ^n/n, where $|\rho| \le 1$. Thus, the series need not any acceleration, if $|\rho| \ll 1$, i.e., $|\bar{z}_1 - \bar{z}_2| \gg 1$. In the same time, series $\sum \rho^n/n$ can be summarized analytically and the sum is an elementary function, which has analytic singularity proportional to $\ln(1-\rho)$. The series similar to $\sum \rho^n/n$ can be extracted term by term from the right-hand side of (1.24) and the result is series of the kind $\sum p_n^{(1)}$, where $p_n^{(1)}$ are some numbers possessing property $p_n^{(1)} = O\left(\rho^n/n^2\right)$. Only the last series needs numerical calculation after that. This is essential progress, because the last series is at least absolutely convergence. Nevertheless, its convergence is still too slow for to be called the summation efficient. The above-explained extraction can be continued with terms ρ^n/n^m, $m = 2,3,4,\ldots$, but, unfortunately, the series $\sum \rho^n/n^m$ are not representable by elementary functions for $m \ge 2$. Perhaps, this fact prevented the mentioned above authors from such extraction and based on it acceleration of series (1.24) convergence.

Nevertheless, we managed (see [11]) to obtain for any fixed $m = 2,3,4,\ldots$ the representation of the kind $\tilde{G}_0(\bar{g}_1,\bar{g}_2,\kappa,\Phi) = S_m + \sum p_n^{(m)}$, where S_m and $p_n^{(m)}$ are expressed by means of elementary functions of $\bar{g}_1$, $\bar{g}_2$, κ and Φ, and $p_n^{(m)} = O(\rho^n/n^m)$. Actually, we even found the relevant recurrent algorithm, which avoids

the necessity of knowing and direct calculation of (rather bulky for big m) analytic expressions of S_m. As well, the number m of the extracted terms, as it is explained above, is regulated dependently on value $|\bar{z}_1 - \bar{z}_2|$: it is maximal for $|\bar{z}_1 - \bar{z}_2| = 0$ (i.e., when $|\rho| = 1$), and any extraction is not necessary for $|\bar{z}_1 - \bar{z}_2| \gg 1$. Thus, the problem of fast calculation of $\tilde{G}_0(\bar{g}_1, \bar{g}_2, \kappa, \Phi)$ (and its derivatives of any finite order) is completely solved.

From modified as above-mentioned formula (1.24) and from (2.305) and (2.304), it follows immediately that $\tilde{G}_0(\bar{g}_1, \bar{g}_2, \kappa, \Phi)$ and $M_D(\bar{g}_1)$ are 2π-quasi-periodic function with respect to $\bar{g}_1$ – in the sense of (2.297) – and $\tilde{G}_0(\bar{g}_1, \bar{g}_2, \kappa, \Phi)$ is 2π-quasi-periodic function in the same sense, but with the negated (i.e., $-\Phi$) parameter of quasi-periodicity:

$$M_D(\bar{y} + 2\pi, \bar{z}) = e^{i2\pi\Phi} M_D(\bar{y}, \bar{z}) \,;\, \bar{g} = \{\bar{y}, \bar{z}\} \in \bar{\mathbf{S}}_x, \tag{2.307}$$

$$\tilde{G}_0(\bar{y}_1 + 2\pi j, \bar{z}_1, \bar{y}_2 + 2\pi s, \bar{z}_2, \kappa, \Phi) = e^{i2\pi(j-s)\Phi} \tilde{G}_0(\bar{y}_1, \bar{z}_1, \bar{y}_2, \bar{z}_2, \kappa, \Phi);$$

$$\{\bar{y}_1, \bar{z}_1\}, \ \{\bar{y}_2, \bar{z}_2\} \in \mathbf{R}^2. \tag{2.308}$$

In accordance with the standard approach, we will consider (2.306) from now as the integral equation for the unknown function $M_D(\bar{y}, \bar{z})$. It can be proved that if this function has been found, then one can obtain the scattered field in every point by means of the integral representation (2.304).

Using the parameterization $\eta(\vartheta) \equiv \{\bar{y}(\vartheta), \bar{z}(\vartheta)\}$ of contour $\bar{\mathbf{S}}_x$, one can easily reduce the integral equation (2.306) on contour $\bar{\mathbf{S}}_{x,0}$ to an ordinary integral equation on interval $[-\pi;\pi]$ by means of the substitutions

$$\bar{y}_1 = \bar{y}(\tau), \ \bar{z}_1 = \bar{z}(\tau) \,;\, \tau \in [-\pi;\pi], \tag{2.309}$$

$$\bar{y}_2 = \bar{y}(\vartheta), \ \bar{z}_2 = \bar{z}(\vartheta) \,;\, \vartheta \in [-\pi;\pi] \tag{2.310}$$

and direct definition of new functions

$$\mu^0(\tau) = M_D(\bar{y}(\tau), \bar{z}(\tau)) \,;\, \tau \in [-\pi;\pi], \tag{2.311}$$

$$G^0(\vartheta,\tau) = l(\tau) \tilde{G}_0(\bar{y}(\vartheta), \bar{z}(\vartheta), \bar{y}(\tau), \bar{z}(\tau), \kappa, \Phi) \,;\, \vartheta,\tau \in [-\pi;\pi], \tag{2.312}$$

where the fixed parameters κ and Φ are omitted for the sake of brevity. Such a direct way has the following drawback. Due to formulas (2.307) and (2.308), these new functions $\mu^0(\tau)$ and $G^0(\vartheta,\tau)$ are 2π-quasi-periodical ones and are not 2π-periodical, in general. We are going to use Fourier series of these functions. Unfortunately, Fourier coefficients of a function $\mu^0(\tau)$, defined in the way (2.311), tend to zero very slowly (due to the nonperiodicity of the function), and, which is the most important, the same holds for the function $G^0(\vartheta,\tau)$ that brings a very strong limitation on the efficiency of any algorithm thus constructed. Moreover, the behavior

of Fourier coefficients of function $G^0(\vartheta,\tau)$ does not allow us to obtain anyhow an algebraic system of the second kind, which is our final goal.

That is why, we define other – just 2π-periodic – functions:

$$\tilde{\mu}(\tau) = e^{-i\Phi\tau} M_D(\bar{y}(\tau), \bar{z}(\tau)), \tag{2.313}$$

$$\tilde{G}(\vartheta,\tau) = e^{i\Phi(\tau-\vartheta)} \tilde{G}_0(\bar{y}(\vartheta), \bar{z}(\vartheta), \bar{y}(\tau), \bar{z}(\tau), \kappa, \Phi), \tag{2.314}$$

$$\tilde{f}(\vartheta) = -e^{-i\Phi\vartheta} \tilde{U}_p^i(\bar{y}(\vartheta), \bar{z}(\vartheta), \kappa). \tag{2.315}$$

Using formulas (2.313), (2.314), and (2.315) one can rewrite equation (2.306) after some obvious transformations into the following integral equation of the first kind for the unknown function $\tilde{\mu}(\tau)$:

$$\int_{-\pi}^{\pi} \tilde{\mu}(\tau)\, \tilde{G}(\vartheta,\tau)\, l(\tau)\, d\tau = \tilde{f}(\vartheta);\ \vartheta \in [-\pi;\pi]. \tag{2.316}$$

One can consider the function $\tilde{\mu}(\tau)$ on the interval $(-\infty;\infty)$ as the result of its 2π-periodic continuation from $[-\pi;\pi]$. As it follows from formulas (2.314), (2.315), (2.312), (2.308), and (2.315), functions $\tilde{G}(\vartheta,\tau)$, $\tilde{\mu}(\tau)$, and $\tilde{f}(\vartheta)$ are 2π-periodical ones for $\vartheta,\tau\in(-\infty;\infty)$.

2.6.3 Investigation of the Differential Properties of the Integral Equation Kernel

Before any attempt to solve the integral equation (2.316) and a choice of a proper method for such a purpose, it is necessary to investigate the differential and singular properties of the kernel $\tilde{G}(\vartheta,\tau)\, l(\tau)$.

First of all, $\tilde{G}(\vartheta,\tau)$ is an infinitely smooth function for $0 < |\vartheta-\tau| < 2\pi$, because $\tilde{G}_0(\bar{y}_1, \bar{z}_1, \bar{y}_2, \bar{z}_2, \kappa, \Phi)$ is infinitely smooth for $\{\bar{y}_1,\bar{z}_1\} \neq \{\bar{y}_2,\bar{z}_2\}$ as a solution of the homogeneous Helmholtz equation. An explanation of the differential properties of $\tilde{G}(\vartheta,\tau)$ for small $|\vartheta-\tau|$ and $|2\pi - |\vartheta - \tau||$ requires the formulation of a few definitions as follows.

The function $\psi(\vartheta)$, $\vartheta\in[-\pi;\pi]$ belongs to class $\mathbf{C}_Q^m(\mathbf{R}^1)$, if it is m times continuously differentiable after its 2π-periodic continuation on $(-\infty;\infty)$ (in particular, $\psi^{(k)}(-\pi+0) = \psi^{(k)}(\pi-0)$, $k = 0,1,\ldots,m$).

The function $\psi(\vartheta,\tau)$, $\vartheta,\tau\in[-\pi;\pi]$ belongs to class $\mathbf{C}_Q^m(\mathbf{R}^2)$, if all its partial and mixed derivatives of orders $k = 0,1,\ldots,m$ exist and are continuous after the function 2π-periodic continuation with respect to both variables on $(-\infty,\infty) \times (-\infty,\infty)$.

The function $\psi(\vartheta)$, $\vartheta\in[-\pi;\pi]$ belongs to the Hölder-like 2π-periodical class $\mathbf{C}_Q^{m,\alpha}(\mathbf{R}^1)$, if $\psi \in \mathbf{C}_Q^m(\mathbf{R}^1)$ and such fixed constants $\alpha\in(0;1)$ and $C > 0$ exist that

$$\left|\psi^{(m)}(\vartheta_1)-\psi^{(m)}(\vartheta_2)\right|\le C\left|2\sin\frac{\vartheta_1-\vartheta_2}{2}\right|^{\alpha};\ \vartheta_1,\ \vartheta_2\in[-\pi;\pi],\tag{2.317}$$

where $\psi^{(m)}(\vartheta)$ is the derivative of order m of function $\psi(\vartheta)$.

The function $\psi(\vartheta,\tau)$, $\vartheta,\tau\in[-\pi;\pi]$ belongs to the Hölder-like 2π-periodical class $\mathbf{C}_Q^{m,\alpha}\left(\mathbf{R}^2\right)$, if $\psi\in\mathbf{C}_Q^m\left(\mathbf{R}^2\right)$ and such fixed constants $\alpha\in(0;1)$ and $C>0$ exist that

$$\left|\frac{\partial^m\left[\psi(\vartheta_1,\tau_1)-\psi(\vartheta_2,\tau_2)\right]}{\partial^{m_1}\vartheta\,\partial^{m_2}\tau}\right|\le C\left|2\sin\frac{\vartheta_1-\tau_1}{2}\right|^{\alpha}\left|2\sin\frac{\vartheta_2-\tau_2}{2}\right|^{\alpha},\tag{2.318}$$

for any $m_1\ge 0$ and $m_2\ge 0$ that $m=m_1+m_2$.

The corresponding classes $\mathbf{C}_Q^{\infty}\left(\mathbf{R}^1\right)$ and $\mathbf{C}_Q^{\infty}\left(\mathbf{R}^2\right)$ are defined in standard way:

$$\mathbf{C}_Q^{\infty}\left(\mathbf{R}^1\right)=\bigcap_{m=0}^{\infty}\mathbf{C}_Q^m\left(\mathbf{R}^1\right)\ \text{and}\ \mathbf{C}_Q^{\infty}\left(\mathbf{R}^2\right)=\bigcap_{m=0}^{\infty}\mathbf{C}_Q^m\left(\mathbf{R}^2\right).\tag{2.319}$$

For any $p=0,1,2,\ldots$, we introduce 2π-periodical functions:

$$\widehat{\Phi}_{2p}(\tau)=-(-1)^p(2p)!\sum_{n=1}^{\infty}\frac{\cos n\tau}{n^{2p+1}},\tag{2.320}$$

$$\widehat{\Phi}_{2p+1}(\tau)=-(-1)^p(2p+1)!\sum_{n=1}^{\infty}\frac{\sin n\tau}{n^{2p+2}}.\tag{2.321}$$

In particular,

$$\widehat{\Phi}_0(\tau)=\ln\left|2\sin\frac{\tau}{2}\right|.\tag{2.322}$$

The functions $\widehat{\Phi}_m(\tau)$ possess the properties

$$\widehat{\Phi}_m(\tau)\in\mathbf{C}_Q^{m-1}\left(\mathbf{R}^1\right);\ m\ge 1;\ \widehat{\Phi}_m(\tau)-\left(2\sin\frac{\tau}{2}\right)^m\ln\left|2\sin\frac{\tau}{2}\right|\in\mathbf{C}_Q^{m+1}\left(\mathbf{R}^1\right),\tag{2.323}$$

$$\frac{d}{d\tau}\widehat{\Phi}_m(\tau)=m\,\widehat{\Phi}_{m-1}(\tau).\tag{2.324}$$

Thus, functions $\widehat{\Phi}_m(\tau)$, $m=0,1,2,\ldots$, form a sequence of functions, where each next function is more smooth than the preceding one.

It can be shown that for any fixed finite number $N=2,3,4,\ldots$ the following singular expansion of the function $\tilde{G}(\vartheta,\tau)$ is valid:

$$\tilde{G}(\vartheta,\tau)-\frac{1}{2\pi}\sum_{n=1}^{N}A_n(\vartheta)\,\widehat{\Phi}_n(\delta)\in\mathbf{C}_Q^N\left(\mathbf{R}^2\right).\tag{2.325}$$

Here, $\delta = \tau - \vartheta$ and $A_n(\vartheta)$ are some infinitely smooth functions:

$$A_n(\vartheta) \in \mathbf{C}^{\infty}(-\infty;\infty). \tag{2.326}$$

After some calculation one can obtain the analytic form of the first few functions $A_n(\vartheta)$. In particular,

$$A_0(\vartheta) \equiv 1, A_1(\vartheta) = i\Phi = \text{const}, A_2(\vartheta) = -\frac{\Phi^2}{2} - \frac{\kappa^2 l^2(\vartheta)}{4}. \tag{2.327}$$

This singular expansion completely describes the singular properties of $\tilde{G}(\vartheta,\tau)$. In particular, from it follows that $\tilde{G}(\vartheta,\tau)$ has singularities in points $\{\vartheta,\tau\}$ where $\vartheta - \tau = 0$ or $\vartheta - \tau = \pm 2\pi$ and in these points only.

Having constructed the singular expansion as above, we can try to derive the analytic regularization method similar to the construction in Section 2.1, because the principal singularities of the kernels are similar. This idea encounters an obstacle in the form of the function $l(\tau)$ appearing as a factor in the integral equation kernel. The simplest remedy for this is the introduction of a new unknown function $\tilde{\mu}_{\gamma}(\tau)$ by the relation $\tilde{\mu}(\tau) = \tilde{\mu}_{\gamma}(\tau)[l(\tau)]^{\gamma-1}$ for any number γ, and multiplication of both sides of integral equation (2.316) by $[l(\vartheta)]^{-\gamma}$. This leads to a similar integral equation with unknown function $\tilde{\mu}_{\gamma}(\tau)$, but with a new kernel of the form $[l(\tau)]^{\gamma}[l(\vartheta)]^{-\gamma}\tilde{G}(\vartheta,\tau)$. According to (2.325), (2.327), and (2.322), the principal singularity of this kernel is $(1/2\pi)\ln\left|2\sin(\vartheta-\tau)/2\right|$, and the same algorithm as the one in Section 2.1 (given for the example in that section) for the analytic regularization method construction is applicable, in principle. Nevertheless, a much better algorithm can be constructed. Indeed, as we see, $A_1(\vartheta) \neq 0$. That is why application of the mentioned algorithm has a strong limitation on the rate of decay of the Fourier coefficients of the kernel. Thus, if it is possible to include the subordinate singularity $(1/2\pi)A_1(\vartheta)\widehat{\Phi}_1(\delta)$ into the principal one (extracted from the kernel – see below), then a much more efficient algorithm can be constructed. The coefficient $A_1(\vartheta)$ in (2.325) is constant, and for such a singularity its necessary inclusion can be achieved easily – see below. At the same time, for any $\gamma \neq 0$, the corresponding term $(1/2\pi)A_1(\vartheta)\widehat{\Phi}_1(\delta)$ of the singular expansion of kernel $[l(\tau)]^{\gamma}[l(\vartheta)]^{-\gamma}\tilde{G}(\vartheta,\tau)$ will include functions $l(\vartheta)$ and $dl(\vartheta)/d\vartheta$ that are not constants in general. That is why, it is necessary to take $\gamma = 0$ and to introduce the new unknown function

$$\tilde{\mu}_0(\tau) = l(\tau)\tilde{\mu}(\tau), \tag{2.328}$$

and consider it as a solution of integral equation

$$\int_{-\pi}^{\pi} \tilde{G}(\vartheta,\tau)\tilde{\mu}_0(\tau)\,d\tau = \tilde{f}(\vartheta);\ \vartheta \in [-\pi;\pi], \tag{2.329}$$

with $\tilde{\mu}_0$ and $\tilde{f}$ belonging to the relevant sets:

$$\tilde{\mu}_0 \in \mathbf{H}^{-1/2} \cap \mathbf{C}_Q^{0,\alpha}\left(\mathbf{R}^1\right), \tilde{f} \in \mathbf{H}^{1/2} \cap \mathbf{C}_Q^{1,\alpha}\left(\mathbf{R}^1\right). \tag{2.330}$$

The sets $\mathbf{H}^{-1/2} \cap \mathbf{C}_Q^{0,\alpha}\left(\mathbf{R}^1\right)$ and $\mathbf{H}^{1/2} \cap \mathbf{C}_Q^{1,\alpha}\left(\mathbf{R}^1\right)$ are defined in the same manner as sets $\mathbf{H}^{-1/2} \cap \mathbf{C}^{0,\alpha}[-\pi;\pi]$ and $\mathbf{H}^{1/2} \cap \mathbf{C}^{1,\alpha}[-\pi;\pi]$ in Section 2.1, with the only difference that here we directly request the 2π-periodicity of $\tilde{\mu}_0$ and $\tilde{f}$ functions. As it follows from the below, instead of $\mathbf{H}^{-1/2} \cap \mathbf{C}_Q^{0,\alpha}\left(\mathbf{R}^1\right)$ and $\mathbf{H}^{1/2} \cap \mathbf{C}_Q^{1,\alpha}\left(\mathbf{R}^1\right)$ in (2.330) we can, as well, use corresponding Sobolev spaces $\mathbf{H}^{-1/2}$ and $\mathbf{H}^{1/2}$ of 2π-periodical functions for the integral equation (2.329) posing, and this change does not influence anyhow the algorithm of the equation solving. Nevertheless, we will use posing (2.330) for simplicity and convenience of our reader.

2.6.4 Additive Splitting of the Integral Equation Kernel into a Sum of Main Singular Part and Some More Smooth Function

The kernel $\tilde{G}(\vartheta,\tau)$ can be additively splitted now into a sum of the principal singularity and a relatively smooth part as follows:

$$\tilde{G}(\vartheta,\tau) = \frac{1}{2\pi}\left\{\left[\left(-\frac{1}{2} + \ln\left|2\sin\frac{\vartheta-\tau}{2}\right|\right) + i\Phi\,\widehat{\Phi}_1(\tau-\vartheta)\right] + K_0(\vartheta,\tau)\right\}. \tag{2.331}$$

The expression in round brackets is the main singularity, the next term in square brackets is the subordinate singularity, and the next term in figure brackets is the relatively smooth part of the kernel.

Formally, we can now construct the analytic regularization method for equation (2.329) with its kernel splitting (2.331), and the construction is simple because double Fourier series for both principal and subordinated extracted singularities have diagonal form (see Section 2.1 and below). Nevertheless, something more should be done for calculation efficiency. Namely, the function $\widehat{\Phi}_1(\tau-\vartheta)$ is known to be nonrepresentable in elementary functions. That is why, its calculation requires some extra effort, which is not necessary if we can construct another function having equivalent singular behavior, but representable itself by means of elementary functions, and with its Fourier coefficients also representable by means of elementary functions.

To this end, let us consider the simplest function $\Psi(\vartheta)$ of the necessary kind:

$$\Psi_1(\vartheta) = -\sum_{n=2}^{\infty}\Psi_n \sin n\vartheta = i\frac{1}{2}\sum_{n=-\infty}^{\infty}\Psi_n \mathrm{sign}(n)\,\mathrm{e}^{in\vartheta};\ \vartheta \in [-2\pi;2\pi], \tag{2.332}$$

$$\Psi_n = \begin{cases} 0; & |n| \le 1 \\ \left(n^2-1\right)^{-1}; & |n| \ge 2 \end{cases}, \ \mathrm{sign}(n) = \begin{cases} 1; & n > 0 \\ 0; & n = 0 \\ -1; & n < 0 \end{cases}. \tag{2.333}$$

The Fourier coefficients $(i/2)\Psi_n \mathrm{sign}(n)$ of function $\Psi_1(\vartheta)$ are expressed by means of elementary functions already. As well, the function $\Psi_1(\vartheta)$ itself can easily be expressed by means of elementary functions (we leave this calculation to the reader). It is evident that $\Psi_1, \ \widehat{\Phi}_1 \in \mathbf{C}_Q^{0,\alpha}\left(\mathbf{R}^1\right)$, but $\Psi_1 - \widehat{\Phi}_1 \in \mathbf{C}_Q^{2,\alpha}\left(\mathbf{R}^1\right)$, and substitution of $\Psi_1(\vartheta)$ instead of $\widehat{\Phi}_1(\tau - \vartheta)$ in the singular expansion (2.325) does not influence the next term of the expansion, but changes only the term $n = 3$.

Let us make a splitting of the kernel $\tilde{G}(\vartheta,\tau)$ similar to (2.331), but now with $-\Psi_1(\vartheta - \tau) = \Psi_1(\tau - \vartheta)$ instead of $\widehat{\Phi}_1(\tau - \vartheta)$:

$$\tilde{G}(\vartheta,\tau) = \frac{1}{2\pi}\left\{\left[\left(-\frac{1}{2} + \ln\left|2\sin\frac{\vartheta-\tau}{2}\right|\right) - i\Phi\Psi_1(\vartheta-\tau)\right] + K_D(\vartheta,\tau)\right\}. \tag{2.334}$$

One can consider formula (2.334) as definition of the function $K_D(\vartheta,\tau)$. From singular expansion (2.325) and formulas (2.332) and (2.334) it immediately follows that:

$$K_D(\vartheta,\tau) \in \mathbf{C}^1\left((-\infty;\infty)\times(-\infty;\infty)\right), \tag{2.335}$$

$$\frac{\partial^2 K_D(\vartheta,\tau)}{\partial\vartheta\partial\tau}, \ \frac{\partial^2 K_D(\vartheta,\tau)}{\partial\vartheta^2}, \ \frac{\partial^2 K_D(\vartheta,\tau)}{\partial\tau^2} \ \in \ \mathbf{L}_2\left([-\pi;\pi]\times[-\pi;\pi]\right). \tag{2.336}$$

Using formula (2.334), one can reduce integral equation (2.329) to the view:

$$\begin{gathered}\frac{1}{2\pi}\int_{-\pi}^{\pi}\tilde{\mu}_0(\tau)\left\{\ln\left|2\sin\tfrac{\vartheta-\tau}{2}\right| - i\Phi\Psi_1(\vartheta-\tau) + K_D(\vartheta,\tau)\right\}d\tau = \tilde{f}(\vartheta); \\ \vartheta\in[-\pi;\pi].\end{gathered} \tag{2.337}$$

2.6.5 Reduction of the Integral Equation to an Infinite System of Linear Algebraic Equations of the First Kind

Now one can make Fourier transform of all functions in formula (2.337). According to formulas (2.334) and (2.335), function $K(\vartheta,\tau)$ can be expanded into its double Fourier series and is representable by this series:

$$K_D(\vartheta,\tau) = \sum_{s=-\infty}^{\infty}\sum_{j=-\infty}^{\infty} K_{sj}^D e^{i(s\vartheta+j\tau)}; \ \vartheta, \ \tau\in[-\pi;\pi]. \tag{2.338}$$

The following identity can be proved:

$$-\frac{1}{2} + \ln\left|2\sin\frac{\vartheta-\tau}{2}\right| \ = \ -\frac{1}{2}\sum_{n=-\infty}^{\infty}\frac{e^{in(\vartheta-\tau)}}{\tau_n^2}; \ \tau_n = \max\left(1,|n|^{1/2}\right). \tag{2.339}$$

The unknown and given functions $\mu(\vartheta)$ and $f(\vartheta)$, respectively, are representable by their Fourier series:

$$\tilde{\mu}_0(\tau) = \sum_{n=-\infty}^{\infty} \mu_n \exp(in\vartheta);\ \vartheta \in [-\pi;\pi], \tag{2.340}$$

$$-2\tilde{f}(\vartheta) = \sum_{n=-\infty}^{\infty} f_n \exp(in\vartheta);\ \vartheta \in [-\pi;\pi]. \tag{2.341}$$

We define infinite vector columns μ^D and f^D of Fourier coefficients of unknown and given functions and of the infinite matrix W^D, which is formed by Fourier coefficients of function $K(\vartheta,\tau)$, as follows:

$$\mu^D = \{\mu_n\}_{n=-\infty}^{\infty}, f^D = \{f_n\}_{n=-\infty}^{\infty}, W^D = \left\{w_{sn}^D\right\}_{s,n=-\infty}^{\infty}, w_{sn}^D = -2K_{s,-n}^D. \tag{2.342}$$

Substituting series (2.338), (2.339), (2.340), and (2.341) into equation (2.437) and using the orthogonality properties of the system of functions $\{\exp(is\tau)\}_{s=-\infty}^{\infty}$ on $[-\pi;\pi]$, one obtains after simple manipulation the following series equation:

$$\sum_{n=-\infty}^{\infty} \mu_n \left(\tau_n^D\right)^{-2} e^{in\vartheta} + \sum_{n=-\infty}^{\infty} \left(W^D\mu^D\right)_n e^{in\vartheta} = \sum_{n=-\infty}^{\infty} f_n e^{in\vartheta};\ \vartheta \in [-\pi;\pi]. \tag{2.343}$$

Here,

$$\tau_n^D = \tau_n (1 - \Phi n\psi_n)^{-1/2};\ \tau_n^D = |n|^{1/2}\left[1 + O\left(n^{-1}\right)\right] \text{ for } n \to \infty, \tag{2.344}$$

and $(W^D\mu^D)_n$ is the nth component of the infinite vector column $W^D\mu^D$. According to (2.298), $|\Phi| \leq 1/2$. From here and definitions (2.332) and (2.339) of ψ_n and τ_n, respectively, one can conclude that $\tau_n > 0$ and $1-\Phi n\psi_n > 0$. Consequently, the values $\tau_n^D > 0$ are correctly definite for every $n = 0,\pm1,\pm2,\ldots$.

Taking into account the equality of Fourier coefficients of left- and right-hand sides in equation (2.343), one obtains the following infinite set of linear algebraic equations:

$$\mu_s \left(\tau_s^D\right)^{-2} + \left(W^D\mu^D\right)_s = f_s;\ s = 0, \pm 1, \pm 2,\ldots \tag{2.345}$$

The system of linear algebraic equations (2.349) is evidently one of the first kind [see (2.344)]. Our next purpose is to transform it to an equation of the second kind in the space l_2 of square-summable sequences.

2.6.6 Construction of an Infinite System of Linear Algebraic Equations of the Second Kind

Let us define new unknown and known coefficients

$$\widehat{\mu}_s = \mu_s/\tau_s^D,\ \widehat{f}_s = \tau_s^D f_s, \tag{2.346}$$

$$\widehat{w}_{s,n}^D = \tau_s^D \tau_n^D w_{sn}^D = -2\tau_s^D \tau_n^D K_{s,-n}^D, \tag{2.347}$$

and corresponding vector columns $\widehat{\mu}$ and $\widehat{f}$ and matrix operator $\widehat{W}$:

$$\widehat{\mu} = \left\{\widehat{\mu}_n\right\}_{n=-\infty}^{\infty},\ \widehat{f} = \left\{\widehat{f}_n\right\}_{n=-\infty}^{\infty};\ \widehat{W}^D = \left\{\widehat{w}_{sn}^D\right\}_{s,n=-\infty}^{\infty}. \tag{2.348}$$

Multiplying every equation (2.345) by τ_s^D and using the new coefficients $\widehat{\mu}_s$ and $\widehat{f}_s$, one obtains after a simple transformation the new algebraic system of the kind

$$\widehat{\mu}_s + \left(\widehat{W}^D \widehat{\mu}\right)_s = \widehat{f}_s;\ s = 0, \pm 1, \pm 2, ..., \tag{2.349}$$

which can be rewritten in the operator form

$$\left[E + \widehat{W}^D\right]\widehat{\mu} = \widehat{f};\ \widehat{\mu},\ \widehat{f} \in l_2. \tag{2.350}$$

It follows (see [11]) from (2.335) and (2.336) that $\widehat{W}$ is a compact operator in l_2 and even more: the coefficients of the matrix operator $\widehat{W}$ satisfy the inequality

$$\sum_{s=-\infty}^{\infty} \sum_{n=-\infty}^{\infty} (1 + |s|)(1 + |n|) \left|\widehat{w}_{sn}^D\right|^2 < \infty. \tag{2.351}$$

Thus, the Dirichlet BVP considered is reduced to the infinite algebraic system (2.350), which forms a functional equation of the second kind in the space l_2 with the compact in l_2 operator $\widehat{W}^D$.

2.6.7 The Neumann Diffraction Problem

The Neumann BVP posing is the same as the one for the Dirichlet BVP, but with the replacement of the Dirichlet boundary condition (2.305) by the Neumann one:

$$\frac{\partial \tilde{U}^{s(\pm)}(\bar{g}, \kappa)}{\partial \vec{n}_{\bar{g}}} + \frac{\partial \tilde{U}_p^i(\bar{g}, \kappa)}{\partial \vec{n}_{\bar{g}}} = 0;\ \bar{g} \in \bar{\mathbf{S}}_x. \tag{2.352}$$

By means of standard technique of Green's formulas, one obtains that the scattering field $\tilde{U}^{s(\pm)}(\bar{g},\kappa)$ has the following representation:

$$\tilde{U}^{s(\pm)}(\bar{g}_1,\kappa)=\int\limits_{\mathbf{S}_{x,0}}\frac{\partial\tilde{G}_0(\bar{g}_1,\bar{g}_2,\kappa,\Phi)}{\partial\vec{n}_{\bar{g}_2}}M_N(\bar{g}_2)\,dl_{\bar{g}_2}=0;\ \bar{g}_1\in\mathbf{R}^2\backslash\bar{\mathbf{S}}_x, \tag{2.353}$$

$$M_N(\bar{g})=\tilde{U}^{s(-)}(\bar{g},\kappa)-\tilde{U}^{s(+)}(\bar{g},\kappa);\ \bar{g}\in\bar{\mathbf{S}}_x. \tag{2.354}$$

The contour $\bar{\mathbf{S}}_x$ is assumed to be smooth. Consequently, there are such a number $H>0$ and an open vicinity $\mathbf{V}_H$ of $\bar{\mathbf{S}}_x$ such that $\bar{\mathbf{S}}_x\subset\mathbf{V}_H$ and for any point $\bar{g}_h\in\mathbf{V}_H$ the point $\bar{g}\in\bar{\mathbf{S}}_x$ (which is known as the projection of $\bar{g}_h$ onto $\bar{\mathbf{S}}_x$) and the number h with $|h|<H$ exist that $\bar{g}_h$ has the unique representation of the kind

$$\bar{g}_h=\bar{g}+h\vec{n}_{\bar{g}};\quad\bar{g}\in\bar{\mathbf{S}}_x. \tag{2.355}$$

Here, $\vec{n}_{\bar{g}}$ is unit outward (oriented from $\mathbf{R}^{2(+)}$ to $\mathbf{R}^{2(-)}$) normal to $\bar{\mathbf{S}}_x$ in the point $\bar{g}\in\bar{\mathbf{S}}_x$. Thus, any point $\bar{g}_h\in\mathbf{V}_H$ has view (2.355) with $\vec{n}_{\bar{g}}$ uniquely defined by $\bar{g}$. That is why, derivative $\partial\big/\partial\vec{n}_{\bar{g}}$ is correctly defined in $\mathbf{V}_H$.

Applying this derivative to both sides of (2.353), one obtains that

$$\begin{aligned}&\tfrac{\partial\tilde{U}^{s(\pm)}(\bar{g}_h,\kappa)}{\partial\vec{n}_{\bar{g}}}=\tfrac{\partial}{\partial\vec{n}_{\bar{g}}}\int\limits_{\mathbf{S}_{x,0}}\tfrac{\partial\tilde{G}_0(\bar{g}_h,\bar{g}_2,\kappa,\Phi)}{\partial\vec{n}_{\bar{g}_2}}M_N(\bar{g}_2)\,dl_{\bar{g}_2};\\&\bar{g}_h\in\left(\mathbf{V}_H\backslash\bar{\mathbf{S}}_x\right).\end{aligned} \tag{2.356}$$

According to (2.302), there exist uniform on $\bar{\mathbf{S}}_x$ limits $\lim\limits_{h\to\pm0}\partial\tilde{U}^{s(\pm)}(\bar{g}_h,\kappa)\big/\partial\vec{n}_{\bar{g}}$. Consequently, substitution of (2.356) for $h\to\pm0$ into boundary conditions (2.352) brings the identity

$$\lim_{h\to\pm0}\frac{\partial}{\partial\vec{n}_{\bar{g}}}\int\limits_{\mathbf{S}_{x,0}}\frac{\partial\tilde{G}_0(\bar{g}_h,\bar{g}_2,\kappa,\Phi)}{\partial\vec{n}_{\bar{g}_2}}M_N(\bar{g}_2)\,dl_{\bar{g}_2}=-\frac{\partial\tilde{U}_p^i(\bar{g},\kappa)}{\partial\vec{n}_{\bar{g}}};\ \bar{g}\in\bar{\mathbf{S}}_x. \tag{2.357}$$

Using parameterization $\eta(\vartheta)\equiv\{\bar{y}(\vartheta),\bar{z}(\vartheta)\}$ of the contour $\bar{\mathbf{S}}_x$ [see (2.291), (2.292), (2.293), (2.294), and (2.295)] and being based on the analogy to the treatment made above for the Dirichlet problem, one can define the following functions:

$$\tilde{D}_h(\bar{g},\bar{g}_2)=\frac{\partial^2\tilde{G}_0\left(\bar{g}+h\vec{n}_{\bar{g}},\bar{g}_2,\kappa,\Phi\right)}{\partial\vec{n}_{\bar{g}}\partial\vec{n}_{\bar{g}_2}};\ \bar{g},\ \bar{g}_2\in\bar{\mathbf{S}}_{x,0}, \tag{2.358}$$

$$D_h(\vartheta,\tau)=e^{i\Phi(\tau-\vartheta)}\tilde{D}_h(\bar{g},\bar{g}_2)\Big|_{\bar{g}=\eta(\vartheta),\ \bar{g}_2=\eta(\tau)}, \tag{2.359}$$

$$\nu(\tau)=e^{-i\Phi\tau}M_N(\eta(\tau)), \tag{2.360}$$

$$\tilde{g}\,(\vartheta) = -\mathrm{e}^{-i\Phi\vartheta}\,\frac{\partial \tilde{U}_p^i\,(\bar{g},\kappa)}{\partial \vec{n}_{\bar{g}}}\bigg|_{\bar{g}=\eta(\vartheta)}. \tag{2.361}$$

Functions $D_h(\vartheta,\tau)$, $\nu(\tau)$, and $\tilde{g}\,(\vartheta)$ are periodical ones, as this evidently follows from their definitions.

Using formulas (2.359), (2.360), and (2.361), one can rewrite identity (2.357) in parameterized form:

$$\lim_{h\to\pm 0}\int_{-\pi}^{\pi} D_h\,(\vartheta,\tau)\,\nu\,(\tau)\,l\,(\tau)\,d\tau = \tilde{g}\,(\vartheta)\,;\ \vartheta\in[-\pi;\pi]\,. \tag{2.362}$$

Identity (2.362) is not suitable for further analysis and transformation, because it involves limits $h\to\pm 0$. Direct substitution of $h=0$ in (2.362) is illegal even because the integral in (2.362) is divergent for $h=0$. Thus, the problem of analytic "calculation" of these limits, i.e., of their expression in terms of some elementary operations arises. It is clear that function $D_0(\vartheta,\tau)$ (i.e., $D_h(\vartheta,\tau)$ for $h=0$) must somehow appear in any result of such limit "calculation." That is why we need an investigation of the differential and singular properties of $D_0(\vartheta,\tau)$.

First of all, $D_0(\vartheta,\tau)$ is evidently smooth function everywhere on $[-\pi;\pi]\times[-\pi;\pi]$, but with exception of the points $\{\vartheta,\tau\}$ under relations $\vartheta=\tau$ or $|\vartheta-\tau|=2\pi$. Detailed investigation results into the singular expansion

$$\begin{aligned} D_0\,(\vartheta,\tau) \;-\; \tfrac{1}{2\pi l(\vartheta)l(\tau)}\,\Bigg\{ \tfrac{1}{4\sin^2\frac{\vartheta-\tau}{2}} \;+\; i\Phi\,\tfrac{1}{2}\mathrm{ctg}\,\tfrac{\tau-\vartheta}{2} \;+ \\ +\sum_{m=0}^{M} B_m\,(\vartheta)\,\widehat{\Phi}\,(\tau-\vartheta)\Bigg\} \;\in\; \mathbf{C}_Q^M\left(\mathbf{R}^2\right), \end{aligned} \tag{2.363}$$

which is valid for any fixed $M=0,\pm1,\pm2,\ldots$, and where $B_m(\vartheta)$ are some functions of the kind $B_m\in\mathbf{C}_Q^\infty\left(\mathbf{R}^1\right)$. In particular,

$$B_0\,(\vartheta) = \frac{[\kappa l\,(\vartheta)]^2}{2},\; B_1\,(\vartheta) \;=\; \frac{1}{4}\frac{d\,[\kappa l\,(\vartheta)]^2}{d\vartheta} \;+\; i\Phi\frac{[\kappa l\,(\vartheta)]^2}{2}. \tag{2.364}$$

Taking into account formulas (2.320) and (2.322), one obtains after elementary calculations that

$$\frac{1}{4\sin^2\frac{\vartheta-\tau}{2}} = \frac{d^2}{d\vartheta^2}\ln\left|2\sin\frac{\vartheta-\tau}{2}\right|, \tag{2.365}$$

$$\frac{d^2}{d\vartheta^2}\ln\left|2\sin\frac{\vartheta-\tau}{2}\right| \approx \frac{1}{2}\sum_{n=-\infty}^{\infty}|n|\mathrm{e}^{in(\vartheta-\tau)}; \tag{2.366}$$

$$\frac{1}{2}\mathrm{ctg}\frac{\vartheta-\tau}{2} = -\frac{1}{2}\mathrm{ctg}\frac{\tau-\vartheta}{2} = -\frac{d}{d\vartheta}\ln\left|2\sin\frac{\vartheta-\tau}{2}\right|, \tag{2.367}$$

$$-\frac{d}{d\vartheta}\ln\left|2\sin\frac{\vartheta-\tau}{2}\right| \;\approx\; i\frac{1}{2}\sum_{n=-\infty}^{\infty}\operatorname{sign}(n)\,e^{in(\vartheta-\tau)}. \tag{2.368}$$

The series (2.366) and (2.368) are formal ones, because they are divergent. Nevertheless, the sense of the Fourier series of corresponding 2π-periodical generalized functions (distributions) can be given to them, and most right-hand sided expressions in (2.365) and (2.367) have sense of the regularization of these generalized functions. Without going into such far from the main topic details, we note only herein that these series are really useful for better understanding of the features of $D_0(\vartheta,\tau)$ as the kernel of the differential integral equation that we will consider below.

One can conclude from (2.363) that $D_0(\vartheta,\tau)$ has nonintegrable singularity of the type $(\tau–\vartheta)^2$, and consequently, the exchange of the order of limiting operation and integration in (2.362) is indeed illegal.

It follows from (2.360), (2.354), and (2.300) that $\nu(\vartheta)\in\mathbf{C}_Q^{1,\alpha}\left(\mathbf{R}^1\right)$. As the result of rather bulky and nontrivial calculation, based on the relevant singular expansion of the function similar to $D_h(\vartheta,\tau)$, $h\geq 0$, but generated by nonperiodical Green's function $(-i/4)\,H_0^{(1)}(\kappa|g-g_0|)$, and under the same assumption for $\nu(\vartheta)$, the limit of the type (2.362) has been calculated – see [11] and the references therein. The similar, in some respect, calculation of the limits (2.362) results into the relation of the kind:

$$\begin{aligned}\lim_{h\to\pm 0}\int_{-\pi}^{\pi}D_h(\vartheta,\tau)\,\nu(\tau)\,d\tau \;&=\; \tfrac{1}{2\pi l(\vartheta)}\left\{\left[\tfrac{1}{2}\int_{-\pi}^{\pi}\nu(\tau)\,d\tau+\right.\right.\\ &\left.\left.+\left(\tfrac{d^2}{d\vartheta^2}-i\Phi\tfrac{d}{d\vartheta}\right)\int_{-\pi}^{\pi}\ln\left|2\sin\tfrac{\vartheta-\tau}{2}\right|\nu(\tau)\,d\tau\right]+\int_{-\pi}^{\pi}K_N(\vartheta,\tau)\,\nu(\tau)\,d\tau\right\};\\ &\vartheta\in[-\pi;\pi].\end{aligned} \tag{2.369}$$

Here, function $K_N(\vartheta,\tau)$, $\vartheta,\tau\in[-\pi;\pi]$, is defined by the following equality:

$$D_0(\vartheta,\tau) \;=\; \frac{1}{2\pi l(\vartheta)\,l(\tau)}\left\{\frac{1}{2}+\frac{1}{4\sin^2\frac{\vartheta-\tau}{2}}+i\Phi\frac{1}{2}\operatorname{ctg}\frac{\tau-\vartheta}{2}+K_N(\vartheta,\tau)\right\}. \tag{2.370}$$

Substitution of (2.369) into (2.362) and multiplying the result by $l(\vartheta)$ bring the identity:

$$\begin{aligned}&\tfrac{1}{2\pi}\left\{\left[\tfrac{1}{2}\int_{-\pi}^{\pi}\nu(\tau)d\tau+\left(\tfrac{d^2}{d\vartheta^2}-i\Phi\tfrac{d}{d\vartheta}\right)\int_{-\pi}^{\pi}\ln\left|2\sin\tfrac{\vartheta-\tau}{2}\right|\nu(\tau)d\tau\right]+\right.\\ &\left.+\int_{-\pi}^{\pi}K_N(\vartheta,\tau)\,\nu(\tau)\,d\tau\right\}=l(\vartheta)\,g(\vartheta);\;\vartheta\in[-\pi;\pi].\end{aligned} \tag{2.371}$$

In accordance with standard approach, we will consider identity (2.371) from now as the differential–integral equation to unknown function $\nu(\tau)$ under assumptions:

$$\nu(\tau) \in \mathbf{H}^{1/2} \cap \mathbf{C}_Q^{1,\alpha}\left(\mathbf{R}^1\right), l(\vartheta)\, g(\vartheta) \in \mathbf{H}^{-1/2} \cap \mathbf{C}_Q^{0,\alpha}\left(\mathbf{R}^1\right). \tag{2.372}$$

It can be proved that if the equation is solved and function $\nu(\vartheta)$ is found, then one can obtain the scattered field by means of the integral representation (2.353), where function $M_N(\bar{g})$ is given by inversion of formulas (2.360), namely, $M_N(\bar{g}) = \left[e^{i\Phi\tau}\nu(\tau)\right]\big|_{\tau=\eta^{-1}(\bar{g})}$ – function $\eta(\tau)$ is constructed above as an invertible one.

As one can see, domains of definition and image of the differential operator in (2.371) are exchanged in comparison with the same domains, but for integral operator generated by the Dirichlet BVP – see (2.330) for comparison. This exchange is in the proper agreement with physical and mathematical senses of functions $\nu(\tau)$ and $\mu(\tau)$ correspondingly – see (2.305) and (2.354) also. It is possible to say that operators of equations (2.329) and (2.371) have somewhat opposite qualities: the kernel of the first one is too smooth, but the kernel of the second is too singular for making the operators boundedly invertible in space $\mathbf{L}_2[-\pi,\pi]$.

The structure of the differential–integral equation in (2.371) is in some respects similar to one of (2.337). Namely, the expression in square brackets in (2.371) is the singularity extracted from the operator and, as well as in (2.337), it involves the first two principal singularities as corresponding derivatives of logarithmic singularity (the very first integral in (2.371) is extracted for the only convenience to have the extracted singularity to be formally invertible).

The rest of the necessary transforms is almost the same as for the Dirichlet problem. Namely, let us expand $\nu(\vartheta)$, $l(\vartheta)\,\tilde{g}(\vartheta)$, and $K_N(\vartheta,\tau)$ into their Fourier series:

$$\nu(\vartheta) = \sum_{n=-\infty}^{\infty} \nu_n e^{in\vartheta},\ l(\vartheta)\,\tilde{g}(\vartheta) = \sum_{n=-\infty}^{\infty} g_n e^{in\vartheta}, \tag{2.373}$$

$$K_N(\vartheta,\tau) = \sum_{s=-\infty}^{\infty}\sum_{n=-\infty}^{\infty} K_{sn}^N e^{i(s\vartheta+n\tau)}. \tag{2.374}$$

Substituting these series into (2.371), making term by term integration, and term by term differentiation, when necessary (all these operations can be mathematically justified – see [11]), one arrives into the series equation similar to (2.343), from which (2.345) follows. Exactly in the same manner, one derives from the series equation just obtained an algebraic equation similar to (2.345), but of the kind:

$$\left(\tau_s^N\right)^2 \nu_s + \sum_{n=-\infty}^{\infty} w_{sn}^N \nu_n = g_s;\ s = 0, \pm 1, \pm 2... \tag{2.375}$$

Here,

$$\tau_s^N = \tau_s \left[1 - \Phi \operatorname{sign}(n) / \tau_n^2\right]^{1/2} = \begin{cases} 1; \, n = 0 \\ \tau_n \left[1 - \Phi / n\right]^{1/2}; \quad n = \pm 1, \pm 2, \ldots \end{cases}, \tag{2.376}$$

$$w_{sn}^N = 2K_{s,-n}^N. \tag{2.377}$$

Values $\tau_s^N > 0$ for any $s = 0, \pm 1, \pm 2, \ldots$, due to the same reason as $\tau_s^D > 0$ (see the previous section), and $\tau_n^N = O(|n|)$ for $n \to \pm\infty$. The last means evidently that equation (2.375) is one of the first kind in space l_2, where its matrix operator is unbounded.

The analytic regularization of equation (2.375) is trivial now. Indeed, let us define vector columns

$$\widehat{v} = \left\{\widehat{v}_n\right\}_{n=-\infty}^{\infty}; \; \widehat{v}_n = \tau_n^N v_n, \; \widehat{g} = \left\{\widehat{g}_s\right\}_{s=-\infty}^{\infty}; \; \widehat{g}_s = g_s / \tau_s^N \tag{2.378}$$

and matrix operator

$$\widehat{W}^N = \left\{\widehat{w}_{sn}\right\}_{s,n=-\infty}^{\infty}; \; \widehat{w}_{sn} = \left(\tau_s^N \tau_n^N\right)^{-1} w_{sn}^N, \tag{2.379}$$

and divide each equation (2.375) by τ_s^N. As the result, we obtain an algebraic equation in l_2 of the kind

$$\left[E + \widehat{W}^N\right] \widehat{v} = \widehat{g}; \; \widehat{v}, \; \widehat{g} \in l_2. \tag{2.380}$$

It can be shown that

$$\sum_{s=-\infty}^{\infty} \sum_{n=-\infty}^{\infty} (1 + |s|)(1 + |n|) \left|w_{sn}^N\right|^2 < \infty. \tag{2.381}$$

It is noteworthy that matrix operator for $\widehat{W}^N$ satisfies exactly the same inequality (2.381) as matrix operator $\widehat{W}^D$ does – see (2.351).

Thus, the Neumann BVP considered is reduced to the infinite algebraic system (2.380), which forms functional equation of the second kind in space l_2 with compact in l_2 operator $\widehat{W}^N$.

We wish to emphasize again that more complicated transmission BVP can be solved in similar way.

Chapter 3
C-Method: From the Beginnings to Recent Advances

Abstract C-method – is simple and rather clear for code implementation and it enables to resolve efficiently diverse applied problems of optics and spectroscopy. Although the method cannot be treated as completely mathematically rigorous, in the case when the principal characteristics of grating are required, the C-method provides the data of applied interest with engineering accuracy.

In this chapter the principal ideas making the background of classical C-method and its latest modifications have been described concisely. The physical results demonstrating the considerable potentialities of the method for resolving actual fundamental and applied problems of electromagnetic theory of gratings are also presented.

3.1 Introduction

The C-method was developed in the 1980s in Clermont-Ferrand, France, from the need to solve rigorously diffraction problems at corrugated periodic surfaces in the resonance regime. The main difficulty of such problems is the matching of boundaries conditions. It is obvious that any method aimed at solving Maxwell's equation is all the more efficient since it is able to fit the geometry of the problem. For that purpose, J. Chandezon et al. [151, 152] introduced the so-called translation coordinate system u, v, w deduced from the Cartesian coordinate system x, y, z by the relations $u = x$, $v = y$, and $w = z - f(y)$, where $z = f(y)$ is a continuously differentiable function describing the surface profile. Since the boundary of the physical problem coincides with coordinate surface $w = 0$, writing boundary conditions is as simple as it is for classical problems in Cartesian, cylindrical, or spherical coordinates. This is the first ingredient of C-method. The second one is to write Maxwell's equation under the covariant form. This formulation comes from relativity where the use of curvilinear nonorthogonal coordinate system is essential and natural. The main feature of this formalism is that Maxwell's equations remain invariant in any coordinate system, the geometry being shifted into the constitutive relations. J. Chandezon et al. derived their 3-D formulation from the general 4-D

Y.K. Sirenko, S. Ström (eds.), *Modern Theory of Gratings*, Springer Series in Optical Sciences 153, DOI 10.1007/978-1-4419-1200-8_3,

relativistic Post's formalism [153] and evidently used tensorial calculus. Although it is with no doubt the most elegant and efficient way to deal with electromagnetic field in general curvilinear coordinates it is also probably the reason why the theory appeared difficult to understand to many scientists. The third ingredient of C-method is that it is a modal method. This nice property is linked with the translation coordinate system in which a grating diffraction problem may be expressed as an eigenvalue–eigenvector problem with periodic boundary conditions. The last feature of C-method is that it is a numerical method. The matrix operator is obtained by expanding field components into Floquet–Fourier or spatial harmonics and by projecting Maxwell's equations onto quasi-periodic exponential functions. The above four features may be resumed by saying that C-method is a curvilinear coordinate modal method by Fourier expansion.

Since the original papers, the C-method has gone through many stages of extension and improvement. The original theory was formulated for uncoated perfectly conducting gratings in classical mount. Various authors extended the method to conical diffraction mountings [154–156]. G. Granet et al. [157], T.W. Preist et al. [158], and L. Li et al. [159] allowed the various profiles of a stack of gratings to be different from each other, although keeping the same periodicity. Solving the vertical faces case in a simple manner, J.P. Plumey et al. [160] have showed that the method can be applied to overhanging gratings. T.W. Preist et al. obtained the same results by applying the usual coordinate transformation to oblique coordinates [161]. In the numerical context, L. Li [162] and N.P.K. Cotter et al. [163] improved the numerical stability of the C-method by using the S-matrix propagation algorithm for multilayer gratings.

It is seen that C-method has been applied to a large class of surface relief gratings and multilayer coated gratings. In this chapter, we concentrate on two main points. On the one hand, we present C-method in a simple way without tensorial calculus and on the other hand, we show that the motivation for choosing a coordinate system may be dictated by other reasons than pure geometrical ones. It may be a rather simple tool to improve effectiveness of existing methods.

Sections 3.2 and 3.3 of this chapter are devoted to the presentation of C-method in an easy understandable way so that it can become more useful to a large community.

Section 3.4 considers parametric C-method and adaptive spatial resolution.

The subject of Section 3.5 is to show how the ideas of the C-method can be applied to perfectly conducting curved strip gratings.

In Section 3.6, we discuss several mathematical issues concerning the C-method that are in the focus of the present book: the continuation of diffraction problems into the complex plane of frequency parameters and a comparative investigation of diffraction and spectral problems.

3.2 Classical C-Method

In this section, we introduce all the steps of the C-method from the change of coordinates to the formulation in terms of an eigenvector–eigenvalue problem and its

numerical solution in truncated Fourier space. We assume a time dependence of $\exp(-ikt)$, $k = 2\pi/\lambda$, λ is the wavelength in a free space, t is the time parameter – it is the product of the natural time and the velocity of the propagation of light in vacuum. The problem of finding the electromagnetic field in a source-free, homogeneous, isotropic region is solved once general solutions to the scalar Helmholtz equation are known. The main feature of C-method is to make surfaces of break of properties of medium coincide with coordinate surfaces. Therefore the solution of a modulated surface diffraction problem with C-method shares many common steps with the solution of a similar planar problem. In the next sections we will solve Helmholtz equation in Cartesian coordinates and in translation coordinates. For simplicity, we restrict our analysis to two-dimensional problems ($\partial/\partial x = 0$).

3.2.1 Modal Equations in Cartesian Coordinates and Quasi-periodic Green Function

In Cartesian coordinates and in a medium with the relative complex-valued permittivity $\tilde{\varepsilon}$, the E- and H-polarized quasi-periodic (with respect to y-axis) fields described by the following boundary value problem in Floquet channel $\mathbf{R} = \left\{g \in \mathbf{R}^2 \colon 0 < y < l\right\}$ [see also formula (1.20)]:

$$\begin{cases} \left[\frac{\partial^2}{\partial y^2} + \frac{\partial^2}{\partial z^2} + \tilde{\varepsilon}k^2\right]\tilde{U}(g,k) = \tilde{f}(g,k); \qquad g = \{y,z\} \in \mathbf{R} \\ \tilde{U}\left\{\frac{\partial \tilde{U}}{\partial y}\right\}(l,z,k) = \mathrm{e}^{2\pi i\Phi}\tilde{U}\left\{\frac{\partial \tilde{U}}{\partial y}\right\}(0,z,k) \end{cases}. \tag{3.1}$$

Here, Φ is some real-valued parameter (Floquet channel parameter), $\tilde{U} = \tilde{E}_x$ for E-polarization ($\tilde{E}_y = \tilde{E}_z = \tilde{H}_x = 0$) and $\tilde{U} = \tilde{E}_x$ for H-polarization ($\tilde{H}_y = \tilde{H}_z = \tilde{E}_x = 0$), $\vec{E} = \left\{\tilde{E}_x,\tilde{E}_y,\tilde{E}_z\right\}$, and $\vec{H} = \left\{\tilde{H}_x,\tilde{H}_y,\tilde{H}_z\right\}$ are the vectors of electromagnetic field (factor $\exp(-ikt)$ is omitted). Within the strip $\mathbf{R}$ the support of function

$$\tilde{f}(g,k)\colon\ \tilde{f}\left\{\frac{\partial \tilde{f}}{\partial y}\right\}(l,z,k) = \mathrm{e}^{2\pi i\Phi}\tilde{f}\left\{\frac{\partial \tilde{f}}{\partial y}\right\}(0,z,k), \tag{3.2}$$

that gives current sources of the field, is bounded.

Let $\tilde{f}(g,k) \equiv 0$. Then general solution to the problem (3.1) and (3.2) can be presented (see Section 1.1.4) in the form

$$\tilde{U}(g,k) = \tilde{U}^+(g,k) + \tilde{U}^-(g,k), \tag{3.3}$$

where

$$\tilde{U}^{\pm}(g,k) = \sum_{n=-\infty}^{\infty}\left\{\begin{matrix} A_n^+(k) \\ A_n^-(k) \end{matrix}\right\}\mathrm{e}^{i[\Phi_n y \pm \Gamma_n z]};\ \Phi_n = 2\pi(\Phi + n)/l,\ \Gamma_n = \sqrt{k^2\tilde{\varepsilon} - \Phi_n^2},$$
$$\operatorname{Re}\Gamma_n \operatorname{Re}k \geq 0,\ \operatorname{Im}\Gamma_n \geq 0. \tag{3.4}$$

Relations (3.3) and (3.4) are derived by the means of separation of variables in the problem (3.1). The orthonormal (at the interval [0;l]) system $\{\mu_n(y)\}_{n=-\infty}^{\infty}$ of the transversal functions $\mu_n(y) = l^{-1/2}\exp(i\Phi_n y)$, complete in the space $\mathbf{L}_2(0;l)$, is determined by nontrivial solutions to the homogeneous (spectral) problem

$$\begin{cases} \left[\frac{d^2}{dy^2} + \Phi_n^2\right]\mu_n(y) = 0; \qquad 0 < y < l \\ \\ \mu_n\left\{\frac{d\mu_n}{dy}\right\}(l) = \mathrm{e}^{2\pi i\Phi}\mu_n\left\{\frac{d\mu_n}{dy}\right\}(0) \end{cases}, \tag{3.5}$$

while the spatial amplitudes $\{u_n(z)\}_{n=-\infty}^{\infty}$: $u_n(z) = \exp(\pm i\Gamma_n z)$ of the field $\tilde{U}(g,k)$ are given by the solutions of the following differential equations:

$$\left[\frac{\partial^2}{\partial z^2} - \Phi_n^2 + k^2\tilde{\varepsilon}\right]u_n(z) = 0,\ n = 0, \pm 1, \pm 2,... \tag{3.6}$$

The word "orthonormal" relative to the system $\{\mu_n(y)\}_{n=-\infty}^{\infty}$ means that

$$\langle\mu_n,\mu_m\rangle = \int_0^l \mu_n(y)\,\mu_m^*(y)\,dy = \begin{cases} 0; & n \neq m \\ 1; & n = m \end{cases}. \tag{3.7}$$

The relations (3.4) are called Rayleigh expansions and the Γ_n are referred to as Rayleigh eigenvalues. Since the eigenvalues are deduced from their squared number, there are two sets of modes, the number of which are equal: those propagating or decaying in the positive direction of z and those propagating or decaying in the opposite direction. We denote these modes by the superscripts + (plus) and − (minus), respectively. Hence, $A_n^+(k)$ and $A_n^-(k)$ are constant modal-field amplitudes that correspond to forward and backward waves, respectively. In the context of concrete boundary value problem, such amplitudes are determined from boundary conditions. Unfortunately, expansions of (3.4) type do not allow to calculate Rayleigh coefficients $A_n^+(k)$ and $A_n^-(k)$ directly from boundary conditions when they have to be written at some modulated surface. This is the reason why we are seeking other expansions and other approaches for their realization.

In the case that the field is radiated by a known quasi-periodic distribution of sources, it may be calculated with the help of Green function $\tilde{G}_0(g,g_0,k,\Phi)$, which is the solution of the problem (3.1) with

$$\tilde{f}(g,k) = \delta(z - z_0)\sum_{n=-\infty}^{\infty}\delta(y - y_0 - nl)\,\mathrm{e}^{2\pi i n\Phi}; \qquad 0 \le y_0 < l, \tag{3.8}$$

where $\delta(...)$ is the δ-Dirac function. In addition to (3.1), $\tilde{G}_0(g,g_0,k,\Phi)$ has to satisfy the radiation conditions for $z \to \pm\infty$ – only outgoing waves may participate in Fourier series expansion

$$\tilde{G}_0\,(g,g_0,k,\Phi) = \sum_{n=-\infty}^{\infty} g_n\,(z)\,e^{i\Phi_n y}.$$

It can be proved (see, for example [10]), that function

$$\tilde{G}_0\,(g,g_0,k,\Phi) = -\frac{i}{2\,l}\sum_{n=-\infty}^{\infty} e^{i[\Phi_n(y-y_0)+\Gamma_n|z-z_0|]}\Gamma_n^{-1}. \tag{3.9}$$

meets all above-mentioned conditions.

3.2.2 New Coordinate System

In Euclidean space with origin in zero and basis vectors $\vec{x}$, $\vec{y}$, and $\vec{z}$, let us consider an infinite cylindrical surface $\mathbf{S}^{\varepsilon,\mu,\sigma}$ whose generatrices are parallel to the x-axis. This surface separates two linear homogeneous and isotropic media denoted **I** and **II**. In Cartesian coordinates x, y, z, such a surface can be described by equation $z = f\,(y)$. Any electromagnetic field interacting with this particular geometry obstacle satisfies some boundary conditions. For instance, the tangential (relative to $\mathbf{S}^{\varepsilon,\mu,\sigma}$) components of the electric field vector and the magnetic field vector are continuous at the surface. The point is that boundary conditions involve quantities that obviously depend on the position at which they are considered on the surface. We are thus led to think about a coordinate system that fit the problem and make it more readily soluble than it is in Cartesian coordinates framework. One such system is the so-called translation coordinate system u, v, w introduced by J. Chandezon and defined from the Cartesian coordinate system x, y, z by the direct and inverse transformations

$$u = x,\, v = y,\, w = z - f\,(y) \tag{3.10}$$

and

$$x = u,\, y = v,\, z = w + f\,(y)\,. \tag{3.11}$$

It makes the surface $\mathbf{S}^{\varepsilon,\mu,\sigma}$ coincide with the coordinate surface $w = 0$. A point $p = \{x,y,z = f\,(y)\}$ on the surface $\mathbf{S}^{\varepsilon,\mu,\sigma}$ is now referenced by the triplet $p_{tr} = \{u,v,0\}$. The coordinate surface $w = \text{const}$ is obtained by translating each point on surface $\mathbf{S}^{\varepsilon,\mu,\sigma}$ with vector $w\vec{z}$, hence the name given by J. Chandezon to this particular coordinate system: translation coordinate system. The Jacobian matrices of the inverse and direct transformation are inverse one of the other. Let us denote by J the Jacobian matrix of the direct transformation. Then

$$J = \frac{\partial(x,y,z)}{\partial(u,v,w)} = \begin{bmatrix} \frac{\partial x}{\partial u} & \frac{\partial x}{\partial v} & \frac{\partial x}{\partial w} \\ \frac{\partial y}{\partial u} & \frac{\partial y}{\partial v} & \frac{\partial y}{\partial w} \\ \frac{\partial z}{\partial u} & \frac{\partial z}{\partial v} & \frac{\partial z}{\partial w} \end{bmatrix} = \begin{bmatrix} 1 & 0 & 0 \\ 0 & 1 & 0 \\ 0 & f' & 1 \end{bmatrix} \tag{3.12}$$

and

$$J^{-1} = \frac{\partial(u,v,w)}{\partial(x,y,z)} = \begin{bmatrix} \frac{\partial u}{\partial x} & \frac{\partial u}{\partial y} & \frac{\partial u}{\partial z} \\ \frac{\partial v}{\partial x} & \frac{\partial v}{\partial y} & \frac{\partial v}{\partial z} \\ \frac{\partial w}{\partial x} & \frac{\partial w}{\partial y} & \frac{\partial w}{\partial z} \end{bmatrix} = \begin{bmatrix} 1 & 0 & 0 \\ 0 & 1 & 0 \\ 0 & -f' & 1 \end{bmatrix}. \tag{3.13}$$

Here and below, $f' = df\,(y)\big/dy$.

3.2.3 Modal Equation in the Translation Coordinate System

In this section, we derive the main operator of C-method by following the same steps as in [164]. The new coordinates u, v, w are linked to the Cartesian coordinates x, y, z by the transformation that may be considered as a change of variable. For the change of variables $u = x$, $v = y$, $w = z - f\,(y)$ the rule of chain for derivatives has the form:

$$\begin{cases} \frac{\partial}{\partial x} = \frac{\partial u}{\partial x}\frac{\partial}{\partial u} + \frac{\partial v}{\partial x}\frac{\partial}{\partial v} + \frac{\partial w}{\partial x}\frac{\partial}{\partial w} = \frac{\partial}{\partial u} \\ \frac{\partial}{\partial y} = \frac{\partial u}{\partial y}\frac{\partial}{\partial u} + \frac{\partial v}{\partial y}\frac{\partial}{\partial v} + \frac{\partial w}{\partial y}\frac{\partial}{\partial w} = \frac{\partial}{\partial v} - f'\frac{\partial}{\partial w} \\ \frac{\partial}{\partial z} = \frac{\partial u}{\partial z}\frac{\partial}{\partial u} + \frac{\partial v}{\partial z}\frac{\partial}{\partial v} + \frac{\partial w}{\partial z}\frac{\partial}{\partial w} = \frac{\partial}{\partial w} \end{cases}. \tag{3.14}$$

Substituting derivatives (3.14) into the homogeneous ($\tilde{f}\,(g,k) \equiv 0$) problem (3.1) gives

$$\left[\frac{\partial^2}{\partial v^2} - \frac{\partial}{\partial v}f'\frac{\partial}{\partial w} - f'\frac{\partial}{\partial w}\frac{\partial}{\partial v} + \left[1 + \left(f'\right)^2\right]\frac{\partial^2}{\partial w^2} + k^2\tilde{\varepsilon}\right]\tilde{U}_{tr}\,(g_{tr},k) = 0,$$

$$g_{tr} = \{v,w\} \in \mathbf{R}_{tr} = \{g_{tr}\colon 0 < v < l\}, \tag{3.15}$$

$\tilde{U}_{tr}\,(l,w,k) = \mathrm{e}^{2\pi\mathrm{i}\Phi}\,\tilde{U}_{tr}\,(0,w,k)$ and

$$\left[\frac{\partial}{\partial v} - f'\frac{\partial}{\partial w}\right]\tilde{U}_{tr}\,(v,w,k)\Big|_{v=l} = \mathrm{e}^{2\pi\mathrm{i}\Phi}\left[\frac{\partial}{\partial v} - f'\frac{\partial}{\partial w}\right]\tilde{U}_{tr}\,(v,w,k)\Big|_{v=0}. \tag{3.16}$$

Let $\tilde{U}(g,k) = \tilde{U}^{+}(g,k) + \tilde{U}^{-}(g,k)$ be a general solution of (3.1) (see formula (3.4)). Substituting in it y for v, and z for $w + f(v)$, we obtain

$$\tilde{U}(g_{tr},k) = \tilde{U}^{+}(g_{tr},k) + \tilde{U}^{-}(g_{tr},k), \tag{3.17}$$

where

$$\tilde{U}^{\pm}(g_{tr},k) = \sum_{n=-\infty}^{\infty} \begin{Bmatrix} A_n^{+}(k) \\ A_n^{-}(k) \end{Bmatrix} e^{i[\Phi_n v \pm \Gamma_n (w+f(v))]};\ \Phi_n = 2\pi(\Phi + n)/l,$$

$$\Gamma_n = \sqrt{k^2\tilde{\varepsilon} - \Phi_n^2}, \operatorname{Re}\Gamma_n \operatorname{Re} k \geq 0, \operatorname{Im}\Gamma_n \geq 0. \tag{3.18}$$

Functions (3.17) and (3.18) give the general solution to problem (3.15) and (3.16). It is not difficult to check that each component of this solution respondent to any index n satisfies the boundary conditions at the walls $v = 0$ and $v = l$ of the Floquet channel $\mathbf{R}_{tr}$. Indeed, if in (3.17) one replaces values $\pm\Gamma_n$ for arbitrary values $\Gamma_{n,N}^{\pm}$ these conditions are still valid. But expansions (3.18) are infinite and one may wonder if they are still valid when only a finite number of spatial Fourier harmonics is retained. In other words, is $\tilde{U}(g_{tr},k)$, as expressed by (3.17) and (3.18), with n running from $-N$ to N, where N is some integer, still a solution of (3.15) and (3.16) when $\Gamma_n^2 + \Phi_n^2 = k^2\tilde{\varepsilon}$? The response is negative, but elementary quasi-periodical "solutions" to (3.15) do exist

$$\tilde{U}_n^{\pm}(g_{tr};N) = V_n(v;N)\, W_n^{\pm}(w;N),\ W_n^{\pm}(w;N) = \exp\left[i\Gamma_{n,N}^{\pm} w\right],$$

$$V_n(v;N) = \sum_{m=-N}^{N} v_{nm}\mu_m(v),\ \mu_n(v) = l^{-1/2}\exp(i\Phi_n v),$$

$$\Phi_n = 2\pi(\Phi + n)/l. \tag{3.19}$$

Functions $\tilde{U}_n^{\pm}(g_{tr};N)$ from (3.19) do not meet the second boundary condition from (3.16), but with N increasing this discrepancy decreases and $\Gamma_{n,N}^{\pm} \to \pm\Gamma_n$. The solution to the spectral problem

$$\begin{bmatrix} \left(\frac{\partial^2}{\partial v^2} + k^2\tilde{\varepsilon}\right) & 0 \\ 0 & 1 \end{bmatrix} \begin{bmatrix} V(v) \\ \Gamma V(v) \end{bmatrix} = \Gamma \begin{bmatrix} i\left(f'\frac{\partial}{\partial v} + \frac{\partial}{\partial v}f'\right) + \left[1 + \left(f'\right)^2\right] & \\ 1 & 0 \end{bmatrix} \begin{bmatrix} V(v) \\ \Gamma V(v) \end{bmatrix} \tag{3.20}$$

brings the proof of this statement. We derive the homogeneous functional equation (3.20) from (3.15) by substituting the unknown function in the form

$$\tilde{U}(g_{tr}) = V(v)\exp(i\Gamma w),\ V(v) = \sum_{m=-N}^{N} v_m \mu_m(v). \tag{3.21}$$

In terms of Fourier coefficients $v = \{v_m\}_{m=-N}^{N}$ of unknown function $V(v)$ the problem (3.20) can be reduced to the following matrix form:

$$\begin{bmatrix} k^2\tilde{\varepsilon}E - E_\Phi E_\Phi & 0 \\ 0 & 1 \end{bmatrix} \begin{bmatrix} v \\ \Gamma v \end{bmatrix} = \Gamma \begin{bmatrix} -F'E_\Phi - E_\Phi F' & E + F'F' \\ 1 & 0 \end{bmatrix} \begin{bmatrix} v \\ \Gamma v \end{bmatrix}. \tag{3.22}$$

Here, E is identity matrix, $E_\Phi = \left\{\Phi_n \delta_m^n\right\}_{n,m=-N}^{N}$, $F' = \left\{f'_{nm}\right\}_{n,m=-N}^{N}$ – is the Toeplitz matrix formed by the Fourier coefficients of $f'(v)$ according to the following rule:

$$f'_{nm} = \int_0^l f'(v) \mathrm{e}^{i(\Phi_n - \Phi_m)v} dv. \tag{3.23}$$

In the above relations, we have added a number N to indicate the truncation dependence. Indeed, in practice, the truncation number in (3.22) has to be chosen large enough so that the computed eigenvalues $\Gamma_{n,N}^{\pm}$ that respond to eigenvectors $v_n^{\pm} = \{v_{nm}\}_{m=-N}^{N}$ coincide with a great accuracy with their Rayleigh counterparts $\pm\Gamma_n$. In that case, provided that the eigenvalue is not degenerated, up to a multiplicative constant coefficient, the associated computed eigenvector $\tilde{U}_n^{\pm}(g_{tr};N)$ tend to the corresponding plane wave expressed in terms of variables v and w.

In conclusion, we may write the common solution of the propagation equation in translation coordinates and in truncated Fourier space as

$$\tilde{U}(g_{tr},k;N) = \tilde{U}^{+}(g_{tr},k;N) + \tilde{U}^{-}(g_{tr},k;N);$$

$$\tilde{U}^{\pm}(g_{tr},k;N) = \sum_{n=-N}^{N} \begin{Bmatrix} A_n^{+}(k) \\ A_n^{-}(k) \end{Bmatrix} \exp\left[i\Gamma_{n,N}^{\pm} w\right] \sum_{m=-N}^{N} v_{nm}^{\pm} \mu_m(v), \tag{3.24}$$

or, in matrix form, as

$$\tilde{U}(g_{tr},k;N) = \gamma^{+}(w) V^{+} \mu(v) + \gamma^{-}(w) V^{-} \mu(v). \tag{3.25}$$

Here, $V^{\pm} = \left\{v_{nm}^{\pm}\right\}_{n,m=-N}^{N}$ is the $(2N+1) \times (2N+1)$ matrix, $\mu(v) = \{\mu_m(v)\}_{m=-N}^{N}$ the $(2N+1) \times 1$ matrix (column vector), and $\gamma^{\pm}(w) = \left\{A_n^{\pm} \exp\left(i\Gamma_{n,N}^{\pm} w\right)\right\}_{n=-N}^{N}$ the $1 \times (2N+1)$ matrix (row vector).

3.3 Diffraction of a Plane Wave by a Modulated Surface Grating

3.3.1 Formulation of the Problem

In Cartesian coordinates x, y, z, we consider an infinite cylindrical surface $\mathbf{S}^{\varepsilon,\mu,\sigma}$ (or $\mathbf{S}$) whose generatrices are parallel to the x-axis and give in the crossing with the

plane $x = 0$ the line $z = f(y)$: $\max\ f(y) = 0, \quad \min f(y) = -h$. The periodic function $f(y)$ of period l is assumed to be continuously differentiable. Surface $\mathbf{S}^{\varepsilon,\mu,\sigma}$ separates an air and a homogeneous isotropic medium with relative permittivity $\tilde{\varepsilon}$. The particular case when the cylindrical surface is the perfectly conducting surface $\mathbf{S}$ will also be considered. Let one of these surfaces be illuminated from air with a unit amplitude monochromatic plane wave $\tilde{U}_0^i(g,k) = \exp\left[i\left(\Phi_0 y - \Gamma_0 z\right)\right]$, $\operatorname{Im}\Gamma_0 = 0$ of wavelength $\lambda = 2\pi/k$. The Cartesian components of vector $\vec{k}$ are

$$k_y = k\sin\alpha_0^i \text{ and } k_z = -k\cos\alpha_0^i,\ \alpha_0^i = \arcsin\left(\Phi_0/k\right). \tag{3.26}$$

Since the incident plane wave and the geometry of the system are x invariant, Maxwell's equations for total field $\left\{\vec{E},\vec{H}\right\}$ are split into two independent systems of equations with unknown functions $\tilde{E}_x, \tilde{H}_y, \tilde{H}_z$ and $\tilde{H}_x, \tilde{E}_y, \tilde{E}_z$, respectively. In grating theory these two sets are referred to as E- and H-polarization set, respectively. They are given below for the nonmagnetic medium (see also Section 1.1.1):

$$\frac{\partial\tilde{E}_x}{\partial z} = ik\eta_0\tilde{H}_y,\ \frac{\partial\tilde{E}_x}{\partial y} = -ik\eta_0\tilde{H}_z,\ \frac{\partial\tilde{H}_z}{\partial y} - \frac{\partial\tilde{H}_y}{\partial z} = -ik\tilde{\varepsilon}\eta_0^{-1}\tilde{E}_x \tag{3.27}$$

(E-polarized field) and

$$\eta_0\frac{\partial\tilde{H}_x}{\partial z} = -ik\tilde{\varepsilon}\tilde{E}_y,\ \eta_0\frac{\partial\tilde{H}_x}{\partial y} = ik\tilde{\varepsilon}\tilde{E}_z,\ \frac{\partial\tilde{E}_z}{\partial y} - \frac{\partial\tilde{E}_y}{\partial z} = ik\eta_0\tilde{H}_x \tag{3.28}$$

(H-polarized field). Here $\eta_0 = (\mu_0/\varepsilon_0)^{1/2}$ is the free space impedance, ε_0 and μ_0 are electric and magnetic vacuum constants, respectively.

It is elementary to show that $\tilde{E}_x$ and $\tilde{H}_x$ obey the same Helmholtz equation:

$$\left(\frac{\partial^2}{\partial y^2} + \frac{\partial^2}{\partial z^2} + k^2\tilde{\varepsilon}\right)\tilde{U}(g,k) \equiv \left(\Delta_{y,z} + k^2\tilde{\varepsilon}\right)\tilde{U}(g,k) = 0,\ g = \{y,z\}, \tag{3.29}$$

where $\tilde{U}(g,k)$ designates $\tilde{E}_x$ or $\tilde{H}_x$ (accordingly, $\tilde{U}_0^i(g,k) = \tilde{E}_x^i$ or $\tilde{U}_0^i(g,k) = \tilde{H}_x^i$). In order to write easily boundary condition we move to the translation coordinate system u, v, w [see (3.10), (3.11), (3.12), (3.13), and (3.14)] where we have derived the expression of $\tilde{U}(g_{tr},k)$, $g_{tr} = \{v,w\}$, in terms of a linear combination of eigenvectors of a finite-size matrix, the amplitude coefficients of which have to calculated from the boundary conditions at surface $\mathbf{S}^{\varepsilon,\mu,\sigma}$ (or $\mathbf{S}$). Boundary conditions involve the tangential components of vector fields $\vec{E}$ and $\vec{H}$. So far, for E-polarization, (respectively, for H-polarization) we have the tangential component of electric field (respectively, magnetic field). The subject of next section is the derivation of the missing tangential components.

3.3.2 Tangential Component of a Vector Field at a Coordinate Surface

Let $\vec{V}(p)$, $p = \{x,y,z\}$, be a vector field with components V_x, V_y, V_x. The tangential components of $\vec{V}(p)$ at point p_s on coordinate surface are the perpendicular projections of $\vec{V}(p_s)$ onto this surface. At this point, the unit vectors of the tangent to the curve $z = f(y)$ are $\vec{x}$ and $\vec{\eta} = \vec{y}\cos\varphi + \vec{z}\sin\varphi$ with

$$\mathrm{tg}\varphi = f', \qquad \cos\varphi = \frac{1}{\sqrt{1+\left(f'\right)^2}}, \qquad \sin\varphi = \frac{f'}{\sqrt{1+\left(f'\right)^2}}.$$

Then the two tangential components of $\vec{V}(p)$ at point p_s are V_x and $V_\eta = \left(\vec{V}\cdot\vec{\eta}\right)$. The first one corresponds to the only component of the vector $\vec{V}(p)$, whereas the other one mixes components V_y and V_z:

$$V_\eta = V_y\cos\varphi + V_z\sin\varphi = \frac{1}{\sqrt{1+\left(f'\right)^2}}\left(V_y + f'\,V_z\right). \tag{3.30}$$

In practice, it is more suitable to introduce another quantity proportional to V_η

$$\tilde{W} = V_\eta\sqrt{1+\left(f'\right)^2} = V_y + f'\,V_z. \tag{3.31}$$

In tensorial formulation of C-method, the $\tilde{W}$-function is a covariant component of the electric or magnetic field. We have to express V_y and V_z in terms of $\tilde{U}(g,k)$. Consider E-polarization. Then $\tilde{U}(g,k)$ is $\tilde{E}_x$, while V_y and V_z [see (3.30) and (3.31)] are $\tilde{H}_y$ and $\tilde{H}_z$, respectively. Starting from Maxwell's equations [see (3.27) and (3.28)] and using chain rules for partial derivatives (3.14), we get:

$$\begin{aligned}\tilde{W} &= \tilde{H}_y + f'\,\tilde{H}_z = -\frac{i}{k\eta_0}\frac{\partial\tilde{E}_x}{\partial z} + \frac{i}{k\eta_0}f'\,\frac{\partial\tilde{E}_x}{\partial y} = \\ &= -\frac{i}{k\eta_0}\left[\frac{\partial}{\partial w} - f'\left(\frac{\partial}{\partial v} - f'\,\frac{\partial}{\partial w}\right)\right]\tilde{E}_x(v,w).\end{aligned} \tag{3.32}$$

Similar expression holds for H-polarization:

$$\tilde{W} = \tilde{E}_y + f'\,\tilde{E}_z = \frac{i\eta_0}{k\tilde{\varepsilon}}\left[\frac{\partial}{\partial w} - f'\left(\frac{\partial}{\partial v} - f'\frac{\partial}{\partial w}\right)\right]\tilde{H}_x(v,w). \tag{3.33}$$

Taking into account the modal expansion (3.25) for $\tilde{U}(g_{tr},k;N)$, $\tilde{W}$ may be written under the form:

$$\tilde{W} = \tilde{W}(g_{tr},k;N) = a\left[\gamma^+(w)\,\tilde{V}^+\mu(v) + \gamma^-(w)\,\tilde{V}^-\mu(v)\right]. \tag{3.34}$$

Here (see also Section 3.2.3),

$$\tilde{V}^{\pm} = \left\{\tilde{v}^{\pm}_{nm}\right\}^{N}_{n,m=-N} = E^{\pm}_{\Gamma} V^{\pm} \left(E + \tilde{F}'\tilde{F}'\right) - V^{\pm} E_{\Phi} \tilde{F}', \tag{3.35}$$

$E_{\Phi} = \left\{\Phi_n \delta^n_m\right\}^{N}_{n,m=-N}$ and $E^{\pm}_{\Gamma} = \left\{\Gamma^{\pm}_{n,N}\delta^n_m\right\}^{N}_{n,m=-N}$ are the diagonal matrices, $V^{\pm} = \left\{v^{\pm}_{nm}\right\}^{N}_{n,m=-N}$ is the $(2N+1)\times(2N+1)$ matrix, $\mu(v) = \{\mu_m(v)\}^{N}_{m=-N}$ the $(2N+1)\times 1$ matrix, $\gamma^{\pm}(w) = \left\{A^{\pm}_n \exp\left(i\Gamma^{\pm}_{n,N} w\right)\right\}^{N}_{n=-N}$ the $1\times(2N+1)$ matrix, and $\tilde{F}' = \left\{\tilde{f}'_{nm}\right\}^{N}_{n,m=-N}$ the $(2N+1)\times(2N+1)$ matrix with the elements

$$\tilde{f}'_{nm} = \int_0^l f'(v) e^{i(\Phi_m - \Phi_n)v} dv = f'_{mn},$$

$a = (k\eta_0)^{-1}$ for E-polarized field and $a = -\eta_0 (k\tilde{\varepsilon})^{-1}$ for H-polarized field.

3.3.3 Boundary Conditions

Since we have modal expansions in truncated Fourier space for every tangential components in medium **I** and **II**, writing boundary conditions at coordinate surface $w = \text{const}$ (see Section 1.1.2) is elementary. In the previously derived expressions, we add an index **I** or **II** to indicate the medium. Boundary conditions at $\mathbf{S}^{\varepsilon,\mu,\sigma}$ (the boundary between free space and medium with the permittivity $\tilde{\varepsilon}$) or at **S** (the boundary of the perfect conductor), we write [see formulas (3.32), (3.33), (3.34), and (3.35)] in such a form:

$$\left\{\begin{array}{l} \tilde{U}^{\mathbf{I}}(g_{tr},k;N) = \tilde{U}^{\mathbf{II}}(g_{tr},k;N) \\ \tilde{W}^{\mathbf{I}}(g_{tr},k;N) = \tilde{W}^{\mathbf{II}}(g_{tr},k;N) \end{array}\right|_{g_{tr}\in\mathbf{S}^{\varepsilon,\mu,\sigma}} \text{and} \tag{3.36}$$

$$\tilde{U}^{\mathbf{I}}(g_{tr},k;N) = 0\Big|_{g_{tr}\in\mathbf{S}} \tag{3.37}$$

for E-polarization, and

$$\left\{\begin{array}{l} \tilde{U}^{\mathbf{I}}(g_{tr},k;N) = \tilde{U}^{\mathbf{II}}(g_{tr},k;N) \\ \tilde{W}^{\mathbf{I}}(g_{tr},k;N) = \tilde{W}^{\mathbf{II}}(g_{tr},k;N) \end{array}\right|_{g_{tr}\in\mathbf{S}^{\varepsilon,\mu,\sigma}} \text{and} \tag{3.38}$$

$$\tilde{W}^{\mathbf{I}}(g_{tr},k;N) = 0\Big|_{g_{tr}\in\mathbf{S}} \tag{3.39}$$

for H-polarization.

From relations (3.36), (3.37), (3.38), and (3.39), we may calculate the scattering matrices

$$S^{\varepsilon,\mu,\sigma} = \begin{bmatrix} S_{11} & S_{12} \\ S_{21} & S_{22} \end{bmatrix} \text{ and } S = S_{11} \tag{3.40}$$

for boundaries $\mathbf{S}^{\varepsilon,\mu,\sigma}$ and $\mathbf{S}$, respectively. These matrices defined in the following way:

$$\begin{bmatrix} A_{\mathbf{I}}^{+} \\ A_{\mathbf{II}}^{-} \end{bmatrix} = \begin{bmatrix} S_{11} & S_{12} \\ S_{21} & S_{22} \end{bmatrix} \begin{bmatrix} A_{\mathbf{I}}^{-} \\ A_{\mathbf{II}}^{+} \end{bmatrix} \text{ and } A_{\mathbf{I}}^{+} = SA_{\mathbf{I}}^{-}. \tag{3.41}$$

Here, $A_{\mathbf{I}}^{\pm} = \left\{A_n^{\pm}(\mathbf{I})\right\}_{n=-N}^{N}$ and $A_{\mathbf{II}}^{\pm} = \left\{A_n^{\pm}(\mathbf{II})\right\}_{n=-N}^{N}$ are the $(2N+1) \times 1$ matrices (column vectors).

The result is

$$S^{\varepsilon,\mu,\sigma} = \begin{bmatrix} V_T^{+}(\mathbf{I}) & -V_T^{-}(\mathbf{II}) \\ \tilde{V}_T^{+}(\mathbf{I}) & -b\tilde{V}_T^{-}(\mathbf{II}) \end{bmatrix}^{-1} \begin{bmatrix} -V_T^{-}(\mathbf{I}) & V_T^{+}(\mathbf{II}) \\ -\tilde{V}_T^{-}(\mathbf{I}) & b\tilde{V}_T^{+}(\mathbf{II}) \end{bmatrix} \text{ and}$$

$$S = -\left[V_T^{+}(\mathbf{I})\right]^{-1} V_T^{-}(\mathbf{I}) \ (E-\text{case}) \text{ or}$$

$$S = -\left[\tilde{V}_T^{+}(\mathbf{I})\right]^{-1} \tilde{V}_T^{-}(\mathbf{I}) \ (H-\text{case}). \tag{3.42}$$

Here, $V_T^{\pm}$ and $\tilde{V}_T^{\pm}$ are the transposed matrices $V^{\pm}$ and $\tilde{V}^{\pm}$ (see the previous section), $b = 1$ for E-polarized field and $b = \tilde{\varepsilon}^{-1}$ for H-polarized field.

Let us recall that in presentation (3.24) for total field $\tilde{U}(g_{tr},k;N)$ the components $\tilde{U}_n^{\pm}(g_{tr},k;N) = A_n^{\pm}\exp\left[i\Gamma_{n,N}^{\pm}w\right]V_n(v;N)$, $n = 0, \pm 1, \ldots, \pm N$ describe the plane waves propagating without ($\operatorname{Im}\Gamma_n^{\pm} = 0$) or with ($\operatorname{Im}\Gamma_n^{\pm} > 0$) decay toward increasing (sign +) or decreasing (sign –) values of w, then we can see clearly that formulas (3.40), (3.41), and (3.42) give the most complete solution to the problem, connected with determination of diffraction characteristics of the surfaces $\mathbf{S}^{\varepsilon,\mu,\sigma}$ and $\mathbf{S}$.

In this solution by wavepackets, $\left\{A_n^{-}(\mathbf{I})\exp\left[i(\Phi_n y - \Gamma_n z)\right]\right\}_{n=-N}^{N}$, $z > 0$ (domain $\mathbf{A}$), and $\left\{A_n^{+}(\mathbf{II})\exp\left[i(\Phi_n y + \Gamma_n(z+h))\right]\right\}_{n=-N}^{N}$, (domain $\mathbf{B}$), are defined the waves coming onto the boundary $z = f(y)$ from above and from below. By wavepackets, $\left\{A_n^{+}(\mathbf{I})\exp\left[i(\Phi_n y + \Gamma_n z)\right]\right\}_{n=-N}^{N}$, $z > 0$ and $\left\{A_n^{-}(\mathbf{II})\exp\left[i(\Phi_n y - \Gamma_n(z+h))\right]\right\}_{n=-N}^{N}$, $z < -h$, are defined the scattered field in reflection (domain $\mathbf{A}$) and transmission (domain $\mathbf{B}$) domains of periodic structure.

In the case when $A_n^{-}(\mathbf{I}) = \delta_0^n$ and $A_n^{+}(\mathbf{II}) = 0$ for all $n = 0, \pm 1, \ldots, \pm N$, we arrive to the problem formulated in Section 3.3.1. Complex amplitudes $A_n^{+}(\mathbf{I}) = R_{n0}^{\mathbf{AA}}$ and $A_n^{-}(\mathbf{II}) = T_{n0}^{\mathbf{BA}}$, that are the solutions to it, are called conventionally coefficients of reflection and transition, respectively.

3.4 Adaptive Spatial Resolution

Among the existing grating methods the C-method and the modal method by Fourier expansion (MMFE) are certainly the simplest because they involve only elementary mathematics and numerical techniques. Indeed, the solution of Maxwell's equations

is reduced to the solution of an algebraic eigenvalue problem in discrete Fourier space. The derivation of the matrix operator involves two steps: the electromagnetic field is expanded into Floquet–Fourier series and the periodic coefficients of boundary value problem for Maxwell's equations are expanded into Fourier series. In the MMFE, the periodic coefficient is the permittivity function, whereas in the C-method it is the derivative of the grating profile function. When the above-mentioned functions are discontinuous, the Fourier method is known to converge slowly. In the MMFE, this happens with high-contrast permittivity profiles and in the C-method with profiles that have sharp edges. This weakness remains even when the correct Fourier factorization of products of discontinuous periodic functions, as given by L. Li, is applied. The reason for slow convergence is that the spatial resolution of the Fourier expansion remains uniform within a grating period whatever the permittivity or the grating profile function may be. In this section, we overcome this limitation by choosing a coordinate system in such a way that the mapping of space fits the variation of the periodic function of interest. Then, the matrix operator takes into account the new information, and truly dramatic improvement of the convergence rate is achieved [165–167]. So, a new reason for choosing new coordinates is to realize adaptive spatial resolution. We will show the effectiveness of this new approach by considering a trapezoidal grating modeled with C-method and a lamellar grating with high-contrast permittivity function modeled with MMFE.

We consider the electromagnetic problem in which a grating, periodic in the y-direction, is illuminated from above by a linear polarized monochromatic plane wave with vacuum wavelength λ and wave number $k = 2\pi/\lambda$. The incident medium is assumed to be air, and the wave vector inclined at α_0^i to the z-axis has the following Cartesian components: $k_y = k \sin \alpha_0^i$ and $k_z = -k \cos \alpha_0^i$. Time dependence is expressed by the factor $\exp(-ikt)$. Such a problem is reduced to the study of the two fundamental cases of polarization, and the unknown function $\tilde{U}(g,k)$, $g = \{y,z\}$, is the x-component of the electric or the magnetic field for E- and H-polarization, respectively.

3.4.1 Trapezoidal Grating

We have believed for a long time that sharp edges were an intrinsic limitation of the C-method. Here we present the contrary example. The chosen grating is shown in Fig. 3.1. Its profile function $z = f(y)$ is described by five parameters: period l, groove depth h, and the abscissas of three vertices, assuming that one of the lower vertices is located at the origin of the rectangular Cartesian coordinate system. The slow convergence observed for deep gratings can be easily understood from the following simple explanation. When the slope of $f(y)$ becomes steeper, the portion of the graph of $f'(y)$ that corresponds to the slope becomes narrower and taller (or deeper). Therefore, the accurate representation of $f'(y)$ requires more and more terms of the Fourier series. Since $f'(y)$ is an intrinsic characteristic of the profile, the only way to make its spectrum narrower is to modify the representation of y by introducing a new function $y = g(v)$: $g(0) = 0$, $g(l) = l$. Let us present the coordinate y as a function of v and denote the transition points by y_p in the y-space

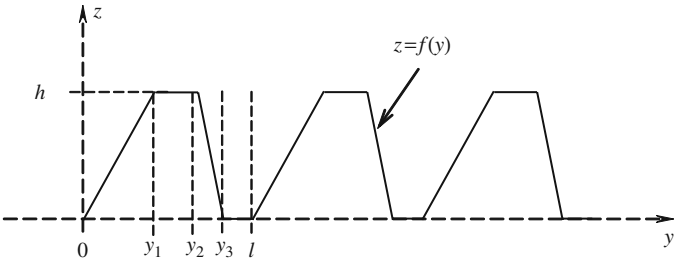

Fig. 3.1 Trapezoidal grating

and by v_p in v-space. Between transitions p and $p-1$, we use the function $y_p\,(v)$ for the mapping between spaces:

$$y_p(v) = y_{p-1} + \frac{y_p - y_{p-1}}{v_p - v_{p-1}}\left[1 - \eta\frac{v_p - v_{p-1}}{2\pi}\sin\frac{2\pi\left(v - v_p\right)}{v_p - v_{p-1}}\right]; \qquad p = 1,2,3,4. \tag{3.43}$$

The distance between two transition points in v-space is proportional to the length of the corresponding facet:

$$v_p - v_{p-1} = \frac{L_p}{L}; \qquad p = 1,2,3,4, \tag{3.44}$$

where L_p is the length of the pth facet and L is the total length of the surface profile, $L = L_1 + L_2 + L_3 + L_4$. Function $z\,(v)$ becomes:

$$z_1(v) = \frac{h}{v_1}y_1(v),\; z_2\,(v) = h,\; z_3\,(v) = h - \frac{h}{v_3 - v_2}y_3(v),\; z_4\,(v) = 0. \tag{3.45}$$

The η parameter between 0 and 1 controls the density of coordinate lines around the transition points. It allows to stretch space thinner where discontinuities of coefficients in Maxwell's equations occur.

Let us now derive the new propagation equations when the translation coordinate system is obtained by

$$x = u, \qquad y = g(v), \qquad z = w + h(v),\; h\,(v) = f\left[g\,(v)\right]. \tag{3.46}$$

The Jacobian matrices of the direct transformation and of the inverse transformation are

$$J = \frac{\partial(x,y,z)}{\partial(u,v,w)} = \begin{bmatrix} \frac{\partial x}{\partial u} & \frac{\partial x}{\partial v} & \frac{\partial x}{\partial w} \\ \frac{\partial y}{\partial u} & \frac{\partial y}{\partial v} & \frac{\partial y}{\partial w} \\ \frac{\partial z}{\partial u} & \frac{\partial z}{\partial v} & \frac{\partial z}{\partial w} \end{bmatrix} = \begin{bmatrix} 1 & 0 & 0 \\ 0 & g' & 0 \\ 0 & h' & 1 \end{bmatrix} \tag{3.47}$$

and

$$J^{-1} = \frac{\partial(u,v,w)}{\partial(x,y,z)} = \begin{bmatrix} \frac{\partial u}{\partial x} & \frac{\partial u}{\partial y} & \frac{\partial u}{\partial z} \\ \frac{\partial v}{\partial x} & \frac{\partial v}{\partial y} & \frac{\partial v}{\partial z} \\ \frac{\partial w}{\partial x} & \frac{\partial w}{\partial y} & \frac{\partial w}{\partial z} \end{bmatrix} = \begin{bmatrix} 1 & 0 & 0 \\ 0 & \left(g'\right)^{-1} & 0 \\ 0 & -h'\left(g'\right)^{-1} & 1 \end{bmatrix},$$

$$\left(g'\right)^{-1} = 1/\left(\partial g\left(v\right)/\partial v\right). \tag{3.48}$$

For the change of variables (3.46), (3.47), and (3.48), the rule of chain for derivatives has the form:

$$\begin{cases} \frac{\partial}{\partial x} = \frac{\partial u}{\partial x}\frac{\partial}{\partial u} + \frac{\partial v}{\partial x}\frac{\partial}{\partial v} + \frac{\partial w}{\partial x}\frac{\partial}{\partial w} = \frac{\partial}{\partial u} \\ \frac{\partial}{\partial y} = \frac{\partial u}{\partial y}\frac{\partial}{\partial u} + \frac{\partial v}{\partial y}\frac{\partial}{\partial v} + \frac{\partial w}{\partial y}\frac{\partial}{\partial w} = \left(g'\right)^{-1}\frac{\partial}{\partial v} - h'\left(g'\right)^{-1}\frac{\partial}{\partial w} \\ \frac{\partial}{\partial z} = \frac{\partial u}{\partial z}\frac{\partial}{\partial u} + \frac{\partial v}{\partial z}\frac{\partial}{\partial v} + \frac{\partial w}{\partial z}\frac{\partial}{\partial w} = \frac{\partial}{\partial w} \end{cases}. \tag{3.49}$$

Substituting these derivatives into the homogeneous ($\tilde{f}\left(g,k\right) \equiv 0$) equation of problem (3.1) gives

$$\left\{\left[\left(g'\right)^{-1}\frac{\partial}{\partial v}\right]^2 + \left[h'\left(g'\right)^{-1}\frac{\partial}{\partial w}\right]^2 + \frac{\partial^2}{\partial w^2} - \left(g'\right)^{-1}\frac{\partial}{\partial v}h'\left(g'\right)^{-1}\frac{\partial}{\partial w} - \right.$$
$$\left. -h'\left(g'\right)^{-1}\frac{\partial}{\partial w}\left(g'\right)^{-1}\frac{\partial}{\partial v} + k^2\tilde{\varepsilon}\right\}\tilde{U}\left(g_{tr},k\right) = 0,\ g_{tr} = \{v,w\}. \tag{3.50}$$

Starting from (3.50) we may iterate all operations carried out in Sections 3.2.3 and 3.3 and construct the effective algorithm for calculation of the diffraction characteristics of the considered periodic surface. The crucial stage in constructions of this kind is the conversion of the new propagation equations in translation coordinates [see, for example, (3.50)] to the spectral problems for eigenvectors

$$\tilde{U}\left(g_{tr}\right) = V\left(v\right)\exp\left(i\Gamma w\right),\ V\left(v\right) = \sum_{m=-N}^{N} v_m \mu_m\left(v\right) \tag{3.51}$$

and eigenvalues Γ in truncated Fourier space. In case under consideration such a problem may be produced in the following form:

$$\Gamma\begin{bmatrix} i\left(\left(g'\right)^{-1}\dfrac{\partial}{\partial v}h'\left(g'\right)^{-1} + h'\left(g'\right)^{-1}\left(g'\right)^{-1}\dfrac{\partial}{\partial v}\right) & \left(\left[h'\left(g'\right)^{-1}\right]^2 + 1\right) \\ 1 & 0 \end{bmatrix} \times$$

$$\times\begin{bmatrix} V\left(v\right) \\ \Gamma V\left(v\right) \end{bmatrix} = \begin{bmatrix} \left(\left[\left(g'\right)^{-1}\dfrac{\partial}{\partial v}\right]^2 + k^2\tilde{\varepsilon}\right) & 0 \\ 0 & 1 \end{bmatrix}\begin{bmatrix} V\left(v\right) \\ \Gamma V\left(v\right) \end{bmatrix}. \tag{3.52}$$

In order to illustrate the improvement in terms of convergence rate of the present formulation compared with the usual one, let us consider the following grating configuration: $h = l = 2\lambda$, $y_1 = 0.25\lambda$, $y_2 = \lambda$, $y_3 = 1.25\lambda$, $\alpha_0^i = 45°$, $\tilde{\varepsilon} = (0.3 + i7.0)^2$. The η parameter is set to zero. Figure 3.2 shows the convergence of the specularly reflected order in *H*-polarization versus the inverse of truncation order when classical formulation is used and when the distance between transition points in the transformed coordinates is proportional to the length of the facets. The improvement of convergence with the new formulation is remarkable. We suggest a geometrical interpretation. Suppose that the profile is to be represented by some samples. Then the present parametric representation allows us to put samples with a density proportional to the length of the facets, whereas in the classical representation, the steeper the slope, the fewer the points on it. Figure 3.3 shows the importance of having a η parameter that permits the discontinuities of the derivative of the profile to be taken into account. When η is close to one, samples are accumulated in the neighborhood of the vertices. Here, we have modified the vertices y_1 and y_2 in order to have two nearly vertical facets. By choosing $y_1 = 0.001\lambda$ and $y_2 = y_3 - 0.0001\lambda$ the slope is 89.9 degrees. Another code based on modal method by Fourier expansion in Cartesian coordinates shows that the reflected specular efficiency in *H*-polarization is $W_{00}^R = 0.129$ for a true lamellar grating (values $W_{n0}^R = \left|R_{n0}^{\mathbf{AA}}\right|^2 \mathrm{Re}\,\Gamma_n/\Gamma_0$ and $W_{n0}^T = \left|T_{n0}^{\mathbf{BA}}\right|^2 \mathrm{Re}\,\Gamma_n/\Gamma_0$ determine energy content of the harmonics, that is the relative part of the energy that is directed by the structure into the relevant spatial radiation channel; see Section 1.2.1). From the practical point of view, one can say that C-method with adaptive spatial resolution is able to handle vertical facets.

3.4.2 Lamellar Grating and Adaptive Spatial Resolution

In this section, we consider the case of a lamellar grating configuration as shown in Fig. 3.4. A grating layer separates the vacuum $\tilde{\varepsilon}_1 = 1$ and an

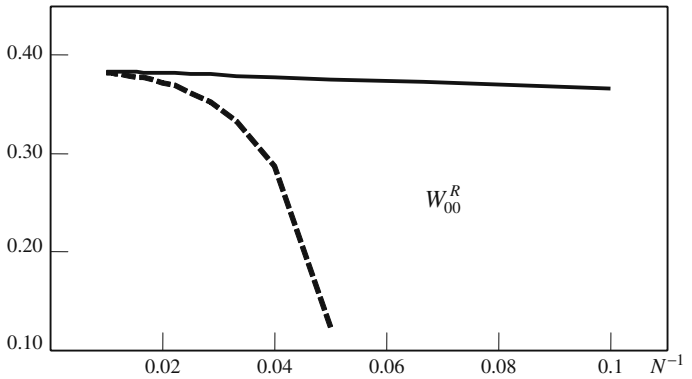

Fig. 3.2 Convergence of specular reflected order calculated without parametric representation of the trapezoidal profile (*dashed line*) and with parametric representation of the trapezoidal profile (*solid line*)

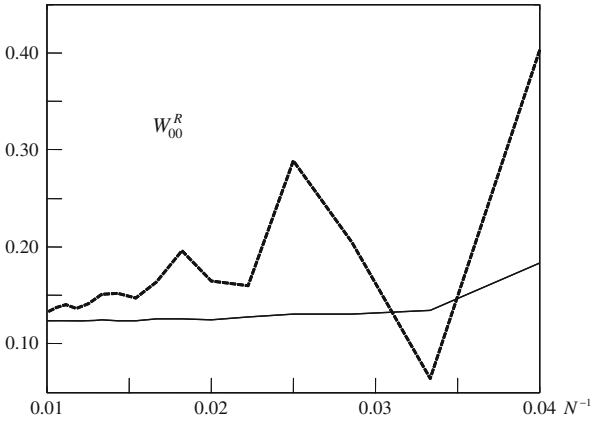

Fig. 3.3 Convergence of specular reflected order in the case of nearly vertical facets. *Dashed line* – calculation without parametric representation; *solid line* – calculation with parametric representation

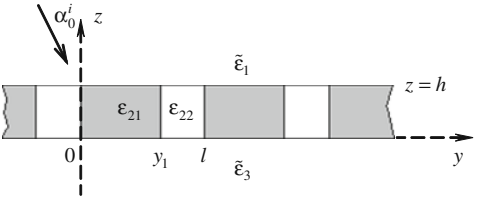

Fig. 3.4 Geometry of a lamellar diffraction problem

homogeneous isotropic media with refractive index $\tilde{\varepsilon}_3$. The layer consists of a piecewise homogeneous medium with thickness h, characterized by a x-invariant, y-periodic with period l, and permeability function

$$\tilde{\varepsilon}_2(y) = \begin{cases} \varepsilon_{21}; & 0 < y < y_1 \\ \varepsilon_{22}; & y_1 < y < l \end{cases}.$$

The unknown function $\tilde{U}(g,k)$ is the x-component of the magnetic field in the case of H-polarization of the electric field in the case of E-polarization. In each region, which we refer to by the index $j = 1,2,3$, the field $\tilde{U}_j(g,k)$ can be represented by superposition of eigenfunctions

$$\tilde{U}_{nj}^{\pm}(g,k) = A_{nj}^{\pm}(k) \exp\left(\pm i\Gamma_{nj} z\right) \mu_{nj}(y), \; n = 0, \pm 1, \pm 2, ..., \; g = \{y,z\} \tag{3.53}$$

computed from the following spectral problems (see also Section 3.2.1):

$$\begin{cases} \left[L_j + \dfrac{\partial^2}{\partial z^2}\right] \tilde{U}_j(g,k) = 0; \qquad g = \{y,z\} \in \mathbf{R}^2 \\ \tilde{U}_j\left\{\frac{\partial \tilde{U}_j}{\partial y}\right\}(y + l,z,k) = \mathrm{e}^{2\pi i \Phi} \tilde{U}_j\left\{\frac{\partial \tilde{U}_j}{\partial y}\right\}(y,z,k) \end{cases}. \tag{3.54}$$

Here,

$$L_j \equiv \frac{\partial^2}{\partial y^2} + \tilde{\varepsilon}_j k^2 \; (E - \text{case}), \text{ and } L_j \equiv \tilde{\varepsilon}_j \frac{\partial}{\partial y} \frac{1}{\tilde{\varepsilon}_j} \frac{\partial}{\partial y} + \tilde{\varepsilon}_j k^2 \; (H - \text{case}). \tag{3.55}$$

In deriving operator L_j for $j = 2$ we have to take care of the representation of the permittivity coefficient in truncated Fourier space. Indeed, let us assume functions $f(y)$ and $h(y)$ be linked by a third one $g(y)$ that acts as a multiplicative operator. Provided that $g(y)$ is nonnull, the two relations

$$f(y) = g(y)h(y) \text{ and } \frac{1}{g(y)} f(y) = h(y) \tag{3.56}$$

are completely equivalent. In truncated Fourier space this is not the case. Here, the equivalent pairs are

$$F = GH, \; G^{-1}F = H \text{ and } \tilde{G}F = H, \; F = \tilde{G}^{-1}H;$$

$$G = \left\{g_{pm}\right\}_{p,m=-N}^{N}, \; \tilde{G} = \left\{\tilde{g}_{pm}\right\}_{p,m=-N}^{N}, \; F = \left\{f_m\right\}_{m=-N}^{N},$$

$$H = \left\{h_m\right\}_{m=-N}^{N}, \ldots . g_{pm} = \left\langle g(y), \mu_{m-p}(y) \right\rangle, \; \tilde{g}_{pm} = \left\langle g^{-1}(y), \mu_{m-p}(y) \right\rangle,$$

but $G \neq \tilde{G}^{-1}$ and $G^{-1} \neq \tilde{G}$.

Let $f(y)$ and $h(y)$ in (3.56) represent the field components and the function $g(y)$ – the properties of the piecewise homogeneous medium. At some coordinate surface $y = \text{const}$, functions $f(y)$ and $h(y)$ satisfied some boundary conditions according to whether they are tangential components or normal components at that surface. We postulate that matrix operator that links two components and respond

to the function $g(y)$ should always be defined in such a way that it operates on the continuous component. Thus, for example, in the case that $\tilde{\varepsilon}$ is a function of y, the relation between vectors $\vec{D}$ (vector of electric flux density) and $\vec{E}$ we write:

$$\tilde{D}_x(y) = \varepsilon_0 \tilde{\varepsilon}(y) \tilde{E}_x(y),\ \frac{1}{\tilde{\varepsilon}(y)} \tilde{D}_y(y) = \varepsilon_0 \tilde{E}_y(y),\ \tilde{D}_z(y) = \varepsilon_0 \tilde{\varepsilon}(y) \tilde{E}_z(y).$$

We are seeking now some change of variable $y = g(v)$ that realizes adaptive spatial resolution. The function of v is chosen in such a way that spatial resolution is increased around $y = 0$ and $y = y_1$ where the permittivity function is discontinuous. Around these points a given variation Δv of v should result in a very much lower variation Δy of y. A possible change of variable is the one that was successfully used in the case of trapezoidal grating and C-method (see Section 3.4.1):

$$y_p(v) = y_{p-1} + \frac{y_p - y_{p-1}}{v_p - v_{p-1}} \left(v - v_p - \eta \frac{v_p - v_{p-1}}{2\pi} \sin \frac{2\pi \left(v - v_p \right)}{v_p - v_{p-1}} \right); \qquad p = 1,2.$$

The new defined function v is periodic with the same period as the permittivity function and its derivative is minimum at the discontinuities.

To show the improvement in terms of convergence of the present formulation over the usual one, let us consider the geometry depicted in Fig. 3.4 with the following parameters: $v_1 = 0.4$, $\alpha_0^i = 29°$, $l = 1.0$, $\lambda = 1.0$, $\varepsilon_{21} = 4.0$, and $\varepsilon_{22} = 25$. The convergence behavior of the second-smallest eigenvalue is illustrated in Fig. 3.5 for the case of H-polarization. The error $\log_{10} \left| \Gamma_{exact} - \Gamma_N \right/ \Gamma_{exact} \left|\right.$ is plotted versus the truncation order N for three values of the η parameter. The exact value Γ_{exact} of Γ is computed by use of a transcendental eigenvalue equation.

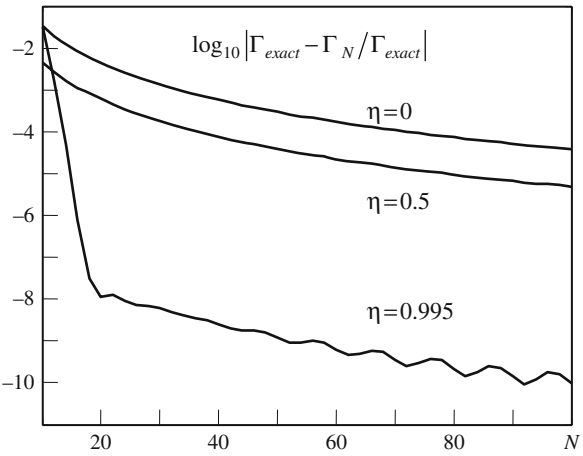

Fig. 3.5 Convergence of the second-smallest real eigenvalue for H-polarization. The exact eigenvalue is found to be 2.81329903403930

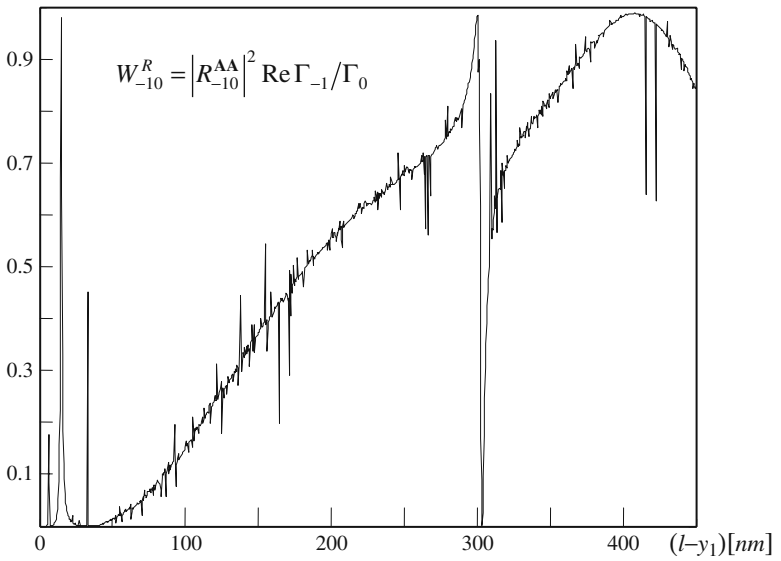

Fig. 3.6 Groove width dependence of the minus first-order diffraction efficiency. Computation is done by using classical Fourier modal method with a truncation order $N = 15$: $\varepsilon_{21} = -100$, $\varepsilon_{22} = 1.0$, $\tilde{\varepsilon}_3 = -100$, H-polarization

We consider another example that has been investigated in the literature (see papers [167, 168]). It consists of a lossless grating with a negative permittivity $\varepsilon_{21} = -100$ for which classical MMFE produces noisy data due to apparition of spurious modes in the numerical calculation (see Fig. 3.6 that reproduces the numerical results obtained in [167]). The grating period l and depth h are 500 [nm], the wavelength λ is 632.8 [nm], and the incidence angle $\alpha_0^i = 30°$. Figure 3.7 shows the same configuration computed with Fourier modal method and adaptive spatial resolution. It is seen that all instabilities have disappeared.

3.5 Curved Strip Gratings

Strip gratings can model such devices as photolithographic masks or frequency-selective surfaces either in the optical or in the microwave domain. Likewise, by deposition of a periodic strip at the surface of a dielectric or a metal, one obtains a selective surface waveguide or even in certain conditions new materials with negative refractive index, the so-called metamaterials. This last application has renewed the interest for numerical modeling of strip gratings. The problem of the diffraction of electromagnetic waves by strip gratings has been extensively studied in the past. A possible way to obtain the solution is to express the fields in terms of the Rayleigh expansions above and below the strips and to apply the combined boundary conditions method (CBCM) introduced in [169]. The key feature

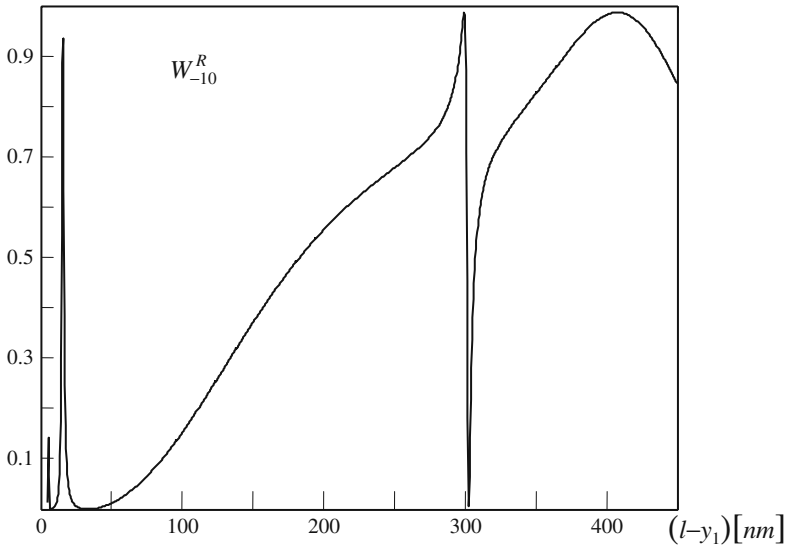

Fig. 3.7 Groove width dependence of the minus first-order diffraction efficiency. The physical parameters are the same as in Fig. 3.6. Adaptive spatial resolution is achieved with $v_1 = 0.5$ and $\eta = 1$. The truncation number is $N = 40$

of this differential approach is that it combines the continuity equations of the electric and magnetic fields in a unified equation that holds over one full period. The advantage of this method is its simplicity due to the use of Fourier series. Furthermore, it offers the numerical possibility to easily mix strip gratings and other gratings provided that they share the same periodicity and they are analyzed with any method that uses Fourier expansions. However, the main drawback of most Fourier-based methods is that they are not able to describe efficiently electromagnetic fields with sharp variations. As a consequence, convergence is achieved with rather huge matrices. Here, the tangential component of the field that points toward the axis of periodicity is singular at the edge of the strips! Of course, such problems can be overcome by intricate mathematics [45, 74, 79, 170] but also by the very simple technique of adaptive spatial resolution [171]. By using a nonuniform sampling scheme that places more points around the edge of the strip, we have shown that the convergence speed was dramatically improved. Our purpose in the present section is to further demonstrate the versatility, the effectiveness, and the complementarily of C-method, adaptive spatial resolution, and combined boundary conditions.

The structure under study is depicted in Fig. 3.8. It consists of a 1-D periodic surface $\mathbf{S}^{\varepsilon,\mu,\sigma}$, with period l, separating the air (the medium **I**) and the dielectric (with relative permittivity $\tilde{\varepsilon}$) homogeneous and isotropic medium **II** and over which is deposited an infinitely thin perfectly conducting strip grating **S** of the same shape and period. The surface $\mathbf{S}^{\varepsilon,\mu,\sigma}$ is invariant along the x-direction, and described by

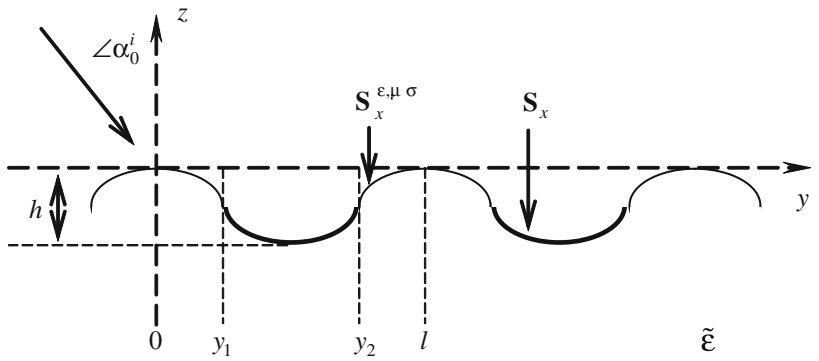

Fig. 3.8 Geometry of a strip grating diffraction problem

the function $z = f(y)$: $\max f(y) = 0$, $\min f(y) = -h$. The part of the grating covered by the strip is within the interval $[y_1;y_2]$. The grating is illuminated from the upper domain **A** ($z > 0$) with a unit amplitude monochromatic plane wave $\tilde{U}_0^i(g,k) = \exp[i(\Phi_0 y - \Gamma_0 z)]$, $\mathrm{Im}\Gamma_0 = 0$, of wavelength $\lambda = 2\pi/k$. The Cartesian components of vector $\vec{k}$ are $k_y = k\sin\alpha_0^i$ and $k_z = -k\cos\alpha_0^i$; $\alpha_0^i = \arcsin(\Phi_0/k)$. The unknowns of the problem are the reflected (to domain **A**) and transmitted (to domain **B**: $z < -h$) fields.

The ingredients of the method that we use to solve the present problem have already been presented elsewhere but never combined together in the context of strip gratings. Before going into details, we briefly recall the two main ideas behind our formalism. Any numerical method aimed at solving Maxwell's equations is all the more efficient since it is able to fit the geometry of the problem. One way to do so is to use a coordinate transformation. The C-method that was developed in the 1980s is precisely one such method. Following, the C-method, we introduce a new coordinate system u, v, w deduced from the Cartesian coordinate system by the relations $u = x$, $v = y$, and $w = z - f(y)$. Hence, the surface profile of the grating becomes the coordinate surface $w = 0$. Then we have to write Maxwell's equation in terms of the new variables. The boundary conditions at $w = 0$ impose that:

- the tangential components of the electric field must be continuous over a whole period;
- the tangential components of the electric field must be null over the strips;
- the tangential components of the magnetic field must be continuous over the complementary of the strips.

In order to introduce adaptive spatial resolution, we adopt a parametric representation of the profile function $z = f(y)$:

$$x = u, \quad y = g(v), \quad z = w + f(g(v)),\ g(v):\ g(0) = 0,\ g(l) = l. \tag{3.57}$$

Here,

$$g(v) = \begin{cases} \frac{4v_1}{l}\left(v + \frac{l}{4\pi}\sin\left(\frac{4\pi v}{l}\right)\right); & 0 \le v \le 0.25\,l \\ v_1 + \frac{2(v_2-v_1)}{l}\left((v-0.25\,l) - \frac{l}{4\pi}\sin\left(\frac{8\pi(v-0.25\,l)}{l}\right)\right); & \\ \qquad 0.25\,l \le v \le 0.75\,l & \\ v_2 + \frac{4(l-v_2)}{l}\left((v-0.75\,l) - \frac{l}{4\pi}\sin\left(\frac{4\pi(v-0.75\,l)}{l}\right)\right); & 0.75 \le v \le l \end{cases} \tag{3.58}$$

The above change of coordinates introduces a metric factor $\partial y/\partial v$ along the y-direction. Hence, the width of the strip becomes $v_2 - v_1$ instead of $y_2 - y_1$. Furthermore, at the edges of the strip ($v = v_1$ and $v = v_2$) where a singularity of the field occurs, the metric factor is null. Therefore spatial resolution is infinite and an accurate representation of the field at these points is possible. It is also to be emphasized that the transition points in v-space are equally spaced. Modal solution of Maxwell's equations in a similar coordinate system and in truncated Fourier space has already be given in Section 3.4.1. The only remaining task is to write boundary conditions.

These conditions write (see Section 3.3.3):

$$\begin{cases} \tilde{U}^{\mathbf{I}}(g_{tr},k;N) = \tilde{U}^{\mathbf{II}}(g_{tr},k;N)\big|_{g_{tr}\in\mathbf{S}^{\varepsilon,\mu,\sigma}} \\ \tilde{U}^{\mathbf{I}}(g_{tr},k;N) = \tilde{U}^{\mathbf{II}}(g_{tr},k;N) = 0\big|_{g_{tr}\in\mathbf{S}} \\ \tilde{W}^{\mathbf{I}}(g_{tr},k;N) = \tilde{W}^{\mathbf{II}}(g_{tr},k;N)\big|_{g_{tr}\in\mathbf{S}^{\varepsilon,\mu,\sigma}\setminus\mathbf{S}} \end{cases} \tag{3.59}$$

(in the case of E-polarization) and

$$\begin{cases} \tilde{W}^{\mathbf{I}}(g_{tr},k;N) = \tilde{W}^{\mathbf{II}}(g_{tr},k;N)\big|_{g_{tr}\in\mathbf{S}^{\varepsilon,\mu,\sigma}} \\ \tilde{W}^{\mathbf{I}}(g_{tr},k;N) = \tilde{W}^{\mathbf{II}}(g_{tr},k;N) = 0\big|_{g_{tr}\in\mathbf{S}} \\ \tilde{U}^{\mathbf{I}}(g_{tr},k;N) = \tilde{U}^{\mathbf{II}}(g_{tr},k;N)\big|_{g_{tr}\in\mathbf{S}^{\varepsilon,\mu,\sigma}\setminus\mathbf{S}} \end{cases} \tag{3.60}$$

(in the H-case). Equations (3.59) and (3.60) can be recast to the following sets of two relations:

$$\begin{cases} \tilde{U}^{\mathbf{I}}(g_{tr},k;N) = \tilde{U}^{\mathbf{II}}(g_{tr},k;N) \\ \tilde{U}^{\mathbf{I}}(g_{tr},k;N)\,\chi(v) + [1-\chi(v)]\left[\tilde{W}^{\mathbf{I}}(g_{tr},k;N) - \tilde{W}^{\mathbf{II}}(g_{tr},k;N)\right] = 0 \end{cases}\Bigg|_{g_{tr}\in\mathbf{S}^{\varepsilon,\mu,\sigma}} \tag{3.61}$$

(in the case of E-polarization) and

$$\begin{cases} \tilde{W}^{\mathbf{I}}(g_{tr},k;N) = \tilde{W}^{\mathbf{II}}(g_{tr},k;N) \\ \tilde{W}^{\mathbf{I}}(g_{tr},k;N)\,\chi(v) + [1-\chi(v)]\left[\tilde{U}^{\mathbf{I}}(g_{tr},k;N) - \tilde{U}^{\mathbf{II}}(g_{tr},k;N)\right] = 0 \end{cases}\Bigg|_{g_{tr}\in\mathbf{S}^{\varepsilon,\mu,\sigma}} \tag{3.62}$$

(in the H-case). Here, $\chi(v)$ is the characteristic function of the strips, i.e., $\chi(v) = 1$ over the strip and zero elsewhere.

The conditions (3.61) and (3.62) have the same form as conditions (3.36), (3.37), (3.38), and (3.39). That is why, for constructing the generalized scattering matrixes in truncated Fourier space in order to resolve the problem (to find out the sets of complex amplitudes $A_n^+(\mathbf{I}) = R_{n0}^{\mathbf{AA}}$ и $A_n^-(\mathbf{II}) = T_{n0}^{\mathbf{BA}}$, $n = 0, \pm 1, ..., \pm N$, of scattered field in domains **A** and **B**) it is necessary to repeat all those steps that we have already done in Section 3.3.3 going to (3.42). Indeed, by defining scattering matrix S^{grt} by relations

$$S^{grt} = \begin{bmatrix} S_{11} & S_{12} \\ S_{21} & S_{22} \end{bmatrix}; \begin{bmatrix} A_{\mathbf{I}}^+ \\ A_{\mathbf{II}}^- \end{bmatrix} = \begin{bmatrix} S_{11} & S_{12} \\ S_{21} & S_{22} \end{bmatrix} \begin{bmatrix} A_{\mathbf{I}}^- \\ A_{\mathbf{II}}^+ \end{bmatrix},$$

from (3.61) and (3.62) we derive:

$$S^{grt} = \begin{bmatrix} V_T^+(\mathbf{I}) & -V_T^-(\mathbf{II}) \\ \left[C_T^+(\mathbf{I}) + \tilde{D}_T^+(\mathbf{I})\right] & -\tilde{D}_T^-(\mathbf{II}) \end{bmatrix}^{-1} \begin{bmatrix} -V_T^-(\mathbf{I}) & V_T^+(\mathbf{II}) \\ -\left[C_T^-(\mathbf{I}) + \tilde{D}_T^-(\mathbf{I})\right] & \tilde{D}_T^+(\mathbf{II}) \end{bmatrix}$$

(for *E*-polarized field) and

$$S^{grt} = \begin{bmatrix} \tilde{V}_T^+(\mathbf{I}) & -\tilde{\varepsilon}^{-1}\tilde{V}_T^-(\mathbf{II}) \\ \left[\tilde{C}_T^+(\mathbf{I}) + D_T^+(\mathbf{I})\right] & -D_T^-(\mathbf{II}) \end{bmatrix}^{-1} \times$$

$$\times \begin{bmatrix} -\tilde{V}_T^-(\mathbf{I}) & \tilde{\varepsilon}^{-1}\tilde{V}_T^+(\mathbf{II}) \\ -\left[\tilde{C}_T^-(\mathbf{I}) + D_T^-(\mathbf{I})\right] & D_T^+(\mathbf{II}) \end{bmatrix}$$

(for *H*-polarized field). Here, $V_T^{\pm}$ and $\tilde{V}_T^{\pm}$ are the transposed matrices $V^{\pm}$ and $\tilde{V}^{\pm}$ (see Section 3.3.3); $C_T^{\pm}$, $\tilde{C}_T^{\pm}$, $D_T^{\pm}$, and $\tilde{D}_T^{\pm}$ are the transposed matrices $C^{\pm} = V^{\pm}\bar{K}$, $\tilde{C}^{\pm} = \tilde{V}^{\pm}\bar{K}$, $D^{\pm} = V^{\pm}\underline{K}$, and $\tilde{D}^{\pm} = \tilde{V}^{\pm}\underline{K}$; $\bar{K} = \{\bar{\chi}_{nm}\}_{n,m=-N}^{N}$ and $\underline{K} = \{\underline{\chi}_{nm}\}_{n,m=-N}^{N}$; and

$$\overline{\chi}_{n,m} = \int_0^l \chi(v) e^{i(\Phi_m - \Phi_n)v} dv, \; \underline{\chi}_{n,m} = \int_0^l [1 - \chi(v)]\, \mathrm{e}^{i(\Phi_m - \Phi_n)v} dv.$$

Now we provide some numerical results to illustrate the effectiveness of the presented method. Let us first emphasize that the convergence of the method has been checked against usual criteria such as energy conservation (up to 10^{-9}) and reciprocity laws (see Section 1.2.1). We begin by considering flat gratings, and ascertain, that we have managed to repeat [171] the rigorous results obtained with the method of the Riemann–Hilbert problem (see [45] and Section 2.2). For *E*- and *H*-polarization, for various angles of incidence α_0^i within wide range of frequency

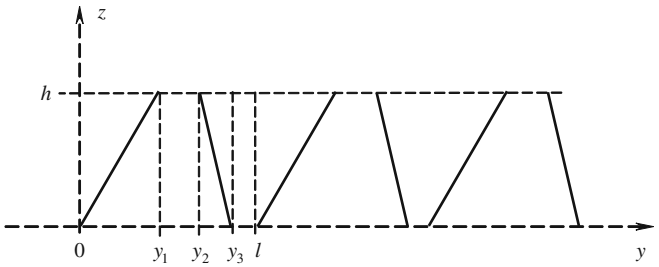

Fig. 3.9 Schematic view of a nonplanar strip grating

$\kappa = l/\lambda$, the absolute values of the difference $R_{n0}^{\mathbf{AA}} - \tilde{R}_{n0}^{\mathbf{AA}}$ between the present method ($R_{n0}^{\mathbf{AA}}$) and rigorous analysis ($\tilde{R}_{n0}^{\mathbf{AA}}$) are less than $6 \cdot 10^{-4}$.

In the second example, and for the purpose of validation, we compare our results to those obtained by an integral approach [172]. The profile is trapezoidal as depicted in Fig. 3.9 and the metal is deposited along the lateral sides of the trapezium. As can be seen from Fig. 3.10, where the reflected efficiencies are drawn as functions of the parameter $\kappa = l/\lambda$, our results coincide exactly with those of [172]. Furthermore, we verified that by setting the strips on one horizontal part of the trapezium we recover the results computed by use of the classical planar CBCM.

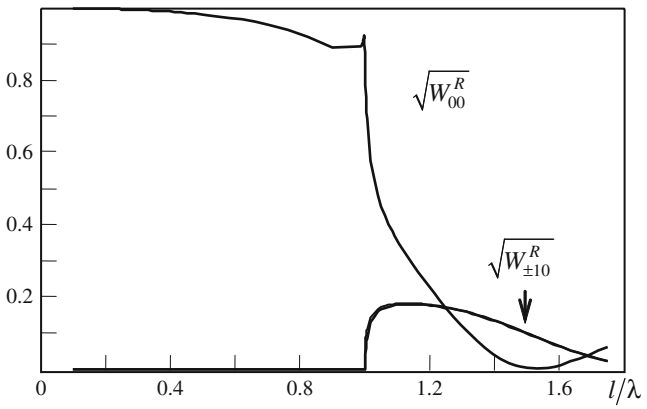

Fig. 3.10 *E*-polarization. Evolution of the square root of the reflected efficiencies W_{n0}^R, $n = 0, \pm 1$ versus $\kappa = l/\lambda$, $\alpha_0^i = 0.1°$. The structure is depicted in Fig. 3.9. The strips are assumed to be deposed on the inclined facets of a trapezoidal profile with $y_2 = y_1 = l - y_3 = l/3$ and $y_1 = h \operatorname{tg}(\pi/6)$

3.6 Several Issues of Spectral Theory Relevant to C-Method Formalism

Here we shall discuss several mathematical issues concerning the C-method that are in the focus of the present book: the continuation of diffraction problems into the complex plane of frequency parameters and a comparative investigation of diffraction and spectral problems.

There is a wide set of different possibilities to formulate the spectral problems. From mathematical point of view, all of them have equal rights for existence. But, as it often happens in theoretical physics, the correctness of one or another models can be justified by its mathematical consequences only, i.e., by mathematical results following from the formulation, by possibility of their reasonable physical interpretation and their utility level for modeling of corresponding physical processes, as well as for profound understanding of the processes' inner nature. Just this originates the principal reason that made us to choose (among many possibilities) such posing of spectral problem, which is, from one side, strictly connected with excitation problem and, from the other side, is based on the idea of analytic continuation of operator of this excitation problem in relevant complex-valued frequency domain.

It is clear that any correctly formulated diffraction problem (for real-valued frequencies) should have the solution, which is unique. From the other side, there are well-known resonant phenomena, which become apparent, when frequency of excitation field is varying. It is natural to think these phenomena as a result of an existence of some eigenoscillations of electromagnetic field round the obstacle. If such eigenoscillations cannot exist for real frequencies, relevant question arises: do they exist in a domain of complex-valued frequencies? Moreover, are they allowed and are they able to exist? What mathematical object can be treated as such eigenoscillation? It is necessary to outline that within the scope of one of the possible and even traditional way of spectral problems formulation (when eigenfunctions supposed to be square integrable in the space $\mathbf{R}^2$ or $\mathbf{R}^3$) the answers are negative: eigenoscillations are forbidden for complex-valued frequencies.

That is why we have chosen the formulation of spectral problem in which eigenoscillations are allowed to exist and they are in strong connection with solutions of diffraction problem for real-valued frequencies. This strong connection is based on the idea of analytic continuation of diffraction boundary value problem operator from real frequencies into the relevant domain (Riemannian surface) of complex-valued frequencies (see Section 1.3). More exactly, it is necessary to construct the relevant formulation of diffraction problem considered for complex-valued frequencies.

The procedure of analytic continuation of resolvent of corresponding operator in complex-valued domain of spectral parameter, which is frequency in our case, is well known in functional analysis and in the theory of boundary value problems. The presence of poles of this continuation means the absence of uniqueness and existence of nontrivial solution of corresponding homogeneous functional equation for such values of spectral parameter, the residuals of resolvent in

these poles are strictly connected with eigenvectors of the direct initial operator and so on. It can be shown (see [11]) that the approach of analytic continuation of direct operator of boundary value problem, which we are using here, is essentially equivalent to analytic continuation of the above-mentioned operator resolvent.

Thus, the principal step in our way of construction of spectral theory is the formulation of diffraction boundary value problem in relevant domain (infinite-sheeted Riemannian surface) of complex-valued frequencies. We would like to point out once again that the formulation chosen has predetermined the mathematical consequences and the utility for understanding of physical essence of the real diffraction problem – the problem with real-valued frequencies.

3.6.1 The Diffraction Problem Formulation for Real-Valued Frequencies

In this section, we consider the standard formulation of diffraction problem for real-valued wave number $k = 2\pi/\lambda$, where λ is a wavelength of incident field in vacuum, doing in the way similar to [19] (see also Section 1.2.1). After that, in the next section, we discuss the necessary changes in formulation for complex-valued k.

We consider the structure of two dielectric media, which both together fill whole space $\mathbf{R}^3$ (see Fig. 3.11). The structure is homogenous along the x-axis as well as the boundary surface $\mathbf{S}^{\varepsilon,\mu,\sigma}$ between the two media. The smooth and one-connected contour $\mathbf{S}_x^{\varepsilon,\mu,\sigma}$ is a generator of surface in the plane $x = 0$ (i.e., $\mathbf{S}_x^{\varepsilon,\mu,\sigma}$ is the boundary line between two media). Contour $\mathbf{S}_x^{\varepsilon,\mu,\sigma}$ is given by l-periodic function $z = f(y)$, $-h \le f(y) \le 0$, its maximum deviation from the y-axis is equal to $h < \infty$. The upper medium is assumed to be a vacuum and the lower medium have constant complex-valued material parameters $\tilde{\varepsilon}$ and $\tilde{\mu}$.

The incident time harmonic field $\tilde{U}_0^i(g,k) = \exp\left[i(\Phi_0 y - \Gamma_0 z)\right]$, $g = \{y,z\}$, is given in the domain $\mathbf{A}$ (in the domain $z > 0$) and is supposed to be E-polarized:

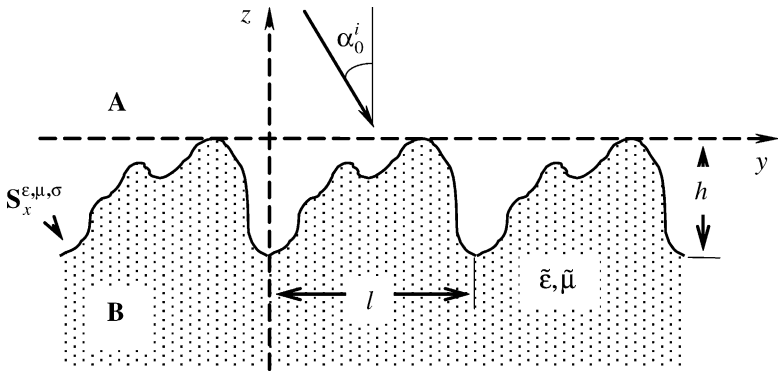

Fig. 3.11 Presentation of the problem

$\tilde{U}_p^i(g,k) = \tilde{E}_x^i(g,k)$ and $\tilde{E}_y^i = \tilde{E}_z^i = \tilde{H}_x^i = 0$ (the case of H-polarized incident field can be investigated in a very similar way). The time factor is chosen as $\exp(-ikt)$, and it is omitted everywhere below. It is evident and can be shown easily that the total field $\tilde{U}(g,k)$ is E-polarized too: $\tilde{E}_x = \tilde{U}$, $\tilde{E}_y = \tilde{E}_z = \tilde{H}_x = 0$, and

$$\begin{cases} \left[\frac{\partial^2}{\partial y^2} + \frac{\partial^2}{\partial z^2} + \tilde{\varepsilon}(g)\,\tilde{\mu}(g)\,k^2\right]\tilde{U}(g,k) = 0; \qquad g = \{y,z\} \in \mathbf{R}^2 \\ \tilde{U}\left\{\frac{\partial \tilde{U}}{\partial y}\right\}(l,z,k) = \mathrm{e}^{2\pi i\Phi}\,\tilde{U}\left\{\frac{\partial \tilde{U}}{\partial y}\right\}(0,z,k) \\ \tilde{U}(g,k) = \begin{cases} \tilde{U}_0^i(g,k) + \sum\limits_{n=-\infty}^{n=\infty} R_{np}^{\mathbf{AA}} \exp\left[i\left(\Phi_n y + \Gamma_n^{\mathbf{A}} z\right)\right]; \qquad z \geq 0 \\ \sum\limits_{n=-\infty}^{n=\infty} T_{np}^{\mathbf{BA}} \exp\left[i\left(\Phi_n y - \Gamma_n^{\mathbf{B}}(z+h)\right)\right]; \qquad z \leq -h \end{cases} \end{cases}, \tag{3.63}$$

$$\tilde{H}_y = \frac{1}{ik\eta_0\tilde{\mu}(g)}\frac{\partial \tilde{U}}{\partial z},\ \tilde{H}_z = -\frac{1}{ik\eta_0\tilde{\mu}(g)}\frac{\partial \tilde{U}}{\partial y}. \tag{3.64}$$

Here, $\Phi_n = 2\pi(\Phi + n)/l$, $\Gamma_n^{\mathbf{A}} = \sqrt{k^2 - \Phi_n^2}$, $\Gamma_n^{\mathbf{B}} = \sqrt{k^2\tilde{\varepsilon}\tilde{\mu} - \Phi_n^2}$, Φ is some real-valued parameter, $\tilde{\varepsilon}(g)$ and $\tilde{\mu}(g)$ are relative permittivity and magnetic conductivity of corresponding dielectric medium, respectively, and is free space impedance. The angle $\alpha_0^i = \arcsin\left(\Phi_0/k\right)$ is an angle of incidence of the excitation wave $\tilde{U}_0^i(g,k)$ on the grating (see Fig. 3.11). The standard boundary conditions on the boundary surface between two media are requirement of continuity of the tangential components of the total electromagnetic field. By means of the formulas (3.64), these conditions can be written in the following standard form:

$$\tilde{U}^{(+)}(g,k) = \tilde{U}^{(-)}(g,k),\ \frac{\partial \tilde{U}^{(+)}(g,k)}{\partial \vec{n}_g} = \frac{1}{\tilde{\mu}}\frac{\partial \tilde{U}^{(-)}(g,k)}{\partial \vec{n}_g},\ g \in \mathbf{S}_x^{\varepsilon,\mu,\sigma}. \tag{3.65}$$

Here, subscripts $(+)$ and $(-)$ denote (uniform on the contour $\mathbf{S}_x^{\varepsilon,\mu,\sigma}$) limits of functions $\tilde{U}(g,k)$ and $\partial\tilde{U}(g,k)/\partial\vec{n}_g$ of arguments $g \pm r\vec{n}_g$ when $r \to +0$, $\vec{n}_g$ is the unit normal to the contour $\mathbf{S}_x^{\varepsilon,\mu,\sigma}$ in a point $g \in \mathbf{S}_x^{\varepsilon,\mu,\sigma}$, which is the direction arbitrarily chosen for the contour and fixed after that.

The essential part of diffraction boundary value problem definition is a radiation condition formulation. Several comments worth to be done about the philosophy and the history of the question before the radiation condition formulating.

We would like to remind the reader that a radiation condition from mathematical point of view is a kind of such closure of the boundary value problem formulation, which guarantees the uniqueness of the solution to the diffraction boundary value problem. At the same time, the radiation condition should be chosen in such a form that this unique solution has reasonable physical sense. Standard choice of the radiation condition is that one, which corresponds to the presence in the secondary (scattered) field of outgoing waves only, without waves coming from the infinity. The last statements above look like something trivial and well known. Nevertheless, it looks like the meaning of the words "outgoing waves" should be explained in

more thoroughly. One of the most fundamental physical principle is the energy conservation law. Thus, outgoing waves, in this context, means that energy of scattered field must always go to the infinity (and never comes from the infinity) independent of the fact in what kind of the medium we are considering the scattering process. The values of the square roots of $\Gamma_n^{\mathbf{A}} = \sqrt{k^2 - \Phi_n^2}$ and $\Gamma_n^{\mathbf{B}} = \sqrt{k^2\tilde{\varepsilon}\tilde{\mu} - \Phi_n^2}$ in formula (3.63) are chosen according to this conception, both for ordinary ($\operatorname{Re}\tilde{\varepsilon}(g) > 0$, $\operatorname{Re}\tilde{\mu}(g) > 0$) and for double-negative ($\operatorname{Re}\tilde{\varepsilon}(g) < 0$, $\operatorname{Re}\tilde{\mu}(g) < 0$) materials.

The physical meaning of radiation conditions for domains **A** ($z > 0$) and **B** ($z < -h$)

$$\tilde{U}(g,k) = \begin{cases} \tilde{U}_0^i(g,k) + \sum\limits_{n=-\infty}^{n=\infty} R_{np}^{\mathbf{AA}} \exp\left[i\left(\Phi_n y + \Gamma_n^{\mathbf{A}} z\right)\right]; & z \geq 0 \\ \sum\limits_{n=-\infty}^{n=\infty} T_{np}^{\mathbf{BA}} \exp\left[i\left(\Phi_n y - \Gamma_n^{\mathbf{B}}(z+h)\right)\right]; & z \leq -h \end{cases} \tag{3.66}$$

is the restriction of scattering field by outgoing and decaying waves only, i.e., elimination of plane waves that bring energy from infinity to some vicinity of the contour $\mathbf{S}_x^{\varepsilon,\mu,\sigma}$. If the contour $\mathbf{S}_x^{\varepsilon,\mu,\sigma}$ is piecewise smooth only and, for example, some point $g_0 \in \mathbf{S}_x^{\varepsilon,\mu,\sigma}$ is an edge point of $\mathbf{S}_x^{\varepsilon,\mu,\sigma}$, then boundary conditions (3.65) cannot be applied in point g_0 (even because normal vector in g_0 is not defined). Without going into too deep mathematical details (connected with the theory of generalized functions and Sobolev's spaces) for more general mathematical posing of the diffraction problem, one may use in the neighborhood **V** of point g_0 the condition of field energy finiteness

$$\int\limits_{\mathbf{V}} \left\{ \left|\tilde{U}(g,k)\right|^2 + \left|\operatorname{grad}\tilde{U}(g,k)\right|^2 \right\} dv < \infty. \tag{3.67}$$

3.6.2 Diffraction Problem for Complex-Valued Frequencies

In this section, we discuss the necessary changes in the problem formulation for complex k. For better understanding the situation, one can consider canonic quasi-periodic Green function (see also Section 3.2.1)

$$\tilde{G}_0(g,g_0,k,\Phi) = -\frac{i}{2l} \sum_{n=-\infty}^{\infty} \mathrm{e}^{i\left[\Phi_n(y-y_0)+\Gamma_n|z-z_0|\right]} \Gamma_n^{-1}. \tag{3.68}$$

The points g and g_0 belong to free space $\mathbf{R}^2$ where $\varepsilon = \mu = 1$ and, respectively, $\Gamma_n = \Gamma_n^{\mathbf{A}} = \sqrt{k^2 - \Phi_n^2}$. For the real-valued k, we have

$$\operatorname{Re}\Gamma_n \operatorname{Re} k \geq 0 \text{ and } \operatorname{Im}\Gamma_n \geq 0 \tag{3.69}$$

that correspond to the radiation condition for outgoing waves.

It can be proved (see Section 1.1.4) that function (3.68), considered as one of argument k, can be analytically continued [by means of the same formula (3.68)]

from real axis $\operatorname{Im} k = 0$ onto Riemannian surface $\mathbf{K}$ with complex plane cuts, which are starting in points $k_n^{\pm} = \pm|\Phi_n|$, $n = 0, \pm 1, \pm 2,...$, and going to infinity like, for example, curves

$$(\operatorname{Re} k)^2 - (\operatorname{Im} k)^2 - \Phi_n^2 = 0,\ n = 0, \pm 1, \pm 2,...,\ \operatorname{Im} k \le 0 \tag{3.70}$$

that are represented in Fig. 1.2a. The function thus obtained is an analytic function for any $k \neq k_n^{\pm}$ in any sheet of Riemannian surface $\mathbf{K}$. The only singular points of this function are $k_n^{\pm}$, $n = 0, \pm 1, \pm 2,...$, and for local (in vicinity of $k = k_n^{\pm}$) variable $\tau_n = \tau_n(k)$ of the kind $\tau_n = \sqrt{k^2 - \left(k_n^{\pm}\right)^2}$ the function has the only simple poles in $\tau_n = 0$ [10]. The first sheet (which sometimes is referred as the physical one) of Riemannian surface $\mathbf{K}$ is defined by conditions (3.69) and complex plane cuts (3.70). The consequent sheets differ from the first one by opposite choice of signs of Γ_n for a few corresponding indices n.

It is necessary to underline that the function $\tilde{G}_0(g,g_0,k,\Phi)$ gives the solution to the "diffraction problem" for the system of quasi-periodic point sources in the absence of obstacles. The question arises: what new quality should one expect in the presence of boundary surface, which separates two different media, when both media are extending to infinity (in the way half-space like)? It is clear that two Green functions are naturally involved now, namely, $\tilde{G}_0(g,g_0,k,\Phi)$ and $\tilde{G}_0\left(g,g_0,k\sqrt{\tilde{\varepsilon}\tilde{\mu}},\Phi\right)$, which satisfy radiation conditions (3.66) in the upper and the lower half-spaces, respectively. Due to this the Riemannian surface $\bar{\mathbf{K}}$ of analytic continuation of the corresponding boundary value problem operator with respect to k be somehow doubled Riemannian surface $\mathbf{K}$. More exactly, it is necessary to consider two sets of branch points

$$k_n^{\pm}(\mathbf{A}) = \pm|\Phi_n| \text{ and } k_n^{\pm}(\mathbf{B}) = \pm\frac{|\Phi_n|}{n_{\mathbf{B}}},\ n = 0, \pm 1, \pm 2,...,$$

where $n_{\mathbf{B}} = \sqrt{\tilde{\varepsilon}\tilde{\mu}}$ is a number calculated according to conception of outgoing waves in the medium whose parameters are $\tilde{\varepsilon}$ and $\tilde{\mu}$ [10, 173–175]. That is why, it is natural to generalize the formulation of diffraction problem (considered in the previous section for real-valued k) for the case of complex-valued k in the following way. At first, we suppose that wave number k belongs to Riemannian surface $\bar{\mathbf{K}}$. At second, radiation conditions (3.66) for each given $k \in \bar{\mathbf{K}}$ have the same form, but the signs of square roots of $\Gamma_n^{\mathbf{A}} = \sqrt{k^2 - \Phi_n^2}$ and $\Gamma_n^{\mathbf{B}} = \sqrt{k^2\tilde{\varepsilon}\tilde{\mu} - \Phi_n^2}$ must be taken according to the rule of sheet, which k is belonging to. At third, all the other conditions are exactly the same as ones for real-valued k.

Thus, the only formal difference in the diffraction problems formulation for complex- and real-valued k is that now we consider k belonging to relevant Riemannian surface, instead of the previous case for $\operatorname{Im} k = 0$. We would like to emphasize the significant difference between the diffraction problem considered and diffraction problem for finite obstacles, where well-known Sommerfeld radiation conditions are traditionally applied. The procedure of analytic continuation

into the domain of complex-valued k requires changing of Sommerfeld condition by Reichardt radiation condition (see details in [10, 11]). However, for the infinite periodic structure under consideration the radiation conditions in form (3.66) are valid (see below) for both real- and complex-valued k as described above. The reason of such difference is that Sommerfeld condition is one of a kind of asymptotic requirement, but Reichardt condition as well as conditions (3.66) are the exact series representations in a vicinity of the infinite point.

As we have had already mentioned earlier, the usefulness of one or another formulation of diffraction problem for complex-valued k is based on the mathematical consequences from such posing, namely, on qualitative properties of the solution and on its connection with the solutions for real-valued k. The detailed explanation of such qualitative mathematical consequences requires a lot of space, and we shall not dwell on it here. We restrict ourselves here by brief explanation of the several facts that justify the formulation chosen above.

Taking into account radiation condition (3.66) and using standard Green's formulas technique, one can represent total field $\tilde{U}(g,k)$, $g \in \mathbf{R}^2 \backslash \mathbf{S}_x^{\varepsilon,\mu,\sigma}$, as an integral over one period of the boundary contour $\mathbf{S}_x^{\varepsilon,\mu,\sigma}$ with integrand formed by the linear combination of the functions

$$\tilde{G}_0(g,g_0,kn,\Phi)\,\frac{\partial \tilde{U}(g_0,k)}{\partial \vec{n}_{g_0}} \text{ and}$$

$$\frac{\partial \tilde{G}_0(g,g_0,kn,\Phi)}{\partial \vec{n}_{g_0}}\,\tilde{U}(g_0,k)\,,\ g_0 \in \mathbf{S}_x^{\varepsilon,\mu,\sigma},\ \ n = n_{\mathbf{A}} = 1 \text{ or } n = n_{\mathbf{B}}.$$

Substitution of this representation into the boundary conditions (3.65) gives the system of two integro-differential equations of the first kind. Analytic regularization method reduces this system to functional equation of the second kind in the way similar to one described in [10, 11]. After that the technique similar to one described in [10] gives the result that a resolvent of a diffraction boundary value problem operator treated as a function of $k \in \bar{\mathbf{K}}$ is a finite-meromorphic operator-function in surface $\bar{\mathbf{K}}$. Function $\tilde{U}(g,k)$, $k \in \bar{\mathbf{K}}$, may have poles of finite multiplicity only, and upper half-plane of first sheet of $\bar{\mathbf{K}}$ has no singularity at all (see more details in Section 1.3). Thus, the diffraction problem formulation that is chosen for the complex-valued k really gives natural analytic continuation of diffraction problem for real-valued k.

Unfortunately, the Riemannian surface $\bar{\mathbf{K}}$ constructed in such way has rather complicated structure, especially if one takes into account complex-valued and (or) negative material parameters $\tilde{\varepsilon}$ and $\tilde{\mu}$. This leads to the rotation of the branch points as well as to the rotation of the contours of the corresponding cuts and, consequently, to crossing of such curves generated by the first (upper) and the second (lower) medium. Thus, it is necessary to change the cuts curves, and it is not easy to make this in a uniform way. From formal mathematical point of view, the positions and shapes of cuts are out of any importance (if the cuts have the same starting and ending points), because all Riemannian surfaces thus obtained are equivalent. But the complexity or the simplicity of the system of these cuts is very important from

practical and, in particular, numerical points of view. The simpler the better, especially when complexity is higher than the limits of our ability to understand, and it seems to us that for cuts structure of a two media we are very near to these limits. That is why we call the formulation of diffraction problem in complex domain, which is described above, as the global one with the only one frequency parameter for both media. The alternative posing is the local one, when for each medium its own spectral parameter is chosen and all others parameters of the other medium are frozen, i.e., are fixed in physical domain of their definition [135]. The local formulation has a few evident advantages in comparison with the global one. The first of them is the simplicity: corresponding Riemannian surface has much more simple structure. The second advantage is that it is possible to investigate influence of the corresponding medium that may essentially simplify the understanding of inner nature of diffraction processes.

3.6.3 Spectral Problem and Its Solution: Some Physical Results

In this section, we formulate and solve numerically the spectral problem for complex-valued k. The spectral problem is strictly connected with corresponding diffraction problem considered in the previous section. As shown in [1, 10] (see also Section 1.3), the diffraction problem for complex-valued k always has the solution and the solution is unique, if only $k \notin \Omega_k$, where $\Omega_k = \left\{\bar{k}_n\right\}$ is the frequency spectrum of the grating as an open periodic resonator. If $k = \bar{k}_n$, the homogeneous diffraction problem ($\tilde{U}_0^i(g,k) \equiv 0$) is solvable in a nontrivial way in $\bar{\mathbf{K}}$, and the corresponding solutions $u_0^{(j)}\left(g,\bar{k}_n\right)$, $j = 1,2,...,J$, have the meaning of free states (oscillations) of the field in the structure at the eigenfrequency $\bar{k}_n$. Here, J is the number of linearly independent eigenfunctions $u_0^{(j)}\left(g,\bar{k}_n\right)$ (the number of different free oscillations of the field) related to the eigenvalue (eigenfrequency) $\bar{k}_n$.

Thus, the following spectral problem naturally arises: it is necessary to find such values $\bar{k}_n \in \bar{\mathbf{K}}$, for which homogeneous (i.e., $\tilde{U}_0^i(g,k) \equiv 0$) boundary value problem has nontrivial solutions $u_0^{(j)}\left(g,\bar{k}_n\right)$. In accordance with the terminology of the previous section, we call the spectral problem described as global spectral problem (one spectral parameter k for both media). For its numerical analysis there was an effective algorithm, grounded on classical C-method and some simple regularizing procedures, suggested and realized in [135]. Below, we briefly comment a number of physical results from this paper.

3.6.3.1 Connection Between Spikes in Diffraction Characteristics and Eigen Regimes

In our investigation of diffraction properties of gratings we followed the approach used in [1, 10], considering the periodic grating as an open periodic resonator (OPR). The assumption that resonant transmission or reflection from the periodic boundary treated as OPR is related to the excitation of regimes close to eigen ones

in the region of the boundary $\mathbf{S}_x^{\varepsilon,\mu,\sigma}$ has been inspired by the following facts: when parameters of the problem are close to ones providing the spikes in diffraction characteristics a decrease in the value of the determinant of the system of equations of corresponding boundary value problem and an increase in the field intensity near the boundary do emerge.

To prove this statement we have studied the frequency responses of the different gratings activated by *E*- and *H*-polarized plane waves and the field patterns formed by gratings in the resonant regimes. The latter are rather interesting and useful characteristics, giving more profound understanding of the resonant phenomena. We would like to attract the attention to the fact that in the case of *H*-polarization, the first resonances appears at much smaller frequency parameter, that is, for more long waves. This resonance exists due to the possibility of excitation of *TEM*-waves that are propagating along the grooves and, under certain parameters, are able to provide the resonance. Naturally, this resonance disappears at certain value of h_{TEM} that corresponds to the minimal depth of grooves that can provide resonance conditions for *TEM*-waves.

The impressive illustration of the correlation between spikes in the diffraction characteristics and excitation in OPR oscillations close to eigen ones can be obtained from the consideration of electromagnetic wave diffraction by the dielectric layer, limited by two periodic boundaries. In Fig. 3.12 we present the curves $W_{n0}^R(k)$ ($W_{n0}^R = \left|R_{n0}^{\mathbf{AA}}\right|^2 \mathrm{Re}\Gamma_n^{\mathbf{A}} \big/ \Gamma_0^{\mathbf{A}}$; see Section 1.2.1) and the table, demonstrating the correspondence of resonances at the real frequencies $k = K_n$ and relevant complex eigenfrequencies $\bar{k}_n$. It is clearly seen here that the values of K_n are close to $\mathrm{Re}\,\bar{k}_n$ and the values of $\mathrm{Im}\,\bar{k}_n$ are very small.

3.6.3.2 Spectral Properties of the Grating with Negative Material Parameters

The above-described solution to the spectral and, naturally, diffraction problem and corresponding complementary algorithms can simulate the electromagnetic field interaction in materials characterized by negative material parameters. Therefore, we are able to provide the feedback study: spectral characteristics $\leftrightarrow$ diffraction characteristics. In order to prove the efficiency and perspective advantages of such a study we shall discuss here one result of the simulation that seems to be rather distinctive for the materials with $\mathrm{Re}\,\tilde{\varepsilon} < 0$ and (or) $\mathrm{Re}\,\tilde{\mu} < 0$.

In Fig. 3.13 there are two characteristic cases of *E*- and *H*-polarized waves diffraction by periodic boundary between two media, when one of them occupying the domain **B** has negative magnetic conductivity ($\mathrm{Re}\,\tilde{\mu} < 0$) and $\tilde{\varepsilon} = 2.25$. Fig.

Fig. 3.12 (continued) The diffraction and spectral characteristics for the dielectric layer with $\tilde{\varepsilon} = 4.4$, $\tilde{\mu} = 1$ of thickness h_{reg} normally excited with *E*-polarized plane wave. The layer limited with the *upper boundary* $z = 0.5 - 4\pi^{-2}\left(\cos(y) + \cos(3y)/9 + \cos(5y)/25\right)$ and the *lower boundary* that is the mirror image of the *upper boundary*. *Solid line* corresponds to $h_{reg} = 0.5\pi$; *dashed line* corresponds to the layer with $h_{reg} = 0.1\pi$

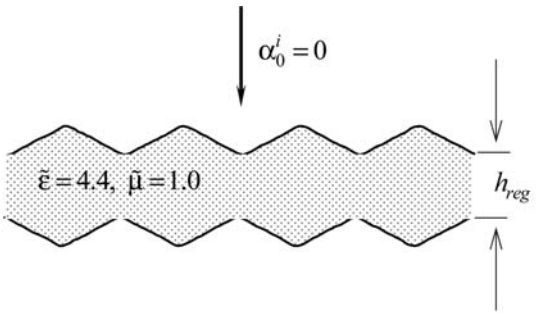

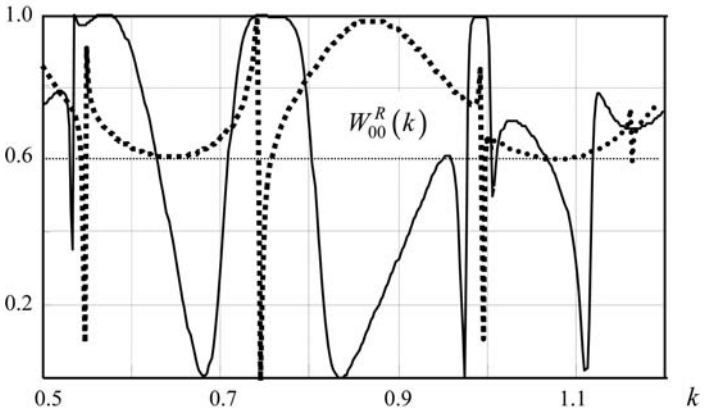

h_{reg}	K_n	$\mathrm{Re}\,\bar{k}_n$	$\mathrm{Im}\,\bar{k}_n$
0.1π	0.549	0.5485	–0.0004
	0.749	0.7455	–0.0000
	0.999	0.9971	–0.0000
	1.171	1.1691	–0.0007
0.5π	0.528	0.5255	–0.0000
	0.680	0.6600	–0.0000
	0.728	0.7085	–0.0484
	0.822	0.8067	–0.0305
	0.972	0.975	–0.0051
	0.981	0.987	–0.0000
	1.03	1.0058	–0.0048
	1.15	1.1144	–0.005

Fig. 3.12 (continued)

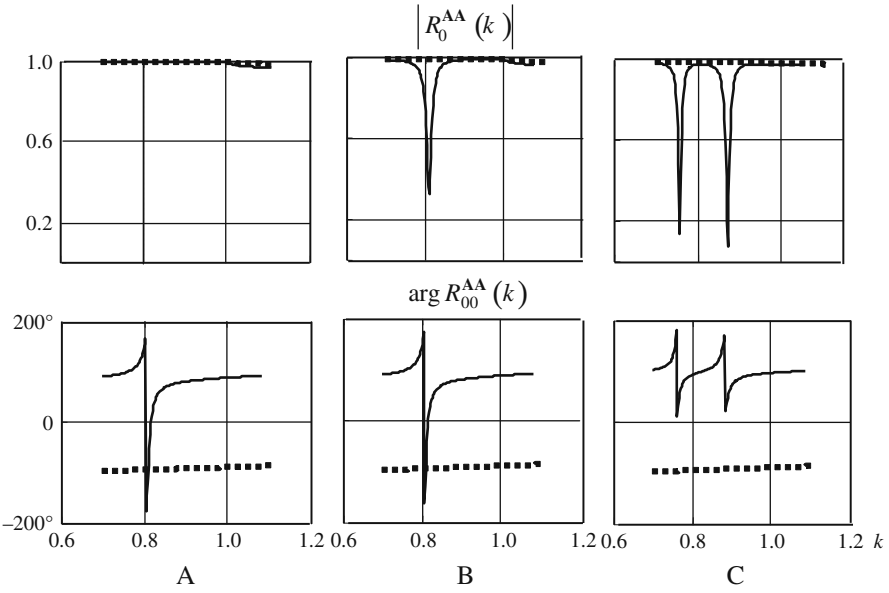

Fig. 3.13 The amplitude and phase of propagating harmonic reflected by boundary $z = 0.4 \times \left[\sin^2(y/2) - 1.0\right]$: $\tilde{\varepsilon} = 2.25$, $\mathrm{Re}\,\tilde{\mu} = -5.0$, *solid curves* correspond to *E*-polarization; *dotted* to *H*-polarization. For *E*-polarization and for $\Phi = 0$, $\mathrm{Im}\,\tilde{\mu} = 0$, the grating has the eigenfrequency $\bar{k} = 0.813 - i0.0$. (**a**) $\mathrm{Im}\,\tilde{\mu} = 0$, $\alpha_0^i = 0$; (**b**) $\mathrm{Im}\,\tilde{\mu} = 0.1$, $\alpha_0^i = 0$; (**c**) $\mathrm{Im}\,\tilde{\mu} = 0.1$, $\alpha_0^i = 5°$

3.13a illustrates the resonance that appears for normal excitation of the boundary, when $\mathrm{Im}\,\tilde{\mu} = 0$. In this case, the resonance may be seen in the curve of $\arg R_{00}^{\mathbf{AA}}(k)$ for *E*-polarized waves only, as we have total reflection of the incident wave, and $\left|R_{00}^{\mathbf{AA}}(k)\right| \approx 1.0$.

By introducing the losses in the second medium we can make the resonance to be manifested for the amplitude of reflection filed also (see Fig. 3.13b). While oblique excitation, even with rather small angles, say $\alpha_0^i = 5.0°$ (see Fig. 3.13c), the resonance splits into two, moving from initial position in frequency into two different directions. The amplitudes of evanescent harmonics in scattering field are suffering pronounced resonant spikes also.

Naturally, similar situation emerges for *H*-polarized wave diffraction by periodic boundary with medium parameters $\mathrm{Re}\,\tilde{\varepsilon} < 0$ and $\mathrm{Re}\,\tilde{\mu} > 0$. In contrast to the resonance appearing for *E*-polarization, that has been discussed above, this resonance does not disappear with depth of grooves h decreasing, even for $h \approx 0.01$ (see Fig. 3.14, where the evolution of resonances with h decreasing and various $\tilde{\varepsilon}$ are presented). It is worthwhile to point out that the Q-factor of this resonance increases when h decreases. That allows us to conclude that resonances of the type are characteristic for periodic boundaries and are connected with excitation of polarizations. All these resonances have corresponding complex eigenfrequencies $\bar{k}$ with $\mathrm{Im}\,\bar{k} \approx 10^{-8}$, that means within the algorithm accuracy these resonances have real eigenfrequencies.

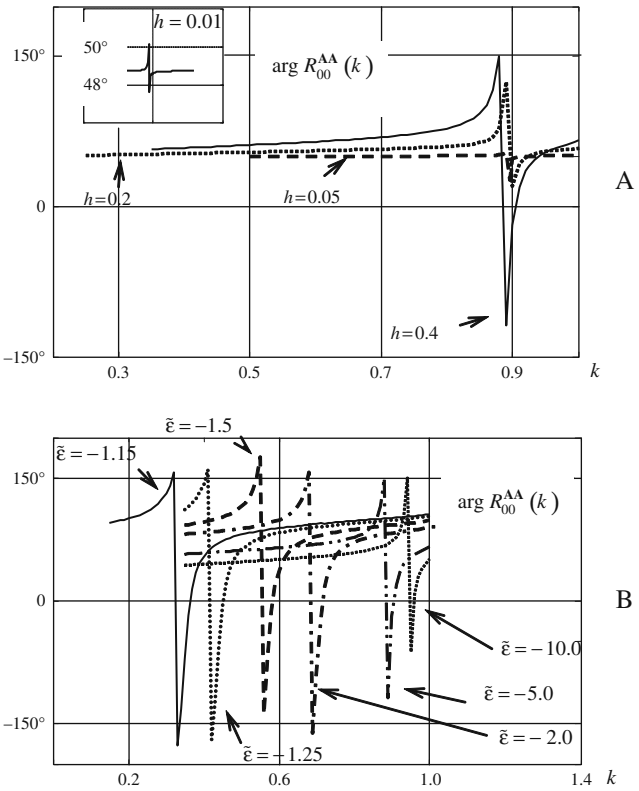

Fig. 3.14 The low-frequency super high-Q resonance of *H*-polarized field for different depths of grating profile $z = h\left[\sin^2(y/2) - 1.0\right]$: $\tilde{\mu} = 1$ and $\Phi = 0$. (**a**) $\tilde{\varepsilon} = -5.0$; (**b**) $h = 0.4$. For grating with $\tilde{\varepsilon} = -5.0$ and $h = 0.4$, the eigenfrequency $\bar{k} = 0.893 - i0.0$

For the special case, say for *H*-polarization, when $\tilde{\varepsilon} < 0$, $\tilde{\mu} > 0$, and $|\tilde{\varepsilon}| > 1.0$, under condition $\delta = h/l \ll 1$, the approximation

$$\operatorname{Re}\bar{k} = \sqrt{\frac{\tilde{\varepsilon}^2 - 1}{\tilde{\varepsilon}\,(\tilde{\varepsilon} - \tilde{\mu})}}\,(1 + O(\delta))\,,\ \left|\operatorname{Im}\bar{k}\right| = O(\delta^2)$$

can be obtained. The fields, corresponding to these eigenfrequencies, are concentrated in the vicinity of the boundary $\mathbf{S}_x^{\varepsilon,\mu,\sigma}$ (see, for example, Fig. 10 in the paper [135], where this type of resonances, supplied with the eigenfield structures for two different shapes of boundary are presented).

Among numerous results of computational experiments carried out for double-negative materials we have chosen to present here the absorption resonance appearing in diffracted field from periodic surface of left-handed material when incident plane electromagnetic wave is almost parallel to the *y*-axis. Figure 3.15a shows the pronounced resonance for rather smooth ($h = 0.1\,l$) periodic surface of left-handed (double negative) material illuminated with *E*-polarized plane wave with

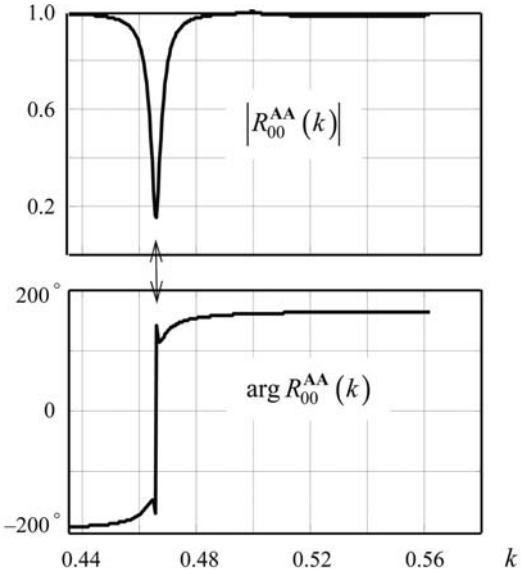

A

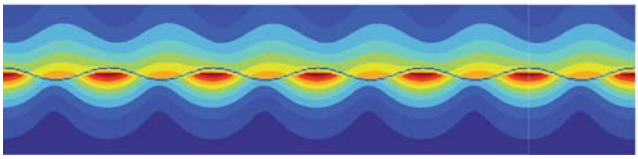

B

Fig. 3.15 (**a**) Reflection coefficient and (**b**) field strength $\left|\tilde{E}_x(g,K)\right| = \text{const}$ computed at frequency of maximal absorption (marked with *arrow*) for the double negative material surface with boundary $z = 0.5\,h\,(\cos(y) - 1)$; $h = 0.1\,l$. *E*-polarization: $\tilde{\varepsilon} = -0.2 + i0.01$, $\tilde{\mu} = -1.5 + i0.01$, incidence angle $\alpha_0^i = 88°$, complex eigenfrequency $\bar{k} = 0.4645 - i0.0012$

incidence angle $\alpha_0^i = 88°$. The real-valued resonant frequency may be estimated for surface with $\delta \ll 1$ from approximate formula

$$\bar{k} \approx 1 \Big/ \left(\sin\left(\alpha_0^i\right) + \sqrt{\left(\tilde{\mu}^2 - 1\right) \Big/ \left(\tilde{\mu}^2 - \tilde{\varepsilon}\tilde{\mu}\right)} \right).$$

For *H*-polarization, the resonance frequency may be defined approximately from

$$\bar{k} \approx 1 \Big/ \left(\sin\left(\alpha_0^i\right) + \sqrt{\left(\tilde{\varepsilon}^2 - 1\right) \Big/ \left(\tilde{\varepsilon}^2 - \tilde{\varepsilon}\tilde{\mu}\right)} \right).$$

When $\delta \ll 1$, these approximate values of resonant frequencies are in good agreement with calculated ones by rigorous solution of problem under consideration. In our case the eigenfrequency $\bar{k} = 0.4645 - i0.0012$ of corresponding natural oscillation that has been found out from the solution to spectral problem is in good correlation with diffraction resonance. Periodic surface eigenfield intensity is concentrated near the boundary at the frequency $k = K = 0.466$, corresponding to maximal electromagnetic energy absorption (see Fig. 3.15b where the field pattern $\left|\tilde{E}_x\,(g,K)\right| = \text{const}$ is presented).

Chapter 4
Modeling and Analysis of Transients in Periodic Structures: Fully Absorbing Boundaries for 2-D Open Problems

Abstract The chapter is concentrated on the description of the construction and implementation of new rigorous methods and techniques oriented to the solution of open initial boundary value problems of the electromagnetic theory of gratings. The formulation and incorporation of explicit absorbing conditions into conventional numerical routines of finite-difference algorithms constitute the basis of the method. An essential point is that such conditions restrict in a correct and efficient way the computational domain without introducing any distortion into the nature of the scattering process, simulated by means of the mathematics.

Study of transient electromagnetic waves [1, 4, 6, 176–180] is a dominating trend in theoretical radio physics today because, first and foremost, many and varied means of communications, electronics, and radiolocation are not possible without profound insights into spatial–temporal and spatial–frequency field transformations in relevant quite sophisticated electromagnetic structures, whereas the potential of traditional frequency domain approaches is to a large extent already exhausted. Additionally, the time domain approaches:

- are free from some frequency domain idealizations;
- are universal, as limitations imposed on geometrical and constitutive parameters of considered objects are at a minimum;
- make possible the construction of explicit and straightforward computational routines (without inversion of any operators) that are rather efficient (limited time and memory resources required) and solve the problem under consideration within a reasonable time;
- furnish results which are easy to translate into a standard set of frequency domain characteristics.

However, in the shift toward time domain approaches we still face problems whose complete and justified solution takes a great deal of analytic efforts. These are, e.g., problems with correct and effective truncation of the computation space in the so-called open problems whose analysis domain tends to infinity along one or several spatial directions, the far-zone treatment, the problems of large and distant sources of the fields, etc. [1, 4]. Problems of this kind are considered in Chapter 4,

Y.K. Sirenko, S. Ström (eds.), *Modern Theory of Gratings*, Springer Series in Optical Sciences 153, DOI 10.1007/978-1-4419-1200-8_4,

in the part concerned with 2-D initial boundary value problems for infinite and finite gratings. The topical themes of Chapter 4 are:

- exact absorbing conditions (EACs) for open initial boundary value problems of diffraction grating theory;
- time domain and frequency domain methods combined in the study of gratings as open resonators;
- spatial–temporal and spatial–frequency transformations of electromagnetic field, including cases of possible resonant wave scattering.

Available heuristic and approximate solutions to problems associated with the finite domain transition in analysis of open time domain problems are mostly based on using of the so-called absorbing boundary conditions (ABCs) [181–183] and the perfectly matched layers (PMLs) [184–186]. A weak point of these solutions is the unpredictable behavior of computational errors when the observation time t is large. As a consequence, the results obtained are not safe to rely upon in the event of the resonant wave scattering.

In this chapter, an approach will be elaborated which allows us to estimate correctly and minimize the errors caused by the translation of open initial boundary problems into corresponding closed problems. It is based on the exact absorbing conditions, on their construction, and on building them into the standard scheme of the finite-difference method. The EACs addition to the starting initial boundary problem turns it into the equivalent closed problem. The history of the approach dates back to 1986, when A.R. Maykov, A.G. Sveshnikov, and S.A. Yakunin first formulated [187] the exact nonlocal conditions for virtual boundaries across a regular semi-infinite hollow waveguide as a channel to transmit signals formed by a waveguide unit. Afterward this approach based on the usage of radiation condition for spatial–time amplitudes of partial components (modes) of nonsinusoidal waves, outgoing from effective sources and scatterers was modified and adapted (refer, e.g., to [1, 40, 188–195]) to a great variety of problems in theoretical and applied radio physics. Its validity and efficiency has been repeatedly proved by numerical experiments and special tests.

4.1 Infinite Gratings: Exact Absorbing Conditions for Plane Parallel Floquet Channel

In Sections 4.1 and 4.2, we obtain some important results relative to the proper truncation of the computational domain in the open 2-D initial boundary value problems of the electromagnetic theory of gratings. By passing on to the some special transforms of the functions describing physically realizable sources, such problems for infinite gratings can be reduced to those of scattering of transient waves by compact inhomogeneities in the plane parallel Floquet channel $\mathbf{R} = \{g \in \mathbf{R}^2 : 0 < y < l\}$

(see Section 1.1.3) or, in other words, in the plane parallel waveguide with specific (quasi-periodic) boundary conditions.

4.1.1 Transformation of Evolutionary Basis of a Signal in a Regular Floquet Channel

Let us rewrite the problems (1.18) for semitransparent infinite gratings (see Fig. 4.1) in the following simplified form (indexes *new* are dropped):

$$\begin{cases} \left[-\varepsilon\mu\frac{\partial^2}{\partial t^2}-\sigma\mu\frac{\partial}{\partial t}+\frac{\partial^2}{\partial y^2}+\frac{\partial^2}{\partial z^2}\right]U(g,t)=F(g,t); \quad g=\{y,z\}\in\mathbf{Q}, \quad t>0 \\ U(g,0)=\varphi(g), \quad \frac{\partial}{\partial t}U(g,t)\big|_{t=0}=\psi(g); \quad g\in\bar{\mathbf{Q}} \\ E_{tg}(p,t)\big|_{p=\{x,y,z\}\in\mathbf{S}}=0; \quad t\geq 0 \\ U\left\{\frac{\partial U}{\partial y}\right\}(l,z,t)=e^{2\pi i\Phi}U\left\{\frac{\partial U}{\partial y}\right\}(0,z,t); \quad t\geq 0 \end{cases} . \tag{4.1}$$

Here, in the *E*-polarization case, $U(g,t)=E_x(g,t)$ and $\mu(g)$ is a piecewise constant function. For the *H*-polarized fields, $U(g,t)=H_x(g,t)$ and $\varepsilon(g)$, $\sigma(g)$ are piecewise constant functions. Φ is a real parameter. The surfaces $\mathbf{S}=\mathbf{S}_x\times[|x|\leq\infty]$ of the perfectly conducting elements in geometry of gratings assumed to be sufficiently smooth. Also, we suppose (here and from this point on) that the continuity conditions for the tangential components of the field strength vectors will be fulfilled in those cases where it is necessary. The analysis domain $\mathbf{Q}$ for problems (4.1) is part of the Floquet channel $\mathbf{R}$ bounded by curves $\mathbf{S}_x$: $\mathbf{Q}=\mathbf{R}\backslash\overline{\text{int}\mathbf{S}_x}$. The complex-valued functions $U(g,t)$, $F(g,t)$, and so on are special images of real functions describing the actual fields and sources (see Section 1.1.3). It is assumed that the functions $F(g,t)$, $\varphi(g)=U^i(g,0)$, $\psi(g)=\partial U^i(g,t)\big/\partial t\big|_{t=0}$ ($U^i(g,t)$ is the incident wave), $\sigma(g)$, $\varepsilon(g)$–1, and $\mu(g)$–1, being finitary in the closure of $\mathbf{Q}$, satisfy the theorem of unique solvability of problems (4.1) in the Sobolev space $\mathbf{W}_2^1(\mathbf{Q}^T)$, $\mathbf{Q}^T=\mathbf{Q}\times(0;T)$, $T<\infty$ (see Statement 1.1 and work [5]). The supports of the functions $F(g,t)$, $\varphi(g)$, and $\psi(g)$ belong to the set $\overline{\mathbf{Q}_L}\backslash\mathbf{L}$, $\mathbf{Q}_L=\{g\in\mathbf{Q}: -L_2-h<z<L_1\}$, $L_1\geq 0$ and $L_2\geq 0$. The regular parts $\mathbf{A}$ and $\mathbf{B}$ of the channel $\mathbf{R}$ (the parts $z>L_1$ and $z<-L_2-h$ of the domain ${}_L\mathbf{Q}=\mathbf{Q}\backslash(\mathbf{Q}_L\cup\mathbf{L})=\mathbf{A}\cup\mathbf{B}$), along which the field formed by the grating propagate infinitely far, are free from the sources and scatterers. Here, $\mathbf{L}=\mathbf{L}_1\cup\mathbf{L}_2$ is the artificial boundary which separates the domain $\mathbf{Q}_L$ from the domain ${}_L\mathbf{Q}$. It is denoted by dashed lines in Fig. 4.1.

Take, for definiteness sake, the upper ($z>L_1$) regular part of the $\mathbf{R}$ channel. Here, $\varepsilon(g)=\mu(g)\equiv 1$ and $\sigma(g)=\varphi(g)=\psi(g)=F(g,t)\equiv 0$. By assuming that the excitation $U(g,t)$ in domain $\mathbf{Q}_L$ has not yet reached the boundary $\mathbf{L}_1$ ($z=L_1$) by the time $t=0$, we obtain via the separation of variables the following representation for the solutions $U(g,t)$ to (4.1):

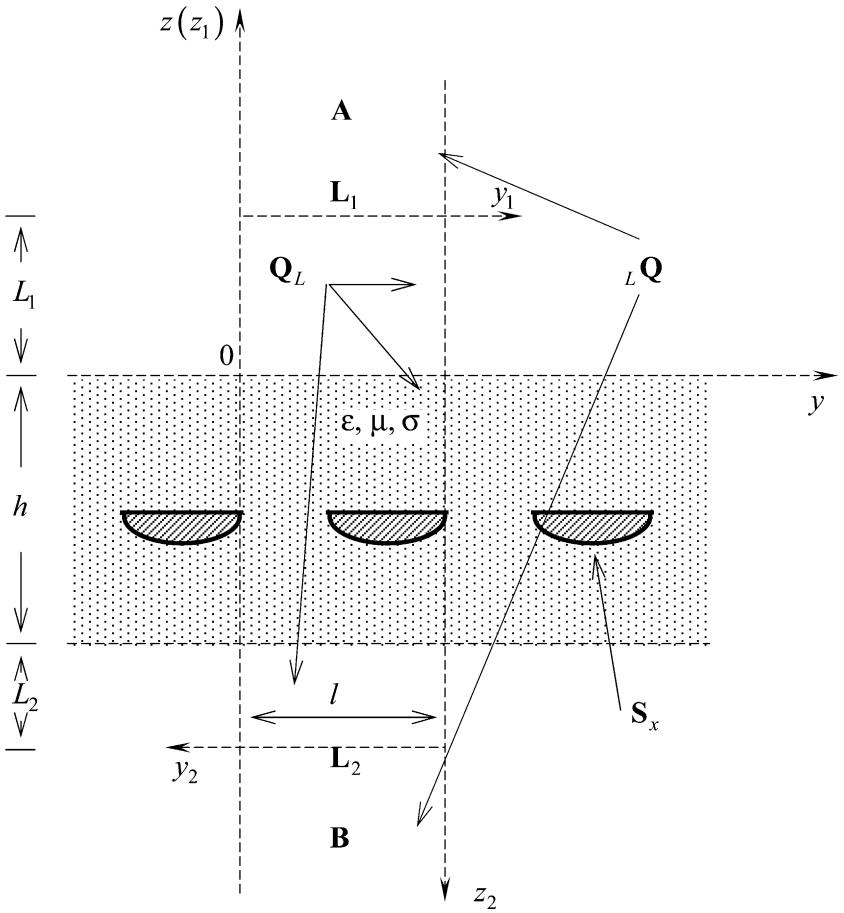

Fig. 4.1 Geometry of model problems (4.1)

$$U(g,t) = \sum_{n=-\infty}^{\infty} u_n(z,t)\,\mu_n(y); \qquad z \geq L_1, \qquad 0 \leq y \leq l, \qquad t \geq 0. \tag{4.2}$$

The orthonormal system $\{\mu_n(y)\}$ of transversal, complete in the space $\mathbf{L}_2(0;l)$ functions of the form $\mu_n(y) = l^{-1/2}\exp(i\Phi_n y)$; $\Phi_n = (n+\Phi)\,2\pi/l$, $n = 0,\pm1,\ldots$ comes from the nontrivial solutions of the homogeneous (spectral) problem

$$\begin{cases} \left[\frac{d^2}{dy^2} + \Phi_n^2\right]\mu_n(y) = 0; \qquad 0 < y < l \\ \mu_n\left\{\frac{d\mu_n}{dy}\right\}(l) = \mathrm{e}^{2\pi i\Phi}\mu_n\left\{\frac{d\mu_n}{dy}\right\}(0) \end{cases}. \tag{4.3}$$

The spatial–time amplitudes $\{u_n(z,t)\}$ (evolutionary basis) of the signal $U(g,t)$ are available from the solutions of the initial boundary value problems

$$\begin{cases} \left[-\frac{\partial^2}{\partial t^2}+\frac{\partial^2}{\partial z^2}-\Phi_n^2\right]u_n\,(z,t)=0; & t>0 \\ u_n\,(z,0)=0, \quad \frac{\partial}{\partial t}u_n\,(z,t)\big|_{t=0}=0 \end{cases}; z\geq L_1,\, n=0,\pm 1,\pm 2,... \quad (4.4)$$

The cosine Fourier transform of (4.4) with respect to $\bar{z}=z-L_1$ on the semi-axis $\bar{z}\geq 0$ (image $\leftrightarrow$ original)

$$\begin{aligned} \tilde{f}\,(\omega)=F_c\left[f\right](\omega)\equiv\sqrt{\tfrac{2}{\pi}}\int\limits_0^\infty f\,(\bar{z})\cos(\omega\,\bar{z})\,d\,\bar{z} \quad \leftrightarrow \\ \leftrightarrow \quad f\,(\bar{z})=F_c^{-1}\left[\tilde{f}\right](\bar{z})\equiv\sqrt{\tfrac{2}{\pi}}\int\limits_0^\infty \tilde{f}\,(\omega)\cos(\omega\,\bar{z})\,d\omega \end{aligned} \quad (4.5)$$

results in the following Cauchy problems for the images $\tilde{u}_n\,(\omega,t)$:

$$\begin{cases} D\left(\sqrt{\Phi_n^2+\omega^2}\right)\left[\tilde{u}_n(\omega,t)\right]\equiv\left[\frac{\partial^2}{\partial t^2}+(\Phi_n^2+\omega^2)\right]\tilde{u}_n\,(\omega,t)=-\sqrt{\tfrac{2}{\pi}}\bar{u}_n'(0,t); \\ \qquad \omega>0, \quad t>0 \\ \tilde{u}_n\,(\omega,0)=0, \quad \frac{\partial}{\partial t}\tilde{u}_n\,(\omega,t)\big|_{t=0}=0; \quad \omega\geq 0 \end{cases}. \quad (4.6)$$

Here, $\tilde{u}_n\,(\omega,t) \quad \leftrightarrow \quad \bar{u}_n\,(\bar{z},t)=u_n\,(z,t)$ and $\bar{u}_n'\,(0,t)=\partial\bar{u}_n\,(\bar{z},t)\big/\partial\,\bar{z}\big|_{\bar{z}=0}$. It has also been considered that

$$-\omega^2\tilde{f}\,(\omega)-\sqrt{\frac{2}{\pi}}\left[\frac{d}{d\,\bar{z}}f\,(\bar{z})\right]\Big|_{\bar{z}=0} \quad \leftrightarrow \quad \frac{d^2}{d\,\bar{z}^2}f\,(\bar{z})\,,$$

and that the wave $U(z,t)$ in the region **A** does not contain components propagating in the sense of decreasing z. The outgoing components toward $z=\infty$ are equal to zero for sufficiently large z at any finite instant of time $t=T$.

By extending the functions $\tilde{u}_n\,(\omega,t)$ with zero on the semi-axis $t<0$, let us pass on to the generalized statement of the Cauchy problems (4.6) [2]:

$$\begin{aligned} D\left(\sqrt{\Phi_n^2+\omega^2}\right)\left[\tilde{u}_n(\omega,t)\right]\equiv\left[\tfrac{\partial^2}{\partial t^2}+(\Phi_n^2+\omega^2)\right]\tilde{u}_n\,(\omega,t)=-\sqrt{\tfrac{2}{\pi}}\bar{u}_n'\,(0,t)+ \\ +\delta^{(1)}\,(t)\,\tilde{u}_n\,(\omega,0)+\delta\,(t)\,\tfrac{\partial}{\partial t}\tilde{u}_n\,(\omega,t)\big|_{t=0}=-\sqrt{\tfrac{2}{\pi}}\bar{u}_n'\,(0,t); \\ \omega>0, \qquad -\infty<t<\infty. \end{aligned} \quad (4.7)$$

Here, $\delta(\ldots)$ is the Dirac delta function and $\delta^{(m)}(\ldots)$ is its generalized mth derivative. The convolution of the fundamental solution $G(\lambda,t)=\chi(t)\lambda^{-1}\sin\lambda t$ of the operator $D(\lambda)$ (see Section 1.1.3 and [1]) with the right-hand side of equation (4.7) gives the following representation of $\tilde{u}_n\,(\omega,t)$:

$$\tilde{u}_n(\omega,t) = -\sqrt{\frac{2}{\pi}} \int_0^t \sin\left[(t-\tau)\sqrt{\Phi_n^2+\omega^2}\right] \frac{\bar{u}_n'(0,\tau)}{\sqrt{\Phi_n^2+\omega^2}} d\tau;\ \omega \geq 0, \qquad t \geq 0. \tag{4.8}$$

After application to (4.8) of the inverse Fourier transform (4.5), we obtain

$$\bar{u}_n(\bar{z},t) = -\int_0 J_0\left[\Phi_n\left((t-\tau)^2-\bar{z}^2\right)^{1/2}\right] \chi\left[(t-\tau)-\bar{z}\right] \bar{u}_n'(0,\tau)\, d\tau; \quad \bar{z} \geq 0,\ t \geq 0, \tag{4.9}$$

from which it follows that

$$u_n(z,t) = -\int_0 J_0\left[\Phi_n\left((t-\tau)^2-(z-L_1)^2\right)^{1/2}\right] \chi\left[(t-\tau)-(z-L_1)\right] u_n'(L_1,\tau)\, d\tau; \quad z \geq L_1,\ t \geq 0. \tag{4.10}$$

The expressions (4.10) displays the general property of the solutions $U(g,t)$ to problems (4.1) in the subdomain ${}_L\mathbf{Q}$, namely, the solutions satisfying zero initial conditions and being free of the components (modes) propagating toward the compact inhomogeneity of the channel $\mathbf{R}$ (toward the domain $\mathbf{Q}_L$). These expressions define the diagonal transport operator $Z_{L_1\to z}(t)$ (see references [1, 40, 196, 197]), which operates according to the rule

$$u(z,t) = \{u_n(z,t)\} = Z_{L_1\to z}(t)\left[u'(L_1,\tau)\right];\ u'(b,\tau) = \left\{u_n'(b,\tau)\right\}, \quad z \geq L_1,\ t \geq \tau \geq 0$$

and enables us to trace changes of the transient wave field during its free propagation along the finite regular section of the $\mathbf{R}$ channel. Here, $J_m(\ldots)$ is the Bessel cylindrical function, $\chi(\ldots)$ is the Heaviside step function,

$$u_n'(b,t) = \left.\frac{\partial u_n(z,t)}{\partial z}\right|_{z=b} = \int_0^l \left.\frac{\partial U(g,t)}{\partial z}\right|_{z=b} \mu_n^*(y)\, dy, \tag{4.11}$$

and the asterisk $*$ stands for the complex conjugation.

4.1.2 Nonlocal Absorbing Conditions

Consider the case when the observation point in (4.10) is on the artificial boundary $\mathbf{L}_1$ ($z = L_1$). Then

$$u_n(L_1,t) = -\int_0 J_0\left[\Phi_n(t-\tau)\right] \chi(t-\tau)\, u_n'(L_1,\tau)\, d\tau;\ t \geq 0. \tag{4.12}$$

Differentiation of (4.12) with respect to t gives

$$\left[\frac{\partial}{\partial t}+\frac{\partial}{\partial z}\right]u_n(z,t)\Big|_{z=L_1}=\Phi_n\int\limits_0 J_1\left[\Phi_n(t-\tau)\right]\chi(t-\tau)\,u_n'(L_1,\tau)\,d\tau;\ t\geq 0 \tag{4.13}$$

on account of the familiar relationships $dJ_0(x)\big/dx=-J_1(x)$, $J_0(0)=1$, and $\chi^{(1)}(t-\tau)=\delta(t-\tau)$, where $\chi^{(1)}(\ldots)$ is the generalized derivative of $\chi(\ldots)$.

Next, the application of the Laplace transform in t (image $\leftrightarrow$ original)

$$\tilde{f}(s)=L\left[f\right](s)\equiv\int\limits_0^\infty f(t)\,\mathrm{e}^{-st}dt\quad\leftrightarrow\quad f(t)=L^{-1}\left[\tilde{f}\right](t)\equiv\frac{1}{2\pi i}\int\limits_{\alpha-i\infty}^{\alpha+i\infty}\tilde{f}(s)\,\mathrm{e}^{st}\,ds \tag{4.14}$$

in view of the familiar formulas $\tilde{f}_1(s)\tilde{f}_2(s)\ \leftrightarrow\ \int\limits_0^t f_1(t-\tau)f_2(\tau)\,d\tau$ (the convolution theorem), $\lambda^2\left[\sqrt{s^2+\lambda^2}\left(\sqrt{s^2+\lambda^2}+s\right)\right]^{-1}\ \leftrightarrow\ \lambda J_1(\lambda t)$ [198], and $s\tilde{f}(s)-f(0)\ \leftrightarrow\ df(t)\big/dt$ gives (in the space of images $\tilde{u}_n(z,s)$)

$$\left[\frac{\partial}{\partial z}+s\right]\tilde{u}_n(z,s)\Big|_{z=L_1}=\frac{\Phi_n^2\,\tilde{u}_n'(L_1,s)}{\sqrt{s^2+\Phi_n^2}\left(\sqrt{s^2+\Phi_n^2}+s\right)}, \tag{4.15}$$

and finally

$$\tilde{u}_n'(L_1,s)=-\left(s+\frac{\lambda_n^2}{s+\sqrt{s^2+\lambda_n^2}}\right)\tilde{u}_n(L_1,s)\,. \tag{4.16}$$

The inverse Laplace transform of (4.16), in view of $\left(s+\sqrt{s^2+\lambda^2}\right)^{-1}\ \leftrightarrow\ (\lambda t)^{-1}J_1(\lambda t)$ [199], allows us to return to the original functions $u_n(z,t)$

$$\left[\tfrac{\partial}{\partial t}+\tfrac{\partial}{\partial z}\right]u_n(z,t)\Big|_{z=L_1}=-\Phi_n\int\limits_0 J_1\left[\Phi_n(t-\tau)\right](t-\tau)^{-1}\chi(t-\tau)\,u_n(L_1,\tau)\,d\tau;\quad t\geq 0. \tag{4.17}$$

The translation of (4.13) into (4.17) [the validity of transformations (4.14)] rests upon the assertion [8] that at some points g of any bounded subdomain inside a **Q** domain, the field $U(g,t)$ from a set of compact support sources cannot grow faster than $\exp(\alpha t)$ as $t\to\infty$, where $\alpha>0$ is a constant. The assertion is true for any electromagnetic structure whose spectrum Ω_k does not contain points $\bar{k}$ of the upper half-plane of the first (physical) sheet of the surface giving the natural variation range of the complex frequency parameter k. This holds for all the gratings considered in Chapter 4 (see Section 1.3.2).

In terms of (4.2) and (4.11), expressions (4.12), (4.13), and (4.17) become

$$U(y,L_1,t) = -\sum_{n=-\infty}^{\infty}\left\{\int_0^t J_0\left[\Phi_n(t-\tau)\right]\left[\int_0^l \frac{\partial U(\tilde{y},z,\tau)}{\partial z}\Big|_{z=L_1}\mu_n^*(\tilde{y})\,d\tilde{y}\right]d\tau\right\}\mu_n(y) =$$
$$= V_1(y,t);\ 0 \le y \le l,\ t \ge 0, \tag{4.18}$$

$$\left[\frac{\partial}{\partial t}+\frac{\partial}{\partial z}\right]U(y,z,t)\Big|_{z=L_1} =$$
$$= \sum_{n=-\infty}^{\infty}\left\{\int_0^t J_1\left[\Phi_n(t-\tau)\right]\left[\int_0^l \frac{\partial U(\tilde{y},z,\tau)}{\partial z}\Big|_{z=L_1}\mu_n^*(\tilde{y})\,d\tilde{y}\right]d\tau\right\}\Phi_n\mu_n(y) =$$
$$= V_2(y,t);\ 0 \le y \le l,\ t \ge 0, \tag{4.19}$$

$$\left[\frac{\partial}{\partial t}+\frac{\partial}{\partial z}\right]U(y,z,t)\Big|_{z=L_1} =$$
$$= -\sum_{n=-\infty}^{\infty}\left\{\int_0^t J_1\left[\Phi_n(t-\tau)\right](t-\tau)^{-1}\left[\int_0^l U(\tilde{y},L_1,\tau)\,\mu_n^*(\tilde{y})\,d\tilde{y}\right]d\tau\right\}\times$$
$$\times\,\Phi_n\mu_n(y) = V_3(y,t);\ 0 \le y \le l,\ t \ge 0. \tag{4.20}$$

Let us consider the possibility of (4.18), (4.19), and (4.20) to play the part of the boundary conditions for restriction of the analysis domain **Q** of open problems (4.1). Using the results from references [1, 2, 5, 40, 187, 200] we advance.

Statement 4.1 *Problems (4.1) and problems (4.1) supplemented with any one of conditions (4.18), (4.19), and (4.20) are equivalent. The requirements that ensure their unique solvability (correctness classes) are identical.*

Formulas (4.18), (4.19), and (4.20) are exact. Hence their addition to the original problems does not actually increase the computation error or distort the process of simulation.

In the problem (4.1) with (4.18), (4.19), and (4.20), the instant (for $\tau = t$) impacts of the function $U(g,\tau)$ that is in the right-hand side functions $V_j(y,t)$ can be entirely excluded. Hence, during the calculation, when "moving" through time layers, the functions $V_j(y,t)$ may be considered as known ones, determined at the previous layers $\tau < t$.

Relations (4.12), (4.13), (4.17) and (4.18), (4.19), and (4.20) constitute the exact radiation conditions for the outgoing transient waves formed by the grating. Formulas (4.12), (4.13), and (4.17) describe the behavior of spatial–temporal amplitudes of all partial components (modes) of the waves guided by the regular channel **R** in the direction $z \to \infty$. The behavior of these wave fields as a whole is governed

by formulas (4.18), (4.19), and (4.20). Therefore, the open problems (4.1) are equivalent to problems (4.1) whose analysis domain $\mathbf{Q}_L$ is finite, with any condition of (4.18), (4.19), and (4.20) types met on the virtual boundaries $\mathbf{L}_1$ and $\mathbf{L}_2$. By the same reason, conditions (4.18), (4.19), and (4.20) can be regarded as exact absorbing conditions: the wave field $U(g,t)$ neither experiences deformation across $\mathbf{L}_1$ boundary nor reflects back into the $\mathbf{Q}_L$ domain, the wave $U(g,t)$ fully transmits to the upper ($z > L_1$) regular part of the $\mathbf{R}$ channel as if it were absorbed by the domain $\mathbf{A}$ or its boundary $\mathbf{L}_1$.

At $V_2(y,t) = V_3(y,t) = 0$, the nonlocal conditions (4.19) and (4.20) coincide with the simplest local classical ABC of the first-order approximation [181, 182]. This means that functions $V_2(y,t)$ and $V_3(y,t)$ determine the ABC residual, or the difference between the exact values of the function $\left[\partial \big/ \partial t + \partial \big/ \partial z\right] U(y,z,t)\big|_{z=L_1}$ and the corresponding figures given in the computational schemes using this approximate absorbing condition. The availability of the residual allows us to estimate the accuracy of the corresponding computational scheme as a whole.

4.1.3 Local Absorbing Conditions

Finite-difference method algorithms employing the nonlocal (both in space and time variables) absorbing conditions (4.18), (4.19), and (4.20) call for substantial memory resources as the $V_j(y,t)$ function databases grow progressively with time. They all are stored to make the next step, proceeding through time layers [40]. The problem can be approached in the following way. We will turn to the local conditions by applying the following scheme which is easy to realize. In view of the representation [201]

$$J_0(x) = \frac{2}{\pi} \int_0^{\pi/2} \cos(x \sin\varphi)\, d\varphi,$$

rewrite (4.12) as

$$u_n(L_1,t) = -\frac{2}{\pi} \int_0^{\pi/2} \left\{ \int_0^{} \cos\left[\Phi_n (t-\tau)\sin\varphi\right] \chi(t-\tau)\, u_n'(L_1,\tau)\, d\tau \right\} d\varphi;\ t \geq 0. \tag{4.21}$$

Introduce

$$w_n(t,\varphi) = -\int_0^{} \frac{\sin\left[\Phi_n (t-\tau)\sin\varphi\right] \chi(t-\tau)\, u_n'(L_1,\tau)}{\Phi_n \sin\varphi}\, d\tau;\ t \geq 0,\ 0 \leq \varphi \leq \pi/2. \tag{4.22}$$

Then

$$\frac{\partial w_n(t,\varphi)}{\partial t} = -\int_0 \cos\left[\Phi_n(t-\tau)\sin\varphi\right]\chi(t-\tau)\,u_n'(L_1,\tau)\,d\tau,$$

and from (4.21) we have

$$u_n(L_1,t) = \frac{2}{\pi}\int_0^{\pi/2} \frac{\partial w_n(t,\varphi)}{\partial t}\,d\varphi;\ t \geq 0. \tag{4.23}$$

The integral form (4.22) is equivalent to the differential formulation below

$$\begin{cases} \left[\frac{\partial^2}{\partial t^2} + \Phi_n^2 \sin^2\varphi\right] w_n(t,\varphi) = -u_n'(L_1,t); & t > 0 \\ w_n(0,\varphi) = \left.\frac{\partial w_n(t,\varphi)}{\partial t}\right|_{t=0} = 0 \end{cases}. \tag{4.24}$$

Indeed, passing from (4.24) to the generalized Cauchy problem and using the fundamental solution $G(\lambda,t) = \chi(t)\lambda^{-1}\sin\lambda t$ of the operator $D(\lambda) \equiv \left[d^2/dt^2 + \lambda^2\right]$ (see Section 1.1.3 and [1]), one easily finds out that (4.22) and (4.24) define one and the same functions $w_n(t,\varphi)$.

Now multiply (4.23) and (4.24) by $\mu_n(y)$ and sum over $n = 0,\pm1,\pm2,\ldots$. On account of

$$\sum_{n=-\infty}^{\infty} \Phi_n^2 w_n(t,\varphi)\mu_n(y) = -\frac{\partial^2 W(y,t,\varphi)}{\partial y^2}$$

for

$$W(y,t,\varphi) = \sum_{n=-\infty}^{\infty} w_n(t,\varphi)\,\mu_n(y)$$

[see problem (4.3)], we obtain

$$U(y,L_1,t) = \frac{2}{\pi}\int\limits_0^{\pi/2} \frac{\partial W(y,t,\varphi)}{\partial t}\, d\varphi;\ t \geq 0,\ 0 \leq y \leq l,$$

$$\begin{cases} \left[\frac{\partial^2}{\partial t^2} - \sin^2\varphi \frac{\partial^2}{\partial y^2}\right] W(y,t,\varphi) = -\left.\frac{\partial U(y,z,t)}{\partial z}\right|_{z=L_1}; \quad 0 < y < l, \quad t > 0. \\ W(y,0,\varphi) = \left.\frac{\partial W(y,t,\varphi)}{\partial t}\right|_{t=0} = 0; \quad 0 \leq y \leq l \\ W\left\{\frac{\partial W}{\partial y}\right\}(l,t,\varphi) = e^{i2\pi\Phi} W\left\{\frac{\partial W}{\partial y}\right\}(0,t,\varphi); \quad t \geq 0 \end{cases} \tag{4.25}$$

This local (both in space and time variable) EAC enables us to efficiently truncate the computation domain when solving problems (4.1) numerically. From here on, $W(y,t,\varphi)$ is an auxiliary function coming from the solution of the separate initial boundary value problem, which is the inner problem with respect to the corresponding condition, and $0 \leq \varphi \leq \pi/2$ is a numerical parameter.

A similar treatment for (4.13) and (4.17) gives the following local EACs, different from (4.25):

$$\left[\frac{\partial}{\partial t} + \frac{\partial}{\partial z}\right] U(y,z,t)\Big|_{z=L_1} = \frac{2}{\pi}\int\limits_0^{\pi/2} W(y,t,\varphi)\cos^2\varphi\, d\varphi; \quad t \geq 0, \quad 0 \leq y \leq l,$$

$$\begin{cases} \left[\frac{\partial^2}{\partial t^2} - \cos^2\varphi \frac{\partial^2}{\partial y^2}\right] W(y,t,\varphi) = -\frac{\partial^2}{\partial y^2}\left[\frac{\partial}{\partial z} U(y,z,t)\Big|_{z=L_1}\right]; \quad 0 < y < l, \quad t > 0 \\ W(y,0,\varphi) = \left.\frac{\partial W(y,t,\varphi)}{\partial t}\right|_{t=0} = 0; \quad 0 \leq y \leq l \\ W\left\{\frac{\partial W}{\partial y}\right\}(l,t,\varphi) = e^{i2\pi\Phi} W\left\{\frac{\partial W}{\partial y}\right\}(0,t,\varphi); \quad t \geq 0, \end{cases} \tag{4.26}$$

$$\left[\frac{\partial}{\partial t} + \frac{\partial}{\partial z}\right] U(y,z,t)\Big|_{z=L_1} = \frac{2}{\pi}\int\limits_0^{\pi/2} \frac{\partial W(y,t,\varphi)}{\partial t}\sin^2\varphi\, d\varphi; \quad t \geq 0, \quad 0 \leq y \leq l,$$

$$\begin{cases} \left[\frac{\partial^2}{\partial t^2} - \cos^2\varphi \frac{\partial^2}{\partial y^2}\right] W(y,t,\varphi) = \frac{\partial^2 U(y,L_1,t)}{\partial y^2}; \quad 0 < y < l, \quad t > 0 \\ W(y,0,\varphi) = \left.\frac{\partial W(y,t,\varphi)}{\partial t}\right|_{t=0} = 0; \quad 0 \leq y \leq l \\ W\left\{\frac{\partial W}{\partial y}\right\}(l,t,\varphi) = e^{i2\pi\Phi} W\left\{\frac{\partial W}{\partial y}\right\}(0,t,\varphi); \quad t \geq 0 \end{cases} . \tag{4.27}$$

Expression (4.26) was obtained by virtue of the formula [202]

$$J_1(x) = \frac{2}{\pi}\int\limits_0^{\pi/2} \sin(x\cos\varphi)\cos\varphi\, d\varphi$$

with the substitutions

$$w_n(t,\varphi) = \Phi_n \int_0 \frac{\sin[\Phi_n(t-\tau)\cos\varphi]\chi(t-\tau)u_n'(L_1,\tau)}{\cos\varphi}\, d\tau;$$
$$t \geq 0,\ 0 \leq \varphi \leq \pi/2.$$

The derivation of (4.27) was through the Poisson integral [201]

$$J_1(x) = \frac{2x}{\pi} \int_0^{\pi/2} \cos(x\cos\varphi)\sin^2\varphi\, d\varphi$$

and

$$w_n(t,\varphi) = -\Phi_n \int_0 \frac{\sin[\Phi_n(t-\tau)\cos\varphi]\chi(t-\tau)u_n(L_1,\tau)}{\cos\varphi}\, d\tau;$$
$$t \geq 0,\ 0 \leq \varphi \leq \pi/2.$$

Under the assumption $W(y,t,\varphi) \equiv 0$ (which cannot be justified), (4.26) and (4.27) reduce to the classical ABC of first-order approximation. Using the trapezoidal rule, the integral in (4.26) is replaced by a finite sum and we end up with an approximate condition that agrees well with that from [183].

By invoking the formulas [202]

$$J_0(x) = \frac{1}{2\pi}\int_{-\pi}^{\pi} \exp(ix\sin\varphi)\, d\varphi \text{ and } J_1(x) = \frac{1}{\pi}\int_0^{\pi} \sin(x\sin\varphi)\sin\varphi\, d\varphi,$$

one also arrives at the following local EACs:

$$U(y,L_1,t) = -\tfrac{1}{2\pi}\int_{-\pi}^{\pi} W(y,t,\varphi)\, d\varphi; \qquad 0 \leq y \leq l, \qquad t \geq 0,$$
$$\begin{cases} \left[\frac{\partial}{\partial t} - \sin\varphi\frac{\partial}{\partial y}\right] W(y,t,\varphi) = \frac{\partial}{\partial z}U(y,z,t)\Big|_{z=L_1}; \quad 0 < y < l, \quad t > 0 \\ W(y,0,\varphi) = \frac{\partial W(y,t,\varphi)}{\partial t}\Big|_{t=0} = 0; \quad 0 \leq y \leq l \\ W\left\{\frac{\partial W}{\partial y}\right\}(l,t,\varphi) = e^{i2\pi\Phi} W\left\{\frac{\partial W}{\partial y}\right\}(0,t,\varphi); \quad t \geq 0 \end{cases}, \tag{4.28}$$

$$\left[\frac{\partial}{\partial t} + \frac{\partial}{\partial z}\right] U(g,t)\Big|_{z=L_1} = \frac{1}{\pi}\int_0^{\pi} W(y,t,\varphi)\, d\varphi; \qquad 0 \leq y \leq l, \qquad t \geq 0,$$
$$\begin{cases} \left[\frac{\partial^2}{\partial t^2} - \sin^2\varphi\frac{\partial^2}{\partial y^2}\right] W(y,t,\varphi) = -\sin^2\varphi\frac{\partial^2}{\partial y^2}\left[\frac{\partial U^s(g,t)}{\partial z}\Big|_{z=L_1}\right]; \\ \qquad 0 < y < l, \quad t > 0 \\ W(y,0,\varphi) = \frac{\partial W(y,t,\varphi)}{\partial t}\Big|_{t=0} = 0; \quad 0 \leq y \leq l \\ W\left\{\frac{\partial W}{\partial y}\right\}(l,t,\varphi) = e^{i2\pi\Phi} W\left\{\frac{\partial W}{\partial y}\right\}(0,t,\varphi); \quad t \geq 0 \end{cases}. \tag{4.29}$$

Conditions (4.28), (4.29) are concerned with (4.12), (4.13) and (4.18), (4.19) in the same way as (4.25), (4.26). Here, we have made the substitutions

$$w_n(t,\varphi) = \int_0^t \exp\left[i\Phi_n(t-\tau)\sin\varphi\right] u_n'(L_1,\tau)\,d\tau;\ |\varphi| \le \pi, \tag{4.30}$$

$$w_n(t,\varphi) = \Phi_n \sin\varphi \int_0^t \sin\left[\Phi_n(t-\tau)\sin\varphi\right] u_n'(L_1,\tau)\,d\tau;\ 0 \le \varphi \le \pi,$$

to derive conditions (4.28) and (4.29), respectively. Note the new technical detail – the differential form $\left[\partial \big/ \partial t - i\Phi_n \sin\varphi\right] w_n(t,\varphi) = u_n'(L_1,\tau)$ [from which follows the equation with respect to $W(y,t,\varphi)$ in the inner initial boundary value problem in (4.28)], which is equivalent to the integral form (4.30), has been constructed with the help of the fundamental solution $G(\lambda,t) = \chi(t)\exp(-\lambda t)$ of the operator $[d/dt + \lambda]$ (see Section 1.1.3 and [1]).

We return now to the representation (4.2) for the lower regular part $z < -L_2 - h$ of the **R** channel as well as for its upper part and construct the following initial boundary value problems similar to (4.4):

$$\begin{cases} \left[-\frac{\partial^2}{\partial t^2} + \frac{\partial^2}{\partial z^2} - \Phi_n^2\right] u_n(z,t) = 0, & t > 0 \\ u_n(z,0) = 0, \quad \frac{\partial}{\partial t} u_n(z,t)\big|_{t=0} = 0 \end{cases}; z \le -L_2 - h,\ n = 0, \pm 1, \pm 2, \ldots \tag{4.31}$$

for the evolutionary basis elements $u_n(z,t)$ of the signal $U(g,t)$, $g \in \mathbf{B}$. The problems (4.4) generates three types of nonlocal EACs [formulas (4.18), (4.19), and (4.20)] and five types of the local EACs [(4.25), (4.26), (4.27), (4.28), and (4.29)]. A comparison between (4.4) and (4.31) shows how all these EAC formulas can be rewritten in terms of boundary $\mathbf{L}_2$. In what follows, conditions (4.19) and (4.26) will be used. Taking into account the change both in the direction of free propagation of pulsed waves (toward $z \to -\infty$ instead of $z \to +\infty$) and in the position of the artificial boundary $\mathbf{L}_2$ ($z = -L_2 - h$ instead of $z = L_1$), we have

$$\begin{aligned} &\left[\frac{\partial}{\partial t} - \frac{\partial}{\partial z}\right] U(y,z,t)\Big|_{z=-L_2-h} = \\ &\quad = -\sum_n \left\{ \int_0^t J_1\left[\Phi_n(t-\tau)\right] \left[\int_0^l \frac{\partial U(\tilde{y},z,\tau)}{\partial z}\Big|_{z=-L_2-h} \mu_n^*(\tilde{y})\,d\tilde{y} \right] d\tau \right\} \Phi_n \mu_n(y); \\ &\quad 0 \le y \le l,\ t \ge 0 \end{aligned} \tag{4.32}$$

and

$$\left[\frac{\partial}{\partial t}-\frac{\partial}{\partial z}\right]U(y,z,t)\Big|_{z=-L_2-h}=\frac{2}{\pi}\int\limits_0^{\pi/2}W(y,t,\varphi)\cos^2\varphi\,d\varphi;\qquad t\geq 0,\qquad 0\leq y\leq l,$$

$$\begin{cases}\left[\frac{\partial^2}{\partial t^2}-\cos^2\varphi\frac{\partial^2}{\partial y^2}\right]W(y,t,\varphi)=\frac{\partial^2}{\partial y^2}\left[\frac{\partial}{\partial z}U(y,z,t)\Big|_{z=-L_2-h}\right];\\ \qquad 0<y<l,\qquad t>0\\ W(y,0,\varphi)=\frac{\partial W(y,t,\varphi)}{\partial t}\Big|_{t=0}=0;\qquad 0\leq y\leq l\\ W\left\{\frac{\partial W}{\partial y}\right\}(l,t,\varphi)=\mathrm{e}^{i2\pi\Phi}W\left\{\frac{\partial W}{\partial y}\right\}(0,t,\varphi);\qquad t\geq 0\end{cases}. \tag{4.33}$$

Now we can formulate the main result of the section.

Statement 4.2 *The open problems (4.1) with the analysis domain* $\mathbf{Q}$ *are equivalent to closed problems (4.1) with the analysis domain* $\mathbf{Q}_L$ *and nonlocal or local EACs (4.18), (419) and (4.20), (4.25), (4.26), (4.27), (4.28) and (4.29), (4.32), and (4.33) on its outer boundary* $\mathbf{L}=\mathbf{L}_1\cup\mathbf{L}_2$. *For the auxiliary functions* $W(y,z,\varphi)$, *the inner initial boundary value problems in (4.25), (4.26), (4.27), (4.28), (4.29), and (4.33) are well posed.*

4.1.4 The Problems of Large and Remote Field Sources

Earlier, formulating the initial boundary value problem and specifying $\mathbf{Q}$ and $\mathbf{Q}_L$ domains, we assumed that the functions describing the sources which excite the gratings (see Section 4.1.1) are finitary in the closure of the complete analysis domain $\mathbf{Q}$ and their supports belong to $\overline{\mathbf{Q}_L}\backslash\mathbf{L}$ for all times $0\leq t\leq T$. The advantage is that the conditions on the virtual boundaries $\mathbf{L}$ can be formulated in terms of the total field $U(g,t)$. The limitations introduced by these assumptions can be partially or completely removed by enclosing a certain part of the current and/or the instant sources in the ${}_L\mathbf{Q}$ domain. The only concern is that one should exclude the incoming primary wave $U^i(g,t)$, generated by this source, from the field $U(g,t)$ on $\mathbf{L}$. To this end, the scattered (secondary) field $U^s(g,t)=U(g,t)$–$U^i(g,t)$ is introduced. The final equations for the modified problem can be formulated either in terms of the total field $U(g,t)$ or in terms of the secondary field $U^s(g,t)$. The first alternative is preferred to the second as the formally true separation of the field $U(g,t)$ into $U^s(g,t)$ and $U^i(g,t)$ can be physically invalid in partial subdomains of the domain $\mathbf{Q}$.

The problems (4.34) stated below

$$\begin{cases}\left[-\varepsilon\mu\frac{\partial^2}{\partial t^2}-\sigma\mu\frac{\partial}{\partial t}+\frac{\partial^2}{\partial y^2}+\frac{\partial^2}{\partial z^2}\right]U(g,t)=F(g,t)+\tilde{F}(g,t);\\ \qquad g=\{y,z\}\in\mathbf{Q},\qquad t>0\\ U(g,0)=\varphi(g)+\tilde{\varphi}(g),\qquad \frac{\partial}{\partial t}U(g,t)\Big|_{t=0}=\psi(g)+\tilde{\psi}(g);\qquad g\in\bar{\mathbf{Q}}\\ E_{tg}(p,t)\Big|_{p=\{x,y,z\}\in\mathbf{S}}=0;\qquad t\geq 0\\ U\left\{\frac{\partial U}{\partial y}\right\}(l,z,t)=\mathrm{e}^{2\pi i\Phi}U\left\{\frac{\partial U}{\partial y}\right\}(0,z,t);\qquad t\geq 0\end{cases} \tag{4.34}$$

differs from (4.1) by the existence of the functions $\tilde{F}(g,t)$, $\tilde{\varphi}(g)$, and $\tilde{\psi}(g)$ which are finitary in the domain $\mathbf{Q}$. It is assumed that the supports of these functions and the corresponding sources belong to the domain $\mathbf{A} = \{g \in \mathbf{Q}\colon\ z > L_1\}$ (see Fig. 4.1). The domain $\mathbf{B} = \{g \in \mathbf{Q}\colon\ z < -L_2 - h\}$ carries, as before, no sources or efficient scatterers.

In $\mathbf{A}$, the total field can be written as $U(g,t) = U^i(g,t)+U^s(g,t)$, where $U^i(g,t)$ is the field in the channel $\mathbf{R}$ from the sources $\tilde{F}(g,t)$, $\tilde{\varphi}(g)$, and $\tilde{\psi}(g)$:

$$\begin{cases} \left[-\frac{\partial^2}{\partial t^2} + \frac{\partial^2}{\partial y^2} + \frac{\partial^2}{\partial z^2}\right] U^i(g,t) = \tilde{F}(g,t); \qquad g \in \mathbf{R}, \qquad t > 0 \\ U^i(g,0) = \tilde{\varphi}(g), \qquad \frac{\partial}{\partial t} U^i(g,t)\big|_{t=0} = \tilde{\psi}(g); \qquad g \in \mathbf{R} \\ U^i\left\{\frac{\partial U^i}{\partial y}\right\}(l,z,t) = \mathrm{e}^{2\pi i \Phi} U^i\left\{\frac{\partial U^i}{\partial y}\right\}(0,z,t); \qquad t \geq 0 \end{cases} . \tag{4.35}$$

In order to find $U^s(g,t)$ in $\mathbf{A}$ and $U(g,t)$ in $\mathbf{B}$, we may consider now the following homogeneous initial boundary value problems:

$$\begin{cases} \left[-\frac{\partial^2}{\partial t^2} + \frac{\partial^2}{\partial y^2} + \frac{\partial^2}{\partial z^2}\right] \begin{Bmatrix} U^s(g,t) \\ U(g,t) \end{Bmatrix} = 0; \qquad g \in \begin{Bmatrix} \mathbf{A} \\ \mathbf{B} \end{Bmatrix}, \qquad t > 0 \\ \begin{Bmatrix} U^s(g,0) \\ U(g,0) \end{Bmatrix} = 0, \qquad \frac{\partial}{\partial t} \begin{Bmatrix} U^s(g,t) \\ U(g,t) \end{Bmatrix}\Big|_{t=0} = 0; \qquad g \in \begin{Bmatrix} \bar{\mathbf{A}} \\ \bar{\mathbf{B}} \end{Bmatrix} \\ \begin{Bmatrix} U^s \\ U \end{Bmatrix} \left\{ \begin{Bmatrix} U^s \\ U \end{Bmatrix} \Big/ \partial y \right\}(l,z,t) = \mathrm{e}^{2\pi i \Phi} \begin{Bmatrix} U^s \\ U \end{Bmatrix} \left\{ \begin{Bmatrix} U^s \\ U \end{Bmatrix} \Big/ \partial y \right\}(0,z,t); \\ \qquad \begin{Bmatrix} z > L_1 \\ z < -L_2 - h \end{Bmatrix}, \qquad t \geq 0 \end{cases} \tag{4.36}$$

It is assumed that the perturbation caused by the sources concentrated in $\mathbf{Q}_L$ have not reached the boundaries $\mathbf{L}_1$ and $\mathbf{L}_2$ of the domains $\mathbf{A}$ and $\mathbf{B}$ at the time $t = 0$. The solutions of problems (4.36) – the function $U(g,t)$ in $\mathbf{B}$ and the function $U^s(g,t)$ in $\mathbf{A}$ – determine the outgoing waves traveling in the $z \to -\infty$ and $z \to +\infty$ directions, respectively. Therefore we will prove that (see Sections 4.1.1, 4.1.2 and 4.1.3)

$$\begin{aligned} U(y,L_1,t) - U^i(y,L_1,t) = \\ = -\sum_{n=-\infty}^{\infty} \left\{ \int_0^t J_0[\Phi_n(t-\tau)] \left[\int_0^l \frac{\partial\left[U(\tilde{y},z,\tau) - U^i(\tilde{y},z,\tau)\right]}{\partial z}\Big|_{z=L_1} \mu_n^*(\tilde{y})\, d\tilde{y} \right] d\tau \right\} \times \\ \times \mu_n(y); \ 0 \leq y \leq l, t \geq 0, \end{aligned} \tag{4.37}$$

$$\begin{aligned} U(y,-L_2-h,t) = \sum_{n=-\infty}^{\infty} \left\{ \int_0^t J_0[\Phi_n(t-\tau)] \left[\int_0^l \frac{\partial U(\tilde{y},z,\tau)}{\partial z}\Big|_{z=-L_2-h} \mu_n^*(\tilde{y})\, d\tilde{y} \right] d\tau \right\} \times \\ \times \mu_n(y); \ 0 \leq y \leq l, t \geq 0, \end{aligned} \tag{4.38}$$

and

$$U(y,L_1,t) - U^i(y,L_1,t) = \frac{2}{\pi}\int\limits_0^{\pi/2} \frac{\partial W(y,t,\varphi)}{\partial t}\, d\varphi;\ t \ge 0,\ 0 \le y \le l,$$

$$\begin{cases} \left[\frac{\partial^2}{\partial t^2} - \sin^2\varphi \frac{\partial^2}{\partial y^2}\right] W(y,t,\varphi) = -\left.\frac{\partial\left[U(y,z,t)-U^i(y,z,t)\right]}{\partial z}\right|_{z=L_1}; \\ \qquad 0 < y < l, \qquad t > 0 \\ W(y,0,\varphi) = \left.\frac{\partial W(y,t,\varphi)}{\partial t}\right|_{t=0} = 0; \qquad 0 \le y \le l \\ W\left\{\frac{\partial W}{\partial y}\right\}(l,t,\varphi) = e^{i2\pi\Phi} W\left\{\frac{\partial W}{\partial y}\right\}(0,t,\varphi); \qquad t \ge 0 \end{cases}, \tag{4.39}$$

$$U(y,-L_2-h,t) = \frac{2}{\pi}\int\limits_0^{\pi/2} \frac{\partial W(y,t,\varphi)}{\partial t}\, d\varphi;\ t \ge 0,\ 0 \le y \le l,$$

$$\begin{cases} \left[\frac{\partial^2}{\partial t^2} - \sin^2\varphi \frac{\partial^2}{\partial y^2}\right] W(y,t,\varphi) = \left.\frac{\partial U(y,z,t)}{\partial z}\right|_{z=-L_2-h}; \qquad 0 < y < l, \qquad t > 0 \\ W(y,0,\varphi) = \left.\frac{\partial W(y,t,\varphi)}{\partial t}\right|_{t=0} = 0; \qquad 0 \le y \le l \\ W\left\{\frac{\partial W}{\partial y}\right\}(l,t,\varphi) = e^{i2\pi\Phi} W\left\{\frac{\partial W}{\partial y}\right\}(0,t,\varphi); \qquad t \ge 0 \end{cases}. \tag{4.40}$$

Here, as before, $W(y,t,\varphi)$ are certain auxiliary functions.

The couple (4.37) and (4.39) are exact (nonlocal and local) absorbing conditions on the boundary $\mathbf{L}_1$ in the region $\mathbf{A}$ cross-section at $z = L_1$. The couple (4.38) and (4.40) represents the same conditions for the boundary $\mathbf{L}_2$ in the region $\mathbf{B}$ cross-section at $z = -L_2 - h$. They are direct analogues of conditions (4.18) and (4.25) constructed in Sections 4.1.2 and 4.1.3. It is evident that the other nonlocal and local conditions from these sections may be adjusted for the situation considered here.

In $\mathbf{Q}_L$, the function $U(g,t)$ is defined by the equations

$$\begin{cases} \left[-\varepsilon\mu\frac{\partial^2}{\partial t^2} - \sigma\mu\frac{\partial}{\partial t} + \frac{\partial^2}{\partial y^2} + \frac{\partial^2}{\partial z^2}\right] U(g,t) = F(g,t); \qquad g \in \mathbf{Q}_L, \qquad t > 0 \\ U(g,0) = \varphi(g), \qquad \left.\frac{\partial}{\partial t}U(g,t)\right|_{t=0} = \psi(g); \qquad g \in \overline{\mathbf{Q}}_L \\ \left.E_{tg}(p,t)\right|_{p=\{x,y,z\}\in\mathbf{S}} = 0; \qquad t \ge 0 \\ U\left\{\frac{\partial U}{\partial y}\right\}(l,z,t) = e^{2\pi i\Phi} U\left\{\frac{\partial U}{\partial y}\right\}(0,z,t); \qquad t \ge 0 \end{cases}. \tag{4.41}$$

Statement 4.3 *Problems (4.34) and problems (4.41) with conditions (4.37) and (4.38) or (4.39) and (4.40) in the domain* $\mathbf{Q}_L$ *have the same solutions* $U(g,t)$ *for an arbitrary observation time* $t\in[0;T]$. *In the modified problems, the functions* $U^i(g,t)$

involved in the EACs of (4.37) and (4.39) type for the virtual boundary $\mathbf{L}_1$ *act as real sources outside the bounded analysis domain* $\mathbf{Q}_L$.

The EACs of the (4.37) and (4.39) type allow us to confine the calculation space $\mathbf{Q}_L$ to a reasonable size when working the problem of the type (4.34) with large and/or distant sources of transient waves $U^i(g,t)$. These sources – $\tilde{F}(g,t)$, $\tilde{\varphi}(g)$, and $\tilde{\psi}(g)$ – are merely enclosed in the ${}_L\mathbf{Q}$ domain. Their contribution to the total field $U(g,t)$ is considered via the boundary values of the functions $U^i(g,t)$, $t\in[0;T]$ and their normal derivatives on the $\mathbf{L}$ boundaries. All information relevant for the realization of the scheme is provided by the solution of problem (4.35), which is quite simple computationwise. Also, the problem is explicitly solved using the mirror image technique. The Poisson formula governing the given source field in a free 2-D space (in the space $\mathbf{R}^2$) readily admits the boundary wall condition of the Floquet channel $\mathbf{R}$ [2, 10].

Where and how the primary $U^i(g,t)$ wave is excited is usually no problem for standard scattering analysis of infinite periodic gratings (see Section 4.4). Nor does it need $U^i(g,t)$ values at all observation time $t\in[0;T]$ and at all points g from $\mathbf{A}$. A proper numerical experiment only needs $U^i(g,t)\big|_{g\in L_1}$ and $\left[\partial U^i(g,t)\big/\partial z\right]\big|_{g\in L_1}$ values for all times $t\in[0;T]$. Yet these values must be in agreement with the boundary values of some function $U^i(g,t)$ that governs in the domain $\mathbf{A}$ a transient electromagnetic wave running on the virtual boundary $\mathbf{L}_1$ (principle of causality). On the $\mathbf{L}_1$ boundary separating the domains $\mathbf{Q}_L$ and $\mathbf{A}$, this requirement complies with the functions

$$U_p^i(y,L_1,t) = v_p(L_1,t)\,\mu_p(y),\ \left[\partial U_p^i(y,z,t)\big/\partial z\right]\Big|_{z=L_1} = v_p'(L_1,t)\,\mu_p(y);\quad 0\le y\le l,\ p=0,\pm1,\pm2,\ldots, \tag{4.42}$$

whose amplitudes $v_p(L_1,t)$ and $v_p'(L_1,t)$ are related as follows:

$$v_p(L_1,t) = \int_0 J_0\left[\Phi_p(t-\tau)\right]\chi(t-\tau)\,v_p'(L_1,\tau)\,d\tau;\ t\ge 0. \tag{4.43}$$

It is evident that (4.42) and (4.43) give boundary values of the function $U_p^i(g,t) = v_p(z,t)\,\mu_p(y)$ describing a transient wave running on the boundary $\mathbf{L}_1$ from the $\mathbf{A}$ region. This is so because (4.43) comes from (4.10), taking into account the changes in the direction of propagation of the wave under discussion.

4.2 Finite Gratings: Exact Conditions for Rectangular Artificial Boundaries

4.2.1 Statement of the Problems

In Section 4.2, we analyze 2-D model configurations involving finite periodic structures (see, for example, Fig. 4.2). The models proceed from the following real-valued scalar problems:

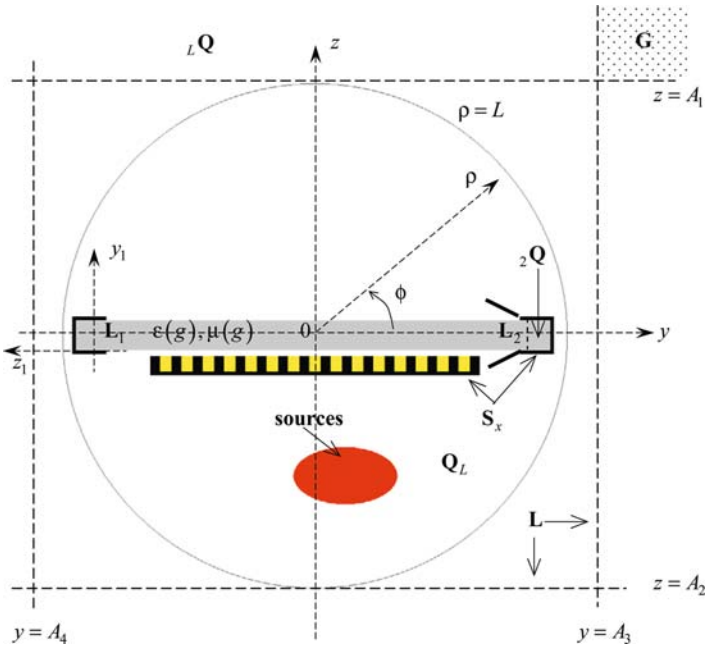

Fig. 4.2 Geometry of model problems (4.44)

$$\begin{cases} \left[-\varepsilon\mu\frac{\partial^2}{\partial t^2} - \sigma\mu\frac{\partial}{\partial t} + \frac{\partial^2}{\partial y^2} + \frac{\partial^2}{\partial z^2}\right] U(g,t) = F(g,t); \quad g = \{y,z\} \in \mathbf{Q}, \quad t > 0 \\ U(g,t)|_{t=0} = \varphi(g), \quad \frac{\partial}{\partial t}U(g,t)\big|_{t=0} = \psi(g); \quad g \in \overline{\mathbf{Q}} \\ E_{tg}(p,t)\big|_{p=\{x,y,z\}\in\mathbf{S}} = 0; \quad t \geq 0 \\ D_j\left[U(g,t) - U^{i(j)}(g,t)\right]\big|_{g\in\mathbf{L}_j} = 0; \quad j = 1,2,...,N, \quad t \geq 0 \end{cases} . \tag{4.44}$$

Here, $U(g,t) = E_x(g,t)$ for E-polarization of the field ($E_y = E_z = H_x = 0$ and $\mu(g)$ is a piecewise constant function) and $U(g,t) = H_x(g,t)$ for H-polarization ($H_y = H_z = E_x = 0$ and $\varepsilon(g)$ and $\sigma(g)$ are piecewise constant functions). The analysis domain $\mathbf{Q}$, part of the plane $\mathbf{R}^2$, is limited by curves $\mathbf{S}_x$ and virtual boundaries (ports) $\mathbf{L}_j$; $\mathbf{S} = \mathbf{S}_x \times [|x| \leq \infty]$ are surfaces of perfectly conducting elements as given by the device geometry. The functions $F(g,t)$, $\varphi(g)$, $\psi(g)$, $\sigma(g)$, $\varepsilon(g)$–1, and $\mu(g)$–1 are finitary in $\mathbf{Q}$. For all observation times $0 \leq t \leq T$, their supports belong to the closure of the domain $\mathbf{Q}_L = \{g \in \mathbf{Q}: A_4 < y < A_3; A_2 < z < A_1\}$ (see Fig. 4.2). Above (below, on the right/left of) the artificial boundary $z = A_1$ ($z = A_2$, $y = A_3$, $y = A_4$) there are neither sources nor scatterers. The continuity conditions of the tangential components of the field strength vectors are satisfied when the situation so requires, and all initial data are such that (4.44) have a unique solution in the space $\mathbf{W}_2^1(\mathbf{Q}^T)$, $\mathbf{Q}^T = \mathbf{Q} \times (0;T)$, $T < \infty$ (see Statement 1.1 and [5]).

The difference between problems (4.44) and compact (in the free space $\mathbf{R}^2$) inhomogeneity problems (3.12) [1] is only that the former admits perturbation sources in the ${}_j\mathbf{Q}$ domains that are regular, l_j wide virtual plane parallel waveguides immediately adjacent to the $\mathbf{Q}_L$ domain lengthwise of the boundaries (ports) $\mathbf{L}_j$ (see Fig. 4.2). These sources produce pulsed waves $U^{i(j)}(g,t)$ running on the boundaries $\mathbf{L}_j$ from ${}_j\mathbf{Q}$. Owing to the ${}_j\mathbf{Q}$ waveguides, the object modeling in terms of infinite regular boundaries $\mathbf{S}$ leaves us in a more convenient yet more physically relevant contexts, which are valid, strictly speaking, only for compact inhomogeneities in free space. Also, it is very important that this expedient allows the object modeling in the regime of the excitation from the waveguide feed line by giving on one or more boundaries $\mathbf{L}_j$ the primary signal $U^{i(j)}(g,t)$ from the current or the instant sources whose supports are within the virtual ${}_j\mathbf{Q}$ domain.

The exact absorbing conditions

$$D_j\left[U(g,t) - U^{i(j)}(g,t)\right]\Big|_{g\in\mathbf{L}_j} = 0; \qquad t \geq 0 \tag{4.45}$$

for the plane parallel waveguide ${}_j\mathbf{Q}$ are derived in the same way as the EACs are derived for $\mathbf{A}$ as part of the plane parallel Floquet channel $\mathbf{R}$. The results from Section 4.1 are easily modified to fit the situation considered now. All we need to do is to substitute the solutions $\{\Phi_n\}$ and $\{\mu_n(y)\}$ of problems (4.3) by the solutions $\{\lambda_{nj}\}$ and $\{\mu_{nj}(y_j)\}$ of the spectral problems

$$\begin{cases} \left[\frac{d^2}{dy_j^2} + \lambda_{nj}^2\right]\mu_{nj}(y_j) = 0; \qquad 0 < y_j < l_j \\ \mu_{nj}(0) = \mu_{nj}(l_j) = 0 \qquad (E-\text{case}) \qquad \text{or} \\ d\mu_{nj}(y_j)/dy_j\big|_{y_j=0,l_j} = 0 \qquad (H-\text{case}) \end{cases}$$

and change from the local coordinates $g_j = \{y_j, z_j\}$ associated with the waveguide ${}_j\mathbf{Q}$ (see Fig. 4.2) to the general coordinates $g = \{y,z\}$. Thus, for the structure shown in Fig. 4.2 and excited by the E-polarized wave $U^{i(2)}(g,t)$ from the second virtual waveguide, the EACs of the type (4.37), (4.38), (4.39), and (4.40) on the boundaries $\mathbf{L}_1$ ($y = -L_1$) and $\mathbf{L}_2$ ($y = L_2$) take the form

$$\begin{aligned} &U(L_2,z,t) - U^{i(2)}(L_2,z,t) = U^{s(2)}(L_2,z,t) = \\ &\quad = -\sum_{n=1}^{\infty}\left\{\int_0^t J_0\left[\lambda_n(t-\tau)\right]\left[\int_{a_2}^{b_2}\frac{\partial U^{s(2)}(y,\tilde{z},\tau)}{\partial y}\Big|_{y=L_2}\mu_{n2}(\tilde{z})\,d\tilde{z}\right]d\tau\right\}\mu_{n2}(z); \\ &\quad a_2 \leq z \leq b_2,\ t \geq 0, \end{aligned} \tag{4.46}$$

$$\begin{aligned} &U(-L_1,z,t) = \sum_{n=1}^{\infty}\left\{\int_0^t J_0\left[\lambda_n(t-\tau)\right]\left[\int_{a_1}^{b_1}\frac{\partial U(y,\tilde{z},\tau)}{\partial y}\Big|_{y=-L_1}\mu_{n1}(\tilde{z})\,d\tilde{z}\right]d\tau\right\}\mu_{n1}(z); \\ &\quad a_1 \leq z \leq b_1,\ t \geq 0 \end{aligned} \tag{4.47}$$

and

$$U(L_2,z,t) - U^{i(2)}(L_2,z,t) = \frac{2}{\pi}\int\limits_0^{\pi/2} \frac{\partial W(z,t,\varphi)}{\partial t}\, d\varphi;\ t \geq 0,\ a_2 \leq z \leq b_2,$$

$$\begin{cases} \left[\frac{\partial^2}{\partial t^2} - \sin^2\varphi \frac{\partial^2}{\partial z^2}\right] W(z,t,\varphi) = -\left.\frac{\partial\left[U(y,z,t) - U^{i(2)}(y,z,t)\right]}{\partial y}\right|_{y=L_2}; \\ \qquad a_2 \leq z \leq b_2, \qquad t > 0 \\ W(z,0,\varphi) = \left.\frac{\partial W(z,t,\varphi)}{\partial t}\right|_{t=0} = 0; \qquad a_2 \leq z \leq b_2 \\ W(a_2,t,\varphi) = W(b_2,t,\varphi) = 0; \qquad t \geq 0 \end{cases}, \tag{4.48}$$

$$U(-L_1,z,t) = \frac{2}{\pi}\int\limits_0^{\pi/2} \frac{\partial W(z,t,\varphi)}{\partial t}\, d\varphi;\ t \geq 0,\ a_1 \leq z \leq b_1,$$

$$\begin{cases} \left[\frac{\partial^2}{\partial t^2} - \sin^2\varphi \frac{\partial^2}{\partial z^2}\right] W(z,t,\varphi) = \left.\frac{\partial U(y,z,t)}{\partial y}\right|_{y=-L_1}; \qquad a_1 \leq z \leq b_1, \qquad t > 0 \\ W(z,0,\varphi) = \left.\frac{\partial W(z,t,\varphi)}{\partial t}\right|_{t=0} = 0; \qquad a_1 \leq z \leq b_1 \\ W(a_1,t,\varphi) = W(b_1,t,\varphi) = 0; \qquad t \geq 0 \end{cases}. \tag{4.49}$$

Here, $\lambda_{nj} = n\pi/l_j, n = 1,2,\ldots; \{\mu_{nj}(z)\}$ are the complete systems of orthonormalized transverse functions $\mu_{nj}(z) = \sqrt{2/l_j}\sin\left[n\pi\left(z - a_j\right)/l_j\right]$, $l_j = b_j – a_j$ is the height of the waveguide ${}_j\mathbf{Q}$, $z = a_j$ and $z = b_j$ are the planes corresponding to the waveguide upper and lower walls, respectively.

4.2.2 Truncation of the Analysis Domain to a Band

In the domain ${}_L\mathbf{Q}$, the functions $U(g,t)$ are associated with the outgoing waves crossing the boundary $\mathbf{L}$ in one direction only. They comply with the homogeneous problems

$$\begin{cases} \left[-\frac{\partial^2}{\partial t^2} + \frac{\partial^2}{\partial y^2} + \frac{\partial^2}{\partial z^2}\right] U(g,t) = 0; \qquad g = \{y,z\} \in_L \mathbf{Q}, \qquad t > 0 \\ U(g,t)|_{t=0} = 0, \qquad \frac{\partial}{\partial t} U(g,t)\big|_{t=0} = 0; \qquad g \in \overline{{}_L\mathbf{Q}} \end{cases}. \tag{4.50}$$

Subject the $U(g,t)$ function from (4.50) to the Fourier transform

$$u_y(\lambda,z,t) = \frac{1}{2\pi}\int\limits_{-\infty}^{\infty} U(y,z,t)e^{i\lambda y}dy \quad \leftrightarrow \quad U(y,z,t) = \int\limits_{-\infty}^{\infty} u_y(\lambda,z,t)e^{-i\lambda y}d\lambda,$$

$$u_z(y,\mu,t) = \frac{1}{2\pi}\int\limits_{-\infty}^{\infty} U(y,z,t)e^{i\mu z}dz \quad \leftrightarrow \quad U(y,z,t) = \int\limits_{-\infty}^{\infty} u_z(y,\mu,t)e^{-i\mu z}d\mu$$

and employ the technique checked in Sections 4.1.1 and 4.1.2 as applied to homogeneous problems (4.4) for one-dimensional Klein–Gordon equations. Then

$$\left[\frac{\partial}{\partial t} \pm \frac{\partial}{\partial z}\right] u_y(\lambda,z,t) = \pm\lambda \int_0^t J_1(\lambda(t-\tau)) \frac{\partial u_y(\lambda,z,\tau)}{\partial z} d\tau; \qquad \begin{cases} z \geq A_1 \\ z \leq A_2 \end{cases}, \quad (4.51)$$

$$\left[\frac{\partial}{\partial t} \pm \frac{\partial}{\partial y}\right] u_z(y,\mu,t) = \pm\mu \int_0^t J_1(\mu(t-\tau)) \frac{\partial u_z(y,\mu,\tau)}{\partial y} d\tau; \qquad \begin{cases} y \geq A_3 \\ y \leq A_4 \end{cases}. \quad (4.52)$$

After a sequence of simple operations (see Section 4.1.2: Laplace transform in $t \rightarrow$ solution of the operational equations with respect to the derivatives in the spatial coordinates of the u_y and u_z images $\rightarrow$ inverse Laplace transform), equations (4.51) and (4.52) can be written in the following equivalent form:

$$\left[\frac{\partial}{\partial t} \pm \frac{\partial}{\partial z}\right] u_y(\lambda,z,t) = -\lambda \int_0^t \frac{J_1(\lambda(t-\tau))}{t-\tau} u_y(\lambda,z,\tau)\, d\tau; \qquad \begin{cases} z \geq A_1 \\ z \leq A_2 \end{cases}, \quad (4.53)$$

$$\left[\frac{\partial}{\partial t} \pm \frac{\partial}{\partial y}\right] u_z(y,\mu,t) = -\mu \int_0^t \frac{J_1(\mu(t-\tau))}{t-\tau} u_z(y,\mu,\tau)\, d\tau; \qquad \begin{cases} y \geq A_3 \\ y \leq A_4 \end{cases}. \quad (4.54)$$

The nonlocal conditions (4.51), (4.52), (4.53), and (4.54), written in terms of the Fourier amplitudes of the field $U(g,t)$, truncate the analysis domain of problems (4.44) to the band $A_2 < z < A_1$ or $A_4 < y < A_3$. We will seek now relations that are local in time and space. Let us begin with formulas (4.53) and (4.54) and follow the scheme tried in Section 4.1.3. Here we apply the Poisson integral formula [201]

$$J_1(x) = \frac{2x}{\pi} \int_0^{\pi/2} \cos(x\cos\varphi)\sin^2\varphi\, d\varphi,$$

the substitutions

$$v_y = -\lambda \int_0^t \frac{\sin(\lambda(t-\tau)\cos\varphi)}{\cos\varphi} u_y\, d\tau, \; \frac{\partial v_y}{\partial t} = -\lambda^2 \int_0^t \cos(\lambda(t-\tau)\cos\varphi)\, u_y\, d\tau, \quad (4.55)$$

and the fundamental solution $G(a,t) = \chi(t)\sin(at)\,a^{-1}$ of the operator $D(a) \equiv \left[d^2/dt^2 + a^2\right]$, in order to go from the integral forms (4.55) to the equivalent differential forms

$$\begin{cases} \left[\frac{\partial^2}{\partial t^2} + \lambda^2\cos^2\varphi\right] v_y = -\lambda^2 u_y; \qquad t > 0 \\ \left.\frac{\partial v_y}{\partial t}\right|_{t=0} = \left. v_y\right|_{t=0} = 0 \end{cases}.$$

As a result we obtain:

$$\left[\frac{\partial}{\partial t}\pm\frac{\partial}{\partial z}\right]u_y(\lambda,z,t)=\frac{2}{\pi}\int\limits_0^{\pi/2}\frac{\partial v_y(\lambda,z,t,\varphi)}{\partial t}\sin^2\varphi d\varphi;\qquad t\geq 0,$$
$$\begin{cases}\left[\frac{\partial^2}{\partial t^2}+\lambda^2\cos^2\varphi\right]v_y(\lambda,z,t,\varphi)=-\lambda^2u_y(\lambda,z,t);\qquad t>0\\ \left.\frac{\partial v_y(\lambda,z,t,\varphi)}{\partial t}\right|_{t=0}=v_y(\lambda,z,t,\varphi)|_{t=0}=0\end{cases},\begin{cases}z\geq A_1\\ z\leq A_2\end{cases},\tag{4.56}$$

$$\left[\frac{\partial}{\partial t}\pm\frac{\partial}{\partial y}\right]u_z(y,\mu,t)=\frac{2}{\pi}\int\limits_0^{\pi/2}\frac{\partial v_z(y,\mu,t,\varphi)}{\partial t}\sin^2\varphi d\varphi;\qquad t\geq 0,$$
$$\begin{cases}\left[\frac{\partial^2}{\partial t^2}+\mu^2\cos^2\varphi\right]v_z(y,\mu,t,\varphi)=-\mu^2u_z(y,\mu,t);\qquad t>0\\ \left.\frac{\partial v_z(y,\mu,t,\varphi)}{\partial t}\right|_{t=0}=v_z(y,\mu,t,\varphi)|_{t=0}=0\end{cases},\begin{cases}y\geq A_3\\ y\leq A_4\end{cases}.\tag{4.57}$$

Let

$$V_1(g,t,\varphi)=\int\limits_{-\infty}^{\infty}v_y(\lambda,z,t,\varphi)e^{-i\lambda y}d\lambda,\ V_2(g,t,\varphi)=\int\limits_{-\infty}^{\infty}v_z(y,\mu,t,\varphi)e^{-i\mu z}d\mu.$$

Subject (4.56) and (4.57) to the inverse Fourier transform. Then the local EACs reducing the analysis domain of the original problems (4.44) to a band in $\mathbf{R}^2$ takes the form

$$\left[\frac{\partial}{\partial t}\pm\frac{\partial}{\partial z}\right]U(g,t)=\frac{2}{\pi}\int\limits_0^{\pi/2}\frac{\partial V_1(g,t,\varphi)}{\partial t}\sin^2\varphi d\varphi;\qquad |y|\leq\infty,\qquad t\geq 0,$$
$$\begin{cases}\left[\frac{\partial^2}{\partial t^2}-\cos^2\varphi\frac{\partial^2}{\partial y^2}\right]V_1(g,t,\varphi)=\frac{\partial^2}{\partial y^2}U(g,t);\qquad |y|<\infty,\qquad t>0\\ \left.\frac{\partial V_1(g,t,\varphi)}{\partial t}\right|_{t=0}=V_1(g,t,\varphi)|_{t=0}=0;\qquad |y|\leq\infty\end{cases};\begin{cases}z\geq A_1\\ z\leq A_2\end{cases}\tag{4.58}$$

and

$$\left[\frac{\partial}{\partial t}\pm\frac{\partial}{\partial y}\right]U(g,t)=\frac{2}{\pi}\int\limits_0^{\pi/2}\frac{\partial V_2(g,t,\varphi)}{\partial t}\sin^2\varphi d\varphi;\qquad |z|\leq\infty,\qquad t\geq 0,$$
$$\begin{cases}\left[\frac{\partial^2}{\partial t^2}-\cos^2\varphi\frac{\partial^2}{\partial z^2}\right]V_2(g,t,\varphi)=\frac{\partial^2}{\partial z^2}U(g,t);\qquad |z|<\infty,\qquad t>0\\ \left.\frac{\partial V_2(g,t,\varphi)}{\partial t}\right|_{t=0}=V_2(g,t,\varphi)|_{t=0}=0;\qquad |z|\leq\infty\end{cases};\begin{cases}y\geq A_3\\ y\leq A_4\end{cases}.\tag{4.59}$$

4.2.3 The Corner Points: Proper Formulation of the Inner Initial Boundary Value Problems in the Exact Local Absorbing Conditions

Each of the four expressions (4.58) and (4.59) generates the EAC which truncates the analysis domain down to the half-plane $z<A_1$, $z>A_2$, $y<A_3$ or $y>A_4$. The inner

differential (Cauchy) problems for the functions $V_1(g,t,\varphi)$ (z is some parameter) and $V_2(g,t,\varphi)$ (y is some parameter) are well posed.

When the so truncated domain is of rectangular shape, all the four equations of (4.58) and (4.59) must be taken into account. At the same time, the inner differential problems must be completed with the conditions at the ends where the boundaries $z = \text{const}$ and $y = \text{const}$ meet. There are several analytic ways to treat this problem (the problem of the corner points). One of them, supposedly the clearest, is examined below.

Initially, consider the first equations (with the plus signs) from conditions (4.58) and (4.59). In Fig. 4.2, the $\mathbf{R}^2$ plane quadrant, where these equations are valid simultaneously, is dotted. In this quadrant, single out the region

$$\mathbf{G} = \{g = \{y,z\} : A_3 < y < A_3 + 2\pi;\ A_1 < z < A_1 + 2\pi\}$$

and use here the following representation:

$$f(g,t) \in \mathbf{W}_2^1(\mathbf{G}^\infty,\beta) = \left\{f(g,t) : f(g,t)\exp(-\beta t) \in \mathbf{W}_2^1(\mathbf{G}^\infty)\right\}:$$

$$\begin{gathered} f(g,t) = \frac{1}{2\pi i}\int\limits_{\alpha-i\infty}^{\alpha+i\infty}\sum_{n,m=-\infty}^{\infty}\tilde{f}(n,m,s)e^{i(ny+mz)+st}ds;\quad \mathrm{Re}\, s \geq \beta \geq 0 \leftrightarrow \\ \leftrightarrow\quad \tilde{f}(n,m,s) = \frac{1}{4\pi^2}\int\limits_0^\infty\int\limits_{A_1}^{A_1+2\pi}\int\limits_{A_3}^{A_3+2\pi} f(g,t)e^{-i(ny+mz)-st}dydzdt. \end{gathered} \tag{4.60}$$

For the amplitudes $\tilde{u} = \tilde{u}(n,m,s)$, $\tilde{v}_j(\varphi) = \tilde{v}_j(n,m,s,\varphi)$, and $\tilde{w}_j(\varphi) = \tilde{w}_j(n,m,s,\varphi)$, $j = 1,2$, of the functions $U(g,t)$, $V_j(g,t,\varphi)$, and $W_j(g,t,\varphi) = V_j(g,t,\varphi)\cos^2\varphi + U(g,t)$, we obtain:

$$(s+im)\tilde{u} = \frac{2s}{\pi}\int\limits_0^{\pi/2}\sin^2\varphi\,\tilde{v}_1 d\varphi,\ (s+in)\tilde{u} = \frac{2s}{\pi}\int\limits_0^{\pi/2}\sin^2\varphi\,\tilde{v}_2 d\varphi, \tag{4.61}$$

$$\tilde{w}_1 = \frac{s^2}{s^2+n^2\cos^2\varphi}\tilde{u},\quad \tilde{w}_2 = \frac{s^2}{s^2+m^2\cos^2\varphi}\tilde{u}, \tag{4.62}$$

$$\tilde{v}_1 = -\frac{n^2}{s^2+n^2\cos^2\varphi}\tilde{u},\quad \tilde{v}_2 = -\frac{m^2}{s^2+m^2\cos^2\varphi}\tilde{u}, \tag{4.63}$$

$$s^2 + m^2 + n^2 = 0. \tag{4.64}$$

Now address the function

$$in\tilde{w}_1(\varphi) = in\tilde{u}\frac{s^2}{s^2+n^2\cos^2\varphi} = \frac{s^2}{s^2+n^2\cos^2\varphi}\left[-s\tilde{u} + \frac{2s}{\pi}\int\limits_0^{\pi/2}\sin^2\gamma\tilde{v}_2(\gamma)\,d\gamma\right] =$$
$$= -s\tilde{u}\frac{s^2}{s^2+n^2\cos^2\varphi}\left[1 + \frac{2\sin^2\varphi}{\pi}\int\limits_0^{\pi/2}\frac{\sin^2\gamma}{\cos^2\varphi+\sin^2\varphi\cos^2\gamma}d\gamma\right] +$$
$$+\frac{2}{\pi}\int\limits_0^{\pi/2} s\tilde{u}\frac{s^2}{s^2+m^2\cos^2\gamma}\times\frac{\sin^2\gamma}{\cos^2\varphi+\sin^2\varphi\cos^2\gamma}d\gamma =$$
$$= -\frac{s}{\cos\varphi}\tilde{w}_1(\varphi) + \frac{2}{\pi}\int\limits_0^{\pi/2} s\tilde{w}_2(\gamma)\frac{\sin^2\gamma}{\cos^2\varphi+\sin^2\varphi\cos^2\gamma}d\gamma. \tag{4.65}$$

Here, a successive usage was made of equations (4.62), (4.61), and (4.63), the equality

$$\frac{s^2}{s^2+an^2}\times\frac{s^2}{s^2+bm^2} = \frac{a}{a+(1-a)\,b}\times\frac{s^2}{s^2+an^2} + \frac{b}{a+(1-a)\,b}\times\frac{s^2}{s^2+bm^2}$$

is valid only if (4.64) holds, and, once again, equation (4.62).

The inverse transform of (4.65) yields

$$\left[\frac{\partial}{\partial t} + \cos\varphi\frac{\partial}{\partial y}\right]W_1(g,t,\varphi) = \frac{2\cos\varphi}{\pi}\int\limits_0^{\pi/2}\frac{\sin^2\gamma}{\cos^2\varphi+\sin^2\varphi\cos^2\gamma}\frac{\partial W_2(g,t,\gamma)}{\partial t}d\gamma;$$
$$z \geq A_1, \qquad y \geq A_3.$$

The upper boundaries $z = A_1 + 2\pi$ and $y = A_3 + 2\pi$ of the region **G**, where the mentioned equation holds, are not mentioned, because the region **G** may be arbitrary in size.

Performing the operations described above for the function $im\tilde{w}_2(\varphi)$, which is the object of the present study, we obtain

$$\left[\frac{\partial}{\partial t} + \cos\varphi\frac{\partial}{\partial z}\right]W_2(g,t,\varphi) = \frac{2\cos\varphi}{\pi}\int\limits_0^{\pi/2}\frac{\sin^2\gamma}{\cos^2\varphi+\sin^2\varphi\cos^2\gamma}\frac{\partial W_1(g,t,\gamma)}{\partial t}d\gamma;$$
$$z \geq A_1, \quad y \geq A_3.$$

The expressions relating the auxiliary functions $W_1(g,t,\varphi)$ and $W_2(g,t,\varphi)$ in all the four **G**-like regions resolve the problem of corner points. The inner initial boundary value problems in (4.58) and (4.59) equipped by the corresponding relation are well posed within the finite sections of the outer boundary **L** surrounding the rectangular domain $\mathbf{Q}_L$. The relevant complete system of equations truncating the analysis

domain $\mathbf{Q}$ down to the region $\mathbf{Q}_L$ is

$$\left[\frac{\partial}{\partial t} \pm \frac{\partial}{\partial z}\right] U(g,t) = \frac{2}{\pi} \int\limits_0^{\pi/2} \frac{\partial V_1(g,t,\varphi)}{\partial t} \sin^2\varphi d\varphi; \quad A_4 \le y \le A_3, \qquad t \ge 0,$$

$$\begin{cases} \left[\dfrac{\partial^2 V_1(g,t,\varphi)}{\partial t^2} - \dfrac{\partial^2 W_1(g,t,\varphi)}{\partial y^2}\right] = 0; & A_4 < y < A_3, \quad t > 0 \\ \left.\dfrac{\partial V_1(g,t,\varphi)}{\partial t}\right|_{t=0} = V_1(g,t,\varphi)|_{t=0} = 0; & A_4 \le y \le A_3 \end{cases}; \quad \begin{cases} z = A_1 \\ z = A_2 \end{cases}, \tag{4.66}$$

$$\left[\frac{\partial}{\partial t} \pm \frac{\partial}{\partial y}\right] U(g,t) = \frac{2}{\pi} \int\limits_0^{\pi/2} \frac{\partial V_2(g,t,\varphi)}{\partial t} \sin^2\varphi d\varphi; \quad A_2 \le z \le A_1, \qquad t \ge 0,$$

$$\begin{cases} \left[\dfrac{\partial^2 V_2(g,t,\varphi)}{\partial t^2} - \dfrac{\partial^2 W_2(g,t,\varphi)}{\partial z^2}\right] = 0; & A_2 < z < A_1, \quad t > 0 \\ \left.\dfrac{\partial V_2(g,t,\varphi)}{\partial t}\right|_{t=0} = V_2(g,t,\varphi)|_{t=0} = 0; & A_2 \le z \le A_1 \end{cases}; \quad \begin{cases} y = A_3 \\ y = A_4 \end{cases}, \tag{4.67}$$

$$\begin{cases} \left[\frac{\partial}{\partial t} \pm \cos\varphi \frac{\partial}{\partial y}\right] W_1(g,t,\varphi) = \dfrac{2\cos\varphi}{\pi} \displaystyle\int\limits_0^{\pi/2} \frac{\sin^2\gamma}{\cos^2\varphi + \sin^2\varphi\cos^2\gamma} \frac{\partial W_2(g,t,\gamma)}{\partial t} d\gamma \\ \left[\frac{\partial}{\partial t} \pm \cos\varphi \frac{\partial}{\partial z}\right] W_2(g,t,\varphi) = \frac{2\cos\varphi}{\pi} \displaystyle\int\limits_0^{\pi/2} \frac{\sin^2\gamma}{\cos^2\varphi + \sin^2\varphi\cos^2\gamma} \frac{\partial W_1(g,t,\gamma)}{\partial t} d\gamma \end{cases}; \\ \begin{Bmatrix} + \\ + \end{Bmatrix} \to g = \{A_3, A_1\}, \quad \begin{Bmatrix} + \\ - \end{Bmatrix} \to \{A_3, A_2\}, \quad \begin{Bmatrix} - \\ + \end{Bmatrix} \to \{A_4, A_1\}, \quad \begin{Bmatrix} - \\ - \end{Bmatrix} \to \{A_4, A_2\}. \end{cases} \tag{4.68}$$

Actually, the three formulas (4.66), (4.67), and (4.68) should be considered together, for only taken together they can determine the exact local absorbing condition over the entire artificial coordinate boundary $\mathbf{L}$. Equations (4.68) act here as boundary conditions in the inner initial boundary value problems of (4.66) and (4.67). The symbol

$$\begin{Bmatrix} + \\ + \end{Bmatrix} \to g = \{A_3, A_1\}$$

chooses the signs in the upper and lower equations for different corner points $g = \{y,z\}$.

Statement 4.4 *Problems (4.44), the analysis domain* $\mathbf{Q}$ *and problems (4.44), the analysis domain* $\mathbf{Q}_L = \{g \in \mathbf{Q}: A_4 < y < A_3; A_2 < z < A_1\}$ *and conditions (4.66), (4.67), and (4.68) on the outer rectangular boundary* $\mathbf{L}$ *are equivalent.*

The inner initial boundary value problems in (4.66), (4.67), and (4.68) for the functions $W_1(g,t,\varphi)$ and $W_2(g,t,\varphi)$ are well posed.

4.2.4 The Far Zone Problem: Radiation Conditions for Outgoing Cylindrical Waves and Exact Conditions for Artificial Boundaries in Polar Coordinates

Let a circle of radius L with its center in the point $g = \{y,z\} = \{0,0\}$ be inscribed in the rectangular $\mathbf{Q}_L$ domain. Let this circle have all field sources and $\mathbf{R}^2$ space inhomogeneities inside (see Fig. 4.2). Then within $\rho > L$, $0 \le \phi \le 2\pi$ ($g = \{\rho,\phi\}$ are polar coordinates) the solutions $U(g,t)$ of the initial boundary value problems (4.44) represent outgoing transient waves crossing the boundary $\rho = L$ only in one ($\rho \to \infty$) direction, and

$$\begin{cases} \left[-\frac{\partial^2}{\partial t^2} + \frac{1}{\rho}\,\frac{\partial}{\partial \rho}\rho\frac{\partial}{\partial \rho} + \frac{1}{\rho^2}\frac{\partial^2}{\partial \phi^2}\right] U(g,t) = 0; \qquad \rho > L, \qquad t > 0 \\ U(g,t)|_{t=0} = 0, \quad \frac{\partial}{\partial t}U(g,t)\big|_{t=0} = 0; \qquad \rho \ge L \\ U(\rho,\phi,t) = U(\rho,\phi + 2\pi,t); \qquad t \ge 0 \end{cases} . \tag{4.69}$$

Separation of the ϕ-variable in (4.69) yields

$$U(\rho,\phi,t) = \sum_n \bar{u}_n(\rho,t)\,\bar{\mu}_n(\phi); \qquad \rho \ge L, \qquad t \ge 0, \tag{4.70}$$

where $\bar{\mu}_n(\phi) = (2\pi)^{-1/2}\exp(in\phi)$, $n = 0,\pm1,\pm2,\ldots$, is the orthonormal system of transverse functions, complete in the space $\mathbf{L}_2(0 < \phi < 2\pi)$. The spatial–temporal amplitudes $\bar{u}_n(\rho,t)$ (the evolutionary bases $\bar{u}(\rho,t) = \{\bar{u}_n(\rho,t)\}$) of the waves $U(\rho,\phi,t)$ are available from the solutions of the initial boundary value problems

$$\begin{cases} \left[-\frac{\partial^2}{\partial t^2} + \frac{1}{\rho}\,\frac{\partial}{\partial \rho}\rho\frac{\partial}{\partial \rho} - \frac{n^2}{\rho^2}\right] \bar{u}_n(\rho,t) = 0; \qquad \rho > L, \qquad t > 0 \\ \bar{u}_n(\rho,0) = 0, \quad \frac{\partial}{\partial t}\bar{u}_n(\rho,t)\big|_{t=0} = 0; \qquad \rho \ge L \end{cases} . \tag{4.71}$$

The expansion (4.70) refers to an analysis in the space of complex functions $\bar{u}_n(\rho,t)$. We can (through a slight analytic complication) translate the analysis into a real space, thereby saving computer resources. An important point is that the scheme for constructing the radiation conditions is identical within both approaches.

Let us multiply (4.71) by $\chi(\rho–L)$ and then apply the Hankel transformation in ρ on the semi-axis $\rho \ge 0$ (image $\leftrightarrow$ original):

$$\begin{aligned}&\tilde{f}_n(\omega) = H\left[f_n\right](\omega) \equiv \int_0^\infty f_n(\rho)\,\rho\,J_{|n|}(\rho\omega)\,d\rho \quad \leftrightarrow \\ &\leftrightarrow \quad f_n(\rho) = H^{-1}\left[\tilde{f}_n\right](\rho) \equiv \int_0^\infty \tilde{f}_n(\omega)\,\omega\,J_{|n|}(\rho\omega)\,d\omega.\end{aligned} \tag{4.72}$$

Finally, for the images $\tilde{Z}_n(\omega,t)$ of the functions $Z_n(\rho,t) = \bar{u}_n(\rho,t)\,\chi(\rho - L)$ we have,

$$\begin{cases}\left(\frac{\partial^2}{\partial t^2} + \omega^2\right)\tilde{Z}_n(\omega,t) = L\left[\bar{u}_n(L,t)\,J'_{|n|}(\omega L) - \bar{u}'_n(L,t)\,J_{|n|}(\omega L)\right]; \\ \qquad \omega > 0, \qquad t > 0 \\ \tilde{Z}_n(\omega,0) = \frac{\partial}{\partial t}\tilde{Z}_n(\omega,t)\big|_{t=0} = 0; \qquad \omega \geq 0\end{cases}. \tag{4.73}$$

Here,

$$\bar{u}'_n(L,t) = \frac{\partial}{\partial\rho}\bar{u}_n(\rho,t)\Big|_{\rho=L} \text{ and } J'_{|n|}(\omega L) = \frac{\partial}{\partial\rho}J_{|n|}(\omega\rho)\Big|_{\rho=L}.$$

The derivation of (4.73) uses the familiar formula [201]

$$-\omega^2\tilde{f}_n(\omega) \quad \leftrightarrow \quad \left[\frac{d^2}{d\rho^2} + \frac{d}{\rho d\rho} - \frac{n^2}{\rho^2}\right] f_n(\rho)$$

and the chain of evident equalities

$$\begin{aligned}&\chi(\rho - L)\left[\tfrac{1}{\rho}\,\tfrac{\partial}{\partial\rho}\rho\tfrac{\partial}{\partial\rho}\right]\bar{u}_n(\rho,t) = \chi(\rho - L)\left[\tfrac{1}{\rho}\,\tfrac{\partial}{\partial\rho} + \tfrac{\partial^2}{\partial\rho^2}\right]\bar{u}_n(\rho,t) = \\ &= \left[\tfrac{1}{\rho}\,\tfrac{\partial}{\partial\rho} + \tfrac{\partial^2}{\partial\rho^2}\right]Z_n(\rho,t) - \delta(\rho - L)\left[\tfrac{1}{\rho} + \tfrac{\partial}{\partial\rho}\right]\bar{u}_n(\rho,t) - \\ &- \tfrac{\partial}{\partial\rho}\left[\delta(\rho - L)\,\bar{u}_n(\rho,t)\right],\end{aligned}$$

and, also, the equality $(\partial^\alpha f,\gamma) = (-1)^{|\alpha|}(f,\partial^\alpha\gamma)$ defining the generalized derivative $\partial^\alpha f$ of the generalized function $f \in \tilde{\mathbf{D}}(\mathbf{R}^n)$ (see Section 1.1.3).

Problems (4.73) are similar to (4.6) in Section 4.1.1. Their solutions

$$\tilde{Z}_n(\omega,t) = \frac{L}{\omega}\int_0^t \sin\left[\omega(t - \tau)\right]\left[\bar{u}_n(L,\tau)\,J'_{|n|}(\omega L) - \bar{u}'_n(L,\tau)\,J_{|n|}(\omega L)\right]d\tau$$

after inverse Hankel transform (4.72) become

$$\begin{aligned}&\bar{u}_n(\rho,t) = L\int_0^t\left[\bar{u}_n(L,\tau)f'_n(L,\rho,t - \tau) - \bar{u}'_n(L,\tau)f_n(L,\rho,t - \tau)\right]d\tau; \\ &\rho \geq L,\ t \geq 0.\end{aligned} \tag{4.74}$$

Formula (4.74) describes spatial–time amplitude variations of outgoing transient cylindrical waves (4.70), propagating from the circle $\rho = L$ to $\rho \geq L$. Here,

$$f_n(r,\rho,t-\tau)=\int_0^{\infty}\sin[\omega(t-\tau)]\,J_{|n|}(\omega r)J_{|n|}(\omega\rho)\,d\omega \tag{4.75}$$

and

$$f_n'(L,\rho,t-\tau)=\frac{\partial}{\partial r}f_n(r,\rho,t-\tau)\bigg|_{r=L}.$$

The integration in (4.75) is converted to the calculation of the first and the second kind Legendre functions $P_{|n|-1/2}(a)$ and $Q_{|n|-1/2}(-a)$ for the argument $a_{r,\rho}=\left[r^2+\rho^2-(t-\tau)^2\right]/(2\rho r)$ [1]:

$$f_n(r,\rho,t-\tau)=\begin{cases}0; & 0<t-\tau<\rho-r\\ P_{|n|-1/2}\left(a_{r,\rho}\right)\Big/\left[2(r\rho)^{1/2}\right]; & \rho-r<t-\tau<\rho+r\\ Q_{|n|-1/2}\left(-a_{r,\rho}\right)\cos(n\pi)\Big/\left[\pi(r\rho)^{1/2}\right]; & \rho+r<t-\tau\end{cases}=$$
$$=\chi[(t-\tau)-(\rho-r)]\,Q_{|n|-1/2}\left(-a_{r,\rho}\right)\cos(n\pi)\Big/\left[\pi(r\rho)^{1/2}\right];\qquad 0<t-\tau.$$

The final step is the use of the familiar property of the Legendre functions [202]

$$P_\nu(x)=\cos(\nu\pi)\,P_\nu(-x)-\frac{2}{\pi}\sin(\nu\pi)\,Q_\nu(-x).$$

Formula (4.74) in problems (4.44) acts in the same manner as (4.10) does in the infinite grating problems (4.1). Following the previous line of rearrangements, one finally gets the exact radiation conditions for the total field $U(g,t)$ in the region $\rho>L$. Considering [7, 202] that the value of $Q_{|n|-1/2}(-a_{r,\rho})$ at $t-\tau=\rho-r$ is $Q_{|n|-1/2}(-1)=\pi P_{|n|-1/2}(1)\big/2\cos(n\pi)=\pi\big/2\cos(n\pi)$, while $\partial\chi[(t-\tau)-(\rho-r)]\big/\partial r=\delta[(t-\tau)-(\rho-r)]$, upon differentiation in (4.74) and summation of the results in accordance with (4.70), we obtain for $\rho\geq L$ and $t\geq 0$:

$$\begin{aligned}&U(\rho,\phi,t)=\\ &=\tfrac{1}{2}\sqrt{\tfrac{L}{\rho}}\,U(L,\phi,t-\rho+L)+\tfrac{1}{\pi}\sqrt{\tfrac{L}{\rho}}\sum_n(-1)^n\bar{\mu}_n(\phi)\int_0^{t-(\rho-L)}\Big\{\tfrac{\bar{u}_n(L,\tau)}{2L}\times\\ &\times\left[Q'_{|n|-1/2}\left(-a_{L,\rho}\right)\left(\tfrac{\rho^2-L^2-(t-\tau)^2}{L\rho}\right)-Q_{|n|-1/2}\left(-a_{L,\rho}\right)\right]-\\ &-\bar{u}'_n(L,\tau)\,Q_{|n|-1/2}\left(-a_{L,\rho}\right)\Big\}\,d\tau.\end{aligned} \tag{4.76}$$

On the artificial boundary $\rho=L$, the exact absorbing condition coming from (4.76) takes the form

$$U(L,\phi,t) = \frac{2}{\pi}\sum_{n}(-1)^n\bar{\mu}_n(\phi)\left[\int_0^t\left[\bar{u}_n(L,\tau)\,\xi_n(t-\tau) - \bar{u}'_n(L,\tau)\,\eta_n(t-\tau)\right]d\tau\right];$$
$$0 \le \phi \le 2\pi, \qquad t \ge 0. \tag{4.77}$$

In (4.76) and (4.77) the following notations have been introduced:

$$Q'_{|n|-1/2}(-a) = \frac{\partial}{\partial x}Q_{|n|-1/2}(x)\big|_{x=-a},$$
$$\xi_n(t-\tau) = \left[2Q'_{|n|-1/2}\left(-a_{L,L}\right)\left(a_{L,L}-1\right) - Q_{|n|-1/2}\left(-a_{L,L}\right)\right](2L)^{-1},$$
$$\text{and } \eta_n(t-\tau) = Q_{|n|-1/2}\left(-a_{L,L}\right).$$

The expression (4.76) suggests the exact radiation condition for an outgoing transient waves $U(\rho,\phi,t)$ and solves the far-zone problem by extending the originally compact grating problems (4.44) to the situation in which the calculation space is bounded with EACs (4.66), (4.67), and (4.68).

4.3 Time Domain Methods in the Study of Gratings and Compact Grating Structures as Open Resonators

The exact absorbing conditions properly bounding the calculation space of initial boundary value problems suggest versatile and stable computational schemes aimed at a wide diversity of problems in electromagnetic resonant scattering [1, 4, 40, 193–195]. How can we benefit from these schemes in the spectral study of different electromagnetic objects, in particular, those from Sections 4.1 and 4.2? How is it possible to find out information about certain high-quality free oscillations of the field from the database representing the transient dynamics in some open (periodic, compact, or guiding) resonators? Or how is it possible to distinguish these oscillations in the response that the resonance structure gives to the excitation by broadband or quasi-monochromatic signals? In Sections 4.3.1 and 4.3.2, these questions will be discussed by considering some elementary problems in the theory of infinite periodic gratings. The reported results are easy to extend to more complicated problems in this theory and also to problems for compact grating structures (see Sections 4.2, 4.3.3, and papers [203, 204]).

4.3.1 Spatial–Frequency Representations of Transient Fields and Preliminary Qualitative Analysis

The initial boundary value problems and the boundary value problems given in equations (4.78) and (4.79) below

$$\begin{cases} \left[-\varepsilon\mu\frac{\partial^2}{\partial t^2}-\sigma\mu\frac{\partial}{\partial t}+\frac{\partial^2}{\partial y^2}+\frac{\partial^2}{\partial z^2}\right]U(g,t)=F(g,t); \\ \qquad g=\{y,z\}\in\mathbf{Q}=\mathbf{R}\backslash\overline{\mathrm{int}\mathbf{S}_x}, \qquad t>0 \\ U(g,0)=\varphi(g), \qquad \frac{\partial}{\partial t}U(g,t)\big|_{t=0}=\psi(g); \qquad g\in\bar{\mathbf{Q}}, \\ E_{tg}(p,t)\big|_{p=\{x,y,z\}\in\mathbf{S}}=0; \qquad t\geq 0 \\ U\left\{\frac{\partial U}{\partial y}\right\}(l,z,t)=U\left\{\frac{\partial U}{\partial y}\right\}(0,z,t); \qquad t\geq 0 \end{cases} \tag{4.78}$$

$$\begin{cases} \left[\frac{\partial^2}{\partial y^2}+\frac{\partial^2}{\partial z^2}+\tilde{\varepsilon}\mu k^2\right]\tilde{U}\left(g,k,\tilde{f}\right)=\tilde{f}(g,k); \qquad g\in\mathbf{Q} \\ \tilde{E}_{tg}(p,k)\big|_{p=\{x,y,z\}\in\mathbf{S}}=0 \\ \tilde{U}\left\{\frac{\partial\tilde{U}}{\partial y}\right\}(l,z,k)=\tilde{U}\left\{\frac{\partial\tilde{U}}{\partial y}\right\}(0,z,k) \\ \tilde{U}(g,k)=\sum\limits_{n=-\infty}^{n=\infty}\left\{\begin{matrix}A_n(k)\\B_n(k)\end{matrix}\right\}\mathrm{e}^{i[\Phi_n y\pm\Gamma_n(z\mp a)]}; \qquad \left\{\begin{matrix}z\geq a\\z\leq -a\end{matrix}\right\} \end{cases} . \tag{4.79}$$

describe transient and stable processes going on in 1-D periodic gratings, or, more precisely, in the Floquet channels $\mathbf{R}$ whose compact discontinuities scatter the waves owing to sources confined in the region $\mathbf{Q}_a=\{g\in\mathbf{Q}:\ |z|<a\}\in\mathbf{Q}_L$. These are (1.18) [or (4.1)] and (1.20), (1.22) problems (indices *new* are dropped) for $\Phi=0$ – $\mathrm{Im}U(g,t)\equiv 0$, if only $\mathrm{Im}F(g,t)=\mathrm{Im}\varphi(g)=\mathrm{Im}\psi(g)\equiv 0$. Their solutions $\tilde{U}(g,k)$ (for $\mathrm{Im}k>0$) and $U(g,t)$ ($t\geq 0$) obey the formulas (see Section 1.1.4)

$$U(g,t)=\frac{1}{2\pi}\int\limits_{i\alpha-\infty}^{i\alpha+\infty}\tilde{U}(g,k)\mathrm{e}^{-ikt}dk,\ \tilde{U}(g,k)=\int\limits_0^{\infty}U(g,t)\mathrm{e}^{ikt}dt. \tag{4.80}$$

All $\bar{k}$ poles of the resolvents $A^{-1}(k)$ of the (4.79) type problem $A(k)\left[\tilde{U}\left(g,k,\tilde{f}\right)\right]=\tilde{f}(g,k)$, $g\in\bar{\mathbf{Q}}$, on the first – physical – sheet $\mathbf{C}_k$ of the $\mathbf{K}$ surface are localized in the region $\mathrm{Im}k\leq 0$ (see Sections 1.1.4 and 1.3.2). Assuming that elements $\bar{k}$ of the set Ω_k do not accumulate in the neighborhood of the axis $\mathrm{Im}k=0$ as $|\mathrm{Re}k|\to\infty$, we can deform the integration contour $|\mathrm{Re}k|<\infty$, $\mathrm{Im}k=\alpha>0$ in (4.80) downward to $\mathrm{Im}k=-\beta<0$. Narrow loops of the new contour $\mathbf{P}$ go the branch points $k_n^{\pm}$ around and descent along the two sides of the branch cuts of the surface $\mathbf{K}$ (see Fig. 1.2a). In the result,

$$
\begin{aligned}
U(g,t) &= \frac{1}{2\pi}\int\limits_{i\alpha-\infty}^{i\alpha+\infty}\left[A^{-1}(k)\left[\tilde{f}(g,k)\right]\right]\mathrm{e}^{-ikt}dk = \\
&= \frac{1}{2\pi}\int\limits_{i\alpha-\infty}^{i\alpha+\infty}\left[\int\limits_{\mathbf{Q}}\tilde{G}(g,g_0,k)\tilde{f}(g_0,k)\,dg_0\right]\mathrm{e}^{-ikt}dk = \\
&= \frac{1}{i}\left\{\sum_n\int\limits_{\mathbf{Q}}\operatorname*{Res}_{k=\bar{k}_n}\left[\tilde{G}(g,g_0,k)\tilde{f}(g_0,k)\,\mathrm{e}^{-ikt}\right]dg_0 + \right. \\
&\left. + \sum_m\int\limits_{\mathbf{Q}}\operatorname*{Res}_{k=\underline{k}_m}\left[\tilde{G}(g,g_0,k)\tilde{f}(g_0,k)\,\mathrm{e}^{-ikt}\right]dg_0\right\} + R(g,t)\,; \\
&g\in\mathbf{Q}_L,\ t>0.
\end{aligned}
\tag{4.81}
$$

Here:

- $\tilde{G}(g,g_0,k)$, $g_0\in Q_a$, is the Green function of problem (4.79), or the kernel of the operator-function $A^{-1}(k)$;
- $\bar{k}_n \in \Omega_k$ are the characteristic numbers of the operator $A(k)$ (eigenfrequencies of the open periodic resonator) which are situated on the first sheet of the **K** surface over the contour **P** and numbered so that $\mathrm{Im}\bar{k}_{n+1} \le \mathrm{Im}\bar{k}_n$; these eigenfrequencies are finite in number;
- $\underline{k}_m$ are the poles of the function $\tilde{f}(g,k)$ which do not coincide with the elements of the spectral set Ω_k; all they are assumed to belong to the plane $\mathbf{C}_k$ over the contour **P**;
- the function $R(g,t) = \frac{1}{2\pi}\int\limits_{\mathbf{P}}\tilde{U}(g,k)\,\mathrm{e}^{-ikt}dk$ summarizes the contributions from the singularities of the function $\tilde{U}\left(g,k,\tilde{f}\right)$, $k\in\mathbf{K}$, which have not been encircled in the deformation of the integration contour in expression (4.80); $\|R(g,t)\|_{\mathbf{W}_2^1(\mathbf{Q}_a)} = O\left(t^{-1}\right)$ as $t\to\infty$ [10].

The identity $\tilde{\varepsilon}(-k^*) = \tilde{\varepsilon}^*(k)$ suggests

Statement 4.5

$$
\tilde{G}(g,g_0,k) = \tilde{G}(g_0,g,k) = \tilde{G}^*\left(g,g_0,-k^*\right). \tag{4.82}
$$

On the basis of (4.82) and assuming that $\tilde{f}(g,-k^*) = \tilde{f}^*(g,k)$, which is true for all real current and instant sources of practical interest, we can rewrite (4.81) in the form

$$
\begin{aligned}
U(g,t) &= 2\mathrm{Im}\left\{\sum_n\int\limits_{\mathbf{Q}}\operatorname*{Res}_{k=\bar{k}_n:\,\mathrm{Re}\bar{k}_n>0}\left[\tilde{G}(g,g_0,k)\tilde{f}(g_0,k)\,\mathrm{e}^{-ikt}\right]dg_0 + \right. \\
&\left. + \sum_m\int\limits_{\mathbf{Q}}\operatorname*{Res}_{k=\underline{k}_m:\,\mathrm{Re}\,\underline{k}_m>0}\left[\tilde{G}(g,g_0,k)\tilde{f}(g_0,k)\,\mathrm{e}^{-ikt}\right]dg_0\right\} + R(g,t)\,; \\
&g\in\mathbf{Q}_L,\ t>0.
\end{aligned}
\tag{4.83}
$$

A complete analytic description of the deformations experienced by the $U(g,t)$ pulses inside open periodic resonators (gratings) is scarcely possible without relevant computations whose results should be properly considered. In these structures, the transients develop very fast, and multiple factors have an influence on them. Therefore, a strong background of computational experiment is necessary. Sometimes some features of the results have to be to a certain extent predicted beforehand – you should be prepared to what is going to come out, in order to be able to recognize it. Of benefit here can be analytic representations of the type (4.81) and (4.83). They certainly refine the process, leaving the main participants alone on the stage. Yet having traced these components in the actual database, one can feel more confident when taking up the interpretation of the physical sense of the obtained results. Also, the analysis of field transients in open periodic resonators cannot be fruitful if one leaves aside the results of the spectral theory and the theory of resonant scattering of sinusoidal waves. The achievements of the kind can suggest a reasonable scheme for numerical experiment in the time domain, ridding us off a direct, little-efficiency item-by-item examination of probable situations. All this are general phrases. Now, proceed to expressions (1.23) from Statement 1.3 and (4.81) and (4.83) to have some particular corollaries facilitating the numerical experiments and the interpretation of their results [203, 204].

Assume that all poles $k = \bar{k} \in \mathbf{C}_k$ of the Green function $\tilde{G}(g,g_0,k)$ of problem (4.79) are simple. This assumption is supported by Statement 1.6 and also, as shown in Section 1.3.2, by the numerical results in frequency domain. Yet otherwise (say, for example, the point $k = \bar{k}$; $\mathrm{Re}\bar{k} > 0$, $\mathrm{Im}\bar{k} < 0$ is a second-order pole) the corresponding term

$$2\mathrm{Im}\int\limits_{\mathbf{Q}} \operatorname*{Res}_{k=\bar{k}} \left[\tilde{G}(g,g_0,k)\tilde{f}(g_0,k)\,\mathrm{e}^{-ikt}\right] dg_0 =$$

$$= 2\mathrm{Im}\left\{-it\mathrm{e}^{-i\bar{k}t}\int\limits_{\mathbf{Q}} G_{-2}\left(g,g_0,\bar{k}\right) f_0\left(g_0,\bar{k}\right) dg_0 + \right.$$

$$\left. +\mathrm{e}^{-i\bar{k}t}\int\limits_{\mathbf{Q}} \left[G_{-2}\left(g,g_0,\bar{k}\right) f_1\left(g_0,\bar{k}\right) + G_{-1}\left(g,g_0,\bar{k}\right) f_0\left(g_0,\bar{k}\right)\right] dg_0 \right\}$$

in the expansion (4.83) when $\tilde{f}(g,k) = ik\tilde{\varepsilon}(g)\,\mu(g)\,\varphi(g) - \varepsilon(g)\,\mu(g)\,\psi(g)$ (the grating is excited by a transient wave $U^i(g,t)$) will grow until $t = T_1 < T$, faster than the general energy ratios permit (see, for example, formula (1.31) in [1]). From this point on, $G_l(g,g_0,\eta)$ and $f_l(g_0,\eta)$ are the coefficients of the terms $(k–\eta)^l$ in the Laurent expansion of the functions $\tilde{G}(g,g_0,k)$ and $\tilde{f}(g_0,k)$ about a point $k = \eta$.

Without loss of generality, every characteristic number $\bar{k}$ can be assumed to correspond to one eigen element $u_0^{(1)}(g) = u_0\left(g,\bar{k}\right)$ of the operator-function $A(k)$. The eigen element $w_0^{(1)}(g)$ of the operator-function $\bar{A}(k)$ (see Statement 1.3) is denoted by $w_0\left(g,\bar{k}^*\right)$ when it refers to the characteristic number $\bar{k}^*$.

Under these assumptions, the principal part $\Xi\tilde{G}$ of the Green function $\tilde{G}(g,g_0,k)$ [see (1.23)] in the vicinity of the characteristic number $k = \bar{k}$ is

$$\Xi\tilde{G}\left(g,g_0,k\right)=\frac{G_{-1}\left(g,g_0,\bar{k}\right)}{k-\bar{k}}=\frac{u_0\left(g,\bar{k}\right)w_0^*\left(g_0,\bar{k}^*\right)}{k-\bar{k}},\tag{4.84}$$

and it follows from (4.82) and (4.84) that eigen elements u_0 and w_0 are connected by the relations

$$u_0\left(g,\bar{k}\right)=w_0^*\left(g,\bar{k}^*\right),\ u_0\left(g,\bar{k}\right)w_0^*\left(g_0,\bar{k}^*\right)=-u_0^*\left(g,-\bar{k}^*\right)w_0\left(g_0,-\bar{k}\right).\tag{4.85}$$

Now consider some indicative situations **A** to **E**. Using (4.83), (4.84), and (4.85) we will derive for them certain analytic representations to facilitate analysis of the numerical results as applied to problems (4.78).

Situation **A**: The function $\tilde{f}\left(g,k\right)$ has no singularities on the sheet $\mathbf{C}_k$. From (4.83), it follows that

$$\begin{aligned}U\left(g,t\right)\approx 2\mathrm{Im}\left[\sum_{n:\,\mathrm{Re}\bar{k}_n>0}u_0\left(g,\bar{k}_n\right)\mathrm{e}^{-i\bar{k}_nt}\int\limits_{\mathbf{Q}}u_0\left(g_0,\bar{k}_n\right)\tilde{f}\left(g_0,\bar{k}_n\right)dg_0\right]=\\ =2\sum_{n:\,\mathrm{Re}\bar{k}_n>0}\mathrm{e}^{t\mathrm{Im}\bar{k}_n}\left|u_0\left(g,\bar{k}_n\right)\right|\left|C\left(\tilde{f},\bar{k}_n\right)\right|\sin\left[\arg u_0\left(g,\bar{k}_n\right)+\right.\\ \left.+\arg C\left(\tilde{f},\bar{k}_n\right)-t\mathrm{Re}\bar{k}_n\right];\ g\in\mathbf{Q}_L,\ 0<T_1<t<T.\end{aligned}\tag{4.86}$$

Here, (0;T) is the observation time, T_1 is specified by the experimental conditions, and

$$C\left(f,\bar{k}\right)=\int\limits_{\mathbf{Q}}u_0\left(g_0,\bar{k}\right)f\left(g_0,\bar{k}\right)dg_0.\tag{4.87}$$

From (4.86) it follows that the near field $U(g,t)$ of a periodic open resonator is a superposition of the free oscillation fields $u_0\left(g,\bar{k}\right)$ corresponding to real and complex eigenfrequencies $\bar{k}$. The lifetime of each oscillation in the $\mathbf{Q}_L$ domain and the velocity of its decay are determined by $\left|\mathrm{Im}\bar{k}\right|$ (or by the quality $Q=\mathrm{Re}\bar{k}/2\left|\mathrm{Im}\bar{k}\right|$). The initial state (or the excitation level) is governed by the $C\left(\tilde{f},\bar{k}\right)$ function estimating the degree of the linkage between the amplitude–spatial and the amplitude–frequency characteristics of the field $u_0\left(g,\bar{k}\right)$ on one side and the source function $\tilde{f}\left(g,k\right)$ on the other.

Situation **B**: In the right half-plane of the $\mathbf{C}_k$ sheet, the function $\tilde{f}\left(g,k\right)$ has one simple pole that is located at a point $k=\underline{k}$ and does not coincide with any element $\bar{k}$ from the set Ω_k. From (4.83) we have

$$U(g,t) \approx 2\mathrm{Im}\left\{\sum_{n:\,\mathrm{Re}\bar{k}_n>0} u_0\left(g,\bar{k}_n\right)\mathrm{e}^{-i\bar{k}_n t}\int\limits_{\mathbf{Q}} u_0\left(g_0,\bar{k}_n\right)\tilde{f}\left(g_0,\bar{k}_n\right)dg_0 + \right.$$
$$\left. +\mathrm{e}^{-i\underline{k}t}\int\limits_{\mathbf{Q}}\tilde{G}\left(g,g_0,\underline{k}\right)f_{-1}\left(g_0,\underline{k}\right)dg_0\right\} = 2\left\{\sum_{n:\,\mathrm{Re}\bar{k}_n>0}\mathrm{e}^{t\mathrm{Im}\bar{k}_n}\left|u_0\left(g,\bar{k}_n\right)\right|\times\right.$$
$$\times\left|C\left(\tilde{f},\bar{k}_n\right)\right|\sin\left[\arg u_0\left(g,\bar{k}_n\right)+\arg C\left(\tilde{f},\bar{k}_n\right)-t\mathrm{Re}\bar{k}_n\right]+$$
$$\left.+\mathrm{e}^{t\mathrm{Im}\underline{k}}\left|\tilde{U}\left(g,\underline{k},f_{-1}\right)\right|\sin\left[\arg\tilde{U}\left(g,\underline{k},f_{-1}\right)-t\mathrm{Re}\underline{k}\right]\right\};$$
$$g\in\mathbf{Q}_L,\ 0<T_1<t<T. \tag{4.88}$$

The expression (4.88) contains a new term for the field whose oscillation frequency is $\mathrm{Re}\underline{k}$. The spatial field configuration is determined by the solution $\tilde{U}\left(g,\underline{k},f_{-1}\right)$ of the elliptic problem $A\left(\underline{k}\right)\left[\tilde{U}\left(g,\underline{k},f_{-1}\right)\right]=f_{-1}\left(g,\underline{k}\right)$. The amplitude decreases as $\exp\left(t\mathrm{Im}\underline{k}\right)$. If $\mathrm{Im}\bar{k}_n<0$ for all n, then for $\mathrm{Im}\,\underline{k}=0$ and a sufficiently large t this term will dominate in the field $U(g,t)$, setting the so-called limiting amplitude principle.

Situation **C**: In the right half-plane of the $\mathbf{C}_k$ sheet, the function $\tilde{f}\,(g,k)$ possesses one second-order pole. It is located at a point $k=\underline{k}$ and coincides with none of $\bar{k}$ elements of the set Ω_k. In this case,

$$U(g,t)\approx 2\mathrm{Im}\left\{\sum_{n:\,\mathrm{Re}\bar{k}_n>0}u_0\left(g,\bar{k}_n\right)\mathrm{e}^{-i\bar{k}_n t}\int\limits_{\mathbf{Q}}u_0\left(g_0,\bar{k}_n\right)\tilde{f}\left(g_0,\bar{k}_n\right)dg_0-\right.$$
$$-it\mathrm{e}^{-i\underline{k}t}\int\limits_{\mathbf{Q}}\tilde{G}\left(g,g_0,\underline{k}\right)f_{-2}\left(g_0,\underline{k}\right)dg_0+$$
$$\left.+\mathrm{e}^{-i\underline{k}t}\int\limits_{\mathbf{Q}}\left[\tilde{G}\left(g,g_0,\underline{k}\right)f_{-1}\left(g_0,\underline{k}\right)+G_1\left(g,g_0,\underline{k}\right)f_{-2}\left(g_0,\underline{k}\right)\right]dg_0\right\}=$$
$$=2\left\{\sum_{n:\,\mathrm{Re}\bar{k}_n>0}\mathrm{e}^{t\mathrm{Im}\bar{k}_n}\left|u_0\left(g,\bar{k}_n\right)\right|\sin\left[\arg u_0\left(g,\bar{k}_n\right)+\arg C\left(\tilde{f},\bar{k}_n\right)-t\mathrm{Re}\bar{k}_n\right]\times\right.$$
$$\times\left|C\left(\tilde{f},\bar{k}_n\right)\right|-t\mathrm{e}^{t\mathrm{Im}\underline{k}}\left|\tilde{U}\left(g,\underline{k},f_{-2}\right)\right|\cos\left[\arg\tilde{U}\left(g,\underline{k},f_{-2}\right)-t\mathrm{Re}\underline{k}\right]+$$
$$+\mathrm{e}^{t\mathrm{Im}\underline{k}}\left|\tilde{U}\left(g,\underline{k},f_{-1}\right)+\tilde{U}_1\left(g,\underline{k},f_{-2}\right)\right|\sin\left[\arg\left[\tilde{U}\left(g,\underline{k},f_{-1}\right)+\tilde{U}_1\left(g,\underline{k},f_{-2}\right)\right]-\right.$$
$$\left.-\ t\mathrm{Re}\underline{k}\right]\right\};\ g\in\mathbf{Q}_L,0<T_1<t<T. \tag{4.89}$$

Here,

$$\tilde{U}_l\left(g,\eta,f\right)=\int\limits_{\mathbf{Q}}G_l\left(g,g_0,\eta\right)f\left(g_0,\eta\right)dg_0.$$

For $\operatorname{Im}\underline{k} = 0$ and sufficiently large t, the contribution from the free oscillations corresponding to complex eigenfrequencies $\bar{k}$ to the $U(g,t)$ field can be dropped. Even against the background of steady-state free oscillations corresponding to real eigenfrequencies $\bar{k}$, the field of the $k = \underline{k}$ frequency oscillation will dominate then. The spatial configuration of this field is given by the solution $\tilde{U}\left(g,\underline{k},f_{-2}\right)$ of the elliptic problem $A(\underline{k})\left[\tilde{U}\left(g,\underline{k},f_{-2}\right)\right] = f_{-2}\left(g,\underline{k}\right)$, and the amplitude grows proportionally with t. Although at a small $\left|\operatorname{Im}\underline{k}\right| > 0$, the contrast ceases to be so striking, the pattern (for a certain finite time t of observation) will be practically the same.

Situation **D**: Simple poles $k = \underline{k}$ and $k = \bar{k}$ of the functions $\tilde{f}(g,k)$ and $\tilde{G}(g,g_0,k)$ coincide ($\bar{k} = \underline{k}$). In this case,

$$
\begin{aligned}
U(g,t) \approx 2\operatorname{Im}\Bigg\{ & \sum_{n:\,\operatorname{Re}\bar{k}_n>0;\ \bar{k}_n\neq\bar{k}} u_0\left(g,\bar{k}_n\right)\mathrm{e}^{-i\bar{k}_n t}\int\limits_{\mathbf{Q}} u_0\left(g_0,\bar{k}_n\right)\tilde{f}\left(g_0,\bar{k}_n\right)dg_0 - \\
& -it\mathrm{e}^{-i\bar{k}t}u_0\left(g,\bar{k}\right)\int\limits_{\mathbf{Q}} u_0\left(g_0,\bar{k}\right)f_{-1}\left(g_0,\bar{k}\right)dg_0 + \mathrm{e}^{-i\bar{k}t}u_0\left(g,\bar{k}\right)\times \\
& \times\int\limits_{\mathbf{Q}} u_0\left(g_0,\bar{k}\right)f_0\left(g_0,\bar{k}\right)dg_0 + \mathrm{e}^{-i\bar{k}t}\int\limits_{\mathbf{Q}} G_0\left(g,g_0,\bar{k}\right)f_{-1}\left(g_0,\bar{k}\right)dg_0\Bigg\} = \\
= 2\Bigg\{ & \sum_{n:\,\operatorname{Re}\bar{k}_n>0;\ \bar{k}_n\neq\bar{k}} \mathrm{e}^{t\operatorname{Im}\bar{k}_n}\left|u_0\left(g,\bar{k}_n\right)\right|\left|C\left(\tilde{f},\bar{k}_n\right)\right|\times \\
& \times\sin\left[\arg u_0\left(g,\bar{k}_n\right)+\arg C\left(\tilde{f},\bar{k}_n\right)-t\operatorname{Re}\bar{k}_n\right]- \\
& -t\mathrm{e}^{t\operatorname{Im}\bar{k}}\left|u_0\left(g,\bar{k}\right)\right|\left|C\left(f_{-1},\bar{k}\right)\right|\cos\left[\arg u_0\left(g,\bar{k}\right)+\arg C\left(f_{-1},\bar{k}\right)-t\operatorname{Re}\bar{k}\right]+ \\
& +\mathrm{e}^{t\operatorname{Im}\bar{k}}\left|u_0\left(g,\bar{k}\right)\right|\left|C\left(f_0,\bar{k}\right)\right|\sin\left[\arg u_0\left(g,\bar{k}\right)+\arg C\left(f_0,\bar{k}_n\right)-t\operatorname{Re}\bar{k}\right]+ \\
& +\mathrm{e}^{t\operatorname{Im}\bar{k}}\left|\tilde{U}_0\left(g,\bar{k},f_{-1}\right)\right|\sin\left[\arg\tilde{U}_0\left(g,\bar{k},f_{-1}\right)-t\operatorname{Re}\bar{k}\right]\Bigg\} \\
& g\in\mathbf{Q}_L,\ 0<T_1<t<T.
\end{aligned}
\tag{4.90}
$$

As soon as a singularity of the Green function of problem (4.79) and a source function $\tilde{f}(g,k)$ singularity coincide, the corresponding free oscillation becomes dominant in the $U(g,t)$ field. How long the field

$$
W(g,t) = -2t\mathrm{e}^{t\operatorname{Im}\bar{k}}\left|u_0\left(g,\bar{k}\right)\right|\left|C\left(f_{-1},\bar{k}\right)\right|\cos\left[\arg u_0\left(g,\bar{k}\right)+\arg C\left(f_{-1},\bar{k}\right)-t\operatorname{Re}\bar{k}\right] \tag{4.91}
$$

can hold that position depends on the $\left|\operatorname{Im}\bar{k}\right|$ and $\left|C\left(f_{-1},\bar{k}\right)\right|$ values and, also, on whether the free oscillations $u_0\left(g,\bar{k}_n\right)$ include oscillations of real eigenfrequencies.

Situation **E**: Simple poles $\bar{k}$ and $\underline{k}$ of the functions $\tilde{G}(g,g_0,k)$ and $\tilde{f}(g,k)$ do not coincide but $\left|\bar{k}-\underline{k}\right| \ll 1$. In this case,

$$U(g,t) \approx 2\left\{ \sum_{n:\,\mathrm{Re}\bar{k}_n>0;\ \bar{k}_n\neq\bar{k}} \mathrm{e}^{t\mathrm{Im}\bar{k}_n} \left|u_0\left(g,\bar{k}_n\right)\right| \left|C\left(\tilde{f},\bar{k}_n\right)\right| \times \right.$$
$$\times \sin\left[\arg u_0\left(g,\bar{k}_n\right) + \arg C\left(\tilde{f},\bar{k}_n\right) - t\mathrm{Re}\bar{k}_n\right] -$$
$$-\mathrm{Im}\left[it\mathrm{e}^{-i\bar{k}t} u_0\left(g,\bar{k}\right) \int\limits_{\mathbf{Q}} u_0\left(g_0,\bar{k}\right) f_{-1}\left(g_0,\underline{k}\right) dg_0 - \mathrm{e}^{-i\bar{k}t} u_0\left(g,\bar{k}\right) \times \right.$$
$$\left.\left. \times \int\limits_{\mathbf{Q}} u_0\left(g_0,\bar{k}\right) f_0\left(g_0,\underline{k}\right) dg_0 - \mathrm{e}^{-i\underline{k}t} \int\limits_{\mathbf{Q}} G_0\left(g,g_0,\bar{k}\right) f_{-1}\left(g_0,\underline{k}\right) dg_0 \right]\right\} +$$
$$+O\left(t^2\left|\bar{k}-\underline{k}\right|\right);\ g\in\mathbf{Q}_L,\ 0<T_1<t<T. \tag{4.92}$$

The representations (4.90) and (4.92) are practically the same. It is only determination of the excitation level for the component

$$W(g,t) = -2t\mathrm{e}^{t\mathrm{Im}\bar{k}}\mathrm{Re}\left[\mathrm{e}^{-it\mathrm{Re}\bar{k}} u_0\left(g,\bar{k}\right) \int\limits_{\mathbf{Q}} u_0\left(g_0,\bar{k}\right) f_{-1}\left(g_0,\underline{k}\right) dg_0\right], \tag{4.93}$$

which at certain circumstances can dominate in the field $U(g,t)$, and for other components, oscillating with the frequencies $\mathrm{Re}\,\underline{k}$ and $\mathrm{Re}\bar{k}_n$, somewhat differs from the one in the previous case.

4.3.2 A Choice of the Field Sources in Numerical Experiments

In reality the upper bound T of the observation time $[0;T]$ is often limited as are the possibilities of present means of computation. When T is not large enough, some special measures must be undertaken to separate the contributions from particular quasi-monochromatic components to the total field $U(g,t)$ in order to examine the spectral characteristics of the open periodic resonator. A variant of the solution of the problem is as follows. We should choose a field source that could unveil one or another oscillation against the background of others, making its properties manifestly more conspicuous for the further investigation.

Begin with the Situation **A**, whose analytic description is given by (4.86). When among other free oscillations of comparable quality, a certain one of eigenfrequency $\bar{k}$ is wanted, then a source $\tilde{f}(g,k)$ is needed such that $\left|C\left(\tilde{f},\bar{k}\right)\right| \gg \left|C\left(\tilde{f},\bar{k}_n\right)\right|$, $\bar{k}_n \neq \bar{k}$. Formula (4.87) suggests the following algorithm for the choice:

- in a considered frequency range, $\tilde{f}(g,k)$, as a function of parameter k, must have a single and well-pronounced amplitude center located in the neighborhood of the point $k=\bar{k}$;

- the function $\tilde{f}\left(g,\bar{k}\right)$, as a member of the space $\mathbf{L}_2(\mathbf{Q}_L)$, must be closely parallel to the element $w_0\left(g,\bar{k}^*\right) = u_0^*\left(g,\bar{k}\right)$ in the same space.

Both these requirements are easily satisfied when $\tilde{f}\,(g,k) \leftrightarrow F\,(g,t)$ (here, as before, the function derived through the Laplace transform is identified with its continuation to the first sheet of the **K** surface), and some information about the spatial structure of the free oscillation field $u_0\left(g,\bar{k}\right)$ is available beforehand.

The excitation source of the open resonator and the observation time length $0 \leq t \leq T$ are very important in the experiment and must comply with the particular problem to be solved. This will be explained in terms of an example. A soft current source

$$F\,(g,t) = P\,(g)\exp\left[-\left(t-\tilde{T}\right)^2\Big/4\tilde{\alpha}^2\right]\cos\left[\tilde{k}\left(t-\tilde{T}\right)\right]\chi\left(\bar{T}-t\right) = P\,(g)\,F_1\,(t) \tag{4.94}$$

for E-polarized waves ($\chi(\ldots)$ is the Heaviside step function) is specified by the five free parameters: $P(g)$, $\tilde{k}$, $\tilde{\alpha}$, $\tilde{T}$, and $\bar{T}$. The first one gives the size and location of the support of the function $F(g,t)$ (in other words, the source geometry) and also a spatial current distribution over this support. The parameter $\tilde{k}$ specifies the amplitude center of the primary signal $U_{\text{prim}}(g,t)$ (and, of course, of the functions $\tilde{F}\,(g,k) \leftrightarrow F\,(g,t)$ and $\tilde{F}_1\,(k) \leftrightarrow F_1\,(t)$, too) in the spectral domain (in the domain of real k; see Fig. 4.3a), i.e., the maximum point of the module of the function

$$\tilde{U}_{\text{prim}}\left(g,k,\tilde{f}\right) = \int_0^T U_{\text{prim}}\,(g,t)e^{ikt}dt \quad \leftrightarrow \quad \begin{cases} U_{\text{prim}}\,(g,t)\,; & t \leq T \\ 0; & t > T \end{cases}.$$

Here $U_{\text{prim}}(g,t)$ is the field of the source $F(g,t)$ in free space. The parameters $\tilde{k}$ and $\tilde{\alpha}$ establish the band $\left[\tilde{k}-b\big/\tilde{\alpha};\tilde{k}+b\big/\tilde{\alpha}\right]$ of real frequencies k, where the normalized spectral amplitudes of the field $U_{\text{prim}}(g,t)$ ($\left|\tilde{U}_{\text{prim}}\,(g,k)\right|\Big/\left|\tilde{U}_{\text{prim}}\left(g,\tilde{k}\right)\right|$ values) do not fall below the γ level. On the t–axis, the signal $U_{\text{prim}}(g,t)$ occupies the interval $\tilde{T}-c\tilde{\alpha} \leq t \leq \tilde{T}+c\tilde{\alpha}$, and $\left|U_{\text{prim}}\,(g,t)\right|\Big/\left|U_{\text{prim}}\left(g,\tilde{T}\right)\right| \leq \gamma$ beyond it. Table 4.1 lists the coefficients b and c which are available due to the well-known analytic representations [40] for several γ levels. The parameters $\tilde{T}$ and $\bar{T} \geq 2\tilde{T}$ control the delay of signal $U_{\text{prim}}(g,t)$ and its duration.

Now it is time to ask what requirements should be imposed on the above-mentioned parameters to benefit from the study of the general frequency characteristics of the open periodic resonator? Evidently the frequency $\tilde{k}$ should be close to the central point of the frequency band of interest. The parameter $\tilde{\alpha}$ is picked so that the level of normalized spectral amplitudes of the signal $U_{\text{prim}}(g,t)$ [of the function $F(g,t)$] in this band would not be lower than 0.1. In fact, it would be better to keep it not less than 0.5. Then the ultimate picture we could observe if the

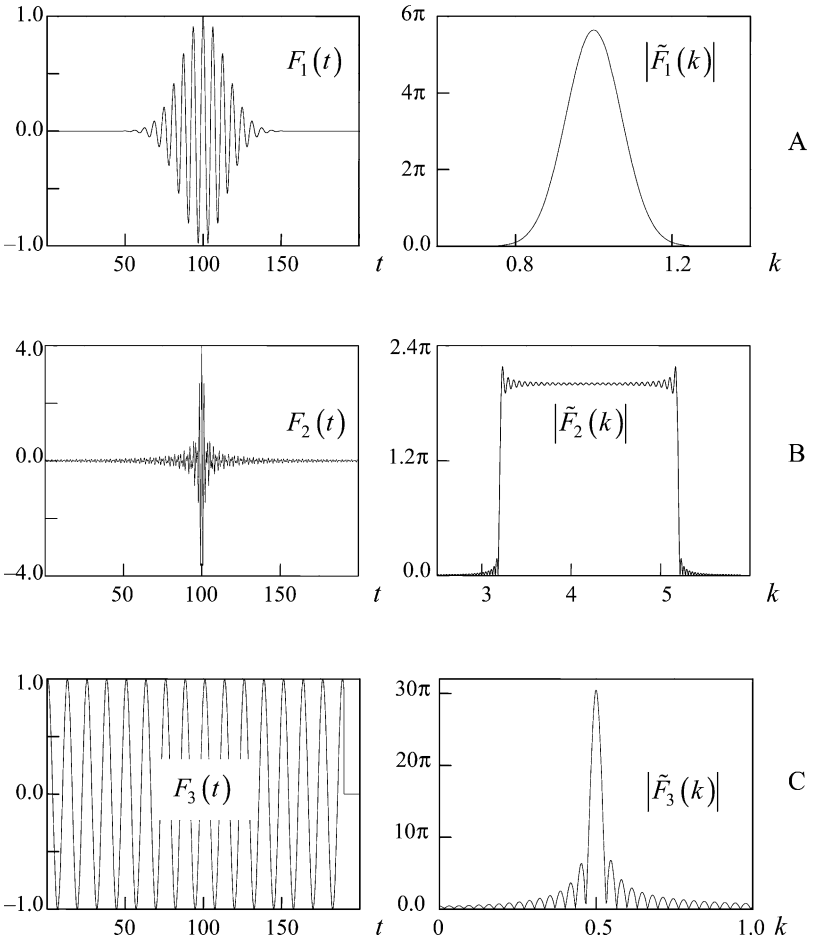

Fig. 4.3 Dynamical and spectral characteristics of current sources for pulsed waves: (**a**) Source (4.94), $\tilde{k} = 1.0$, $\tilde{\alpha} = 1.0$, $\tilde{T} = 100$, and $\bar{T} = 200$; (**b**) source (4.95), $\tilde{k} = 4.2$, $\Delta k = 1$, $\tilde{T} = 100$, $\bar{T} = 200$; (**c**) source (4.96), $\tilde{k} = 0.5$, $\tilde{T} = 0.5$, and $\bar{T} = 190$

Table 4.1 Determination of parameters for the source given by (4.94)

	$\gamma = 0.001$	$\gamma = 0.01$	$\gamma = 0.1$	$\gamma = 0.5$
$b\approx$	2.63	2.14	1.52	0.83
$c\approx$	5.25	4.29	3.04	1.66

value $\left|\tilde{U}_{\text{prim}}(g,k)\right|$ did not suffer changes throughout the band of interest would be most true. To cut down the overall computation time T, the left end of the interval $\tilde{T} - c\tilde{\alpha} \le t \le \tilde{T} + c\tilde{\alpha}$ is put at the point $t = 0$. And to secure the expected spectral characteristics of the source, the level of $\left|U_{\text{prim}}(g,0)\right|$ should be small

($0.001 \le \gamma \le 0.01$). This condition and the chosen $\tilde{\alpha}$ establish the effective spatial duration $0 \le t \le 2\tilde{T}$ of the primary signal and its delay time $\tilde{T}$.

At the stage related to the study of resonator frequency characteristics, of interest are, as a rule, all mode types corresponding to the relevant symmetry class. Hence, in its spatial structure, the function $\tilde{f}(g,k)$ [the function $F(g,t)$] must be of the same symmetry class and provide approximately the same coefficient values $C\left(\tilde{f},\bar{k}\right)$ [see formula (4.87)] for all free oscillations.

The excitation efficiency of quasi-monochromatic components of the field $U(g,t)$ depends on the source volume [see representations (4.86), (4.87), (4.88), (4.89), (4.90), (4.91), (4.92), and (4.93)]. Making the support of the function $F(g,t)$ bigger, one can substantially reduce the overall computation time T. The bottom $T = 5\tilde{T}$ of the possible T value is controlled by the following evident requirements. Within $0 \le t \le T$, the open periodic resonator has to:

- work in the forced oscillation mode for some time ($0 \le t \le 2\tilde{T}$);
- exclude (by the radiation into free space) those $U(g,t)$ field components that cannot form stable oscillations in the resonance volume ($2\tilde{T} \le t \le 3\tilde{T}$);
- allow high-Q modes to reveal themselves against the background of low-Q oscillations ($3\tilde{T} \le t \le 5\tilde{T}$).

With these requirements met, the study of the grating spectral characteristics over a frequency band consists in the search of the field $U(g,t)$ as a function of the time $t \in [0;T]$ at a fixed point $g \in \mathbf{Q}_L$ and the analysis of the image $\tilde{U}(g,k) \quad \leftrightarrow \quad U(g,t)$; $\mathrm{Im}k = 0$ (see Section 7.4.1 in [1]). Evidently the point g must not fall into a field node of a high-Q oscillation $u_0\left(g,\bar{k}\right)$. If so, the resonator characteristics will be distorted – the function $\tilde{U}(g,k)$ will fail to consider frequency $\bar{k}$ as a member of the spectral set Ω_k.

The examination of a particular free oscillation $u_0\left(g,\bar{k}\right)$ (see, for example, Fig. 7.16 in [1]) implies that $\tilde{k} \approx \mathrm{Re}\bar{k}$. One must guard against other resonance points in the interval $\left[\tilde{k} - b/\tilde{\alpha};\tilde{k} + b/\tilde{\alpha}\right]$ and be careful that the level of spectral amplitudes of the signal $U_{\mathrm{prim}}(g,t)$ is insignificant at this interval ends. Otherwise the choice of the source parameters in (4.94) still follows above-formulated rules.

The source

$$F(g,t) = 4\frac{\sin\left[\Delta k\left(t-\tilde{T}\right)\right]}{\left(t-\tilde{T}\right)}\cos\left[\tilde{k}\left(t-\tilde{T}\right)\right]\chi\left(\bar{T}-t\right)P(g) = F_2(t)\,P(g) \quad (4.95)$$

produces signals $U_{\mathrm{prim}}(g,t)$ with a trapezoidal distribution of spectral amplitudes (see Fig. 4.3b), which is very suitable for the study of frequency characteristics of open resonators. Within the frequency range $\left[\tilde{k} - \Delta k;\tilde{k} + \Delta k\right]$, the module of the function $\tilde{F}_2(k) \quad \leftrightarrow \quad F_2(t)$ remains almost unchanged. Off it, $\left|\tilde{F}_2(k)\right| \approx 0$ for all $k > 0$.

The spectral characteristics of the source

$$F(g,t) = P(g)\cos\left[\tilde{k}\left(t-\tilde{T}\right)\right]\chi\left(\bar{T}-t\right) = P(g)\,F_3(t) \tag{4.96}$$

for quasi-monochromatic signals $U_{\text{prim}}(g,t)$ (see Fig. 4.3c) are controlled by the parameters $\tilde{k}$, $\bar{T}$, and $\tilde{T}$. The first two determine the central frequency and duration of the signal and also its effective width in the spectral domain. The parameter $\tilde{T}$ smoothes the switch-on process of the source if necessary.

The information on singularities of the $\tilde{f}(g,k)$ functions for sources of the type (4.94) and (4.95) is unavailable for the direct analysis. The existence of $\underline{k}$ poles of these functions in the lower half-plane of the $\mathbf{C}_k$ sheet, the order and location of these poles can be judged only by circumstantial evidence, considering the $\tilde{f}(g,k)$ behavior in the domain of real k. A better adjustment to a particular point $\underline{k}$ can be via a $F(g,t)$ source with, for example, the following time dependence [201]:

$$F(t) = \frac{1}{\mathrm{Re}\underline{k}}\mathrm{e}^{t\mathrm{Im}\underline{k}}\sin\left(t\mathrm{Re}\underline{k}\right) \quad \leftrightarrow \quad \tilde{F}(k) = -\frac{1}{\left(k-\underline{k}\right)\left(k+\underline{k}^*\right)}. \tag{4.97}$$

4.3.3 Compact Grating Structures

The initial boundary value and the boundary value problems

$$\begin{cases} \left[-\varepsilon\mu\frac{\partial^2}{\partial t^2} - \sigma\mu\frac{\partial}{\partial t} + \frac{\partial^2}{\partial y^2} + \frac{\partial^2}{\partial z^2}\right]U(g,t) = F(g,t); \\ \qquad g = \{y,z\} \in \mathbf{Q} = \mathbf{R}^2\backslash\overline{\mathrm{int}\mathbf{S}_x}, \qquad t > 0 \\ U(g,t)\big|_{t=0} = \varphi(g), \qquad \frac{\partial}{\partial t}U(g,t)\big|_{t=0} = \psi(g); \qquad g \in \overline{\mathbf{Q}} \\ E_{tg}(p,t)\big|_{p=\{x,y,z\}\in\mathbf{S}} = 0; \qquad t \geq 0 \end{cases}, \tag{4.98}$$

$$\begin{cases} \left[\frac{\partial^2}{\partial y^2} + \frac{\partial^2}{\partial z^2} + \tilde{\varepsilon}\mu k^2\right]\tilde{U}(g,k) = \tilde{f}(g,k); \qquad g \in \mathbf{Q} \\ \tilde{E}_{tg}(p,k)\big|_{p=\{x,y,z\}\in\mathbf{S}} = 0 \\ \tilde{U}(g,k) = \sum\limits_{n=-\infty}^{\infty} a_n(k)\,H_n^{(1)}(k\rho)\,\mathrm{e}^{in\phi}; \qquad \rho \geq a, \qquad 0 \leq \phi \leq 2\pi \end{cases} \tag{4.99}$$

describe transient and steady-state processes in compact grating structures and, certainly, in any open compact resonator as well. Here, $H_n^{(1)}(...)$ are the Hankel cylindrical functions and $\{\rho,\phi\}$ are polar coordinates in the $y0z$ plane. All scattering inhomogeneities of the free space $\mathbf{R}^2$ and wave sources exciting these inhomogeneities are enclosed in the domain $\rho < L$ (see Fig. 4.2). Problems (4.98) are nothing but (4.44) without virtual waveguides ${}_j\mathbf{Q}$. Their solutions $U(g,t)$ relate to the solutions $\tilde{U}(g,k)$; $\mathrm{Im}k > 0$, of problems (4.99) by formula (1.21). The last equation in (4.99) represents the radiation condition acting in the same way as condition (1.22)

in problems (1.20) and (4.79) (see Statement 1.2). All the key qualitative conclusions of the spectral theory of open periodic resonators (see Statements 1.3 and 1.4) and all the results from Sections 4.3.1 and 4.3.2 remain true and almost unchanged for problems (4.98) and (4.99) [11, 47–49, 203, 204]. However, we must mention the following essential difference existing between infinite periodic resonators and open compact resonators with grating structures (or compact resonators for short).

- The surface $\mathbf{K}$ of the analytic continuation of the solutions $\tilde{U}(g,k)$; $\mathrm{Im}k > 0$, of problems (4.99) to the complex domain k: $\mathrm{Im}k \leq 0$ coincides with the surface of the analytic continuation of the function $\ln k$: $k = 0$ is the logarithmic branch point and the surface sheets are cut along the negative axis $\mathrm{Re}k = 0$ [11].
- The spectrum $\{\bar{k}_n\} = \Omega_k$ of open compact resonators does not contain any points $\bar{k} \in \mathbf{C}_k$ ($\mathbf{C}_k$ is the first – physical – sheet of the surface $\mathbf{K}$) such that $\mathrm{Im}\bar{k} = 0$ [8, 9, 11].
- In the case of compact resonators bounded by sufficiently smooth convex contours $\mathbf{S}_x$, for dielectric and metal objects, in the case of absorbing insertions, the value $\left|\mathrm{Im}\bar{k}\right|$ of the elements $\bar{k} \in \mathbf{C}_k$ increase as $\left|\mathrm{Re}\bar{k}\right|$ grows, at least as fast as $\ln\left|\mathrm{Re}\bar{k}\right|$ [8, 205].

We take up now [203, 204] some simple compact resonators with dispersion mirrors furnished by reflection or semitransparent gratings and start with the spectral characteristics of the structure whose geometrical and constituent parameters are given by the equation

$$\sigma(g) = 2.19 \cdot 10^{10} \chi(4 - |y|)\left[\chi(-z)\,\chi(z + 0.1) + \chi(6.6 - z)\,\chi(z - 6.5)\right]. \tag{4.100}$$

Equation (4.100) applies to a Fabry–Perot resonator with parallel metal (copper) mirrors (see Fig. 4.4a). The E-polarized wave source

$$\begin{aligned} F(g,t) &= \chi(3 - |y|)\,\chi(6 - z)\,\chi(z - 3)\cos\left(\tilde{k}z\right) F_2(t) = P(g)\,F_2(t); \\ \tilde{k} &= 8.5,\ \Delta k = 5,\ \tilde{T} = 20,\ \bar{T} = 150 \end{aligned} \tag{4.101}$$

occupying the frequency band $3.5 < k < 13.5$ excites symmetrical about the main, $y = 0$ axis oscillations alone in the resonator of the kind (see Fig. 4.5a). One of these oscillations ($H_{0,1,18}$-oscillation; see Fig. 4.6a) corresponds to eigenfrequency $\bar{k} \approx 8.5 - i0.0015$. The $\mathrm{Re}\bar{k}$ and $\mathrm{Im}\bar{k}$ values have been inferred from the behavior of the field $U(g,t) = U(\tau)$, $\tau = t - 2\tilde{T} > 0$ in the resonator excited by the narrowband current source for E-polarized waves

$$F(g,t) = 10P(g)\,F_1(t);\ \tilde{k} = 8.5,\ \tilde{\alpha} = 30,\ \tilde{T} = 90,\ \bar{T} = 180. \tag{4.102}$$

This source switches off at the time $t = 2\tilde{T} = 180$. According to (4.86), for all times $\tau > 0$ at any fixed point $g \in \mathbf{Q}_L$, we have

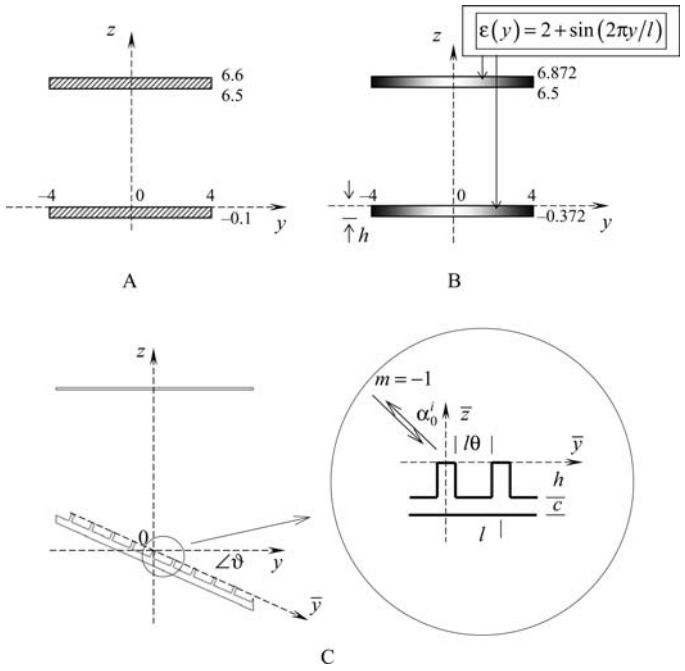

Fig. 4.4 (**a**) Fabry–Perot resonator and (**b** and **c**) dispersive open resonators; (**b**) resonator with semitransparent dielectric mirrors; and (**c**) resonator with a reflective grating

$$U(g,t) = U(\tau) \approx A \exp\left(\tau \mathrm{Im}\bar{k}\right) \cos\left(\tau \mathrm{Re}\bar{k} + a\right). \tag{4.103}$$

A correlation of (4.103) with the features of $U(g,t)$ (see the right-hand fragment in Fig. 4.6a) yields the quantities $\mathrm{Re}\bar{k} \approx \tilde{k}$, $\mathrm{Im}\bar{k}$, and also the values $A \approx \pm 18.2$ and $a \approx 0.79$.

For the resonator (4.100), the elements $\bar{k}_n$ of the spectrum Ω_k corresponding to sufficiently high-quality oscillations are presented by an almost equidistant system of points $k \approx \mathrm{Re}\bar{k}_n$ on the axis $\mathrm{Im}k = 0$ (see Fig. 4.5a). At these points, the level $\left|\tilde{U}\left(g,k,\tilde{f}\right)\right|$ of spectral amplitudes of the field $U(g,t)$ is governed by the quality of the corresponding free oscillations and the quantity $C\left(\tilde{f},\bar{k}_n\right)$ [see formula (4.87)] displaying the response of the amplitude–spatial characteristics of the free oscillation field to the source function $\tilde{f}(g,k) \leftrightarrow F(g,t)$.

In the examination of the $H_{0,1,18}$-oscillation of the resonator (4.100) described above, the contribution from the other free oscillations to the $U(g,t)$ field was made infinitesimally small owing to the fine tuning of the source and the absence of other resonator eigenfrequencies in the $\bar{k}$ neighborhood. The analysis becomes complicated when some two eigenfrequencies $\bar{k}_1$ and $\bar{k}_2$ are so close that even an essential narrowing of the band of the signal $U_{\mathrm{prim}}(g,t)$ in the spectral domain (this narrowing

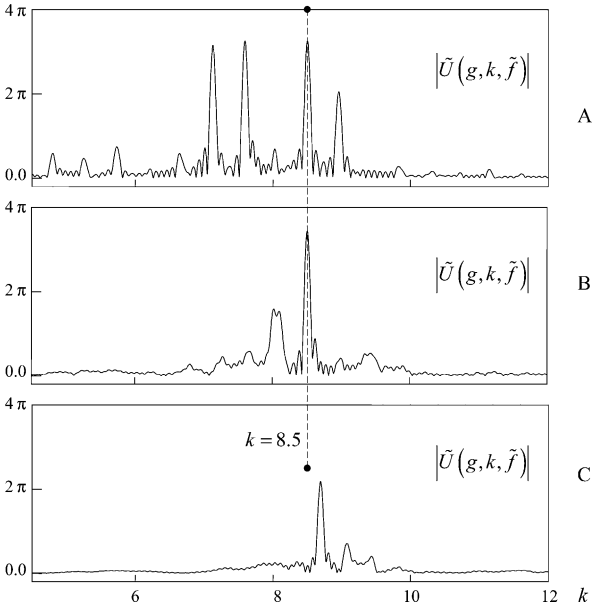

Fig. 4.5 Spectral amplitudes of field $U(g,t)$ produced by current source (4.101) in resonators: (**a**) (4.100) for $g = \{0,6.28\}$; (**b**) (4.106) for $g = \{0.0,6.3\}$; and (**c**) (4.108) for $g = \{0.0,6.32\}$

evidently increases $\tilde{T}$ and T, the experiment duration increases substantially) is not helpful when it comes to an extraction of one of them accurately enough.

This statement can be illustrated by a simple example (see Fig. 4.7 and [204]). The confocal resonator

$$\sigma(g) = 2.19 \cdot 10^{10} \chi\left[5 - |y|\right] \chi\left[4 - |z|\right] \chi\left[z^2 + (|y| + 4.5)^2 - 9^2\right]$$

is excited by the current source

$$F(g,t) = 10\chi\left[3.5 - |y|\right] \chi\left[1.5 - |z+1|\right] \cos\left(\beta_1 \tilde{k} y + \beta_2\right) \exp\left[-\left(t - \tilde{T}\right)^2 \Big/ 4\tilde{\alpha}^2\right] \times$$
$$\times \cos\left[\tilde{k}\left(t - \tilde{T}\right)\right] \chi\left(\bar{T} - t\right); \tilde{k} = 4.235, \tilde{\alpha} = 50, \tilde{T} = 150, \bar{T} = 2\tilde{T},$$
$$\beta_1 = 1, \beta_2 = 0.785$$

for E-polarized transient waves. The frequency characteristics of the source and its spatial configuration are such that at any instant $0 < t < 2500$ one can observe oscillations of the two types, $H_{0,12,1} - \mathrm{Re}\bar{k}_1 \approx 4.2212$ and $H_{0,11,3} - \mathrm{Re}\bar{k}_2 \approx 4.239$, in the field $U(g,t)$. In support of this statement see Fig. 4.7a for the $E_x(g,t)$ spatial distribution in the free oscillation field. The dependence $U(g,t)$ at the point $g = \{0.82,0.0\}$, $t > \bar{T}$, is plotted in Fig. 4.7b.

We now make use of representation (4.86) and describe the behavior of the field $U(g,t)$ using the following simplified formula:

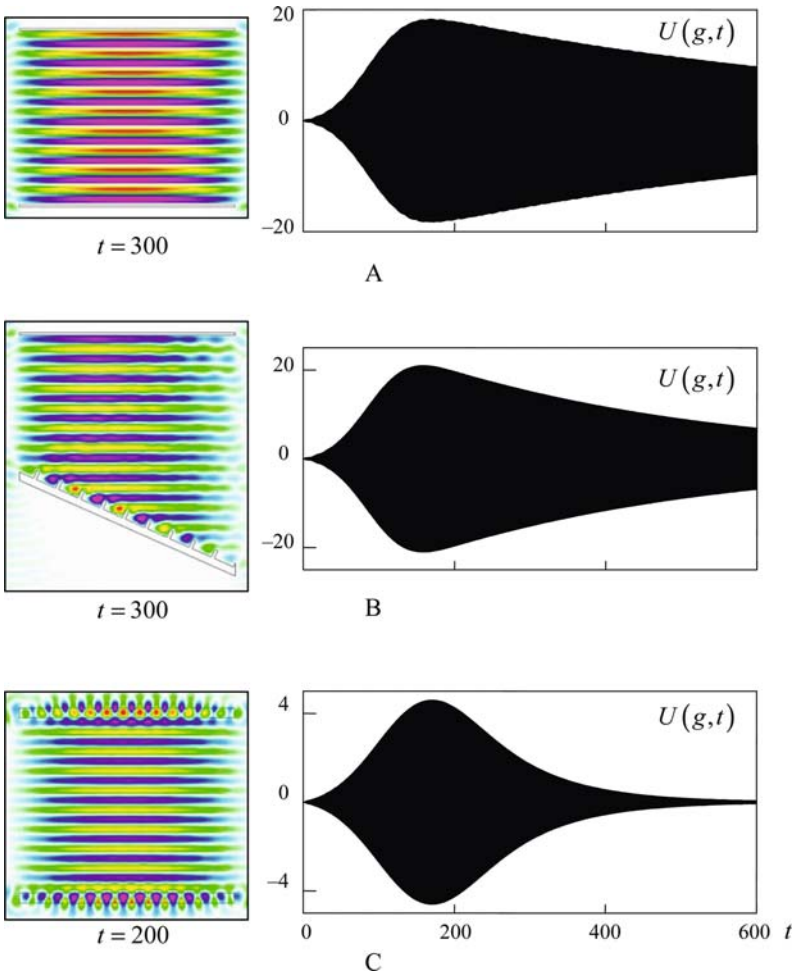

Fig. 4.6 The $H_{0,1,18}$-oscillations in (**a**) Fabry–Perot resonator (4.100) and in resonators (**b**) (4.106) and (**c**) (4.108): $g = \{0.0,6.32\}$

$$U(g,t) = U(\tau) \approx U_1(\tau) + U_2(\tau) = A\exp\left(\tau \mathrm{Im}\bar{k}_1\right)\cos\left(\tau \mathrm{Re}\bar{k}_1\right) + \\ +B\exp\left(\tau \mathrm{Im}\bar{k}_2\right)\cos\left(\tau \mathrm{Re}\bar{k}_2 + b\right);\ \tau = t - \bar{T} > 0. \tag{4.104}$$

Introduce the notation $\Gamma_0(\tau) = \cos\left[\tau\left(\mathrm{Re}\bar{k}_2 - \mathrm{Re}\bar{k}_1\right) + b\right]$ and refer to the model situation – $\mathrm{Re}\bar{k}_1 = 5.1$, $\mathrm{Re}\bar{k}_2 = 5.2$, $A = 0.9$, $\mathrm{Im}\bar{k}_1 = -0.002$, $B = -6.0$, $\mathrm{Im}\bar{k}_2 = -0.005$, $b = 0.8$ – expressed in Fig. 4.7c. It is easy to check that:

- the curves

$$\Gamma_1^{\pm}(\tau) = \pm\left[|A|\exp\left(\tau \mathrm{Im}\bar{k}_1\right) - |B|\exp\left(\tau \mathrm{Im}\bar{k}_2\right)\right]$$

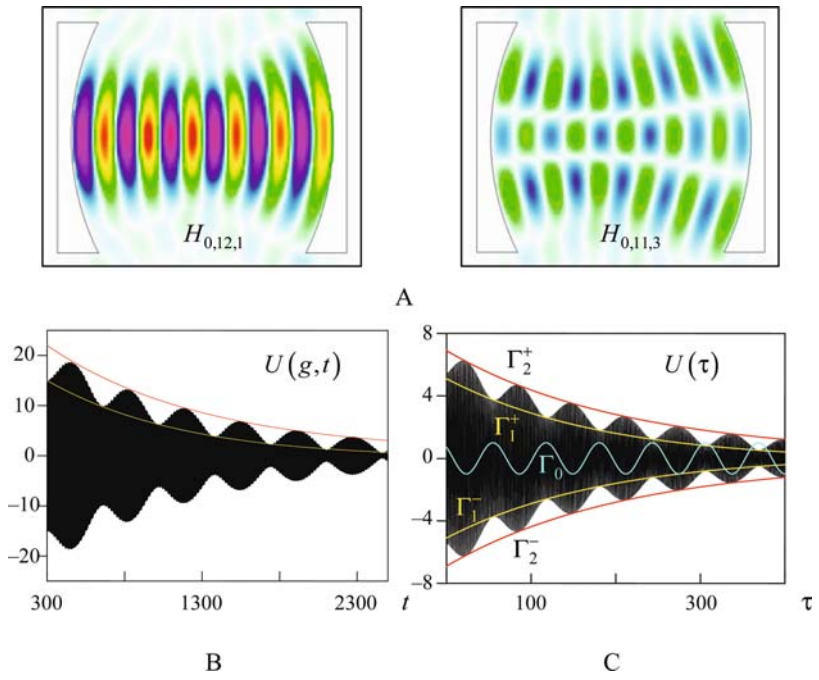

Fig. 4.7 Determination of parameters of free oscillations with neighboring eigenfrequencies $\bar{k}_1$ and $\bar{k}_2$: (**a** and **b**) Analyzed situation; and (**c**) model situation

and

$$\Gamma_2^{\pm}(\tau) = \pm\left[|A|\exp\left(\tau \mathrm{Im}\bar{k}_1\right) + |B|\exp\left(\tau \mathrm{Im}\bar{k}_2\right)\right]$$

represent global interior and global superior envelopes of the dependence $U(\tau)$;

- for $A > 0$, $B > 0$, at the points of contact of the $U(\tau)$ and $\Gamma_2^{\pm}(\tau)$ curves

$$\Gamma_0(\tau) = 1 \text{ and } \cos\left(\tau \mathrm{Re}\bar{k}_1\right) = \cos\left(\tau \mathrm{Re}\bar{k}_2 + b\right) = \pm 1$$

and at the points of contact of the $U(\tau)$ and $\Gamma_1^{\pm}(\tau)$ curves,

$$\Gamma_0(\tau) = -1 \text{ and } \cos\left(\tau \mathrm{Re}\bar{k}_1\right) = -\cos\left(\tau \mathrm{Re}\bar{k}_2 + b\right) = \pm 1;$$

- when $A < 0$, $B < 0$, at the points of contact of the $U(\tau)$ and $\Gamma_2^{\pm}(\tau)$ curves,

$$\Gamma_0(\tau) = 1 \text{ and } \cos\left(\tau \mathrm{Re}\bar{k}_1\right) = \cos\left(\tau \mathrm{Re}\bar{k}_2 + b\right) = \pm 1$$

and at the points of contact of $U(\tau)$ and $\Gamma_1^{\pm}(\tau)$ curves,

$$\Gamma_0(\tau) = -1 \text{ and } \cos\left(\tau \mathrm{Re}\bar{k}_1\right) = -\cos\left(\tau \mathrm{Re}\bar{k}_2 + b\right) = \mp 1;$$

- when $A > 0$, $B < 0$, at the points of contact of the $U(\tau)$ and $\Gamma_1^{\pm}(\tau)$ curves,

$$\Gamma_0(\tau) = 1 \text{ and } \cos\left(\tau \mathrm{Re}\bar{k}_1\right) = \cos\left(\tau \mathrm{Re}\bar{k}_2 + b\right) = \pm 1,$$

and at the points of contact of $U(\tau)$ and $\Gamma_2^{\pm}(\tau)$ curves,

$$\Gamma_0(\tau) = -1 \text{ and } \cos\left(\tau \mathrm{Re}\bar{k}_1\right) = -\cos\left(\tau \mathrm{Re}\bar{k}_2 + b\right) = \pm 1;$$

- when $A < 0$, $B > 0$ at the points of contact of the $U(\tau)$ and $\Gamma_1^{\pm}(\tau)$ curves,

$$\Gamma_0(\tau) = 1 \text{ and } \cos\left(\tau \mathrm{Re}\bar{k}_1\right) = \cos\left(\tau \mathrm{Re}\bar{k}_2 + b\right) = \mp 1,$$

and at the points of contact of $U(\tau)$ and $\Gamma_2^{\pm}(\tau)$ curves,

$$\Gamma_0(\tau) = -1 \text{ and } \cos\left(\tau \mathrm{Re}\bar{k}_1\right) = -\cos\left(\tau \mathrm{Re}\bar{k}_2 + b\right) = \mp 1.$$

These conclusions suggest that the behavior of the function $U(g,t)$, $t > \bar{T}$ (behavior of $U(\tau) = U(g,t)$, $\tau = t - \bar{T} > 0$) makes it possible to uniquely determine all main parameters of the field free oscillations corresponding to some neighboring eigenfrequencies $\bar{k}_1$ and $\bar{k}_2$. Thus, in the case whose analysis results can be seen in Figs. 4.7a and b, we have $\mathrm{Re}\bar{k}_2 - \mathrm{Re}\bar{k}_1 \approx 0.0178$, $A \approx 3.5$, $\mathrm{Im}\bar{k}_1 \approx -0.0005$, $B \approx 18.5$, $\mathrm{Im}\bar{k}_2 \approx -0.00105$, and $b \approx 2.91$.

The spectrum of a classical open resonator can be rarefied by changing its nonselective mirrors for grating mirrors [10, 16, 206–208]. For an open resonator, the model synthesis scheme [1, 40, 41] based on the so-called principle of prototype [10, 40] predicts the relevant changes of the spectral characteristics and allows us to find the eigenfrequency allocation over the working range and the field configuration of high-Q oscillations to an accuracy desired [40, 203, 204]. Following this scheme, we substitute the lower mirror of resonator prototype (4.100) by a finite metal grating (see Fig. 4.4c) of the type

$$\sigma(g) = 2.19 \cdot 10^{10} \chi(4 - |y|)\left\{\chi(-\bar{z})\,\chi(\bar{z} + h)\,\chi\left[\cos\left(2\pi\bar{y}/l\right) - \cos(\pi(1-\theta))\right] + \right.$$
$$\left. + \chi(-\bar{z} - h)\,\chi(\bar{z} + h + c)\right\};\ \bar{y} = y\cos\vartheta - z\sin\vartheta,\ \bar{z} = y\sin\vartheta + z\cos\vartheta. \tag{4.105}$$

This is a metal comb with the period $l = 0.9$, the groove width $l\theta = 0.765$ ($\theta = 0.85$), the depth $h = 0.315$, and the substrate thickness $c = 0.3$. The upper plane of the periodic structure (plane $\bar{z} = 0$) is turned clockwise at an angle $\vartheta \approx 24.25°$ with respect to the plane $z = 0$.

As is known (see [10, 16, 18] and Section 1.2.1), when an infinite reflection grating of the kind is excited with the plane monochromatic wave $\tilde{U}_0^i(\bar{g},k) = \exp\left[ik\left(\bar{y}\sin\alpha_0^i - \bar{z}\cos\alpha_0^i\right)\right]$, $\bar{g} = \{\bar{y},\bar{z}\}$, $\left|\alpha_0^i\right| < 90°$, the secondary field

$$\tilde{U}^s(\bar{g},k) = \tilde{U}(\bar{g},k) - \tilde{U}_0^i(\bar{g},k) = \sum_{n=-\infty}^{\infty} R_{n0}^{\mathbf{AA}} \exp\left[i(\Phi_n \bar{y} + \Gamma_n \bar{z})\right];$$
$$\Phi_n = 2\pi n/l + k\sin\alpha_0^i,\ \Gamma_n = \sqrt{k^2 - \Phi_n^2},\ \mathrm{Re}\Gamma_n \geq 0, \mathrm{Im}\Gamma_n \geq 0,$$

in the zone $\bar{z} > 0$ contains a finite number of spatially traveling harmonics with $\mathrm{Im}\Gamma_n = 0$, where n is the harmonic number. Each harmonic accumulates the portion $W_{n0}^R(k) = \left|R_{n0}^{\mathbf{AA}}\right|^2 \mathrm{Re}\Gamma_n/\Gamma_0$ of the energy arriving to the channel whose orientation in space is given by the angle $\alpha_n = -\arcsin\left(2\pi n/lk + \sin\alpha_0^i\right)$ (counterclockwise reading from the $\bar{z}$-axis). With the condition $kl\sin\left(\alpha_p^i\right) = \pi m$ satisfied, the component $R_{-m0}^{\mathbf{AA}}(k)\exp\left[i(\Phi_{-m}\bar{y} + \Gamma_{-m}\bar{z})\right]$ of the field $\tilde{U}^s(\bar{g},k)$ travels toward the incident wave. This regime is known as autocollimation reflection on the minus mth spatial harmonic. If $W_{-m0}^R(k) \approx 1$ in this regime, the effect of total autocollimation reflection is achieved.

For an infinite grating of the type (4.105), the reflection efficiency of an E-polarized plane wave into the minus first autocollimating harmonic tends to one within the frequency region $7.68 < k < 9.77$ ($W_{-10}^R(k) \approx 1$; see Fig. 133 in [18]). Therefore the modified resonator, or the resonator

$$\sigma(g) = 2.19\cdot 10^{10}\chi(4-|y|)\left\{\chi(-\bar{z})\chi(\bar{z}+h)\chi\left[\cos\left(2\pi\bar{y}/l\right) - \cos(\pi(1-\theta))\right] + \right.$$
$$\left. +\chi(-\bar{z}-h)\chi(\bar{z}+h+c) + \chi(6.6-z)\chi(z-6.5)\right\}, \tag{4.106}$$

at the frequency $k = 8.5$, with $\arg R_{-10}^{\mathbf{AA}}(k) \approx \pi$ must keep (in the main) the electromagnetic characteristics of the resonator of the type (4.100) (see the principle of prototype in [10, 40]). The results presented in Figs. 4.5b and 4.6b confirm the statement: the resonator with a reflection grating maintains the free oscillation of the same type ($H_{0,1,18}$-oscillation) that the Fabry–Perot resonator does. The spectrum of the dispersive open resonator is perceptibly and predictably rarefied (a detailed description of the selection mechanism for the dispersive resonator with grating mirrors can be found in [10, 40]), the quality of the discussed oscillation is almost halved. In this case, $\mathrm{Im}\bar{k} \approx -0.0026$: when the resonator is excited with a narrow-band current source of the type (4.102), the behavior of the field $U(\tau) = U(g,t)$, $\tau = t - \bar{T}$ is such that $\Gamma_1^{\pm}(\tau) = \Gamma_2^{\pm}(\tau) \approx \pm 20.4\exp(-0.0026\tau)$.

The periodic dielectric layer

$$\varepsilon(g) = 1 + \chi(-z)\chi(z+0.372)\left[1 + \sin(10.13y)\right] \tag{4.107}$$

(period length $l = 0.62$, layer thickness $h = 0.372$) excited with a normally incident monochromatic wave $\tilde{U}_0^i(g,k) = \exp(-ikz)$ produces the secondary field

$$\tilde{U}^s(g,k) = \begin{cases} \sum\limits_{n=-\infty}^{\infty} R_{n0}^{\mathbf{AA}}(k)\exp\left[i(\Phi_n y + \Gamma_n z)\right]; & z > 0 \\ \sum\limits_{n=-\infty}^{\infty} T_{n0}^{\mathbf{BA}}(k)\exp\left[i(\Phi_n y - \Gamma_n(z+h))\right]; & z < -h \end{cases}$$

in the reflection ($z > 0$) and transmission ($z < -h$) zones. At the $k = 8.5$ frequency, $W_{00}^{R}(k) \approx 1$ (see Fig. 5.5 in [10] for regimes of the total resonance reflection of plane waves from semitransparent dielectric structures) and all the scattered energy is accumulated in the principal reflection harmonic $R_{00}^{\mathbf{AA}}(k)\exp\left[i\left(\Phi_0 y + \Gamma_0 z\right)\right]$ of the grating spatial spectrum. But at this frequency, $\arg R_{00}^{\mathbf{AA}}(k)$ is different from π. That is why the substitution of the metal mirrors in the resonator (4.100) for finite dielectric gratings of the type (4.107), that is the passage to the dispersive open resonator

$$\varepsilon(g) = 1 + \chi(4 - |y|)\left[\chi(-z)\,\chi(z + 0.372) + \chi(6.872 - z)\,\chi(z - 6.5)\right] \times \times \left[1 + \sin(10.13y)\right] \tag{4.108}$$

(see Fig. 4.4b), drastically changes the eigenfrequency $\bar{k}$ corresponding to the $H_{0,1,18}$-oscillation: $\mathrm{Re}\,\bar{k}$ moves toward the point $k \approx 8.7$ (see Fig. 4.5c). It is at this point the rule applies that the phase of the resonant wave recovers in a complete cycle of propagation along the longitudinal axis of resonator (4.108). $\mathrm{Im}\bar{k} \approx -0.011$: when the dispersion open resonator is excited with a narrowband current source

$$F(g,t) = 10\chi(3 - |y|)\,\chi(4.75 - z)\,\chi(z - 1.75)\cos\left(\tilde{k}z + 1.75\right)F_1(t)\,;\ \tilde{k} = 8.7,$$
$$\tilde{\alpha} = 40,\ \tilde{T} = 120,\ \bar{T} = 180,\ T = 600,$$

the field $U(\tau) = U(g,t)$, $\tau = t - \bar{T} > 0$ (see Fig. 4.6c) behaves so that $\Gamma_1^{\pm}(\tau) = \Gamma_2^{\pm}(\tau) \approx \pm 3.3\exp(-0.011\tau)$. The quality of the oscillation decreases, as at the frequency $k \approx \mathrm{Re}\bar{k}$ the semitransparent mirrors of the resonator (4.108) transmit a substantial part of energy into free space. For a grating of the type (4.107), $W_{00}^{R}\left(\mathrm{Re}\bar{k}\right) \approx W_{00}^{T}\left(\mathrm{Re}\bar{k}\right) \approx 0.5$. Evidently the situation can be recovered and the $H_{0,1,18}$-oscillation can be restored to the previous parameters. For this, the dispersive open resonator should be extended lengthwise, or what is the same, the resonance conditions for the quasi-optical volume should match the resonance conditions for the periodic dielectric layer.

4.4 Infinite Gratings: Resonant Wave Scattering

The standard discretization of the 2-D initial boundary value problems considered in Sections 4.1 and 4.2 by the finite-difference method [4, 5] using a uniform rectangular mesh attached to Cartesian coordinates $g = \{y,z\}$ leads to explicit computational schemes with uniquely defined mesh functions $U(j,k,m) \approx U\left(y_j,z_k,t_m\right)$. The approximation error is $O(\bar{h}^2)$, $\bar{h}$ is the mesh step in spatial coordinates, $\bar{l} = \bar{h}/2$ for $\vartheta = \max\limits_{g\in\mathbf{Q}_L}\left[\varepsilon(g)\,\mu(g)\right] < 2$ or $\bar{l} < \bar{h}/2$ for $\vartheta \geq 2$ is the mesh step in time variable t; $y_j = j\bar{h}$, $z_k = k\bar{h}$, and $t_m = m\bar{l}$. The range of the j, k, and m integers depends on the size of the $\mathbf{Q}_L$ areas and the length of the interval $[0;T]$ of the observation time

t: $g_{jk} \in \overline{\mathbf{Q}_L}$ and $t_m \in [0;T]$, $g_{jk} = \{y_j, z_k\}$. The condition providing uniform boundedness of the approximate solutions $U(j,k,m)$ with decreasing $\bar{h}$ and $\bar{l}$ is met (see, for example, formula (1.50) in [1]). Hence [5] the finite-difference computational schemes are stable, and the mesh functions $U(j,k,m)$ tend to the solutions $U(g_{jk},t_m)$ of the original problems. The relevant test problems solution and other independent results serve to confirm the statement (see, for example, Section 4.5.1 and 4.6.1 in [1]).

4.4.1 Electrodynamical Characteristics of Gratings

The analysis of infinite single-periodic gratings rests on the numerical solution of problems of the type (4.34). The passage to the finite domain of analysis $\mathbf{Q}_L$ is assisted by exact absorbing conditions (4.39) and (4.40).

Let us represent the total field $U(g,t)$ in the form $U(g,t) = U^i(g,t)+U^s(g,t)$, $g \in \mathbf{A}$, and $U(g,t) = U^s(g,t)$, $g \in \mathbf{B}$, where $U^i(g,t)$ is the field produced in the channel $\mathbf{R}$ by some sources $\tilde{F}(g,t)$, $\tilde{\varphi}(g)$, and $\tilde{\psi}(g)$. Then [see formulas (4.2) and (4.42)],

$$\begin{cases} U^s(g,t) = \sum\limits_{n=-\infty}^{\infty} u_n(z,t)\,\mu_n(y) \\ U^i(g,t) = \sum\limits_{n=-\infty}^{\infty} v_n(z,t)\,\mu_n(y) \end{cases}; \; t \geq 0. \tag{4.109}$$

$U(g,t) = E_x(g,t)$ or $U(g,t) = H_x(g,t)$ depending on whether the field is E- or H-polarized, respectively. In the domain ${}_L\mathbf{Q} = \mathbf{A} \cup \mathbf{B}$ [see (1.6) and (1.8)],

$$\partial \begin{Bmatrix} H_y \\ E_y \end{Bmatrix} \Big/ \partial t = \mp \eta_0^{\mp 1} \frac{\partial U}{\partial z},\; \partial \begin{Bmatrix} H_z \\ E_z \end{Bmatrix} \Big/ \partial t = \pm \eta_0^{\mp 1} \frac{\partial U}{\partial y};\; \begin{Bmatrix} E-\text{case} \\ H-\text{case} \end{Bmatrix}. \tag{4.110}$$

Then [cf. the representation (4.109)],

$$\begin{Bmatrix} H^s_{y(z)} \\ E^s_{y(z)} \end{Bmatrix} = \sum_{n=-\infty}^{\infty} u_n^{y(z)}(z,t)\,\mu_n^{y(z)}(y), \; \begin{Bmatrix} H^i_{y(z)} \\ E^i_{y(z)} \end{Bmatrix} = \sum_{n=-\infty}^{\infty} v_n^{y(z)}(z,t)\,\mu_n^{y(z)}(y); \quad \begin{Bmatrix} E-\text{case} \\ H-\text{case} \end{Bmatrix}. \tag{4.111}$$

The spatial–temporal amplitudes $u_n(z,t)$, $v_n(z,t)$, etc., in the representations (4.109) and (4.111) are also called the evolutionary basis elements of the corresponding signals [196, 197]. They fully describe the dynamics of the $U^s(g,t)$ ($U(g,t)$) and $U^i(g,t)$ pulsed waves traveling along the Floquet channel, their mode and spectral contents.

In the $\mathbf{Q}_L$ domain, the simulated process dynamics is estimated upon the time dependences $U(g,t)$ referring to particular points $g \in \mathbf{Q}_L$ as well as the point set $\mathbf{Q}_L$ as a whole. In the latter case, current values of the complex quantities $U(g,t)$ are

specified by the color of pixels (spatial mesh cells) throughout the computational domain $\mathbf{Q}_L$. In the **.exe** files (see captions in Chapter 4) and the figures related to Section 4.4, the data mapping is executed using a circular color scale graded in the two variables (Fig. 4.8a): $|U(g,t)|$ (10 layers) and $\arg U(g,t)$ (20 layers). The quantity $U_{\max}(t)$ responsible for the starting (exterior) layer can be chosen in two ways. In the first, each time layer is attached to its own current value $U_{\max}(t) = \max\limits_{g\in\mathbf{Q}_L} |U(g,t)|$. In the second, a value of $U_{\max}(t)$ is fixed and kept constant on a certain interval of the time variable t. If in the second regime, the $|U(g,t)|$ magnitude at some point in the $\mathbf{Q}_L$ domain exceeds the $U_{\max}(t)$ level, this point (a spatial mesh cell) will be colored as $U_{\max}(t)$ is colored.

Attach the **A** and **B** domains each to the local coordinate system $g_j = \{y_j, z_j \geq 0\}$, $j = 1,2$, the boundary $\mathbf{L}_j$ lies in the plane $z_j = 0$. Then, starting from the values on the boundary $\mathbf{L}_j$, the diagonal transport operator $Z_{0\to z_j}(t)$ (see Section 4.1.1 and Fig. 4.1) will calculate the spatial–temporal amplitudes $u(z_j,t) = \{u_n(z_j,t)\}$ for any $z_j \geq 0$ section of the corresponding regular channel **R**. This means that [see also (4.109), (4.110), and (4.111)] any electrodynamical characteristic of the grating is established by the amplitude sets $\left\{u_n(z_j,t)\right\}\big|_{z_j=0}$, $j = 1,2$, of the secondary pulsed field $U^s(g,t)$ on the virtual boundaries $\mathbf{L}_j$.

Now let the grating be excited by a pulsed wave $U_p^i(g_1,t) = v_p(z_1,t)\,\mu_p(y_1)$ coming from the area **A**, the $\mathbf{Q}_L$ domain has no current sources. In this case, the relationship

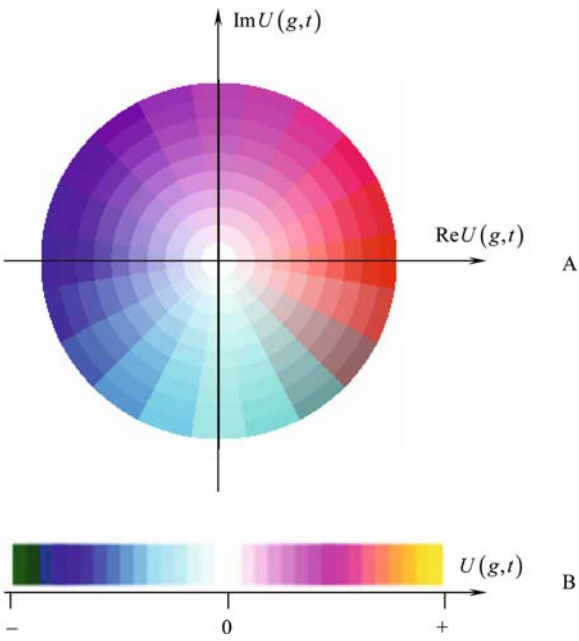

Fig. 4.8 The color scale for current (**a**) complex and (**b**) real $U(g,t)$ values in the computational domain $\mathbf{Q}_L$, $0 < t < T$

$$\underbrace{P_1^s + P_2^s + P_1^{i\times s}}_{1} + \underbrace{\frac{1}{2}\frac{\partial}{\partial t}\int\limits_{\mathbf{Q}_L}(\eta_0\mu\left|\vec{H}\right|^2 + \frac{\varepsilon}{\eta_0}\left|\vec{E}\right|^2)dg}_{2} + \underbrace{\frac{1}{\eta_0}\int\limits_{\mathbf{Q}_L}\sigma\left|\vec{E}\right|^2 dg}_{3} = -P_1^i \tag{4.112}$$

($dg = dydz$) governs the balance of instant powers of the electromagnetic field. Namely, the instant power arriving at $\mathbf{Q}_L$ across the boundary $\mathbf{L}_1$ is the sum of the total instant power (1) radiated across the $\mathbf{L}_j$ boundaries into the ${}_L\mathbf{Q}$ domain, the instant power (2) accumulative in the $\mathbf{Q}_L$ domain and the instant accepted power (3). Here,

$$P_j^{s(i)}(t) = \int\limits_{\mathbf{L}_j}\left([\vec{E}^{s(i)}\times\vec{H}^{s(i)}]\cdot\vec{n}_j\right)dy_j,$$
$$P_1^{i\times s}(t) = \int\limits_{\mathbf{L}_1}\left[\left([\vec{E}^s\times\vec{H}^i] + [\vec{E}^i\times\vec{H}^s]\right)\cdot\vec{n}_1\right]dy_1,$$

$\vec{n}_j$ is the outward normal to the $\mathbf{Q}_L$ domain at the boundary $\mathbf{L}_j$, $\vec{E}^{s(i)}$ and $\vec{H}^{s(i)}$ are the electric and magnetic fields of the waves $U^s(g,t)$ ($U^i(g,t)$) in the $\mathbf{A}$ and $\mathbf{B}$ domains.

The amplitude–frequency characteristics $\tilde{f}(k)$ (where $k = 2\pi/\lambda$; $\mathrm{Re}k > 0$, $\mathrm{Im} = 0$, is the wavenumber, or some frequency parameter or simple frequency, and λ is the free space wavelength) come from the time characteristics $f(t)$ by virtue of the integral transformation

$$\tilde{f}(k) = \int\limits_0^T f(t)\,\mathrm{e}^{ikt}dt \quad \leftrightarrow \quad f(t) \tag{4.113}$$

(image $\leftrightarrow$ original, T is the upper limit of the interval $[0;T]$ of the observation time t: for all $t > T$, the function $f(t)$ is assumed to be zero).

The frequency domain traditional characteristics $R_{np}^{\mathbf{AA}}(k)$ and $T_{np}^{\mathbf{BA}}(k)$ (see also Section 1.2.1, where $\mathbf{A} = \{g = \{y,z\} \in \mathbf{R}\colon\ z > 0\}$ and $\mathbf{B} = \{g \in \mathbf{R}\colon\ z < -h\}$) represent the conversion coefficients. The former indicates how the pth mode incident from the part $\mathbf{A}$ of the Floquet channel $\mathbf{R}$ converts into the nth reflection mode (synonymous with reflection coefficient). The latter shows how the pth mode arriving from the $\mathbf{A}$ domain transforms to the nth mode in the $\mathbf{B}$ domain (transition coefficient). Specifically,

$$R_{np}^{\mathbf{AA}}(k) = \left.\frac{\tilde{u}_n(z_1,k)}{\tilde{v}_p(z_1,k)}\right|_{z_1=0},\ T_{np}^{\mathbf{BA}}(k) = \frac{\tilde{u}_n(z_2,k)|_{z_2=0}}{\tilde{v}_p(z_1,k)|_{z_1=0}}. \tag{4.114}$$

When the grating is excited by a traveling ($\mathrm{Im}\Gamma_p = 0$) or damped ($\mathrm{Im}\Gamma_p > 0$) monochromatic wave $\tilde{U}_p^i(g,k) = \exp\left[i\left(\Phi_p y - \Gamma_p(z - L_1)\right)\right]$, the total field in the domain $\mathbf{Q}_L = \mathbf{A}\cup\mathbf{B}$ is

$$\tilde{U}(g,k)=\begin{cases}\tilde{U}_p^i(g,k)+\sum\limits_{n=-\infty}^{n=\infty}R_{np}^{\mathbf{AA}}\exp\left[i\left(\Phi_n y+\Gamma_n(z-L_1)\right)\right]; & g\in\mathbf{A}\\ \sum\limits_{n=-\infty}^{n=\infty}T_{np}^{\mathbf{BA}}\exp\left[i\left(\Phi_n y-\Gamma_n(z+h+L_2)\right)\right]; & g\in\mathbf{B}\end{cases},$$

and the coefficients $R_{np}^{\mathbf{AA}}(k)$ and $T_{np}^{\mathbf{BA}}(k)$ are related according to

$$\sum_{n=-\infty}^{\infty}\left[\left|R_{np}^{\mathbf{AA}}\right|^2+\left|T_{np}^{\mathbf{BA}}\right|^2\right]\begin{Bmatrix}\mathrm{Re}\Gamma_n\\ \mathrm{Im}\Gamma_n\end{Bmatrix}=\begin{Bmatrix}\mathrm{Re}\Gamma_p+2\mathrm{Im}R_{pp}^{\mathbf{AA}}\mathrm{Im}\Gamma_p\\ \mathrm{Im}\Gamma_p-2\mathrm{Im}R_{pp}^{\mathbf{AA}}\mathrm{Re}\Gamma_p\end{Bmatrix}-\frac{k^2\beta_0}{l}\begin{Bmatrix}W_1\\ W_2\end{Bmatrix}. \tag{4.115}$$

Here (see also Sections 1.1.4 and 1.2.1), $\Phi_n=2\pi(\Phi+n)/l$, $\Gamma_n=\sqrt{k^2-\Phi_n^2}$, and

$$W_2=\begin{Bmatrix}+\\ -\end{Bmatrix}\int\limits_{\mathbf{Q}_L}\left[\mu\mu_0\left|\vec{H}\right|^2-\mathrm{Re}\tilde{\varepsilon}\varepsilon_0\left|\vec{E}\right|^2\right]dg=\begin{Bmatrix}+\\ -\end{Bmatrix}\int\limits_{\mathbf{Q}_L}\left[\mu\mu_0\left|\vec{H}\right|^2-\varepsilon\varepsilon_0\left|\vec{E}\right|^2\right]dg,$$
$$\beta_0=\begin{Bmatrix}\eta_0^2\\ \eta_0^{-2}\end{Bmatrix};\qquad\begin{Bmatrix}E-\text{case}\\ H-\text{case}\end{Bmatrix}.$$

Provided that $\mathrm{Im}\Gamma_p=0$, the values

$$W=W_1\frac{k^2\beta_0}{l\Gamma_p}=\frac{k\beta_0}{l\Gamma_p}\int\limits_{\mathbf{Q}_L}\sigma\varepsilon_0\left|\vec{E}\right|^2dg,\ W_{np}^R=\left|R_{np}^{\mathbf{AA}}\right|^2\frac{\mathrm{Re}\Gamma_n}{\Gamma_p},\ W_{np}^T=\left|T_{np}^{\mathbf{BA}}\right|^2\frac{\mathrm{Re}\Gamma_n}{\Gamma_p} \tag{4.116}$$

are the relative parts of energy lost by absorption and given to the open channels (each propagating mode of the Floquet channel) taking it away from the $\mathbf{Q}_L$ domain. The relationships (4.115) reduce to the expressions (1.29) if the virtual boundaries $\mathbf{L}_1$ and $\mathbf{L}_2$ lie in the planes $z=0$ and $z=-h$.

The nonlocal and local absorbing conditions derived for problems (4.1) and (4.34) were tested to find out [1, 40, 189] that the errors introduced by their incorporation into the explicit finite-difference schemes of the second-order approximation do not exceed the standard sampling error. They are much smaller than the errors caused by the use of the classical approximate absorbing boundary conditions [181–183] of the first, second, and third orders of approximation. And, by contrast, they almost do not grow at all with time t.

4.4.2 Semitransparent Gratings

A grating will be called semitransparent if the geometry and constitutive parameters permit an electromagnetic wave transition from the zone $z>0$ to the zone $z<-h$ (see, for example, Figs. 1.1b and 4.1). The state of the art of the theory of these gratings originates with the book [16]. For a long time, it used to be a unique source whose

value is difficult to overestimate for the top quality and exceptional completeness of the factual material on the physics of resonant wave scattering by periodic structures of classical geometry. After a lapse of 13 years, the book [18] appeared. However, it sometimes duplicates the results from [16], and the level of the presentation is fairly different. In [18], an analysis is given of classes of structures sharing certain scattering properties. The observed effects and spatial–frequency electromagnetic field transformations of practical interest have been given a comprehensive description, opening certain possibilities to pose and effectively solve problems of synthesis of periodic structures with desired electrodynamical characteristics. In the book [10] the results of [16, 18] with respect to the resonant nature of the concerned effects are confirmed and new results based on the spectral theory of gratings are added. On this basis [10, 16, 18], the book [1] briefly summarizes the central achievements of the electrodynamical theory of gratings. The study of transient processes such as spatial–time transformations of pulsed waves traveling along regular and irregular Floquet channels, which is undertaken in the book [1], leans in an essential way upon fundamental results from the frequency domain. Sections 4.4.2, 4.4.3, and 4.4.4 of the present book does not present results different in kind from the material worked out in [1, 10, 16, 18]. Rather, we seek to demonstrate possibilities of some new approaches and techniques to open up a new chapter in the study of gratings.

Let a pulsed E-polarized wave

$$\begin{aligned} U_0^i(g,t) &= v_0(z,t)\,\mu_0(y)\,;\ g=\{y,z\}\in\mathbf{A},\ \Phi=0.1,\\ v_0(L_1,t) &= 4\frac{\sin\left[\Delta k(t-\tilde{T})\right]}{(t-\tilde{T})}\cos\left[\tilde{k}\left(t-\tilde{T}\right)\right]\chi\left(\bar{T}-t\right)=F_2(t)\,;\\ \tilde{k} &= 1.15,\ \Delta k=0.75,\ \tilde{T}=50,\bar{T}=100 \end{aligned} \tag{4.117}$$

(or, for short, the wave $U_0^i(g,t)$: $\Phi=0.1$; $v_0(L_1,t)=F_2(t)$; $\tilde{k}=1.15$, $\Delta k=0.75$, $\tilde{T}=50$, $\bar{T}=100$) be incident on semitransparent gratings whose geometry is sketched in Fig. 4.9. The parameters $\tilde{k}$, Δk, $\tilde{T}$, and $\bar{T}$ establish (see formula (4.95) and Fig. 4.3b) the central frequency of the signal (4.117), its spectral bandwidth ($0.4\le k\le 1.9$), the delay time (the moment the principal part of the pulse $U_0^i(g,t)$ crosses the boundary $\mathbf{L}_1$), and the duration. When $k\in[0.4;1.9]$, one (for $k<k_{-1}^+$ the value of N in the joint qualitative characteristic $\{N,M\}$ introduced in Section 1.2.1 is equal to one), two ($k_{-1}^+<k<k_1^+$, $N=2$), or three ($k>k_1^+$, $N=3$) spatial propagating harmonics can be maintained (without attenuation) in the Floquet channel $\mathbf{R}$. Here, $k_n^{\pm}=\pm|\Phi_n|$ are the threshold points of the periodic structure, or the branch points of the surface $\mathbf{K}$ (see Sections 1.1.4 and 1.2.1): $k_0^+\approx 0.156$, $k_{-1}^+\approx 1.41$, $k_1^+\approx 1.72$, and $k_{-2}^+=2.97$.

The time domain data obtained in terms of the initial boundary value model problems are translated into the amplitude–frequency characteristics [see the representation (4.113)] with an accuracy that depends on the observation time period $[0;T]$ and the Q-factor of the free field oscillations in the gratings, excited by pulses of finite duration. In the considered case (see Fig. 4.9), the observation time is taken to be as long as $T=500$ for geometry 2 and $T=2500$ for geometry 3, providing highly accurate $W_{n0}^R(k)$ and $W_{n0}^T(k)$ functions: a routine check shows that the energy

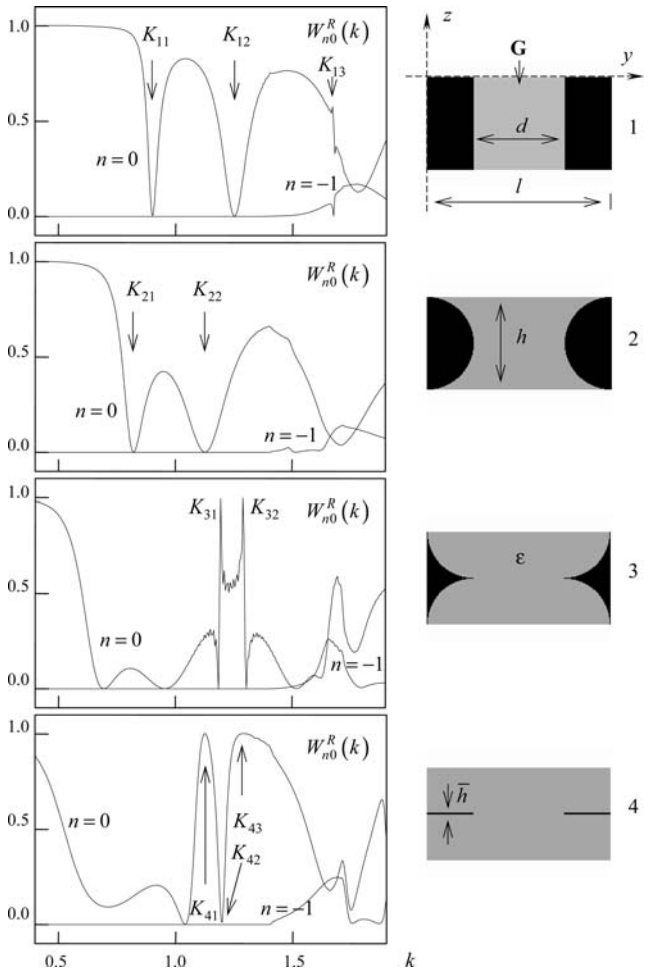

Fig. 4.9 *E*-polarization. Functions $W^R_{n0}(k)$ of different semitransparent gratings of perfectly conducting bars inside a $\varepsilon = 4.0$ dielectric layer. Geometries 1–4: grating period $l = 4.02$, height $h = 2.0$, period open part is $d = 2.0$ long, metal strips are $\bar{h} = 0.02$ thick, $L_1 = L_2 = 5.0$ Look: 4-09-1.exe, 4-09-2.exe, 4-09-3.exe, 4-09-4.exe – the $E_x(g,t)$ spatial–time distribution, $g \in \mathbf{Q}_L$, $50 \le t \le 65$ (forced oscillations mode; $U_{\max}(t) = 1.0$) in the excitation of gratings 1–4 by pulsed wave (4.117)

All **.exe** files which enable to watch in dynamics the space–time transformations of the electromagnetic field close to finite and infinite periodic structures one may download from the http://www.ire.kharkov.ua/downloads/Figures_EXE_Files.zip

conservation law on propagating harmonics is fulfilled with a related error not exceeding 1% throughout the interval $0.4 \le k \le 1.9$ [see formula (4.115)]. The maximum error for geometry 1 is observed at $k \approx K_{13} = 1.675$ (resonance on H_{02}-waves in the d-wide parallel-plate waveguide segments within parameters' domain $\{N,M\}$; $N = M = 2$). For geometry 2, it is at the threshold points $k \approx k^+_{-1}$ and $k \approx k^+_1$. For

geometry 3 – at $k \approx K_{31} = 1.19$ and $k \approx K_{32} = 1.29$ (high-Q resonances providing fast switch regimes with utmost $W_{00}^{R}(k)$ and $W_{00}^{T}(k)$ values). For geometry 4, it is at $k \approx K_{41} = 1.13$ and $k \approx K_{43} = 1.29$ (total resonant reflection), $k \approx K_{42} = 1.2$ (total resonant transition), $k \approx k_{-1}^{+}$, and $k \approx k_{1}^{+}$.

At the points $k \approx K_{11} = 0.9$, $k \approx K_{12} = 1.22$, and $k \approx K_{21} = 0.82$, $k \approx K_{22} = 1.13$ on the frequency interval $k_0^+ < k < k_{-1}^+$ coming under $N = 1$, the functions $W_{00}^{R}(k)$ vanish in the case of metal gratings of rectangular or circular bars (see Fig. 4.9). In these cases, the plane monochromatic wave

$$\tilde{U}_0^i(g,k) = \exp\left[i\left(\Phi_0 y - \Gamma_0(z - L_1)\right)\right];\ g = \{y,z\} \in \mathbf{A} \tag{4.118}$$

transmits to the domain **B** without reflection, $\left|R_{00}^{\mathbf{AA}}(k)\right| = 0$ and $\left|T_{00}^{\mathbf{BA}}(k)\right| = 1$. It is known [1, 10] that these grating regimes at frequencies $k = K$ are induced by the excitation of some sufficiently high-Q oscillations whose field highly resembles the field of free oscillations complying with complex eigenfrequencies $\bar{k}$ such that $\mathrm{Re}\bar{k} \approx K$. Thus, in the case of rectangular metal gratings, these are oscillations on the H_{0m}-waves propagating in the **G** domain, or the H_{0mn}-oscillations.

Let us have a closer look at the total transition effect occurring at frequency $k \approx K_{11} = 0.9$, geometry 1 (see Fig. 4.10). Following the recommendations from Section 4.3, we illuminate the grating with the quasi-monochromatic pulsed wave

$$U_0^i(g,t):\ \Phi = 0.1;\ v_0(L_1,t) = \cos\left[\tilde{k}\left(t - \tilde{T}\right)\right]\chi\left(\bar{T} - t\right) = F_3(t);\ \tilde{k} = 0.9,\ \tilde{T} = 0.5,\ \bar{T} = 100 \tag{4.119}$$

(see Fig. 4.10a). The analysis of the $U(g,t)$ field for the quasi-monochromatic component responsible for the resonance regime of interest leads to the H_{011}-oscillation (see Fig. 4.10d). The analysis of the dynamical properties of $U(\tau)$, $\tau = t - \bar{T} > 0$ (see Fig. 4.10b) provides its essential characteristics: the complex eigenfrequency $\bar{k} \approx 0.899 - i0.026$ and the quality factor $Q = \mathrm{Re}\bar{k}/2\left|\mathrm{Im}\bar{k}\right| \approx 17.3$.

Similar results were obtained for the total transition effects at frequencies $k \approx K_{12}$ (geometry 1) and K_{21}, K_{22} (geometry 2). These effects in gratings are associated with the excitation of the first-family oscillations H_{011} and H_{012} (see Fig. 4.11 and Section 1.3.4). Their Q-factor is modest and the suitable eigenfrequencies $\bar{k}$ are sparse. Hence, the examination of these resonant regimes admits employing rather narrow monochromatic signals, and, consequently, the observation time $[0;T]$ need not be long.

The pattern is quite different when semitransparent gratings maintain low-attenuation oscillations of the second family in the band $k_0^+ < k < k_{-1}^+$ ($N = 1$). When the frequency k approaches the real values of the complex eigenfrequencies $\bar{k}$ suitable for the free H_{02n}-oscillations of the field, the plane monochromatic wave of the type (4.118) type is totally reflected: $\left|R_{00}^{\mathbf{AA}}(k)\right| = 1$, $\left|T_{00}^{\mathbf{BA}}(k)\right| = 0$, and the field in the domain **B** is formed only by evanescent spatial harmonics. As a rule, the total

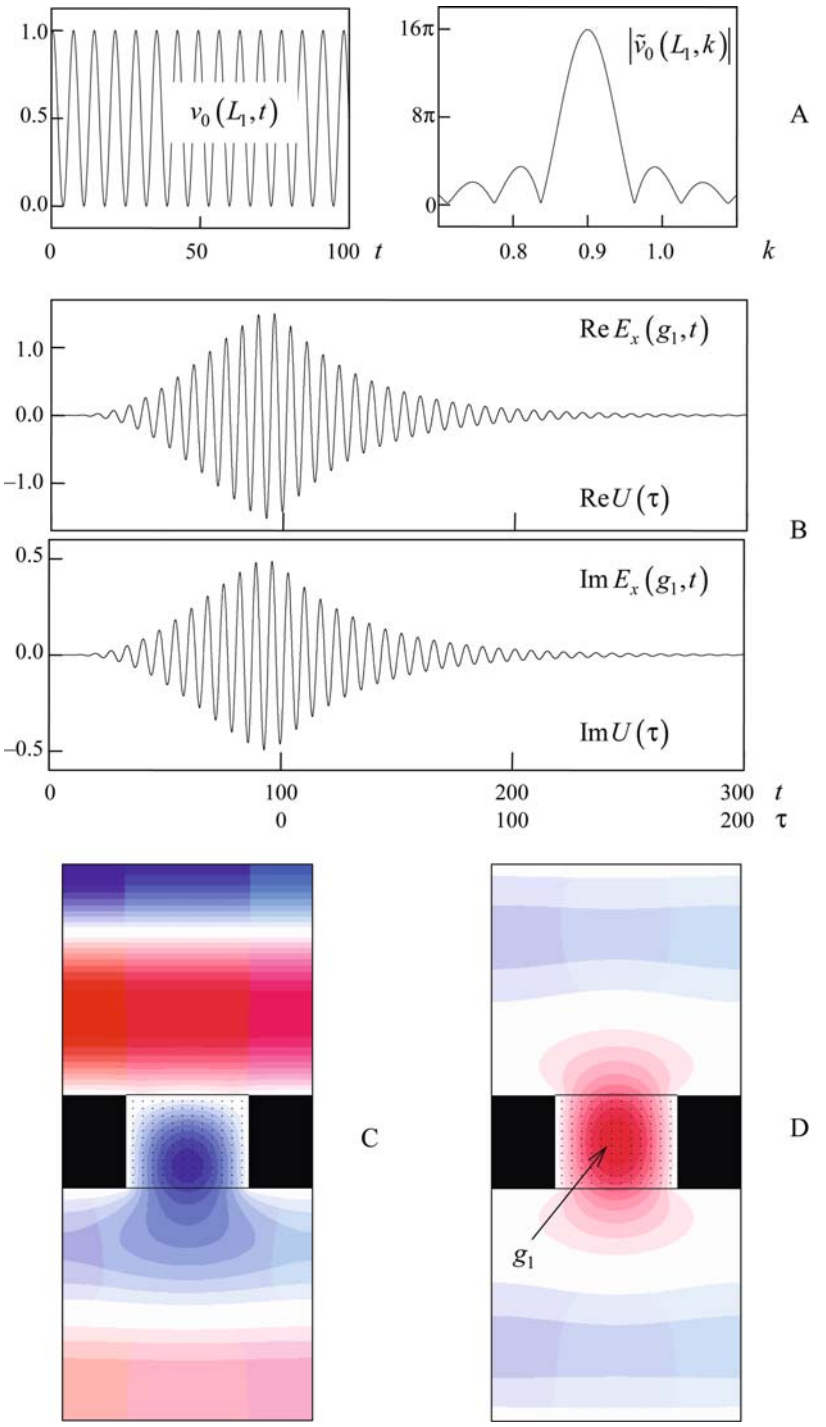

Fig. 4.10 (continued)

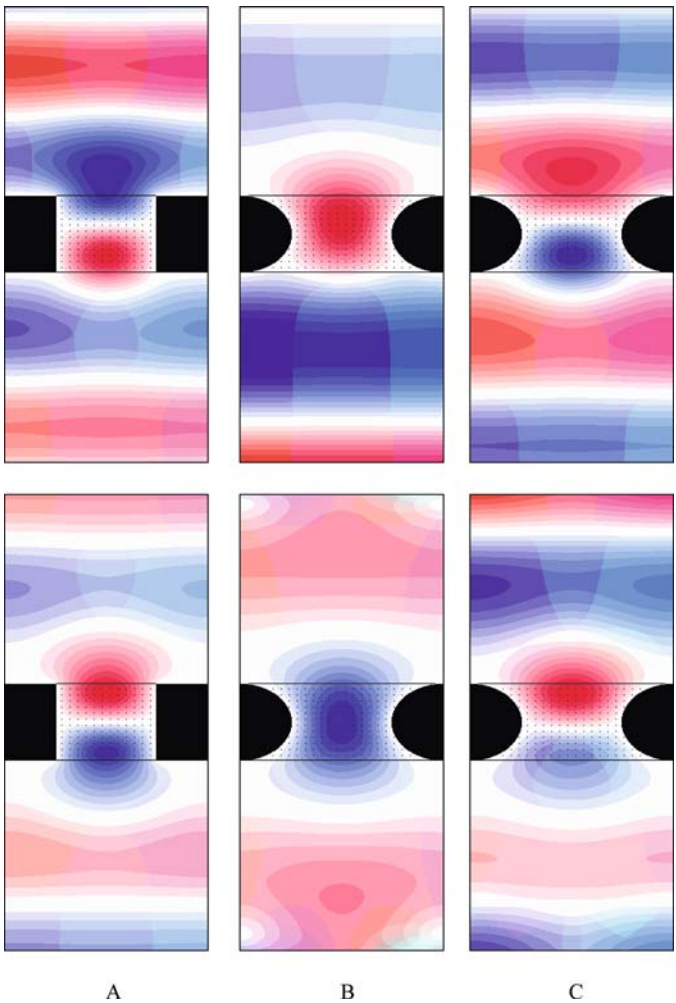

Fig. 4.11 The grating excitation by quasi-monochromatic wave (4.119) with the central frequency: (**a**) $\tilde{k} = K_{12}$; (**b**) $\tilde{k} = K_{21}$; and (**c**) $\tilde{k} = K_{22}$: the $E_x(g,t)$ spatial distribution, $g \in \mathbf{Q}_L$ at the time $t \approx 80$ (the *upper row*; forced oscillations of the field) and $t \approx 205$ (the *lower row*; free oscillations of the field)

Fig. 4.10 (continued) Geometry 1. The grating excitation by quasi-monochromatic wave (4.119) with the central frequency $\tilde{k} = K_{11}$: (**a**) Temporal and spectral amplitudes of the $U_0^i(g,t)$ wave on virtual boundary $\mathbf{L}_1$; (**b**) complex-valued function $E_x(g_1,t)$; (**c** and **d**) the $E_x(g,t)$ spatial distribution, $g \in \mathbf{Q}_L$ at the time $t \approx 80$ (forced oscillations of the field) and $t \approx 205$ (free oscillations)
Look: the $E_x(g,t)$ spatial–time distribution, $g \in \mathbf{Q}_L$; 4-10-C.exe – forced oscillations mode ($75 \le t \le 90$); 4-10-D.exe – free oscillations mode ($200 \le t \le 210$)

reflection effect of the nature is accompanied by the total transition effect. Together they make up the so-called double resonance (for details, see Section 6.3.2 in [1]).

The double resonances and the resonances giving rise to the total reflection effects are illustrated in Fig. 4.9, for points $k \approx K_{31}$, K_{32} (geometry 3) and $k \approx K_{41}$, K_{43} (geometry 4). We take a closer look at the situation corresponding to the frequency $k \approx K_{31}$ (see Fig. 4.12). Now the bandwidth factually occupied by signal (4.119) with the central frequency $\tilde{k} = K_{31} = 1.19$ turns out to be too wide to accurately identify in the field $U(g,t)$ oscillations responsible for the double resonance. Any substantial extension of the quasi-monochromatic signal practically serves no purpose. In this situation it is more efficient to use the pulsed wave

$$U_0^i(g,t): \Phi = 0.1;\ v_0(L_1,t) = \exp\left[-\frac{(t-\tilde{T})^2}{4\tilde{\alpha}^2}\right]\cos\left[\tilde{k}\left(t-\tilde{T}\right)\right]\chi\left(\bar{T}-t\right) = F_1(t);$$
$$\tilde{k} = 1.19,\ \tilde{\alpha} = 40,\ \tilde{T} = 150,\ \bar{T} = 300 \tag{4.120}$$

(see Fig. 4.12a; the dashed line shows the module of the spectral amplitude of the pulsed wave as given by formula (4.119) for $\tilde{k} = 1.19$ and $\bar{T} = 300$). In

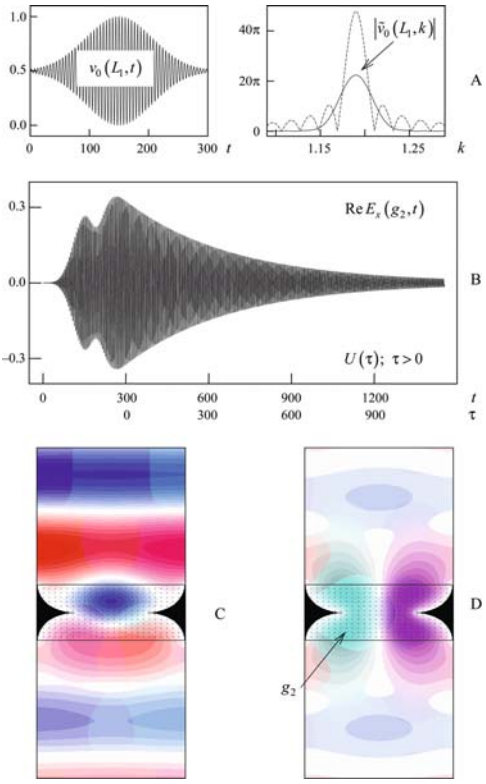

Fig. 4.12 Geometry 3. The grating excitation by pulsed wave (4.120) with the central frequency $\tilde{k} = K_{31}$: (**a**) The temporal and the spectral amplitudes of the wave $U_0^i(g,t)$ on virtual boundary $\mathbf{L}_1$; (**b**) function Re$E_x(g_2,t)$; (**c** and **d**) the $E_x(g,t)$ spatial distribution, $g \in \mathbf{Q}_L$ at the time $t \approx 159$ (forced oscillations of the field) and $t \approx 515$ (free oscillations of the field) Look: the $E_x(g,t)$ spatial–time distribution, $g \in \mathbf{Q}_L$; 4-12-C.exe – forced oscillations mode ($150 \le t \le 165$); 4-12-D.exe – free oscillations mode ($510 \le t \le 520$)

the field $U(g,t)$, arising as the grating is excited by a wave (4.120), at a time $t > 400$, a quasi-monochromatic component dominates which can be identified to be an H_{021}-oscillation (see Fig. 4.12d). This oscillation field builds up strength while the perturbation source is acting. But this growth is not monotonous (see Fig. 4.12b), suggesting (see Section 4.3) that the real part $\mathrm{Re}\bar{k}$ of the complex eigenfrequency $\bar{k}$ complying with the free H_{021}-oscillation of the grating field does not coincide with the central frequency of the signal (4.120). Yet the difference $\mathrm{Re}\bar{k} - \tilde{k}$ is not large. The spectral characteristics of the free oscillation can be obtained by analysis of the function $U(\tau)$, $\tau = t$–$300 > 0$ at a node of this oscillation field. They are $\mathrm{Re}\bar{k} \approx 1.1885$, $\mathrm{Im}\bar{k} \approx 0.0025$, and $Q \approx 237.7$.

In [10], one finds eigenfrequency behavior research for the first three families of the free field oscillations in a rectangular metal grating under changes of the parameter $\mathrm{Im}\ \tilde{\varepsilon}(g)$ ($\tilde{\varepsilon}(g) = \varepsilon(g) + i\sigma(g)/k$) specifying the value $W(k)$ of the related energy part absorbed by a lossy dielectric [see formula (4.116)] to fill the domain **G** connecting the reflection and transition zones of periodic structures. In particular, it has been shown that as $|\mathrm{Im}\ \tilde{\varepsilon}(g)|$ grows, the oscillation field configuration and the $\mathrm{Re}\bar{k}$ part of the eigenfrequency $\bar{k}$ change little. At the same time, $\mathrm{Im}\bar{k}$ increases proportionally with the $|\mathrm{Im}\ \tilde{\varepsilon}(g)|$ and uniformly with the other independent parameters. By and large this pattern holds, also, in parameter ranges where the Q-factor of free oscillations can change anomalously (see Section 1.3.4). How should this knowledge be applied to the analysis of wave scattering by semitransparent gratings with lossy dielectric insertions? First of all, it is safe to say that if $|\mathrm{Im}\ \tilde{\varepsilon}|$ is not very large, the resonant regimes will be practically at the same place as in the case $\mathrm{Im}\ \tilde{\varepsilon} = 0$ (see Figs. 4.9 and 4.13, where all geometrical parameters of the gratings with geometry 1 coincide). Second, the function $W(k)$ must have been at its maximum in the $\mathrm{Re}\bar{k}$ vicinity. But in case $\mathrm{Im}\ \tilde{\varepsilon}$ varies, this $W(k)$ behavior cannot be attributed one to one only to the growth of the square of the electric field amplitude in the **G** domain [see formula (4.116)]. The field strength of free oscillations still depends markedly on their Q-factors, which decrease with increasing $|\mathrm{Im}\ \tilde{\varepsilon}|$. In support of this statement, refer to Fig. 4.13. The field changes in the domain **A** are more pronounced than in the domain **B**, the influence mostly concerns the amplitudes $R_{00}^{\mathbf{AA}}(k)$ and $T_{00}^{\mathbf{BA}}(k)$ of the propagating harmonics whose k value approaches $\mathrm{Re}\bar{k}$.

4.4.3 Reflective Gratings

The structure of the reflective grating field can be effectively controlled by a few geometrical and (or) constitutive parameters [10, 16, 18, 19]. Effects that come to light in modeling and analysis of these gratings excite great interest in a variety of practical applications. As a rule, their implementation does not take long but it means new optical and spectroscopic devices, radar and antenna units, solid state and vacuum electronics applications, new trends in high-power electronics. Below some effects of that nature will be discussed. We emphasize that all

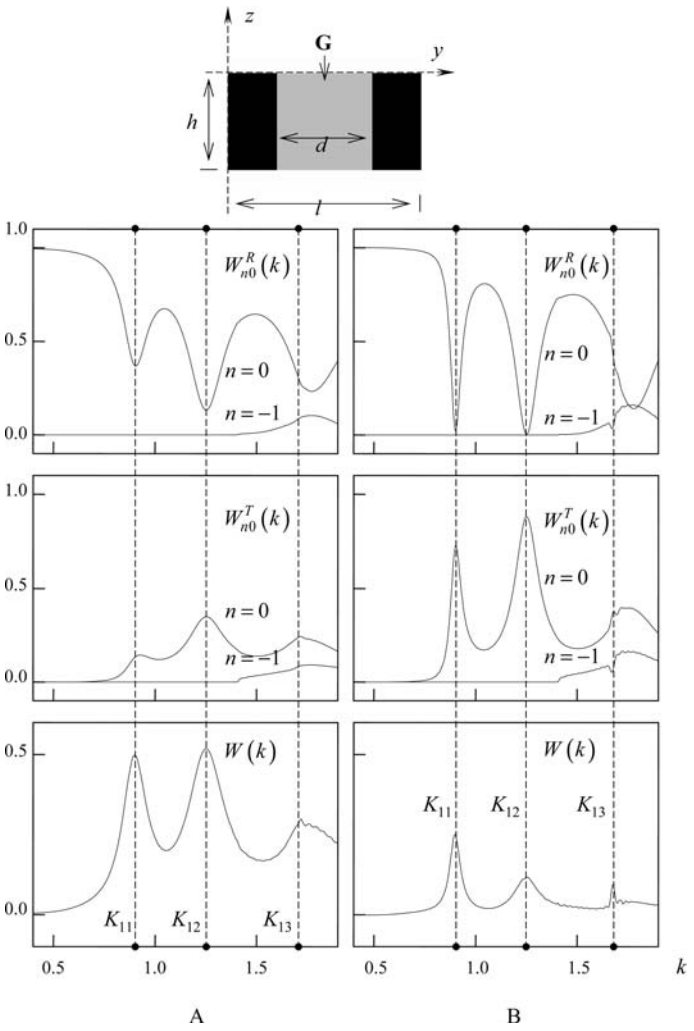

Fig. 4.13 The amplitude–frequency characteristics of a semitransparent grating of rectangular metal bars inside a dielectric layer with relative dielectric permittivity $\varepsilon = 4.0$ and specific conductivity σ_0: (**a**) $\sigma_0 = 0.001$ and (**b**) $\sigma_0 = 0.0001$; $l = 4.02$, $h = 2.0$, $d = 2.0$, $L_1 = L_2 = 5.0$

they can be extracted from commonly used reflective gratings of ordinary geometry, conventional dispersive and selective components in both optical and radio wavelengths.

Let an echelette grating like that depicted in Fig. 4.14a be illuminated by *H*-polarized pulsed waves

$$U_0^i(g,t): \Phi = 0;\ v_0(L_1,t) = F_2(t);\ \tilde{k},\ \Delta k = 0.7,\ \tilde{T} = 50,\ \bar{T} = 100. \qquad (4.121)$$

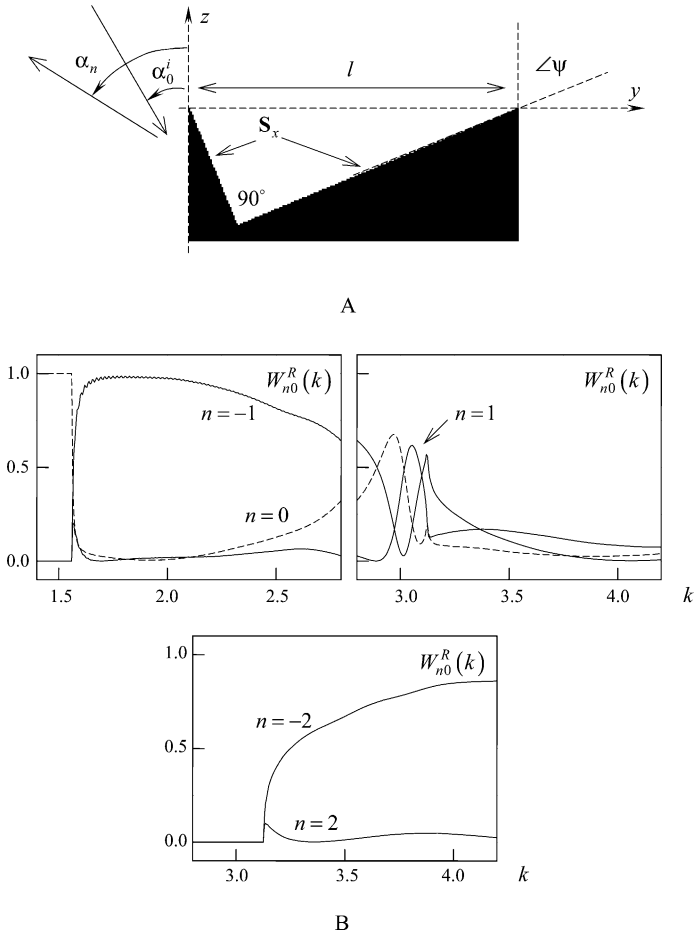

Fig. 4.14 (**a**) The echelette geometry and (**b**) its electrodynamical characteristics in the frequency band $1.4 \le k \le 4.2$: H-polarization, $\alpha_0^i = 0$ ($\Phi = 0$), $l = 4.02$, $\psi = 67.5°$, $L_1 = 8.4$

Having solved the corresponding initial boundary value problems for any time $0 \le t \le T$, $T = 500$, we can obtain the electrodynamical characteristics of the structure (see Fig. 4.14b) in the frequency bands $1.4 \le k \le 2.8$ (the central frequency of signal (4.121) is $\tilde{k}$ =2.1) and $2.8 \le k \le 4.2$ ($\tilde{k} = 3.5$). Why do we halve the analyzed frequency interval $1.4 \le k \le 4.2$? Thus, the free oscillation field $U(g,t)$, $g \in \mathbf{Q}_L$, $t > \bar{T}$ (see Fig. 4.15) rids of the contribution from the threshold effect taking place at one of the branch points of the surface $\mathbf{K}$: $k_{\pm 1}^{+} \approx 1.56$ (for $\tilde{k} = 3.5$) or $k_{\pm 2}^{+} \approx 3.13$ (for $\tilde{k} = 2.1$).

In the frequency band $1.7 \le k \le 2.0$ past the threshold point $k_{\pm 1}^{+} \approx 1.56$ (where first high-order spatial propagating harmonics appear), the echelette grating

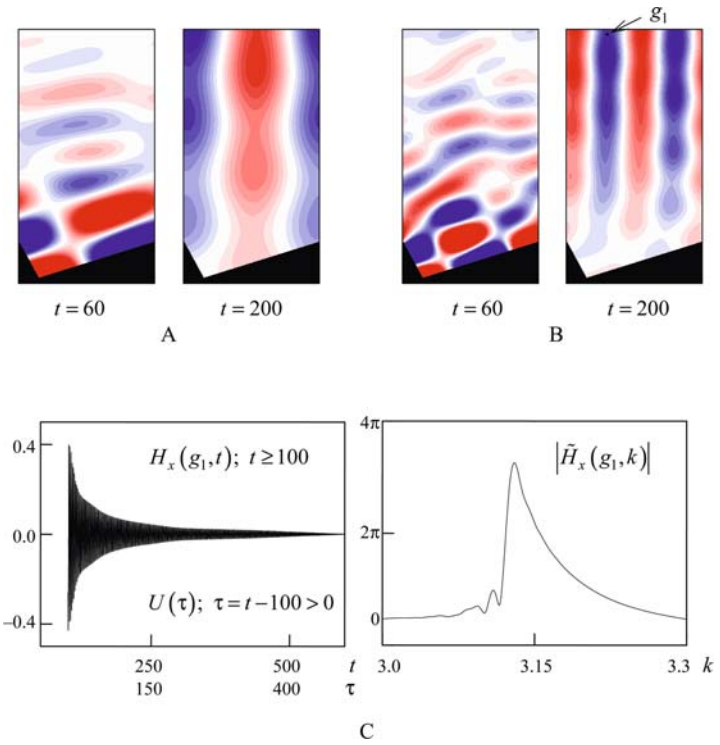

Fig. 4.15 The echelette excitation by pulsed H-polarized wave (4.121) with the central frequency (**a**) $\tilde{k} = 2.1$ and (**b** and **c**) $\tilde{k} = 3.5$: (**a** and **b**) The $H_x(g,t)$ spatial distribution, $g \in \mathbf{Q}_L$ at the time $t = 60$ (forced oscillations) and $t = 200$ (free oscillations); (**c**) the temporal and the spectral amplitudes of the H_x-field component at the point $g = g_1$
Look: the $H_x(g,t)$ spatial–time distribution, $g \in \mathbf{Q}_L$; 4-15-A.exe and 4-15-B.exe – forced oscillations mode ($50 \leq t \leq 70$; $U_{\max}(t) = 1.0$); 4-15-A-F.exe and 4-15-B-F.exe – free oscillations mode ($200 \leq t \leq 210$)

manages to concentrate over 98% of the applied energy delivered by normally incident H-polarized plane wave (4.118) into one of these harmonics (specifically, the minus first one) (see Fig. 4.14b). For these k values, the angle $\alpha_{-1} = -\arcsin\left(\Phi_{-1}/k\right)$ at which the $R^{\mathbf{AA}}_{-10}(k)$-amplitude harmonic departs from the grating is $\alpha_{-1} = 66.8°$ to $\alpha_{-1} = 51.4°$. Past the second threshold point $k^{+}_{\pm 2} \approx 3.13$, a substantial part of the incident energy is given to the minus second spatial harmonic. But its $W^{R}_{-20}(k)$ function does not grow as fast as $W^{R}_{-10}(k)$ does, and it cannot achieve anomalously high values.

At the frequency $k = 2.89$, all the energy is equally distributed between the principal and the minus first spatial harmonics ($W^{R}_{-10}(k) = W^{R}_{00}(k) = 0.5$ and $W^{R}_{10}(k) = 0$; $\alpha_0 = 0$ and $\alpha_{-1} = 32.7°$), compare with $W^{R}_{10}(k) = W^{R}_{00}(k) \approx 0.49$, $W^{R}_{-10}(k) \approx 0.02$, and $\alpha_1 = -31.2°$ at the frequency $k = 3.015$. From an asymmetric echelette grating, we can also get symmetric channels to radiate the input

energy. Thus, $W_{10}^R \approx W_{-10}^R \approx 0.46$, $W_{00}^R(k) \approx 0.08$, and $\alpha_{\mp 1} = \pm 30.3°$ at the point $k = 3.098$.

The energy flows that the reflective grating under the action of a normally incident E- or H-polarized quasi-monochromatic wave $U_0^i(g,t)$ directs to side channels can be visualized via the calculation of the spatial–time distribution of the values of $H_z(g,t)$ or $E_z(g,t)$ corresponding to the field $U(g,t)$, $g \in \mathbf{Q}_L$. Indeed, the excitation with a quasi-monochromatic wave whose spectral amplitudes decrease rapidly as the frequency k departs from $k = \tilde{k}$ makes it possible to minimize the angular widening of the side channels. Then the z-components of the incident wave field $U_0^i(g,t)$ and of the total field $U(g,t)$ part traveling toward it are identically equal to zero. Figure 4.16 plots the solution results of the initial boundary value problems of the echelette grating excitation by the quasi-monochromatic wave

$$U_0^i(g,t) : \Phi = 0;\ v_0(L_1,t) = F_3(t);\ \tilde{k},\ \tilde{T} = 0.5,\ \bar{T} = 300 \tag{4.122}$$

with the central frequencies $\tilde{k} = 1.85$ (Fig. 4.16a) and $\tilde{k} = 2.89$ (Fig. 4.16b). Let us remember (see above) that $W_{-10}^R(k) > 0.98$ and $\alpha_{-1} = 57.7°$ at the frequency $k = 1.85$ and $W_{-10}^R(k) = 0.5$ and $\alpha_{-1} = 32.7°$ at $k = 2.89$. These α_{-1} values are shown in those parts of Fig. 4.16 which are plotting the spatial distribution of $E_z(g,t)$, $g \in \mathbf{Q}_L$, $t = 101$. They give a sufficiently accurate picture of the orientation of the side channels drawing energy away from the grating.

Evidently in the H-polarized field case, the spectrum Ω_k (see Section 1.3.2) of the perfectly conducting plane $z = 0$ on the first sheet of the surface $\mathbf{K}$ carries real-valued $\bar{k}$ points coinciding with the branch points $k_n^{\pm} = \pm|\Phi_n|$, $n = 0,\pm1,\pm2,\ldots$. These eigenvalues $\bar{k}$ meet the field free oscillations $u_0(g,\bar{k}) = u_0(g,k_n^{\pm}) = \exp(i\Phi_n y)$, $\Phi_n = 2\pi(\Phi+n)/l$ with infinitely large Q-factor. If a "smooth" deformation of the plane $z = 0$ is started to shape it into the surface $\mathbf{S} = \mathbf{S}_x \times [|x| \le \infty]$ of some reflective grating, then the oscillations $u_0(g,\bar{k})$ and the relevant elements $\bar{k}$ of the spectral set Ω_k will vary in the same "smooth" manner so that no element in the bounded part of the surface $\mathbf{K}$ will ever disappear (see [10] and Statement 1.5). Therefore, in the H-polarized field case, the amplitude–frequency characteristics of

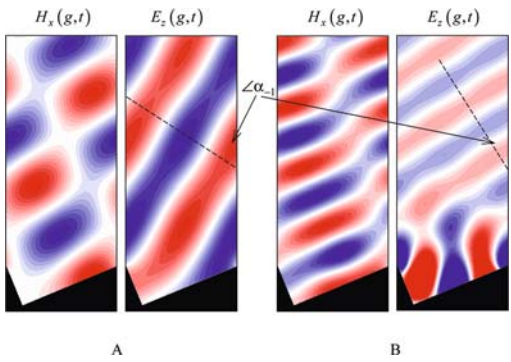

Fig. 4.16 The echelette excitation by quasi-monochromatic pulsed wave (4.122) with the central frequency: (**a**) $\tilde{k} = 1.85$ and (**b**) $\tilde{k} = 2.89$. The $H_x(g,t)$ and $E_z(g,t)$ spatial distributions, $g \in \mathbf{Q}_L$ at the time $t = 101$ Look: 4-16-A.exe and 4-16-B.exe – the $H_x(g,t)$ spatial–time distribution, $g \in \mathbf{Q}_L$, $100 \le t \le 110$

reflective gratings demonstrate the threshold effects (Wood's anomalies) far more intensively than in the *E*-case. The reason is that the action of the branch points $k_n^{\pm}$ of the surface **K** (in small vicinities of the $k_n^{\pm}$ points, the local variable of the surface **K** is $\left(k - k_n^{\pm}\right)^{1/2}$ [1, 10]) is enhanced by the resonances associated with the excitation of sufficiently high-Q oscillations of the field. These oscillations fit, as a rule, eigenfrequencies $\bar{k}$ whose difference $\mathrm{Re}\bar{k} - k_n^{\pm}$ is not large. For instance, the free oscillation field $U(g,t)$, $g \in \mathbf{Q}_L$, $t > 100$, maintained by a metal echelette grating excited by a pulsed wave (4.121), clearly demonstrates [see expression (4.86)] certain characteristic features of free oscillation fields $u_0\left(g,k_n^{+}\right) = \exp\left(i\Phi_n y\right) = \exp\left(i2\pi n y/l\right)$. $n = \pm 1$ (Fig. 4.15a) and $n = \pm 2$ (Fig. 4.15b). The spectral amplitudes of the H_x-field component at the node of one of these oscillations (see Fig. 4.15c) reach their maxima in the vicinity of the point $k = 3.13$ ($k_{\pm 2}^{+} \approx 3.13$). A second local maximum of the function $\left|\tilde{H}_x\left(g_3,k\right)\right|$ exists near $k = 3.11$. These seem to be right $\mathrm{Re}\bar{k}$ values of the eigenfrequencies $\bar{k}$ to fit the deformed free oscillations $u_0\left(g,k_n^{+}\right)$, $n = \pm 2$.

Reflective gratings excited by an oblique incident ($\sin\alpha_0^i = \Phi_0/k \neq 0$) *E*- or *H*-polarized plane wave (4.118) can concentrate most of the applied energy into one of high-order spatial harmonics $R_{n0}^{\mathbf{AA}}(k)\exp\left[i\left(\Phi_n y + \Gamma_n\left(z - L_1\right)\right)\right]$. $n \neq 0$, of the secondary field $\tilde{U}^s(g,k) = \tilde{U}(g,k) - \tilde{U}_0^i(g,k)$; $g = \{y,z\} \in \mathbf{A}$ (see [16, 18, 19] and Section 1.2.1). The propagation direction of this harmonic according to the angle $\alpha_n = -\arcsin\left(\Phi_n/k\right)$ is different from the direction of the specular reflection wave $R_{00}^{\mathbf{AA}}(k)\exp\left[i\left(\Phi_0 y + \Gamma_0\left(z - L_1\right)\right)\right]$, $\alpha_0 = -\alpha_0^i$. If $W_{n0}^R(k) = 1$, we say that the total nonspecular reflection effect takes place. Let $n = -m$ and

$$W_{-m0}^R(k) = 1,\ kl\sin\left(\alpha_0^i\right) = \pi m. \tag{4.123}$$

If condition (4.123) holds for some k values, it is said that the effect of total autocollimation reflection takes place on the minus *m*th spatial harmonic, implying that all the energy is concentrated into the plane wave traveling toward the incident wave $\tilde{U}_0^i(g,k)$. In the autocollimation regime $\Phi = m/2$, the propagation constants Γ_n of the specular ($n = 0$) and autocollimation ($n = -m$) harmonics coincide at the same time as $\Phi_0 = -\Phi_{-m}$.

The effect of total or nearly total autocollimation reflection on the minus first spatial harmonic can both be spread over wide a band and retained within a narrow band. For example, Fig. 4.17b shows that for geometry 1 the $0.85 \leq k \leq 1.85$ bandwidth where $W_{-10}^R(k) \geq 0.95$ amounts to 74%. In the first case, the effect is due to the low-Q oscillations of the first family in the **G** domain, namely, the oscillations on *TEM*- or H_{01}-waves in the *d*-wide parallel-plate waveguide segments. In the second case, the responsibility for maintaining the effect rests with larger-Q oscillations on the E_{0n}- ($n \geq 1$) or H_{0n}-waves ($n \geq 2$). But in any case, the limit value $W_{-10}^R(k) = 1.0$ can only be reached when no more than two – the zeroth and the minus first – spatial harmonics propagate without attenuation in the reflection zone of the periodic structure.

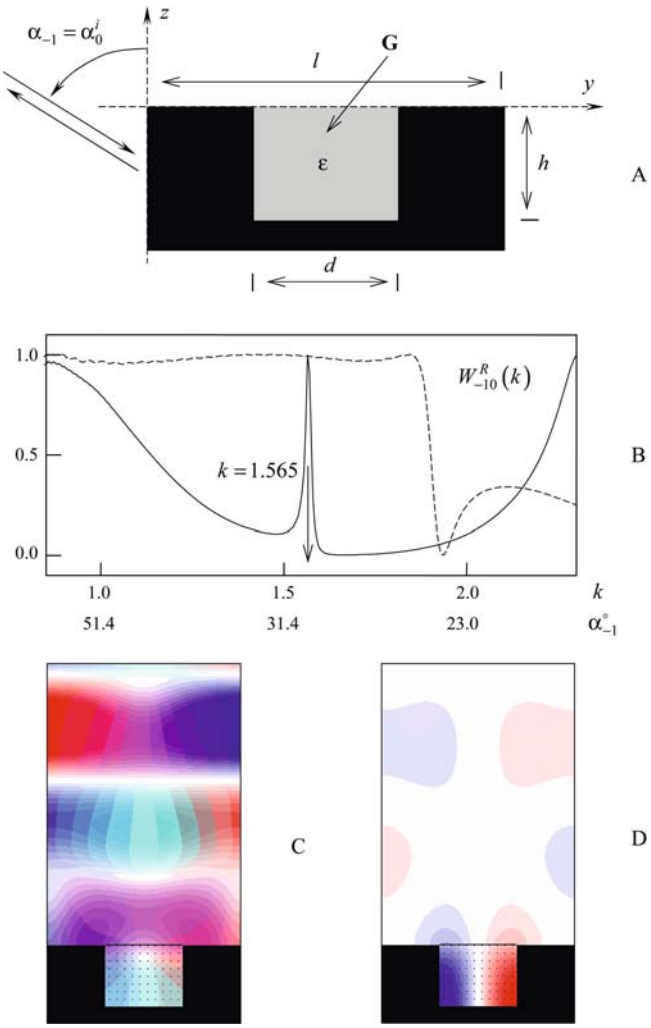

Fig. 4.17 *H*-polarization. The autocollimation reflection on the minus first spatial harmonic: (**a**) Grating geometry (1 – $l = 4.02$, $h = 1.0$, $d = 2.02$, $\varepsilon = 1$; 2 – $l = 4.02$, $h = 1.28$, $d = 1.62$, $\varepsilon = 2$); (**b**) reflection efficiency (geometry 1 – *dots* and geometry 2 – *solid line*); (**c** and **d**) the $H_x(g,t)$ spatial distribution, $g \in \mathbf{Q}_L$ at the time $t = 65$ and $t = 205$ in the excitation of grating with geometry 2 by a pulsed wave (4.124), $L_1 = 8.4$
Look: 4-17-C.exe and 4-17-D.exe – the $H_x(g,t)$ spatial–time distribution, $g \in \mathbf{Q}_L$, $50 \le t \le 70$ ($U_{\max}(t) = 1.0$) and $200 \le t \le 210$

The data reported in Fig. 4.17 were obtained by studying the grating response to the excitation with the pulsed *H*-polarized wave

$$U_0^i(g,t): \Phi = 0.5;\ v_0(L_1,t) = F_2(t);\ \tilde{k} = 1.55,\ \Delta k = 0.75,\ \tilde{T} = 50,\ \bar{T} = 100. \tag{4.124}$$

The band $0.85 \le k \le 2.3$, where the spectral amplitudes of the signal (4.124) reach their maxima, does not include the branch points $k_0^+ = k_{-1}^+ \approx 0.782$ and $k_1^+ = k_{-2}^+ \approx 2.35$. Therefore, in the free oscillation field $U(g,t)$, $t > 100$, the oscillation on E_{01}-waves is clear enough (see Fig. 4.17d), and it is evidently a single oscillation characterized by a sufficiently high Q-factor whose complex eigenfrequency $\bar{k}$ is under the segment $0.85 \le k \le 2.3$ of the real axis $k > 0$ of the first sheet of the surface **K**. It seems to be precisely that this oscillation is responsible for the total autocollimation reflection at the frequency $k = 1.565$ (see Fig. 4.17b). This possibility gains substance from the analysis of the grating response to the excitation by a quasi-monochromatic H-polarized wave $U_0^i(g,t)$ with the central frequency $\tilde{k} = 1.565$ (see Fig. 4.18). The spectral amplitudes of the function $U(\tau)$ are at their maxima in the small vicinity of the point $k = 1.569$, its envelope $f(\tau)$ obeys the equation $f(\tau) = \pm 3.12\exp(-0.0088\tau)$. This means (see Section 4.3) that the free oscillation on the E_{01}-waves (see Fig. 4.18b) fits the eigenfrequency $\bar{k} \approx 1.569 - i0.0088$. The field $U(g,t)$ becomes real valued as soon as the perturbation source is turned off (see Fig. 4.18c). Therein lies a specific character of the boundary value and the initial boundary value problems with a half-integer Φ [10, 18]. Namely, in the case of gratings symmetric about the planes $y = l/2+nl$, $n = 0,\pm 1,\pm 2,\ldots$, the problems of this kind can be reduced to the inhomogeneity problems of a parallel-plate waveguide with electrical and magnetic walls $y = 0$ and $y = l$.

Reflective gratings can be used as dispersive elements to do effective polarization selection of signals. Refer to the situation reported in Fig. 4.19. At the frequency $k = 0.775$, 99% of the applied energy is drawn toward the incident plane wave when it is H-polarized and only 1% when the incident plane wave is E-polarized. At the frequency $k = 1.005$, the main channels of energy withdrawal on E- and H-polarized waves are interchanged: $W_{-10}^R(k) = 0.05$ for the H-polarization and $W_{-10}^R(k) = 1.0$ for the E-polarization. At the frequency $k = 0.667$, $W_{-10}^R(k) = 0.92$ for both polarizations. The portion of energy given away to the specular reflection spatial harmonics comes from the equation $W_{-10}^R(k) + W_{00}^R(k) = 1.0$: in the band $0.5 < k < 1.5$, only the principal and the minus first harmonics of the secondary field $\tilde{U}^s(g,k)$ travel without attenuation in the domain **A**.

A grating formed by thin metal strips lying on a dielectric substrate backed by a perfectly conducting screen fully separates polarizations when the autocollimation reflection regime comes about on the minus first spatial harmonic. Figure 4.20 shows that at $k = 1.565$, all the energy delivered by the E-polarized wave goes to the minus first spatial harmonic ($W_{-10}^R(k) = 1.0$). When the incident wave is H-polarized, all the energy concentrates into the specular reflection harmonic ($W_{-10}^R(k) = 0.0$). At $k = 2.0$, the separation of polarizations is not so fine. Here $W_{-10}^R(k) = 1.0$ in the case of H-polarization of the field and $W_{-10}^R(k) = 0.02$ ($W_{00}^R(k) = 0.98$) in the E-case.

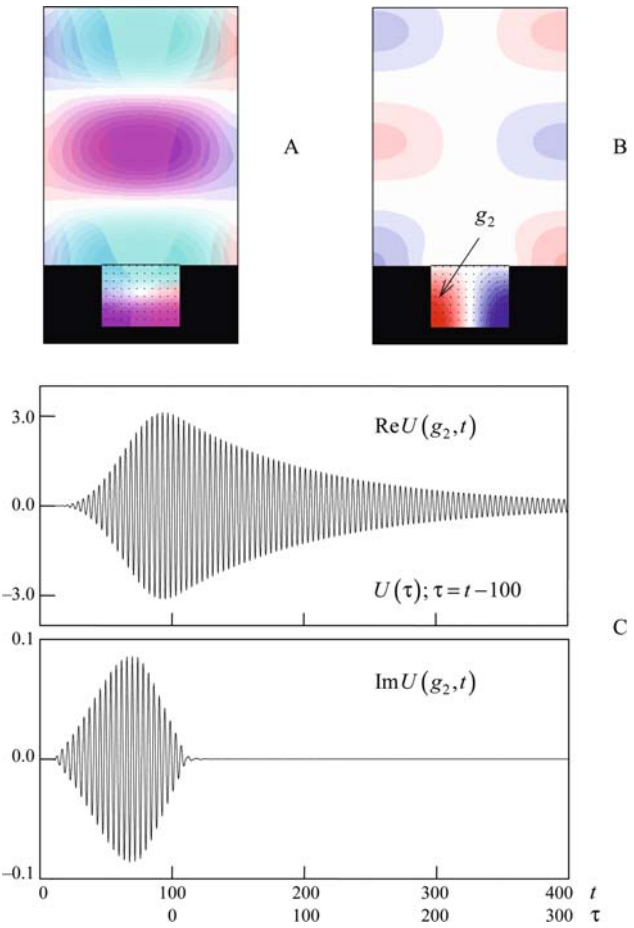

Fig. 4.18 The reflective grating excitation (geometry 2) by an H-polarized quasi-monochromatic wave $U_0^i(g,t)$: $\Phi = 0.5$; $v_0(L_1,t) = F_3(t)$; $\tilde{k} = 1.565$, $\tilde{T} = 0.5$, $\bar{T} = 100$: (**a** and **b**) The $H_x(g,t)$ spatial distribution, $g \in \mathbf{Q}_L$ at the time $t = 90$ and $t = 205$: (**c**) functions $U(g_2,t)$ and $U(\tau)$
Look: 4-18-A.exe and 4-18-B.exe – the $H_x(g,t)$ spatial–time distribution, $g \in \mathbf{Q}_L$, $80 \le t \le 95$ and $200 \le t \le 210$

4.4.4 Gratings in a Pulsed Wave Field

It is evident that a fairly complete analytic description of pulse deformations in regular and irregular Floquet channels is impossible without proper computational work. The figures obtained must be adequately interpreted. A treatment of this kind

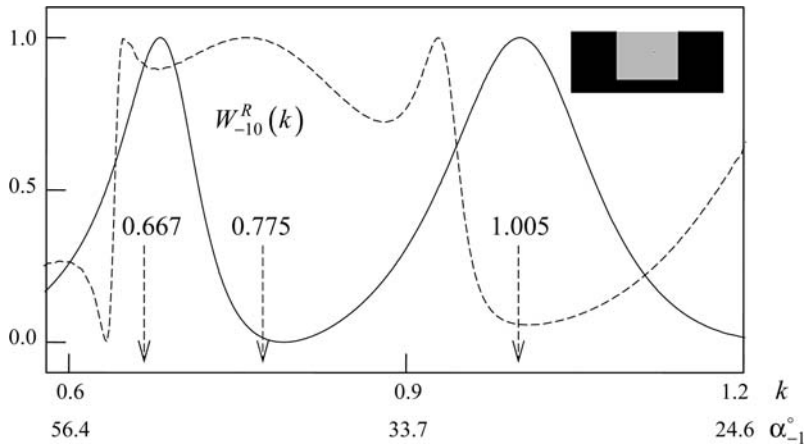

Fig. 4.19 The autocollimation reflection efficiency on the minus first spatial harmonic: *H*-polarization – *dots*; *E*-polarization – *solid line* ($l = 2\pi$, $h = 4.3$, $d = 3.8$, $\varepsilon = 2$)

originated in references [1, 40, 209]. Here, we discuss some recent results based on the methods reported in Section 4.1.

The four plane *E*-polarized sinusoidal waves $\tilde{U}^i_0(g,k) = \exp(-ikz)$, $\tilde{U}_0(g,k) = \exp(ikz)$, $\tilde{U}_1(g,k) = -\exp(iky)$, and $\tilde{U}_{-1}(g,k) = -\exp(-iky)$ traveling in free space result in the field $\tilde{E}_x(g,k)$ whose null surfaces at $k = k^+_{\pm 1} = 2\pi/l$ can be brought into coincidence with the surface $\mathbf{S} = \mathbf{S}_x \times [|x| \le \infty]$ of a symmetric echelette grating (see Fig. 4.14a: $\psi = 45°$). This means that the total field originating as the echelette grating excited by the wave $\tilde{U}^i_0(g,k)$ coincides (everywhere above the contour $\mathbf{S}_x$) with the field $\tilde{U}(g,k) = \tilde{U}^i_0(g,k) + \sum_{n=0,1,-1} \tilde{U}_n(g,k)$. In this case, the waves $\tilde{U}_n(g,k)$, $n = 0,\pm 1$, play the parts of principal, plus and minus first spatial harmonics of the secondary field $\tilde{U}^s(g,k) = \tilde{U}(g,k) - \tilde{U}^i_0(g,k)$. Usually in this way a reason is given for an explicit analytic solution to problem (1.26), the existence of the solution is attributed to the so-called geometrical resonances [18]. Later on, we will see what the mentioned geometrical resonance (a frequency domain effect) tells us about the solution of the corresponding scattering problem in the time domain.

Suppose that a symmetric echelette grating is excited by the *E*-polarized quasi-monochromatic wave $U^i_0(g,t)$: $\Phi = 0$; $v_0(L_1,t) = F_3(t)$; $\tilde{k} = 1.563 \approx k^+_{\pm 1}$, $\tilde{T} = 0.5$, $\bar{T} = 200$ (see Figs. 4.21 and 4.22). Next compare between the spatial–temporal amplitudes of the signal $U^i_0(g,t)$ and the principal spatial harmonics $U_n(g,t) = u_n(z,t)\,\mu_n(y)$, $n = 0,\pm 1$, caused by this signal in the reflection zone of the grating. The function $v_0(L_1,t)$, whose related spectral amplitudes do not exceed 0.3 beyond the narrow frequency band $1.54 < k < 1.586$, has a simple envelope and vanishes for all $t > \bar{T}$. The effective spatial duration of the signals $U_0(g,t)$ and

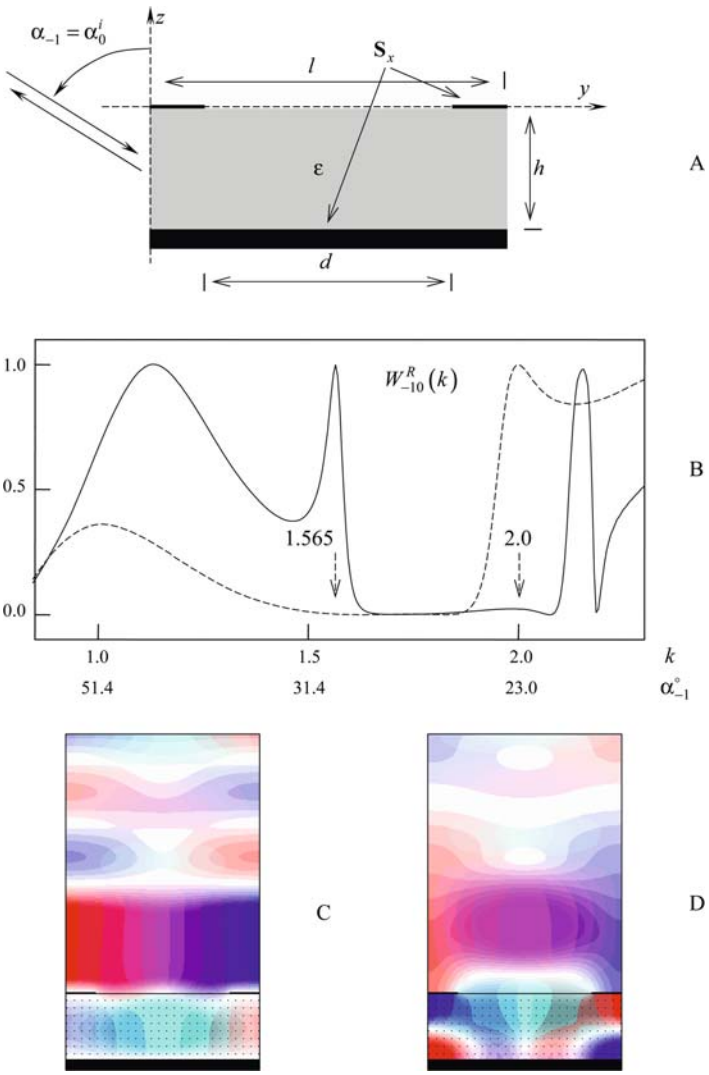

Fig. 4.20 The autocollimation reflection efficiency on the minus first spatial harmonic: (**a**) Grating geometry ($l = 4.02$, $h = 1.42$, $d = 2.78$, $\varepsilon = 2$, perfectly conducting strips thickness is 0.04, $L_1 = 8.4$); (**b**) reflection efficiency (*H*-polarization – *dots*; *E*-polarization – *solid line*); (**c** and **d**) the $E_x(g,t)$ and $H_x(g,t)$ spatial distributions, $g \in \mathbf{Q}_L$ at the time $t = 60$ in the grating excitation by a pulsed *E*- and *H*-polarized wave (4.124)
Look: 4-20-C.exe and 4-20-D.exe – the $E_x(g,t)$ and $H_x(g,t)$ spatial–time distributions, $g \in \mathbf{Q}_L$, $50 \le t \le 70$ (forced oscillations mode; $U_{\max}(t) = 1.0$)

$U_0^i(g,t)$ is practically the same, but the $U_0(g,t)$ amplitude gradually increases by the action of the perturbation source. The main part of the pulse $u_0(L_1,t)$ is followed by a short, fast decaying tail. The tails of the pulses $u_{\pm 1}(L_1,t)$ are more powerful, which is probably caused by the fact that the plus and the minus first

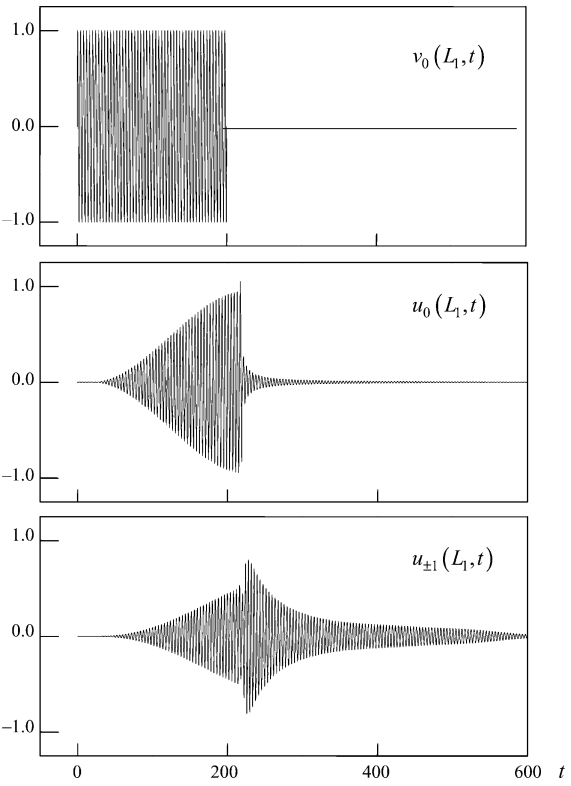

Fig. 4.21 The excitation of a symmetric echelette ($\psi = 45°$, $l = 4.02$, $L_1 = 7.8$) by a normally incident E-polarized quasi-monochromatic wave $U_0^i(g,t)$. The spatial–temporal amplitudes are shown for the $U_0^i(g,t)$ wave and the principal spatial harmonics of the secondary field $U^s(g,t)$ on the virtual boundary $\mathbf{L}_1$

harmonics are the principal components of the free oscillation field complying with the eigenfrequency $\bar{k}$ which is such that $\mathrm{Re}\bar{k}$ is in a small vicinity of the branch point $k_{\pm1}^{+} \approx 1.563$.

The main carriers of the $H_z(g,t)$-component of the field $U(g,t)$ are the waves $U_{\pm1}(g,t)$. The $H_y(g,t)$ main carriers are the waves $U_0^i(g,t)$ and $U_0(g,t)$. The spatial distribution of the values $E_x(g,t)$, $g \in \mathbf{Q}_L$, corresponding to the field $U(g,t)$ is equally governed by all these waves. At some time moments, it is practically no different from the distribution resulting (at $k = k_{\pm1}^{+}$) from the interference of the sinusoidal waves $\tilde{U}_0^i(g,k)$ and $\tilde{U}_n(g,k)$, $n = 0,\pm1$. The distinctions decrease monotonously with the time t provided that the central frequency $\tilde{k}$ of the quasi-monochromatic wave $U_0^i(g,t)$ having a sufficiently large spatial duration $\bar{T}$ coincides exactly with $k_{\pm1}^{+}$. Thus in this situation, the limiting amplitude principle [1, 10] is realized, and the transient gradually takes on properties of the established process.

Now let us excite a symmetrical echelette grating by the E-polarized wideband signal $U_0^i(g,t)$: $\Phi = 0$; $v_0(L_1,t) = F_1(t)$; $\tilde{k} = 1.6$, $\tilde{\alpha} = 1.3$, $\tilde{T} = 15$, $\bar{T} = 30$ (see Fig. 4.23: the bandwidth is given by $0.4 < k < 2.8$, where the normalized spectral

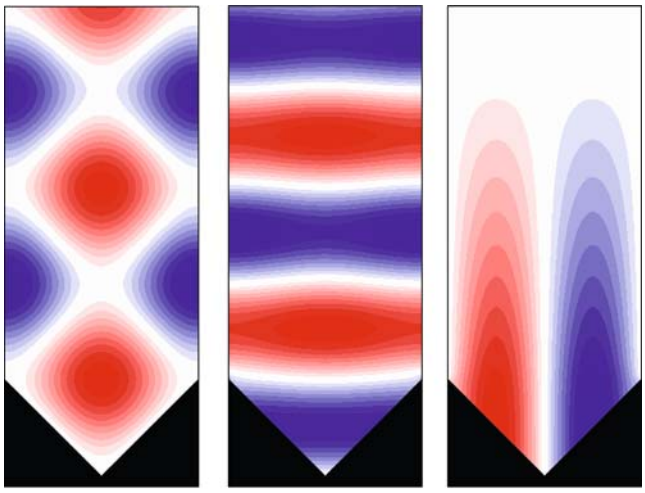

Fig. 4.22 (Complementation to Fig. 4.21). The $E_x(g,t)$, $H_y(g,t)$, and $H_z(g,t)$ spatial distributions, $g \in \mathbf{Q}_L$, $t = 189.75$
Look: 4-22.exe and 4-22-F.exe – the $E_x(g,t)$ spatial–time distribution, $g \in \mathbf{Q}_L$, $180 \le t \le 195$ (forced oscillations mode) and $450 \le t \le 460$ (free oscillations mode)

amplitudes of the function $v_0(L_1,t)$ are no less than 0.1, is equal to 150%). The spectral amplitudes of the pulses $u_0(L_1,t)$ and $v_0(L_1,t)$ differ little from each other everywhere except on the frequency interval past the branch point $k_{\pm 1}^{+}$. And it is on this frequency interval that the amplitudes of the pulses $u_{\pm 1}(L_1,t)$ are at their maxima. As in the case of a grating excitation by a monochromatic signal $U_0^i(g,t)$, all features of the functions $u_n(L_1,t)$ and $|\tilde{u}_n(L_1,k)|$ originate from the threshold effect in the frequency domain and the redistribution of the applied energy among the spatial harmonics of the field $\tilde{U}^s(g,k)$.

The phenomenon of the strong conversion of the sinusoidal H_{01}-waves to the H_{0m}-waves, $m > 1$ that takes place on inclined H-plane plugs in rectangular waveguides (see Fig. 12 in [210]) can be interpreted in superwideband signal terms as follows. The pulsed H_{01}-wave with spectral amplitudes evenly distributed across the range $k_2 < k < k_M$ (k_m is the H_{0m}-wave cutoff) is reflected from the plug to produce a series of the pulsed H_{0m}-waves, $m = 2, \ldots, M$–2, each occupying its own band $k_m < k < k_{m+2}$ in the range. In this band, the function $W_{m1}(k)$ describing the applied energy part transferred to the reflected H_{0m}-wave first monotonously increases from zero up to $\max\limits_{k} W_{m1}(k) = W_{m1}(k_{m+1}) \approx 1$, then monotonously decreases down to $W_{m1}(k_{m+2}) \ll 1$.

Phenomena of this kind attend the scattering of superwideband TE_{01}-pulses from cone-shaped plugs in circular and coaxial circular waveguides [211] and also the scattering of E-polarized pulsed waves normally incident on a symmetric metal echelette grating with obtuse teeth (see Figs. 4.24 and 4.25). The

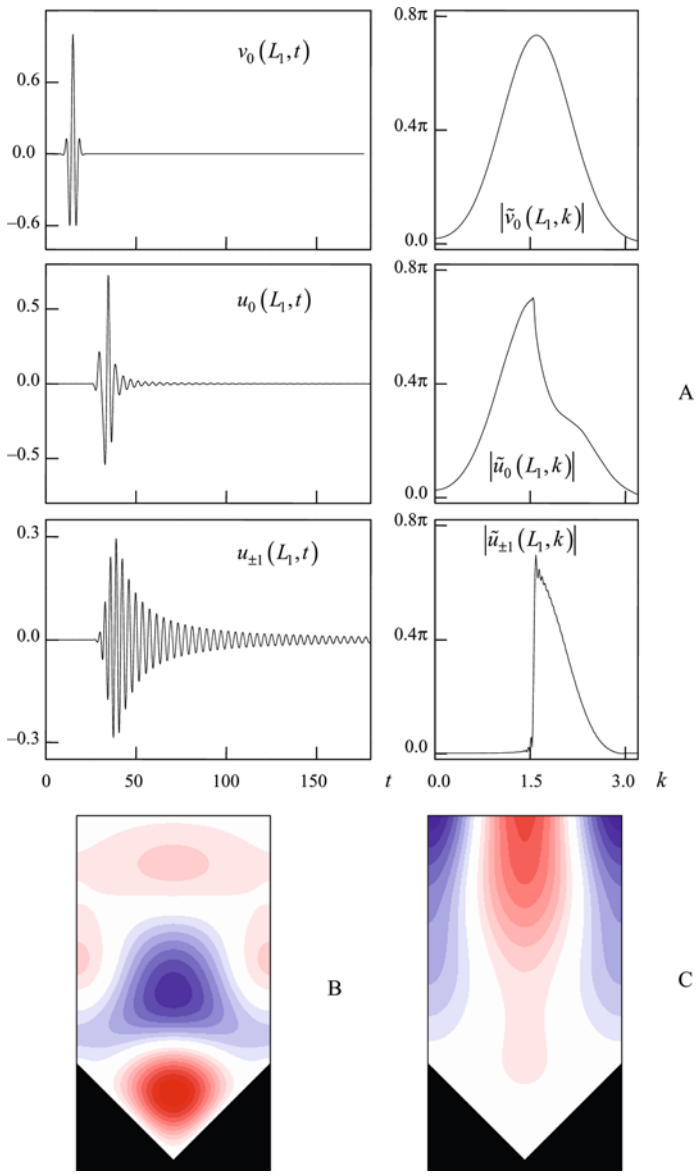

Fig. 4.23 The symmetric echelette excitation by a normally incident *E*-polarized Gaussian pulse $U_0^i(g,t)$: (**a**) The spatial–temporal and the spectral amplitudes are shown for the $U_0^i(g,t)$ wave and the principal spatial harmonics of the secondary field $U^s(g,t)$ on the virtual boundary $\mathbf{L}_1$; (**b** and **c**) the $E_x(g,t)$ spatial distribution, $g \in \mathbf{Q}_L$, $t = 26$ and $t = 55$
Look: 4-23-B.exe and 4-23-C.exe – the $E_x(g,t)$ spatial–time distribution, $g \in \mathbf{Q}_L$, $15 \le t \le 40$ (forced oscillations mode) and $50 \le t \le 60$ (free oscillations mode)

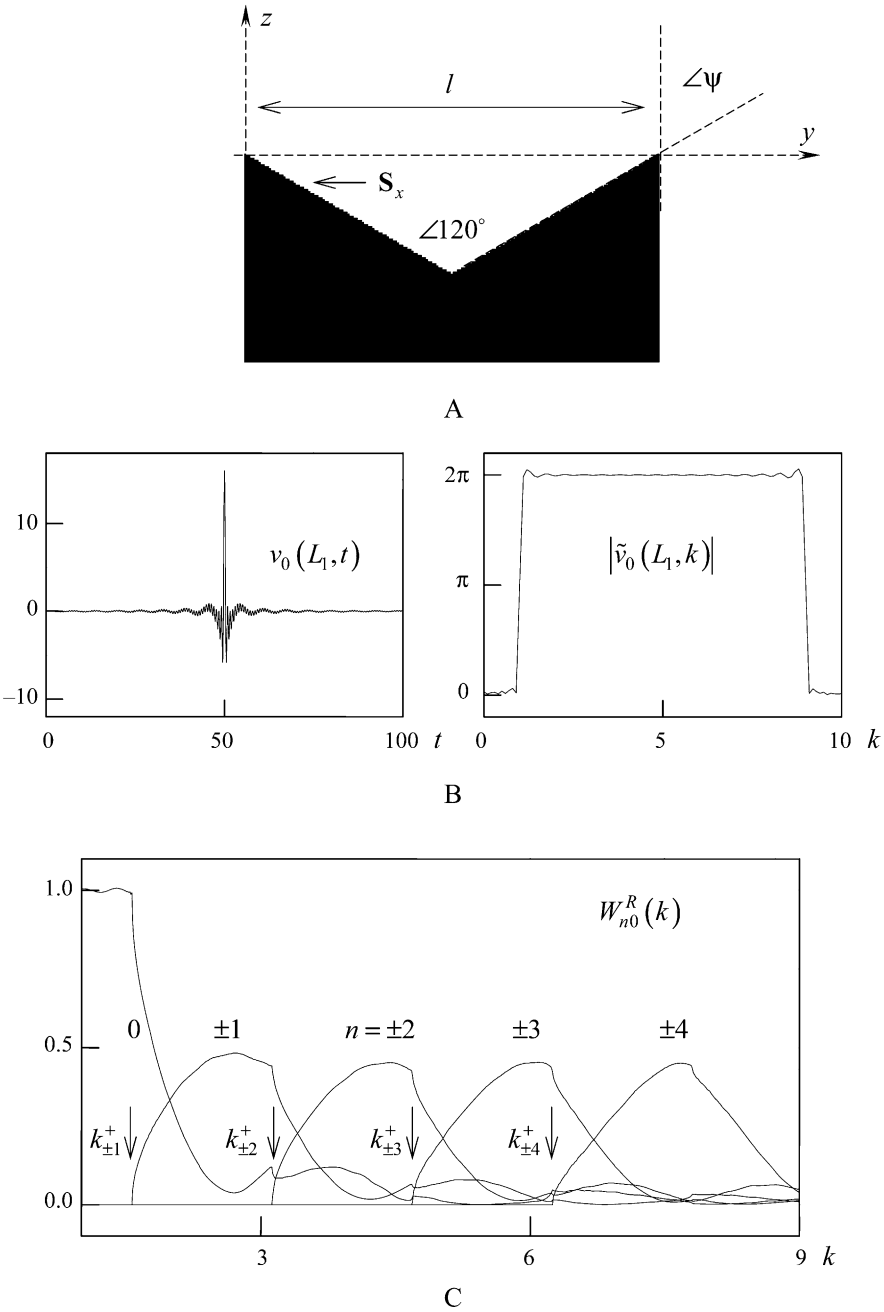

Fig. 4.24 The mode-frequency exfoliation of a superbroadband pulse: (**a**) Grating geometry ($\psi = 60°$, $l = 4.02$, $L_1 = 8.0$); (**b**) the amplitudes of the incident E-polarized pulsed wave $U_0^i(g,t)$ ($\Phi = 0$); (**c**) the energy distribution among spatial harmonics of the field $\tilde{U}^s(g,k)$ in the structure reflection zone

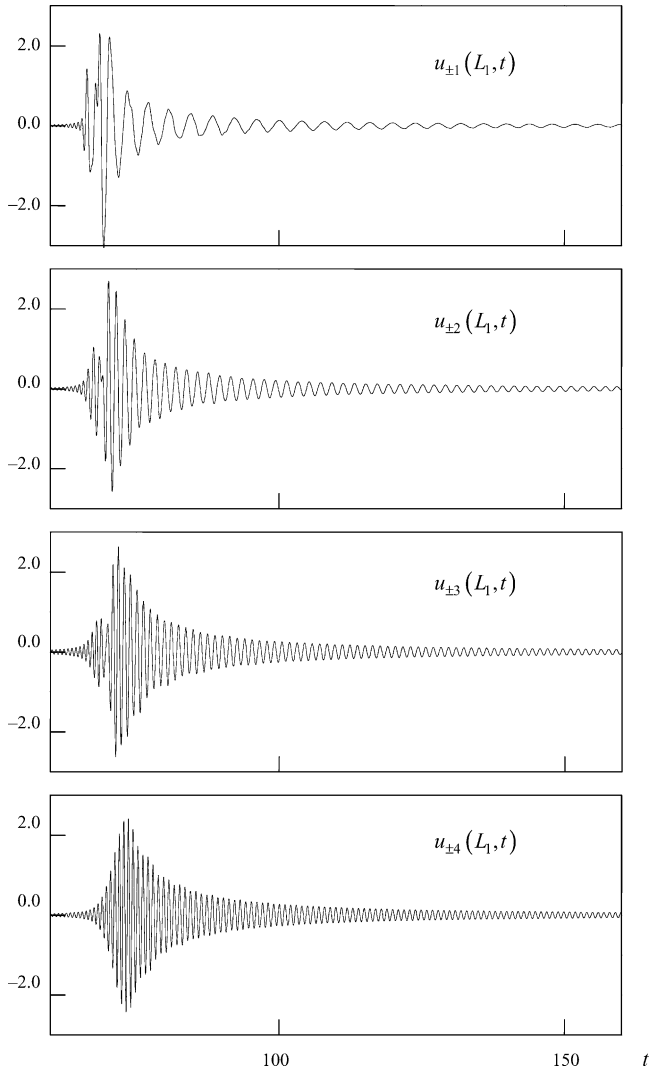

Fig. 4.25 (Complementation to Fig. 4.24). The amplitudes of high-order spatial harmonics of the field $U^s(g,t)$ on the virtual boundary $\mathbf{L}_1$

result is that a superwideband pulse of one type (for echelette gratings, it is the pulsed wave $U_0^i(g,t)$) changes into an ordered sequence of narrowband pulses of other types (pulsed spatial harmonics $U_n(g,t)$, $|n| \geq 1$). This effect is the modal frequency exfoliation of a superwideband signal. Particular bands occupied by each pair $U_{\pm n}(g,t)$ of pulsed waves and the $W_{n0}(k) = W_{-n0}^R(k) + W_{n0}^R(k)$ distributions across these bands remain basically the same as in the case of the H_{0n}-waves of a rectangular waveguide. The reflected pulses $U_{\pm n}(g,t)$ with a higher

$|n|$ have a larger central frequency $\tilde{k}_n \approx k^+_{\pm(n+1)}$. It tells clearly on the oscillating character of the spatial–temporal amplitudes $u_{\pm n}(z,t)$ as a function of t (see Fig. 4.25).

In the H-polarization case, the effect is not so evident. The formation of the pairs $U_{\pm n}(g,t)$ of the reflected pulses fitting the above-mentioned notion of the modal frequency exfoliation begins only past the point $k = k^+_{\pm 3}$ – the grazing point for the plus and minus third spatial harmonics of the field $\tilde{U}^s(g,k)$. But now the top value of the energy characteristic $W_{n0}(k)$ can fall over a 0.85 level for none of the pairs. Distinctions from the E-case are mainly caused by different intensities of the threshold phenomena (Wood's anomalies) in the vicinities of the first three branch points $k = k^+_{\pm n}$.

4.5 2-D Models of Compact Grating Structures: Spatio-frequency and Spatio-temporal Field Transformations

4.5.1 Basic Definitions and Numerical Tests of New Exact Conditions

Plane models are classical in electrodynamics. They start from some universally adopted assumptions that simplify the solution of urgent theoretical and applied problems and, at the same time, take care of the substance of processes and phenomena that these problems seek to describe. In Section 4.5, we deal with plane models of compact grating structures (see Fig. 4.2 and Section 4.2) in the field of E-polarized waves. Models of this kind proceed from the scalar initial boundary value problems of the type (4.44) for $U(g,t) = E_x(g,t)$. By virtue of the exact absorbing conditions (4.66), (4.67), and (4.68), analysis domains $\mathbf{Q}$ extending to infinity are truncated to the finite domains $\mathbf{Q}_L$. In the electrodynamical scheme of the objects treated in these problems, the regular parallel-plate waveguides ${}_j\mathbf{Q}$ feeding the structure or drawing away electromagnetic energy are thought of as virtual boundaries (ports) $\mathbf{L}_j$. On these boundaries, exact absorbing conditions of the type (4.46), (4.47), (4.48), and (4.49) must be met.

Assume that a compact grating structure ($j = 1,2,\ldots, N$) is excited by some current and momentary sources $F(g,t)$, $\varphi(g)$, $\psi(g)$ and, simultaneously, by the pulsed wave $U^{i(q)}(g,t)$ from the waveguide ${}_q\mathbf{Q}$. Then the general solution of problem (4.44) in the free propagation domains is given as

$$U(g,t) = U(\rho,\phi,t) = \sum_{n=-\infty}^{\infty} \bar{u}_n(\rho,t)\,\bar{\mu}_n(\phi);\ \rho \geq L,\ 0 \leq \phi \leq 2\pi, \tag{4.125}$$

$$U\left(g_j,t\right) = U^{s(j)}\left(g_j,t\right) + \delta^q_j U^{i(q)}\left(g_q,t\right);\ g_j \in_j \mathbf{Q},\ j = 1,2,\ldots,N.$$

Here,

$$U^{s(j)}\left(g_j,t\right)=\sum_{n=1}^{\infty}u_{nj}\left(z_j,t\right)\mu_{nj}\left(y_j\right),\ U^{i(q)}\left(g_q,t\right)=\sum_{n=1}^{\infty}v_{nq}\left(z_q,t\right)\mu_{nq}\left(y_q\right);\quad(4.126)$$

$g_j=\{y_j,z_j\}$ is the local coordinate system attached to the waveguide ${}_j\mathbf{Q}$ (see Fig. 4.2); $\rho=L$ is a circle that does not overflow the boundary $\mathbf{L}$ and surrounds all the inhomogeneities of the space $\mathbf{R}^2$ and the sources $F(g,t)$, $\varphi(g)$, $\psi(g)$; ρ and ϕ are the polar coordinates; $\bar{\mu}_n(\phi)=(2\pi)^{-1/2}\exp(in\phi)$, $n=0,\pm1,\pm2,\ldots$, is the complete orthonormal system of transverse functions in the free space $\mathbf{R}^2$, and $\bar{u}_n(\rho,t)$ are the spatial–temporal amplitudes (the evolutionary basis $\bar{u}(\rho,t)=\{\bar{u}_n(\rho,t)\}$) of the wave $U(\rho,\phi,t)$ (see Section 4.2.4).

The amplitude–frequency characteristics $\tilde{f}(k)$ ($k=2\pi/\lambda$ is the wavenumber, frequency parameter, or mere frequency and λ is the free space wavelength) are obtained from the time characteristics $f(t)$ via the integral transformation (4.113).

If $F(g,t)\equiv0$, $\varphi(g)=\psi(g)\equiv0$ and $U^{i(q)}\left(g_q,t\right)=U_p^{i(q)}\left(g_q,t\right)=v_{pq}\left(z_q,t\right)\times$ $\times\mu_{pq}\left(y_q\right)$, then the formulae

$$R_{np}^{qq}(k)=\left.\frac{\tilde{u}_{nq}\left(z_q,k\right)}{\tilde{v}_{pq}\left(z_q,k\right)}\right|_{z_q=0}\ \text{and}\ T_{np}^{jq}(k)=\frac{\tilde{u}_{nj}\left(z_j,k\right)\big|_{z_j=0}}{\tilde{v}_{pq}\left(z_q,k\right)\big|_{z_q=0}}\qquad(4.127)$$

give us the reflection coefficient $R_{np}^{qq}(k)$ describing the transformation of the pth incident monochromatic wave to the nth reflected and the transition coefficient $T_{np}^{jq}(k)$ tracing the transformation of the pth mode of the waveguide ${}_q\mathbf{Q}$ to the nth mode of the waveguide ${}_j\mathbf{Q}$, $j\neq q$.

When, in addition, $\sigma(g)\equiv0$ and $\mathrm{Im}\gamma_{pq}=0$, the efficiency $\eta(k)$ of the open unit as a monochromatic wave radiator is expressed by the formula

$$\eta(k)=1-\sum_{n,j}W_{np}^{jq}(k);\quad W_{np}^{qq}(k)=\left|R_{np}^{qq}(k)\right|^2\frac{\mathrm{Re}\gamma_{nq}}{\gamma_{pq}},\ W_{np}^{jq}(k)=\left|T_{np}^{jq}(k)\right|^2\frac{\mathrm{Re}\gamma_{nj}}{\gamma_{pq}}.\qquad(4.128)$$

Here, $\gamma_{nj}=\left(k^2-\lambda_{nj}^2\right)^{1/2}$; $\mathrm{Re}\gamma_{nj}\geq0$ and $\mathrm{Im}\gamma_{nj}\geq0$; λ_{nj} are the transverse eigenumbers of the waveguide ${}_j\mathbf{Q}$ (see Section 4.2.1); $W_{np}^{jq}(k)$ is the relative energy of the nth mode that is reflected or enters the waveguide ${}_j\mathbf{Q}$ as the structure is excited across the $\mathbf{L}_q$ boundary by the propagating wave $\tilde{U}_p^{i(q)}\left(g_q,k\right)$ ($\mathrm{Im}\gamma_{pq}=0$).

The pulsed near field $U(g,t)$ is worked out in the immediate calculation space $\mathbf{Q}_L$. The far field is found by the field $U(g,t)$ conversion from the arc $\rho=L$ to the arc $\rho=M>L$, a proper distance away from the virtual boundary $\mathbf{L}$ (see Section 4.2.4). Such a possibility gives us the exact radiation conditions for outgoing cylindrical waves (4.125) [see formulas (4.74) and (4.76)] resulting in a transport operator $Z_{L\to\rho}(t)$ such that

$$\bar{u}(\rho,t) = \{\bar{u}_n(\rho,t)\} = Z_{L\to\rho}(t)\left[\partial\bar{u}(\rho,\tau)\big/\partial\rho\big|_{\rho=L}, \bar{u}(L,\tau)\right];\ \rho \geq L,\ t \geq \tau \geq 0.$$

Having obtained the spatial–temporal amplitudes $\bar{u}_n(\rho,t)$ of the field $U(g,t)$ on the circle $\rho = L$, we proceed to finding also the far monochromatic field $\tilde{U}(\rho,\phi,k) \leftrightarrow U(\rho,\phi,t)$; $\rho = M > L$. Make use of the spectral representations

$$\bar{u}_n(\rho,t) \leftrightarrow \tilde{\bar{u}}_n(\rho,k) = a_n(k)\, H_n^{(1)}(k\rho);\ n = 0, \pm 1, \pm 2..., \tag{4.129}$$

owing to the partial radiation conditions for outgoing cylindrical waves [see Section 4.3.3 and formula (4.99)]. From (4.129), the sets of complex amplitudes $a_n(k)$ are obtained, and invoking the radiation conditions we have the $\tilde{U}(M,\phi,k)$ value.

The function

$$D(\phi,k,M) = \frac{\left|\tilde{U}(M,\phi,k)\right|^2}{\max\limits_{\phi_1<\phi<\phi_2}\left|\tilde{U}(M,\phi,k)\right|^2} \tag{4.130}$$

describes the normalized radiation pattern produced by the compact grating structures on the portion $0 \leq \phi_1 \leq \phi \leq \phi_2 \leq 360°$ of the arc $\rho = M \geq L$; $K_1 \leq k \leq K_2$. The main lobe is directed at the angle $\bar{\phi}(k)$: $D\left(\bar{\phi}(k), k, M\right) = 1$; $\phi_{0.5}(k)$ is the lobe width at the level $D(\phi,k,M) = 0.5$, with M indicating the zone (near, medium or far) where the diagram $D(\phi,k,M)$ is computed. Assume that the near zone is limited by $M = L$, and the far-zone boundary is specified by such a value of M that the function $D(\phi,k,M)$ barely changes as M increases for all k considered.

When dealing with spatial–time transformations of broadband signals, a good deal of information can be gained from the characteristics associated with the normalized pulse diagram [193]

$$D_P(\phi,t,M) = \frac{U(M,\phi,t)}{\max\limits_{\phi_1<\phi<\phi_2,\ t}|U(M,\phi,t)|} \tag{4.131}$$

on the portion $0 \leq \phi_1 \leq \phi \leq \phi_2 \leq 360°$ of the arc $\rho = M \geq L$; $T_1 \leq t \leq T_2 \leq T + M$. The pulse radiation efficiency $\xi = 1–W$; $0 \leq \xi \leq 1$ for nonabsorbing ($\sigma(g) \equiv 0$) compact grating structures excited from the waveguide ${}_q\mathbf{Q}$ is obtained by integrating the instant power flows of the primary $U^{i(q)}(g_q,t)$ and the secondary $U^{s(j)}(g_j,t)$ pulsed waves on the virtual boundaries $\mathbf{L}_j$. Here, W is the related energy stored by all the $U^{s(j)}(g_j,t)$ waves. The integral is taken over $0 \leq t \leq T$, where T is the upper limit of the observation time $t\in[0;T]$.

The analysis of the time dependences $U(g,t) = E_x(g,t)$, both pointwise, at separate g points in the domain $\mathbf{Q}_L$ and also with the $\mathbf{Q}_L$ domain thought of as a unit, yields the character of the simulated processes. Current values of the real quantities $U(g,t)$ in the computation domain $\mathbf{Q}_L$ are mapped throughout all the **.exe** files and figures related to Section 4.5 by means of a linear color scale (see Fig. 4.8b) providing a 19-layer gradation from $–U_{\max}(t)$ to $U_{\max}(t)$. The algorithm for the $U_{\max}(t)$ choice is the same as in the case of infinite periodic gratings (see Section 4.4.1).

The faithfulness of the obtained electrodynamical characteristics primarily depends on the step dimension $\bar{h} \geq 2\bar{l}$ of the spatial mesh, at which nodes the mesh functions $U(j,k,m) \approx U\left(y_j,z_k,t_m\right)$, $y_j = j\bar{h}$, $z_k = k\bar{h}$, $t_m = m\bar{l}$, are specified. The overall size of the computation space $\mathbf{Q}_L$, the way in which conditions (4.66), (4.67), and (4.68) are realized, etc., are less important. Among the induced errors, those are distinguished that are caused by the standard finite-difference approximation of the original initial boundary value problems (scheme errors) and those introduced by enclosing the analysis in the finite domain $\mathbf{Q}_L$ (boundary errors). The boundary errors are usually an order of magnitude less and decay faster than the scheme errors. These estimations and others regarding convergence and stability of the computational schemes upon the standard sampling of the original initial boundary problems equipped with exact absorbing conditions follow from the solution of various test problems [1, 40, 189]. Below, we will comment briefly one of these problems just to identify the basic points of the test scheme, assuming no comparison with familiar and well-proved results.

The problem geometry is shown in Fig. 4.26a. A soft current source of the kind

$$F(g,t) = \chi(y)\,\chi(0.04 - y)\,\chi(-z)\,\chi(z + 0.04)\,F(t)$$

(see Fig. 4.26b) produces a divergent pulsed wave $U(g,t)$ in the homogeneous ($\varepsilon(g) = \mu(g) \equiv 1$, $\sigma(g) \equiv 0$, $\overline{\text{int}\mathbf{S}_x} = \varnothing$) space $\mathbf{R}^2$. Denote by $U_L\left(j,k,m,\bar{h}\right)$ the mesh function obtained by the numerical solution of the problem within the $\mathbf{Q}_L$ domain and approximating the exact values $U(g_{jk},t_m)$, $g_{jk} = \{y_j,z_k\}$, of the sought function $U(g,t)$; the step dimension of the mesh is $\bar{h} = 2\bar{l}$. The numerical solution of this problem in a larger domain $\mathbf{Q}_p \supset \mathbf{Q}_L$ is designated as $U_P\left(j,k,m,\bar{h}\right)$. The size of the new domain is large enough so that the perturbation cannot reach its outer boundary $\mathbf{P}$ within the observation time $0 \leq t \leq T$. We analyze the functions (here N is the number of the nodes g_{jk} in the $\mathbf{Q}_L$ domain):

$$V_L\left(g_{jk},t_m,\bar{h}\right) = U_L\left(j,k,m,\bar{h}\right),$$

$$M_{LP}\left(g_{jk},t_m,\bar{h}\right) = \left|U_L\left(2j,2k,2m,0.5\bar{h}\right) - U_L\left(j,k,m,\bar{h}\right)\right|,$$

$$\bar{M}_{LP}\left(g_{jk},t_m,\bar{h}\right) = \frac{1}{N}\sum_{g_{jk}\in\mathbf{Q}_L} M_{LP}\left(g_{jk},t_m,\bar{h}\right),$$

$$M_L\left(t_m,\bar{h}\right) = \max_{j,k:\ g_{jk}\in\mathbf{Q}_L}\left|U_L\left(j,k,m,\bar{h}\right) - U_P\left(j,k,m,\bar{h}\right)\right|,$$

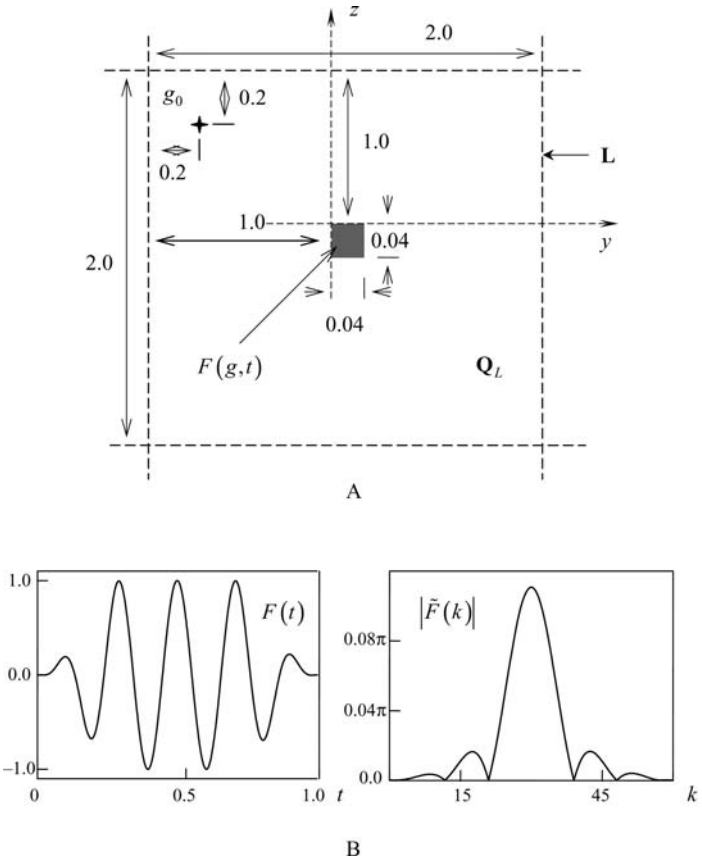

Fig. 4.26 (**a**) Test problem geometry and (**b**) dynamical and spectral characteristics of the source $F(g,t)$

$$\bar{M}_L\left(t_m,\bar{h}\right) = \frac{1}{N}\sum_{j,k:\ g_{jk}\in\mathbf{Q}_L}\left|U_L\left(j,k,m,\bar{h}\right) - U_P\left(j,k,m,\bar{h}\right)\right|,$$

$$M_P\left(t_m,\bar{h}\right) = \max_{j,k:\ g_{jk}\in\mathbf{Q}_L}\left|U_P\left(2j,2\,k,2m,0.5\bar{h}\right) - U_P\left(j,k,m,\bar{h}\right)\right|,$$

$$\bar{M}_P\left(t_m,\bar{h}\right) = \frac{1}{N}\sum_{j,k:\ g_{jk}\in\mathbf{Q}_L}\left|U_P\left(2j,2\,k,2m,0.5\bar{h}\right) - U_P\left(j,k,m,\bar{h}\right)\right|,$$

and others. The results are partly represented in Fig. 4.27. On this basis, it is possible to estimate (see, for example, reference [17]):

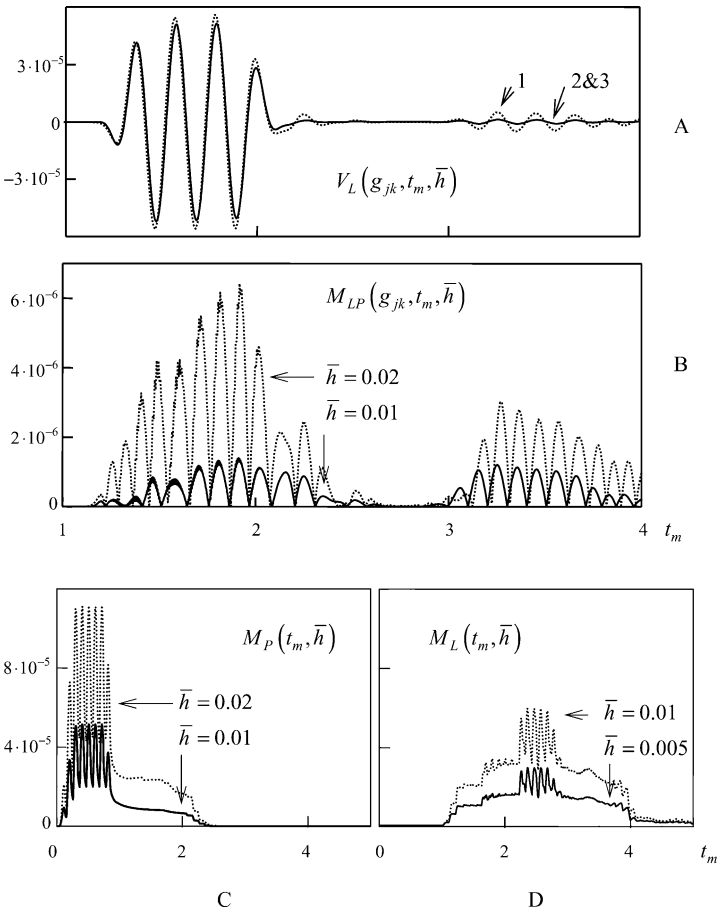

Fig. 4.27 Test problem solution results: (**a**) Functions $V_L\left(g_{jk},t_m,\bar{h}\right)$; $g_{jk}=g_0$ for $\bar{h}=0.02$ (*curve* 1), $\bar{h}=0.01$ (2), and $\bar{h}=0.005$ (3) – *curves* 2 and 3 are difficult to distinguish; (**b**) functions $M_{LP}\left(g_{jk},t_m,\bar{h}\right)$; $g_{jk}=g_0$ for two different $\bar{h}$ values; (**c**) scheme error functions $M_P\left(t_m,\bar{h}\right)$; (**d**) boundary error functions $M_L\left(t_m,\bar{h}\right)$

- the actual rate of convergence of the method (governed by the functions $V_L\left(g_{jk},t_m,\bar{h}\right)$, $M_{LP}\left(g_{jk},t_m,\bar{h}\right)$, and $\bar{M}_{LP}\left(g_{jk},t_m,\bar{h}\right)$ for a number of decreasing $\bar{h}$ values);
- the actual error of virtual boundaries **L** and the rate of its decrease (governed by the functions $M_L\left(t_m,\bar{h}\right)$ and $\bar{M}_L\left(t_m,\bar{h}\right)$ for a number of decreasing $\bar{h}$ values);
- the real error of the finite-difference scheme itself and the rate of its decrease (governed by the functions $M_P\left(t_m,\bar{h}\right)$ and $\bar{M}_P\left(t_m,\bar{h}\right)$ for a number of decreasing $\bar{h}$ values).

The examinations of this kind need substantial computation time and computer resources. However, a full measure of research is demanded only when a new method or algorithm or software package is tried before being launched. In everyday treatment, one or two simple tests will suffice to check the operational stability of the scheme, the convergence of the approximation, etc.

4.5.2 Finite and Infinite Periodic Structures: Similarities and Differences

The secondary field

$$\tilde{U}^s(g,k) = \begin{cases} \tilde{U}(g,k) - \tilde{U}_0^i(g,k); & g \in \mathbf{A} \\ \tilde{U}(g,k); & g \in \mathbf{B} \end{cases},$$

produced by the semitransparent (Fig. 1.1b) or reflective (Fig. 1.1c) infinite grating excited by a homogeneous E-polarized plane wave $\tilde{U}_0^i(g,k)$ from the domain $\mathbf{A}$ contains a finite number of propagating spatial harmonics. Each harmonic gets some part of the energy applied to the periodic structure (see Section 1.2.1). Consider the pairs $\left\{W_{n0}^R(k);\alpha_n(k)\right\}$ and $\left\{W_{n0}^T(k);\alpha_n(k)\right\}$, where $\alpha_n(k) = -\arcsin\left(\Phi_n/k\right)$ refers to the grating reflection zone harmonics and $\alpha_n(k) = \pi + \arcsin\left(\Phi_n/k\right)$ to the transmission zone harmonics (all the $\alpha_n(k)$ angles are measured anticlockwise from the z-axis in the plane $y0z$). They define the so-called beam pattern characterizing the energy distribution among the plane waves traveling in the space $\mathbf{R}^2$ in the directions $\phi = \phi_n = \alpha_n + 90°$ (ρ and ϕ are polar coordinates). With all things the same, the beam pattern of an infinite grating and the radiation pattern $D(\phi,k,\infty)$ [see formula (4.130)] of its finite analog give qualitatively the same picture of spatial–frequency transformations of the electromagnetic field. This speculation is postulated (sometimes without grounds and even against available facts) in the majority of applied problems of electrodynamical theory of gratings. This line leaves open the question about how safe it is to quantitatively describe finite gratings leaning upon infinite grating analysis estimates. Evidently it can only be answered by solving many model boundary and initial boundary value problems for various compact grating structures.

Let us simulate the finite semitransparent grating excited by a normally incident pulsed wave with a finite and almost plane wavefront. In so doing, 20 circular perfectly conducting metal bars (see Fig. 4.28a) are put in the field of the current source

$$F(g,t) = \chi(4.11 - y)\,\chi(y + 4.11)\,\chi(2.26 - z)\,\chi(z - 2.04)\,F_2(t); \quad \tilde{k} = 9,\ \Delta k = 7,\ \tilde{T} = 30,\ \bar{T} = 60. \tag{4.132}$$

This source, occupying the frequency band $2 \le k \le 16$, produces a pulsed wave whose field spot covers 10–12 grating elements. Within $6 \le k \le 16$, the lobes of the pattern $D(\phi,k,\infty)$ of the periodic structure transition zone $180° < \phi < 360°$

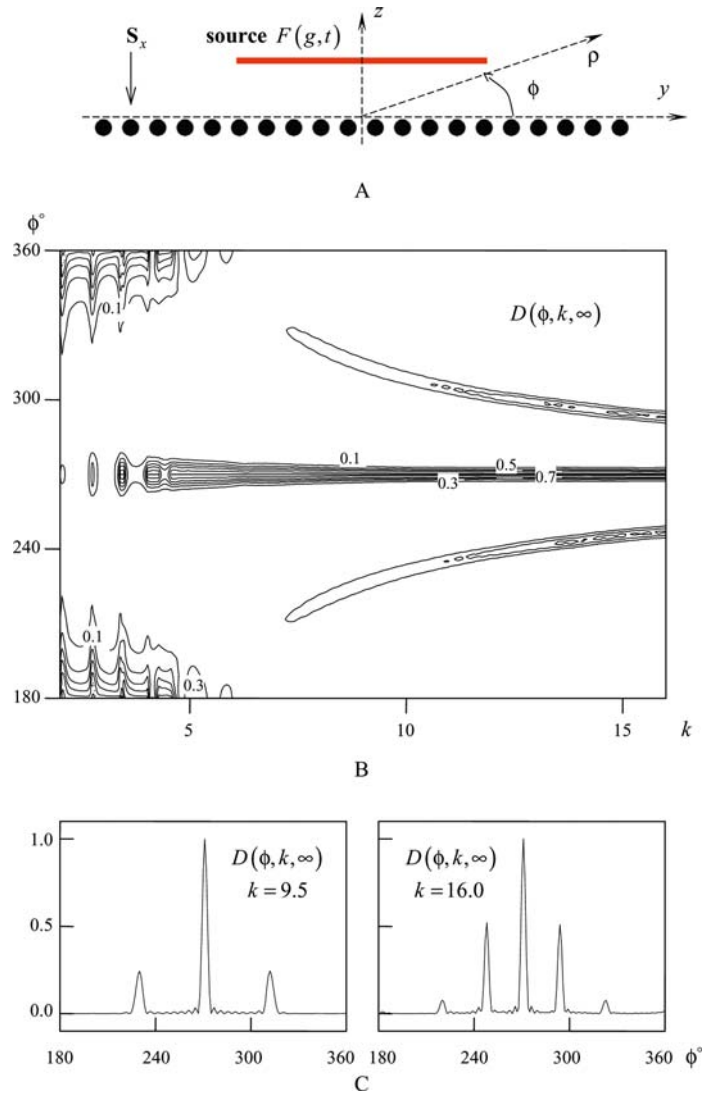

Fig. 4.28 A finite (20-element) grating in the field of current source (4.132): (**a**) Problem geometry ($l = 1$, circular metal bar diameter is 0.62, source length is 9.22 and source width 0.22, the source–grating distance is 2.04); (**b**) the radiation pattern in the grating transition zone; (**c**) the functions $D(\phi,k,\infty)$ for two k frequency values
Look: 4-28.exe – the $E_x(g,t)$ spatial–time distribution, $g \in \mathbf{Q}_L$, $30 \le t \le 45$

(see Figs. 4.28b and c) are directed in the same way as the propagating spatial harmonics of the infinite grating placed in the field of normally incident plane monochromatic wave (4.118) (see Fig. 4.29c). They differ only in the related energy amounts concentrated in analogous lobes and similar harmonics. Thus, for $k = 9.5$,

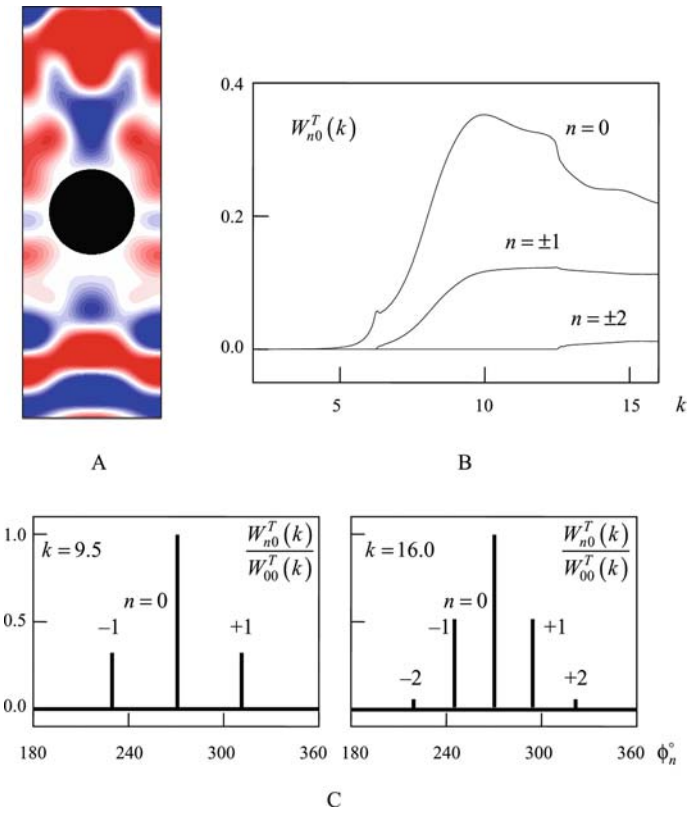

Fig. 4.29 (Complementation to Fig. 4.28). An infinite grating ($l = 1$, $L_1 = 1.19$) in the field of a pulsed wave $U_0^i(g,t)$: $\Phi = 0$; $v_0(L_1,t) = F_2(t)$; $\tilde{k} = 9$, $\Delta k = 7$, $\tilde{T} = 12.5$, $\bar{T} = 25$. (**a**) The $E_x(g,t)$ spatial distribution, $g \in \mathbf{Q}_L$, $t = 15.5$; (**b** and **c**) the functions $W_{n0}^T(k)$ ($k_{\pm1}^+ \approx 6.28$, $k_{\pm2}^+ \approx 12.57$) and ray radiation patterns $W_{n0}^T(k)/W_{00}^T(k)$; $k = 9.5$ and $k = 16.0$, for spatial harmonics propagating in the grating transition zone
Look: 4-29-A.exe – the $E_x(g,t)$ spatial–time distribution, $g \in \mathbf{Q}_L$, $12.5 \le t \le 16.25$ ($U_{\max}(t) = 1.0$)

it is seen that $\phi_{\pm1} \approx 270^\circ \pm 41^\circ$, $D(\phi_{\pm1},k,\infty) = 0.25$, and $W_{\pm1,0}^T(k) \Big/ W_{00}^T(k) \approx 0.32$. For $k = 16.0$, we have $\phi_{\pm1} = 270^\circ \pm 23^\circ$, $\phi_{\pm2} \approx 270^\circ \pm 52^\circ$, $D(\phi_{\pm1},k,\infty) = 0.52$, $D(\phi_{\pm2},k,\infty) = 0.08$, and $W_{\pm1,0}^T(k) \Big/ W_{00}^T(k) \approx 0.51$, $W_{\pm2,0}^T(k) \Big/ W_{00}^T(k) \approx 0.05$. Hence, with a source whose field spot covers 16–18 grating elements, the corresponding characteristics do not come any closer together.

An infinite grating of rectangular dielectric bars (see Fig. 4.30a) fully reflects a normally incident E-polarized plane wave $\tilde{U}_0^i(g,k)$, $g \in \mathbf{A}$, at the points $k = K_1 \approx 7.6$, $K_2 \approx 8.7$, and $K_3 \approx 10.22$ falling within the frequency range $6.5 \le k \le 11.5$. For all these points, the value of N in joint qualitative characteristic $\{N,M\}$ introduced in Section 1.2.1 is equal to 1 ($k_{\pm1}^+ \approx 10.3$), whereas the value of M is equal to 2 [18]. The finite analog (see Fig. 4.30b, all components of the system "source – periodic

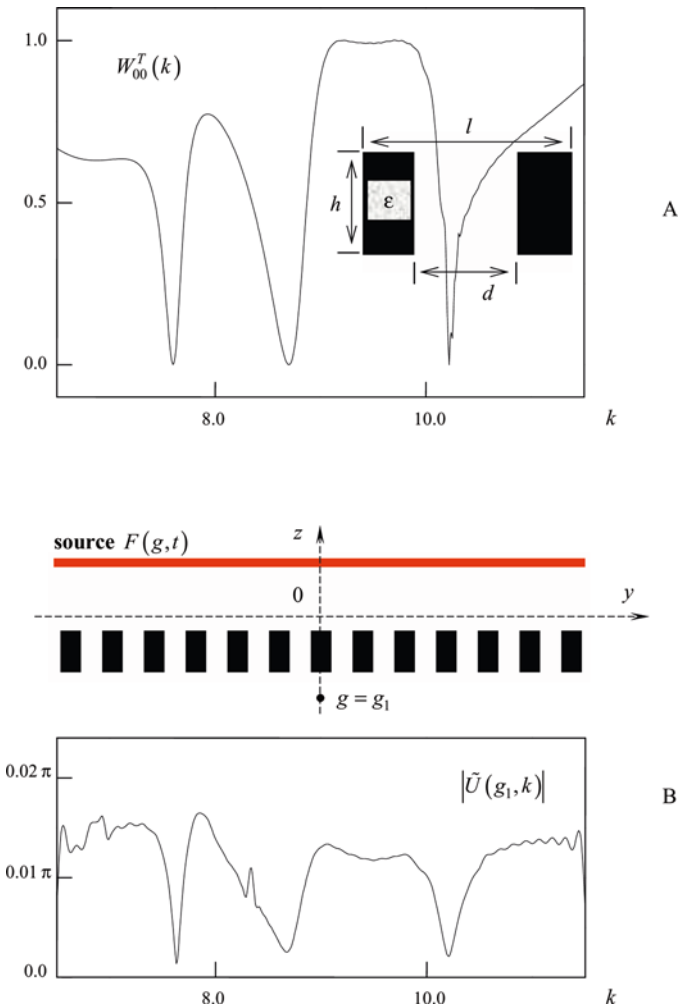

Fig. 4.30 The functions (**a**) $W_{00}^{T}(k)$; $\Phi = 0$, and (**b**) $|\tilde{U}(g_1,k)|$ characterizing the transparency of the infinite (**a**) ($l = 0.61$, $h = 0.61$, $d = 0.31$ and $\varepsilon = 5.0$) and (**b**) finite (13 periods) dielectric gratings

structure" are drawn to scale) placed in the field of the current source $F(g,t) = P(g)\ F_2(t)$; $\tilde{k} = 9.0$, $\Delta k = 2.5$, $\tilde{T} = 50$, $\bar{T} = 100$, $T = 150$ (the function $P(g)$ determines the source geometry and location) effectively blocks the $U(g,t)$ wave monochromatic components corresponding to the frequencies $k \approx 7.63$, 8.68, and 10.21 and keep them from the lower space. No principal distinctions between the finite and infinite periodic structures are observed.

Another behavior is demonstrated by dielectric gratings whose elements are depicted in Fig. 4.31a. The infinite periodic structure fully reflects the normally

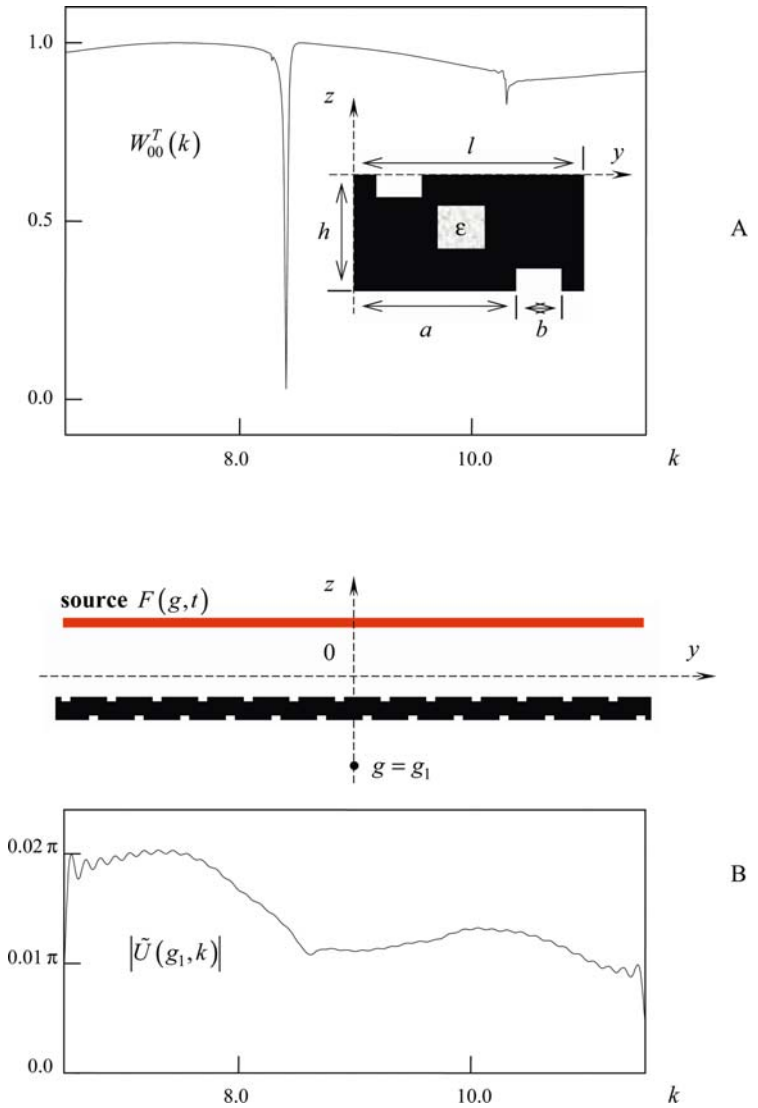

Fig. 4.31 The same as in Fig. 4.30 but for a dielectric grating of $l = 0.61$, $h = 0.31$, $a = 0.43$, $b = 0.12$, and $\varepsilon = 2.0$

incident E-polarized plane wave $\tilde{U}_0^i(g,k)$ at the point $k = K_4 \approx 8.4$. But this effect practically does not influence the transparency of the finite structure (see Fig. 4.31b, the experimental conditions are the same as for the system sketched in Fig. 4.30b). Why are those excellent range characteristics of a simple dielectric grating (see Fig. 4.31a) affected so much in a situation that is so easy to realize not only in theory but

also in practice, too? In an effort to answer this question, let us excite an infinite grating by the plane pulsed wave $U_0^i(g,t)$: $\Phi = 0$; $v_0(L_1,t) = F_1(t)$; $\tilde{\alpha} = 15$, $\tilde{k} = 8.34$, $\tilde{T} = 75$, $\bar{T} = 150$ (see Fig. 4.32a). We trace the spatial–time transformations of the field $U(g,t)$, $g \in \mathbf{Q}_L$, $0 < t < T = 600$. From the time $t = \bar{T}$, the source being off and till $t \approx 300$, it is a quasi-monochromatic component corresponding to the free oscillation $u_0\left(g,\bar{k}_1\right)$, $\bar{k}_1 \approx 8.404 - i0.0135$ (see Sections 1.3.2 and 1.3.4) that dominates in the field $U(g,t)$. It turns out to be the H_{021}-oscillation, the field nodes align themselves in the directions $y = nl$ and $y = 0.5l + nl$, $n = 0,\pm1,\ldots$ (see Fig. 4.32b), and it is this oscillation that is responsible for the total resonant reflection effect at the frequency $k = K_4 \approx 8.4$. Again, at the moments of time $t > 375$, a quasi-monochromatic component corresponding to the H_{021}-oscillation dominates in the field $U(g,t)$. But now it is another, $u_0\left(g,\bar{k}_2\right)$ oscillation. Its Q-factor is practically unbounded ($\mathrm{Re}\bar{k}_2 \approx 8.28$ and $\mathrm{Im}\bar{k}_2 \approx 0$), and the field nodes are placed along the lines $y = \pm0.25l + nl$, $n = 0,\pm1,\ldots$ (see Fig. 4.32c). At the intermediate moments of time $300 < t < 375$, the field $U(g,t)$ is featured by both $u_0\left(g,\bar{k}_1\right)$ and $u_0\left(g,\bar{k}_2\right)$ characteristics. Here the amplitudes of the quasi-monochromatic components corresponding to these oscillations are comparable (see Figs. 4.32b and c). It seems possible that the conditions providing the existence and the special properties of the oscillations $u_0\left(g,\bar{k}_1\right)$ and $u_0\left(g,\bar{k}_2\right)$ (and, indirectly, the effect of the total reflection of a normally incident E-polarized wave) are interrelated (note, for example, the intermode coupling effect described in the books [1, 10] and in Section 1.3.4). Finite gratings cannot maintain persistent free oscillations of the field (see Section 4.3.3). This point appears to stop the cause-and-effect chain that for the infinite structure leads to the effect given by the analytic formula $W_{00}^R(k) = 1 - W_{00}^T(k) = 1.0$.

4.5.3 Radiating Apertures with Quasi-periodic Field Structure

A most important component of the models that is investigated and discussed below is a planar dielectric waveguide (see, for example, Fig. 4.33a) – an open segment of a regular parallel-plate waveguide. Near the plugged (on the side of the $\mathbf{Q}_L$ domain) ends, the parallel-plate waveguide has a port $\mathbf{L}_1$ to excite the examined systems by the pulsed H_{01}-wave

$$U_1^{i(1)}(g,t) = v_{11}(y,t)\,\mu_{11}(z)\,;\; v_{11}(g \in \mathbf{L}_1,t) = F_2(t)\,;\; \tilde{k} = 4.5,\; \Delta k = 2.1,\; \tilde{T} = 25,\; \bar{T} = 100 \tag{4.133}$$

(see Section 4.2.1 and formula (4.117)), and a port $\mathbf{L}_2$ to receive signals crossing the zone open for radiation into the free space. In the parallel-plate waveguide can propagate without attenuation one ($k_1 < k < k_2$; $k_1 \approx 2.17$, $k_2 \approx 4.33$; k_m is the H_{0m}-wave cutoff), two ($k_2 < k < k_3$; $k_3 \approx 6.5$), or three ($k > k_3$) H_{0m}-waves in the frequency band $2.4 < k < 6.6$ occupied by the pulse (4.133). For frequencies $2.5 < k < 6.0$, the loss by radiation from the finite segment of the planar waveguide does

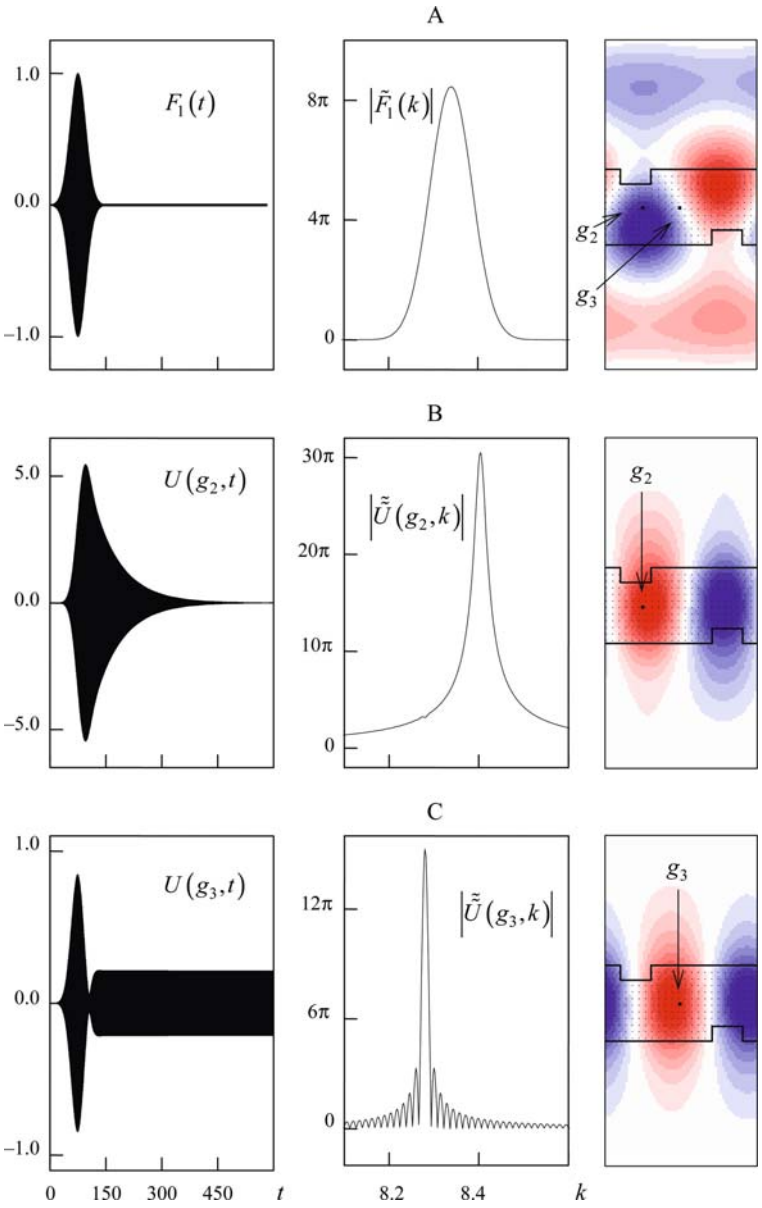

Fig. 4.32 The dynamical and the spectral characteristics of (**a**) wave $U_0^i(g,t)$ $(L_1 = L_2 = 1.0)$ and (**b** and **c**) field $U(g,t)$ at the points (**b**) $g = g_2$ and (**c**) $g = g_3$. Here [see transformation (4.113)] $\tilde{\tilde{f}}(k) \leftrightarrow \begin{cases} 0; & t \le \bar{T} \\ f(t); & t > \bar{T} \end{cases}$. The last right fragments in the rows depict the $U(g,t) = E_x(g,t)$ spatial distributions within the $\mathbf{Q}_L$ domain at the time (**a**) $t = 76$, (**b**) $t = 250$, and (**c**) $t = 400$

not exceed 15% (see Fig. 4.33b) and 25% – within all of the considered bands 2.5 $< k <$ 6.5. The H_{02}-wave of the parallel-plate waveguide is never excited because the symmetry classes of the structure and the primary wave coincide. Therefore the function $\eta(k)$ characterizing the radiation efficiency is unresponsive to the passage of the cutoff $k = k_2$, and it starts changing only when the point $k = k_3$ is approached.

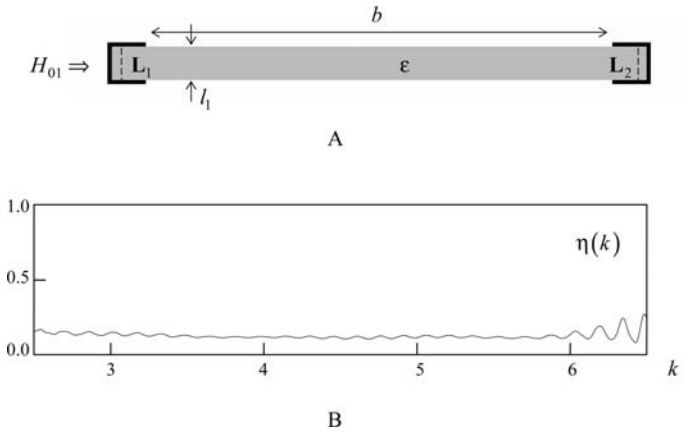

Fig. 4.33 (**a**) A planar dielectric waveguide ($l_1 = 1$, $b = 13.58$, $\varepsilon = 2.1$, all proportions of the actual object are retained) and (**b**) its loss by the radiation into the free space

Assuming that $\Phi_0(k) = \beta_p(k)$ ($\beta_p(k)$ is a longitudinal wavenumber of some propagating wave of the open guiding channel in the system "planar waveguide – grating"; see, for example, Figs. 4.34a and 4.35a) and modeling the grating excitation by the plane nonhomogeneous (Im $\Gamma_0 > 0$) wave $\tilde{U}_0^i(g,k) = \exp\left[i(\Phi_0 y - \Gamma_0 z)\right]$, $g = \{y,z\} \in \mathbf{A}$, one gets the complex amplitudes $R_{n0}^{\mathbf{AA}}(k)$ for the first traditional step of the solution of the synthesis problem of a pattern-generating (PG) plane grating structure [1, 40, 41, 212–215]. That is to compute (in the given field approximation) the energy characteristics of the channels to radiate the energy into free space. The figures obtained in this way cannot be reliable enough – for the primary wave attenuation during its y-propagation is ignored, as well as a possible emergence of other propagating waves of the guide, etc. A full-scale experiment is needed and its success largely depends on the validity of the corresponding theoretical predictions. Quite satisfactory data can be obtained by the approach developed in Section 4.2. In support of this statement, refer to the examples considered below.

Fig. 4.34 (continued) (**a**) Geometry ($l_1 = 1$, $\varepsilon = 2.1$, $\varepsilon_1 = 4$, $l = 1$, $\theta = 0.5$), (**b** and **d**) radiation patterns, and (**c**) efficiency of the pattern-generating plane structure
Look: 4-34.exe – the radiator excitation by a pulsed wave (4.133) ($E_x(g,t)$, $g \in \mathbf{Q}_L$, $25 < t < 55$; $U_{\max}(t) = 0.5$)

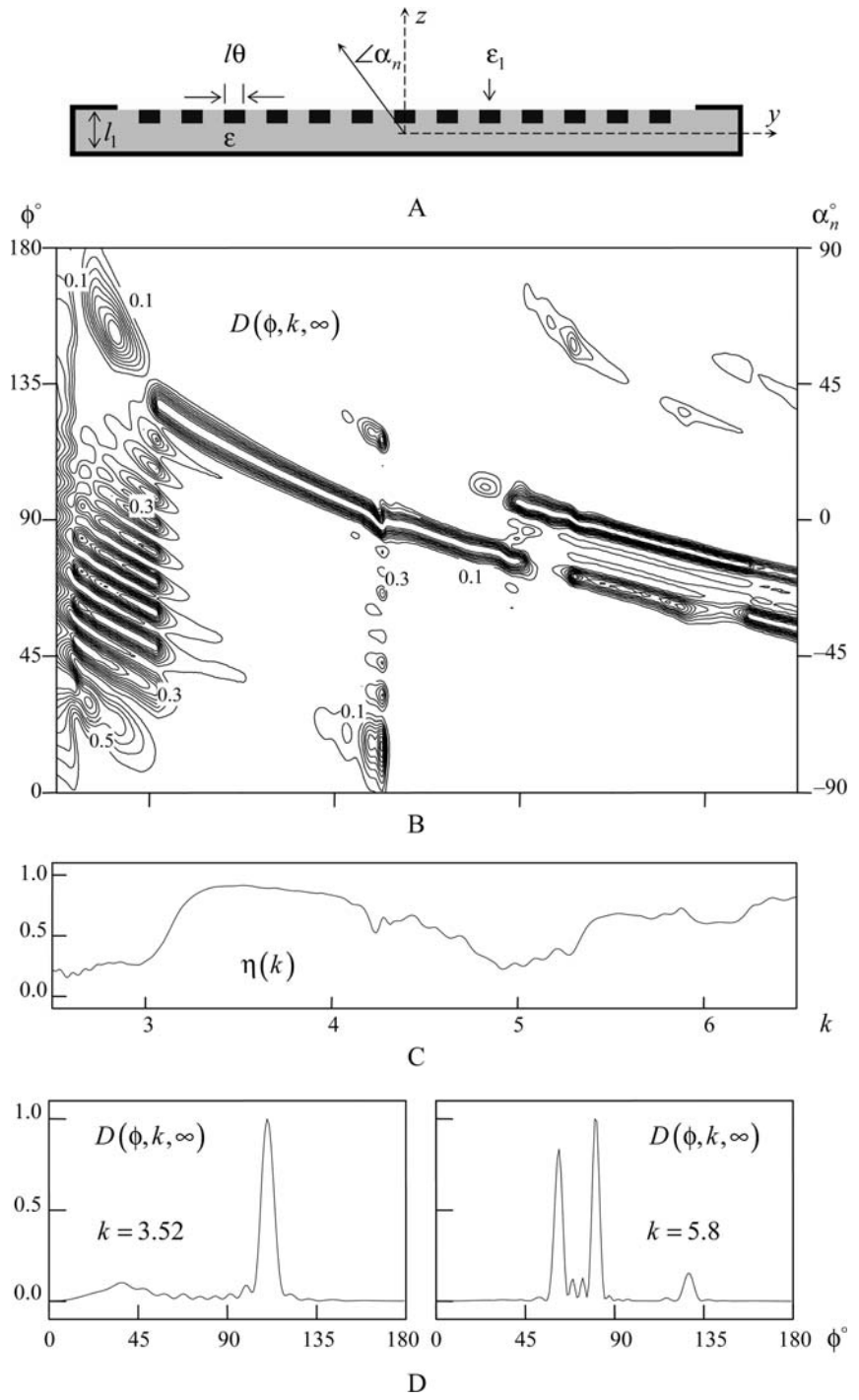

Fig. 4.34 (continued)

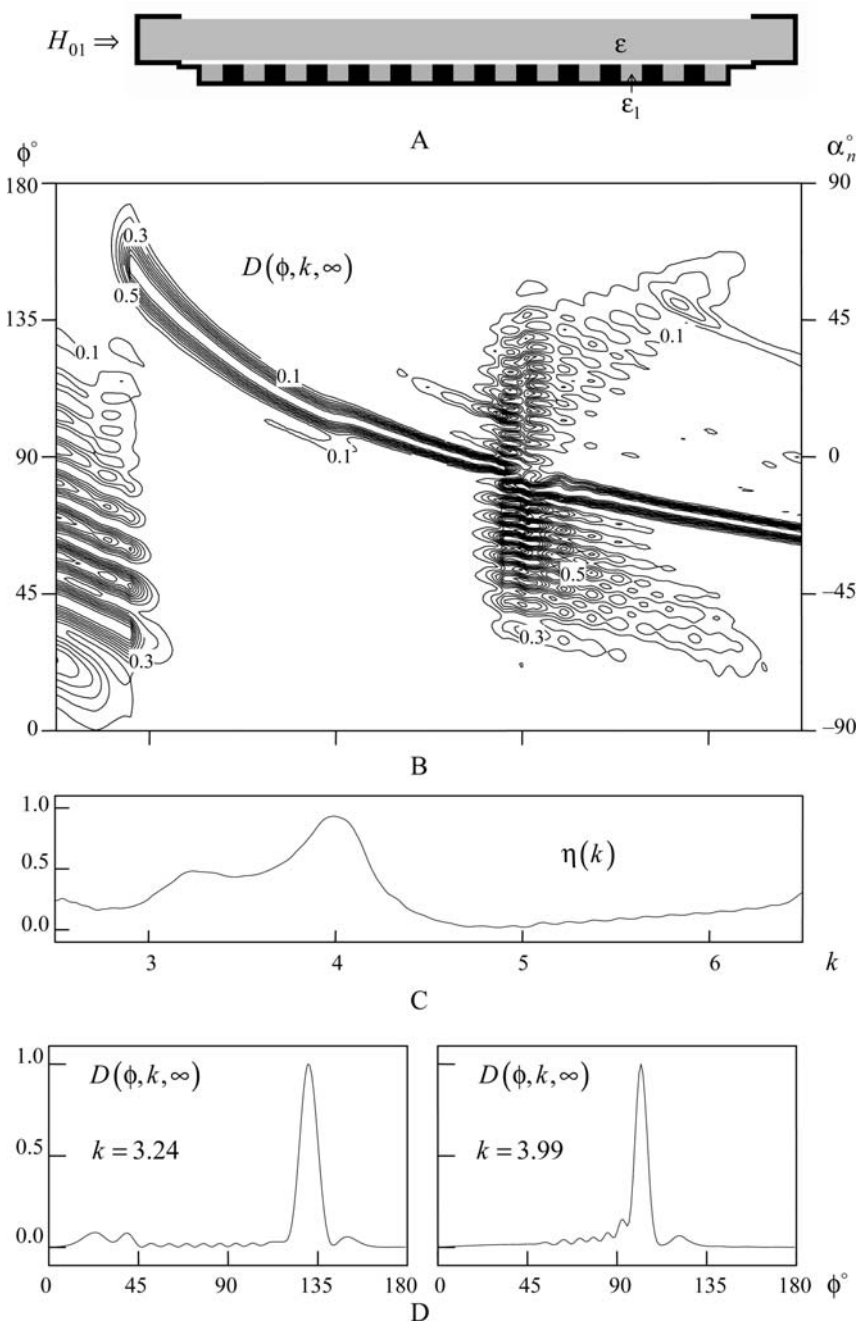

Fig. 4.35 (**a**) Geometry ($\varepsilon = 2.1$, $\varepsilon_1 = 4$, $l = 1$), (**b** and **d**) radiation patterns, and (**c**) efficiency of the pattern-generating plane structure

Look: 4-35-1.exe and 4-35-2.exe – the radiator excitation by a pulsed wave (4.133) and a quasi-monochromatic wave $U_1^{i(1)}(g,t) : v_{11}(g \in L_1,t) = F_3(t)$; $\tilde{k} = 3.99$, $\tilde{T} = 0.5$, $\bar{T} = 100$ ($E_x(g,t)$, $g \in \mathbf{Q}_L$, $25 < t < 55$; $U_{\max}(t) = 0.5$)

Figure 4.34 sketches a planar waveguide backed with a metal substrate and having 13 slots 0.32 deep and 0.5 wide filled with a material of dielectric permittivity $\varepsilon_1 = 4$. The grating period is $l = 1.0$. The structure is drawn to scale. Within the band $3.25 < k < 4.05$ (its width equals 22%), this plane PG structure produces a single-beam radiation pattern, $\eta(k) > 0.8$ and $95^\circ < \bar{\phi}(k) < 120^\circ$ (see Fig. 4.34b and c). At the point $k = 3.52$ of the band, $\eta(k) = 0.914$, $\bar{\phi}(k) = 110^\circ$, and $\phi_{0.5}(k) = 7.5^\circ$ (see Fig. 4.34d).

Assume that the function $\Phi_0(k) = \beta_1(k)$ is defined by the value $\gamma_1(k)$, with $\gamma_m(k) = \sqrt{k^2\varepsilon - \left(\pi m / l_1\right)^2}$ being the longitudinal wavenumbers of the H_{0m}-waves of the parallel-plate waveguide. In this case, the minus first spatial harmonic of the grating is responsible for the pattern main lobe. The substitution $\Phi_0(k) = \gamma_1(k)$ (a very rough approximation) is good enough to sketch the situation quite fairly. But the quantitative results differ from the exact figures substantially. Thus, this approximation yields $\bar{\phi}(k) = 129.9^\circ$ at $k = 3.52$.

In the frequency band $5.4 < k < 6.5$, the radiator efficiency is $\eta(k) > 0.6$, and the radiation pattern has a new main lobe (see Figs. 4.34b and d) whose appearance is also caused by the radiation of the minus first spatial harmonic. But in this case, $\Phi_0(k) = \beta_2(k)$ – another cutoff point has been passed, and the next propagating wave has been excited in the planar guiding structure. At the point $k = 5.8$ of this band, $\bar{\phi}(k) = 80^\circ$ and $\phi_{0.5}(k) = 4^\circ$, and the side lobe direction is $\underline{\phi}(k) = 62^\circ$. A qualitative analysis of the situation tolerates $\Phi_0(k) = \gamma_1(k)$ and $\Phi_0(k) = \gamma_2(k)$. But this approximation is too rough for computations and causes great errors. Thus, at the point $k = 5.8$, we have $\bar{\phi}(k) \approx 96^\circ$ and $\underline{\phi}(k) \approx 73.2^\circ$.

At the beginning of the considered range ($2.5 < k < 3$), the radiation efficiency is not over 28%. Multilobe radiation patterns are formed by particular components of the grating, rather than by the grating as a unit. The traveling wave of the planar waveguide excites each of the grating components, not generating any spatial traveling harmonics.

For the structure whose electrodynamical characteristics are plotted in Fig. 4.35, the passage to multilobe patterns has the same reasons. Thus, in the frequency band $4.9 < k < 5.2$, this passage is caused by the fact that the high-order propagating wave of the planar dielectric waveguide appears sooner than the corresponding $\Gamma_{-1}(k)$ becomes real valued. All structure components in Fig. 4.35a are drawn to scale. A metal comb is placed under a planar dielectric waveguide 0.1 apart. The dielectric permittivity of the slot filling is $\varepsilon_1 = 4$, the period length is $l = 1.0$, the slots are 0.5 wide and 0.4 deep. At the point $k = 3.99$ of the observed frequency interval, the radiation efficiency amounts 94%, $\bar{\phi}(k) = 102^\circ$ (in the $\Phi_0(k) = \gamma_1(k)$ approximation, $\bar{\phi}(k) = 111^\circ$) and $\phi_{0.5}(k) = 7^\circ$.

A truncated H-plane bend of rectangular waveguide (see Fig. 4.36)with a lateral matching aperture at the input converts (at certain geometrical and frequency parameters) the H_{01}-wave of the narrow waveguide (waveguide 1) to the H_{0m}-wave, $m = 2,3,\ldots,20$ of the broad waveguide (waveguide 2). The conversion efficiency is 86% ($m = 20$, $W^{21}_{20,1} \approx 0.86$; $W^{jq}_{mp}(k)$ is the relative part of energy given to the mth mode of the jth waveguide when the structure is excited by the pth propagating

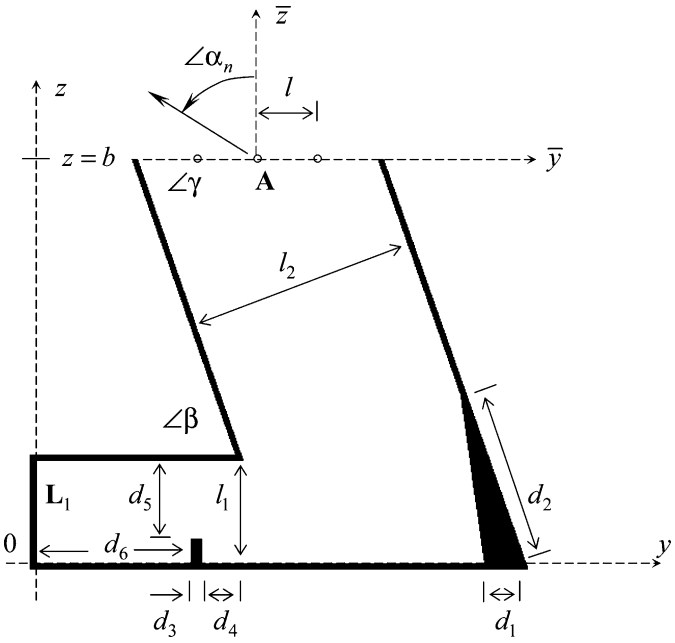

Fig. 4.36 The geometry of the converting and radiating waveguide unit

wave from the qth waveguide) to 99.99% ($m = 2$) [216]. The strict $H_{01} \rightarrow H_{0m}$ conversion is a narrowband effect. But off the corresponding band, the same unit acts as $H_{01} \rightarrow H_{0m-1}$ or $H_{01} \rightarrow H_{0m+1}$ transducer. Here the conversion purity characterized by the quantity $W^{21}_{m-1,1}$ or $W^{21}_{m+1,1}$ and the coefficients of the transformation to the reflected and the same-direction waves are only little worse than the optimized special unit offers [210, 216].

The mentioned properties of the $H_{01} \rightarrow H_{0m}$ transducers can be employed in antennas whose radiation pattern is controlled by varying the operation frequency (passage to the conversion regime $H_{01} \rightarrow H_{0m-1}$ or $H_{01} \rightarrow H_{0m+1}$), the angle γ at which the broad waveguide gets open into free space, and (or) by special bifurcations of the broad waveguide (see Fig. 4.36; **A** is the radiation aperture). In the aperture **A**, the H_{0m}-wave traveling along the broad waveguide produces a quasi-periodic system of the secondary field sources that form their radiation pattern at a sufficiently large m obeying rules legitimate for periodic structures of all types. The results validating this assumption are seen in Figs. 4.37 and 4.38. The units are excited by the quasi-monochromatic H_{01}-wave

$$U_1^{i(1)}(g,t): v_{11}(g \in \mathbf{L}_1, t) = \cos\left[\tilde{k}\left(t - \tilde{T}\right)\right] P(t) = F_4; \tilde{k} = 5.03, \tilde{T} = 0.5,$$
$$P(t): 0.1 - 5 - 75 - 80, \tag{4.134}$$

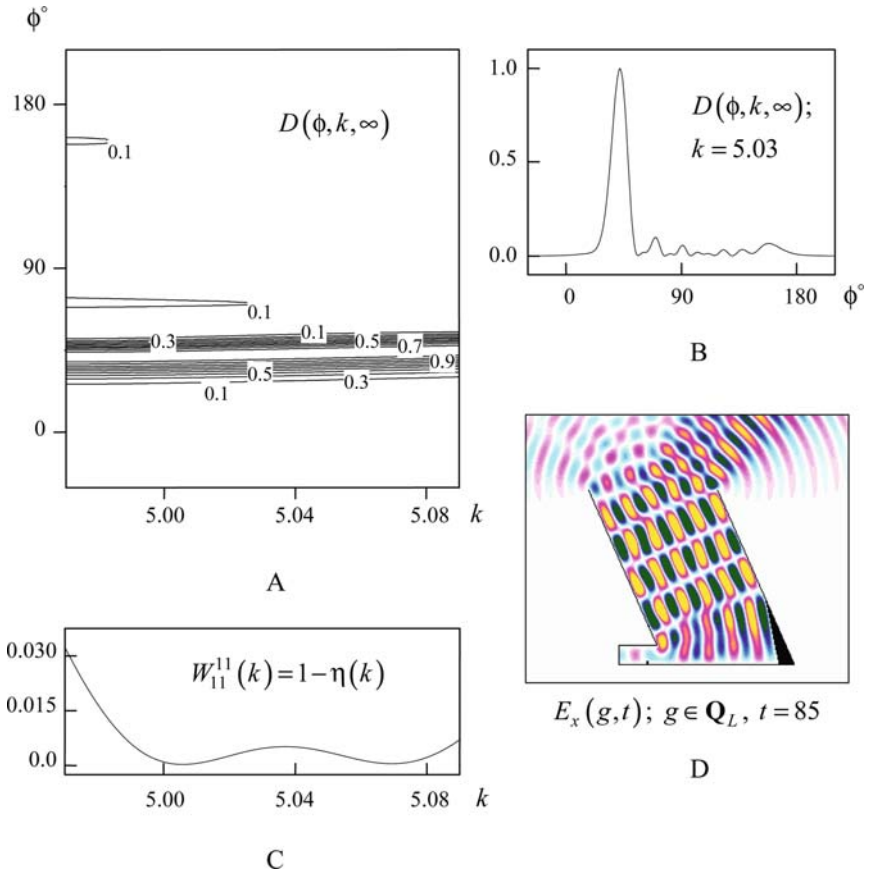

Fig. 4.37 The radiator providing a strong H_{01}- to $H_{0,10}$-wave conversion ($l_1 = 1$, $l_2 = 6.56$, $b = 9.8$, $d_1 = 0.84$, $d_2 = 3.91$, $d_3 = 0.1$, $d_4 = 0.53$, $d_5 = 0.83$, $d_6 = 1.5$, $\beta = 66.3°$, the unit walls are 0.05 thick). The radiator excitation by a quasi-monochromatic wave (4.134): (**a** and **b**) Radiation patterns in a frequency band and at the frequency $k = 5.03$; (**c**) the dependence $W_{11}^{11}(k) = 1 - \eta(k)$ characterizing the radiation efficiency; (**d**) the $E_x(g,t)$ spatial distribution, $g \in \mathbf{Q}_L$, $t = 85$
Look: 4-37-D.exe – the $E_x(g,t)$ spatial–time distribution, $g \in \mathbf{Q}_L$, $60 < t < 70$ ($U_{\max}(t) = 0.5$)

where $P(t)$:t_1–t_2–t_3–t_4 is the trapezoidal envelope that vanishes for $t < t_1$ and $t > t_4$ and equals unity for $t_2 < t < t_3$, and $k = 5.03$ is the design frequency for the $H_{01} \to H_{0m}$ transducers considered here [216].

For the radiator whose analysis results are plotted in Fig. 4.37, $\gamma = \beta = 66.3°$ and $l = 0.716$ (one-tenth the length of the aperture **A**). The phase incursion of the field per period l in the aperture **A** approximates 2.71. The module of the field amplitude is practically unchanged when going from one period to another. In such a case, two harmonics, the zeroth and the minus first, propagate without attenuation over the infinite periodic structure. For them, $\alpha_0 = -49°$ and $\alpha_{-1} = 83°$, which in view of the

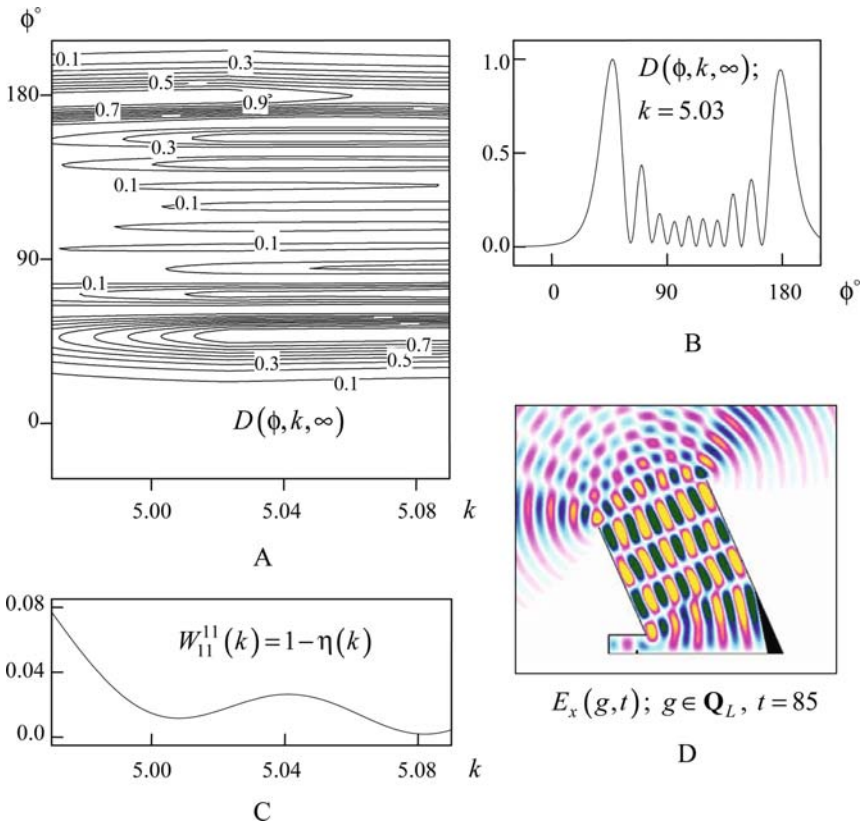

Fig. 4.38 The same as in Fig. 4.37 except that the radiator wide waveguide has a *right cut* (a perpendicular beginning from the point $z = 9.8$ on the *right wall* to the point $z = b = 7.16$ on the *left wall*)
Look: 4-38-D.exe – the radiator excitation by a quasi-monochromatic wave (4.134) ($E_x(g,t)$, $g \in \mathbf{Q}_L$, $60 < t < 70$; $U_{\max}(t) = 0.5$)

evident equality $\phi_n = \alpha_n + 90°$ allows us to predict that the basic directions of the applied energy radiation are $\phi = \phi_0 \approx 41°$ and $\phi = \phi_{-1} \approx 173°$. Actually, at the frequency $k = 5.03$, the main lobe of the pattern is found at the angle $\bar{\phi}(k) = 42°$, and the radiation level in the direction of the minus first harmonic is as low as $D(\phi,k,\infty) < 0.1$. A low radiation level in the direction $\phi = \phi_{-1} \approx 173°$ is attributed to the fact that the minus first spatial harmonic becomes a propagating one only at $k = |\Phi_{-1}|$, while $\Phi_{-1} = -4.99$. The radiation efficiency in the band $4.97 < k < 5.09$ does not fall below 96.8%. So, the $H_{0,10}$-wave propagating along the broad waveguide produces a quasi-periodic system of the secondary sources in the aperture **A**, and the open end of the waveguide really works as a phased antenna array.

The efficiency of the $H_{0,10}$-wave radiation from the broad waveguide segment cut off normal to the walls (see Fig. 4.38; $\gamma = 90°$) is somewhat less than in the

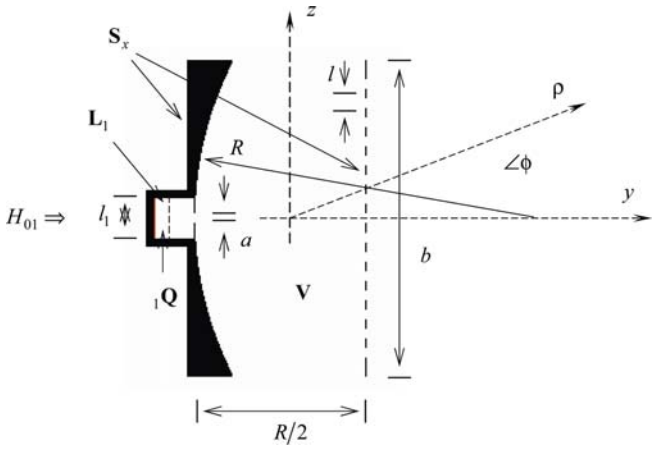

Fig. 4.39 The resonant antenna geometry: $R = 10$, $b = 9.24$, waveguide width is $l_1 = 1.16$, the distance from boundary $\mathbf{L}_1$ to the diaphragm is 1.12, the thickness of the diaphragm and the strip grating (*right mirror*) is $\bar{h} = 0.04$, a is the diaphragm window size, the grating period is $l = 0.56$, $l\theta$ is the length of the period open part

previous case, yet $\eta(k) \geq 0.92$ within the frequency band $4.97 < k < 5.09$. The phase shift of the field of the secondary sources on the period $l = l_2/10 \approx 0.656$ in the aperture **A** approximates 3.14, the expected ϕ_0 and ϕ_{-1} are 42° and 185° ($\phi_n = 90° + \alpha_n + 23.7°$). As a matter of fact, at the frequency $k = 5.03$, the pattern main lobe is observed at $\bar{\phi}(k) = 48°$ (see Fig. 4.38b), the second lobe with a sufficiently high radiation level holds the direction $\phi = 179°$. The difference between the expected and the actual results is bigger than in the previous case. The reason seems to be as follows. Though for some two neighboring channels, defined by the transverse structure of the radiated $H_{0,10}$-wave, the field phases differ practically by a constant, but the module of the field amplitude when going from one channel to another is not constant, the difference amounts to between 4% and 8%.

4.5.4 Resonant Antennas with Semitransparent Grating Mirrors

Distinguishing resonant antennas as a separate class is only reasonable when, in the analyzed frequency region, the structures can maintain slightly damped free oscillations of the electromagnetic field. These oscillations comply with complex eigenfrequencies $\bar{k}_n \in \Omega_k$ (Ω_k is the frequency spectrum; see Section 4.3.3), it is their distribution in the complex space **K** that defines all dynamical features of the basic characteristics of resonant radiators. The operation at a frequency k approaching the real part of one of the eigenfrequencies $\bar{k}$ allows effective control of the radiation pattern (it is bound up with the free oscillation field configuration) as well as the range and the power characteristics of the antenna (they depend on the $k - \mathrm{Re}\bar{k}$

and $\left|\mathrm{Im}\bar{k}\right|$ values and the existence of other eigenfrequencies in the vicinity of the point $\bar{k}$) [217–219].

The efficiency $\eta(k)$ of a resonant antenna becomes satisfactory at the frequency $k = K$ in the near vicinity of the point $k = \mathrm{Re}\,\bar{k}$, where $\bar{k}$ is one of the complex eigenfrequencies of the volume $\mathbf{V}$ that radiates energy into free space. Normally it is expected that at the frequency $k = K$ (or at $k \approx K$ if the k departure from the point $k = K$ is small enough not to noticeably affect the efficiency), the antenna directionality is totally governed by the field spot that the free oscillation complying with eigenfrequency $\bar{k}$ draws on the semitransparent mirror of the resonant volume $\mathbf{V}$. We check this suggestion for the radiator whose overall geometry is given in Fig. 4.39. Excite the radiator by the pulsed H_{01}-wave

$$U_1^{i(1)}(g,t):\ v_{11}(g \in \mathbf{L}_1,t) = F_2(t);\ \tilde{k} = 4.3,\ \Delta k = 0.7,\ \tilde{T} = 50,\ \overline{T} = 100 \tag{4.135}$$

arriving from the parallel-plate waveguide ${}_1\mathbf{Q}$ and occupying the frequency range $3.6 < k < 5.0$ [see formulas (4.117), (4.126), and (4.133)]. For these frequencies, the feeding waveguide is a single-mode one ($k_1 \approx 2.71$, $k_2 \approx 5.42$), and the function $W_{11}^{11}(k) = 1 - \eta(\bar{k})$ characterizing the radiation efficiency has four pronounced local minima (see Fig. 4.40). For geometry 4 (the aperture window connecting the waveguide ${}_1\mathbf{Q}$ and the resonant volume $\mathbf{V}$ is of the size $a = 0.36$; the length of the open part of the strip grating period is $l\theta = 0.2$), peaks of the antenna efficiency $\eta(k)$ are at the points $k = K_j$; $j = 1 \div 4$, and $\eta(K_3) = 1.0$ ($K_1 = 3.823$, $K_2 = 4.147$, $K_3 = 4.443$, $K_4 = 4.769$). For different a and θ parameters (geometries 1–3), the local minima of the functions $W_{11}^{11}(k)$ are slightly shifted from the points $k = K_j$. The radiation efficiency is not better than 50%, 90%, and 85%, respectively. Higher-Q resonances occur in the volume bounded by a strip grating with a shorter open part $l\theta$ of the period l. For this grating within the frequency band $3.6 < k < 5.0$, the module of the reflection coefficient $R_{00}^{\mathbf{AA}}(k)$ [see problem (1.26)] of normally incident wave (4.118) is approximately 0.1 [18]. For a half-filled strip grating (see geometries 1 and 2), $\left|R_{00}^{\mathbf{AA}}(k)\right| \approx 0.3$. The resonance Q-factor, the optimum size a of the diaphragm window, and the radiation efficiency of the applied energy are intimately related. As a rough guide, a better $\eta(k)$ in the case of high-quality resonances comes at a smaller a.

We proceed now to geometry 4 (see Figs. 4.41, 4.42, 4.43, 4.44 and 4.45). Consider the temporal and spectral amplitudes of the field excited by the wave (4.135). The examination of these amplitudes at a point $g = g_1$ located on the radiator axis approximately a quarter of the wavelength $\lambda = 2\pi/k$, $3.6 < k < 5.0$, away from its semitransparent mirror yields the real parts of the eigenfrequencies $\bar{k}$. They are responsible for the realization of resonant regimes in the vicinities of the points $k = K_j$, $j = 1 \div 4$ (see Section 4.3 and Fig. 4.41): $\mathrm{Re}\bar{k}_1 \approx 3.825$, $\mathrm{Re}\bar{k}_2 \approx 4.149$, $\mathrm{Re}\bar{k}_3 \approx 4.445$, $\mathrm{Re}\bar{k}_4 \approx 4.772$. The regimes with peak $\eta(k)$ values appear for lower frequencies, a little earlier than the regimes of possible free oscillations of the field in the volume $\mathbf{V}$.

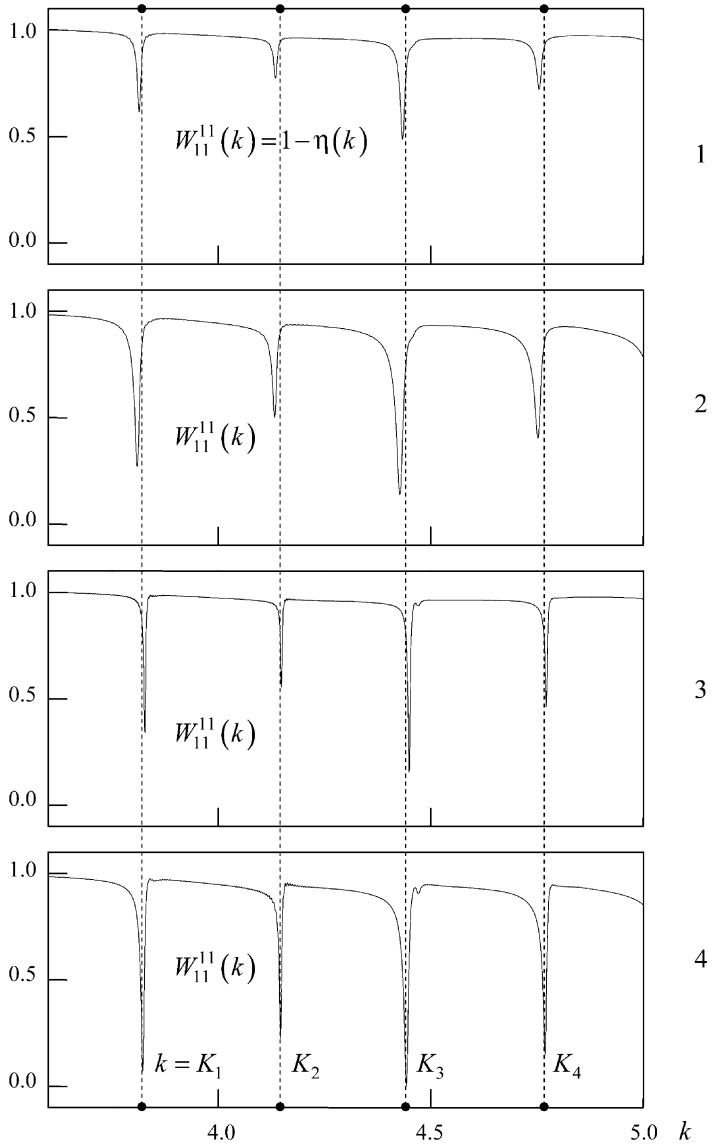

Fig. 4.40 The radiation efficiency characteristic $W_{11}^{11}(k) = 1 - \eta(k)$ for resonant antennas with different-size diaphragm windows and a different length of the open period part of the strip grating (geometries 1–4): 1 – $a = 0.28$ and $\theta = 0.5$; 2 – $a = 0.36$ and $\theta = 0.5$; 3 – $a = 0.28$ and $\theta = 0.36$; 4 – $a = 0.36$ and $\theta = 0.36$

The excitation of the radiator by the quasi-monochromatic H_{01}-wave

$$U_1^{i(1)}(g,t)\text{: } v_{11}(g \in \mathbf{L}_1,t) = \cos\left[\tilde{k}\left(t - \tilde{T}\right)\right] P(t) = F_4,\ \tilde{k},\ \tilde{T} = 0.5,\quad P(t)\text{:}0.1 - 5 - 95 - 99.9 \tag{4.136}$$

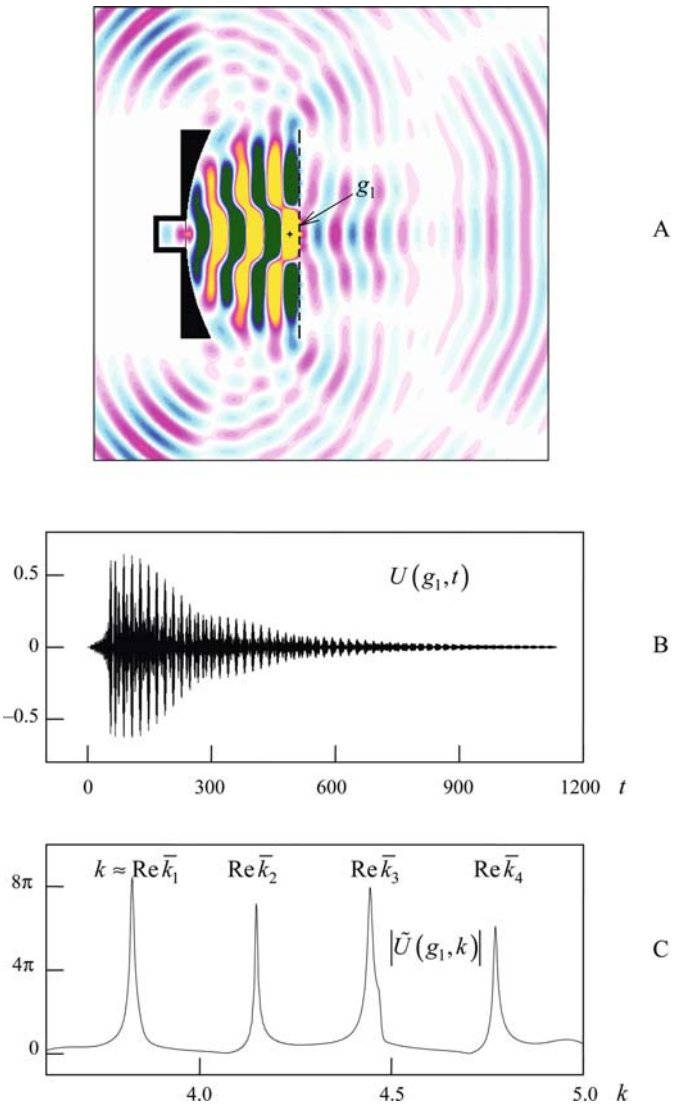

Fig. 4.41 The radiator excitation (geometry 4) by the pulsed H_{01}-wave (4.135): (**a**) The $E_x(g,t)$ spatial distribution, $g \in \mathbf{Q}_L$, $t = 300$; (**b** and **c**) the temporal and the spectral amplitudes of the field at the point $g = g_1$ near the semitransparent mirror of the resonant antenna
Look: 4-41-A.exe and 4-41-A-F.exe – the $E_x(g,t)$ spatial–time distribution, $g \in \mathbf{Q}_L$ at the time $50 < t < 62$ (forced oscillations of the field; $U_{\max}(t) = 0.5$) and $300 < t < 308$ (free oscillations of the field; $U_{\max}(t) = 0.03$)

[see formulas (4.133) and (4.134)] whose central frequency $\tilde{k}$ takes the values $\tilde{k} = K_j$ $j = 1 \div 4$ (see Figs. 4.42, 4.43, 4.44 and 4.45) yields some check points to estimate the quality factor $Q = \mathrm{Re}\bar{k}/2\left|\mathrm{Im}\bar{k}\right|$ of the oscillations corresponding to eigenfrequencies $\bar{k}$, to identify the oscillation type and examine (in the narrow

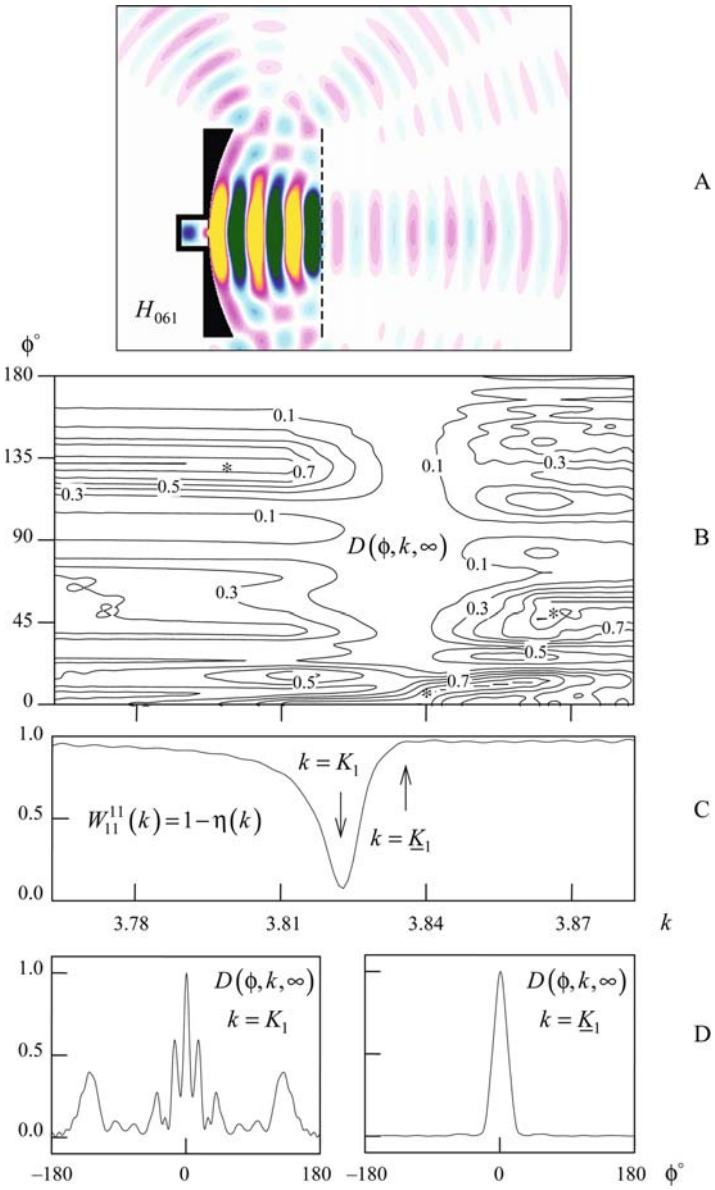

Fig. 4.42 The radiator excitation (geometry 4) by the quasi-monochromatic H_{01}-wave (4.136) with the central frequency $\tilde{k} = K_1$: (**a**) The $E_x(g,t)$ spatial distribution, $g \in \mathbf{Q}_L$, $t = 302$; (**b** and **d**) radiation patterns $D(\phi,k,\infty)$ – from here on, some ϕ and k parameter ranges where $D(\phi,k,\infty) > 0.9$ are asterisked ($*$); (**c**) the function $W_{11}^{11}(k)$ characterizing the radiation efficiency
Look: 4-42-A.exe and 4-42-A-F.exe – the $E_x(g,t)$ spatial–time distribution, $g \in \mathbf{Q}_L$ at the time $80 < t < 92$ (forced oscillations of the field; $U_{\max}(t) = 0.3$) and $300 < t < 308$ (free oscillations of the field; $U_{\max}(t) = 0.2$)

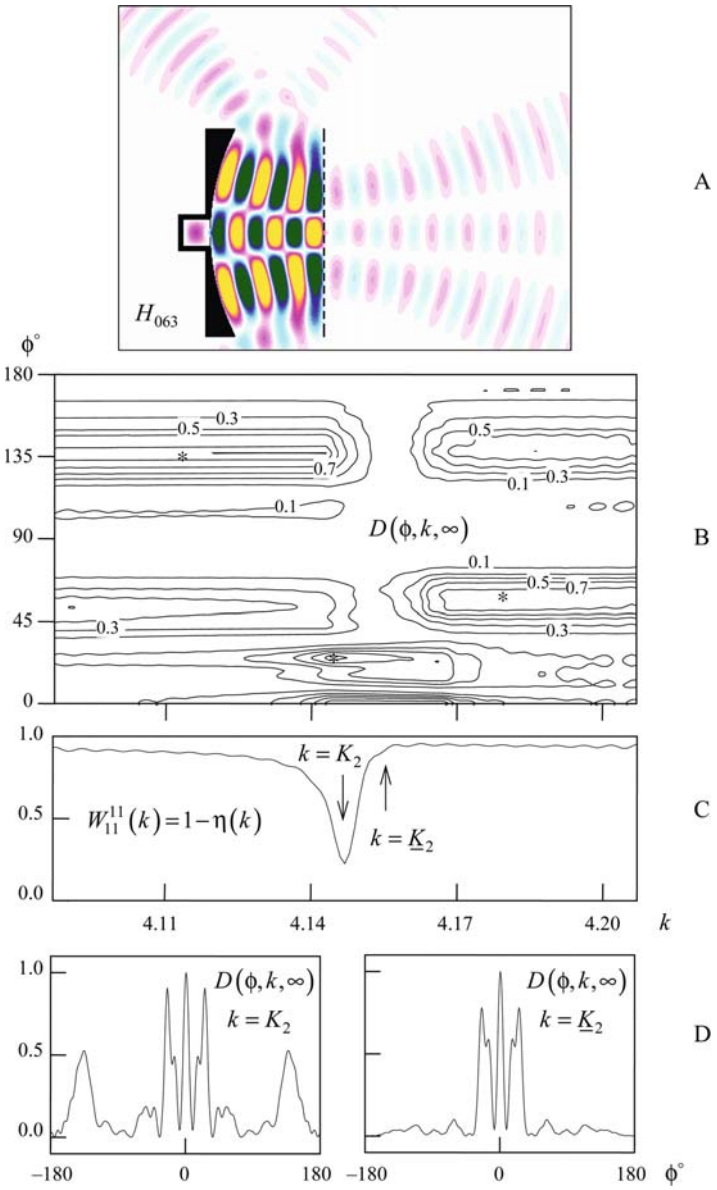

Fig. 4.43 The radiator excitation (geometry 4) by the quasi-monochromatic H_{01}-wave (4.136) with the central frequency $\tilde{k} = K_2$: (**a**) The $E_x(g,t)$ spatial distribution, $g \in \mathbf{Q}_L$, $t = 302$; (**b** and **d**) radiation patterns $D(\phi,k,\infty)$; (**c**) the function $W_{11}^{11}(k)$ characterizing the radiation efficiency
Look: 4-43-A.exe and 4-43-A-F.exe

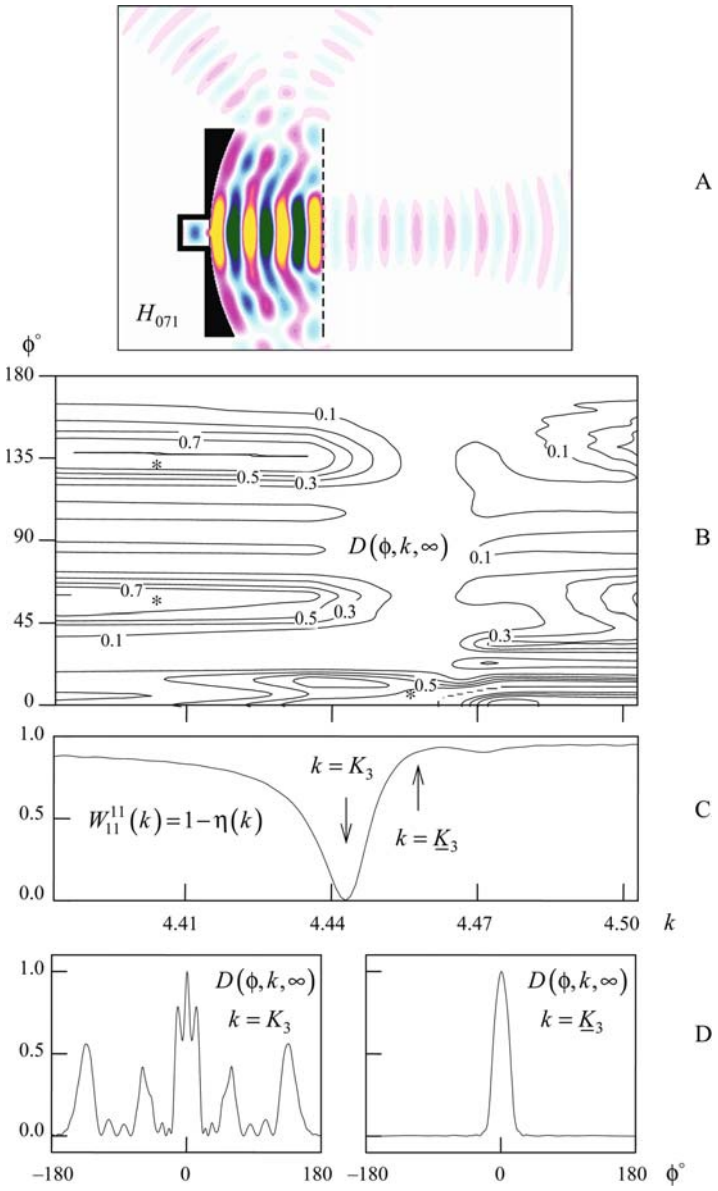

Fig. 4.44 The same as in Fig. 4.42 except that $\tilde{k} = K_3$
Look: 4-44-A.exe and 4-44-A-F.exe

frequency bands $K_j - 0.06 < k < K_j + 0.06$) the behavior of the functions $\eta(k)$ and $D(\phi,k,\infty)$ characterizing the radiation efficiency and its directionality. The resonant change of the pattern $D(\phi,k,\infty)$ – a passage to the pattern exactly corresponding to the field spot of the free oscillation on the semitransparent mirror of the resonant –

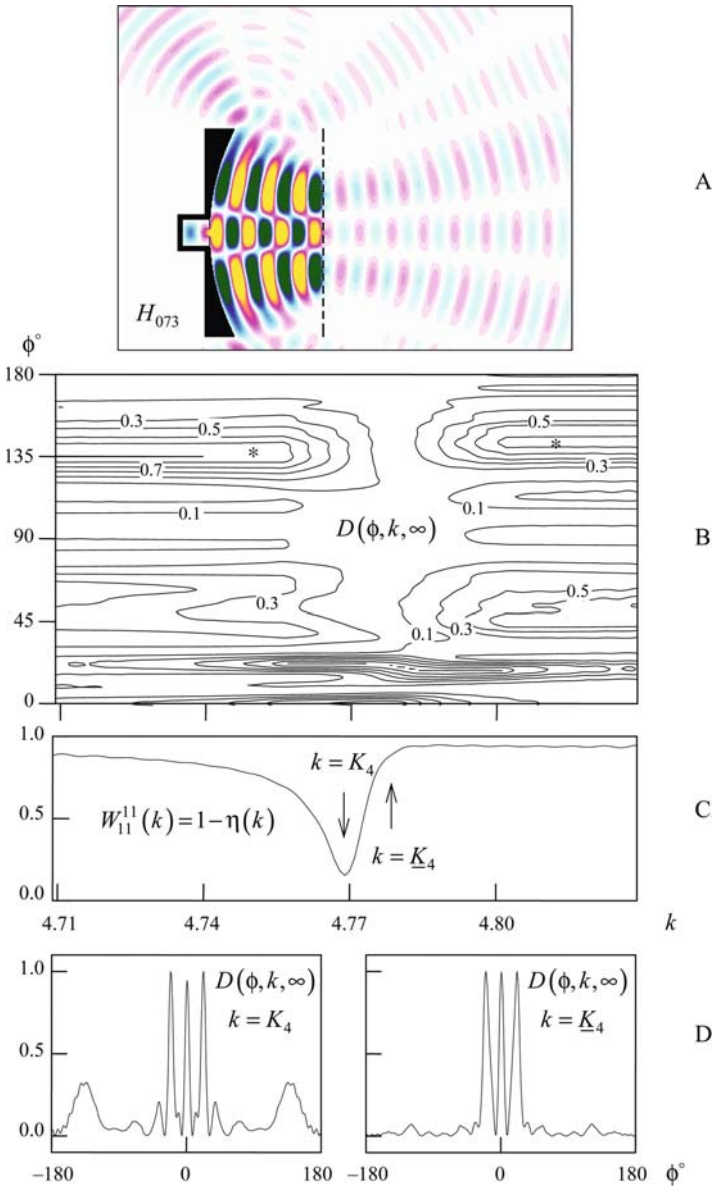

Fig. 4.45 The same as in Fig. 4.42 except that $\tilde{k} = K_4$
Look: 4-45-A.exe and 4-45-A-F.exe

comes too late (along the k-axis) for both maximum $\eta(k)$ regime and for regime of free oscillation of the field. In the case considered, these changes end at the points $k = \underline{K}_j$, $j = 1 \div 4$ ($(\underline{K}_1 = 3.837, \underline{K}_2 = 4.154, \underline{K}_3 = 4.460, \underline{K}_4 = 4.778)$), where the radiation efficiency ($(\eta(\underline{K}_1) \approx 0.05,\ \eta(\underline{K}_2) \approx 0.1,\ \eta(\underline{K}_3) \approx 0.08$, and

$\eta(\underline{K}_4) \approx 0.13)$) is substantially lower than at the points $k = K_j$, $j = 1 \div 4$ ($\eta(K_1) \approx 0.92$, $\eta(K_2) \approx 0.77$, $\eta(K_3) = 1.0$, and $\eta(K_4) \approx 0.85$).

Thus, at particular frequencies, the considered resonant antennas can radiate most of the applied energy into free space. Also, at certain frequencies, the radiation can achieve the predicted directivity. The trouble is that the corresponding frequency sets $k = K_j$ and $k = \underline{K}_j$; $j = 1 \div 4$, differ essentially. The problem is to make the radiation remain efficient enough and yet realize a desired directivity. Let us try one expedient and replace the resonance volume $\mathbf{V}$, open on three sides (see Fig. 4.39), by a resonator, open only on one side where is a semitransparent grating mirror located (see Fig. 4.46a: the scheme of the excitation from the feeding waveguide and the periodic structure are the same as that of the antenna in Fig. 4.39). The resonator size b across is approximately one-third of that before. This is the only way to get over the dramatic crowding of the spectrum Ω_k in the considered band $3.6 < k < 5.0$. Under this band, only eigenfrequencies complying with the H_{0n1}- and H_{0n3}-oscillations can be found. The reason is that no oscillations asymmetric with respect to the longitudinal axis of the resonator (they cannot be excited by the H_{01}-wave of the feeding waveguide), and the H_{0n5}-oscillations arise as soon as the H_{05}-wave becomes propagating when traveling along a b-wide waveguide ($k > k_5 \approx 5.24$).

Let us excite the antenna by a pulsed wave as given by (4.135) and find the functions $W_{11}^{11}(k)$ and $\left|\tilde{U}(g_1,k)\right|$ (the point $g = g_1$ is close to the semitransparent mirror as in the preceding case). Their behavior suggests values for the radiation efficiency $\eta(k) = 1 - W_{11}^{11}(k)$ and the real parts of the eigenfrequencies $\bar{k}$ responsible for the realization of the resonant regimes. The best $\eta(k)$ behavior is for a structure with $a = 0.36$ (the size of the diaphragm window) and $l\theta = 0.28$ (the size of the open part of the grating period). Thus, at the points $k \in [3.6;5.0]$ coinciding with the $\mathrm{Re}\bar{k}$, the antenna efficiency is as high as 95% and more (see Fig. 4.46b and c).

We analyze now in more detail the operation of this system at the frequencies $k \in \left[K_j - 0.06; K_j + 0.06\right]$, $j = 1,2$, $K_1 = \mathrm{Re}\bar{k}_1 = 3.864$, and $K_2 = \mathrm{Re}\bar{k}_2 = 3.972$ (see Figs. 4.47, 4.48 and 4.49). The frequency band beyond which the spectral amplitudes of the wave (4.136) can be neglected turns out to be too wide for the response of the resonant antenna to be formed by only one, $\bar{k}_1$ or $\bar{k}_2$, eigenfrequency. That is why the narrowband Gaussian pulse

$$U_1^{i(1)}(g,t): \; v_{11}(g \in \mathbf{L}_1,t) = F_1(t); \tilde{k}, \tilde{\alpha} = 25, \tilde{T} = 125, \bar{T} = 250 \qquad (4.137)$$

will be used as the exciting H_{01}-wave. Its central frequency $\tilde{k}$ takes on the values $\tilde{k} = K_1$ and $\tilde{k} = K_2$. Outside the band $\left[\tilde{k} - 0.1; \tilde{k} + 0.1\right]$, the absolute value of the normalized spectral amplitudes of this pulse is not above 0.0017.

At the frequencies $k = K_1$ and $k = K_2$, all the energy delivered by the sinusoidal H_{01}-wave to the resonant antenna is radiated into free space, $\eta(K_1) = \eta(K_2) = 1.0$. Such a high efficiency is due to the excitation of the slight-attenuation oscillations on the H_{01}- and H_{03}-waves of the broad parallel-plate waveguide. These oscillations

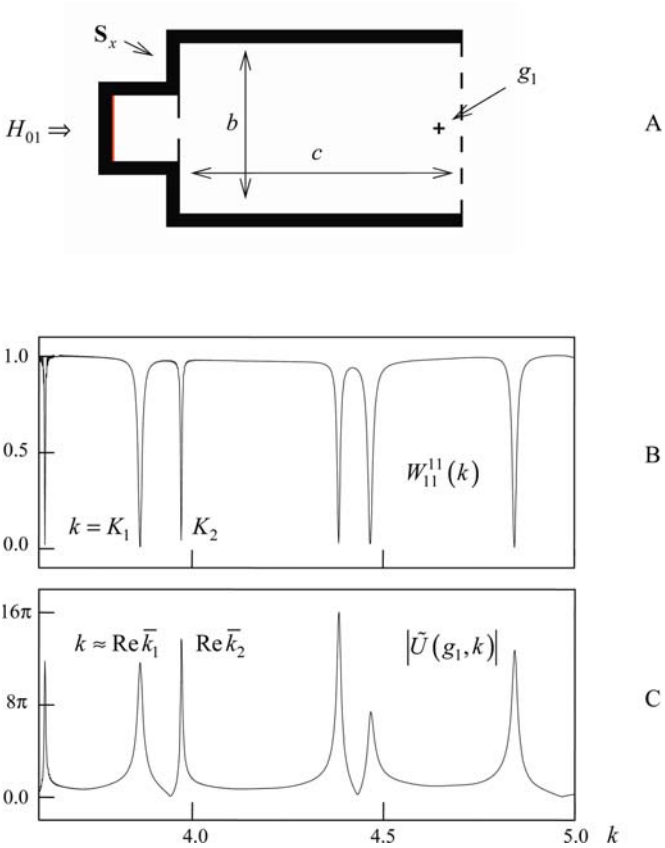

Fig. 4.46 (**a**) The resonant antenna geometry ($b = 3.0$, $c = R/2 = 5.0$, diaphragm window size is 0.36, length of the open part of the grating period is 0.28), its (**b**) energy and (**c**) spectral characteristics in a frequency band

(H_{061} and H_{043}; see Figs. 4.47a and 4.48a) comply with the complex eigenfrequencies $\bar{k}_1 \approx K_1 - i0.0056$ and $\bar{k}_2 \approx K_2 - i0.0019$ whose imaginary parts are uniquely determined by the behavior of the functions $U(\tau) = U(g_1,t)$; $\tau = t - \bar{T} > 0$ (see Section 4.3.3 and Figs. 4.47c and 4.48c).

For all $k \in [K_1 - 0.06;K_1 + 0.06]$, the configuration of the radiation pattern $D(\phi,k,\infty)$ of the resonant antenna complies with the shape of the H_{01}-wave field spot on the semitransparent grating mirror (see Fig. 4.47b). The patterns of the resonant antenna and the nonresonant antenna analog differ only in the width of the main lobe. For example, at the frequency $k = K_1$, it is, respectively, $\phi_{0.5}(k) \approx 36°$ and $\phi_{0.5}(k) \approx 60°$ (see Fig. 4.47d).

In the vicinity of the point $k = K_2$, the resonant antenna radiation pattern changes rather markedly (see Fig. 4.48b): one main lobe at the frequency $k = 3.912$, three lobes at $k = 3.970$, two at $k = 3.998$, and again one at $k = 4.032$

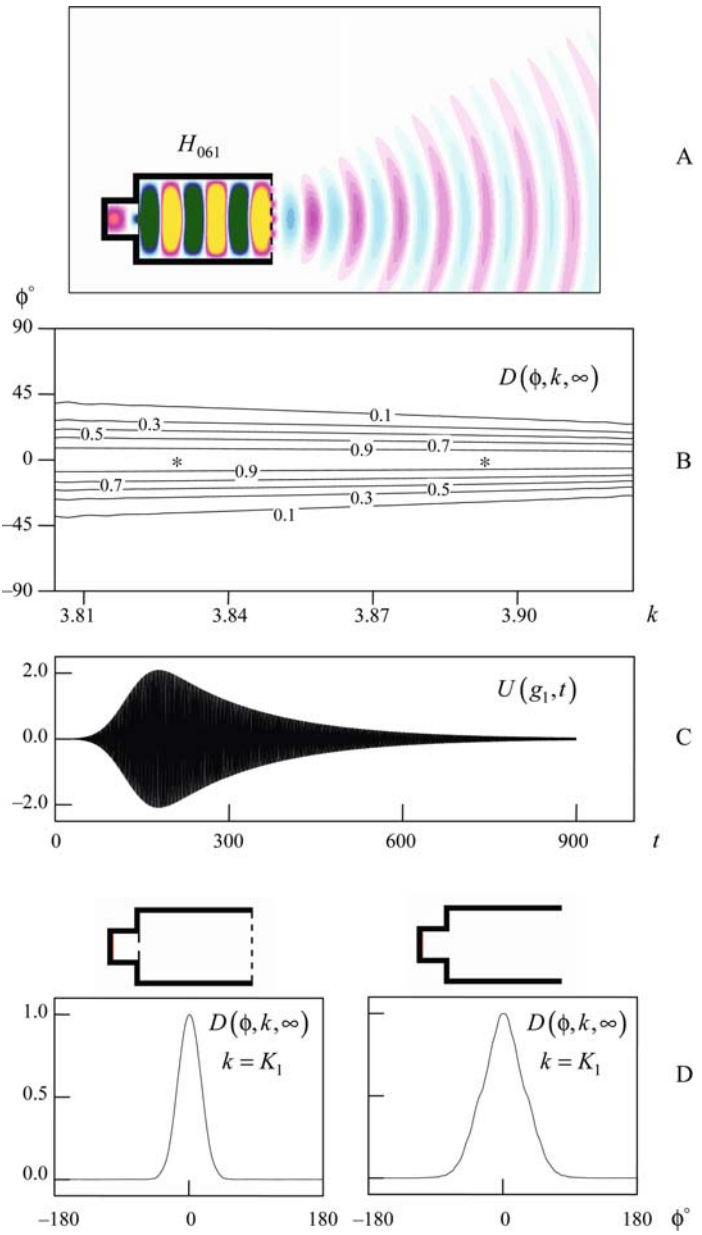

Fig. 4.47 The antenna excitation by a narrowband Gaussian pulse (4.137) with the central frequency $\tilde{k} = K_1$: (**a**) The $E_x(g,t)$ spatial distribution, $g \in \mathbf{Q}_L$, $t = 505$; (**b**) frequency-band radiation pattern $D(\phi,k,\infty)$; (**c**) function $U(g_1,t)$; (**d**) radiation patterns $D(\phi,k,\infty)$ of the resonant and non-resonant antennas at the point $k = K_1$

Look: 4-47-A.exe and 4-47-A-F.exe – the $E_x(g,t)$ space–time distribution, $g \in \mathbf{Q}_L$ at the time $125 < t < 133$ (forced oscillations of the field; $U_{\max}(t) = 0.5$) and $500 < t < 508$ (free oscillations of the field; $U_{\max}(t) = 0.2$)

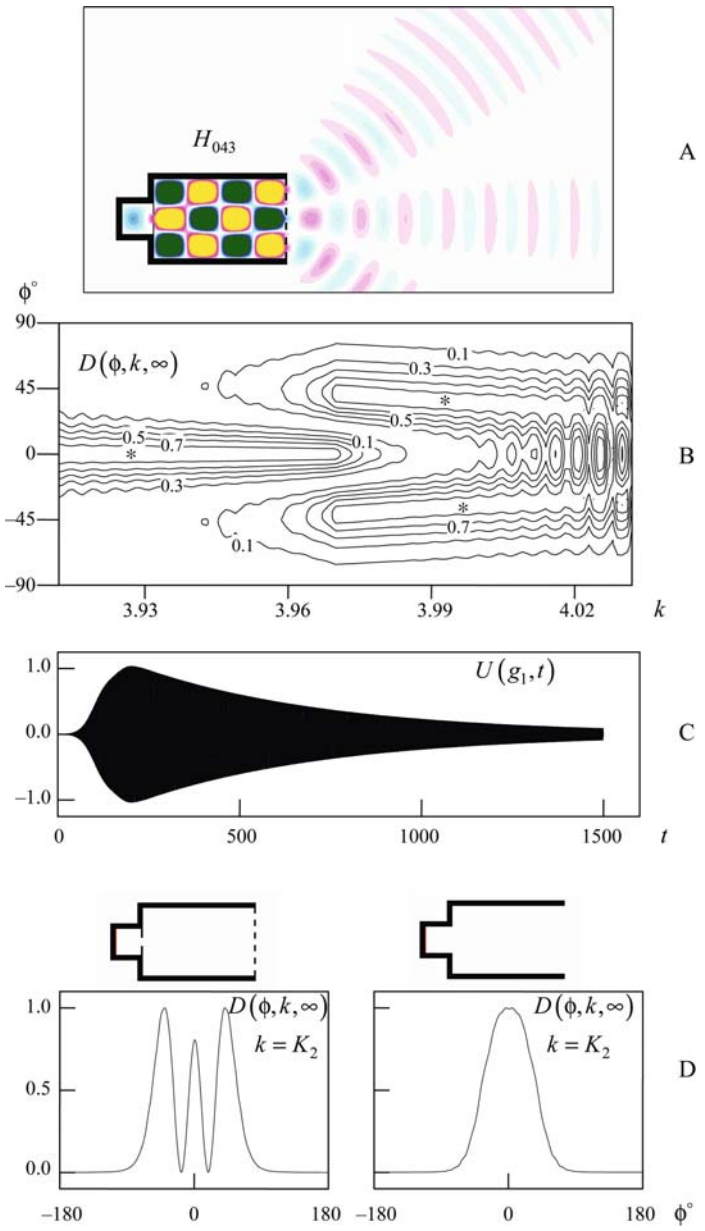

Fig. 4.48 The same as in Fig. 4.47, except that $\tilde{k} = K_2$
Look: 4-48-A.exe and 4-48-A-F.exe

(see Fig. 4.49). Similarly does also the radiation efficiency: from $\eta(k) = 0.02$ to $\eta(k) = 1.0$. Only within the narrow frequency band $k \in [K_2 - 0.008; K_2 + 0.003]$, the configuration of the radiation pattern $D(\phi,k,\infty)$ of the resonant antenna corresponds to the field spot of the resonance-inducing H_{03}-wave on the semitransparent

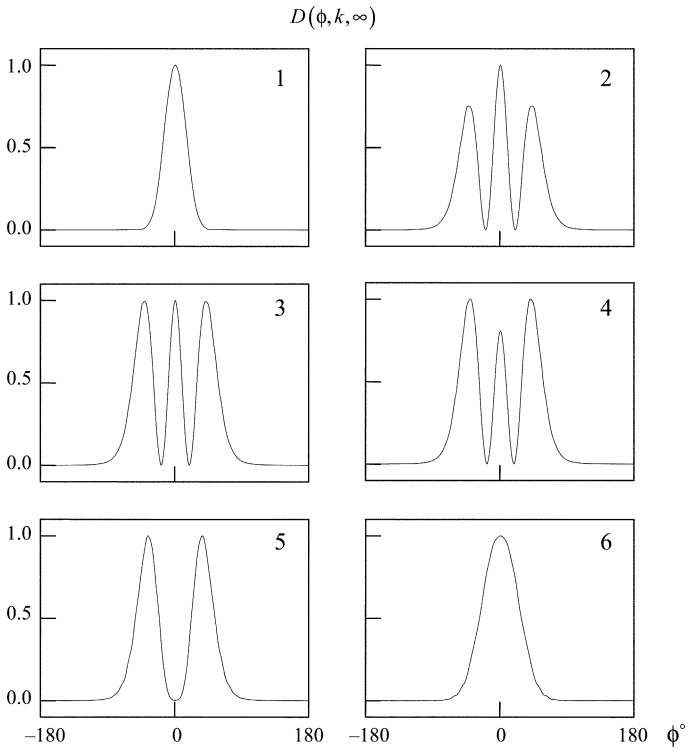

Fig. 4.49 Changes in the radiation pattern $D(\phi,k,\infty)$ and in the radiation efficiency $\eta(k)$ of the resonant antenna upon frequency k slight variations: 1 – $k = 3.912$, $\eta(k) = 0.03$; 2 – $k = 3.968$, $\eta(k) = 0.2$; 3 – $k = 3.970$, $\eta(k) = 0.4$; 4 – $k = 3.972$, $\eta(k) = 1.0$; 5 – $k = 3.998$, $\eta(k) = 0.03$; 6 – $k = 4.032$, $\eta(k) = 0.02$

grating mirror. Here, the $D(\phi,k,\infty)$ value in the ϕ-direction of each of the three lobes is never below $D(\phi,k,\infty) = 0.5$. The radiation pattern of the nonresonant antenna is basically the same as that on the interval $k \in [K_1 - 0.06; K_1 + 0.06]$ (see Fig. 4.48d), the H_{01}-wave running on the open end of the broad parallel-plate waveguide contributes the most to the radiation field.

4.5.5 2-D Models of Phased Arrays

The analysis and synthesis of phased arrays is based mainly on methods and results from the grating theory [220]. Clearly the actual structure design cannot do without sufficiently flexible and reliable 3-D models. Nevertheless, several fundamental aspects, in particular the physics of the processes going in phased antenna arrays, can be treated effectively in terms of simple 2-D models. In what follows, some questions of this nature will be considered with reference to the methods developed in Section 4.2.

First we address problems arising in the case of simple (cheap) phased antenna arrays intended for a certain range $[K_1;K_2]$ of frequencies $k = 2\pi/\lambda = 2\pi\sqrt{\varepsilon_0\mu_0}f$. The main lobe of the radiation pattern has to scan around a circular cone, whose generatrices make a given angle β with its axis. For definiteness' sake, we take $f = 8 \div 12\,[GHz]$ ($k \in [168;251]$, $\lambda \in [0.025;0.0375]$) and $\beta = 45°$. The radiating element of 2-D phased array is a dielectric rod mounted at the open end of the parallel-plate waveguide and excited by the sinusoidal H_{01}-wave (see, for example, Fig. 4.50a).We find the waveguide width a, the permittivity ε of the filling, and the period length $l > a$ of the array composed of N elements (Fig. 4.50b) in the following way.

Assume that the array of Fig. 4.50b extends to infinity, and that the phases of the field produced by the H_{01}-waves running from parallel-plate waveguides on its aperture in the $z = 0$ plane differ (in two neighboring waveguides) by the value of $2\pi\Phi$. In this situation, the electromagnetic field in the $z \geq 0$ area can be written in the following form (see Sections 1.1.4 and 1.2.1):

$$\begin{gathered}\tilde{U}(g,k) = \tilde{E}_x(g,k) = \sum_{n=-\infty}^{n=\infty} A_n(k)\mathrm{e}^{i[\Phi_n y+\Gamma_n z]},\ \tilde{E}_y = \tilde{E}_z = \tilde{H}_x = 0,\\ \tilde{H}_y = \tfrac{1}{ik\eta_0}\tfrac{\partial\tilde{U}}{\partial z},\ \tilde{H}_z = -\tfrac{1}{ik\eta_0}\tfrac{\partial\tilde{U}}{\partial y};\ g = \{y,z\}.\end{gathered} \tag{4.138}$$

Here, $\Phi_n = 2\pi(\Phi + n)/l$; $\Gamma_n = \sqrt{k^2 - \Phi_n^2}$, $\mathrm{Re}\Gamma_n \geq 0$, $\mathrm{Im}\Gamma_n \geq 0$, and $\tilde{U}(y + l,z,k) = \mathrm{e}^{2\pi i\Phi}\tilde{U}(y,z,k)$. The values Φ and k define the departure angles $\alpha_n = -\arcsin(\Phi_n/k)$ at which the propagating spatial harmonics $A_n(k)\exp[i(\Phi_n y + \Gamma_n z)]$ (their numbers n are such that $\mathrm{Im}\Gamma_n = 0$) go from the array into free space. The phased array of this type are usually under the following restrictions imposed on the feeding waveguides cutoffs $k_m = m\pi/\sqrt{\varepsilon}a$, $m = 1,2,\ldots$, and the grazing points $k_n^+ = |2\pi(\Phi + n)/l|$, $n = 0,\pm1,\ldots$, of the infinitely extending periodic structure:

- $k_1 < K_1$ and $k_2 > K_2$;
- $k_0^+ < K_1$ and $k_n^+ > K_2$, with $n \neq 0$ for all $k\in[K_1;K_2]$ and all Φ such that $|\Phi_0| \leq k\sin\beta$.

Neglect of these constraints reduces, as a rule, the array efficiency and enhances side lobes of the radiation pattern because of the threshold effects and certain changes in the operation of the feeding waveguide and the radiating unit. The mentioned restrictions can be converted into the following set of inequalities

$$l < 2\pi[(1 + \sin\beta)K_2]^{-1},\ l > a,\ a\sqrt{\varepsilon} > \frac{\pi}{K_1},\ a\sqrt{\varepsilon} < \frac{2\pi}{K_2}. \tag{4.139}$$

On this basis and assuming that $\varepsilon = 2.5$, one gets the optimum geometrical parameters a and l in the desired range of working frequencies $k\in[168;251]$ and directions $|\alpha_0| \leq 45°$. These are $a = 0.0132$ ($k_1 \approx 151$, $k_2 \approx 301$) and $l = 0.014$.

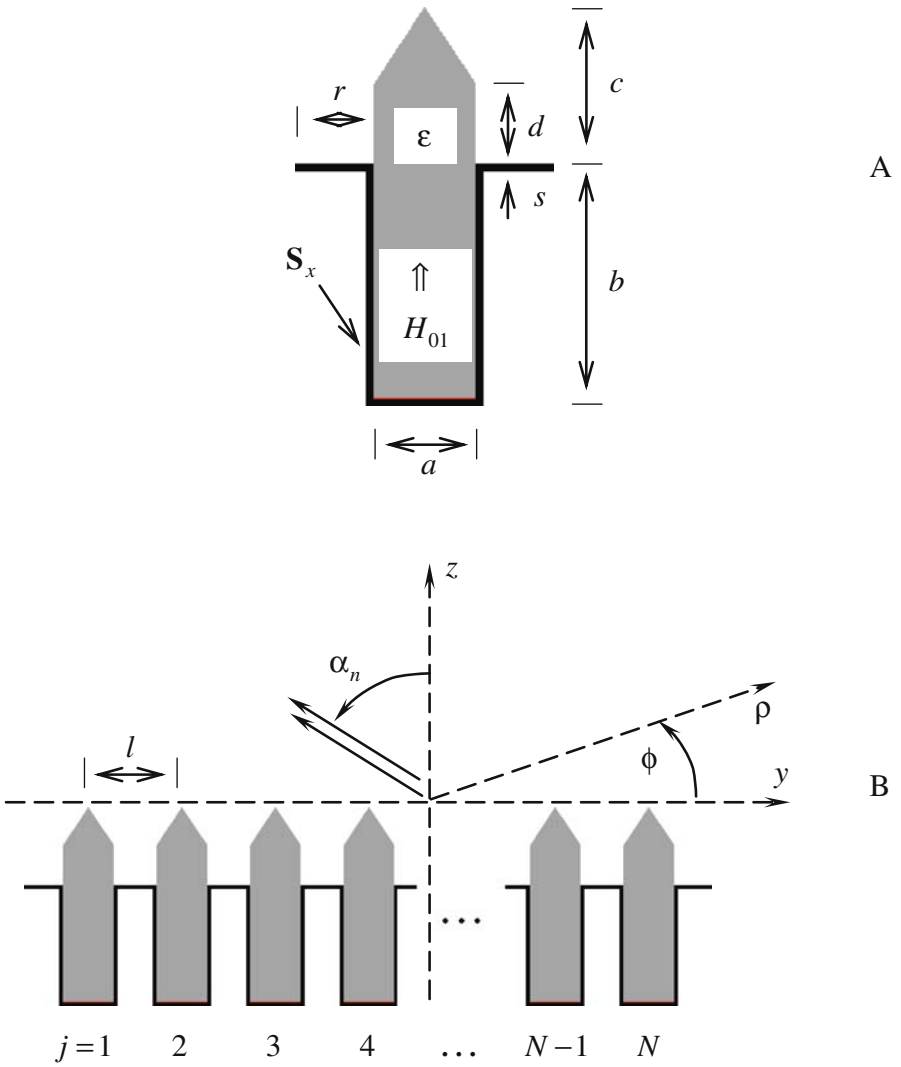

Fig. 4.50 (**a**) The radiating element geometry ($b = 0.03$, $c = 0.02$, $r = 0.01$, $s = 0.001$) and (**b**) the phased array consisting of N elements

The concept of a dielectric rod at the end of the parallel-plate waveguide implies a great variety of radiating elements. How shall we choose among them when designing effective finite-length phased array? This problem will be touched upon, addressing the radiating elements 1–3 with different geometry of the transition "dielectric rod – free space" (see Fig. 4.51). Excite these elements by the pulsed H_{01}-wave

$$U_1^{i(q)}(g,t):\ v_{11}\left(g \in \mathbf{L}_q, t\right) = F_2(t);\ \tilde{k} = 210,\ \Delta k = 42,\ \tilde{T} = 1,\ \bar{T} = 2 \quad (4.140)$$

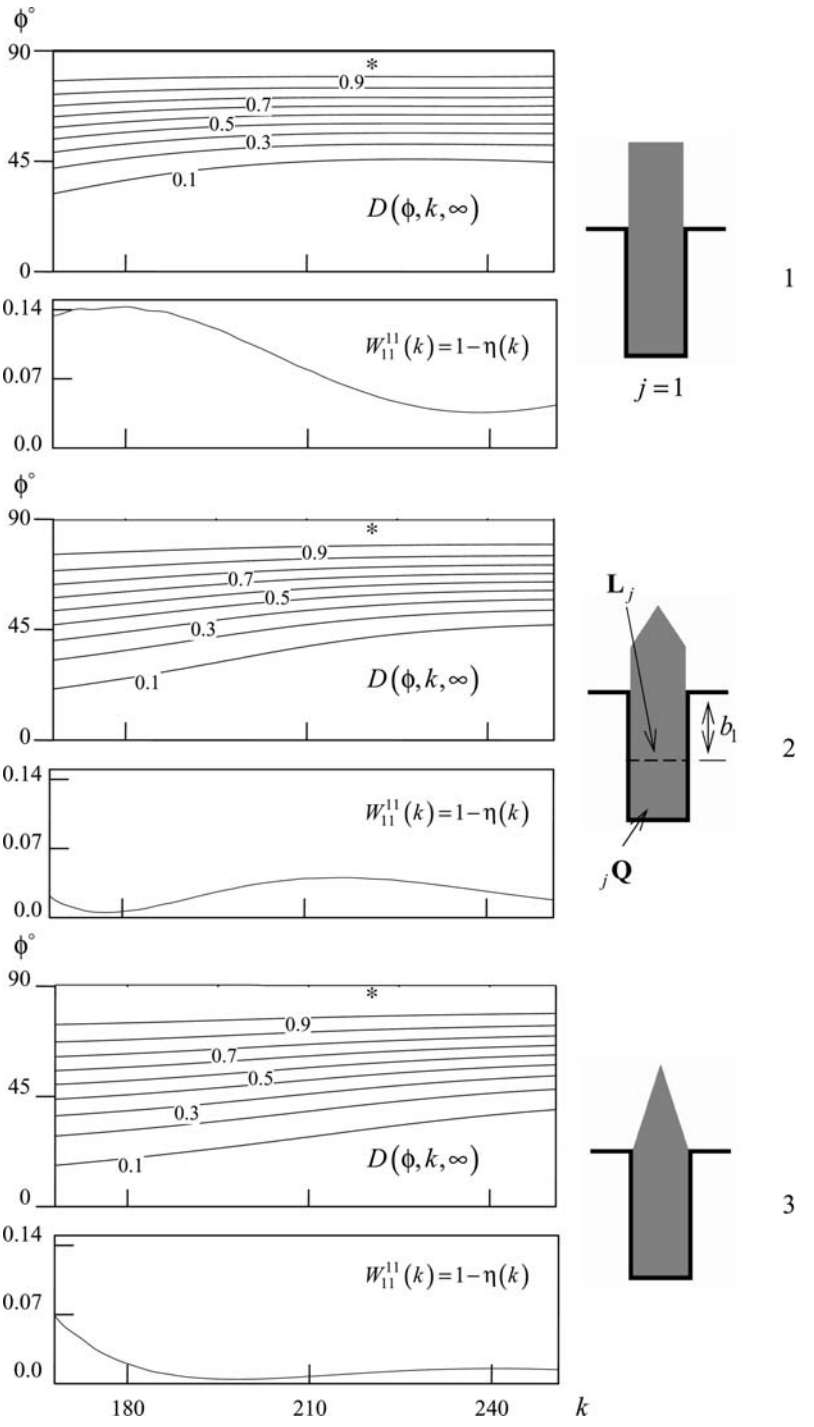

Fig. 4.51 (continued)

($q = 1$) and compare their major electrodynamical characteristics $D(\phi,k,\infty)$ and $\eta(k)$ ($W_{11}^{11}(k)$) within the frequency band $168 \le k \le 251$. As before, $U_p^{i(q)}\left(g_q,t\right) = v_{pq}\left(z_q,t\right)\mu_{pq}\left(y_q\right)$ is the H_{0p}-wave running from the virtual parallel-plate waveguide ${}_q\mathbf{Q}$, $W_{np}^{jq}(k)$ the energy taken away by the sinusoidal H_{0n}-wave reflected or transmitted to the waveguide ${}_j\mathbf{Q}$, $\eta(k) = 1 - \sum\limits_{n,j} W_{np}^{jq}(k)$ the radiation efficiency, and

$$F_2(t) = 4\frac{\sin\left[\Delta k\left(t-\tilde{T}\right)\right]}{\left(t-\tilde{T}\right)}\cos\left[\tilde{k}\left(t-\tilde{T}\right)\right]\chi\left(\bar{T}-t\right).$$

The radiation patterns of all the three radiating elements are identical in kind across the whole band of working frequencies k. Yet configurations 2 and 3 outperform the first one in efficiency. Discard radiator 1. Use radiators 2 and 3 to make up two arrays with a minimum number, $N = 2$, of elements (see Figs. 4.52 and 4.53). One of the elements is active [excited by the pulsed wave (4.140)]. The other is passive. Compare the characteristics $D(\phi,k,\infty)$, $\eta(k) = 1 - W_{11}^{11}(k) - W_{11}^{21}(k)$, and $W_{11}^{21}(k)$ of these arrays within $168 \le k \le 251$. In the case considered, the functions $W_{11}^{21}(k)$ determine the factors of the power coupling between first and second radiating elements [220]. Their behavior, as well as the behavior of the functions $\eta(k)$, does not demonstrate any characteristic features to decide on element 2 or element 3 as the better building block for a multicomponent antenna array. The integral values

$$\bar{\eta} = \frac{1}{K_2 - K_1}\int\limits_{K_1}^{K_2}\eta(k)\,dk \text{ and } \bar{W}_{11}^{21} = \frac{1}{K_2 - K_1}\int\limits_{K_1}^{K_2}W_{11}^{21}(k)\,dk \qquad (4.141)$$

are more informative. For a set of two elements 2, $\bar{\eta} = 0.966$ and $\bar{W}_{11}^{21} = 0.016$. For a set of two elements 3, $\bar{\eta} = 0.975$ and $\bar{W}_{11}^{21} = 0.0077$. On this basis, we discard element 2 and employ element 3. An array consisting of 13 elements 3 is shown in Fig. 4.54a. The radiation patterns of its central radiating element and the coupling coefficients of this element with the rest elements of the structure are shown in Fig. 4.54.

Now excite 5 (case A), 9 (B), and 13 (C) central elements of this grating by the pulsed H_{01}-waves $U_1^{i(q)}(g,t)$ [see formula (4.140)]. This will assist us in tracing the changes of the radiation pattern of the structure [see Fig. 4.55 : for frequency $k = 210$, $\phi_{0.5}(k) \approx 22.5°$ (in the case A), $\phi_{0.5}(k) \approx 12.4°$ (B), and $\phi_{0.5}(k) \approx 8.0°$ (C)]

Fig. 4.51 (continued) Range characteristics of the radiating elements: $a = 0.0132$, $b_1 = b$; $1 - d = c$, $2 - d = 0.5c$, $3 - d = 0$

Look: The radiating element excitation by the pulsed H_{01}-wave (4.140). 4-51-1.exe, 4-51-2.exe, and 4-51-3.exe – the $E_x(g,t)$ spatial–time distribution, $g \in \mathbf{Q}_L$ at the time $1.0 < t < 1.15$ (the pulse major part crosses the computational space $\mathbf{Q}_L$; $U_{\max}(t) = 0.5$)

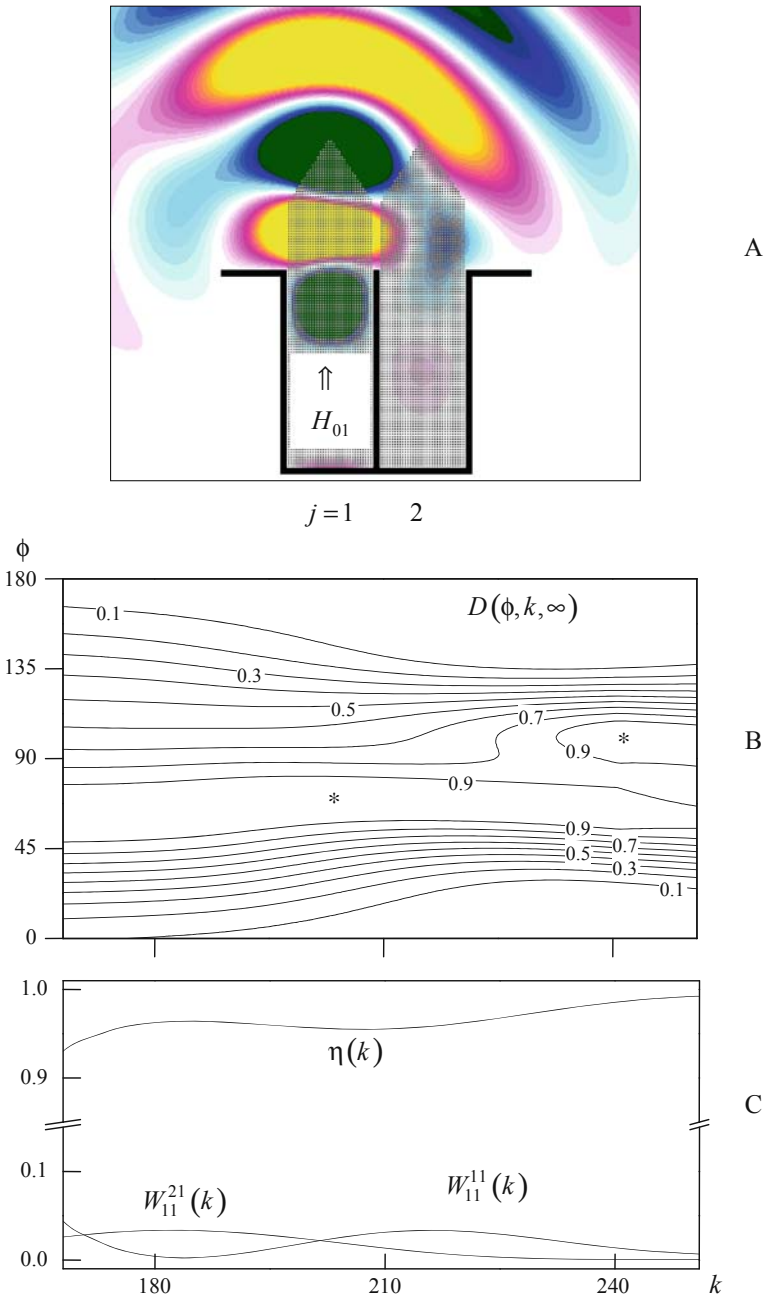

Fig. 4.52 The excitation of a system ($l = 0.014$) of two radiation elements 2 ($d = 0.5c$) by the pulsed H_{01}-wave (4.140): (**a**) The $E_x(g,t)$ spatial distribution, $g \in \mathbf{Q}_L$, $t = 1.1$; (**b**) radiation pattern $D(\phi,k,\infty)$ in the frequency band $168 \le k \le 251$; (**c**) energy characteristics of the system
Look: 4-52-A.exe – the $E_x(g,t)$ spatial–time distribution, $g \in \mathbf{Q}_L$ at the time $1.0 < t < 1.15$ (the pulse major part crosses the computational space $\mathbf{Q}_L$; $U_{\max}(t) = 0.5$)

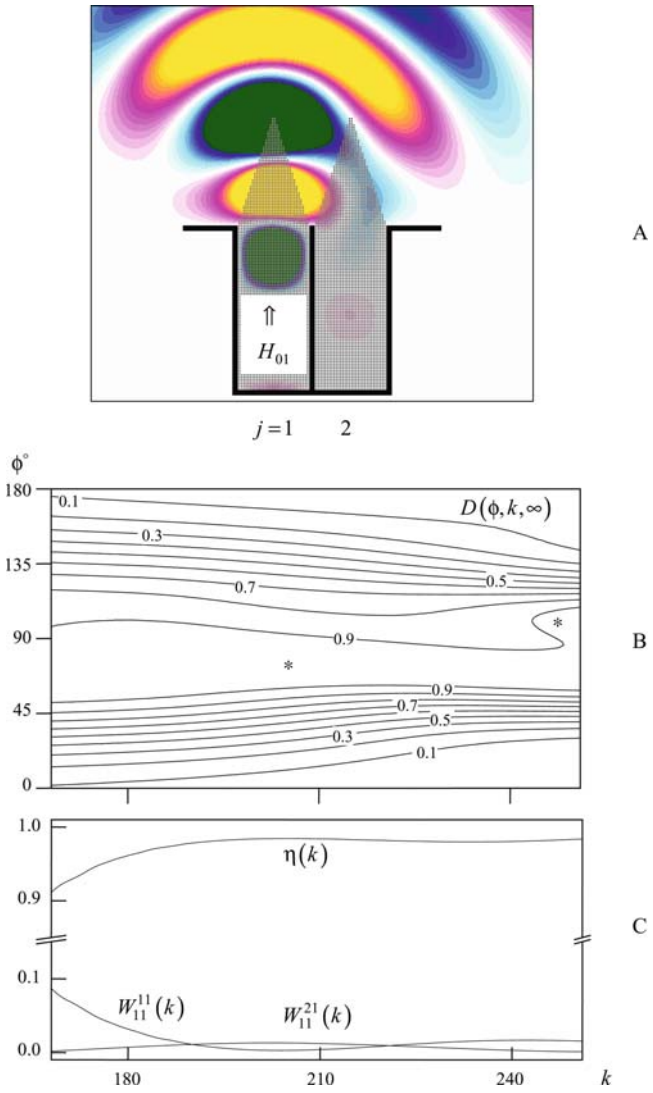

Fig. 4.53 The same as in Fig. 4.52 but for a system of radiating elements 3 ($d = 0$)
Look: 4-53-A.exe

and its efficiency [$\bar{\zeta} \approx 0.95$ (in the case A), $\bar{\zeta} \approx 0.955$ (B), and $\bar{\zeta} \approx 0.957$ (C)]. Here, $\phi_{0.5}(k)$ is the width of the pattern main lobe at the level $D(\phi,k,\infty) = 0.5$, while the integrated efficiency

$$\bar{\zeta} = \frac{1}{K_2 - K_1} \int_{K_1}^{K_2} \zeta(k)\, dk$$

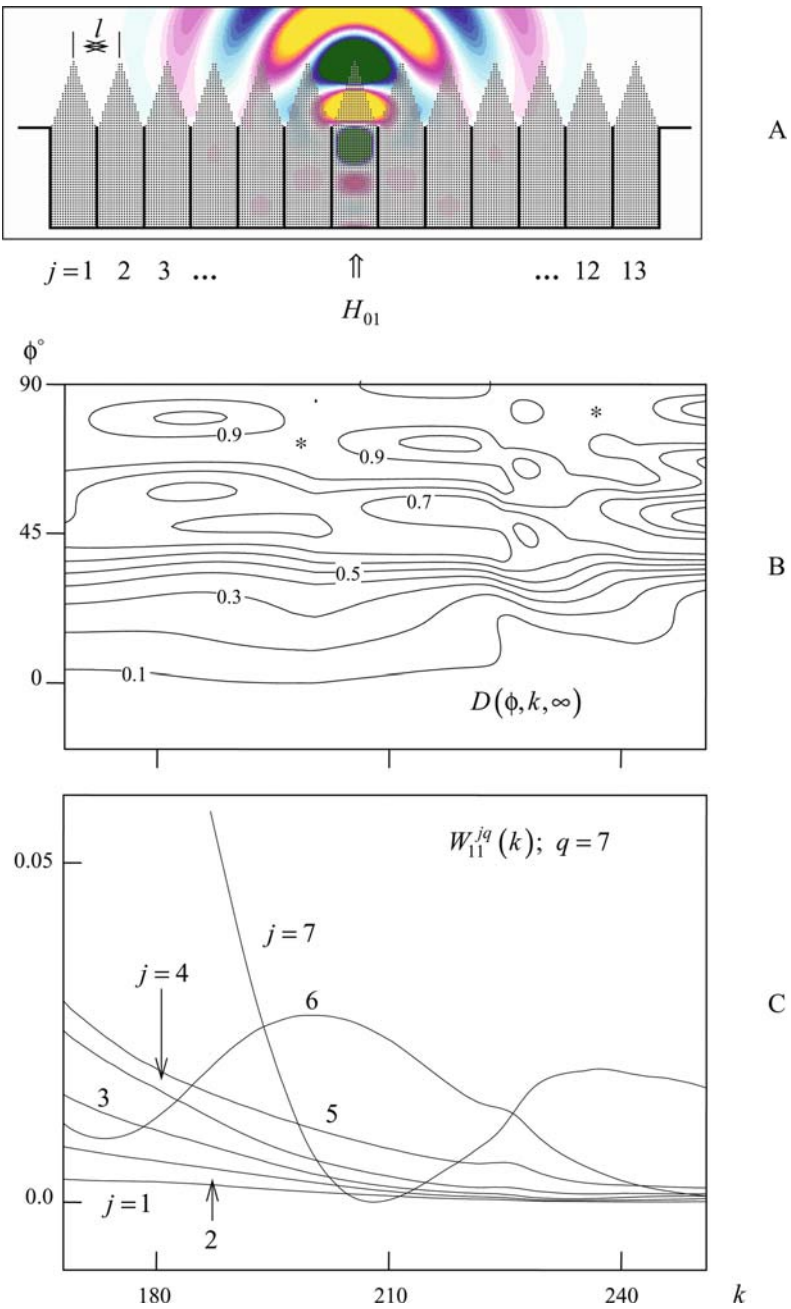

Fig. 4.54 The excitation of a system of 13 radiating elements 3 by the pulsed H_{01}-wave (4.140), $q = 7$: (**a**) The $E_x(g,t)$ spatial distribution, $g \in \mathbf{Q}_L$, $t = 1.1$; (**b**) radiation pattern $D(\phi,k,\infty)$ in the frequency band $168 \le k \le 251$; (**c**) the coefficients of the power coupling between the active ($j = 7$) and passive ($j = 1,2,\ldots,6$) elements

Look: 4-54-A.exe – the $E_x(g,t)$ spatial–time distribution, $g \in \mathbf{Q}_L$ at the time $1.0 < t < 1.3$ (the pulse major part crosses the computational space $\mathbf{Q}_L$; $U_{\max}(t) = 0.5$)

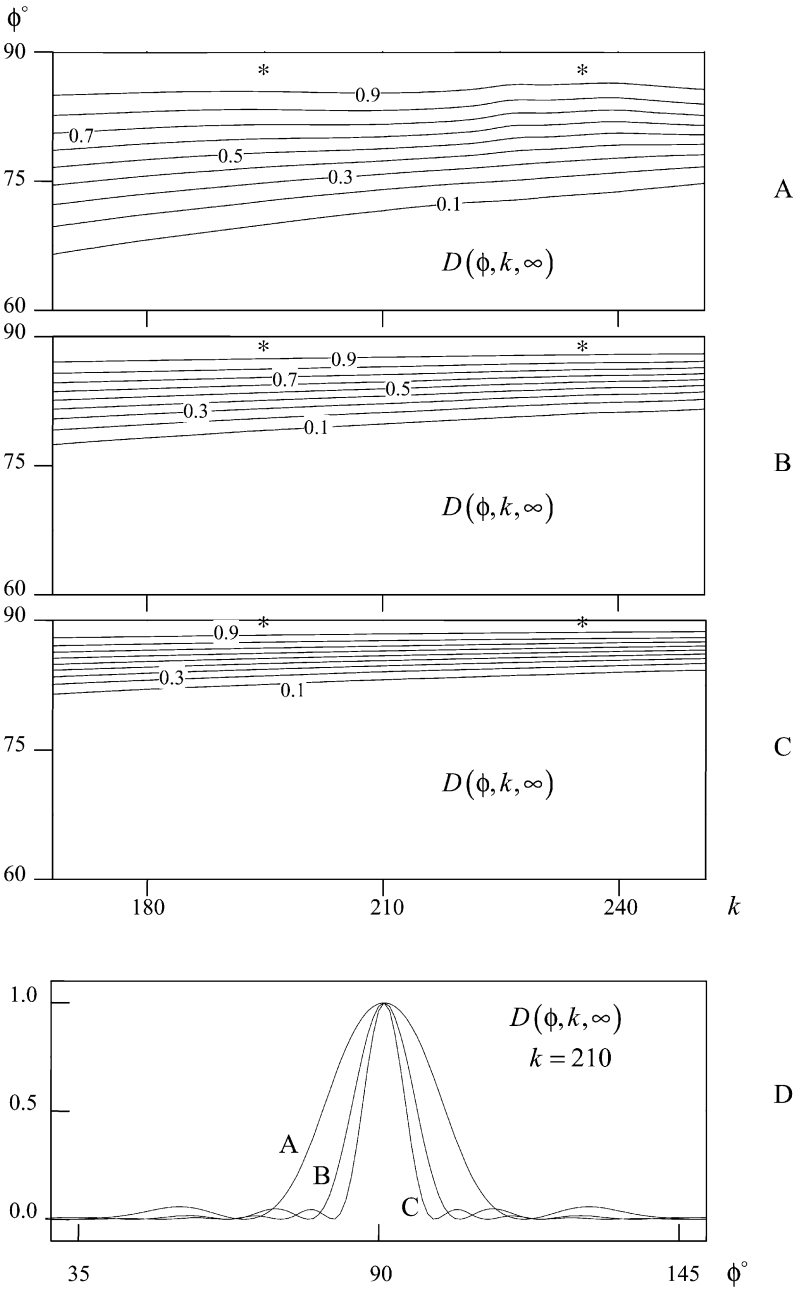

Fig. 4.55 The radiation patterns of a system of 13 radiating elements 3. Pulsed waves (4.140) excite (**a**) 5 central elements; (**b**) 9 central elements; and (**c**) all the 13 elements
Look: 4-55-A.exe, 4-55-B.exe и 4-55-C.exe – the $E_x(g,t)$ spatial–time distribution, $g \in \mathbf{Q}_L$ at the time $1.0 < t < 1.3$ ($U_{\max}(t) = 0.5$)

and the efficiency $\zeta(k)$ clearly generalizes the characteristics $\bar{\eta}$ [see formula (4.141)] and $\eta(k)$ in the case of the excitation of compact grating structures from two, three, and more feeding waveguides.

A failure of one or two radiating elements has practically no effect on the array radiation pattern (see Fig. 4.56). We simulate these regimes by cutting off the energy supply from the corresponding feeding waveguides. At frequency $k = 210$, the main lobe width $\phi_{0.5}(k)$ changes within 0.2°, the side lobes level never exceeds $D(\phi,k,\infty) = 0.1$ for all the cases considered.

Now let the first element of the array be excited by a wave (4.140), while the remaining ones ($q = 2,3,\ldots,13$) are excited by the $U_1^{i(q)}(g,t)$ waves such that $v_{11}\left(g \in \mathbf{L}_q, t + \Delta t\right) = v_{11}\left(g \in \mathbf{L}_{q-1}, t\right)$. One easily checks that in this case, the sinusoidal H_{01}-waves $\tilde{U}_1^{i(q)}(g,k) \leftrightarrow U_1^{i(q)}(g,t)$ [see transformations (1.19) and (4.113)] obey the following quasi-periodicity condition:

$$\tilde{U}_1^{i(q)}\left(g \in {}_q\mathbf{Q}, k\right) = \mathrm{e}^{ik\Delta t}\tilde{U}_1^{i(q-1)}\left(g \in {}_{q-1}\mathbf{Q}, k\right). \tag{4.142}$$

For an infinite array, the fulfillment of condition (4.142) provides an $\alpha_0 = \phi - 90°$ deflection of the beam along which the fundamental spatial harmonic $A_0(k)\exp\left[i\left(\Phi_0 y + \Gamma_0 z\right)\right]$, $\Phi_0 = 2\pi\Phi/l = k\Delta t/l$, propagates in the radiation zone $z > 0$ of the structure [see (4.138) and Sections 1.1.4 and 1.2.1]. The angle $\alpha_0 = \phi - 90°$ is such that

$$-l\sin\alpha_0 = \Delta t. \tag{4.143}$$

Based on relationship (4.143), we model the finite array main lobe steering by time domain methods. In the frequency range $168 \le k \le 251$ and for scan angles $45° \le \phi \le 135°$ (see Figs. 4.57, 4.58 and 4.59), for which the major parameters of the periodic structure have been determined, the radiation efficiency $\zeta(k)$ does not fall below $\zeta(k) = 0.9$. The width $\phi_{0.5}(k)$ of the pattern main lobe varies from 7.0° ($k = 251$, $\phi = 0$) to 13.9° ($k = 168$, $\phi = 90° \pm 45°$). The directivity $\bar{\phi}(k)$ is in full agreement with the predicted value: $\bar{\phi}(k) = 75°$ for $\Delta t = \sin(15°)\,l \approx 0.36$, $\bar{\phi}(k) = 60°$ for $\Delta t = \sin(30°)\,l \approx 0.7$, and $\bar{\phi}(k) = 45°$ for $\Delta t = \sin(45°)\,l \approx 0.99$. The results of this kind encourage further efforts in the modeling of the considered phased array, giving cause for formulating and working out new applied problems. Thus, it could be natural to continue with the analysis and synthesis of the so-called ideal pulse antennas [193, 221] that can directionally radiate broadband radio signals occupying a frequency band up to 40% wide. But now, we go beyond the bounds indicated in the problem formulation with respect to parameters k and (or) ϕ and examine the resulting consequences of such a step. For $\Delta t = \sin(60°)\,l \approx 1.21$ (see Fig. 4.60), the pattern main lobe deflects from the normal through a given angle ($\bar{\phi}(k) = 30°$). The integrated radiation efficiency, which before grew monotonously with Δt from $\bar{\zeta} \approx 0.957$ for $\Delta t = 0$ to $\bar{\zeta} \approx 0.983$ for $\Delta t = 0.99$, now is evidently smaller ($\bar{\zeta} \approx 0.92$). At the short-wavelength piece of the considered range, a side lobe appears. As k increases, it is increasingly more separated from the array plane and concentrates all the more radiation energy into

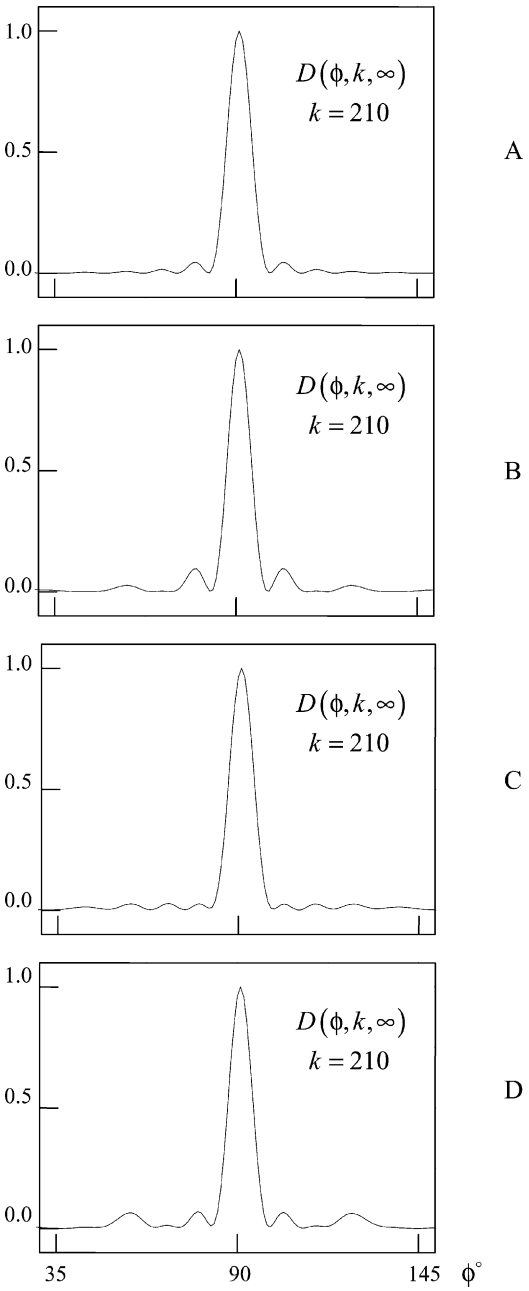

Fig. 4.56 (continued) The radiation patterns of a system of 13 radiating elements 3 at the frequency $k = 210$. Pulsed waves (4.140) excite (**a**) all the 13 elements; (**b**) all the elements but the central one; (**c**) all the elements but the third; and (**d**) all the elements but the central and the third ones

Look: 4-56-B.exe, 4-56-C.exe и 4-56-D.exe – the $E_x(g,t)$ spatial–time distribution, $g \in \mathbf{Q}_L$ at the time $1.0 < t < 1.3$ ($U_{\max}(t) = 0.5$)

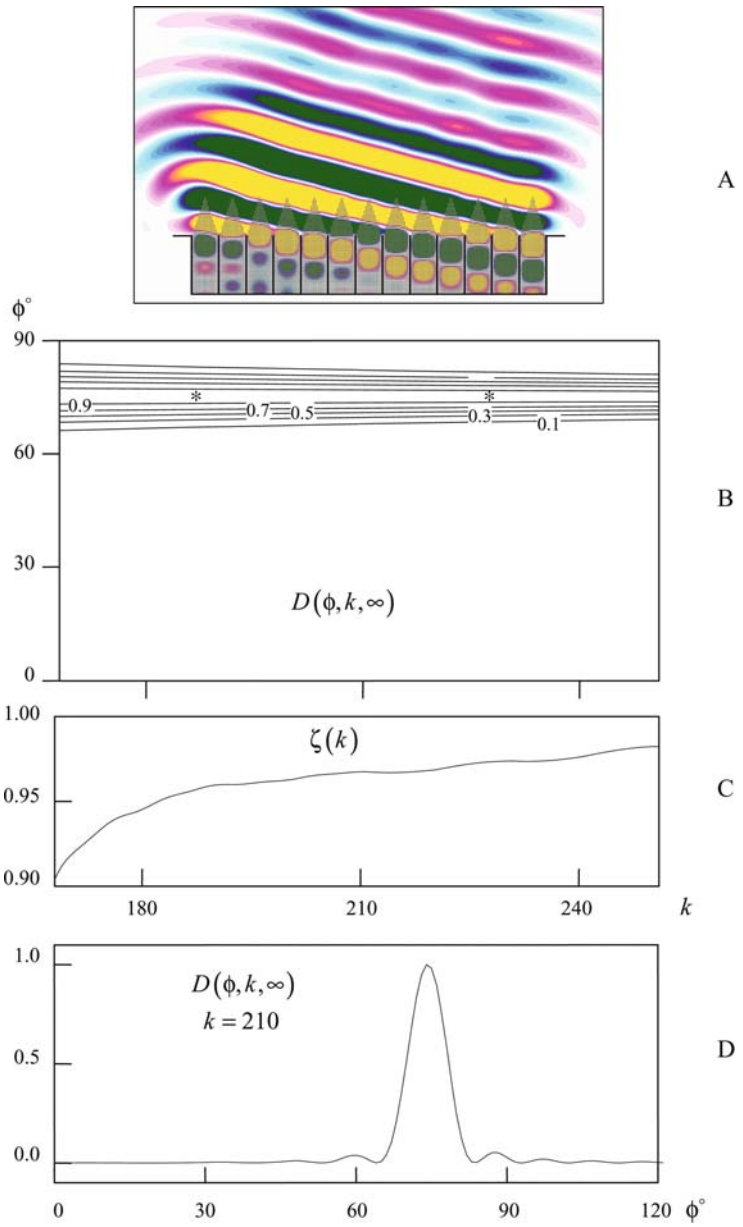

Fig. 4.57 The phased array excitation by a set of pulsed waves $U_1^{i(q)}(g,t)$ satisfying condition (4.142), $\Delta t = \sin(15°)\, l \approx 0.36$: (**a**) The $E_x(g,t)$ spatial distribution, $g \in \mathbf{Q}_L$, $t = 1.1$; (**b**) radiation pattern $D(\phi,k,\infty)$; (**c**) array efficiency in the frequency band $168 \le k \le 251$; and (**d**) radiation pattern $D(\phi,k,\infty)$ at the frequency $k = 210$

Look: 4-57-A.exe – the $E_x(g,t)$ spatial–time distribution, $g \in \mathbf{Q}_L$ at the time $1.0 < t < 1.3$ (the major part of the radiated pulse crosses the computational space $\mathbf{Q}_L$; $U_{\max}(t) = 0.5$)

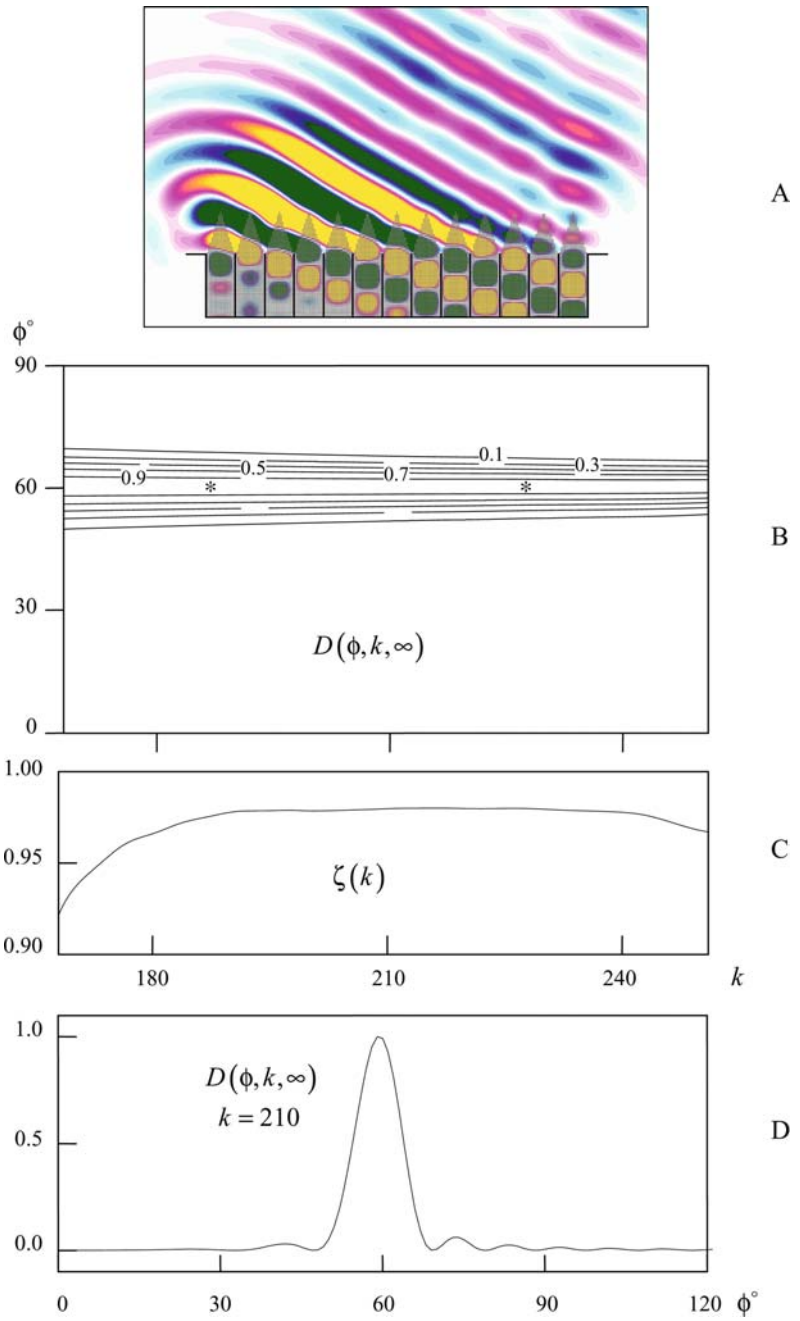

Fig. 4.58 The same as in Fig. 4.57 but for $\Delta t = \sin(30°)\, l \approx 0.7$
Look: 4-58-A.exe

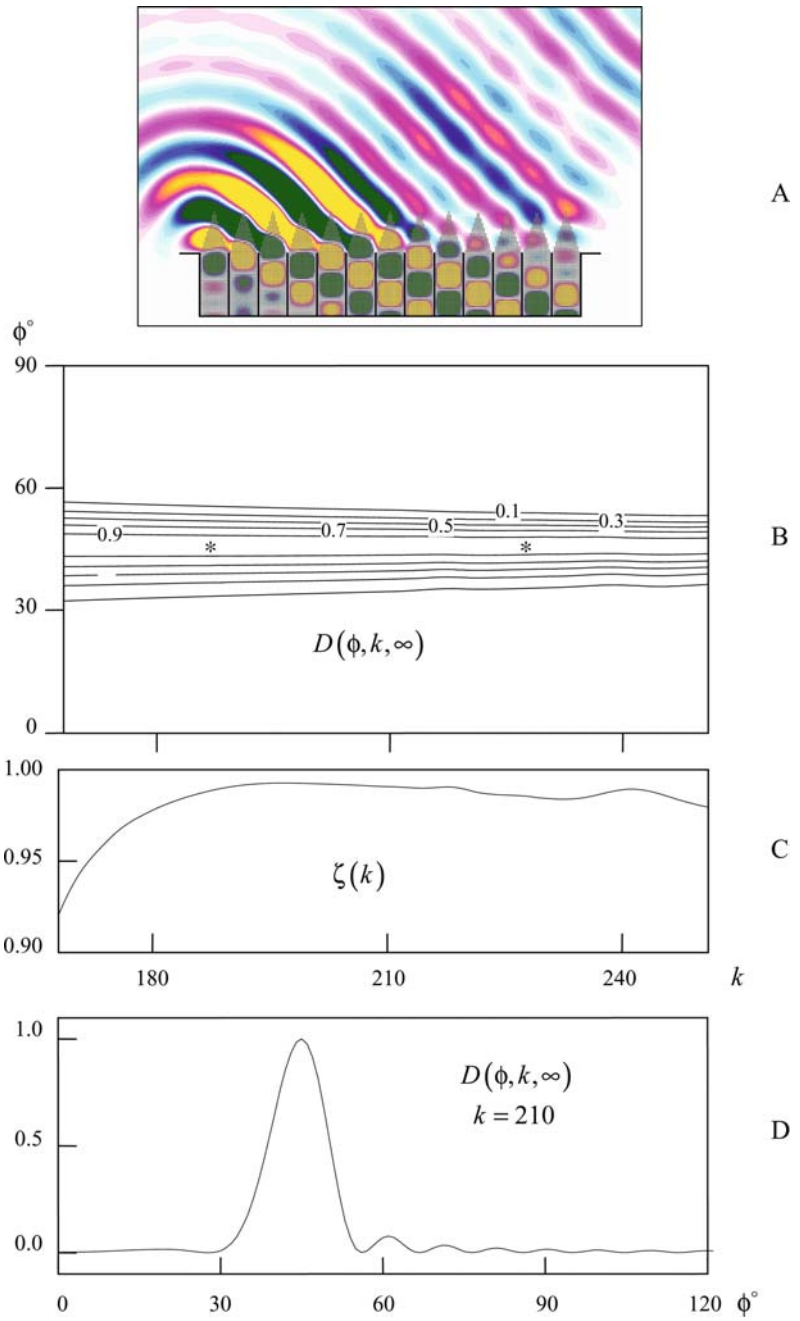

Fig. 4.59 The same as in Fig. 4.57 but for $\Delta t = \sin(45°)\, l \approx 0.99$
Look: 4-59-A.exe

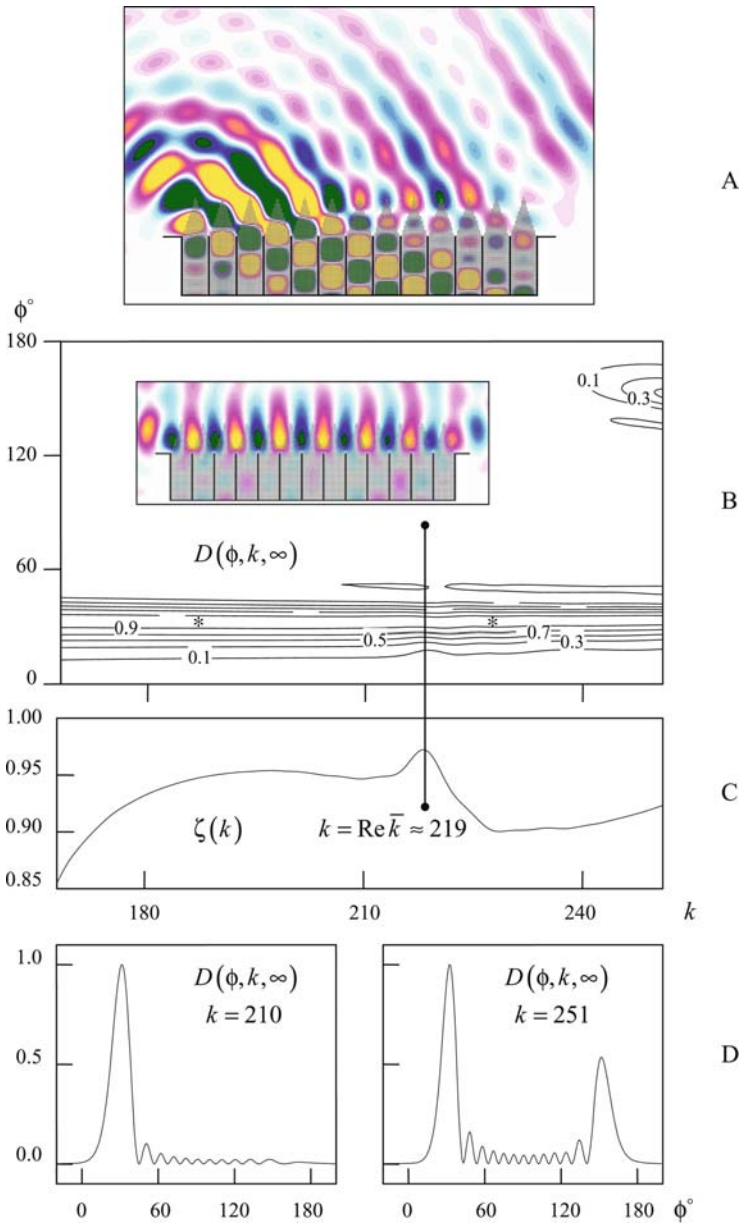

Fig. 4.60 The phased array excitation by a set of pulsed waves $U_1^{i(q)}(g,t)$ satisfying condition (4.142), $\Delta t = \sin(60°)\, l \approx 1.21$: (**a**) The $E_x(g,t)$ spatial distribution; $g \in \mathbf{Q}_L$, $t = 1.1$; (**b**) radiation pattern $D(\phi,k,\infty)$; (**c**) array efficiency in the frequency band $168 \le k \le 251$; (**d**) radiation patterns $D(\phi,k,\infty)$ at the frequencies $k = 210$ and $k = 251$

Look: 4-60-A.exe – the $E_x(g,t)$ spatial–time distribution, $g \in \mathbf{Q}_L$ at the time $1.0 < t < 1.3$ (the major part of the radiated pulse crosses the computational space $\mathbf{Q}_L$; $U_{\max}(t) = 0.5$)

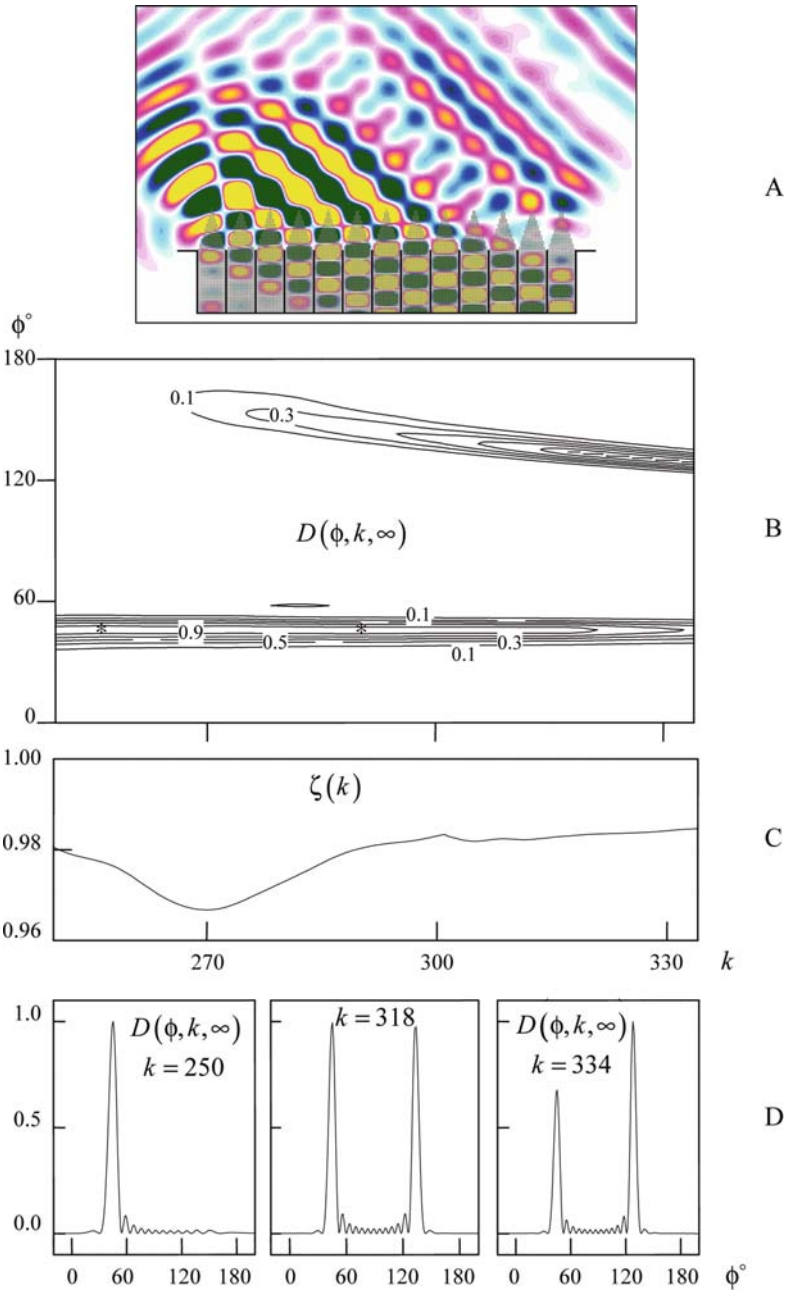

Fig. 4.61 The same as in Fig. 4.60 but for a set of pulsed waves $U_1^{i(q)}(g,t)$ occupying the frequency band $250 < k < 334$ and for $\Delta t = \sin(45°)\, l \approx 0.99$
Look: 4-61-A.exe

itself. In the field of the infinite periodic structure [see formula (4.138)] this lobe complies with the minus first spatial harmonic $A_{-1}(k)\exp\left[i\left(\Phi_{-1}y+\Gamma_{-1}z\right)\right]$. For frequencies k above the threshold $k_{-1}^{+}\approx 241$, this harmonic propagates in the radiation zone $z>0$ of the structure without attenuation and goes away from it at an angle α_{-1} such (see Fig. 4.50b) that $\sin\alpha_{-1}\approx 2\pi/kl-0.866$. At the frequency $k=\mathrm{Re}\bar{k}\approx 219$, the compact grating structure maintains slightly attenuating free oscillations of the field (see Fig. 4.60b for the spatial distribution of $E_x(g,t)$, $t=3.0$). Their excitation sharply enhances the array efficiency and narrows the main lobe somewhat.

For $\Delta t=\sin(45^\circ)\,l\approx 0.99$, the passage to the higher frequencies $250<k<334$ (see Fig. 4.61) is accompanied by the conversion of the decaying H_{02}-wave of the feeding parallel-plate waveguides into a propagating wave ($k>k_2\approx 301$), and also a side lobe appears that complies with the minus first spatial harmonic in the radiation field of the infinite periodic structure ($k_{-1}^{+}\approx 263$). Near the cutoff of the H_{02}-wave, no substantial changes in the array characteristics are observed. The side lobe level goes up with k. Until $k=318$, $\bar{\phi}(k)=45^\circ$. Then the side lobe takes over the part of the main lobe, and $\bar{\phi}(k)\approx 90^\circ+\alpha_{-1}(k)$.

Chapter 5
Finite Scale Homogenization of Periodic Bianisotropic Structures

Abstract This chapter explains how a composite material with a periodic microstructure can be modeled with effective material parameters in the low-frequency limit. In particular, we treat the problem of how to compute the material parameters when the scale of the microstructure is finite compared to the applied wavelength. For lossless anisotropic media, a self-adjoint eigenvalue problem can be formulated to compute the relevant material parameters, whereas a singular value decomposition of Maxwell's equations can be used to treat the general lossy bianisotropic case. The fundamental idea is the number of degrees of freedom: homogenization is possible precisely when the electromagnetic field can only be excited (or observed) corresponding to the degrees of freedom possible in a homogeneous material. When the scale difference is not large, this requires spatial dispersion in the homogenized model.

The chapter deals with the theory of periodic media in the low-frequency limit, where the period is small compared to the wavelength. We treat here the bulk homogenization of composite materials, where the material parameters of the component materials can have bianisotropic properties.

Bulk homogenization concerns under which circumstances the periodic structure can be replaced by a fictitious homogeneous material while maintaining the same large-scale scattering characteristics. In the limit where the scale difference between the period and the wavelength is infinite, this is the classical homogenization problem, which has a long history in many areas of physics, engineering, and mathematics. An introduction to the mathematics is given in [222], a broad overview of applications is given in [24, 223, 224], whereas mathematical rigor and many explicitly solvable cases are found in [225, 226].

We demonstrate how this can be extended to the case where the period and the wavelength are comparable to each other, which corresponds better to the practical problems encountered in real-life applications. Similar problems have been attacked by other authors [227–233], usually in a scalar setting where the effective material parameters can be treated in the effective mass approximation as a derivative of the energy bands of the structure.

Y.K. Sirenko, S. Ström (eds.), *Modern Theory of Gratings*, Springer Series in Optical Sciences 153, DOI 10.1007/978-1-4419-1200-8_5,

For lossless anisotropic media, a self-adjoint eigenvalue problem is formulated to compute the relevant material parameters, whereas a singular value decomposition of Maxwell's equations is used to treat the general lossy bianisotropic case. The mathematical methods employed treat the material case as a perturbation of the vacuum case, which can be solved analytically, and it is shown that important mathematical properties such as compactness of relevant operators can be derived from this perturbation approach. The fundamental idea is the number of degrees of freedom: homogenization is possible precisely when the electromagnetic field can only be excited (or observed) corresponding to the degrees of freedom possible in a homogeneous material, that is, the different polarizations of the electric and magnetic fields. When the scale difference is not infinite, this implies spatial dispersion in the homogenized model. At the end of the chapter, we give examples of results for a few explicit microstructures.

5.1 Fundamental Ideas

The object of this chapter is to demonstrate a method to compute homogenized material parameters for a structure being periodic in three dimensions. The typical application is to compute effective material parameters for composite materials, where the size of the microstructure of the composite is not necessarily infinitely small compared to the free space wavelength.

The fundamental idea is based on the number of degrees of freedom in a homogeneous material. In a homogeneous material, we can in principle only affect the polarizations of the electric and magnetic fields. A pair of electric and magnetic excitation vectors $\vec{E}$ and $\vec{H}$ then have a one-to-one correspondence to a pair of response vectors $\vec{D}$ and $\vec{B}$ according to

$$\begin{pmatrix} \vec{D} \\ \vec{B} \end{pmatrix} = \begin{pmatrix} \varepsilon_0 \bar{\bar{\varepsilon}} & c^{-1} \bar{\bar{\xi}} \\ c^{-1} \bar{\bar{\zeta}} & \mu_0 \bar{\bar{\mu}} \end{pmatrix} \begin{pmatrix} \vec{E} \\ \vec{H} \end{pmatrix},$$

where $c^{-1} = \sqrt{\varepsilon_0 \mu_0}$ is the inverse of the speed of light in vacuum. The material parameters are in general analytic functions of frequency in the complex upper half plane, due to restrictions derivable from causality and energy conservation. This means they satisfy relations similar to the classical Kramers–Kronig relations [234]. In periodic heterogeneous media, the situation is rather that a pair of excitation fields can excite a multitude of possible responses, corresponding to the free oscillations, or eigenwaves, in the structure. The higher the frequency of the excitation, the more modes can be excited.

However, when the signal has a limited frequency content, only a limited number of eigenwaves can be excited, or rather, carry an energy flow. In classical homogenization, the frequency is thought of as being asymptotically close to zero, making it difficult to incorporate dynamic effects of the structure when calculating the material response. In this chapter, we demonstrate that the requirement from classical

homogenization can be relaxed, and we can allow for frequencies high enough to correspond to a wavelength comparable with the periodicity of the structure.

Taking a look first at the classical case of homogenizing permittivity in the limit where the applied wavelength is infinite compared to the microstructure, a physical definition of this quantity can be taken as

$$\langle \vec{D} \rangle = \left\langle \bar{\bar{\varepsilon}} \vec{E} \right\rangle = \bar{\bar{\varepsilon}}^{hom} \langle \vec{E} \rangle,$$

where $\langle ... \rangle$ is a suitably defined averaging operation, smoothing out the small details of the field associated with the microstructure. If the number of degrees of freedom of the electric field is reduced to three, we could write it as

$$\vec{E}(g) = \sum_{n=1}^{3} c_n \vec{E}_n(g), \tag{5.1}$$

where $\vec{E}_n(g)$ are the modes representing the degrees of freedom. The modes can be derived from a local problem, typically defined in a periodic unit cell. When the applied wavelength is infinite compared to the unit cell, the local problem is static and we have $\mathrm{rot}\vec{E} = 0$ which implies $\vec{E} = \vec{E}_0 - \mathrm{grad}\phi$, where $\vec{E}_0$ is a constant vector, and ϕ is a periodic potential with zero mean value. This means that the mean value of the electric field is $\langle \vec{E} \rangle = \vec{E}_0$, which is the large-scale electric field, whereas -gradϕ is the microscopic field, necessary to resolve the boundary conditions in the microstructure. The potential is determined for each fixed $\vec{E}_0$ from the elliptic partial differential equation

$$\mathrm{div}\vec{D} = \mathrm{div}\left[\bar{\bar{\varepsilon}} \left(\vec{E}_0 - \mathrm{grad}\phi \right) \right] = 0$$

and the homogenized permittivity is given by the relation

$$\langle \vec{D} \rangle = \left\langle \bar{\bar{\varepsilon}} \left(\vec{E}_0 - \mathrm{grad}\phi \right) \right\rangle = \bar{\bar{\varepsilon}}^{hom} \vec{E}_0$$

To generalize the classical homogenization, we look for local problems taking the full Maxwell's equations into account. It can then be shown that the modes have some useful orthogonality properties. If these carry over to the averaged vectors in the respect that either $\left(\left\langle \bar{\bar{\varepsilon}} \vec{E}_m \right\rangle \cdot \langle \vec{E}_n^* \rangle \right) = 0$ or $\left(\langle \vec{E}_m \rangle \cdot \langle \vec{E}_n^* \rangle \right) = 0$ when $m \neq n$, we can write up the homogenized matrix as either

$$\bar{\bar{\varepsilon}}^{hom} = \sum_{n=1}^{3} \frac{\left\langle \bar{\bar{\varepsilon}} \vec{E}_n \right\rangle \left\langle \bar{\bar{\varepsilon}} \vec{E}_n \right\rangle^H}{\left\langle \bar{\bar{\varepsilon}} \vec{E}_n \right\rangle^H \langle \vec{E}_n \rangle} \text{ or } \bar{\bar{\varepsilon}}^{hom} = \sum_{n=1}^{3} \frac{\left\langle \bar{\bar{\varepsilon}} \vec{E}_n \right\rangle \langle \vec{E}_n \rangle^H}{\langle \vec{E}_n \rangle^H \langle \vec{E}_n \rangle}$$

depending on which kind of orthogonality is available. Here, $\langle \vec{E} \rangle$ is identified as a column vector and $\langle \vec{E} \rangle^H$ is its hermitian transpose, i.e., the product in the nominator is a dyadic product that is identified as a matrix, whereas the product in the

denominator is a scalar. The correctness of these representations can be checked by simply inserting the expansion (5.1) in $\left\langle \bar{\bar{\varepsilon}}\vec{E} \right\rangle$ and $\langle \vec{E} \rangle$ and use the orthogonality assumptions. The remainder of this chapter will show how to define the averaging operator, how to define suitable modes, and that only a limited number of these modes are excited when the scale of the microstructure becomes small. More precisely, at most six modes, corresponding to the polarizations of the electric and the magnetic fields, will be needed assuming that the currents driving the fields are band-limited in frequency.

5.2 Some Mathematical Properties of Maxwell's Operator

Here, we present some important mathematical properties of Maxwell's operator with periodic boundary conditions in all three dimensions. Most importantly, the compactness of the resolvent operator aids us in formulating decompositions based either on eigenvectors/eigenvalues for lossless media, or a singular value decomposition for general dispersive media.

We start by formulating a six-vector notation which reduces the length and complexity of the chapter. The electromagnetic field is treated as one unified field $\vec{U} = \left\{ \varepsilon_0^{1/2}\vec{E}, \mu_0^{1/2}\vec{H} \right\}^T$, where index T denotes the transpose operation, which permits the interpretation of $\vec{U}$ as a column vector with six elements if $\vec{E}$ and $\vec{H}$ are interpreted as column vectors with three elements. The scaling with the square root of the permittivity and permeability of vacuum makes both the electric and magnetic part of $\vec{U}$ have the same physical dimension of square root of power density. Occasional use of the decomposition $\vec{U}_e = \varepsilon_0^{1/2}\vec{E}$ and $\vec{U}_h = \mu_0^{1/2}\vec{H}$ will be made. The constitutive relation is

$$\begin{pmatrix} \varepsilon_0^{-1/2}\vec{D} \\ \mu_0^{-1/2}\vec{B} \end{pmatrix} = \begin{pmatrix} \bar{\bar{\varepsilon}} & \bar{\bar{\xi}} \\ \bar{\bar{\zeta}} & \bar{\bar{\mu}} \end{pmatrix} \begin{pmatrix} \varepsilon_0^{1/2}\vec{E} \\ \mu_0^{1/2}\vec{H} \end{pmatrix} = \bar{\bar{\bar{M}}}\vec{U}$$

where the scaling of the fluxes $\vec{D}$ and $\vec{B}$ makes all the entries in the material matrix $\bar{\bar{\bar{M}}}$ be dimensionless. The curl operators in Maxwell's equations are denoted by

$$\mathrm{rot} J\vec{U} = \begin{pmatrix} 0 & -\mathrm{rot} \\ \mathrm{rot} & 0 \end{pmatrix} \begin{pmatrix} \vec{U}_e \\ \vec{U}_h \end{pmatrix} = \begin{pmatrix} -\mathrm{rot}\vec{U}_h \\ \mathrm{rot}\vec{U}_e \end{pmatrix}$$

so that Maxwell's equations can be compactly written as $\mathrm{rot} J\vec{U} - ik\bar{\bar{\bar{M}}}\vec{U} = -\vec{F}$, where K is the wave number in vacuum. The excitation currents $\vec{F} = \left\{ \mu_0^{1/2}\vec{J}_e, \varepsilon_0^{1/2}\vec{J}_h \right\}$ satisfy the equation of continuity

$$\mathrm{div}\vec{F} = \begin{pmatrix} \mathrm{div}\mu_0^{1/2}\vec{J}_e \\ \mathrm{div}\varepsilon_0^{1/2}\vec{J}_h \end{pmatrix} = ik \begin{pmatrix} \varepsilon_0^{-1/2}\rho_e \\ \mu_0^{-1/2}\rho_h \end{pmatrix}.$$

Even though the magnetic current and charge density, $\tilde{J}_h$ and $\tilde{\rho}_h$, can be argued to be zero on physical grounds, we still include them here to keep an as general formulation as possible. In a Born-series approach to scattering, they appear in a very natural way, typically $\vec{F} = -ik\left(\overline{\overline{M}} - \overline{\overline{M}}_0\right)\vec{U}_0$, where $\vec{U}_0$ is an applied wave field propagating in a background medium $\overline{\overline{M}}_0$.

We now turn to the description of periodic media. The physical unit cell is denoted by $\mathbf{G}$, and the reciprocal unit cell is $\tilde{\mathbf{G}}$. A vector in the physical unit cell is denoted as $g = \{x,y,z\} \in \mathbf{G}$, and a vector in the reciprocal unit cell is denoted as $\gamma = \{\gamma_x,\gamma_y,\gamma_z\} \in \tilde{\mathbf{G}}$. The three-dimensional space $\mathbf{R}^3$ is tiled by translating the unit cell $\mathbf{G}$ by all possible lattice vectors $g_{n_1,n_2,n_3} = n_1\vec{a}_1 + n_2\vec{a}_2 + n_3\vec{a}_3$, where $\{\vec{a}_1,\vec{a}_2,\vec{a}_3\}$ can be viewed as the sides of the unit cell $\mathbf{G}$. The typical length of one of these vectors is $2\pi a$. The lattice vectors in reciprocal space are represented using the basis $\{\vec{b}_1,\vec{b}_2,\vec{b}_3\}$, with the typical length $1/a$. The two sets of bases are related by $\left(\vec{a}_m \cdot \vec{b}_n\right) = 2\pi\delta_n^m$ where δ_n^m is the Kronecker delta. Using the Floquet–Bloch theorem [235, 236] and the Laplace transform in time, any square integrable field can be written as

$$\vec{U}(g,t) = \frac{1}{2\pi}\int_{i\alpha-\infty}^{i\alpha+\infty}\frac{1}{\left|\tilde{\mathbf{G}}\right|}\int_{\tilde{\mathbf{G}}} \mathrm{e}^{i[(\gamma\cdot g)-kt]}\tilde{U}(g,\gamma,k)\,dv_\gamma dk,$$

where α is large enough so that all poles of the field $\tilde{U}(g,\gamma,k)$ are below the integration path. The Bloch amplitude $\tilde{U}(g,\gamma,k)$ is a $\mathbf{G}$-periodic function of g, and $\exp\left[i(\gamma\cdot g)\right]\tilde{U}(g,\gamma,k)$ is a $\tilde{\mathbf{G}}$-periodic function of γ. It can be expressed in terms of the spatio-temporal field $\vec{U}(g,t)$ as

$$\tilde{U}(g,\gamma,k) = \int_0^\infty \sum_{n_1,n_2,n_3} \vec{U}\left(g + g_{n_1,n_2,n_3},t\right)\mathrm{e}^{i\left[kt-(\gamma\cdot(g+g_{n_1,n_2,n_3}))\right]}dt.$$

We prefer to express the fields in terms of the $\mathbf{G}$-periodic Bloch amplitude $\tilde{U}$ instead of quasi-periodic functions $\exp\left[i(\gamma\cdot g)\right]\tilde{U}(g,\gamma,k)$ in this chapter, since we later on are going to average the fields over the unit cell and it is then very natural to work with the Bloch amplitude. The typical effect is that the nabla operator (divergence) is shifted by $i\gamma$, according to

$$\mathrm{div}\left(\exp\left[i(\gamma\cdot g)\right]\tilde{U}\right) = \exp\left[i(\gamma\cdot g)\right](\mathrm{div} + (i\gamma\cdot))\,\tilde{U}.$$

We use two function spaces in this chapter, each with $\mathbf{G}$-periodic boundary conditions:

$$\mathbf{X} = \left\{\tilde{U} \in \mathbf{L}_2\left(\mathbf{G};\mathbf{C}^6\right):\ \exists(z,\tilde{z}) \in \mathbf{C}^2,\quad (\mathrm{div} + (i\gamma\cdot))\,\tilde{U} = \begin{pmatrix} z\varepsilon_0^{-1/2}\tilde{\rho}_e \\ \tilde{z}\mu_0^{-1/2}\tilde{\rho}_h \end{pmatrix}\right\},$$

$$\mathbf{Y} = \left\{ \tilde{U} \in \mathbf{L}_2\left(\mathbf{G};\mathbf{C}^6\right) : \quad \exists\,(z,\tilde{z}) \in \mathbf{C}^2, \quad (\mathrm{div} + (i\gamma\cdot))\left[\overline{\overline{M}}\tilde{U}\right] = \begin{pmatrix} z\varepsilon_0^{-1/2}\tilde{\rho}_e \\ \tilde{z}\mu_0^{-1/2}\tilde{\rho}_h \end{pmatrix} \right\}.$$

Here, $\mathbf{L}_2\left(\mathbf{G};\mathbf{C}^6\right)$ is the space of square integrable functions taking values in $\mathbf{C}^6$. The shift of the nabla operator means that Maxwell's equations for the Bloch amplitudes are $\left(\mathrm{rot} + \left[i\gamma\times\right]\right) J\tilde{U} - ik\overline{\overline{M}}\tilde{U} = -\tilde{F}$. When considering the function spaces $\mathbf{X}$ and $\mathbf{Y}$, it is convenient to use the notation

$$\left(\tilde{U},\tilde{V}\right) = \frac{1}{|\mathbf{G}|}\int_{\mathbf{G}} \left(\vec{U}\,(g)\cdot\vec{V}^*\,(g)\right) dv_g$$

for the scalar product over the physical unit cell $\mathbf{G}$, and

$$\left\langle \tilde{U} \right\rangle = \frac{1}{|\mathbf{G}|}\int_{\mathbf{G}} \tilde{U}\,(g)\, dv_g \tag{5.2}$$

for the mean value of the field $\tilde{U}$ over the unit cell. Note that when taking the mean value of the Bloch amplitude, the origin of the unit cell is irrelevant since the Bloch amplitude is periodic. Had we taken the mean value of the quasi-periodic function $\exp\left[i\,(\gamma\cdot g)\right]\tilde{U}\,(g,\gamma,k)$ the result would not be translation invariant.

5.2.1 Vacuum Case

We start by considering the source free vacuum case, where Maxwell's equations simplify to

$$\left(\mathrm{rot} + \left[i\gamma\times\right]\right) J\tilde{U} = ik\tilde{U}.$$

This can be considered as an eigenvalue problem for the (bi)curl operator in the left-hand side. The solutions to this equation are easily characterized using a Fourier series representation, and the following statement is easily shown using explicit calculations [237].

Statement 5.1 *The resolvent operator*

$$R_0(k) = \left[\left(\mathrm{rot} + \left[i\gamma\times\right]\right) J - ik\right]^{-1} : \quad \mathbf{X} \to \mathbf{X}$$

is a compact operator for all $k \in \mathbf{C}$ in the resolvent set; i.e., when $R_0(k)$ is bounded, it is also compact. Furthermore, there exists a number $\tilde{k} \in \mathbf{R}^1$, such that $iR_0(\tilde{k})$ is a compact, self-adjoint operator.

It is important to consider the resolvent as an operator on $\mathbf{X}$. If we consider it on the entire space $\mathbf{L}_2\left(\mathbf{G};\mathbf{C}^6\right)$, the resolvent becomes proportional to the identity operator on the subspace consisting of all gradients, since this is the null space of the curl operator. Since the identity operator is compact only on finite-dimensional spaces,

we need the divergence condition in the definition of $\mathbf{X}$ to restrict the dimension of this space. With the divergence condition $(\mathrm{div} + (i\gamma\cdot))\,\tilde{U} = \left[z\varepsilon_0^{-1/2}\tilde{\rho}_e, \tilde{z}\mu_0^{-1/2}\tilde{\rho}_h\right]^T$ for some complex constants z and $\tilde{z}$, at most two linearly independent gradient functions can occur. If the charge densities $\tilde{\rho}_e$ and $\tilde{\rho}_h$ are zero, the only gradient function satisfying the divergence condition is the zero function.

The compactness of the vacuum resolvent constitutes the fundamental result upon which we build our following results. Thanks to the compactness, we know there exist eigenvectors and eigenvalues, and when we have self-adjointness, we also have orthogonality between the eigenvectors. When general bianisotropic material parameters $\overline{\overline{M}}$ are considered, we cannot expect self-adjointness unless the material is lossless.

5.2.2 Material Case

We now show how to use the result for the vacuum operator to deduce information of the material case. The spatial dependence of the material matrix is suppressed in order to emphasize the frequency dependence, that is, when writing $\overline{\overline{M}}(k)$ we really mean $\overline{\overline{M}}(g,k)$.

Statement 5.2 *The generalized resolvent operator*

$$R(k) = \left[\left(\mathrm{rot} + \left[i\gamma\times\right]\right)J - ik\overline{\overline{M}}(k)\right]^{-1} : \quad \mathbf{X} \to \mathbf{Y}$$

is compact for all $k \in \mathbf{C}$ in the resolvent set such that $\overline{\overline{M}}(k)$ is bounded.

Proof. The generalized resolvent operator $R(k)$ can be written in terms of the vacuum resolvent

$$\begin{aligned} R(k) &= \left[\left(\mathrm{rot} + \left[i\gamma\times\right]\right)J - ik\overline{\overline{M}}(k)\right]^{-1} = \left[(R_0(k))^{-1} - ik\left(\overline{\overline{M}}(k) - \overline{\overline{E}}\right)\right]^{-1} \\ &= \left[\overline{\overline{E}} - R_0(k)\,ik\left(\overline{\overline{M}}(k) - \overline{\overline{E}}\right)\right]^{-1} R_0(k), \end{aligned}$$

where $\overline{\overline{E}}$ is the identity matrix. A product of two operators AB is compact if one of the operators is compact and the other is bounded. The operator $\left[\overline{\overline{E}} - R_0(k)\,ik\left(\overline{\overline{M}}(k) - \overline{\overline{E}}\right)\right]^{-1}$ is bounded unless 1 is an eigenvalue of the compact operator $R_0(k)\,ik\left(\overline{\overline{M}}(k) - \overline{\overline{E}}\right)$. It is possible to choose $k = \tilde{k} \in \mathbf{C}$ such that this does not occur. This means $R\left(\tilde{k}\right)$ is compact, and the generalized resolvent equation [238]

$$R(k_1) - R(k_2) = R(k_1)\left(-ik_1\overline{\overline{M}}(k_1) + ik_2\overline{\overline{M}}(k_2)\right)R(k_2)$$

then implies that $R(k)$ is compact for all k in the resolvent set, provided that $\overline{\overline{M}}(k)$ is bounded, which concludes the proof.

Statement 5.2 shows that some fundamental mathematical properties of the vacuum case can be generalized to the material case. The basis of the proof is the fact that the material operator $\overline{\overline{M}}$ is bounded compared to the partial differential operator rot$J$. This is a demonstration of the principle that the well-posedness of a partial differential equation is usually not affected by a change in the model if the principal part, that is, the highest order derivatives are not changed.

5.2.3 Lossless Media: Eigenvalue Decomposition

To gain some intuition about the decomposition of solutions to Maxwell's equations, we start by considering lossless, nondispersive media,

$$\overline{\overline{M}}(g) = \begin{pmatrix} \overline{\overline{\varepsilon}}(g) & 0 \\ 0 & \overline{\overline{\mu}}(g) \end{pmatrix},$$

where the matrices $\overline{\overline{\varepsilon}}$ and $\overline{\overline{\mu}}$ are real-valued, symmetric, and positive definite, but depend on position $g \in \mathbf{G}$. This implies that the generalized resolvent operator $iR(k)$ is self-adjoint for real k, and the eigenvalue problem

$$\left(\text{rot} + \left[i\gamma\times\right]\right) J\tilde{U}_n = ik_n \overline{\overline{M}}(g)\, \tilde{U}_n \tag{5.3}$$

in the function space $\mathbf{Y}$ is well posed for a fixed $\gamma \in \tilde{\mathbf{G}}$. The eigenvectors correspond to waves freely propagating in the periodic structure, representing the natural electromagnetic degrees of freedom in the structure. Using these eigenvectors as a basis, we can expand any square integrable field as

$$\vec{U}(g) = \sum_n \frac{1}{\left|\tilde{\mathbf{G}}\right|} \int_{\tilde{\mathbf{G}}} (\overline{\overline{M}}\tilde{U}, \tilde{U}_n)\tilde{U}_n(g,\gamma) \mathrm{e}^{i(\gamma\cdot g)} dv_\gamma,$$

where $\tilde{U}$ is the Bloch amplitude for $\vec{U}$, and the eigenvectors are orthonormal in the respect $\left(M\tilde{U}_m, \tilde{U}_n\right) = \delta_n^m$. We see that the material parameters appear as a natural weight function in the scalar product of the function space $\mathbf{Y}$.

The time-dependent Maxwell's equations in $\mathbf{R}^3$ with a given excitation current distribution $\vec{F}(g,t)$ is

$$\left(\text{rot}J + \frac{\partial}{\partial t}\overline{\overline{M}}\right) \vec{U} = -\vec{F}. \tag{5.4}$$

By expanding the field $\vec{U}$ in the eigenvectors $\left\{\tilde{U}_n\right\}$, projecting the equations on the same eigenvectors, and solving the resulting ordinary differential equation, we can write the solution as [237]

$$\vec{U}(g,t) = \sum_n \frac{1}{\left|\tilde{\mathbf{G}}\right|} \int_{\tilde{\mathbf{G}}} \mathrm{e}^{i\left[(\gamma\cdot g)-k_n(\gamma)t\right]} \left(-\tilde{F}_{tn},\tilde{U}_n\right) \tilde{U}_n(g,\gamma)\, dv_\gamma,$$

where

$$\tilde{F}_{tn} = \int_{-\infty}^{t} \sum_{n_1,n_2,n_3} \vec{F}\left(g + g_{n_1,n_2,n_3},\tau\right) \mathrm{e}^{i\left[k_n(\gamma)\tau-\left(\gamma\cdot\left(g+g_{n_1,n_2,n_3}\right)\right)\right]} d\tau.$$

As $t \to \infty$, it is clear that $\tilde{F}_{tn} \to \tilde{F}(g,\gamma,k_n(\gamma))$. In the following, we shall see that the infinite sum for $\vec{U}$ becomes finite when the frequency content of the current $\vec{F}$ is limited. We can already see traces of when this happens: as n increases, the eigenfrequencies k_n grow rapidly, and the fast oscillations cannot carry a substantial amount of the available energy if the current $\vec{F}$ is band-limited in frequency.

In this context, it is interesting to look at the contribution of the (at most two) modes where $k_n(\gamma) = 0$ for all $\gamma \in \tilde{\mathbf{G}}$. These are associated with static solutions (where we mean static in the respect that the curl is zero, $\left(\mathrm{rot} + \left[i\gamma\times\right]\right) J\tilde{U}_n = 0$) due to the presence of charge densities ρ_e and ρ_h. Since $k_n(\gamma) = 0$, they cannot contribute to any wave propagation, but they are important to resolve the boundary conditions when free charges are present. When the charge densities are zero, the static modes are zero, but for completeness we include them explicitly in the following.

We enumerate the modes according to $n = 1,2$ for the static modes, and $n \geq 3$ for the other modes, such that the absolute values of the eigenvalues form a nondecreasing sequence, $|k_3| \leq |k_4| \leq |k_5| \leq \ldots$.

Note that if $\tilde{U}_n = \left[\tilde{U}_{ne},\tilde{U}_{nh}\right]^T$ is an eigenvector with eigenvalue k_n, that is,

$$\begin{pmatrix} 0 & -\left(\mathrm{rot} + \left[i\gamma\times\right]\right) \\ \left(\mathrm{rot} + \left[i\gamma\times\right]\right) & 0 \end{pmatrix} \begin{pmatrix} \tilde{U}_{ne} \\ \tilde{U}_{nh} \end{pmatrix} = ik_n \begin{pmatrix} \bar{\bar{\varepsilon}}(g) & 0 \\ 0 & \bar{\bar{\mu}}(g) \end{pmatrix} \begin{pmatrix} \tilde{U}_{ne} \\ \tilde{U}_{nh} \end{pmatrix}$$

then so is $\tilde{U}_{\tilde{n}} = \left[\tilde{U}_{\tilde{n}e},\tilde{U}_{\tilde{n}h}\right]^T = \left[\tilde{U}_{ne}, -\tilde{U}_{nh}\right]^T$ but with eigenvalue $k_{\tilde{n}} = -k_n$. This is seen from

$$\begin{pmatrix} 0 & -\left(\mathrm{rot} + \left[i\gamma\times\right]\right) \\ \left(\mathrm{rot} + \left[i\gamma\times\right]\right) & 0 \end{pmatrix} \begin{pmatrix} \tilde{U}_{ne} \\ -\tilde{U}_{nh} \end{pmatrix} = \begin{pmatrix} \left(\mathrm{rot} + \left[i\gamma\times\right]\right) \tilde{U}_{nh} \\ \left(\mathrm{rot} + \left[i\gamma\times\right]\right) \tilde{U}_{ne} \end{pmatrix} =$$
$$\begin{pmatrix} -ik_n\bar{\bar{\varepsilon}}(g)\,\tilde{U}_{ne} \\ ik_n\bar{\bar{\mu}}(g)\,\tilde{U}_{nh} \end{pmatrix} = -ik_n \begin{pmatrix} \bar{\bar{\varepsilon}}(g) & 0 \\ 0 & \bar{\bar{\mu}}(g) \end{pmatrix} \begin{pmatrix} \tilde{U}_{ne} \\ -\tilde{U}_{nh} \end{pmatrix}.$$

This means we always have pairs of modes with eigenvalues satisfying $k_{2n-1} = -k_{2n}$ corresponding to forward and backward propagating waves. This symmetry property is particular for the lossless case, and is exploited in Section 5.6.3 when looking at an artificial chiral material. One way to see how the symmetry is broken by losses is by considering a material with an electric conductivity, in which case the eigenproblem reads

$$\begin{pmatrix} \overline{\overline{\sigma}}(g) & -\left(\mathrm{rot}+\left[i\gamma\times\right]\right) \\ \left(\mathrm{rot}+\left[i\gamma\times\right]\right) & 0 \end{pmatrix} \begin{pmatrix} \tilde{U}_{ne} \\ \tilde{U}_{nh} \end{pmatrix} = ik_n \begin{pmatrix} \overline{\overline{\varepsilon}}(g) & 0 \\ 0 & \overline{\overline{\mu}}(g) \end{pmatrix} \begin{pmatrix} \tilde{U}_{ne} \\ \tilde{U}_{nh} \end{pmatrix},$$

where the matrix $\overline{\overline{\sigma}}$ is nonnegative. From this equation, it is seen that the operator in the left-hand side is the sum of a symmetric and a skew symmetric operator, which means the eigenvalues ik_{n} must in general be complex valued. A detailed exploration of this eigenvalue problem is given in [239].

5.2.4 Dispersive Media: Singular Value Decomposition

For dispersive media, we cannot conveniently use eigenvectors for the expansion of an arbitrary field $\mathring{U}$, since we typically lose orthogonality. However, since the generalized resolvent operator $R(k)$ is compact, we can use the singular value decomposition, where the associated singular vectors are mutually orthogonal. The following statement is proven in [240], and is an adaptation of a more general representation theorem for compact operators which can be found in, for instance, [241]. The basis for the statement is that $-\left(\mathrm{rot}+\left[i\gamma\times\right]\right)J+ik^*\overline{\overline{M}}^H\colon\ \mathbf{X}\to\mathbf{Y}$ is the adjoint operator of $\left(\mathrm{rot}+\left[i\gamma\times\right]\right)J-ik\overline{\overline{M}}\colon\ \mathbf{Y}\to\mathbf{X}$, and that the null space of each operator is empty for each k in the resolvent set.

Statement 5.3 *For each k in the resolvent set for a fixed $\gamma\in\tilde{\mathbf{G}}$, there exists a sequence of real, positive numbers $\{\sigma_n\}$, arranged in ascending order $0\le\sigma_1\le\sigma_2\le\sigma_3\le\ldots$ with infinity as the only accumulation point, and orthonormal sequences $\left\{\tilde{U}_n\right\}$ in $\mathbf{Y}$ and $\left\{\tilde{V}_n\right\}$ in $\mathbf{X}$ such that*

$$\begin{cases} \left[\left(\mathrm{rot}+\left[i\gamma\times\right]\right)J-ik\overline{\overline{M}}\right]\tilde{U}_n &= \sigma_n\tilde{V}_n \\ \left[-\left(\mathrm{rot}+\left[i\gamma\times\right]\right)J+ik^*\overline{\overline{M}}^H\right]\tilde{V}_n &= \sigma_n\tilde{U}_n \end{cases}. \tag{5.5}$$

For each $\tilde{U}\in\mathbf{Y}$ and $\tilde{V}\in\mathbf{X}$ we have the expansions

$$\tilde{U}=\sum_n(\tilde{U},\tilde{U}_n)\tilde{U}_n \text{ and } \tilde{V}=\sum_n(\tilde{V},\tilde{V}_n)\tilde{V}_n$$

and the action of the operator can be expanded as

$$\left[\left(\mathrm{rot}+\left[i\gamma\times\right]\right)J-ik\overline{\overline{M}}\right]\tilde{U}=\sum_n\sigma_n(\tilde{U},\tilde{U}_n)\tilde{V}_n$$

The numbers $\{\sigma_n\}$ are the singular values for the partial differential operator $\left(\mathrm{rot}+\left[i\gamma\times\right]\right)J-ik\overline{\overline{M}}$.

The singular values are functions of the wave vector $\gamma\in\tilde{\mathbf{G}}$ and the frequency k. They are nonzero except for very particular combinations of γ and k, $k=k_m(\gamma)$

where $\sigma_1(k,\gamma) = \sigma_1(k_m(\gamma),\gamma) = 0$, corresponding to the eigenvalues in the preceding section. Note that due to the ordering of the singular values in a nondecreasing sequence, *all* the eigenvalues of the preceding section are contained in the first singular mode, when considered as a function of both γ and k. Remember that the eigenvalues are not a function of frequency k, they rather define the dispersion relation $k = k_n(\gamma)$, which in the context of singular value decomposition is the particular case when the smallest singular value is zero.

Returning to the solution of Maxwell's equations with sources (5.4), the solution can now be represented as

$$\vec{U}(g,t) = \sum_n \frac{1}{2\pi} \int_{i\alpha-\infty}^{i\alpha+\infty} \frac{1}{\left|\tilde{\mathbf{G}}\right|} \int_{\tilde{\mathbf{G}}} e^{i[(\gamma\cdot g)-kt]} \frac{\left(-\tilde{F},\tilde{V}_n\right)}{\sigma_n(\gamma,k)} \tilde{U}_n(\gamma,g,k)\, dv_\gamma dk.$$

We evaluate the inverse Laplace transform integral using residues, assuming the poles $\left\{\bar{k}_m(\gamma)\right\}$ of $\tilde{F}(\gamma,g,k)$ do not coincide with the poles $\{k_m\}$ of the operator associated with the smallest singular value, $\left(\tilde{V}_1\right)\tilde{U}_1/\sigma_1(\gamma,k)$. These poles are the frequencies $k = k_m(\gamma)$ such that the smallest singular value $\sigma_1(\gamma,k) = 0$. The result is

$$\begin{aligned} U(g,t) = \tfrac{1}{i} \sum_n \tfrac{1}{\left|\tilde{\mathbf{G}}\right|} \int_{\tilde{\mathbf{G}}} \sum_m \operatorname*{Res}_{\{\bar{k}_m(\gamma)\}} \left[e^{i[(\gamma\cdot g)-kt]} \frac{\left(-\tilde{F},\tilde{V}_n\right)}{\sigma_n(\gamma,k)} \tilde{U}_n \right]_{k=\bar{k}_m(\gamma)} dv_\gamma + \\ + \tfrac{1}{i} \tfrac{1}{\left|\tilde{\mathbf{G}}\right|} \int_{\tilde{\mathbf{G}}} \sum_m \operatorname*{Res}_{\{k_m(\gamma)\}} \left[e^{i[(\gamma\cdot g)-kt]} \frac{\left(-\tilde{F},\tilde{V}_1\right)}{\sigma_1(\gamma,k)} \tilde{U}_1 \right]_{k=k_m(\gamma)} dv_\gamma. \end{aligned}$$

This demonstrates the familiar result that the solution is a sum of forced oscillations (first row) and natural resonances (second row). Should the poles of the sources coincide with the poles of the operator, a more detailed analysis must be applied as in [1]. To keep the results in this chapter simple, we refrain from this complication.

5.3 Estimates of the Eigenvalues and Singular Values in the Low-Frequency Limit

In this section, we demonstrate some technical estimates of the eigenvalues $k_n(\gamma)$ and singular values $\sigma_n(\gamma,k)$ derived in the previous section. We shall assume that the frequency is low compared to the periodicity of the structure, i.e., ka is a small number, but not necessarily infinitesimally small.

The inspiration for the behavior of the eigenvalues and singular values is taken from the vacuum case, where they can be explicitly calculated. Using the reciprocal lattice vectors $\gamma_{n_1,n_2,n_3} = n_1\vec{b}_1 + n_2\vec{b}_2 + n_3\vec{b}_3$, the eigenvectors can be written as [237]

$$\tilde{U} = \begin{pmatrix} \gamma_{n_1,n_2,n_3} + \gamma \\ 0 \end{pmatrix} e^{i(\gamma_{n_1,n_2,n_3} \cdot g)} \text{ or } \tilde{U} = \begin{pmatrix} 0 \\ \gamma_{n_1,n_2,n_3} + \gamma \end{pmatrix} e^{i(\gamma_{n_1,n_2,n_3} \cdot g)},$$

$$\tilde{U} = \begin{pmatrix} \widehat{l} \\ \pm \widehat{m} \end{pmatrix} e^{i(\gamma_{n_1,n_2,n_3} \cdot g)} \text{ or } \tilde{U} = \begin{pmatrix} \widehat{m} \\ \mp \widehat{l} \end{pmatrix} e^{i(\gamma_{n_1,n_2,n_3} \cdot g)}$$

where the constant unit vectors $\widehat{l}$ and $\widehat{m}$ are orthogonal to the propagation direction and satisfy $\left[\widehat{l} \times \widehat{m}\right] = (\gamma_{n_1,n_2,n_3} + \gamma)/\left|\gamma_{n_1,n_2,n_3} + \gamma\right|$. We note that the first row corresponds to functions that can be written as gradients, whereas the second row corresponds to functions that can be written as curls. The latter ones correspond to propagating waves, and we see that for a fixed set of indices $\{n_1,n_2,n_3\}$, there are two possible polarizations, $\widehat{l}$ and $\widehat{m}$, and for each polarization there is the possibility of propagation along the positive or negative direction of $\gamma_{n_1,n_2,n_3} + \gamma$ corresponding to the plus or minus sign. Thus, for a fixed propagation direction, there exist four propagating modes. The singular vectors are similar but with slight deviations, we refer to the Appendix in [240] for details.

Using the above explicit representation of the eigenvectors, the eigenvalues for the vacuum case are found as [237]

$$k_{n0}(\gamma) = 0 \text{ for pure gradient functions (statics)},$$

$$k_{n0}(\gamma) = \pm\left|\gamma_{n_1,n_2,n_3} + \gamma\right| \text{ for the others}$$

and the singular values for the vacuum case are [240]

$$\sigma_{n0}(\gamma,k) = |k| \text{ for pure gradient functions (statics)},$$

$$\sigma_{n0}(\gamma,k) = \sqrt{|\mathrm{Im}\, k|^2 + \left(\left|\gamma_{n_1,n_2,n_3} + \gamma\right| \pm |\mathrm{Re}\, k|\right)^2} \quad \text{for the others.}$$

In both cases, the second row has multiplicity two when fixing the sign $\pm$, corresponding to the different polarizations $\widehat{l}$ and $\widehat{m}$. Since the reciprocal basis vectors $\{b_1,b_2,b_3\}$ scale as $1/a$, we see that all eigenvalues and singular values scale as $1/a$ when $a \to 0$, except the ones corresponding to (a) the gradient solutions and (b) the case $n_1 = n_2 = n_3 = 0$. In the enumeration of the eigenvalues and singular values, this corresponds to $n = 1,...,6$. We also see that the smallest singular value can approach zero only when $|\mathrm{Re}\, k| \approx |\gamma|$ and $|\mathrm{Im}\, k| \approx 0$.

For the eigenvalues, it is sufficient to observe that the eigenvalues corresponding to $n_1 = n_2 = n_3 = 0$ are proportional to $|\gamma|$, which make them go to zero as the wave number goes to zero. These are called the acoustic modes, whereas the other modes are called optical modes (see Fig. 5.1 and [242, 243]).

For the singular values, we need a few more delicate estimates. In [240] a more detailed look at the singular vectors for the vacuum case reveals that the requirement

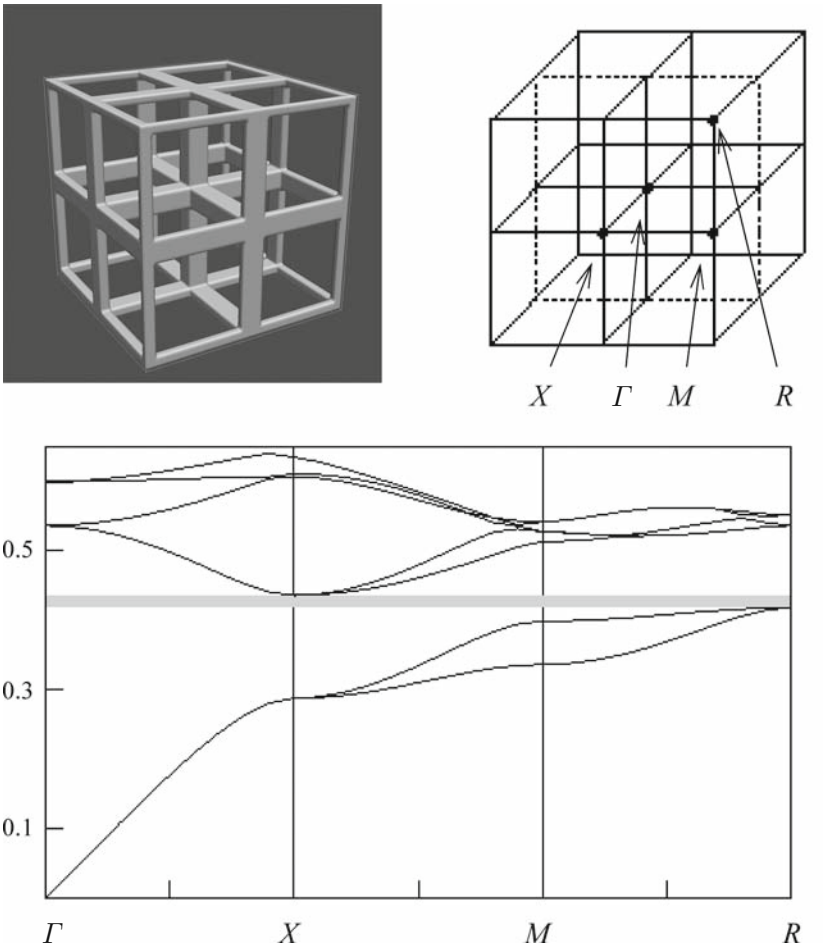

Fig. 5.1 A typical situation for the eigenvalues $k_n(\gamma)$ defined by (5.3). The eigenvalues are plotted as functions of the wave vector γ as this passes through points of symmetry in the reciprocal unit cell. The calculations are made with the program described in [242], and the structure is identical to the one presented in [243]. The thickness of the bars is 20% of the unit cell, and the permittivity in the bars is 12.96

$n_1 = n_2 = n_3 = 0$ allows for six modes, two static and four dynamic. The higher-order singular values can be estimated using the observation that for sufficiently low frequencies, the vacuum singular values for $n > 6$ can be estimated by the size of the reciprocal lattice vectors $\left|\gamma_{n_1,n_2,n_3}\right|$, which has the typical size $1/a$. In the following lemma, D is a dimensionless number such that D/a is the diameter of the largest sphere that can be inscribed in the reciprocal unit cell $\tilde{\mathbf{G}}$ (see Fig. 5.2).

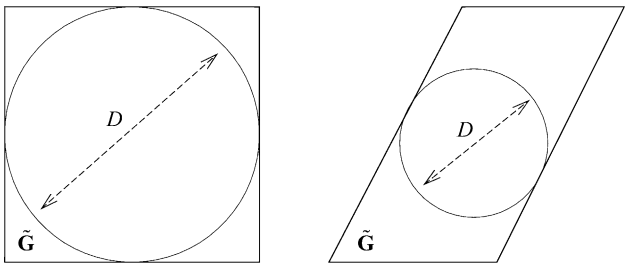

Fig. 5.2 Definition of the diameter D in the reciprocal unit cell. D is the diameter of the largest sphere that can be contained in the unit cell. The unit cell is really three-dimensional, but only 2-D representations are shown here for clarity. Two different unit cells are shown: (**a**) A cubic (quadratic) cell and (**b**) a skew cell

Lemma 5.1 *For each* $C \in (0;D/2)$ *and* $n > 6$ *(with* $n = 1$ *being the smallest singular value) we have*

$$\sigma_n(\gamma,k) \geq \frac{C}{a} \qquad \text{if} \qquad |ka| < \frac{D/2 - C}{\left\|\overline{\overline{M}} - \overline{\overline{E}}\right\| + 1}$$

independent of $\gamma \in \tilde{\mathbf{G}}$.

Proof. From [238] we find the following classical estimate of singular values using the singular values for vacuum,

$$|\sigma_n - \sigma_{n0}| \leq \left\| k\left(\overline{\overline{M}} - \overline{\overline{E}}\right)\right\|_\infty = \sup_{g\in\mathbf{G}} \left| k(\overline{\overline{M}}(g,k) - \overline{\overline{E}})\right|.$$

The higher-order vacuum singular values can be estimated as

$$\sigma_{n0} = \sqrt{|\mathrm{Im}\, k|^2 + \left(\left|\gamma_{n_1,n_2,n_3} + \gamma\right| \pm |\mathrm{Re}\, k|\right)^2} \geq \left|\gamma_{n_1,n_2,n_3} + \gamma\right| - |\mathrm{Re}\, k|.$$

Since the effect of adding γ_{n_1,n_2,n_3} to γ is to shift the origin to a different unit cell in the reciprocal lattice, the absolute value of the vector $\gamma_{n_1,n_2,n_3} + \gamma$ is larger than the absolute value of any vector on the rim of the fundamental reciprocal unit cell $\partial\tilde{\mathbf{G}}$, or

$$\left|\gamma_{n_1,n_2,n_3} + \gamma\right| \geq \inf_{\tilde{\gamma}\in\partial\tilde{\mathbf{G}}} |\tilde{\gamma}| = \frac{D}{2a},$$

when at least one of the indices n_1, n_2, or n_3 is nonzero. This implies

$$\sigma_n \geq \sigma_{n0} - \left\| k\left(\overline{\overline{M}} - \overline{\overline{E}}\right)\right\| \geq \frac{D}{2a} - |\mathrm{Re}k| - |k|\left\|\overline{\overline{M}} - \overline{\overline{E}}\right\| \geq \frac{D}{2a} - |k|\left(\left\|\overline{\overline{M}} - \overline{\overline{E}}\right\| + 1\right).$$

This means that for each $C \in (0;D/2)$, we have

$$\sigma_n \geq \frac{C}{a} \qquad \text{if} \qquad |ka| < \frac{D/2 - C}{\left\| \overline{\overline{M}} - \overline{\overline{E}} \right\| + 1}$$

which concludes the proof.

We now turn to the first six singular values. We do not estimate all of them, it is sufficient to look only at the smallest one, σ_1.

Lemma 5.2 *Let* $k \in \mathbf{C}$ *be such that* $\mathrm{Im}\left(-ik\overline{\overline{M}}\,(g,k)\right)$ *is a definite matrix for each* $g \in \mathbf{G}$. *For each* $\gamma \in \tilde{\mathbf{G}}$, *the smallest singular value* σ_1 *can then be estimated by*

$$\sigma_1(\gamma,k) \leq \left| 1 - \frac{k_n(\gamma)}{|k|} \right| \left\| \mathrm{Im}\left(-ik\overline{\overline{M}}\right) \right\| + C_1 \left\| \mathrm{Re}\left(-ik\overline{\overline{M}}\right) \right\|,$$

where $k_n(\gamma)$ *is a real eigenvalue defined by the eigenproblem*

$$\begin{aligned} \left(\mathrm{rot} + \left[i\gamma\times\right]\right) J\tilde{U} &= ik_n(\gamma)\mathrm{Im}\left(\frac{-ik}{|k|}\overline{\overline{M}}(g,k)\right)\tilde{U}, \\ (\mathrm{div} + (i\gamma\cdot))\left[\mathrm{Im}\left(\frac{-ik}{|k|}\overline{\overline{M}}\,(g,k)\right)\tilde{U}\right] &= 0 \end{aligned} \tag{5.6}$$

and

$$C_1 = 1 + \left| \frac{k_n(\gamma)}{k} \right| \mathrm{cond}\left(\mathrm{Im}\left[-ik\overline{\overline{M}}\right]\right),$$

where the condition number of an invertible matrix A *is* $\mathrm{cond}(\mathrm{A}) = \left\|\mathrm{A}^{-1}\right\| \cdot \|\mathrm{A}\|$.

The proof is quite elaborate and is omitted here (see [240] for details). Notice how an auxiliary self-adjoint eigenvalue problem using only the imaginary part of $-ik\overline{\overline{M}}$ is formulated in order to estimate the singular values. This eigenvalue problem is well posed due to the results previously accounted for in this section and in [237]. This estimate of the singular values is good for materials with small losses, where the singular vectors correspond to only weakly damped waves propagating in the structure. The importance of the estimate is that it provides an upper bound for the singular value, which is necessary to give a lower bound on the energy contained in the first modes. Note how $\mathrm{Re}\left(-ik\overline{\overline{M}}\right)$, corresponding to the losses, enters the estimate of the singular value as an additive term. This is similar to the result in [239], where it is shown that the imaginary part of the spectrum of the corresponding Maxwell operator does not exceed the norm of the conductivity, which is our operator $\mathrm{Re}\left(-ik\overline{\overline{M}}\right)$.

5.4 Reduced Number of Degrees of Freedom in the Low-Frequency Limit

We now demonstrate that the estimates just derived can be used to show that under certain conditions, only a few of the modes indicated by the eigenvalue or singular

value expansion survive. Starting with the eigenvalue expansion, it is seen that the amplitude of mode n is proportional to

$$\tilde{F}_{tn} = \int_{-\infty}^{t} \sum_{n_1,n_2,n_3} \vec{F}(g + g_{n_1,n_2,n_3},\tau) e^{i\left[k_n(\gamma)\tau - \left(\gamma\cdot(g+g_{n_1,n_2,n_3})\right)\right]} d\tau.$$

As $t \to \infty$, it is clear that $\tilde{F}_{tn} \to \tilde{F}\,(g,\gamma,k_n\,(g))$, which is constructed from the temporal Fourier transform of $\vec{F}\,(g,t)$ evaluated at frequency $k_n\,(\gamma)$. For $n > 6$, we have concluded that k_{n} is proportional to $1/a$ ($k_n \propto 1/a$) as $a \to 0$. This means that if the currents are band-limited in frequency, in the respect that $\tilde{F}\,(g,\gamma,k) = 0$ if $|k| > K_0$, then there exists an A such that

$$\tilde{F}\,(g,\gamma,k_n\,(\gamma)) = 0 \qquad \text{for} \quad n > 6 \quad \text{and} \quad a < A.$$

Thus, if we consider the stationary response to a sufficiently band-limited excitation, we have

$$\lim_{t\to\infty} \vec{U}\,(g,t) = \sum_{n=1}^{6} \frac{1}{\left|\tilde{\mathbf{G}}\right|} \int_{\tilde{\mathbf{G}}} e^{i\left[(\gamma\cdot g) - k_n(\gamma)t\right]} \left(-\tilde{F},\tilde{U}_n\right) \tilde{U}_n\,(g,\gamma)\, dv_\gamma$$

that is, the field has only six degrees of freedom, corresponding to the available polarizations of the electric and magnetic fields. The fact that we do not have to let the period a become infinitesimally small is a first indication that we can obtain homogenized material parameters without letting the scale difference between structure and excitation become infinite.

Some words should be said about the relation to real signals. In reality, a signal never exactly satisfies the criterion to be zero for high frequencies, but can often be considered small enough. Also, the limit $t \to \infty$ above does not have to be taken literally, since after some finite time all transient processes can be considered small enough to allow us to focus on the stationary response. We do not give the details of this refined modeling.

Going to the general case of dispersive bianisotropic media, we first consider the classical homogenization, where the scale difference is infinite. The following statement shows that the energy contained in the higher-order modes is negligible compared to the energy in the first six modes.

Statement 5.4 (infinite wavelength) *Let the currents $\vec{F}(g)$ be band-limited in spatial frequency; i.e., the Fourier transform $\widehat{F}\,(\gamma) = 0$ if $|\gamma| > K_0$, where K_0 is a fixed wave number. For a given $C \in (0;D/2)$ with a, k, and K_0 restricted by*

$$|ka| < \frac{D/2 - C}{\left\| \overline{\overline{M}} - \overline{\overline{E}} \right\| + 1} \qquad \text{and} \qquad K_0 a < \frac{D}{2},$$

the estimate

$$\frac{\left\| \sum_{n=7}^{\infty} \int_{\tilde{\mathbf{G}}} \frac{e^{i(\gamma\cdot g)}}{\sigma_n} \left(-\tilde{F},\tilde{V}_n\right) \tilde{U}_n dv_g \right\|^2}{\left\| \sum_{n=1}^{6} \int_{\tilde{\mathbf{G}}} \frac{e^{i(\gamma\cdot g)}}{\sigma_n} \left(-\tilde{F},\tilde{V}_n\right) \tilde{U}_n dv_g \right\|^2} \leq \frac{a^2}{C^2} \left(K_0 + \left\| \overline{\overline{kM}} \right\|\right)^2$$

holds.

This shows that as $K_0 a \to 0$, only the first six modes contribute to the field. This is the regime of classical homogenization, where the wavelength of the applied field is much larger than the size of the microstructure. In order to find information on the situation for finite-scale difference, we need to be a bit more careful with our estimates, and show that the first six modes actually contain more of the electromagnetic energy than the statement above suggests.

We start by demonstrating the typical effect of the lowest singular value, and show that an integral over $\tilde{\mathbf{G}}$ can be estimated from below by an integral over the region where the singular value is small.

Lemma 5.3 *Let $k_n(\gamma)$ be defined from the problem (5.6). Let $\mathbf{\Gamma}$ denote the set of $\gamma \in \tilde{\mathbf{G}}$ such that $k_n(\gamma) = |k|$ for some n, i.e., a surface in $\tilde{\mathbf{G}}$. Assume this set is nonempty and that the eigenvalue function $k_n(\gamma)$ can be linearized near $\gamma_0 \in \mathbf{\Gamma}$ as*

$$\frac{k_n(\gamma)}{|k|} = 1 + \alpha(\gamma_0)\left(\vec{n}\cdot(\gamma-\gamma_0)\right) + o\left(|\gamma-\gamma_0|\right),$$

where $\vec{n}$ is a unit normal to the surface $\mathbf{\Gamma}$. Further assume there exists r such that $|\alpha(\gamma_0)|/a < r$ independent of γ_0 and a. For a dimensionless parameter $\delta > 0$, assume

$$\left(1 + (1+\delta)\,\mathrm{cond}\left\{ \mathrm{Im}\left[-ik\overline{\overline{M}}\right] \right\}\right) \left\| \mathrm{Re}\left[-ik\overline{\overline{M}}\right] \right\| \leq \delta \left\| \mathrm{Im}\left[-ik\overline{\overline{M}}\right] \right\|. \quad (5.7)$$

Then the following estimate holds, under the conditions of Lemma 5.2:

$$\int_{\tilde{\mathbf{G}}} \frac{f(\gamma)\,dv_\gamma}{\sigma_1(\gamma,k)^2} \geq \frac{1}{\delta} \frac{1/r}{2\left\| \mathrm{Im}\left(-ik\overline{\overline{M}}\right) \right\|^2} \frac{1}{a} \int_{\tilde{\mathbf{\Gamma}}} f(\tilde{\gamma}_0) dS_{\tilde{\gamma}_0},$$

where $f(\gamma)$ is a continuous, nonnegative function of γ, and $\tilde{\mathbf{\Gamma}}$ is a set close to $\mathbf{\Gamma}$, satisfying $\mathrm{dist}(\mathbf{\Gamma},\tilde{\mathbf{\Gamma}}) = \sup_{\gamma_0\in\mathbf{\Gamma}} \inf_{\tilde{\gamma}_0\in\tilde{\mathbf{\Gamma}}} |\gamma_0 - \tilde{\gamma}_0| < \delta/(ra)$ *(see Fig. 5.3).*

The proof of the lemma can be found in [240] and is omitted here. The idea of this lemma is to be able to estimate the action of the lowest singular value over the unit cell in a more precise way than the obvious estimate $\int_{\tilde{\mathbf{G}}} f/\sigma_1^2 dv_\gamma \geq \left(\inf \sigma_1^{-2}\right) \int_{\tilde{\mathbf{G}}} f dv_\gamma$, which has the problem that it does not scale favorably with the size of the unit cell and only leads to the classical homogenization case. The lemma states that for a suitably regular function $f(\gamma)$, the integral of f/σ_1^2 over the entire reciprocal unit cell $\tilde{\mathbf{G}}$ is bounded below by a constant multiplying an integral of f

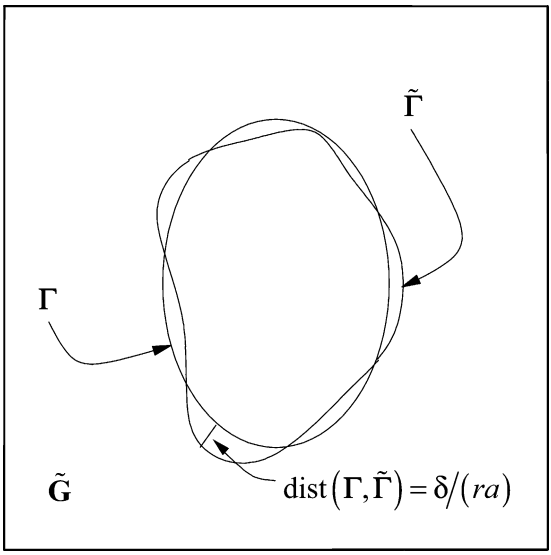

Fig. 5.3 The surfaces $\mathbf{\Gamma}$ and $\tilde{\mathbf{\Gamma}}$ in the reciprocal unit cell $\tilde{\mathbf{G}}$. Only a two-dimensional representation is shown here, making the surfaces become curves. The distance between two surfaces is defined as the supremum of the infimum of the distance between two arbitrary points on each surface. The surface $\mathbf{\Gamma}$ is defined by the equation $k_n(\gamma) = |k|$, δ is a parameter of choice, and r corresponds to the largest linear variation of the eigenvalue $k_n(\gamma)$ orthogonal to the surface $\mathbf{\Gamma}$

over a region close to a surface where σ_1 is small. This means that a large part of the contribution to the integral comes from the region where the singular value σ_1 is small, which makes intuitive sense. The importance of the lemma lies in the possibility of choosing a number $\delta > 0$, which will help in controlling the scaling of the result with unit cell size a. In the following statement, we also assume that the function $f(\gamma) = \left|\left(-\tilde{F},\tilde{V}_1\right)\right|^2 \leq \| \tilde{F}(\cdot,\gamma) \|^2_{\mathbf{L}_2(\mathbf{G})}$ is regular enough to allow the additional estimate $\frac{1}{a}\int_{\tilde{\mathbf{\Gamma}}} f(\gamma)\, dS_\gamma \geq C_f \int_{\tilde{\mathbf{G}}} f(\gamma)\, dv_\gamma$, that is, the integral over the surface $\tilde{\mathbf{\Gamma}}$ can be bounded below by a constant multiplying the integral over the entire reciprocal unit cell. Note that the scaling of the surface integral by $1/a$ makes the constant C_f dimensionless.

Statement 5.5 (finite wavelength) *Choose $\delta > 0$. Let $k \in \mathbf{C}$ be such that $\mathrm{Im}\left(-ik\overline{\overline{M}}(g,k)\right)$ is a definite matrix for each $g \in \mathbf{G}$, (5.7) is satisfied, and*

$$|ka| < \frac{D/2 - C}{\left\|\overline{\overline{M}} - \overline{\overline{E}}\right\| + 1}$$

for some $C > 0$. Further assume that $\left|\left(-\tilde{F},\tilde{V}_1\right)\right|^2$ is a continuous function of γ and there is a dimensionless constant C_f independent of a such that

$$\frac{1}{a}\int_{\tilde{\mathbf{\Gamma}}} \left|(-\tilde{F},\tilde{V}_1)\right|^2 dS_\gamma \geq C_f \int_{\tilde{\mathbf{G}}} \left\|\tilde{F}\right\|^2 dv_\gamma$$

where $\tilde{\mathbf{\Gamma}}$ is defined in Lemma 5.3. Then the estimate

$$\frac{\left\| \sum_{n=7}^{\infty} \int_{\tilde{\mathbf{G}}} \frac{e^{i(\gamma\cdot g)}}{\sigma_n} \left(-\tilde{F},\tilde{V}_n\right) \tilde{U}_n dv_\gamma \right\|^2}{\left\| \sum_{n=1}^{6} \int_{\tilde{\mathbf{G}}} \frac{e^{i(\gamma\cdot g)}}{\sigma_n} \left(-\tilde{F},\tilde{V}_n\right) \tilde{U}_n dv_\gamma \right\|^2} \leq \frac{2ra^2}{C^2 C_f} \left\| \operatorname{Im}\left(-ik\overline{\overline{M}}\right) \right\|^2 \delta$$

holds, where r is defined in Lemma 5.3.

From this estimate we see that the energy can be contained in the first six modes in the limit of vanishing size of the unit cell $a \to 0$ even if $\operatorname{Im}\left(-ik\overline{\overline{M}}\right)$ scales as $1/a$. This requires that we let δ scale as a^ε with $\varepsilon > 0$, which can be done if $\left\| \operatorname{Re}\left(-ik\overline{\overline{M}}\right) \right\| \Big/ \left\| \operatorname{Im}\left(-ik\overline{\overline{M}}\right) \right\| \propto a^\varepsilon$. This is actually a quite common case, and corresponds to the losses becoming zero in the high-frequency limit. Consider for instance the case of a conductivity model, $\overline{\overline{M}}(k) = \overline{\overline{M}}_0 + \overline{\overline{M}}_1/(-ik)$, where $\overline{\overline{M}}_0$ is a positive definite hermitian symmetric matrix, and $\overline{\overline{M}}_1$ is a positive semidefinite hermitian symmetric matrix. For real k, we then have $\operatorname{Re}\left(-ik\overline{\overline{M}}\right) = \overline{\overline{M}}_1$ and $\operatorname{Im}(-ik\overline{\overline{M}}) = -k\overline{\overline{M}}_0$. Letting the frequency scale as $k \propto 1/a$ then implies $\left\| \operatorname{Re}\left(-ik\overline{\overline{M}}\right) \right\| \Big/ \left\| \operatorname{Im}\left(-ik\overline{\overline{M}}\right) \right\| \propto a$, corresponding to $\varepsilon = 1$. This can be seen as letting the scale a become smaller than the skin depth. Additional examples of dispersive models satisfying corresponding relations between the real and imaginary parts are Debye and Lorentz models [240].

The statements of this section have demonstrated a particular combination of circumstances that make the number of modes contributing to the electromagnetic energy in a periodic structure becoming at most six. In short, the result is that if the structure supports propagating waves, a situation which requires small losses, only a few waves can be generated if the frequency is low enough. We now turn to the implications of this, and show that the reduced number of degrees of freedom can be used to compute homogenized material parameters.

5.5 Computation of Homogenized Parameters

Homogenization is the procedure of calculating effective material properties, such that they predict the same large-scale scattering characteristics as the true, microscopic material parameters. This corresponds to forgetting the fine details of the microstructure, but remembering the large, coherent effects. The homogenized material matrix can be defined by the property

$$\left\langle \overline{\overline{M}}\tilde{U} \right\rangle = \overline{\overline{M}}^{hom} \left\langle \tilde{U} \right\rangle, \tag{5.8}$$

where the averaging operator was defined in (5.2). Thanks to the reduced number of degrees of freedom shown previously, the matrix $\overline{\overline{M}}^{hom}$ can not only be defined but also computed, provided the set of averaged modes $\left\{ \left\langle \tilde{U}_n \right\rangle \right\}_{n=1}^{6}$ are linearly independent. That they are linearly independent can be shown by considering the finite sum

$\tilde{U} = \sum_{n=1}^{6} \left(-\tilde{F}, \tilde{V}_n\right) \tilde{U}_n$. If we choose currents that do not vary on the scale of the unit cell, $\tilde{F}(g,\gamma) = \tilde{F}(\gamma)$, this reduces to $\tilde{U} = \sum_{n=1}^{6} - \left(\left\langle \tilde{F} \right\rangle \cdot \left\langle \tilde{V}_n^* \right\rangle\right) \tilde{U}_n$. If $\left\{ \left\langle \tilde{V}_n \right\rangle \right\}_{n=1}^{6}$ were linearly dependent, we could choose currents such that $\left(\left\langle \tilde{F} \right\rangle \cdot \left\langle \tilde{V}_n^* \right\rangle\right) = 0$ for all n. But we know *a priori* from the well-posedness of Maxwell's equations that if $\tilde{F}$ is nonzero, then the electromagnetic field $\tilde{U}$ must also be nonzero, hence the set of constant six-vectors $\left\{ \left\langle \tilde{V}_n \right\rangle \right\}_{n=1}^{6}$ must be linearly independent. In the following sections, we also demonstrate that they are not only linearly independent but also mutually orthogonal.

5.5.1 Lossless Case

In the lossless case, the degrees of freedom can be derived from the eigenvalue problem (5.3). Taking the mean value of this equation and using the definition of the homogenized matrix (5.8) we find

$$\left[i\gamma \times J\left\langle \tilde{U}_n \right\rangle\right] = ik_n \left\langle \overline{\overline{M}} \tilde{U}_n \right\rangle = ik_n \overline{\overline{M}}^{hom} \left\langle \tilde{U}_n \right\rangle, \; n = 1,...,6.$$

This demonstrates that the mean values of the first six eigenvectors are eigenvectors of a generalized eigenvalue problem involving the homogenized matrix $\overline{\overline{M}}^{hom}(\gamma)$ for each fixed $\gamma \in \tilde{\mathbf{G}}$. Remember that the first two modes correspond to the static modes with $k_n(\gamma) = 0$ for all γ. From the above expression it is clear that the mean value of these eigenvectors must be proportional to γ, whereas the mean values $\left\langle \overline{\overline{M}} \tilde{U}_n \right\rangle$ are orthogonal to γ. A continued line of reasoning as in [237] shows that all modes are mutually orthogonal in the respect $\left\langle \overline{\overline{M}} \tilde{U}_m \right\rangle^H \left\langle \tilde{U}_n \right\rangle = 0$ when $m \neq n$, where we identify the mean values of the eigenvectors with ordinary column vectors. Using this orthogonality, the homogenized material parameters can be represented as [237]

$$\overline{\overline{M}}^{hom}(\gamma) = \sum_{n=1}^{6} \frac{\left\langle \overline{\overline{M}} \tilde{U}_n \right\rangle \left\langle \overline{\overline{M}} \tilde{U}_n \right\rangle^H}{\left\langle \overline{\overline{M}} \tilde{U}_n \right\rangle^H \left\langle \tilde{U}_n \right\rangle}.$$

Note that this matrix is defined in terms of averages of the modes, that is, there is an implicit dependence on the eigenvalues $k_n(\gamma)$, and also on the wave vector $\gamma \in \tilde{\mathbf{G}}$.

Considering the special case of propagating waves in nonmagnetic media with no free charges, that is, excluding the static modes, the eigenproblem (5.3) takes the form $\left(\mathrm{rot} + \left[i\gamma\times\right]\right)\left[\left(\mathrm{rot} + \left[i\gamma\times\right]\right)\tilde{E}_n\right] = k_n(\gamma)^2\, \overline{\overline{\varepsilon}} \tilde{E}_n$. It is then straightforward to show that the homogenized permittivity can be written as [244]

$$\overline{\overline{\varepsilon}}^{hom}(\gamma) = \sum_{n=1}^{2} \frac{|\gamma|^2}{k_n(\gamma)^2} \frac{\langle \tilde{E}_n \rangle \langle \tilde{E}_n \rangle^H}{\left| \langle \tilde{E}_n \rangle \right|^2}.$$

Here, the numbering differs from the previous convention, since here only two propagating modes corresponding to the lowest eigenvalues k_n^2 are necessary to represent the permittivity. This demonstrates that the homogenized permittivity is directly associated with the phase slowness $\gamma/k_n(\gamma)$ for each mode. This does not contradict the standard conclusion that it is the group velocity $\partial k_n(\gamma)/\partial\gamma$ which is associated with effective properties for a pulse signal. Since the homogenized material properties $\overline{\overline{\varepsilon}}^{hom}(\gamma)$ depend on the wave vector, it can be shown that the homogenized material satisfies the same dispersion relation as the original heterogeneous structure. Hence, it has the same group velocity as well, which is the relevant velocity for a narrow-band wave packet.

One challenge with the homogenized material properties is that they depend on the wave vector γ, making the medium exhibit spatial dispersion. This is not straightforward to use in scattering problems, since the spatial dispersion implies nonlocal constitutive relations which are not easily implemented in boundary conditions. For a fixed propagation direction $\widehat{\gamma} = \gamma/|\gamma|$, it is formally possible to represent the material in terms of temporal dispersion instead. Assuming the relation $k = k_n(\gamma) = k_n(\widehat{\gamma}|\gamma|) = k_n^{\widehat{\gamma}}(|\gamma|)$ can be inverted to give $|\gamma| = \gamma_n(k)$ (assuming all parameters are real), we can write

$$\overline{\overline{\varepsilon}}^{hom,\widehat{\gamma}}(k) = \sum_{n=1}^{2} \frac{\left[\gamma_n(k)\right]^2}{k^2} \frac{\langle \tilde{E}_n \rangle \langle \tilde{E}_n^H \rangle}{\left| \langle \tilde{E}_n \rangle \right|^2},$$

which, at least formally, can be considered as a temporally dispersive medium. However, the restriction to a fixed propagation direction still implies a spatial dispersion.

The eigenvalue problem defining the modes in the lossless case is well explored, and standard computational tools exist, especially from the photonic bandgap community. Some general-purpose commercial solvers implement periodic boundary conditions and allow for convenient postprocessing, such as calculating the mean of the eigenvectors. In the examples of this section, we make frequent use of the program described in [242], which is a freely available software and works on many platforms.

5.5.2 Dispersive Case

For the general case with dispersive material properties, we have mutual orthogonality between the vectors $\left\{ \langle \tilde{U}_n \rangle \right\}_{n=1}^{6}$ and $\left\{ \langle \tilde{V}_n \rangle \right\}_{n=1}^{6}$, respectively. This can be seen by applying the mean value operator on the equations (5.5) defining the singular values. Having concluded the existence of a homogenized matrix satisfying

$\left\langle \overline{\overline{M}}\tilde{U}_n \right\rangle = \overline{\overline{M}}^{hom} \left\langle \tilde{U}_n \right\rangle$ for the first six modes, the result is

$$\begin{cases} \left[i\gamma \times J \left\langle \tilde{U}_n \right\rangle\right] - ik\overline{\overline{M}}^{hom} \left\langle \tilde{U}_n \right\rangle & = \sigma_n \left\langle \tilde{V}_n \right\rangle \\ -\left[i\gamma \times J \left\langle \tilde{V}_n \right\rangle\right] + ik^* \left(\overline{\overline{M}}^{hom}\right)^H \left\langle \tilde{V}_n \right\rangle & = \sigma_n \left\langle \tilde{U}_n \right\rangle \end{cases}, n = 1,...,6,$$

which is identified as the singular value decomposition of a 6×6 constant matrix $\left[i\gamma \times J\right] - ik\overline{\overline{M}}^{hom}$. This in turn implies that the singular vectors $\left\langle \tilde{U}_n \right\rangle$ and $\left\langle \tilde{V}_n \right\rangle$ are mutually orthogonal, and we can represent the homogenized material matrix as

$$\overline{\overline{M}}^{hom} = \sum_{n=1}^{6} \frac{\left\langle \overline{\overline{M}}\tilde{U}_n \right\rangle \left\langle \tilde{U}_n \right\rangle^H}{\left\langle \tilde{U}_n \right\rangle^H \left\langle \tilde{U}_n \right\rangle}.$$

In contrast to the lossless case, where the local problem from which the homogenized material matrix is computed can be solved with standard methods, there does not seem to exist similar standard methods for computing the singular value decomposition of a partial differential operator. In principle, we could for instance make use of a finite element discretization of the operator, and apply standard linear algebra packages to the resulting system matrix. Since only the first six singular values are actually needed, a method which computes only the lowest singular values should be chosen.

5.6 Results for Sample Structures

To demonstrate the results of the homogenization procedure laid out in this chapter, we look at a few sample structures. At the present level of computational means, only structures consisting of isotropic dielectrics can be treated. However, any general program with periodic (or quasi-periodic) boundary conditions can be used as long as it can export the relevant data. In the following examples, we make frequent use of the freely available program described in [242].

5.6.1 Laminated Media

In [245] it is shown that for a laminated structure, the following analytic expressions for the dispersion relation can be derived for a laminated geometry as in Fig. 5.4, depending on polarization:

$$\cos(k_z a) = \cos(k_1 a_1)\cos(k_2 a_2) - \frac{1}{2}\left(\frac{k_1}{k_2} + \frac{k_2}{k_1}\right)\sin(k_1 a_1)\sin(k_2 a_2)$$

(for *E*-polarization when the electric field is orthogonal to the plane spanned by the propagation direction and the normal direction to the laminates) and

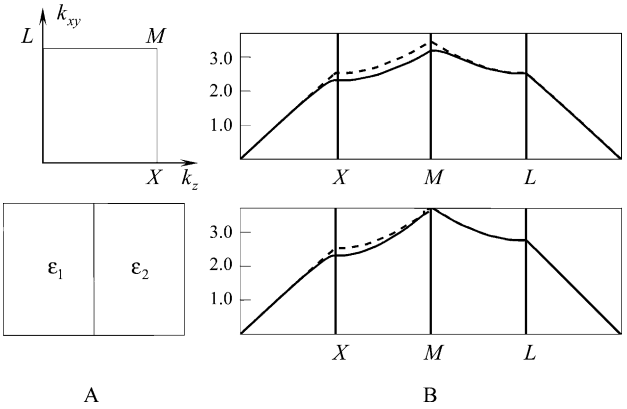

Fig. 5.4 (**a**) Geometry and reciprocal unit cell for the laminated structure. (**b**) The dispersion relations $k_n(\gamma)$ as γ passes through points of symmetry in the unit cell. The exact dispersion relations are the *solid lines*, and the asymptotic approximations leading to (5.9) and (5.10) are the *dashed lines*. The *upper graphs* correspond to *E*-polarization, and the *lower* are for *H*-polarization. The plots are for a low contrast case where $\varepsilon_1/\varepsilon_2 = 2$ and $f_1 = f_2 = 0.5$

$$\cos(k_z a) = \cos(k_1 a_1)\cos(k_2 a_2) - \frac{1}{2}\left(\frac{\varepsilon_2 k_1}{\varepsilon_1 k_2} + \frac{\varepsilon_1 k_2}{\varepsilon_2 k_1}\right)\sin(k_1 a_1)\sin(k_2 a_2)$$

(for *H*-polarization). Here $k_{1,2} = \sqrt{\varepsilon_{1,2}k^2 - k_{xy}^2}$, k_{xy} is the wave number parallel to the laminates, and k_z the wave number in the normal direction to the laminates. These exact relations can be solved asymptotically to find asymptotic formulas for the effective permittivity as

$$\varepsilon^{hom} = f_1\varepsilon_1 + f_2\varepsilon_2 + \frac{1}{12}\frac{(\varepsilon_1 - \varepsilon_2)^2 (f_1 f_2)^2}{f_1\varepsilon_1 + f_2\varepsilon_2}\left(\left(k_{xy}a\right)^2 + (k_z a)^2\right) + O\left(ka^4\right), \quad (5.9)$$

$$\begin{aligned}\varepsilon^{hom} = &\left[\left(\frac{f_1}{\varepsilon_1} + \frac{f_1}{\varepsilon_1}\right)\sin^2\theta + \frac{1}{f_1\varepsilon_1 + f_2\varepsilon_2}\cos^2\theta\right]^{-1} + \frac{1}{12}\frac{(\varepsilon_1 - \varepsilon_2)^2 (f_1 f_2)^2}{f_1\varepsilon_1 + f_2\varepsilon_2}\times \\ &\times\left[\frac{\frac{(f_1\varepsilon_1 + f_2\varepsilon_2)^2}{\varepsilon_1\varepsilon_2}\sin^2\theta - \cos^2\theta}{\left(\frac{f_1}{\varepsilon_1} + \frac{f_1}{\varepsilon_1}\right)(f_1\varepsilon_1 + f_2\varepsilon_2)\sin^2\theta + \cos^2\theta}\right]^2 \\ &\left(\left(k_{xy}a\right)^2 + (k_z a)^2\right) + O\left((ka)^4\right),\end{aligned} \quad (5.10)$$

where the propagation angle θ is defined as

$$\cos^2\theta = \frac{k_z^2}{k_{xy}^2 + k_z^2}.$$

The leading terms in the expressions (5.9) and (5.10) are the effective permittivities predicted by the classical homogenization approach, where the scale difference

is infinite corresponding to $ka \to 0$. It is seen that the leading term in the first expression is isotropic, in the respect that it does not depend on the direction of propagation. This is expected since in this case the electric field is tangential to the laminates, and therefore the leading term is simply the arithmetic mean value of the permittivities, as classical homogenization suggests. In the second expression however, the leading term is identified as the effective permittivity for an extraordinary wave propagating in a uniaxial medium, which does depend on the direction of propagation. The extraordinary wave is composed of two effective permittivities: one with the arithmetic mean of the permittivities, and another with the harmonic mean, where the harmonic mean corresponds to the polarization where the electric field is normal to the laminates.

In both expressions, the correction terms are proportional to $(\varepsilon_1 - \varepsilon_2)^2 f_1 f_2$, which demonstrates that the spatial dispersion is small when the contrast is small or the volume fraction of one of the materials is small. An interesting detail is that the correction term in (5.10) is zero for the particular propagation angle

$$\theta = \text{arc tg}\frac{\sqrt{\varepsilon_1 \varepsilon_2}}{f_1 \varepsilon_1 + f_2 \varepsilon_2}.$$

This means this angle corresponds to a direction of minimal spatial dispersion when the electric field is not orthogonal to the lamination direction. For both polarizations, we see that the correction term is positive, implying that the phase velocity is lowered when ka is small but not negligible.

In Figs. 5.4 and 5.5 we have plotted the exact dispersion relations together with the asymptotic dispersion relations leading to (5.9) and (5.10). It is seen that the asymptotic expressions, keeping only the first-order correction term in ka, approximates the true dispersion relation very well for weak contrasts, whereas it may fail miserably for higher contrasts. We also note that the H-polarization is more sensitive to the spatial dispersion than the E-polarizations.

5.6.2 Validity of Classical Homogenization

Here we give some results for a few structures which can be identified as macroscopically isotropic in the classical homogenization limit [246]. We compare the wave-vector-dependent homogenized material parameters with the classical homogenization results. The following three cases are considered.

- A two-dimensional checker board structure as in Fig. 5.6. This structure has a well-known exact solution in the classical homogenization limit. For electric fields normal to the plane, the effective permittivity is the arithmetic mean, $\varepsilon^{hom} = (\varepsilon_1 + \varepsilon_2)/2$, and for electric fields in the plane, it is the geometric mean $\varepsilon^{hom} = \sqrt{\varepsilon_1 \varepsilon_2}$.
- An assemblage of spherical shells as in Fig. 5.7. This structure is a common engineering case, where the Maxwell–Garnett (also known as Hashin–Shtrikman)

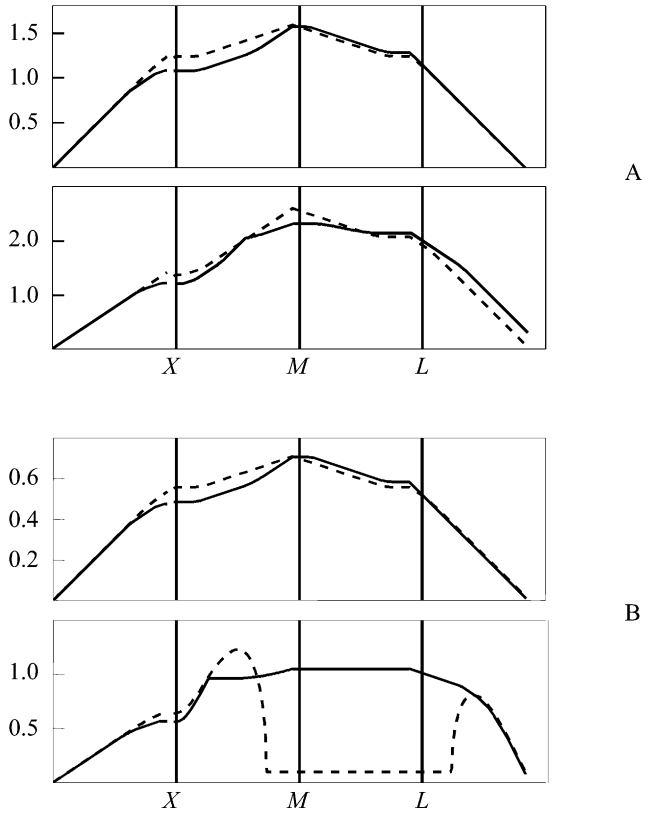

Fig. 5.5 Dispersion relations $k_n(\gamma)$ for a laminated structure corresponding to Fig. 5.4 for the contrasts (**a**) $\varepsilon_1/\varepsilon_2 = 10$ and (**b**) $\varepsilon_1/\varepsilon_2 = 50$. It is seen that for the highest contrast, there is a large region where the asymptotic solution (*dashed curve*) fails to approximate the true dispersion relation for one of the polarizations

mixing formula is often a good approximation in the classical homogenization limit.

- A scaffold structure as in Fig. 5.8. This structure is interesting since it has a bandgap, as illustrated in the previous Fig. 5.1.

The results for finite scale homogenization are computed using postprocessing of data from the freely available program described in [242]. In all three cases, we look at the deviation of the classical homogenization result $\overline{\overline{\varepsilon}}^{hom}(0)$ from the finite scale homogenization result $\overline{\overline{\varepsilon}}^{hom}(\gamma)$, and define the error for the polarization p as $\delta = \left|\varepsilon_p^{hom}(0) - \varepsilon_p^{hom}(\gamma)\right| \Big/ \left|\varepsilon_p^{hom}(\gamma)\right|$, where ε_p^{hom} is the scalar permittivity value corresponding to a fixed polarization p.

For all of these structures, we see that the error when using the classical homogenization method is approximately less than 10% if the contrast is lower than 10

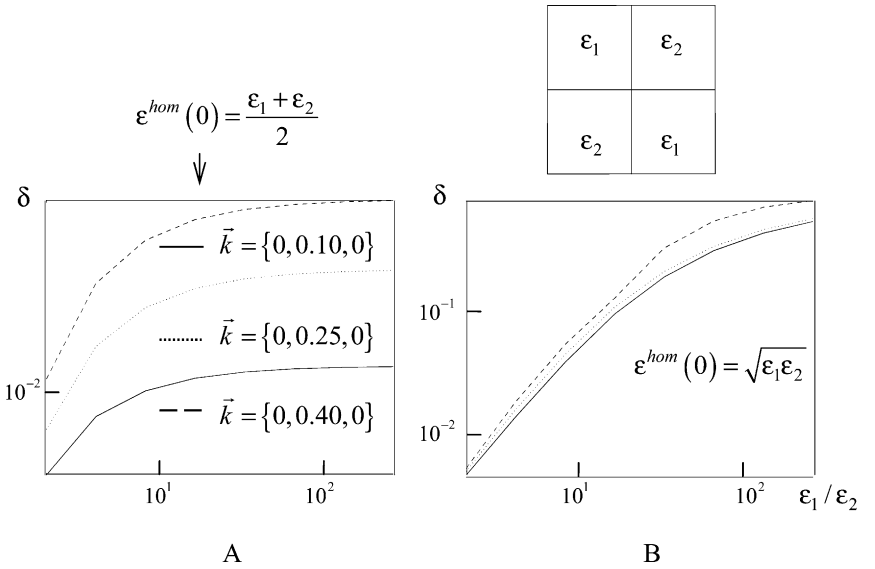

Fig. 5.6 The relative deviations δ depending on $\varepsilon_1/\varepsilon_2$ and $\vec{k} = \{k_x, k_y, k_z\}$: $\left|\vec{k}\right| = k$ for a checkerboard structure. The exact value for the classical homogenization is $(\varepsilon_1 + \varepsilon_2)/2$ for electric fields orthogonal to the plane, and $\sqrt{\varepsilon_1 \varepsilon_2}$ for electric fields in the plane: (**a**) *E*-polarization (**b**) *H*-polarization

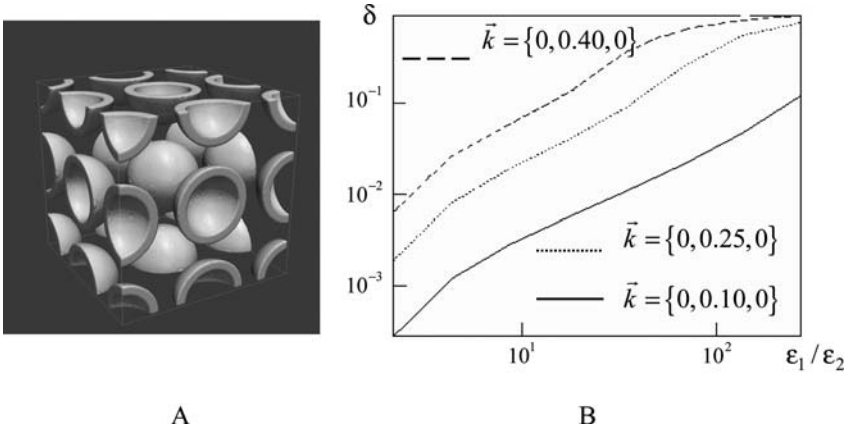

Fig. 5.7 The relative deviations δ depending on $\varepsilon_1/\varepsilon_2$ for a structure of spherical shells: (**a**) The geometry, where spherical shells with outer radius $0.3a$ are arranged in a cubic lattice; (**b**) the results for a wave propagating along a main coordinate axis is given (the results are the same for *E*- and *H*-polarizations due to symmetry)

[246], even when the period is a considerable fraction of the wavelength. This demonstrates that the classical homogenization works surprisingly well even when the wavelength is comparable to the size of the unit cell, provided that the contrast is small. This corresponds well to the analytical results in (5.8) and (5.9), where it

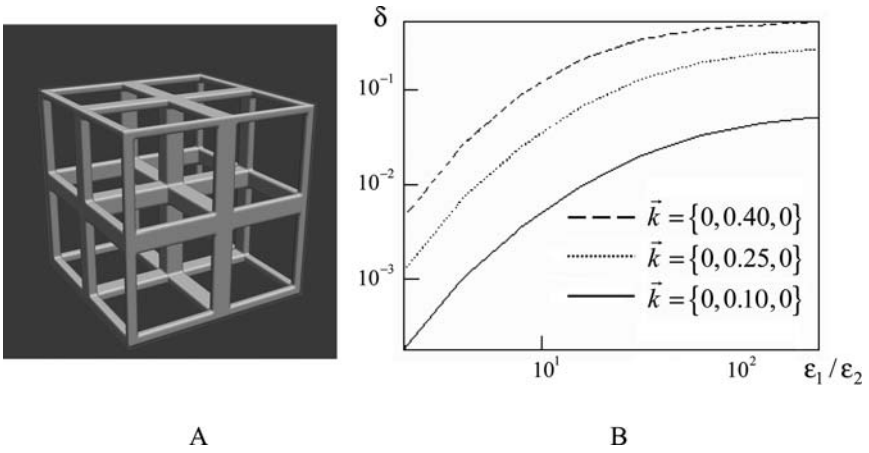

Fig. 5.8 (**a**) Scaffold structure, which is the same as in Fig. 5.1. (**b**) The relative deviations δ depending on $\varepsilon_1/\varepsilon_2$ for a wave propagating along a main coordinate axis. As in Fig. 5.7, the results for *E*- and *H*-polarizations are similar due to symmetry

is seen that the term corresponding to the spatial dispersion is multiplied by a factor directly linked to the contrast.

On the other hand, if we want to design materials which should exhibit *strong* spatial dispersion, we see from these results and the analytic results in equations (5.9) and (5.10) that strong contrasts should be employed. This is natural, since strong contrasts correspond to strong interaction between the electromagnetic field and the structure.

5.6.3 Results for a Chiral Structure

A classical method of synthesizing macroscopically chiral materials is by embedding spiral inclusions in an isotropic background medium. This was first attempted by Lindman in 1914 using metallic coils, all wound the same way as the chiral inclusions [247]. The result was a material with different properties for left- or right-hand circular polarization. In Fig.5.9a, unit cell with similar spirals is shown. This structure is analyzed using the homogenization procedure presented in this chapter.

Chiral structures have classically been modeled in many different ways. In Table 5.1 we list the three most common models for isotropic media, Tellegen/Pasteur,

Table 5.1 Three common models for chiral media. If $\chi \neq 0$ and $\kappa = 0$ we have the Tellegen medium, and if $\chi = 0$ and $\kappa \neq 0$ we have the Pasteur medium, which is what is usually meant by a chiral medium

	Tellegen/Pasteur	Post	Drude-Born-Fedorov
$\vec{D} =$	$\varepsilon_T \vec{E} + (\chi + i\kappa)\,\vec{H}$	$\varepsilon_P \vec{E} + i\xi \vec{B}$	$\varepsilon\left(\vec{E} + \beta \mathrm{rot} \vec{E}\right)$
$\vec{B} =$	$(\chi - i\kappa)\,\vec{E} + \mu_T \vec{H}$	$\mu_P(\vec{H} - i\xi \vec{E})$	$\mu\left(\vec{H} + \beta \mathrm{rot} \vec{H}\right)$

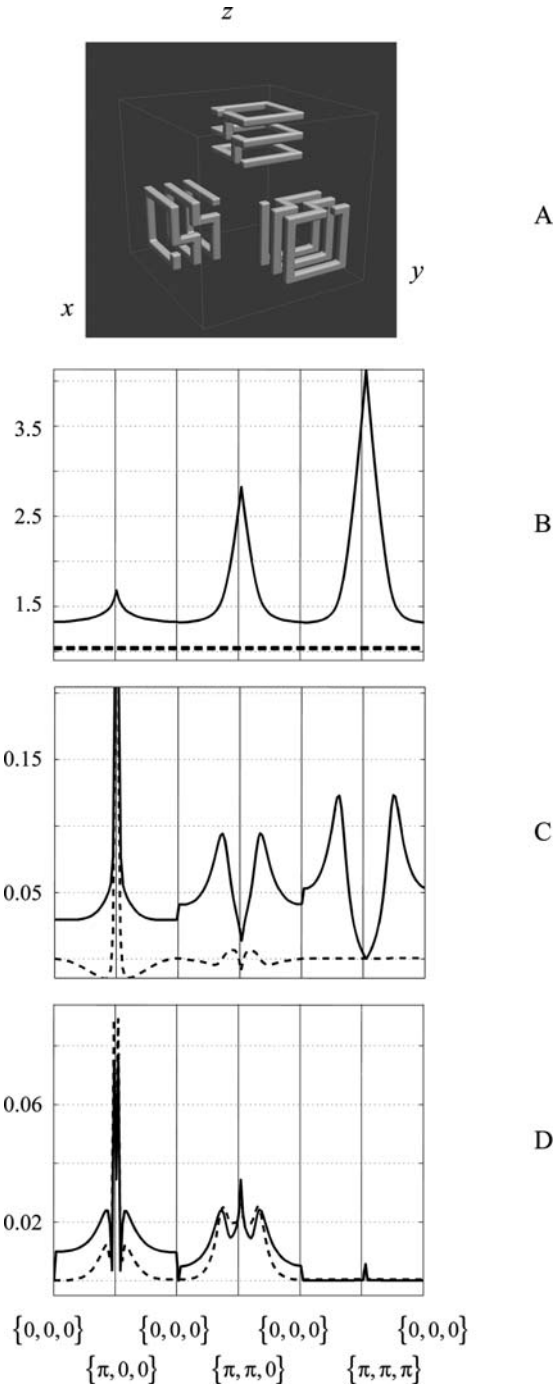

Fig. 5.9 Results for a chiral structure, where the horizontal axis in (**b** to **d**) corresponds to the wave vector γ: (**a**) The analyzed geometry; the computed parameters (**b**) ε (*solid line*), μ (*dashed line*); and (**c**) β_1/a (*solid line*), β_2/a (*dashed line*); (**d**) the errors δ_ε (*solid line*) and δ_μ (*dashed line*) of the parameter fit, which is almost entirely due to the slight non-isotropy of the structure (**a**)

Post, and Drude-Born-Fedorov (DBF). In source-free regions, all three models can be expressed in terms of each other using Maxwell's equations. This presents the interesting question which model should be considered the most correct one.

The Tellegen/Pasteur and Post models differ from the DBF model in the respect that they introduce a coupling between the electric and magnetic fields directly in the constitutive relation, whereas the DBF model introduces a dependence on the spatial derivatives on the fields instead.

We start by demonstrating that when the spirals are made of lossless dielectrics or PEC, the symmetry argument shown in Section 5.2.3 implies that there can be no coupling between the electric and magnetic field in the constitutive relation, in the respect that $\overline{\overline{\xi}}^{hom} = 0$ and $\overline{\overline{\zeta}}^{hom} = 0$ [248]. The symmetry relation states that if $\tilde{U}_n = \left[\tilde{U}_{ne}, \tilde{U}_{nh}\right]^T$ is an eigenvector with eigenvalue k_n, then so is $\tilde{U}_{\tilde{n}} = \left[\tilde{U}_{\tilde{n}e}, -\tilde{U}_{\tilde{n}h}\right]^T$ with eigenvalue $k_{\tilde{n}} = -k_n$. From this relation, it is seen that $\overline{\overline{\xi}}^{hom} = 0$, since we have

$$\begin{aligned}\overline{\overline{\xi}}^{hom} &= \sum_{n=1}^{6} \frac{\left\langle \overline{\overline{\varepsilon}}\tilde{E}_n \right\rangle \left\langle \overline{\overline{\mu}}\tilde{H}_n \right\rangle^H}{\left(\left\langle \overline{\overline{\varepsilon}}\tilde{E}_n \right\rangle^H \left\langle \tilde{E}_n \right\rangle \right) + \left(\left\langle \overline{\overline{\mu}}\tilde{H}_n \right\rangle^H \left\langle \tilde{H}_n \right\rangle \right)} \\ &= \sum_{n=1}^{3} \frac{\left\langle \overline{\overline{\varepsilon}}\tilde{E}_{2n-1} \right\rangle \left\langle \overline{\overline{\mu}}\tilde{H}_{2n-1} \right\rangle^H + \left\langle \overline{\overline{\varepsilon}}\tilde{E}_{2n-1} \right\rangle \left\langle -\overline{\overline{\mu}}\tilde{H}_{2n-1} \right\rangle^H}{\left(\left\langle \overline{\overline{\varepsilon}}\tilde{E}_{2n-1} \right\rangle^H \left\langle \tilde{E}_{2n-1} \right\rangle \right) + \left(\left\langle \overline{\overline{\mu}}\tilde{H}_{2n-1} \right\rangle^H \left\langle \tilde{H}_{2n-1} \right\rangle \right)} = 0\end{aligned}$$

with the same conclusion for $\overline{\overline{\zeta}}^{hom} = 0$. Thus, using this simple symmetry argument, we see that our homogenization method can never predict the Tellegen/Pasteur or Post model of any chiral structure. The only model left for consideration is then the DBF model.

This does not mean that there cannot be any chiral effects. Since the homogenized material parameters depend on the wave number γ, the most general isotropic homogenized permittivity that can be allowed is (where we must subtract $\hat{\gamma}\,\hat{\gamma}$ from the identity matrix in order to account for the fact we only consider polarizations orthogonal to the propagation direction)

$$\overline{\overline{\varepsilon}}^{hom}(\gamma) = \varepsilon \left(\overline{\overline{E}} - \hat{\gamma}\,\hat{\gamma} + \left[\beta i \gamma \times\right] \right).$$

Since an inverse Fourier transform of this implies $\vec{D} = \varepsilon(\vec{E} + \beta \mathrm{rot}\vec{E})$, this is equivalent to the Drude-Born-Fedorov model. With the homogenization method presented in this chapter, the calculation of the homogenized material parameters $\overline{\overline{M}}^{hom}(\gamma) = \left[\overline{\overline{\varepsilon}}^{hom}(\gamma), 0; 0, \overline{\overline{\mu}}^{hom}(\gamma)\right]$ is unbiased by any model. Since the structure is macroscopically isotropic, we attempt to fit the parameters in the models

$$\bar{\bar{\varepsilon}}^{mod}(\gamma) = \varepsilon\left(\bar{\bar{E}} - \hat{\gamma}\,\hat{\gamma} + \left[\beta_1 i\gamma\times\right]\right), \bar{\bar{\mu}}^{mod}(\gamma) = \mu\left(\bar{\bar{E}} - \hat{\gamma}\,\hat{\gamma} + \left[\beta_2 i\gamma\times\right]\right),$$

which are the most general isotropic models orthogonal to the propagation direction. Since $\left[i\gamma \times \langle\tilde{E}\rangle\right]$ corresponds to rot$\vec{E}$, we see that the combination of $\bar{\bar{\varepsilon}}^{mod}(\gamma)$ and $\bar{\bar{\mu}}^{mod}(\gamma)$ corresponds to a generalized DBF model with different β-factors for the electric and magnetic field, respectively. The parameters are calculated from the material parameters $\bar{\bar{\varepsilon}}^{hom}$ and $\bar{\bar{\mu}}^{hom}$ computed from the unbiased finite scale homogenization using the formulas

$$\varepsilon = tr\left(\bar{\bar{\varepsilon}}^{hom}\right)/2,\ \varepsilon\beta_1 = tr\left[i\gamma \times \bar{\bar{\varepsilon}}^{hom}\right]/2,\ \mu = tr\left(\bar{\bar{\mu}}^{hom}\right)/2,\ \mu\beta_2 = tr\left[i\gamma \times \bar{\bar{\mu}}^{hom}\right]/2,$$

which are exact if the model is correct. Here, tr$\left(\bar{\bar{\varepsilon}}^{hom}\right)$ denotes the trace of the matrix $\bar{\bar{\varepsilon}}^{hom}$, i.e., the sum of the diagonal elements. The error in the parameter fit is measured as

$$\delta_\varepsilon = \frac{\left\|\bar{\bar{\varepsilon}}^{mod} - \bar{\bar{\varepsilon}}^{hom}\right\|}{\left\|\bar{\bar{\varepsilon}}^{hom}\right\|},\ \delta_\mu = \frac{\left\|\bar{\bar{\mu}}^{mod} - \bar{\bar{\mu}}^{hom}\right\|}{\left\|\bar{\bar{\mu}}^{hom}\right\|}.$$

The results are depicted in Fig. 5.9. It is seen that in general the chirality parameters β_1 and β_2 are different, and in particular when studying the classical homogenization limit of vanishing wave vector γ we have

$$\beta_1 \to \beta_0 \neq 0 \quad \text{and} \quad \beta_2 \to 0 \quad \text{as} \quad |\gamma| \to 0.$$

The value β_0 is in the order of $0.04a$, and depends on in which direction the origin is approached. This does not contradict the isotropy of the material, since as soon as the propagation direction is fixed and the wave number is not zero, the symmetry is broken. Since the β-factors are multiplied by the wave number, their contribution vanish in the classical homogenization limit where the wave number is taken to be zero.

An interesting note on this result is that this suggests that in the limit of infinite scale difference, our homogenization method predicts a modification of the Drude-Born-Fedorov model

$$\vec{D} = \varepsilon\left(\vec{E} + \beta\text{rot}\vec{E}\right), \vec{B} = \mu_0\vec{H},$$

which is actually Born's original model [249, 250].

In Fig. 5.9 we can see that the magnetic response in terms of the permeability μ is identically one for all wave numbers, whereas the corresponding β-factor varies as a function of the wave vector. The errors in the parameter fit are small, and are mostly due to the fact that the structure is not completely isotropic, since the spirals are realized using rectangular blocks.

5.7 Conclusions

In this chapter, we have presented a means for computing effective material parameters for a broad class of structures. Any bianisotropic structure can in principle be treated, but the range of validity has only been proven in a restricted sense, where the estimates typically depend on the contrast of the materials.

Several examples of applying the method to specific structures have been provided. Most of them are concerned with classical electric material properties, described by a permittivity depending on the wave vector of the applied field, corresponding to spatial dispersion. This may provide useful models for predicting qualitative features of the electromagnetic field, but is not straightforward to apply in a scattering computation, since then the boundary conditions need to be treated with extra care.

As a particular case, we have demonstrated that a chiral structure made up of spirals all wound the same way can be modeled with a modified Drude-Born-Fedorov model, where in the long wavelength limit only the curl of the electric field contributes to the electric flux density but the magnetic properties are not affected. This is Born's original model of optically active media.

Appendix
The List of the Symbols and Abbreviations

$\mathbf{R}^n$ and $\mathbf{G} \subset \mathbf{R}^n$	n-dimensional Euclidean space and domain $\mathbf{G}$ in it
g and p	Points of the space $\mathbf{R}^3$ or $\mathbf{R}^2$; x, y, z – Cartesian coordinates; ρ, ϕ, z – cylindrical coordinates; r, ϑ, ϕ – spherical coordinates
t and τ; $(0;\ T)$, $T < \infty$	Time variables; the observation interval
$\vec{E} \equiv \vec{E}(g,t) = \{E_x,E_y,E_z\}$ and $\vec{H} \equiv \vec{H}(g,t) = \{H_x,H_y,H_z\}$	Vectors of the electrical and magnetic field
$\eta_0 = (\mu_0/\varepsilon_0)^{1/2}$, ε_0, and μ_0	Free space impedance, electric and magnetic vacuum constants
$\sigma_0(g)$, $\varepsilon(g)$, and $\mu(g)$; $\sigma = \eta_0\sigma_0$	Specific conductivity, relative dielectric permittivity, and magnetic conductivity for a locally inhomogeneous, isotropic, nondispersive medium
$\mathbf{Q}$	Unbounded domain of analysis in boundary value and initial boundary value problems; $\mathbf{Q}^T = \mathbf{Q} \times (0;T)$
$\mathbf{R} = \{g \in \mathbf{R}^2 : 0 < y < l\}$ and $\mathbf{R} = \{g \in \mathbf{R}^3 : 0 < x < l_x;\ 0 < y < l_y\}$	Parallel-plane and rectangular Floquet channels
$\mathbf{Q}_a$	Bounded subdomain of the domain $\mathbf{Q}$; ${}_a\mathbf{Q} = \mathbf{Q}\backslash\bar{\mathbf{Q}}_a$ is a complement of $\bar{\mathbf{Q}}_a$ up to $\mathbf{Q}$
$\bar{\mathbf{G}}$, $\mathbf{G} \cup \mathbf{Q}$, $\mathbf{G} \cap \mathbf{Q}$, and $\mathbf{G}\backslash\mathbf{Q}$	Closure, union, intersection, and difference of sets
$\mathbf{C}^n(\mathbf{G})$	Class of functions that are continuous together with all their derivatives including n order in $\mathbf{G}$
$\mathbf{D}(\mathbf{G})$	Sets of finite and infinitely differentiable in $\mathbf{G}$ functions

Y.K. Sirenko, S. Ström (eds.), *Modern Theory of Gratings*, Springer Series in Optical Sciences 153, DOI 10.1007/978-1-4419-1200-8,

$\tilde{\mathbf{D}}(\mathbf{G})$	Space of generalized functions (linearly continuous functionals) on the space of fundamental functions $\mathbf{D}(\mathbf{G})$
(f,γ)	Value of functional (generalized function f) on fundamental function $\gamma \in \mathbf{D}(\mathbf{G})$
$\tilde{\mathbf{D}}_r(\mathbf{G})$	Class of regular (locally integrable) generalized functions
$\mathbf{L}_n(\mathbf{G})$	Space of functions $f(g)$, $g \in \mathbf{G}$, for which function $\lvert f(g)\rvert^n$ is integrable in $\mathbf{G}$
$\mathbf{W}_m^l(\mathbf{G})$	Set of all the elements $f(g)$ from $\mathbf{L}_m(\mathbf{G})$, having generalized derivatives up to the order l, including, from $\mathbf{L}_m(\mathbf{G})$
$\mathbf{L}_{2,1}\left(\mathbf{G}^T\right)$	Space containing all elements $f(g,t) \in \mathbf{L}_1\left(\mathbf{G}^T\right)$ with finite norm $\lVert f\rVert = \int_0^T \left(\int_{\mathbf{G}} \lvert f\rvert^2\, dg\right)^{1/2} dt$
$\overset{\circ}{\mathbf{W}}{}_2^1(\mathbf{G})$	Subspace of space $\mathbf{W}_2^1(\mathbf{G})$, where $\mathbf{D}(\mathbf{G})$ is a dense set
$\mathbf{W}_{2,0}^1\left(\mathbf{G}^T\right)$	Subspace of space $\mathbf{W}_2^1\left(\mathbf{G}^T\right)$, where smooth functions, equal to zero in the vicinity of $\mathbf{P}^T = \mathbf{P} \times (0,T)$ ($\mathbf{P}$ is a boundary of domain $\mathbf{G}$), is a dense set
$\mathbf{C}$	Plane of complex variable w or s
Ø	Empty set
$l_2 = \left\{a = \{a_n\}:\ \sum_n \lvert a_n\rvert^2 < \infty\right\}$, $\tilde{l}_2 = \left\{a:\ \sum_n \lvert a_n\rvert^2 (\lvert n\rvert + 1) < \infty\right\}$, and $l_2(\eta) = \left\{a:\ \sum_n \lvert a_n\rvert^2 (1 + \lvert n\rvert)^\eta < \infty\right\}$	Spaces of infinite sequences $a = \{a_n\}$; $l_2(1) = \tilde{l}_2$
$U(g,t)$ and $\tilde{U}(g,k)$	Unknown functions of 2-D initial boundary value problems and boundary value problems, defining components of vectors of field strength
$v_n(z,t)$, $u_n(z,t)$, and so on	Spatial–temporal amplitudes of pulsed waves

$\tilde{f}(k) \leftrightarrow f(t)$	Functions (image and original), relevant to Laplace transform over $s = -ik$
$k = 2\pi/\lambda$ and λ; $\kappa = l/\lambda$	Wavenumber (frequency parameter or simply frequency) and wavelength in a free space; nondimensional frequency parameter
$U^i(g,t)$ and $\tilde{U}^i(g,k)$	Functions, defining the components of the vectors of the field density of incident wave
$\mathbf{S}$ and $\mathbf{S}^{\varepsilon,\mu,\sigma}$	Surfaces of break of properties of medium where the excitation propagates – boundaries of perfectly conducting and dielectric scatterers
$\mathbf{S}_x$ and $\mathbf{S}_x^{\varepsilon,\mu,\sigma}$	Trace of the surfaces $\mathbf{S}$ and $\mathbf{S}^{\varepsilon,\mu,\sigma}$ in coordinate plane $x = \text{const}$ – boundary contours of inhomogeneouties in 2-D initial boundary value problems and boundary value problems
$\overline{\text{int}\mathbf{S}}$	Closure of the domain, filled with perfectly conducting scatterer or domain, bounded with perfectly conducting surface $\mathbf{S}$
$\tilde{k}$, $\tilde{\alpha}$, $\tilde{\beta}$, $\tilde{T}$, and $\bar{T}$	Parameters of signals
$\varphi(g)$, $\psi(g)$, and $F(g,t)$	Instant ($\varphi(g)$ and $\psi(g)$) and current ($F(g,t)$) sources of signals and pulsed waves
$F_j(t), j = 1,2,3,4$	Functions, defining dynamic characteristic of the sources
$l(2\pi)$ and $h(2\pi\delta)$	The principal geometrical parameters of 1-D periodic gratings: the length of a period and height
$R_{np}^{\mathbf{AA}} \exp\left[i(\Phi_n y + \Gamma_n z)\right]$ and $T_{np}^{\mathbf{BA}} \exp\left[i(\Phi_n y - \Gamma_n (z+h))\right]$, $n = 0, \pm 1, \pm 2, \ldots$	Spatial harmonics of a scattered field in the domain of reflected ($\mathbf{A}$) and transmitted fields ($\mathbf{B}$) of grating; $\Phi_n = 2\pi(\Phi + n)/l$, $\Gamma_n = \sqrt{k^2 - \Phi_n^2}$, $\text{Re}\Gamma_n \text{Re}k \geq 0$, $\text{Im}\Gamma_n \geq 0$
$\mathbf{K}$ and $\mathbf{F}$	Infinitely sheeted Riemann surfaces of variation of complex (nonphysical) values of frequency parameter k and parameter Φ of Floquet channel $\mathbf{R}$
$k_n^{\pm} = \pm\lvert\Phi_n\rvert$ and $\Phi_n^{\pm}$	Branching points of surfaces $\mathbf{K}$ and $\mathbf{F}$ (threshold points)
Ω_k and Ω_Φ	Spectra of open resonators and waveguides (eigenfrequencies and eigen propagation constants)
$\bar{k}_n$ and $\overline{\Phi}_n$	Elements of spectral sets Ω_k and Ω_Φ

$u_0^{(j)}\left(g,\bar{k}_n\right)$ and $u_0^{(j)}\left(g,\bar{\Phi}_n\right)$	Eigenmodes and eigenwaves of periodic open resonators and periodic directing structures
k_m or k_{mj}	Cutoff frequency of mth wave in jth waveguide
$W_{np}^{jq}(k)$	Relative part of energy concentrate in the nth waveguide mode in jth waveguide when pth stimulating mode is coming from qth waveguide
$D(\phi,k,M)$ and $\eta(k)$	Normalized pattern of the radiator and its efficiency
$(f * g)$; $(f \times g)$, $\left(\vec{a}\cdot\vec{b}\right)$, $\left[\vec{a}\times\vec{b}\right]$; f^*	Operation of convolution, direct, scalar and vector products; and complex conjugation
$[a;b]$ and $(a;b)$, $\{a_n\}$	Close and open intervals, set of elements a_n
$\delta(...)$ and $\delta^{(m)}(...)$	δ -Dirac function and its derivative of mth order
δ_m^n	Kronecker symbol
$\chi(...)$	Heaviside step function
$\chi\left[f_1(g)\right]\chi\left[f_2(g)\right]...\chi\left[f_m(g)\right]$	Generalized step function, equal to unity on the intersection $\mathbf{G}$ of sets $\mathbf{G}_j = \left\{g \in \mathbf{R}^n : f_j(g) \geq 0\right\}, j = 1,2,...m$, and equal to zero on $\mathbf{R}^n \backslash \mathbf{G}$
$G(...)$	Fundamental solution (Green function) of differential operator
$J_n(...)$, $N_n(...)$, and $H_n^{(1)}(...)$	Bessel, Neumann, and Hankel cylindrical functions
$P_v(...)$ and $Q_v(...)$ ($P_n^m(...)$ and $Q_n^m(...)$)	Legendre functions (adjoint Legendre functions) of the first and second kind
Re (w) and Im (w)	Real and imaginary parts of the complex value of w
Res $f(w_n)$	Residue of $f(w)$ at a point $w = w_n$
EACs	Exact absorbing conditions
ABCs	Absorbing boundary conditions
PMLs	Perfectly matched layers
FD	Frequency domain
TD	Time domain
BVP	Boundary value problem

References

1. Sirenko, Y.K., Ström, S., Yashina, N.P.: *Modeling and Analysis of Transient Processes in Open Resonant Structures. New Methods and Techniques*. Springer, New York (2007).
2. Vladimirov, V.S.: *Equations of Mathematical Physics*. Dekker, New York (1971).
3. Rothwell, E.J., Cloud, M.J. *Electromagnetics*. CRC Press, New York (2001).
4. Taflove, A., Hagness, S.C.: *Computational Electrodynamics: The Finite-Difference Time-Domain Method*. Artech House, Boston (2000).
5. Ladyzhenskaya, O.A.: *The Boundary Value Problems of Mathematical Physics*. Springer-Verlag, New York (1985).
6. Borisov, V.V.: *Electromagnetic Fields of Transient Currents*. St. Petersburg University Press, St. Petersburg (1996) (in Russian).
7. Vladimirov, V.S. (ed.): *Collected Example Equations of Mathematical Physics*. Nauka, Moscow (1974) (in Russian).
8. Waynberg, B.R.: *Asymptotic Methods in the Equations of Mathematical Physics*. Moscow State University Press, Moscow (1982) (in Russian).
9. Colton, D., Kress, R.: *Integral Equation Methods in Scattering Theory*. Wiley-Interscience, New York (1983).
10. Shestopalov, V.P., Sirenko, Y.K.: *Dynamic Theory of Gratings*. Naukova Dumka, Kiev (1989) (in Russian).
11. Shestopalov, V.P., Tuchkin, Y.A., Poyedinchuk, A.Y., Sirenko, Y.K.: *New Solution Methods for Direct and Inverse Problems of the Diffraction Theory. Analytical Regularization of the Boundary Value Problems in Electromagnetic Theory*. Osnova, Kharkov (1997) (in Russian).
12. Sirenko, Y.K., Shestopalov, V.P.: On the extraction of physical solutions to the wave diffraction problems on one-dimensional periodic gratings. *Rep. Acad. Sci. USSR*, **297**, No.6, 1346–1350 (1987) (in Russian).
13. Sirenko, Y.K., Shestopalov, V.P.: The principles of radiation, limiting absorption and limiting amplitude in the wave diffraction problems on one-dimensional periodic gratings. *J. Comput. Math. Math. Phys.*, **27**, No.10, 1555–1562 (1987) (in Russian).
14. Keldysh, M.V.: On the completeness of eigenfunctions of some classes of not self-adjoint linear operators. *Advances Math. Sci.*, **26**, No.4, 15–41 (1971) (in Russian).
15. Hokhberg, I.Z., Seagul, Y.I.: Operator generalization of the theorem about logarithmic residue and the Rouche theorem. *Coll. Papers Math.*, **84**, No.4, 607–629 (1971) (in Russian).
16. Shestopalov, V.P., Litvinenko, L.N., Masalov, S.A., Sologub, V.G.: *Wave Diffraction by Gratings*. Kharkov State University Press, Kharkov (1973) (in Russian).
17. Shestopalov, V.P., Kirilenko, A.A., Masalov, S.A.: *Matrix Convolution-Type Equations in the Diffraction Theory*. Naukova Dumka, Kiev (1984) (in Russian).
18. Shestopalov, V.P., Kirilenko, A.A., Masalov, S.A., Sirenko, Y.K.: *Resonance Wave Scattering. Vol. 1. Diffraction Gratings*. Naukova Dumka, Kiev (1986) (in Russian).
19. Petit, R. (ed.): *Electromagnetic Theory of Gratings*. Springer-Verlag, New York (1980).

20. Shestopalov, V.P., Kirilenko, A.A., Masalov, S.A.: Reciprocity principle and some physical patterns of wave scattering by diffraction gratings. *Bull. Acad. Sci. Ukrain. SSR*, No.3, 8–18 (1975) (in Russian).
21. Litvinenko, L.N., Prosvirnin, S.L.: *Spectral Scattering Operators in the Problems of the Wave Diffraction by Plane Screens*. Naukova Dumka, Kiev (1984) (in Russian).
22. Masalov, S.A., Sologub, V.G.: A rigorous solution of electromagnetic wave diffraction by some strip structure. *J. Comput. Math. Math. Phys.*, **10**, No.3, 693–715 (1970) (in Russian).
23. Reed, M., Simon, B.: *Methods of Modern Mathematical Physics. IV: Analysis of Operators*. Academic, New York (1978).
24. Sanchez-Palencia, E.: *Non-Homogeneous Media and Vibration Theory*. Springer-Verlag, New York (1980).
25. Sirenko, Y.K., Shestopalov, V.P.: Uniqueness of solutions of spectral problems for one-dimensional periodic lattices. *Soviet Phys. Doklady*, **30**, No.11, 928–930 (1985).
26. Sirenko, Y.K.: Analytical extension of diffraction problems and threshold effects in electromagnetics. *Rep. Acad. Sci. Ukrain. SSR*, **Ser.**A, No.8, 65–68 (1986) (in Russian).
27. Sirenko, Y.K., Shestopalov, V.P.: Free oscillations of electromagnetic field in one-dimensional periodic gratings. *J. Comput. Math. Math. Phys.*, **27**, No.2, 262–271 (1987) (in Russian).
28. Sirenko, Y.K., Shestopalov, V.P., Yatsik, V.V.: A computational algorithm for electromagnetic field quasi-stationary states in waveguide type gratings. *Rep. Acad. Sci. Ukrain. SSR*, **Ser.**A, No.9, 60–64 (1985) (in Russian).
29. Hokhberg, I.Z., Krein, M.G.: *Introduction into the Theory of Linear Not Self-Adjoint Operators*. Nauka, Moscow (1965) (in Russian).
30. Shestopalov, V.P.: *The Morse Critical Points of Dispersion Equations*. Naukova Dumka, Kiev (1992) (in Russian).
31. Sirenko, Y.K., Shestopalov, V.P., Yatsik, V.V.: The Morse critical points of dispersion equations of diffraction gratings. *Ukrain. Phys. J.*, **36**, No.8, 1156–1162 (1991) (in Russian).
32. Poston, T., Steward, I.: *Catastrophe Theory and its Applications*. Pinman, London (1978).
33. Arnold, V.I., Varchenko, A.N., Gussein-Zade, S.M.: *Typical Features of Differentiable Images*. Nauka, Moscow (1982) (in Russian).
34. Melezhik, P.N., Poyedinchuk, A.Y., Tuchkin, Y.A., Shestopalov, V.P.: On the analytical nature of the inter-mode coupling of eigenoscillations. *Rep. Acad. Sci. USSR*, **300**, No.6, 1356–1359 (1988) (in Russian).
35. Kirilenko, A.A., Senkevitch, S.L., Tysik, B.G., Sirenko, Y.K.: On the recovering of scattering matrices of waveguide and periodic structures on the spectrum of complex eigenfrequencies. *Radio-Eng. Electron.*, **34**, No.3, 468–473 (1989) (in Russian).
36. von Hurwitz, A.: *Allgemeine Funktionentheorie und Elliptische Funktionen.* von Courant, R.: *Geometrische Funktionentheorie*. Springer-Verlag, Berlin (1964) (in German).
37. Sirenko, Y.K.: New results in the theory of open periodic directing structures. *Higher school news. Radio-Phys.*, **32**, No.3, 331–338 (1989) (in Russian).
38. Sirenko, Y.K.: A grating in the field of a compact monochromatic source. *Electromagnetics*, **13**, No.3, 255–272 (1993).
39. Dolph, C.L.: Recent developments in some non-self-adjoint problems of mathematical physics. *Bull. Amer. Math. Soc.*, **67**, No.1, 1–69 (1961).
40. Sirenko, Y.K.: *Simulation and Analysis of Transient Processes in Open Periodic, Waveguide, and Compact Resonators*. EDENA, Kharkov (2003) (in Russian).
41. Sirenko, Y.K., Velychko, L.G.: Model synthesis of the grating type absorbing and pattern forming structures. *Electromag. Waves Electron. Syst.*, **7**, No.2, 45–59 (2002) (in Russian).
42. Mittra, R., Lee, S.: *Analitical Techniques in the Theory of Guided Waves*. Macmillan, New York (1971).
43. Galishnikova, T.N., Il'inskiy, A.S.: *Numerical Methods in the Diffraction Problems*. Moscow State University Press, Moscow (1987) (in Russian).

44. Fedoryuk, M.V.: *Saddle-Point Technique*. Nauka, Moscow (1977) (in Russian).
45. Shestopalov, V.P.: *The Method of the Riemann-Hilbert Problem in the Theory of Electromagnetic Wave Diffraction and Propagation*. Kharkov State University Press, Kharkov (1971) (in Russian).
46. Steinschleiger, V.B.: *Effect of Wave Interaction in Electromagnetic Resonators*. Oboronizdat, Moscow (1955) (in Russian).
47. Koshparenok, V.N., Melezhik, P.N., Poyedinchuk, A.Y., Shestopalov, V.P.: Wave interaction in open resonators. *Rep. Acad. Sci. USSR*, **279**, No.5, 1114–1117 (1984) (in Russian).
48. Koshparenok, V.N., Melezhik, P.N., Poyedinchuk, A.Y., Shestopalov, V.P.: The method of the Riemann-Hilbert in the spectral theory of open two-dimensional resonators. 2. Spectral characteristics. *Radio-Eng. Electron.*, **32**, No.2, 238–247 (1987) (in Russian).
49. Melezhik, P.N.: Mode conversion in diffractionally coupled open resonators. *Telecomm. Radio Eng.*, **51**, No.6&7, 54–60 (1997).
50. Svezhentsev, A.E.: Effect of inter-mode coupling of surface waves in partially screened dielectric rod. *Rep. Acad. Sci. Ukrain. SSR*, **Ser.**A, No.7, 58–62 (1986) (in Russian).
51. Pochanina, I.Y., Shestopalov, V.P., Yashina, N.P.: Interaction and degeneration of eigenoscillations in open waveguide resonators. *Rep. Acad. Sci. USSR*, **320**, No.1, 90–95 (1991) (in Russian).
52. Pochanina, I.E., Yashina, N.P.: Electromagnetic properties of open waveguide resonator. *Electromagnetics*, **13**, No.3, 289–300 (1993).
53. Krein, M.G., Lyubarsky, G.Y.: On the theory of the pass bands of periodic waveguides. *Appl. Math. Mech.*, **25**, No.1, 24–37 (1961) (in Russian).
54. Sirenko, Y.K., Yashina, N.P., Schuenemann, K.F.: Synthesis of mode converters in waveguides and gratings based on spectral theory. *J. Electromag. Waves Appl.*, **16**, No.5, 611–628 (2002).
55. Hsiao, G.C., Kleinman, R.E.: Book analysis in numerical solution of acoustic integral equations. *Int. J. Num. Meth.*, **37**, 2921–2933 (1994).
56. Hsiao, G.C., Kleinman, R.E.: Mathematical foundations for book estimation in numerical solutions of integral equations in electromagnetics. *IEEE Trans.*, **AP-47**, No.3, 316–328 (1997)
57. Poyedinchuk, A.Y., Tuchkin, Y.A., Shestopalov, V.P.: New numerical-analytical methods in diffraction theory. *Math. Comput. Modeling*., **32**, No.9, 1029–1046 (2000).
58. Tuchkin, Y.A.: New method in wave diffraction theory by thin screens. *Electromagnetics*, **13**, No.3, 319–338, (1993).
59. Tuchkin, Y.A.: Analytical regularization method for wave diffraction by bowl-shaped screen of revolution. In D. Smith, S.R. Cloude (eds.) *Ultra-Wideband Short-Pulse Electromagnetics* **5**, 153–157. Kluwer Academic/Plenum Publishers, New York (2002).
60. Tuchkin, Y.A.: Method of analytical regularization: State of art and new approaches. *Proc. Fourth Int. Workshop Electromagn. Wave Scatt., Gebze, Turkey*, **2**, 43–49 (2006).
61. Panin, S.B., Smith, P.D., Vinogradova, E.D., Tuchkin, Y.A., Vinogradov, S.S.: Regularization of the Dirichlet problem for Laplace's equation: Surfaces of revolution. *Electromagnetics*, **29**, No.1, 53–76 (2009).
62. Vinogradov, S.S., Smith, P.D., Vinogradova, E.D.: *Canonical Problems in Scattering and Potential Theory. Part 1: Canonical Structures in Potential Theory*. Chapman & Hall/CRC, Boca Raton, FL (2001).
63. Tuchkin, Y.A.: The wave scattering by an unclosed arbitrarily shaped cylindrical screen with Dirichlet boundary condition. *Rep. Acad. Sci. USSR*, **285**, No.6, 1370–1373 (1985) (in Russian).
64. Tuchkin, Y.A.: The wave scattering by an unclosed arbitrarily shaped cylindrical screen with Neumann boundary condition. *Rep. Acad. Sci. USSR*, **293**, No.2, 343–345 (1987) (in Russian).
65. Vinogradov, S.S., Tuchkin, Y.A., Shestopalov, V.P.: Investigation of dual series equations involving Jacoby polynomials. *Rep. Acad. Sci. USSR*, **253**, No.1, 318–321 (1980) (in Russian).

66. Vinogradov, S.S., Tuchkin, Y.A., Shestopalov, V.P.: Summator equations with kernels in the form of Jacobi polynomials. *Soviet Phys. Doklady*, **27**, No.7, 231–232 (1980).
67. Vinogradov, S.S., Shestopalov, V.P.: Solution of a vectorial scattering problem for a sphere with a hole. *Rep. Acad. Sci. USSR*, **237**, No.1, 60–63 (1977) (in Russian).
68. Svischev, Y.V., Tuchkin, Y.A.: Regularization of the problem of diffraction of an arbitrary electromagnetic wave by a perfectly conduction spherical cap. *J. Comput. Math. Math. Phys.*, **38**, No.2, 262–276 (1998) (in Russian).
69. Tikhonov, A.N., Arsenine, V.Y.: *Solutions of Ill-Posed Problems*. Winston, Washington, DC (1977).
70. Kantorovich, L.V., Akilov, G.P.: *Functional Analysis in Normed Spaces*. Pergamon Press, New Work (1982).
71. Wilkinson, J.H.: *The Algebraic Eigenvalue Problem*. Oxford University Press, USA (1988).
72. Krein, S.G.: *Linear Equations in Banach Spaces*. Birkhauser, Boston (1982).
73. Vinogradov, S.S., Tuchkin, Y.A., Shestopalov, V.P.: To the problem of waves diffraction by unclosed screens of spherical shape. *Rep. Acad. Sci. USSR*, **256**, No.6, 1346–1350 (1981) (in Russian).
74. Shestopalov, V.P.: *Summator Equations in Contemporary Diffraction Theory*. Naukova Dumka, Kiev (1983) (in Russian).
75. Poyedinchuk, A.Y., Tuchkin, Y.A., Shestopalov, V.P.: Diffraction by curved strips. *Trans. IEE Jpn.*, **113-A**, No.3, 139–146 (1993).
76. Tversky, V.: On scattering of waves by infinite grating of circular cylinders. *IRE Trans. Anten. Propag.*, **10**, No.6, 757–765 (1962).
77. Veliyev, E.I., Sologub, V.G., Shestopalov, V.P.: Diffraction of -polarized electromagnetic waves by grating composed of cylinders with longitudinal slots. *Rep. Acad. Sci. Ukrain. USSR*, **Ser.**A, No.3, 243–247 (1976) (in Russian).
78. Tarapov, I.Y.: The diffraction problem of an arbitrarily profile grating. *J. Comput. Math. Math. Phys.*, **5**, No.5, 883–893 (1965) (in Russian).
79. Agranovich, Z.S., Marchenko, V.A., Shestopalov, V.P.: Diffraction of electromagnetic waves from plane metallic gratings. *J. Tech. Phys.*, **32**, No.4, 381–394 (1962) (in Russian).
80. Muskhelishvili, N.I.: *Singular Integral Equations*. Dover, New Work (1992).
81. Riesz, M.: L'integrale de Riemann-Liouville et le probleme de Cauchy. *Acta Mathematice*, **81**, No.1&2, 1–223 (1949) (in French).
82. Koshparenok, V.N, Shestopalov, V.P.: The plane electromagnetic wave diffraction by a circular cylinder with a longitudinal slot. *J. Comput. Math. Math. Phys.*, **11**, No.3, 721–729 (1971) (in Russian).
83. Sologub, V.G.: On a solution of some convolution type integral equation with finite limits of integration. *J. Comput. Math. Math. Phys.*, **11**, No.4, 837–845 (1971) (in Russian).
84. Sologub, V.G.: The plane wave diffraction by a strip grating in the short wavelength case. *J. Comput. Math. Math. Phys.*, **12**, No.4, 974–982 (1972) (in Russian).
85. Sologub, V.G.: On some method for studying the problem of diffraction by a finite number of strips in the same plane. *Rep. Acad. Sci. Ukrain. SSR*, **Ser.**A, No.6, 550–556 (1975) (in Russian).
86. Tikhonov, A.N., Samarsky, A.A.: *Mathematical Physical Equations*. Nauka, Moscow (1977) (in Russian).
87. Koshparenok, V.N., Melezhik, P.N., Poyedinchuk, A.Y., Shestopalov, V.P.: A rigorous method for studying the electromagnetic action by a system of several resonant scatterers. *Rep. Acad. Sci. USSR*, **252**, No.2, 328–331 (1980) (in Russian).
88. Koshparenok, V.N., Melezhik, P.N., Shestopalov, V.P.: Helmholtz resonators in electrodynamics. *Rep. Acad. Sci. USSR*, **250**, No.2, 344–347 (1980) (in Russian).
89. Koshparenok, V.N., Melezhik, P.N., Poyedinchuk, A.Y.: Rigorous solution to the 2-D problem of diffraction by a finite number of curved screens. *Comput. Math. Math. Phys.*, **23**, No.1, 140–151 (1983).

90. Koshparenok, V.N., Melezhik, P.N., Poyedinchuk, A.Y., Shestopalov, V.P.: The Riemann-Hilbert method in the spectral theory of open two-dimensional resonators. I. Mathematical model and spectral characteristics. *Radio-Eng. Electron.*, **31**, No.2, 271–278 (1986) (in Russian).
91. Koshparenok, V.N., Melezhik, P.N., Poyedinchuk, A.Y., Shestopalov, V.P.: The spectral theory of open two-dimensional resonators with dielectric insertions. *J. Comput. Maths. Math. Phys.*, **25**, No.4, 562–573 (1985) (in Russian).
92. Poyedinchuk, A.Y., Tuchkin, Y.A., Shestopalov, V.P.: The Riemann-Hilbert problem method in theory of diffraction by shells of arbitrary cross section. *Comput. Math. Math. Phys.*, **38**, No.8, 1260–1273 (1998).
93. Carleman, T.: Sur la resolution de certaines equations integrals. *Arciv Math. Astr. Fys. Bd.*, **16**, No.26, 112–118 (1922) (in French).
94. Lavrentyev, M.A., Shabat, B.V.: *Methods in Theory of Functions of Complex Variable*. Physical and Mathematical Literature Press, Moscow (1958) (in Russian).
95. Bateman, H., Etdelyi, A.: *Higher Transcendental Functions*. McGraw-Hill, New York (1953).
96. Riesz, F., Sz.-Nagy, B.: *Lecons D'Analyse Fonctionnelle*. Akademiai Kiado, Budapest (1972) (in French).
97. Kirilenko, A.A., Masalov, S.A.: The diffraction of *H*-polarized waves by a strip grating of jalousie type. *Higher School News. Radio-Phys.*, **15**, No.1, 83–97 (1972) (in Russian).
98. Kirilenko, A.A., Masalov, S.A., Shestopalov, V.P.: The wave diffraction by a strip grating of jalousie type. *J. Comput. Math. Math. Phys.*, **12**, No.2, 413–428 (1972) (in Russian).
99. Budanov, V.Ye., Kirilenko, A.A.: On radiation of an electron beam over an echelette. *Radio-Eng. Kharkov State Univ. Press*, No.20, 3–11 (1972) (in Russian).
100. Masalov, S.A., Sirenko, Y.K., Shestopalov, V.P.: A solution of plane wave diffraction by a knife grating with a complicated structure of the period. *Radio-Eng. Electron.*, **23**, No.3, 481–487 (1978) (in Russian).
101. Masalov, S.A.: A rigorous solution to the wave diffraction problem for an echelette grating with sharp teeth. *Rep. Acad. Sci. Ukrain. SSR*, **Ser.**A, No.7, 638–642 (1978) (in Russian).
102. Kirilenko, A.A., Masalov, S.A., Rud', L.A.: Wave diffraction by a saw-tooth surface with sharp teeth. *J. Tech. Phys.*, **50**, No.10, 2041–2049 (1980) (in Russian).
103. Masalov, S.A.: Semi-inversion method in the wave diffraction problem of a finite conductivity echelette. *Rep. Acad. Sci. USSR*, **253**, No.5, 1091–1094 (1980) (in Russian).
104. Sirenko, Y.K., Shestopalov, V.P.: Rigorous theory of wave scattering by a diffraction echelette-type grating with absorbing bounds. *Rep. Acad. Sci. USSR*, **263**, No.4, 851–854 (1982) (in Russian).
105. Sirenko, Y.K.: On the validation of the method of semi-inversion of matrix operators in the problems of wave diffraction. *J. Comput. Math. Math. Phys.*, **23**, No.6, 1381–1391 (1983) (in Russian).
106. Kirilenko, A.A., Masalov, S.A.: On truncation method as applied to some infinite system of equations. *J. Comput. Math. Math. Phys.*, **9**, No.4, 934–937 (1969) (in Russian).
107. Masalov, S.A., Sirenko, Y.K., Shestopalov, V.P.: On truncation technique application to some infinite systems of equations. *Rep. Acad. Sci. Ukrain. SSR*, **Ser.**A, No.6, 539–543 (1977) (in Russian).
108. Masalov, S.A.: Semi-inversion method and infinite equation systems in some problems of wave diffraction. *J. Comput. Math. Math. Phys.*, **21**, No.1, 80–88 (1981) (in Russian).
109. Sirenko, Y.K.: On a possibility for analytical solution of some classical problems in diffraction theory. *J. Comput. Math. Math. Phys.*, **23**, No.2, 202–208 (1983) (in Russian).
110. Hokhberg, I.Z., Fel'dman, I.A.: *Convolutional Equations and Projection Methods of Their Solution*. Nauka, Moscow (1971) (in Russian).
111. Gahov, F.D., Cherskiy, Y.I.: *Convolution Type Equations*. Nauka, Moscow (1978) (in Russian).

112. Shestopalov, V.P., Shcherbak, V.V.: Matrix operators in diffraction problems. *Higher school news. Radio-Phys.*, **11**, No.2, 285–305 (1968) (in Russian).
113. Hashimoto, M., Idemen, M, Tretyakov, O.A. (ed.): *Analytical and Numerical Methods in Electromagnetic Wave Theory*. Science House, Tokyo (1993).
114. Petrusenko, I.V.: Basic properties of generalized scattering matrix of waveguide transformers. *Electromagnetics*, **26**, No.8, 601–614 (2006).
115. Hutson, V.C.L., Pym, J.S.: *Applications of Functional Analysis and Operator Theory*. Academic, New York (1980).
116. Cooke, R.G.: *Infinite Matrices and Sequence Spaces*. London University Press, London (1950).
117. Lindell, I.V., Sihvola, A.A., Tretyakov, S.A., Viitanen, A.J.: *Electromagnetic Waves in Chiral and Bi-Isotropic Media*. Artech House Inc., Boston-London (1994).
118. Sihvola, A.A.: *Electromagnetic Mixing Formulas and Applications*. Inst. Elect. Eng., London (1999).
119. Engheta, N., Pelet, P.: Reduction of surface waves in chirostrip antennas. *Electron. Lett.*, **27**, No.1, 5–7 (1991).
120. Bilotti, F., Toscano, A., Vegni, L.: FEM-BEM Formulation for the analysis of cavity-backed patch antennas on chiral substrates. *IEEE Trans.*, **AP-51**, No.2, 306–311 (2003).
121. Bilotti, F., Vegni, L.: Chiral cover effects on microstrip antennas. *IEEE Trans.*, **AP-51**, No.10, 2891–2898 (2003).
122. Wu, T.X., Jaggard, D.L.: Scattering of chiral periodic structure. *IEEE Trans.*, **AP-52**, No.7, 1859–1870 (2004).
123. Panin, S.B., Poyedinchuk, A.Y.: Electromagnetic wave diffraction by a grating with a chiral layer. *Radiophys. Quantum Electron.*, **45**, No.8, 629–639 (2002).
124. Panin, S.B., Smith, P.D., Poyedinchuk, A.Y.: Elliptical to linear polarization transformation by a grating on a chiral medium. *J. Electromag. Waves Appl.*, **21**, No.13, 1885–1899 (2007).
125. Panin, S.B., Poyedinchuk, A.Y.: Polarization properties of a screened chiral layer with a diffraction grating. *Telecomm. Radio Eng.*, **58**, No.3&4, 68–81 (2002).
126. Kusaykin, O.P., Poyedinchuk, A.Y.: Electromagnetic wave diffraction by a chiral layer with a reflecting grating of dielectric filled grooves. *IEEE Microwave Opt. Tech. Lett.*, **36**, No.5, 462–465 (2002).
127. Panin, S.B.: The nonspecular wave reflection from a screened chiral layer with a diffraction grating. *Radiophys. Electron., Proceedings of Institute for Radiophysics and Electronics NASU*, **7**, Special Issue, 288–293, (2002) (in Russian).
128. Kuzu, L., Demir, V., Elsherbeni, A.Z., Arvas, E.: Electromagnetic scattering from arbitrarily shaped chiral objects using the finite difference frequency domain method. *Progress Electromag. Res.*, **67**, 1–24 (2007).
129. Zhang, Y.J., Li, E.P.: Scattering of three-dimensional chiral objects above a perfect conducting plane by hybrid finite element method. *J. Electromag. Waves Appl.*, **19**, No.11, 1535–1546 (2005).
130. Zhang, Y.J., Bauer, A., Li, E.P.: T-matrix analysis of multiple scattering from parallel semicircular channels filled with chiral media in a conducting plane. *Progress Electromag. Res.*, **53**, 299–318 (2005).
131. Tretyakov, S.A.: Electrodynamics of complex media: chiral, biisotropic and some bianisotropic materials. *Radio-Eng. Electron.*, **39**, No.10, 1457–1470 (1994) (in Russian).
132. Meixner, J.: The behaviour of electromagnetic field at edges. *IEEE Trans.* **AP-20**, No.4, 442–446 (1972).
133. Panin, S.B., Poyedinchuk, A.Y.: The solution method of the electromagnetic wave diffraction vector problem for a one-dimensional periodic grating with chiral medium. *Rep. Akad. Sci. Ukraine*, **Ser.**A, No.3, 85–89 (2000) (in Russian).
134. Born, M., Wolf, E.: Principles of Optics. Cambridge University Press, Cambridge (1999).

135. Poyedinchuk, A.Y., Tuchkin, Y.A., Yashina, N.P., Chandezon, J., Granet, G.: C-method: several aspects of spectral theory of gratings. *Progress Electromag. Res.*, **59**, 113–149 (2006).
136. Adonina, A.I., Shcherbak, V.V.: The oblique incidence electromagnetic wave diffraction by a plane metal grating with a screen and a magnetodielectric. *J. Tech. Phys.*, **34**, No.3, 168–173 (1964) (in Russian).
137. Khoroshun, V.V.: The plane electromagnetic wave diffraction by a metal grating with a gyromagnetic medium. *Radio-Eng. Kharkov State Univ. Press*, No.4, 20–25 (1967) (in Russian).
138. Khoroshun, V.V.: The plane electromagnetic wave diffraction by a screened grating with a transversely magnetized real ferrite. *Radio-Eng. Kharkov State Univ. Press*, No.7, 32–37 (1968) (in Russian).
139. Baregamyan, V.A.: The electromagnetic wave diffraction by a plane metal grating with anisotropic dielectric. *Radio-Eng. Kharkov State Univ. Press*, No.1, 108–113 (1965) (in Russian).
140. Tretyakov, O.A., Shestopalov, V.P.: The electromagnetic wave diffraction from a plane metal grating supported by a dielectric layer. *Higher School News. Radio-Phys.*, **6**, No.2, 353–341 (1963) (in Russian).
141. Uehara, M., Yashiro, K., Ohkawa, S.: A method for solving Riemann-Hilbert boundary value problems in nonreciprocal wave propagation. *J. Math. Phys.*, **38**, No.5, 2417–2434 (1997).
142. Uehara, M., Yashiro, K., Ohkawa, S.: Diffraction of waves from a strip grating on a ferrite substrate. *Scripta Technica, Electron Comm. Jap. Pt.2*, **82**, No.7, 41–49 (1999).
143. Nishimura, K., Tsutsumi, M.: Scattering of millimeter waves by metallic strip gratings on an optically plasma-induced semiconductor slab. *IEEE Trans.*, **MTT-44**, No.12, 2231–2237 (1996).
144. Brovenko, A.V., Melezhik, P.N., Poyedinchuk, A.Y.: Diffraction of a plane electromagnetic wave by a metal grating with a magnetoplasma. *Higher School News. Radio-Phys.*, **47**, No.8, 638–649 (2004) (in Russian).
145. Brovenko, A.V., Melezhik, P.N., Poyedinchuk, A.Y., Yashina, N.P., Granet, G.: Surface resonances of a metal stripe grating on a plane metamaterial boundary. *Progress Electromag. Res.*, **63**, 209–222 (2006)
146. Kusaykin, O.P., Melezik, P.N., Poyedinchuk, A.Y., Troschylo, O.S.: Absorbing properties of a negative permittivity layer placed on a reflecting grating. *Progress Electromag. Res.*, **64**, 135–148 (2006).
147. Kusaykin, O.P., Melezik, P.N., Poyedinchuk, A.Y.: Absorption of waves by a grating filled with a metamaterial with a negative dielectric constant. *Telecomm. Radio Eng.*, **66**, No.3, 187–200 (2007).
148. Kusaykin, O.P., Melezik, P.N., Poyedinchuk, A.Y.: Resonance radiation of electromagnetic waves by a diffraction grating filled with metamaterial. *Tech. Phys. Lett.*, **35**, No.1, 13–16 (2009).
149. Krutin', Y.I., Tuchkin, Y.A., Shestopalov, V.P.: Diffraction of -polarized wave by periodic smooth wavy surfaces. *Radio-Eng. Electron.*, **37**, No.2, 202–210 (1992) (in Russian).
150. Krutin', Y.I., Tuchkin, Y.A., Shestopalov, V.P.: Regularization of boundary value problem of wave diffraction by grating which formed by rods of arbitrary profile with Dirichlet boundary condition. *J. Comput. Math. Math. Phys.*, **31**, No.6, 864–876 (1991) (in Russian).
151. Chandezon, J., Maystre, D., Raoult, G.: A new theoretical method for diffraction gratings and its numerical application. *J. Opt. (Paris)*, **11**, No.4, 235–241 (1980).
152. Chandezon, J., Dupuis, M.T., Cornet, G., Maystre, D.: Multicoated gratings: a differential formalism applicable in the entire optical region. *J. Opt. Soc. Am.*, **72**, No.7, 839–846 (1982).
153. Post, E.J.: *Formal Structure of Electromagnetics*. Amsterdam, North-Holland (1962).
154. Popov, E., Mashev, L.: Conical diffraction mounting generalization of a rigorous differential method. *J. Opt. (Paris)*, **17**, No.4, 175–180 (1986).

155. Elston, S.J., Bryan-Brown, G.P., Sambles, J.R.: Polarization conversion from diffraction gratings. *Phys. Rev. B.*, **44**, No.12, 6393–6400 (1991).
156. Plumey, J.P., Granet, G., Chandezon, J.: Differential covariant formalism for solving Maxwell's equations in curvilinear coordinates:oblique scattering from lossy periodic surfaces. *IEEE Trans.*, **AP-43**, No.8, 835–842 (1995).
157. Granet, G., Plumey, J.P., Chandezon, J.: Scattering by a periodically corrugated dielectric layer with non identical faces. *Pure Appl. Opt.*, **4**, No.1, 1–5 (1995).
158. Preist, T.W., Cotter, N.P.K., Sambles, J.R.: Periodic multilayer gratings of arbitrary shape. *J. Opt. Soc. Am. A.*, **12**, No.8, 1740–1749 (1995).
159. Li, L., Granet, G., Plumey, J.P., Chandezon, J.: Some topics in extending the C-method to multilayer-coated gratings of different profiles. *Pure Appl. Opt.*, **5**, No.2, 141–156 (1996).
160. Plumey, J.P., Guizal, B., Chandezon, J.: Coordinate transformation method as applied to asymmetric gratings with vertical facets. *J. Opt. Soc. Am. A.*, **14**, No.3, 610–617 (1997).
161. Preist, T.W., Harris, J.B., Wanstall, N.P., Sambles, J.R.: Optical response of blazed and overhanging gratings using Chandezon transformations. *J. Mod. Opt.*, **44**, No.6, 1073–1080 (1997).
162. Li, L.: Multilayer-coated diffraction gratings: differential method of Chandezon et al. revisited. *J. Opt. Soc. Am. A.*, **11**, No.11, 2816–2828 (1994).
163. Cotter, N.P.K., Preist, T.W., Sambles, J.R.: Scattering matrix approach to multilayer diffraction. *J. Opt. Soc. Am. A.*, **12**, No.5, 1097–1103 (1995).
164. Li, L., Chandezon, J., Granet, G., Plumey, J.P.: Rigorous and efficient grating-analysis method made easy for optical engineers. *Appl. Opt.*, **38**, No.2, 304–313 (1999).
165. Granet, G.: Reformulation of the lamellar grating problem through the concept of adaptive spatial resolution. *J. Opt. Soc. Am. A.*, **16**, No.10, 2510–2516 (1999).
166. Granet, G., Chandezon, J., Plumey, J.P., Raniriharinosy, K.: Reformulation of the coordinate transformation method through the concept of adaptive spatial resolution. Application to trapezoidal gratings. *J. Opt. Soc. Am. A.*, **18**, No.9, 2102–2108 (2001).
167. Watanabe, K.: Study of the differential theory of lamellar gratings made of highly conducting materials. *J. Opt. Soc. Am. A.*, **23**, No.1, 69–72 (2006).
168. Lyndin, N.M., Parriaux, O., Tishenko, A.V.: Modal analysis and suppression of the Fourier modal method instabilities in highly conductive gratings. *JOSA A.*, **24**, No.12, 3781–3788 (2007).
169. Montiel, F., Nevière, M.: Electromagnetic study of the diffraction of light by a mask used in photolithography. *Opt. Commun.*, **101**, No.3–4, 151–156 (1993).
170. Adonina, A.I., Shestopalov, V.P.: The oblique incidence electromagnetic wave diffraction by a plane metal grating with a dielectric layer. *J. Tech. Phys.*, **33**, No.6, 641–651 (1963) (in Russian).
171. Granet, G., Guizal, B.: Analysis of strip gratings using a parametric modal method by Fourier expansions. *Opt. Commun.*, **255**, No.1–3, 1–11 (2005).
172. Hall, R.C., Mittra, R., Mitzner, K.M.: Scattering from finite thickness resistive strip gratings. *IEEE Trans.*, **AP-36**, No.4, 504–510 (1988).
173. Engheta, N., Ziolkowski, R.W.: A positive future for double-negative metamaterials. *IEEE Trans.*, **MTT-53**, No.4, 1535–1556 (2005).
174. Alu, A., Engheta, N., Erentok, A., Ziolkowski, R.W.: Single-negative, double-negative, and low-index metamaterials and their electromagnetic applications. *IEEE Ant. Propag. Mag.*, **49**, No.1, 23–36 (2007).
175. Cakir, M., Cakir, G., Sevgi, L.: A to-dimensional FDTD-based virtual visualization tool for metamaterial-wave interaction. *IEEE Ant. Propag. Mag.*, **50**, No.3, 166–175 (2008).
176. Felsen, L.B. (ed.): *Transient Electromagnetic Fields*. Springer-Verlag, New York (1976).
177. Borisov, V.V.: *Transient Fields in Waveguides*. Leningrad State University Press, Leningrad (1991) (in Russian).
178. Miller, E.K.: Time-domain modeling in electromagnetics. *J. Electromag. Waves Appl.*, **8**, No.9&10, 1125–1172 (1994).

179. He, S., Ström, S., Weston, V.: *Time Domain Wave-Splittings and Inverse Problems*. Oxford University Press, Oxford (1998).
180. Rao, S.M. (ed.): *Time Domain Electromagnetics*. Academic, San Diego (1999).
181. Engquist, B., Majda, A.: Absorbing boundary conditions for the numerical simulation of waves. *Math. Comput.*, **31**, No.139, 629–651 (1977).
182. Mur, G.: Absorbing boundary conditions for the finite difference approximation of the time-domain electromagnetic-field equations. *IEEE Trans.*, **EMC-23**, No.4, 377–382 (1981).
183. Tirkas, P.A., Balanis, C.A., Renaut, R.A.: Higher order absorbing boundary conditions for FDTD-method. *IEEE Trans.*, **AP-40**, No.10, 1215–1222 (1992).
184. Berenger, J.-P.: A perfectly matched layer for the absorption of electromagnetic waves. *J. Comput. Phys.*, **114**, No.1, 185–200 (1994).
185. Berenger, J.-P.: Three-dimensional perfectly matched layer for absorption of electromagnetic waves. *J. Comput. Phys.*, **127**, No.2, 363–379 (1996).
186. Sacks, Z.S., Kingsland, D.M., Lee, R., Lee, J.F.: A perfectly matched anisotropic absorber for use as an absorbing boundary condition. *IEEE Trans.*, **AP-43**, No.12, 1460–1463 (1995).
187. Maikov, A.R., Sveshnikov, A.G., Yakunin, S.A.: Difference scheme for the Maxwell transient equations in waveguide systems. *J. Comput. Math. Math. Phys.*, **26**, No.6, 851–863 (1986) (in Russian).
188. Maikov, A.R., Poezd, A.D., Sveshnikov, A.G., Yakunin, S.A.: Difference scheme of initial boundary-value problems for Maxwell equations in unlimited domain. *J. Comput. Math. Math. Phys.*, **29**, No.2, 239–250 (1989) (in Russian).
189. Perov, A.O., Sirenko, Y.K., Yashina, N.P.: Explicit conditions for virtual boundaries in initial boundary value problems in the theory of wave scattering. *J. Electromag. Waves Appl.*, **13**, No.10, 1343–1371 (1999).
190. Sirenko, Y.K., Pazynin, V.L., Vyazmitinova, A.I., Sirenko, K.Y.: Compact obstacles in free space: virtual boundaries for scalar and vector "open" initial boundary-value problems in electromagnetic wave scattering theory. *Electromag. Waves Electron. Syst.*, **8**, No.11–12, 33–54 (2003) (in Russian).
191. Sirenko, K.Y., Sirenko, Y.K.: Exact "absorbing" conditions in the initial boundary-value problems of the theory of open waveguide resonators. *Comput. Math. Math. Phys.*, **45**, No.3, 490–506 (2005).
192. Sirenko, K.Y.: Transport operators in the axially-symmetrical problems of the electrodynamics of pulsed waves. *Electromag. Waves Electron. Syst.*, **11**, No.11, 15–26 (2006) (in Russian).
193. Sirenko, K.Y., Pazynin, V.L.: Axially-symmetrical radiators of pulsed and monochromatic TE_{0n}- and TM_{0n}-waves. *Success Modern Radioelectron.*, No.4, 52–69 (2006) (in Russian).
194. Pazynin, V.L., Sirenko, K.Y.: The strong approach to analysis of transients in the axially symmetrical waveguide units. *Telecomm. Radio Eng.*, **65**, No.1, 1–18 (2006).
195. Sirenko, K.Y.: Slot resonances in axially symmetric radiators of pulse-modulated and monochromatic TM_{0n}-modes. *Telecomm. Radio Eng.*, **66**, No.1, 9–21 (2007).
196. Sirenko, Y.K., Yashina, N.P.: Nonstationary model problems for waveguide open resonator theory. *Electromagnetics*, **19**, No.5, 419–442 (1999).
197. Sirenko, Y.K., Yashina, N.P.: Time domain theory of open waveguide resonators: canonical problems and a generalized matrix technique. *Radio Sci.*, **38**, No.2, VIC 26-1–VIC 26-12 (2003).
198. Abramowitz, M., Stegun, I.A. (eds.): *Handbook of Mathematical Functions*. Dover, New York (1972).
199. Bateman, H., Erdelyi, A.: *Tables of Integral Transforms*, *Vol.1*. McGraw-Hill, New York (1954).
200. Mikhailov, V.P.: *Partial Differential Equations*. Nauka, Moscow (1976) (in Russian).
201. Korn, G.A., Korn, T.M.: *Mathematical Handbook for Scientists and Engineers*. McGraw-Hill, New York (1961).

202. Gradshteyn, I.S., Ryzhik, I.M.: *Table of Integrals, Series, and Products*. Academic, New York (1994).
203. Sirenko, Y.K., Velychko, L.G., Erden, F.: Time-domain and frequency-domain methods combined in the study of open resonance structures of complex geometry. *Progress Electromag. Res.*, **44**, 57–79 (2004).
204. Velychko, L.G., Sirenko, Y.K., Shafalyuk, O.S.: Time-domain analysis of open resonators. Analytical Grounds. *Progress Electromag. Res.*, **61**, 1–26 (2006).
205. Muravey, L.A.: Analytical extension on the Green function parameter of the outer boundary-value problem for two-dimensional Helmholtz equation. III. *Coll. Papers Math.*, **105**, No.1, 63–108 (1978) (in Russian).
206. Anokhov, S.P., Marusiy, T.Y., Soskin, M.S.: *Tunable Lasers*. Radio and Communication, Moscow (1982) (in Russian).
207. Avtonomov, V.P., Beltyugov, V.N., Ochkin, V.N., Sobolev, N.N., Udalov, Y.B.: Study of the selective properties of an optical resonator with a reflective grating. Academy of Sciences of USSR, Moscow, Preprint PhI; No.80–29 (1980) (in Russian).
208. Belous, O.I., Kirilenko, A.A., Fisun, A.I.: Quasi-single-frequency spectra of an open resonator with a comb grating. *Higher School News. Radio-Electron.*, **41**, No.4, 8–13 (1998) (in Russian).
209. Perov, A.O., Sirenko, Y.K., Yashina, N.P.: Periodic open resonators: peculiarities of pulse scattering and spectral features. *Progress Electromag. Res.*, **46**, 33–75 (2004).
210. Shestopalov, V.P., Kirilenko, A.A., Rud', L.A.: *Resonance Wave Scattering. Vol.2. Waveguide Discontinuities*. Naukova Dumka, Kiev (1986) (in Russian).
211. Sirenko, K.Y.: Splitting of super-broadband pulses by simple inhomogeneities of circular and coaxial waveguide. *Telecomm. Radio Eng.*, **67**, No.16, 1415–1428 (2008).
212. Evdokimov, A.P., Kryzhanovskiy, V.V.: New line of investigation in the antenna array techniques. *Higher School News. Radio-Electron.*, **39**, No.9, 54–61 (1996) (in Russian).
213. Evdokimov, A.P., Kryzhanovskiy, V.V.: The plane antenna arrays with a cosecant directional pattern for 8-mm waves. *Electromag. Waves Electron. Syst.*, **8**, No.10, 52–58 (2003) (in Russian).
214. Evdokimov, A.P., Kryzhanovskiy, V.V.: The plane antenna array with a combined beam scanning. *Electromag. Waves Electron. Syst.*, **10**, No.1–2, 52–56 (2005) (in Russian).
215. Lee, J.W., Eom, H.J., Park, K.H., Chun, W.J.: TM-wave radiation from grooves in a dielectric-covered ground plane. *IEEE Trans.*, **AP-49**, No.1, 104–105 (2001).
216. Kirilenko, A.A., Rud', L.A., Tkachenko, V.I.: Nonsymmetrical *H*-plane corners for TE_{10}–TE_{q0}-mode conversion in rectangular waveguides. *IEEE Trans.*, **MTT-54**, No.6, 2471–2477 (2006).
217. Sauleau, R., Coquet, Ph., Thouroude, D., Daniel, J.-P., Matsui, T.: Radiation characteristics and performance of millimeter-wave horn-fed Gaussian beam antennas. *IEEE Trans.*, **AP-51**, No.3, 378–387 (2003).
218. Sauleau, R., Coquet, Ph., Matsui, T., Daniel, J.-P.: A new concept of focusing antennas using plane-parallel Fabry-Perot cavities with nonuniform mirrors. *IEEE Trans.*, **AP-51**, No.11, 3171–3175 (2003).
219. Guerin, N., Enoch, S., Tayeb, G., Sabouroux, P., Vincent, P., Legay, H.: A metallic Fabry-Perot directive antenna. *IEEE Trans.*, **AP-54**, No.1, 220–224 (2006).
220. Amitay, N., Galindo, V., Wu, C.P.: *Theory and Analysis of Phased Array Antennas*. Wiley & Sons, New York (1972).
221. Montoya, T.P., Smith, G.S.: A study of pulse radiation from several broad-band monopoles. *IEEE Trans.*, **AP-44**, No.8, 1172–1182 (1996).
222. Cioranescu, D., Donato, P.: *An Introduction to Homogenization*. Oxford University Press, Oxford (1999).
223. Bensoussan, A., Lions, J.L., Papanicolaou, G.: *Asymptotic Analysis for Periodic Structures*. North-Holland, Amsterdam (1978).
224. Torquato, S.: *Random Heterogeneous Materials: Microstructure and Microscopic Properties*. Springer-Verlag, Berlin (2002).

225. Jikov, V.V., Kozlov, S.M., Oleinik, O.A.: *Homogenization of Differential Operators and Integral Functionals*. Springer-Verlag, Berlin (1994).
226. Milton, G.W.: *The Theory of Composites*. Cambridge University Press, Cambridge (2002).
227. Conca, C., Orive, R., Vanninathan, M.: Bloch approximation in homogenization and applications. *SIAM J. Math. Anal.*, **33**, No.5, 1166–1198 (2002).
228. Conca, C., Vanninathan, M.: Homogenization of periodic structures via Bloch decomposition. *SIAM J. Appl. Math.*, **57**, No.6, 1639–1359 (1997).
229. Ganesh, S.S., Vanninathan, M.: Bloch wave homogenization of scalar elliptic operators. *Asymptot. Anal.*, **39**, 15–44 (2004).
230. Morgan, R.C., Babuska, I.: An approach for constructing families of homogenized equations for periodic media. I: An integral representation and its consequences. *SIAM J. Math. Anal.*, **22**, No.1, 1–15 (1991).
231. Morgan, R.C., Babuska, I.: An approach for constructing families of homogenized equations for periodic media. II: Properties of the kernel. *SIAM J. Math. Anal.*, **22**, No.1, 16–39 (1991).
232. Santosa, F., Symes, W.W.: A dispersive effective medium for wave propagation in periodic composites. *SIAM J. Appl. Math.*, **51**, No.4, 984–1005 (1991).
233. Sevostyanova, E.V.: Asymptotic expansion of the solution of a second-order elliptic equation with periodic rapidly oscillating coefficients. *Coll. Papers Math.*, **115**, No.2, 204–222 (1981) (in Russian; see also English translation in Math. USSR Sb., 43, No.2, 181–198 (1982)).
234. Jackson, J.D.: *Classical Electrodynamics*. Wiley & Sons, New York (1999).
235. Bloch, F.: Über die Quantenmechanik der Electronen in Kristallgittern. *Z. Phys. Hadrons Nuclei*, **52**, No.7–8, 555–600 (1929) (in German).
236. Floquet, G.: Sur les équations différentielles linéaires à coefficients périodiques. *Ann. École Norm. Sup.*, **12**, No.2, 47–88 (1883) (in French).
237. Sjöberg, D., Engström, C., Kristensson, G., Wall, D.J.N., Wellander, N.: A Floquet-Bloch decomposition of Maxwell's equations applied to homogenization. *Multiscale Model. Simul.*, **4**, No.1, 149–171 (2005).
238. Kato, T.: *Perturbation Theory for Linear Operators*. Springer-Verlag, Berlin (1980).
239. Lassas, M.: The essential spectrum of the nonself-adjoint Maxwell operator in a bounded domain. *J. Math. Anal. Appl.*, **224**, No.2, 201–217 (1998).
240. Sjöberg, D.: Homogenization of dispersive material parameters for Maxwell's equations using a singular value decomposition. *Multiscale Model. Simul.*, **4**, No.3, 760–789 (2005).
241. Kress, R.: *Linear Integral Equations*. Springer-Verlag, Berlin (1999).
242. Johnson, S.G., Joannopoulos, J.D.: Block-iterative frequency-domain methods for Maxwell's equations in a planewave basis. *Opt. Express*, **8**, No.3, 173–190 (2001).
243. Dobson, D.C., Gopalakrishnan, J., Pasciak, J.E.: An efficient method for band structure calculations in 3-D photonic crystals. *J. Comput. Phys.*, **161**, No.2, 668–679 (2000).
244. Sjöberg, D.: Dispersive effective material parameters. *Microwave Opt. Tech. Lett.*, **48**, No.12, 2629–2632 (2006).
245. Sjöberg, D.: Exact and asymptotic dispersion relations for homogenization of stratified media with two phases. *J. Electromag. Waves Appl.*, **20**, No.6, 781–792 (2006).
246. Sjöberg, D., Kristensson, G., Engström, C.: Validity of homogenization using Bloch waves. Proc. Int. Conf. Electromagn. Advan. Appl. (ICEAA), Torino, Italy, 455–458 (2003).
247. Lindman, K.F.: Über eine durch ein isotropes system von spiralförmigen resonatoren erzeugte rotationpolarisation der elektromagnetischen wellen. *Ann. Phys.*, **63**, No.23, 621–644 (1920) (in German).
248. Sjöberg, D.: A modified Drude-Born-Fedorov model for isotropic chiral media, obtained by finite scale homogenization. *J. Phys. D: Appl. Phys.*, **41**, 155412 (6 pp) (2008).
249. Born, M.: Über die natürliche optische aktivität von Flüssigkeiten und Gasen. *Phys. Z.*, **16**, 251–258 (1915) (in German).
250. Born, M.: Über die natürliche optische aktivität der kristalle. *Z. Phys. Hadrons Nuclei*, **8**, No.1, 390–417 (1922) (in German).

Index